The Synthesis of Peptide-Based Tools for Drug Discovery and Chemical-Biology Applications

CARISSA MELANIE LLOYD

The Synthesis of Peptide-Based Tools for Drug Discovery and Chemical-Biology Applications

A Thesis Presented for the Degree of Doctor of Philosophy
The Department of Chemistry
Durham University, Hatfield College

Carissa Melanie Lloyd

Supervised by Professor Steven Cobb and Dr Neil Colgin

2023

The work described in this thesis was carried out at Durham University and Cambridge Research Biochemicals (CRB). It is the work of the author, except where acknowledged by reference, and has not been submitted for any other degree. The copyright of this thesis rests with the author. No quotation or image from it should be published without the author's prior written consent and information derived from it should be acknowledged.

Abstract

Peptidyl mono-fluoromethyl ketones (mFMK) are a class of compounds that have shown potential as protease inhibitors for the treatment of a range of diseases. They have also found application as chemical-biology probes that can be used in the interrogation of cellular processes. Despite the aforementioned applications, the number of synthetically viable routes reported for accessing these compounds is currently rather limited.

To address this issue, the work herein reports the efforts that have been made towards developing a novel synthetic pathway for preparing mFMKs. Initial attempts (**Chapter 2**) involved the formation of a tri-carbonyl system derived from a Boc-protected amino acid and Meldrum's acid, with the intention of subsequently fluorinating, converting to the corresponding *β*-ketoester and coupling to a peptide of choice in solution. The idea was that the resulting substrate could then be saponified and decarboxylated, allowing access to the fluoromethyl ketone (FMK). However, the inherent reactivity of the moisture-sensitive fluorinated tri-carbonyl systems made them difficult to handle and isolate.

Attention was therefore turned towards the direct electrophilic fluorination of *β*-ketoesters, derived from either an *N*-Fmoc (**Chapter 3**) or *N*-Boc-protected (**Chapter 4**) amino acid of choice and formed as the *tert*-butyl ester. Selective mono-fluorination of the resulting 1,3-dicarbonyl was then achieved using $CpTiCl_3$ in conjunction with Selectfluor, through utilisation of adapted literature protocols. The resulting *N*-Fmoc-protected substrate was carefully transformed to the *β*-ketoacid (**Chapter 3**) before attempted resin loading was performed, with the intention of allowing on-resin peptide growth followed by concomitant resin cleavage, global deprotection and decarboxylation to the FMK. However, unsuccessful resin loading attempts, coupled with evidence for premature FMK formation having occurred during these endeavours, suggested the presence of the fluorine atom had significantly reduced the nucleophilicity of the carboxylate, thus favouring decarboxylation over resin loading.

Given the challenges encountered with resin loading, the application of *N*-Boc-protected mono-fluorinated *β*-ketoesters in solution-phase peptide chemistry was explored (**Chapter 4**). Selective removal of the *N*-Boc group in the presence of the *tert*-butyl ester, through the modification of conditions reported in the literature, enabled coupling to a peptide of choice. Subsequent deprotection and decarboxylation led to the desired FMK. Whilst some epimerisation did appear to occur during peptide coupling, this route represents a straightforward approach for accessing these desirable and highly expensive molecular warheads in only 5 steps.

A slightly adapted approach, in which the *N*-Boc protected *β*-ketoester was first decarboxylated to the corresponding FMK prior to peptide coupling in solution, was also trialled (**Chapter 4**). However, this appeared to lead to challenges in purification of the resultant mFMKs, along with an accompanying low yield. Nonetheless, this methodology was successfully adapted and utilised for the synthesis of a peptidyl mono-chloromethyl ketone (mCMK) in only four steps (**Chapter 5**), although epimerisation was apparent. Furthermore, it is believed that extension of this methodology could allow access to other peptide-based C-terminal modified species, such as peptidyl bromomethyl ketones and di-fluoromethyl ketones.

In summary, the methodology developed for accessing both peptidyl mono-fluoromethyl ketones and peptidyl mono-chloromethyl ketones offers ready access to chemical-probes that can be used to interrogate cellular functions in a range of disease relevant systems.

Acknowledgments

I would like to thank my academic supervisor, Professor Steven Cobb, for all his encouragement and support throughout my research at Durham University. His investment of time and resources has been greatly appreciated, and his insight into Chemistry invaluable. I also extend my thanks to the rest of the Cobb group, both past and present (Dr Will Brittain, Dr Diana Gimenez-Ibanez, Yazmin Santos, Hirunika Perera, Diana Kolos, Izzy Zawadzki, Eleanor Taylor-Newman, Katie Dowell, Marc Lennon, Patrick Christie, Liam Beardmore and Lewis Picken) for their help, support and friendship throughout my research. I particularly want to thank Dr Will Brittain for offering his expertise knowledge, and for his willingness to answer my Chemistry-related queries!

A special mention goes to my industrial supervisor, Dr Neil Colgin, and the rest of the staff at CRB (Cambridge Research Biochemicals), including Fraser Lough, who have kindly taken the time to train me up on solid-phase peptide synthesis along with many other skills, for which I am incredibly grateful. Neil has always gone above and beyond to help and support me, and his vast Chemistry knowledge has been invaluable.

I am thankful to the departmental staff running the mass spectrometry (Peter Stokes and Dr Dave Parker), NMR (Dr Alan Kenwright, Dr Juan Aguilar, Dr Eric Hughes and Catherine Heffernan) and X-ray crystallography (Dr Dmitry Yufit) services. Without them, none of this work would have been possible.

I would like to thank my parents, Tim and Carina, for all their prayer, love and support throughout my studies. I so appreciate all the encouragement you have given me through the highs and lows of my research. Thanks for all the cups of tea, hot chocolates, tasty food, IT support and more (the list goes on and on)! I am very grateful to you both and love you both so much!!! Thank you!!! And most of all I am thankful to Jesus for helping me through this work. Without Him nothing would have been possible!

Publications

Lloyd, C.M.; Colgin, N.; Cobb, S.L. Current Synthetic Routes to Peptidyl Mono-Fluoromethyl Ketones (FMKs) and Their Applications. *Molecules* **2020**, *25*, 5601. https://doi.org/10.3390/molecules25235601

Brittain, W.D.G; Lloyd, C.M; Cobb S.L. Synthesis of complex unnatural fluorine-containing amino acids. *J. Fluor. Chem.* **2020**, 239, 109630 https://doi.org/10.1016/j.jfluchem.2020.109630

Abbreviations

AA	Amino acid
Ac	Acyl
BMK	Bromomethyl ketone
Boc	*tert*-butoxycarbonyl
b.p.	Boiling point
Bu	Butyl
Cbz	Carboxybenzyl
CMK	Chloromethyl ketone
COSY	Correlation spectroscopy
CRB	Cambridge Research Biochemicals
CYP	Cytochrome P450
DCM	Dichloromethane
DDI	Drug-drug interaction
DIC	*N*,*N*-Diisopropylcarbodiimide
DIPEA	*N*,*N*-Diisopropylethylamine
DMAP	4-Dimethylaminopyridine
DMF	*N, N*-dimethylformamide
DMSO	Dimethyl sulfoxide
EI	Electron impact (ionisation)
ESI	Electrospray ionisation
Et	Ethyl
EtOAc	Ethyl acetate
EtOH	Ethanol
FDA	Food and Drug Administration
FMK	Fluoromethyl ketone
Fmoc	Fluorenylmethyloxycarbonyl
GCMS	Gas Chromatography Mass Spectrometry
h	Hour (s)
HATU	1-[Bis(dimethylamino)methylene]-1*H*-1,2,3-triazolo[4,5-*b*]pyridinium 3-oxid hexafluorophosphate
HMBC	Heteronuclear multiple-bond correlation spectroscopy

HOAt	1-Hydroxy-7-azabenzotriazole
HOBt	Hydroxybenzotriazole
HPLC	High performance liquid chromatography
HRMS	High-resolution mass spectrometry
HSQC	Heteronuclear single-quantum correlation spectroscopy
***i*-Pr**	Isopropyl
LC	Liquid chromatography
LC-MS	Liquid chromatography – mass spectrometry
LDA	Lithium diisopropylamide
Me	Methyl
MeCN	Acetonitrile
MeOH	Methanol
Mins	Minutes
m.p.	Melting point
MS	Mass spectrometry
MW	Molecular weight
m/z	Mass to charge ratio
NMR	Nuclear magnetic resonance
PG	Protecting group
Ph	Phenyl
pK_a	Logarithmic acid dissociation constant
PMA	Phosphomolybdic acid
ppm	Parts per million
Prep TLC	Preparative thin layer chromatography
PyBOP	(Benzotriazol-1-yloxy)tripyrrolidinophosphonium Hexafluorophosphate
rt	Room temperature
r.t.	Retention time
SelectFluor™	1-Chloromethyl-4-fluoro-1,4-diazoniabicyclo[2.2.2]octane bis(tetrafluoroborate)
S_N2	Bimolecular nucleophilic substitution
SPPS	Solid-phase peptide synthesis
^{t}Bu	Tertiary butyl
TEA	Triethylamine

TFA	Trifluoroacetic acid
TFAA	Trifluoroacetic anhydride
THF	Tetrahydrofuran
TIC	Total ion chromatogram
TIPS	Triisopropylsilane
TLC	Thin layer chromatography
TQD	Triple quadrupole
ToF	Time of flight
TNBS	2,4,6-Trinitrobenzenesulfonic acid
UV	Ultraviolet
UV-VIS	Ultraviolet visible
v/v	Volume concentration
w/v	Mass concentration
w/w	Weight concentration
Z	Carboxybenzyl

Contents

1. Introduction

1.1 Peptides in Chemical-Biology and Medicinal Chemistry

The use of peptide-based molecules in the area of medicinal chemistry has led to the discovery of many novel therapeutics, as well as chemical-biology tools for interrogative applications.[1,2] Peptide-based compounds are now commonly seen in the pharmaceutical industry and many are listed as FDA (Food and Drug Administration) approved drugs,[3] whilst others are undergoing clinical trials.[4–10] Examples range from native peptides derived from natural sources, such as insulin (**1**) for the treatment of diabetes, to modified novel peptide analogues produced synthetically in the laboratory with careful engineering[11], such as Lupron^{TM} (**2**), which is used to treat prostate cancer[6] (**Figure 1.1**).[11] In addition to their use as therapeutics, peptides have also proved to be invaluable tools for probing biological systems in order to gain a greater understanding of cellular activity and for the identification of potential new drug targets.[12] This unique class of compounds, which is elegantly poised between proteins and organic small molecules,[1] exhibits a wide range of desirable properties,[13,14] making them highly attractive candidates for a range of diagnostic[15] and medicinal applications.[16] As a multitude of peptides are naturally occurring within the body and play key roles in many biological processes including signalling, studying their mode of action along with the nature of the targets that they bind and designing mimic compounds accordingly has proved an effective route to accessing new biologically active compounds.[1] Peptides can be modified according to their desired function, and their high binding affinities makes them ideal candidates for drug discovery and cellular interrogation.[13] In addition to this, they often benefit from low toxicity and high specificity towards their targets,[7,17] reducing the likelihood of unwanted interactions with other receptors, avoiding adverse side-effects.

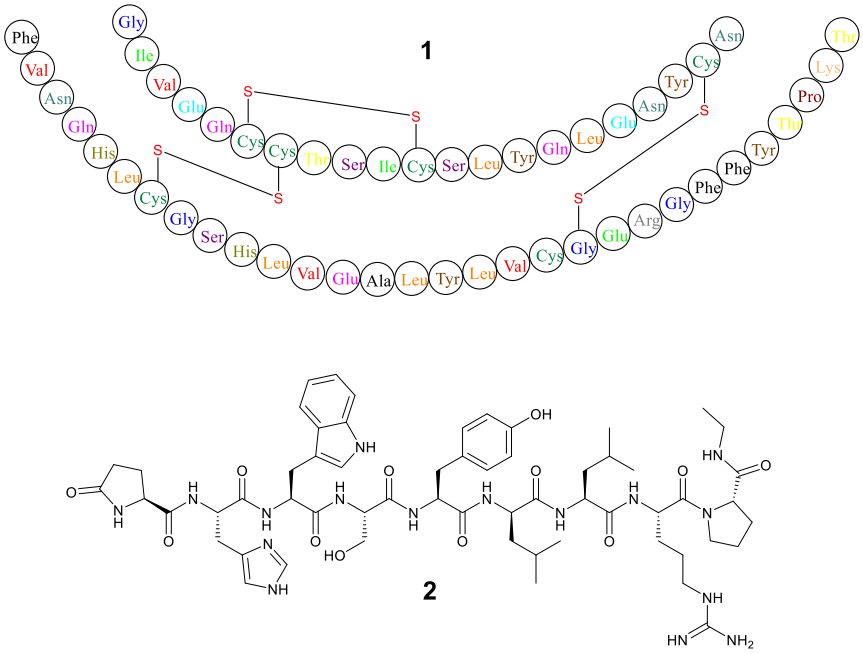

Figure 1.1 – Structure of insulin (**1**); a biopolymer consisting of two peptide chains linked together by disulphide bonds. Chemical structure of Lupron™ (**2**).

Despite the many advantages that peptides offer, the development of this class of compounds has been somewhat hampered by significant drawbacks,[1,13,18] specifically related to poor stability under physiological conditions and challenges in synthesis.[18,19] Peptidase enzymes within the body are able to cleave the amide bonds of the peptides, leaving them obsolete and ineffective towards their targets. The excretory mechanisms within the body also pose a risk to the stability of these compounds. Another cause for concern is the necessity for most peptide-based drugs to be administered intravenously, which may add additional stress to the patient; however significant advances in the oral delivery of peptide therapeutics have been made.[20] For the same reasons already mentioned above, oral ingestion is not viable in most cases due to potential breakdown by salivary enzymes. In addition to this, the cumbersome nature of these relatively large molecules (e.g. MW > 1500 Da) along with the fact that they are strongly polar entities presents intestinal permeability challenges, which has often meant that these types of compounds have been limited to extracellular targets.[13]

Consequently, it is often the case that the focus of drug discovery programmes is directed towards small organic molecules which possess longer plasma half-lives, are typically more synthetically accessible and benefit from improved oral bioavailability.[13] Small molecules also tend to be more permeable with respect to cell membranes, but can suffer from inferior selectivity, a lack of potency and the inability to adopt the necessary conformational changes required when binding peptidic receptors. Furthermore, the susceptibility of these small molecules towards CYP inhibition can lead to unwanted drug-drug interactions (DDIs); a problem rarely observed with peptides. This has highlighted the fact that organic small molecules are not complete substitutes for peptides, and in more recent years, a fresh wave of enthusiasm for peptide therapeutics has emerged.[21,22] This is partly due to the fact that many of the obstacles associated with their use have been successfully overcome through the modification[23–27] of naturally occurring peptides in order to improve their physical properties. The alteration of peptide sequences, the incorporation of unconventional amino acid units and conjugation of certain moieties can lead to more desirable solubility properties, increased stability, or improved selectivity for specific biological targets. In fact, the peptide structure can be specifically tailored to best fit its desired function. The development of novel peptides for binding intracellular targets is now also being explored, which was previously not possible for peptides.

1.2 Covalent Warheads as Probes

The modification of small molecules and peptides to include an electrophilic covalent warhead has been utilised in order to target nucleophilic residues within a range of proteins for use as probes for studying biological systems. A selection of different examples of electrophilic warhead-containing cysteine enzyme inhibitors[28] is summarised in **Figure 1.2**. Acrylamide **3** is known to irreversibly inhibit Bruton's tyrosine kinase (Btk) at the Cys481 residue.[29] It was found to be a potent inhibitor in both *in vitro* and *in vivo* assays, with dose-dependent efficacy evident in a mouse arthritis model. Thus, this work

provides compelling evidence that Btk is a desirable target for the treatment of rheumatoid arthritis.[29] The adaptation of **3** to possess an amide-linked fumarate acid ester (**4**) resulted in a greater degree of selectivity towards Btk, whilst maintaining a substantial amount of reactivity towards the target.[28] This is made possible due to rapid target binding and the occurrence of a slightly slower process of ester cleavage which deactivates the inhibitor, prohibiting even slower reaction with off-target proteins. The addition of an alkyne moiety provided a handle for the possibility of introducing further functionality through click chemistry. Allenamide **5** has also proved effective at irreversibly labelling cysteine residues in proteins through formation of a sulfonyl vinyl complex.[30] The probe (**5**) was found to selectively target thiols whilst leaving amine and hydroxyl groups untouched. Mono-fluoromethyl ketones (mFMKs) such as modified peptide **6** have demonstrated their ability to irreversibly inhibit cysteine protease enzymes. This particular substrate (**6**) was found to be a potent and selective covalent binder of MALT1 paracaspase.[31] Furthermore, diazomethyl ketone **7** was used as a probe for detection of a cathepsin B-like precursor produced by breast-tumour cells in culture due to its ability to irreversibly inhibit cysteine residues.[32]

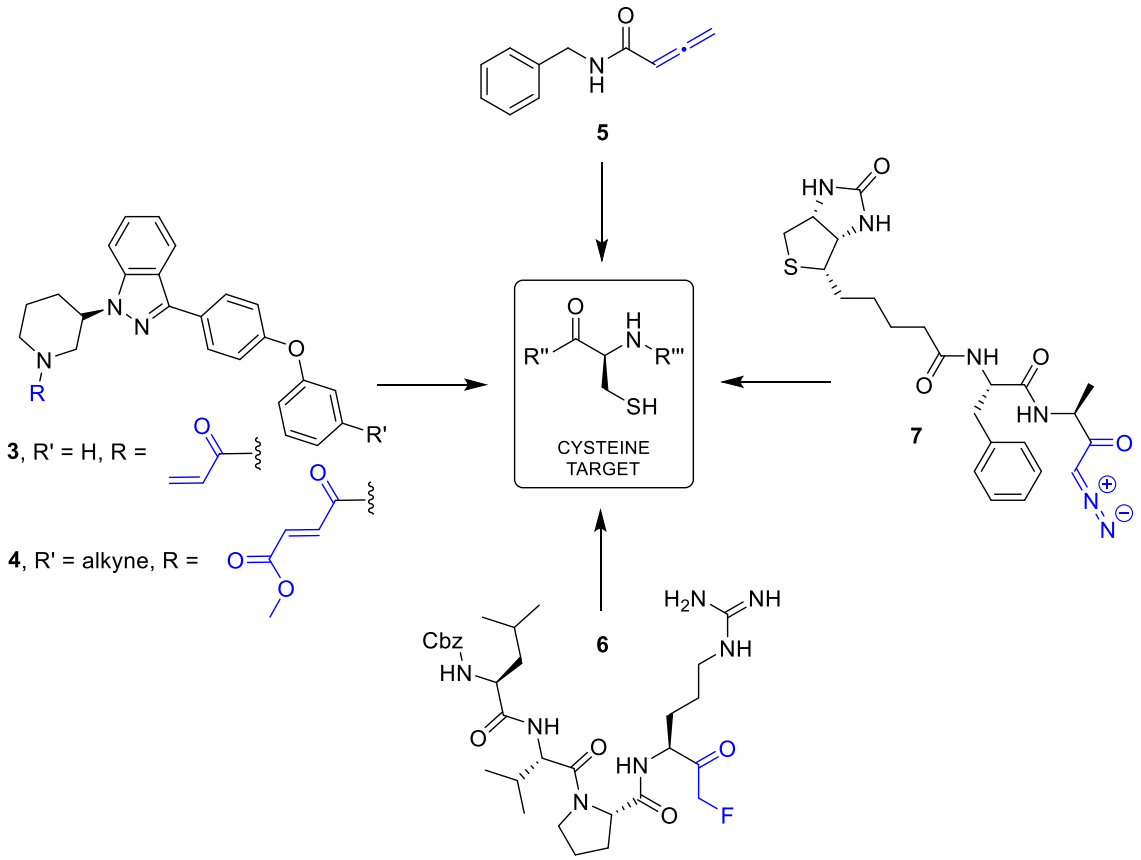

Figure 1.2 – Examples of cysteine enzyme inhibitors.[28–32]

Covalent inhibitors have also been designed to target other nucleophilic protease enzymes such as serine (**Figure 1.3**). A selection of sulfonyl fluorides, including 2-phenylethane-1-sulfonyl fluoride (**8**), was first shown to act as irreversible inhibitors of serine protease enzymes such as chymotrypsin by Fahrney and Gold in 1963.[33] Additionally, peptidyl chloromethyl ketone **9** has been reported as a covalent irreversible inhibitor of serine proteinase K,[34] whilst biotinylated isocoumarin **10** was able to label human leukocyte elastase (HLE) irreversibly.[35] Di- and tri-fluoromethyl ketones (dFMKs and tFMKs) **11** and **12** were found to act as rapidly reversible competitive and slow-binding reversible competitive inhibitors of α-chymotrypsin respectively, with the trifluorinated analogue being the more potent of the two.[36]

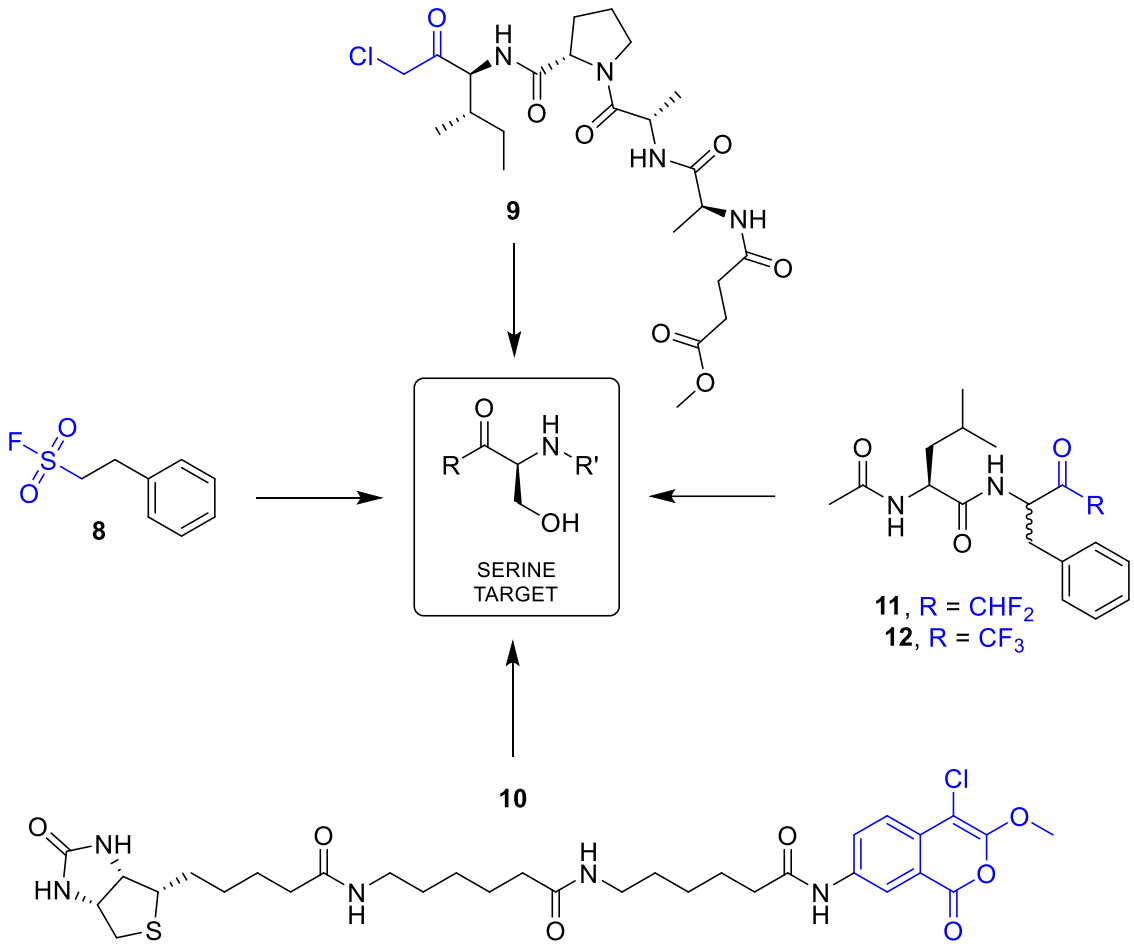

Figure 1.3 – Examples of serine protease inhibitors.[33–36]

1.3 Peptidyl Halomethyl Ketones

Peptidyl halomethyl ketones can act as covalent inhibitors due to their electrophilic nature rendering them prone to attack by nucleophiles such as the active thiol and alcohol functionalities present in cysteine and serine protease enzymes respectively. One type is peptidyl chloromethyl ketones (CMKs),[37,38] an example of which is shown in **Figure 1.4** (**13**). This particular substrate was reported to irreversibly inhibit matriptase-2 activity, making it a useful probe for detection of the active serine enzyme.[39] CMKs have also been used as inhibitors[39] of elastase, a serine protease.[40] Additionally, a selection of fluorinated examples has been reported in the literature, including mono-fluoromethyl ketones (mFMKs), di-fluoromethyl ketones (dFMKs) and tri-fluoromethyl ketones (tFMKs). mFMKs tend to act as irreversible cysteine protease enzyme inhibitors, for example **14** (**Figure**

1.4) is able to complex with human calpain I.[41] mFMKs have also been developed as probes for targeting cathepsins, caspases, SENPs, PKACα and *N*-glucanase.[42] Given the increased reactivity associated with the installation of further fluorine atoms, dFMKs and tFMKs are able to inhibit serine protease enzymes, often in a reversible competitive manner. dFMK **15** demonstrated its ability to inhibit elastase[36] whilst tFMK **16** was able to inhibit human leukocyte elastase (HLE).[43]

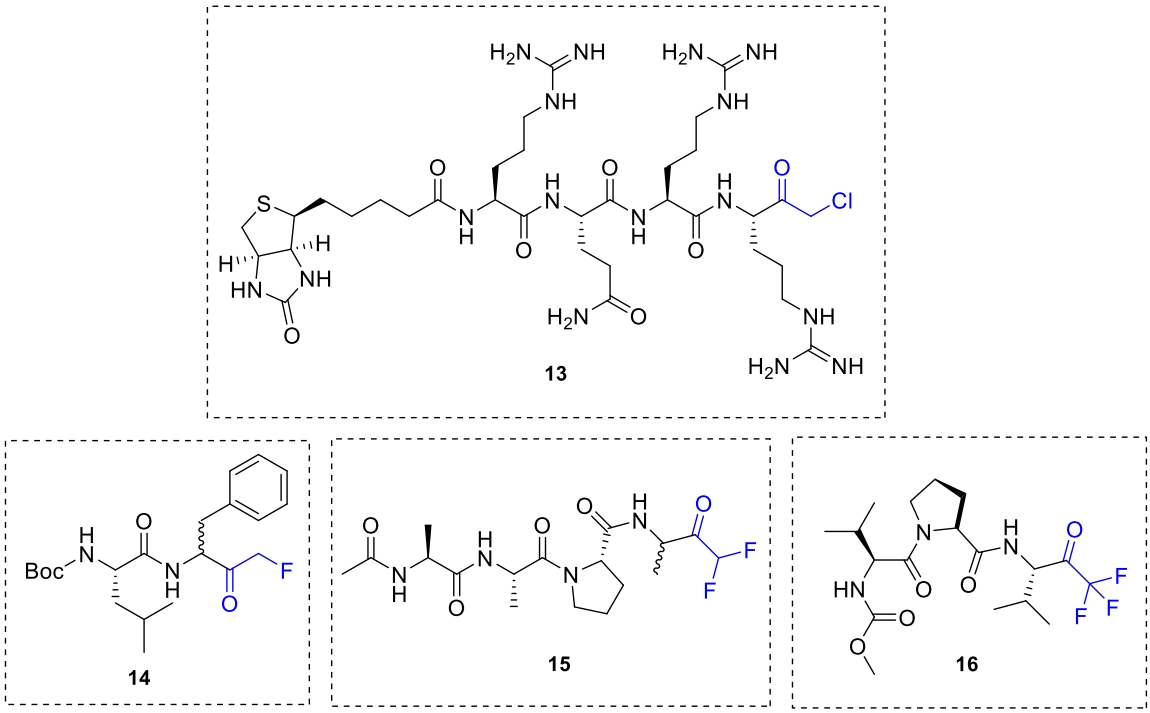

Figure 1.4 – Example of a CMK (**13**),[39] mFMK (**14**),[41] dFMK[36] (**15**) and tFMK (**16**).[43]

1.4 Peptidyl Fluoromethyl Ketones (FMKs)

1.4.1 Introduction to Peptidyl-FMKs

As already highlighted, one particular class of modified peptides which have sparked particular interest are mono- (**17**), di- (**18**) and tri- (**19**) peptidyl fluoromethyl ketones (FMKs) in which the C-terminus of the peptide has been altered to include a $COCH_2F$, $COCHF_2$ or $COCF_3$ functional group respectively (**Figure 1.5**).[44,45] FMKs are known for their potential in drug therapeutics[46] and have also been identified as probes[47]

for the interrogation of cellular activity and biological systems. This is primarily due to their ability to act as potent and selective inhibitors towards a range of hydrolytic protease enzyme targets,[42] enhanced by the presence of electronegative fluorine providing increased electrophilicity. Peptidyl mono-FMKs are predominantly known to inhibit cysteine proteases irreversibly, whilst di- and tri-FMKs are also able to inhibit serine protease enzymes due to their enhanced electrophilicity. The peptidyl sequence of the molecule can be varied in order to encourage selectivity towards specific enzymes within broader protease classes such as caspases or cathepsins, with the amino acid residue adjacent to the electrophilic FMK group (P_1) being most sensitive to change.[42] Additionally, variation of the amino acid residues (**Figure 1.5**) present in the peptide sequence can act to either improve or hamper activity towards the target.[42,48–50]

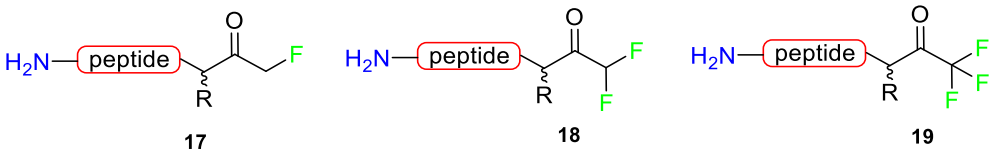

Figure 1.5 – General chemical structures of mono- (**17**), di- (**18**) and tri- (**19**) fluoromethyl ketones (FMKs). R = amino acid sidechain of choice.

One particular advantage of peptidyl-FMKs over the analogous peptidyl-chloromethyl ketones (CMKs) such as **13** (**Figure 1.4**) and **20** (**Figure 1.6**), which have also been synthesised and identified as potential protease inhibitors,[34,51–55] is the improved selectivity that they offer.[52] Peptidyl-FMKs are much less prone to non-specific alkylations due to the intrinsic strength of the C-F bond (**Figure 1.6**) making them significantly more selective.[50,56] Thus, it is suggested that peptidyl-FMKs form a promising class of compounds with unique and desirable properties worth pursuing further.

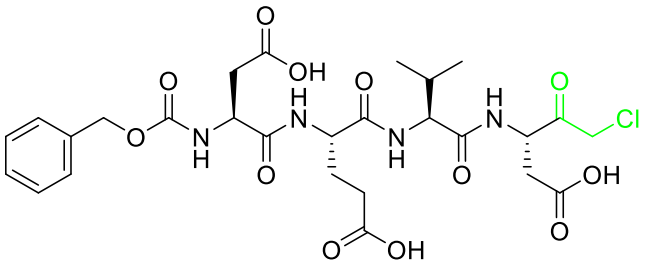

20

Cbz-Asp-Glu-Val-Asp-CMK

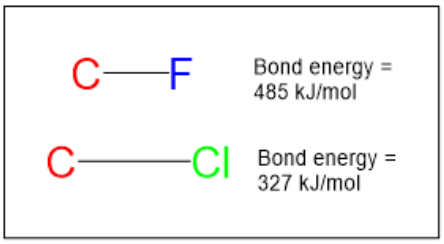

Figure 1.6 – [Left] Example of a peptidyl-chloromethyl ketone (**20**). [Right] Comparison of C-F and C-Cl bond strengths.

Despite their known effectiveness as biologically active warheads, the number of viable synthetic routes to peptidyl-FMKs such as **22** (**Figure 1.7**) is still rather limited, especially for the mono-fluorinated analogues, and the building blocks used to access them (e.g. **21**) can be expensive (**Figure 1.7**). In addition, whilst a number of solution-phase synthetic routes to mono-FMKs exist,[57,58,45] only two solid-phase techniques have been reported in the literature, with both inconveniently requiring the use of a linker for some substrates.[59] Additionally, the majority of the established synthetic pathways to FMKs suffer from long-winded procedures, the use of hazardous materials such as diazomethane and/or fall victim to low-yielding steps. The rest of this chapter will focus on examples of FMKs showing promise for biomedical applications,[62] discuss their mode of action[52] and provide a comprehensive overview of how these molecules are currently made.[60]

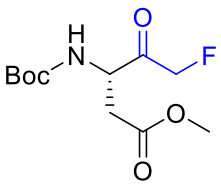

21

Boc-Asp(OMe)-FMK
3 mg = £849 (Sigma-Aldrich)

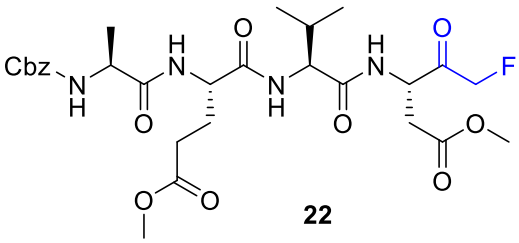

22

Cbz-Ala-Glu(OMe)-Val-Asp(OMe)-FMK
1 mg = £398 (Sigma-Aldrich)

Figure 1.7 – FMK building block **21** suitable for solution-phase peptide coupling in the synthesis of peptidyl-FMKs such as **22**. Prices given are from Sigma-Aldrich, correct as of March 2023.

1.4.2 The Biomedical Importance of Peptidyl mono-FMKs

Peptidyl mono-FMKs have shown potential for use in drug therapeutics as well as for probing cellular activity and investigating promising druggable targets.[42,59] In particular, FMKs have proven to be effective as covalent inhibitors of cysteine proteases for the treatment of a wide range of diseases, including rheumatoid arthritis through their ability to reduce the severity of inflammation and inhibit the extent of bone and cartilage damage.[61–63] The hydrolysis of peptide bonds by protease enzymes[64] within living organisms is of paramount importance for optimum bodily function. In fact, protease enzymes play a key role in many physiological processes such as blood coagulation, digestion and the healing of wounds.[65,66] Despite this, if the cleavage occurs in a disorderly and uncontrollable manner, harmful effects can be observed,[67] leading to all kinds of illnesses ranging from arthritis to cancer and Alzheimer's disease.[42] For this reason, the ability of certain inhibiting molecules to bind selectively to the proteases, preventing them from performing these unwanted cleavages can prove hugely beneficial in the treatment of the patient. In addition to this, protease inhibitors are also useful for fighting viral particles such as HIV,[68] as these too rely on proteolysis to be able to function properly. Peptidyl FMKs are capable of binding to these viral protease enzymes,[46] blocking proteolytic cleavage and therefore preventing the maturation of infectious viral particles. This hinders replication, thus helping to combat disease.

1.4.3 Mechanism of Action for Protease Inhibition by Peptidyl FMKs

The mechanism of action for protease inhibition is very much dependent on the type of protease enzyme being targeted, along with the nature of the inhibitor.[7,24,38,73] The active sites for serine and cysteine protease enzymes have a number of similarities, including a nucleophilic residue and a general base (histidine), both of which assist with proteolytic cleavage i.e. peptide hydrolysis, an otherwise slow process.[50] However, this

active site is also often the site of inhibition, and is therefore shown in **Figure 1.8** and **Figure 1.9** for serine and cysteine protease enzymes respectively.[69]

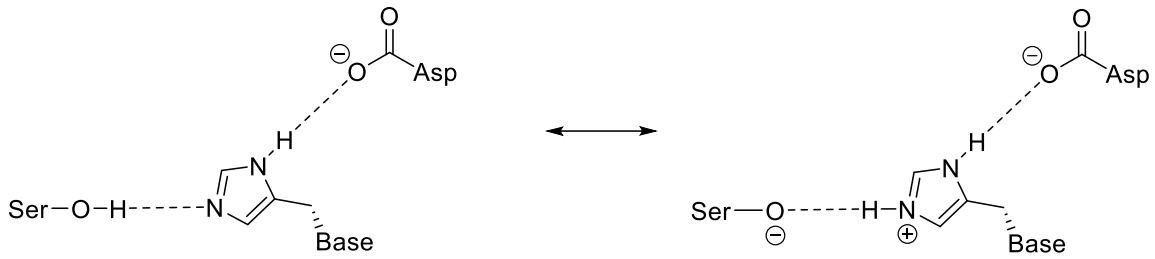

Figure 1.8 – Active site residues for serine protease enzyme.

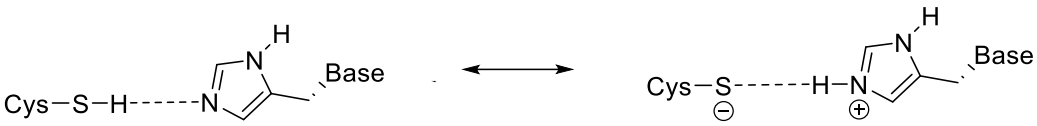

Figure 1.9 – Active site residues for cysteine protease enzyme.

The exact mechanism for the irreversible inhibition of cysteine proteases by peptidyl mono-fluoromethyl ketones is still uncertain; however it is thought to proceed via one of two possible pathways shown in **Scheme 1.1**.[69] The first option (Pathway 1) involves the formation of the covalent thioether adduct **24** through direct attack of the thiolate anion from the cysteine proteases' active site on the C-F bond of the FMK, causing displacement of fluoride as a leaving group. An alternative mechanism is illustrated by Pathway 2. This involves the nucleophilic attack of the thiolate anion on the carbonyl group of the FMK, causing generation of a thiohemiketal (**25**), followed by consequent expulsion of fluoride, giving a three-membered ring (**26**). This intermediate (**26**) species then collapses to give the thioether (**24**).

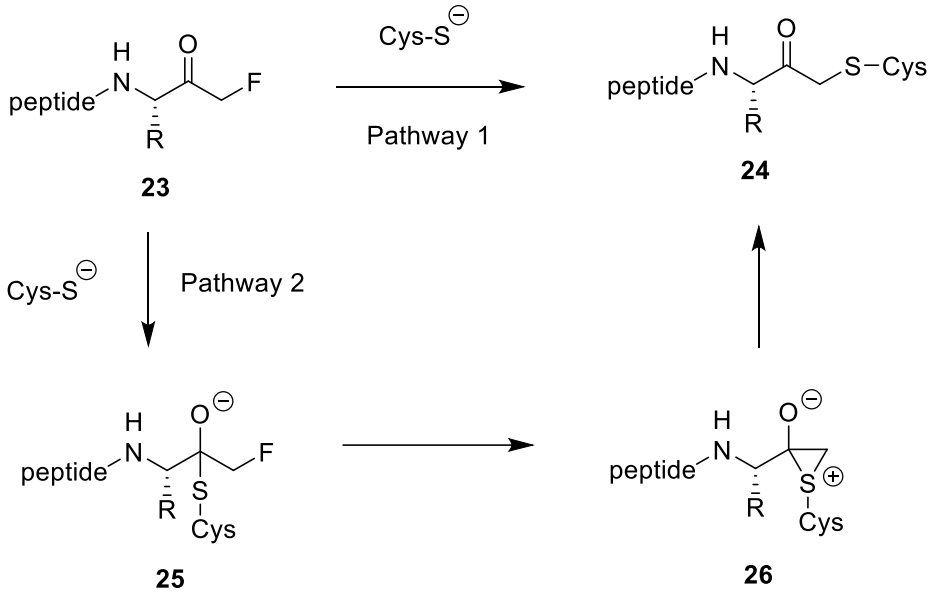

Scheme 1.1 – Possible covalent irreversible cysteine protease inhibition mechanisms by mFMKs.

Whilst peptidyl mono-FMKs tend to target cysteine proteases, inhibition of serine proteases by these molecules has been reported.[36,70] The proposed mechanism for irreversible inhibition of serine protease enzymes by some alkyl mono-FMKs as well as CMKs is expected to proceed via a stable tetrahedral hemiketal and involves the active site histidine residue, as shown in **Scheme 1.2a**.[52,69] Again, two possible mechanisms have been proposed; a single and a double displacement route. However, the latter of the two pathways is thought to be correct. Whilst both agree on the first step involving generation of hemiketal intermediate **28**, Pathway 1 then suggests direct displacement of fluoride or chloride through attack on the C-F or C-Cl bond respectively by the active site histidine residue from the protease enzyme, generating the alkylated species which is able to interconvert rapidly between two forms (**29** and **30**), as shown. Pathway 2, the currently accepted mechanism, involves the formation of a three-membered ring (epoxy ether **31**) through displacement of fluoride or chloride (after initial generation of hemiketal **28**) and subsequent epoxide ring opening through attack of histidine at the least substituted position. Hemiketal intermediate **28** possesses stability as a result of the free energy released from the binding of the peptide chain of the inhibitor to the protease enzyme.

tFMKs and many dFMKs have been shown to act as reversible slow-binding competitive inhibitors of serine proteases according to **Scheme 1.2b**.[42] Alternatively, the ability of some tFMKs and dFMKs to easily hydrate, forming stable geminal-diols (**Scheme 1.2c**, **34**), has enabled them to act exclusively as rapidly competitive reversible transition-state analogue inhibitors (**Scheme 1.2c**) due to the similarities shared by hydrated FMK **34** and the enzyme-substrate tetrahedral adduct transition state formed during amide bond hydrolysis.[42] In most cases, it is thought that a dual inhibition mechanism is adopted (**Scheme 1.2a** and **Scheme 1.2c**) due to the presence of a mixture of the hydrated (**34**) and non-hydrated forms (**32**) of the tFMK or dFMK.[42]

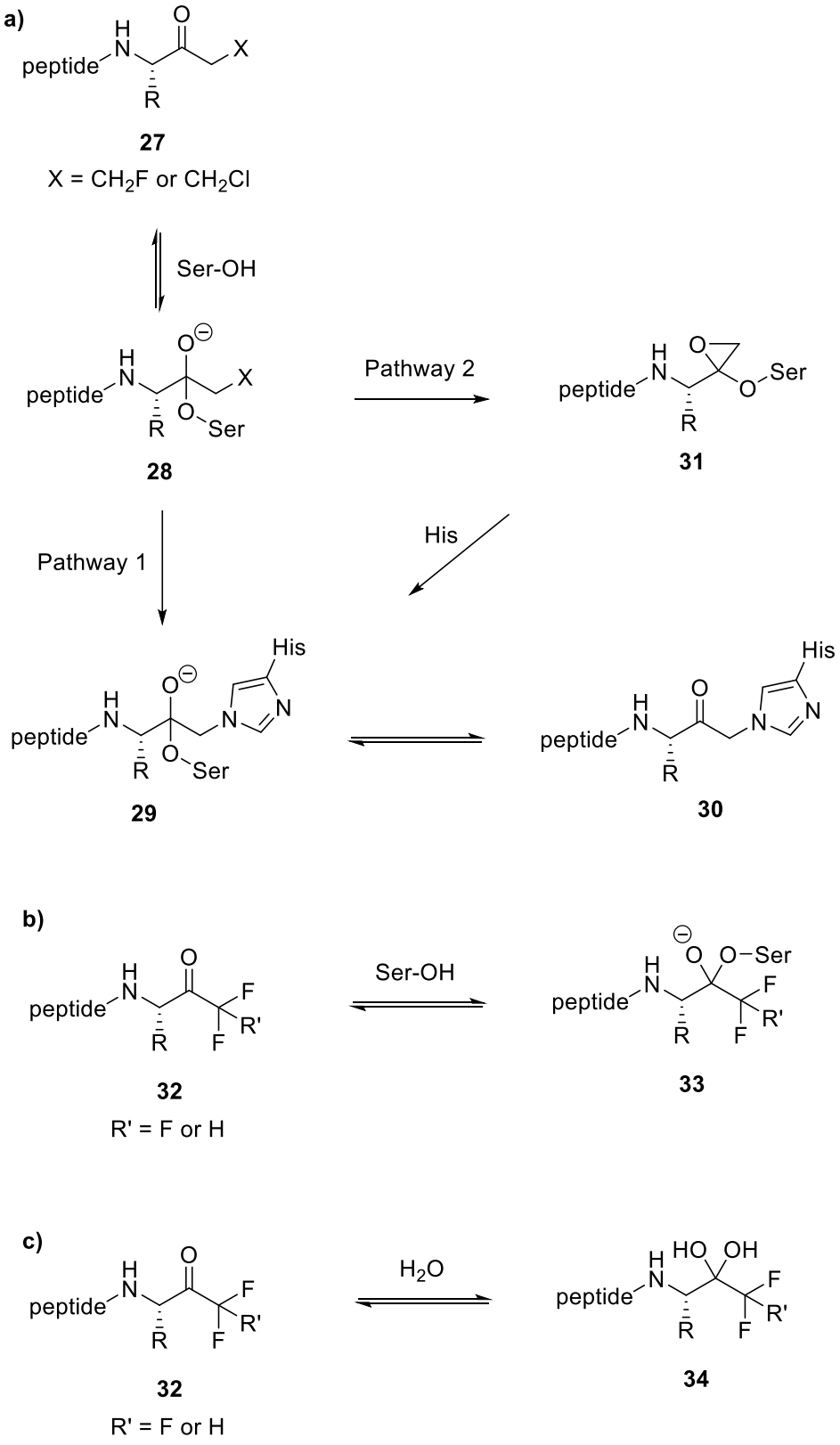

Scheme 1.2 – (a) Proposed mechanisms for the irreversible inhibition of serine proteases by mCMKs and some mFMKs. (b) Proposed mechanism for the slow-binding competitive reversible inhibition of dFMKs and tFMKs. (c) Proposed mechanism for the rapidly competitive reversible hydration of dFMKs and tFMKs enabling **34** to act as a transition-state analogue inhibitor.[42]

1.4.4 Peptidyl mono-FMKs as Potential Therapeutics

1.4.4.1 Peptidyl mono-FMKs as Cathepsin Inhibitors

The use of peptidyl FMKs for the treatment of rheumatoid arthritis has been studied and subsequently reported in the literature.[61,71,72] FMKs have been designed that are able to irreversibly inhibit cysteine protease enzyme cathepsin B,[48,50,56,69,70] thus helping to reduce the extent of inflammation and combat cartilage and bone damage. The extracellular matrix of cartilage consists of proteoglycan and collagen molecules assembled in such a way that a rigid gel is formed, enabling joints to function properly. The development of arthritis has been associated with the release of cathepsins into inflamed tissues,[73] causing destruction of the matrices because of proteoglycan and collagen degradation.[61] This can have detrimental effects on the organism, leading to a loss of optimal joint function.

A selection of peptidyl FMK inhibitors, each consisting of a Phe-Ala moiety with variable *N*-terminal blocking groups (**Table 1.1**, **35a** - **f**), was synthesized and found to be effective irreversible inhibitors *in vitro*.[61] The treatment of rats with a single oral dose of 25 mg/kg resulted in a 22-91% reduction in liver and kidney cathepsin B levels over a period of just 4 hours (**Table 1.1**). The change in inhibition observed as a result of varying the *N*-terminal blocking group suggests that it has a significant effect on the interaction of the inhibitors with cathepsin B. The importance of stereochemistry was later highlighted by Esser *et al*, who demonstrated that Z-L-Phe-L-Val-CH_2F was much more effective as a Cathepsin B inhibitor than the corresponding diastereoisomer Z-L-Phe-D-Val-CH_2F which possesses an unnatural amino acid.[72] It has also been suggested that the ability of FMKs to inhibit NF-κB dependent gene expression may also play a significant role in the treatment of Rheumatoid arthritis.[74,75]

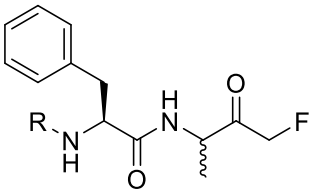

35

R	% inhibition in liver homogenates	% inhibition in kidney homogenates	R	% inhibition in liver homogenates	% inhibition in kidney homogenates
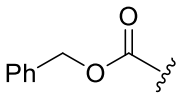 **35a**	70.5	39.0	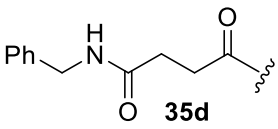 **35d**	81.8	75.4
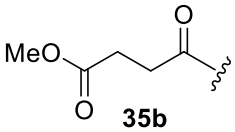 **35b**	86.9	57.3	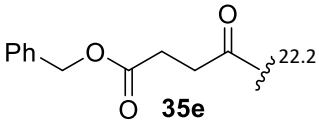 **35e**	22.2	29.8
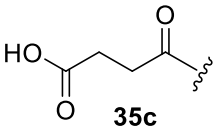 **35c**	28.3	24.2	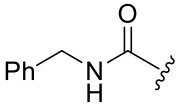 **35f**	91.2	78.8

Table 1.1 - % Inhibition of cathepsin B in liver and kidney tissue homogenates treated with 25 mg/kg of a selection of peptidyl FMKs (**35a**-**f**).[61]

Cathepsin B has also been associated with the development of other pathological conditions such as autoimmune diseases and tumours,[76] and thus peptidyl FMKs may play a role in the treatment of these illnesses as well. Additionally, Denhardt and co-workers indirectly demonstrated that Z-Phe-Ala-FMK can inhibit Cathepsin L,[49] a protease enzyme involved in metastatic processes.[42,77] Furthermore, Gly-Phe-FMK and Ala-Phe-FMK were identified as being effective inhibitors of Cathepsin C,[78] a protease enzyme responsible for activating serine protease zymogens within cells derived from bone marrow.[78] Interestingly, in this particular case, the protease enzyme later regained most of its activity, indicating that inhibition had occurred in a reversible manner. This is in contrast to the majority of cases in the literature which show peptidyl mono-FMKs adopting an irreversible mechanism. It has also been reported that the ability of peptidyl mono-FMKs to inhibit cathepsins could show promise for the treatment of renal cancer.[79,80]

1.4.4.2 Peptidyl mono-FMKs as Calpain Inhibitors

Calcium-activated neutral proteases (Calpains) are a class of cysteine protease enzymes found ubiquitously in mammals. The onset and progression of certain neurological diseases such as Alzheimer's, strokes and epilepsy has been associated with the presence of activated calpain I in the body.[81] During a stroke, the intracellular Ca^{2+} concentration increases as a result of various biochemical events. This subsequently leads to the activation of calpain I which is responsible for degradation of neuronal structural proteins. For this reason, the development of calpain I inhibitors[82] is desirable in order to prevent neurodegeneration, thus combating neurological disorders.[41] A selection of mono-FMK dipeptides with varying amine protecting groups was synthesised and found to be potent irreversible inhibitors of calpain I.[81,83] Interestingly, changing the *N*-capping group could be used to enhance the selectivity of the compound in favour of inhibiting calpain I over cathepsin B and L, along with altering potency. The absence of a protecting group was found to give poor inhibition, whilst *t*-Boc appeared to give the best selectivity for calpain I over cathepsin B. Additionally, a hydrophobic group was preferred at the P_1 position in order for potent inhibition to occur. The importance of Leu or Val at P_2 was also notable from the results reported. The most potent compound tested (k = 276,000 M^{-1} s^{-1}) (**36**) along with the FMKs showing the greatest calpain I selectivity (**37** and **38**) can be seen in **Figure 1.10**. In addition to exhibiting good activity in an assay, these compounds were found to be cell permeable and capable of inhibiting intracellular recombinant human calpain I.

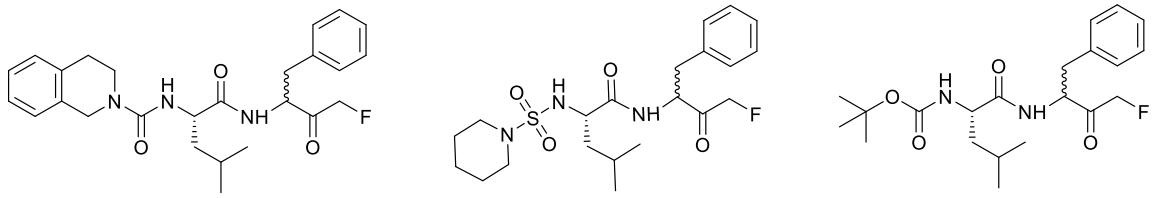

36 **37** **38**

Figure 1.10 - Peptidyl FMKs capable of inhibiting calpain I.[81]

Calpain II requires higher levels of Ca^{2+} in order to be activated[84] and has also been identified as a potentially druggable target through its ability to be inhibited by peptidyl mono-FMKs.[85]

1.4.4.3 Peptidyl FMKs as Inhibitors of MALT1 Paracaspase

The paracaspase enzyme MALT1 plays a key role in immune response through the activation of lymphocytes and other immune cells.[86] Despite the importance of these processes for healthy bodily function, if they occur in an abnormal manner, this can lead to the development of lymphoid malignancies. For this reason, the synthesis of inhibitors which target MALT1 proteases has proved an attractive method for the treatment of these tumors. Peptidyl-FMKs such as **6** (**Figure 1.11**) have shown potential for this purpose. The P_1 Arg residue was found to be essential due to its interaction with the acidic residues in the target protein whilst Leu at P_4 helped by occupying a hydrophobic pocket. Although potent inhibitors have now been successfully developed for targeting MALT1 enzymes *in vivo*, the acquisition of orally available inhibitors remains an ongoing challenge.

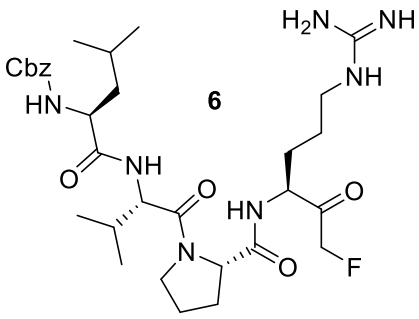

Figure 1.11 - Peptidyl FMK (**6**) capable of inhibiting the paracaspase enzyme MALT1.[86]

1.4.4.4 Dipeptidyl Glutaminyl FMKs as SARS-CoV Inhibitors

In 2003, an outbreak of SARS (Severe Acute Respiratory Syndrome)[87] occurred as a result of the spread of coronavirus pathogen SARS-CoV. The virus, which leads to respiratory difficulties, was responsible for causing nearly 800 deaths; a value close to 10% of all confirmed cases in 2003. In 2006, S. X. Cai *et al* synthesised a selection of

dipeptidyl glutaminyl FMKs to be investigated as potential SARS-CoV inhibitors.[88] The viral cysteine protease enzyme M^{pro} is essential for viral replication (through its ability to enable the release of functional polypeptides from polyproteins through proteolytic processing) and thus was identified as a possible drug target.[89,90] Antiviral activity was evaluated through CPE inhibition in SARS-CoV infected Vero and CaCo2 cultures. Cbz-Leu-Gln(NMe_2)-FMK (**39a**) was found to be the most potent inhibitor, with an EC_{50} value of 2.5 μM in Vero cells (infected with strain 6109), low cellular toxicity and a selectivity index of >40 (**Table 1.2**). FMKs **39b** and **39c** also showed some promising EC_{50} values (**Table 1.2**), and **39c** was also found to exhibit low toxicity in mice, suggesting the inhibitors should possess good safety profiles for further efficacy studies to be performed in animals.

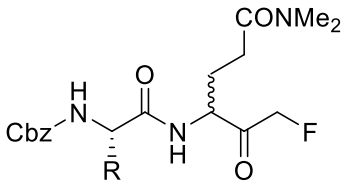

39

Entry	Compound	R	EC_{50} (μM)			CC_{50} (μM)	SI
			Vero		CaCo2	Vero	
			FFM1	6109	FFM1		
1	**39a**		3.6 ± 1.3	2.5 ± 0.4	2.4 ± 0.56	> 100	> 40
2	**39b**		8.9 ± 2.9	5.3 ± 1.7	8.8 ± 2.5	> 100	> 18
3	**39c**		6.2 ± 1.9	6.6 ± 3.0	12.6 ± 4.1	> 100	> 15

Table 1.2 - EC_{50}, CC_{50} and SI values for a selection of dipeptidyl glutaminyl FMKs in SARS-CoV infected Vero and CaCo2 cultures.[88]

It is also notable that the SARS-CoV-2 M^{pro}, which is responsible for COVID-19, possesses genetic similarities with the SARS-CoV M^{pro} which caused the SARS-CoV outbreak.[91,92] In fact, the amino acid sequence of SARS-CoV-2 M^{pro} possesses 96% similarity with that of

SARS-CoV, with differences between the two viruses occurring at 12 residues.[93] More recently, Zaki *et al* released images depicting theoretically predicted binding of a selection of peptidyl FMKs with the SARS-CoV-2 active site using molecular docking simulations.[94] A number of the diagrams, such as the ones shown in **Figure 1.12** (**a**) and (**b**) for Cbz-Val-Ala-Asp(OMe)-FMK (**40**) and Cbz-Phe-Ala-FMK (**41**) respectively, reportedly show how the phenyl ring of the Cbz protecting group provides a crucial hydrophobic binding interaction with an arginine residue present in the active site of the viral protease.[94] However, the fact that a pi-stacking interaction is not reported between arginine and the phenyl ring, as would be expected, does seem somewhat dubious.

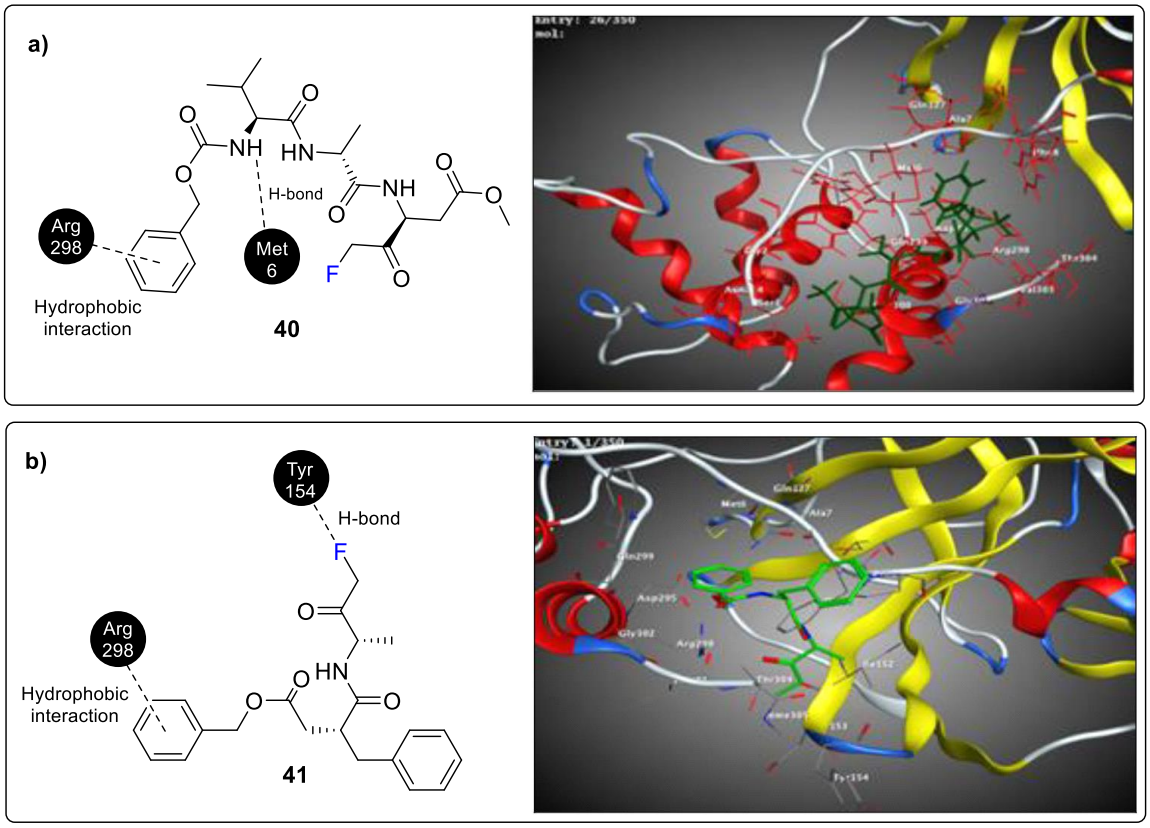

Figure 1.12 – Molecular docking simulations for the binding of (**a**) Z-VAD(OMe)-FMK (**40**) and (**b**) Z-FA-FMK (**41**) with the SARS-CoV-2 active site.[94]

A crystal structure showing the main protease of SARS-CoV-2 complexed with Z-VAD(OMe)-FMK (**40**) was also released in 2021, as shown in **Figure 1.13**.[95,96] Another example in which a viral protease has been targeted by peptidyl mono-FMKs was reported

by Malcolm and co-workers in which irreversible inhibition of hepatitis A virus $3C^{pro}$ was observed.[97]

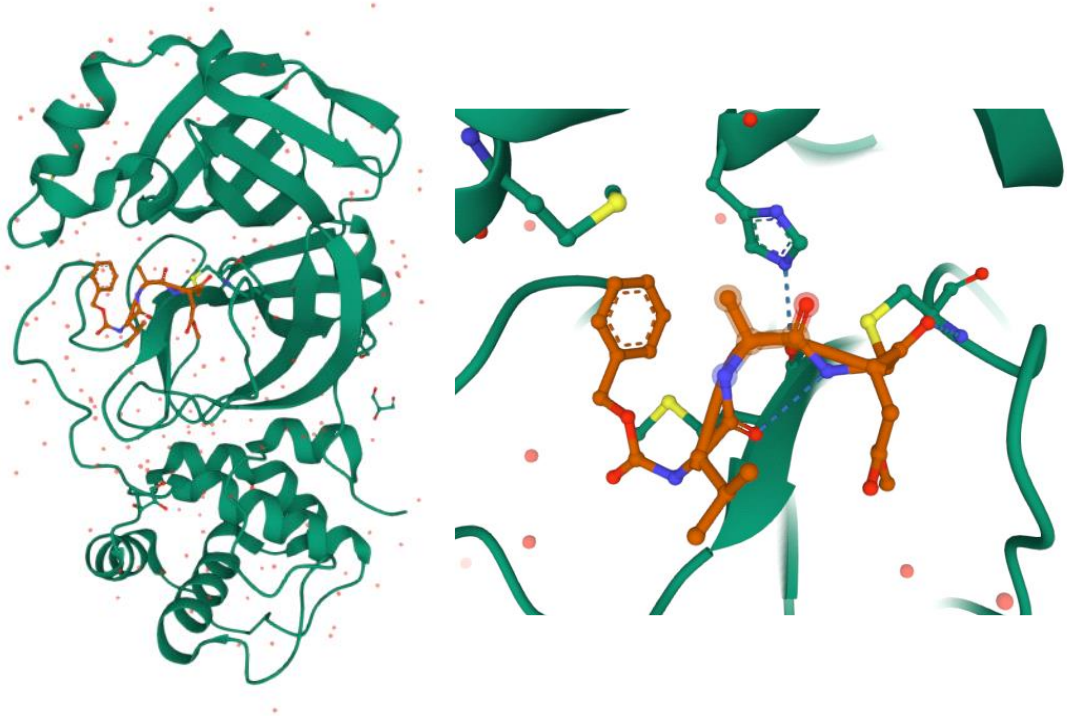

Figure 1.13 – Wide-angle view [left] and close-up view [right] showing the main protease of SARS-CoV-2 complexed with Z-VAD(OMe)-FMK (**40**).[95,96] Crystal structure (7CUT) can be found in the RCSB Protein Data Bank (PDB) (http://doi.org/10.2210/pdb7CUT/pdb).

1.4.4.5 Inhibition of T-Cell Proliferation by Peptidyl mono-FMKs

In a study reported by Lawrence *et al*,[74] Z-Phe-Ala-FMK (**41**, **Figure 1.14**) proved effective as an immunosuppressant of primary human T-cell proliferation[98] *in vitro*; a process brought about by mitogens and cytokine IL-2. This is achieved through the FMK's ability to bring about suppression of cytokine production (IL-2 and IFN-γ), a significant reduction in CD25 expression, inhibition of NF-κB signalling, hindrance to the cell cycle and inhibition of caspase-8 and caspase-3 activation. Additionally, the authors describe a study in which the activity of the FMK was investigated in a mouse model involving pneumococcal disease, an illness in which T cells play a substantial role. This resulted in a significant increase in pneumococcal loads in both lungs and blood, indicating that the FMK is also an effective immunosuppressant *in vivo*. Further to this, caspase inhibitor Z-

Val-Ala-Asp-FMK (**42**, **Figure 1.14**) has also been identified as a blocker of T cell proliferation.[99–101]

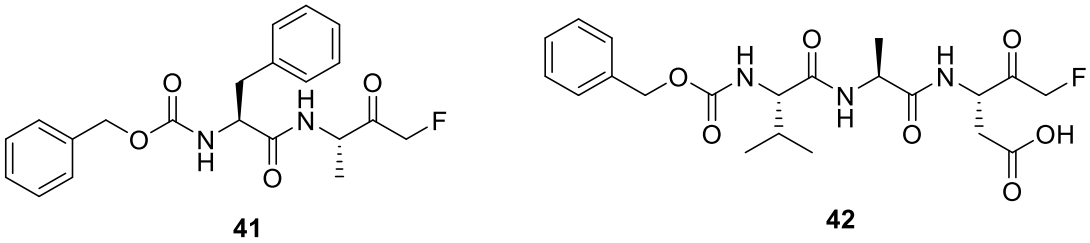

41 **42**

Figure 1.14 – Structure of Z-Phe-Ala-FMK (**41**) and Z-Val-Ala-Asp-FMK (**42**).

1.4.4.6 Peptidyl mono-FMKs as Caspase Inhibitors

Caspases (Casps) are a class of cysteine protease enzymes which plays a key role in cellular homeostasis through regulation of inflammation and cell death.[102–105] They are capable of nucleophilically attacking and cleaving a target protein, but this can only occur after an aspartic acid (Asp) residue. Whilst Casps start off as monomers (pro-Casps), they dimerise after signalling events which subsequently results in either activation or inactivation of substrates, leading to a series of apoptotic events or alternatively the manufacture of pro-inflammatory cytokines.[106] Dysregulation of Casp activity can often be associated with a wide range of conditions including inflammatory disorders, cancer, cardiovascular diseases and Alzheimer's.[42] For this reason, identifying selective Casp inhibitors may prove beneficial for the treatment of these conditions.[107] Because proteolysis of protein targets by Casps only occurs after an Asp residue (involving attachment of the Asp residue to the Casp via a saline bridge), Casp inhibitors are usually designed in such a way that an Asp residue is positioned in the P_1 position.[42,107] In some cases the methyl ester is chosen as opposed to the free acid to improve cell membrane permeability and stability.[108] This is then removed by cytoplasmic esterases, affording the desired functional inhibitor.[109] An example includes Boc-Asp(OMe)-FMK (**43**, **Figure 1.15**) which may prove beneficial after hypoxic-ischemic events in the developing brain which play a role in the onset of cerebral palsy.[110] It has also shown the ability to

prevent neuronal death *in vitro*[111,112] and help spinal motor neurons in neonatal rats to survive after root avulsion.[113] Furthermore, this warhead was shown to block apoptosis in a couple of examples presented in the literature,[114,115] whilst Graham and co-workers demonstrated its ability to delay neuron death caused as a result of traumatic brain injury in rats.[116]

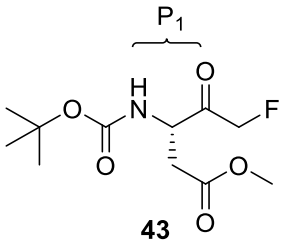

43

Figure 1.15 – Chemical structure of Boc-Asp(OMe)-FMK (**43**).

Various studies have also been carried out to explore the effect of varying the amino acid residue at the P_2 position on potency and selectivity.[117–120] Valine was demonstrated to be the best candidate for potent inhibition of Casp-3 (**44**, **Figure 1.16**), whilst the presence of an additional methyl group in the α-position of the P_2 amino acid was somewhat detrimental to its potency (**45**, **Figure 1.16**).[117] Additional studies have shown that varying the *N*-terminal protecting group can also act to either enhance or hinder activity.[119] A selection of tripeptidyl mono-FMKs has also demonstrated antiapoptotic activity through Casp inhibition,[105,121–142] showing potential against a range of illnesses including liver damage,[143,144] pneumococcal meningitis[145] and multiple sclerosis.[146]

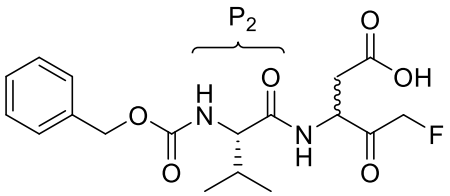

44

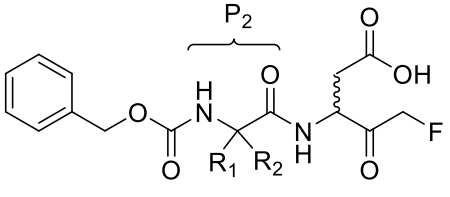

45 $R_1 = CH(CH_3)_2$
$R_2 = CH_3$

Figure 1.16 – Dipeptidyl mono-FMKs **44** and **45** tested as Casp-3 inhibitors.[117]

. The addition of a fourth amino acid residue to give a tetrapeptidyl mono-FMK has potential to allow increased selectivity towards the desired Casp target;[147] however, cell permeability is significantly reduced and thus the methyl ester analogue is employed for any amino acids possessing an acidic proton in the sidechain. An example includes Cbz-Asp(OMe)-Glu(OMe)-Val-Asp(OMe)-FMK (**46**, **Figure 1.17**)[106,121,122,124,132,148–151] which has demonstrated activity against neuronal degeneration in Parkinson's disease models.[106,152]

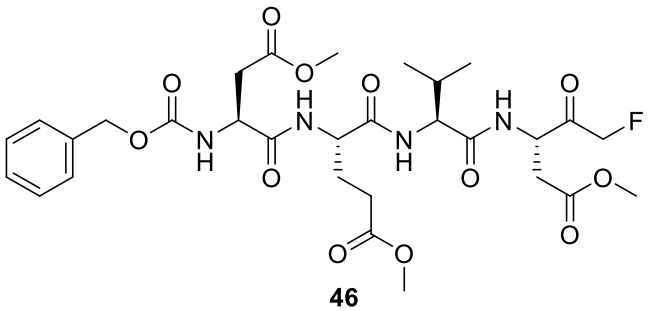

46

Figure 1.17 – Cbz-Asp(OMe)-Glu(OMe)-Val-Asp(OMe)-FMK (**46**).

1.4.4.7 Peptidyl mono-FMKs as Inhibitors of Protozoan Cysteine Proteases

The potential use of peptidyl FMKs for the treatment of infectious diseases caused by protozoan parasites has also been reported in the literature. A selection of FMKs was shown to exhibit antimalarial activity[153,154] through inhibition of a cysteine protease enzyme essential for the development of the parasite.[155] Furthermore, Harth *et al* identified two peptidyl FMKs capable of inhibiting cruzain,[156] a cysteine protease enzyme of *Trypanosoma cruzi* which is the parasite responsible for Chagas' disease.[106] In 1997, the structure of cruzain inhibited by Cbz-Arg-Ala-FMK, as determined by X-ray crystallography, was reported (**Figure 1.18**).[157,158]

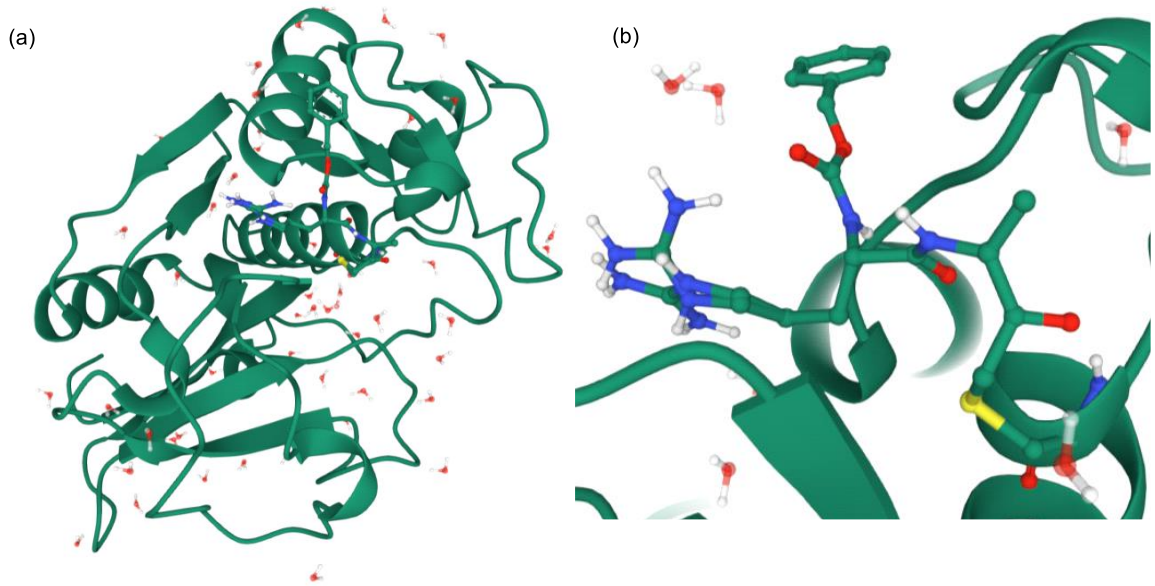

Figure 1.18 – Wide-angle view (**a**) and close-up view (**b**) showing cruzain in complex with Cbz-Arg-Ala-FMK.[157] Crystal structure (2AIM) can be found in the RCSB Protein Data Bank (PDB) (http://doi.org/10.2210/pdb2AIM/pdb).

Cbz-Phe-Ala-FMK (**Figure 1.19**, **41**) is also known to inhibit cruzain through alkylation of a cysteine residue present in the enzyme.[159] **Figure 1.19** shows the catalytic triad residues of cruzain (Cys25, His159 and Asn175) along with the complexed FMK (**38**), as determined by X-ray crystallography.[159] The phenylalanine binds into a hydrophobic pocket of the enzyme, whilst the Cbz moiety makes very few contacts, as evidenced by the lack of electron density surrounding the ring.

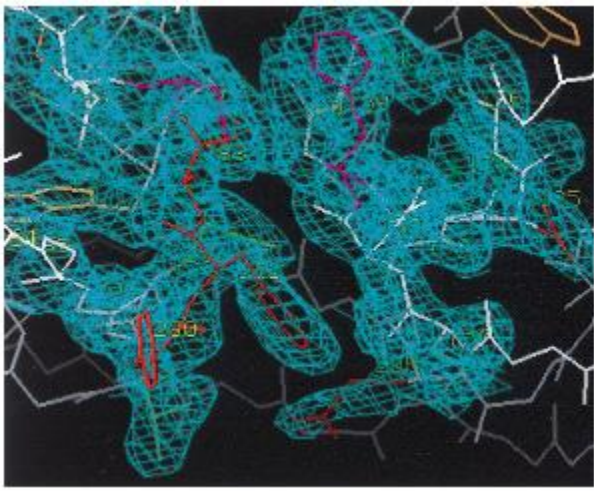

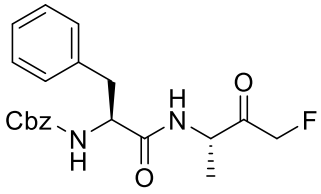

41

Figure 1.19 – [Left] Electron density map showing Cruzain complexed with Cbz-Phe-Ala-FMK **41** [right].[159]

1.4.4.8 Peptidyl mono-FMKs as Inhibitors of ATG4B (Autophagin-1)

ATG4B, otherwise known as autophagin-1, is a cysteine protease enzyme involved in the formation of autophagosomes, which are vesicles responsible for helping to control intracellular catabolic processes.[160] The autophagosomes play a key role in autophagy, in which the removal of unwanted and potentially harmful materials from the cytoplasm occurs to help ensure cell survival.[160,161] Dysregulation of this process has been associated with cancer and viral infections, along with metabolic and neurodegenerative disorders.[162,163] As a result, the desire to discover tools to enable modulation of this process has led to the discovery of certain FMKs as highly potent inhibitors of ATG4B.[57] **Figure 1.20** shows a theoretical model for the predicted binding of FMK **47** (magenta) in the catalytic site of human ATG4B (green). The napthyl group in **47** can be seen to form a π-stacking interaction with the amide backbone of the enzyme.[57]

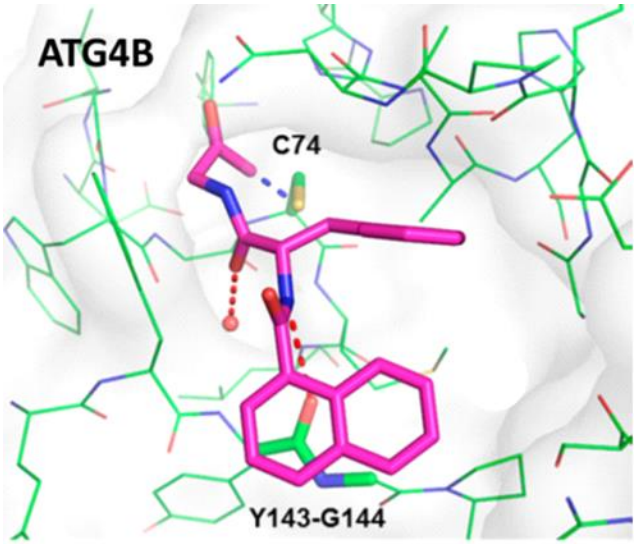

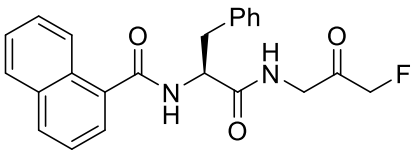

47

Figure 1.20 – [Left] Model showing predicted binding of FMK **47** [right] in the catalytic site of human ATG4B.[57]

1.4.4.9 Peptidyl FMKs as Probes for Cellular Interrogation

In addition to their potential use in the world of therapeutics, peptidyl-FMKs can be used as chemical tools for the study of biological systems,[59] for example the elucidation of the structure and binding requirements for protease receptors in order to design drugs with greater selectivity and potency. Useful information can also be gleaned in relation to the active site selectivity of individual proteases within broader protease classes through observing the nature of the binding interactions when amino acid groups in the peptide region of the FMK chain are varied until the binding requirements are fully satisfied.[50] The conjugation of dyes into the FMK structure (**48**, **Figure 1.21**) has also been explored in order to allow for fluorescent imaging of cellular activity, such as apoptosis (**Figure 1.21**).[47]

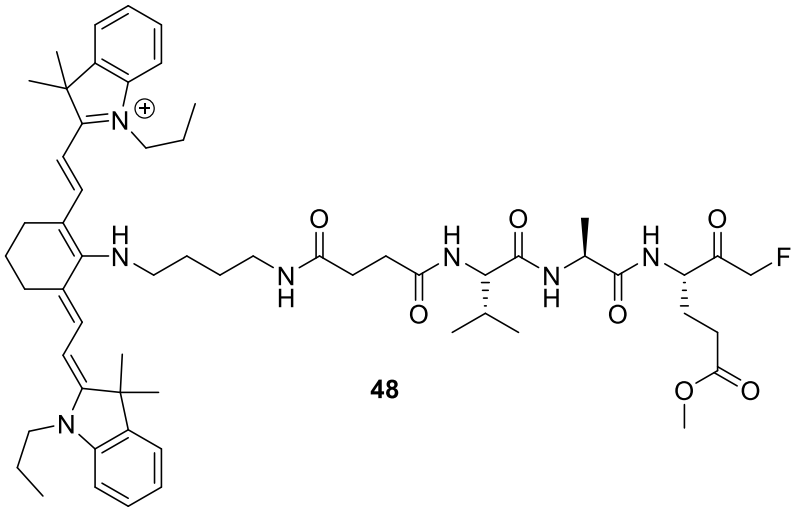

48

Figure 1.21 – Chemical structure of IR780-linker-Val-Ala-Glu(OMe)-FMK (**48**).[47]

Ellis and co-workers describe another example in which peptidyl FMKs are useful for understanding the structural binding requirements and properties of a target enzyme.[164] In this case, inhibitor **49** (**Figure 1.22**) was synthesized and found to be a potent and selective irreversible inhibitor of PKACα, a kinase enzyme. The structure of the inhibitor consists of an electrophilic fluoromethyl ketone moiety attached to a substrate-competitive inhibitor scaffold. This means that if the FMK binds in a region in which a reactive cysteine residue is present, the nucleophilic cysteine will attack the electrophilic FMK, causing inhibition. The nature of the peptide scaffold also plays a key role as it allows the peptide to bind in the vicinity of the reactive cysteine, an essential requirement for successful inhibition. As a result, inhibitor **49** is capable of covalently binding to and modifying a cysteine residue at the binding site of the enzyme. The incorporation of rhodamine B, a fluorescent tag, was employed in order to allow the inhibitor-substrate adduct to be observed, thus helping to confirm that the mechanism of inhibition occurs in an irreversible manner. In this way, the peptidyl FMK developed was found to be a useful tool for studying PKACα activity.

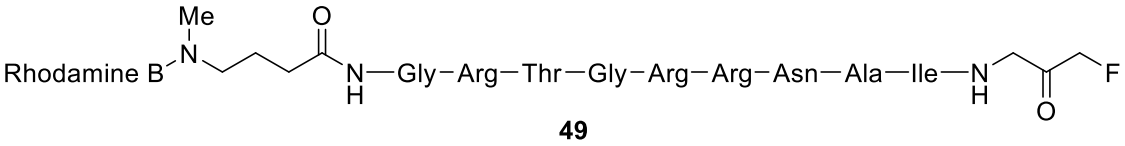

49

Figure 1.22 – Peptidyl FMK (**49**) possessing rhodamine B dye for studying PKACα activity.[164]

Another example of a peptidyl mono-FMK being used as a biological probe was reported by Misaghi *et al* in 2006.[165] *N*-glycanase (PNGase) is a deglycosylating enzyme responsible for degrading misfolded proteins.[166] If this fails to occur, protein folding diseases can result due to endoplasmic reticulum (ER) stress. Cbz-Val-Ala-Asp(OMe)-FMK (**40**, **Figure 1.23**) has been reported as a covalent inhibitor of PNGase[167] and as a result may contribute towards ER stress.[165] For this reason, it has been suggested that it could be used as a useful tool for studying the relationship between ER stress and PNGase inhibition.[165] It has also been used as a probe[168,169] to further analyse the role of PNGase in glycoprotein turnover.[169]

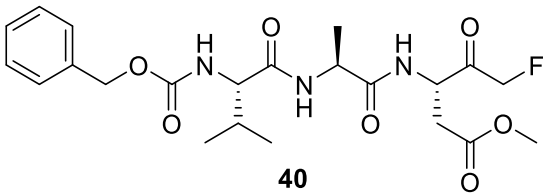

40

Figure 1.23 Cbz-Val-Ala-Asp(OMe)-FMK (**40**) structure.

1.4.5 Current Synthetic Routes to Peptidyl mono-FMKs

The number of synthetic routes to peptidyl mono-FMKs such as **6** and **14** (**Figure 1.24**) is rather limited when compared to the likes of chloromethyl-ketones (**1**, **Figure 1.24**) and tri-fluoromethyl ketones (**50**, **Figure 1.24**) for example.[34,51,53,54,170,171] Various attempts to successfully isolate these compounds in past years have resulted in disappointment and failure. Despite this, it was recognised that the properties exhibited by these biologically active compounds make them a unique class of compounds worth pursuing, and in 1985,[56] the first peptidyl mono-FMKs were isolated, marking a significant

breakthrough. Since then, a relatively small handful of new synthetic pathways have been developed. However, most suffer significant drawbacks such as the implementation of long-winded procedures, the presence of low-yielding steps and the use of hazardous materials, making them less than ideal.

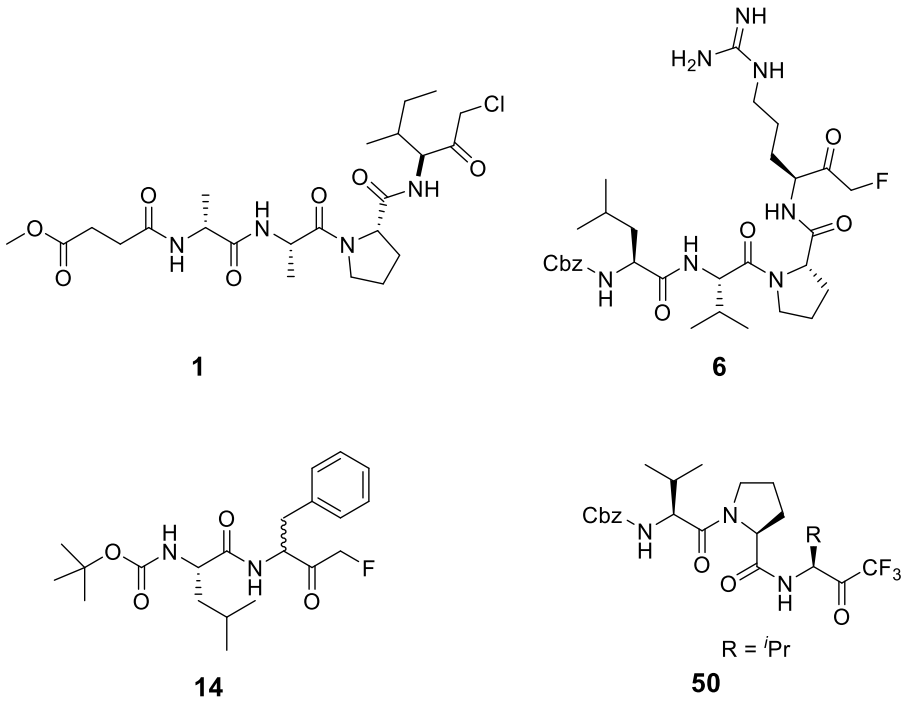

Figure 1.24 – Representative examples of a peptidyl chloromethyl ketone (**1**),[34] peptidyl fluoromethyl ketones (**6**[86] and **14**[41]) and a peptidyl tri-fluoromethyl ketone (**50**).[171]

1.4.5.1. Solution-Phase Synthetic Routes to Peptidyl mono-FMKs

1.4.5.1.1 Halogen-Exchange

An early attempted solution-phase peptidyl-FMK synthesis looked to use the displacement of bromide or chloride with a source of inorganic fluoride in a halogen-exchange reaction. However, this approach did not produce the desired product (**53**) but rather resulted in a non-fluorinated product (**51**) along with various unwanted side-products (**Scheme 1.3**).[56]

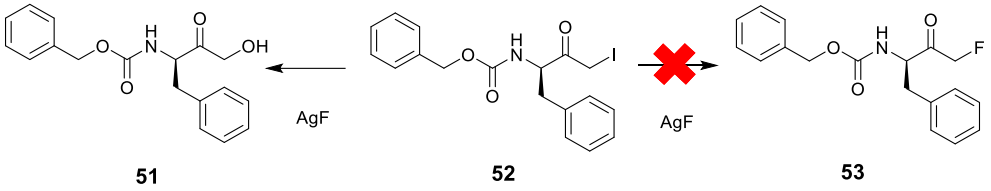

Scheme 1.3 – Attempted formation of a peptidyl mono-FMK (**53**) through a halogen-exchange reaction.[56]

Since then, a successful halogen-exchange method has been developed and was reported by Kolb *et al* in 1986 (**Scheme 1.4**).[172] Initial isolation of 3-phthalimido-1-bromo-4-phenyl-2-butanone (**54**) from *N*-phthaloyl phenylalanine was achieved through generation of the corresponding diazoketone via the acid chloride (not shown). Subsequent bromination of the diazoketone according to previously known conditions[173,174] led to the formation of **54**. Further reaction of **54** with KF/l8-crown-6 led to FMK **55** in a 45% yield (**Scheme 1.4**). Reduction of the ketone with sodium borohydride enabled removal of the phthaloyl protecting group with hydrazine; however, this meant that the ketone functionality had to be reinstalled by Swern oxidation (**56**).[175,176] Vederas *et al* utilised a similar approach for the synthesis of a ^{13}C-labelled peptidyl FMK probe which was used to investigate the mode of action of the HAV 3C enzyme.[97]

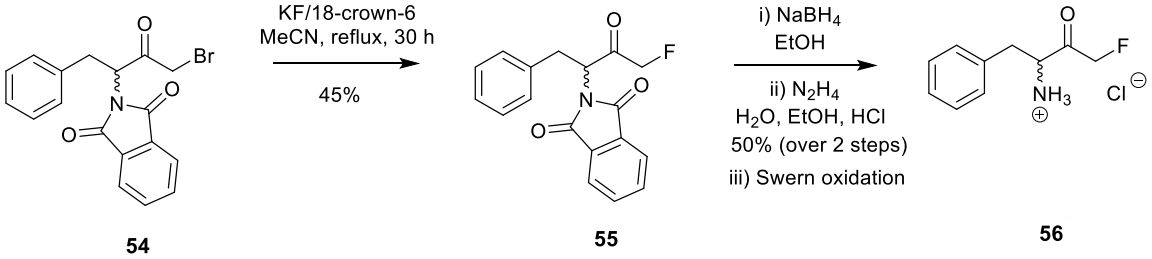

Scheme 1.4 – Formation of FMK **56** via a halogen-exchange reaction.[172]

1.4.5.1.2 Synthesis via Direct Fluorination of a Diazo Intermediate

Another initially unsuccessful attempt involved the reaction of HF with a diazomethyl ketone (**Scheme 1.5a**); a method analogous to that used for the synthesis of CMKs (chloromethyl ketones) and BMKs (bromomethyl ketones). This reaction, which was attempted on Cbz-Phe-CHN_2 (**58**), did not yield the desired FMK (**57**), but instead resulted

in the formation of the cyclic product 1-oxa-3-aza-4-benzylcyclohexan-2,5-dione (**59**).[50,56,177] Replacement of HF with milder HF/pyridine[178] appeared to give the same problem;[50] however, the use of phthaloyl instead of Cbz as a protecting group (**Scheme 1.5b**) prevented unwanted internal cyclisation. Generation of the diazo compound (**61**) was first achieved through the reaction of **60** with diazomethane in the presence of triethylamine and isobutyl chloroformate (**Scheme 1.5b**). Subsequent exposure to HF/pyridine led to the isolation of FMK **62**. Removal of the phthaloyl group under reducing conditions allowed peptide chain extension;[50] however, the FMK carbonyl functionality needed to be regenerated in the final step through oxidation to give **65**.

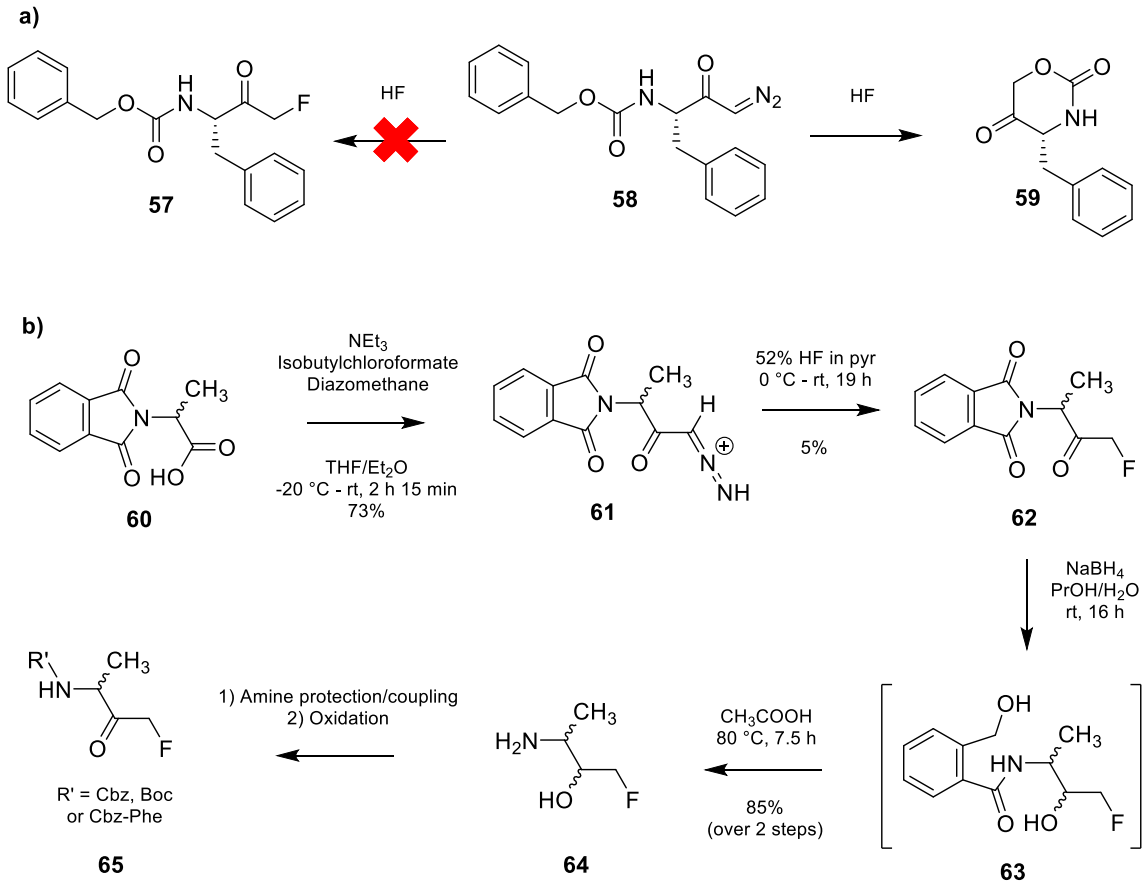

Scheme 1.5 – (**a**) Unwanted formation of cycle **59** instead of FMK **57** in the presence of HF. (**b**) Formation of peptidyl mono-FMK building block **65** via a diazo intermediate (**61**).[50]

As can been seen from the synthetic scheme shown (**Scheme 1.5**), there are a number of significant drawbacks to this approach. Apart from the fact that dealing with HF is hazardous and undesirable, it is unfortunate that once FMK formation has occurred, deprotection to give the free amine (**62** to **64**) requires reduction, which also affects the FMK functionality as already mentioned. As a result, an oxidation step is necessary in order to regenerate the ketone group. The required addition of more steps, especially when a 5% yielding step is already present, renders this a fairly inefficient and undesirable method of synthesis. Additionally, the use of diazomethane poses significant challenges due to its toxicity and potential to explode when heated, shocked or exposed to harsh lighting conditions.

1.4.5.1.3 Dakin-West Modification Method

A commonly used approach for the synthesis of keto-amides, the Dakin–West reactionClick or tap here to enter text.,[180] was modified[56] in order to allow for the synthesis of a selection of peptidyl-FMKs, as shown in **Scheme 1.6** for Bz-DL-Ala-CH_2F (**67**). The isolation of **67** in yields ranging from 20–25% was achieved through reaction of **66** with fluoroacetic anhydride in the presence of triethylamine and catalytic amounts of 4-dimethylaminopyridine. It was; however, noted that racemisation was unavoidable, and the method failed to produce the desired product for the valine analogue. In fact, the authors themselves highlighted the fact that "*isolated yields are low*" and "*purification is tedious due to the large number of side products*".[56]

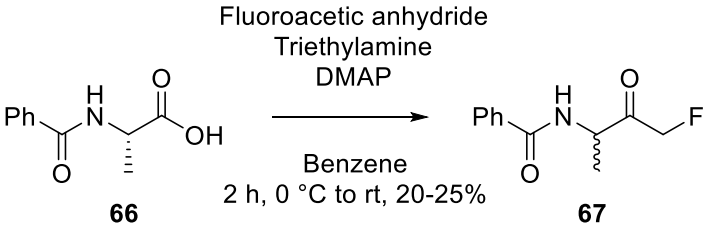

66 **67**

Scheme 1.6 - Formation of peptidyl mono-FMK building block Bz-DL-Ala-CH_2F (**67**) via a modified Dakin–West reaction.[56]

1.4.5.1.4 Epoxide Ring Opening Approach with Fluoride Source

The synthesis of peptidyl FMKs was also reported by Funeriu and co-workers in 2012. This was achieved through epoxide ring opening of epichlorohydrin **68** with a fluoride source (KHF_2) to give **69**, which was then converted to *N*-phthalimid-fluoro-alcohol **70** in the presence of potassium phthalimide[58] (**Scheme 1.7**). Subsequent reaction with hydrazine allowed the generation of the free amine (**71**), which could then be Fmoc protected to give **72**, before oxidation with DMP afforded FMK **73**. Temporary protection of the ketone functionality as a 1,3-dithiane (**74**) followed by Fmoc deprotection was employed in order to allow peptide growth to occur. Regeneration of the ketone group was achieved using bis(trifluoroacetoxy)iodobenzene, giving peptidyl FMK **77** in a quantitative yield. A modified version of this procedure was utilised by Ellis et al. in 2016 in order to access peptidyl FMKs to be studied as irreversible protease inhibitors.[164]

As already highlighted, a key disadvantage to this route is that the FMK functionality is introduced before peptide growth has been achieved, meaning that there is a requirement for protection of the ketone with a dithiane group. Unfortunately this protection, along with other steps in the process, was found to be low yielding, as highlighted in **Scheme 1.7**.

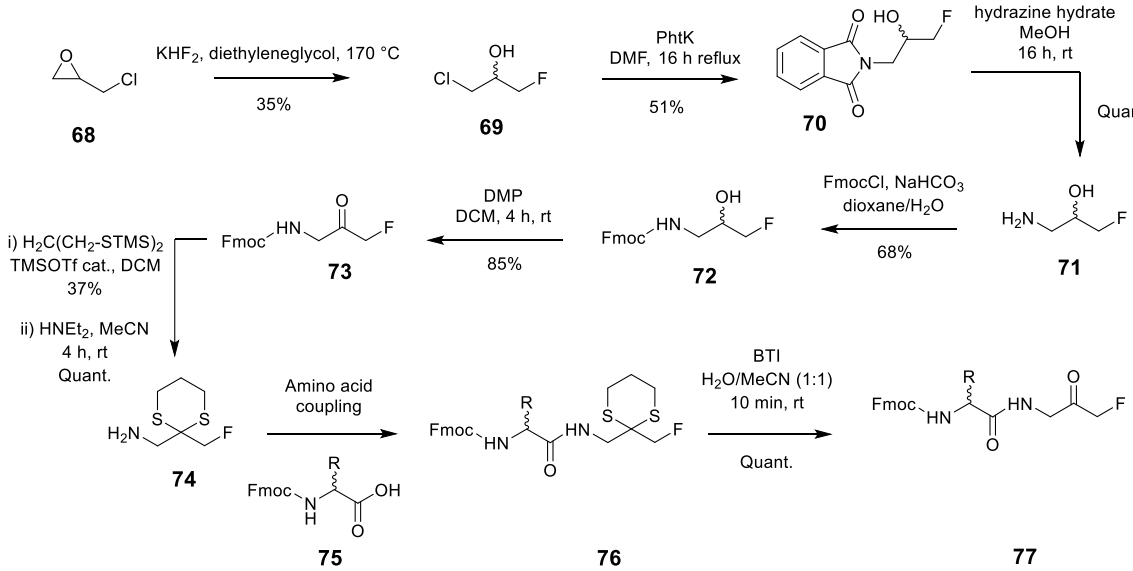

Scheme 1.7 - Synthesis of peptidyl FMK **77** utilising an epoxide ring opening approach.[58]

1.4.5.1.5 Synthetic Pathway Involving Utilisation of a Fluorinated Aldehyde/Hydrate

The application of fluorinated aldehydes/hydrates has also been explored for accessing peptidyl FMKs. One particular example of this involves the formation of *β*-nitroalcohol species **80** derived from nitro alkane **78** reacting with a fluorinated hydrated aldehyde (**79**), catalysed by potassium carbonate (**Scheme 1.8**).[45] Further reduction with Raney nickel at 50 psi of hydrogen pressure followed by treatment with concentrated HCl allowed generation of **81** as a mixture of DL, *threo*, and *erythro* diastereomers. After liberation of the hydrochloride salt, peptide coupling with DCC as the activator afforded **83**. The final step in the process involved a Sarett oxidation, allowing isolation of FMK **84**. This pathway to **84** proceeded with an overall yield of 70–75%. The main drawback with this method is the need for high-pressure during the reduction step, which may be inconvenient and impractical in some settings. Additionally, the use of highly toxic oxidising agent chromium trioxide is far from ideal. A modified version of this method was employed by Revesz *et al* in 1994.[141] Chatterjee and co-workers described the preparation of peptidyl FMKs using a similar procedure,[81] and also introduced a new approach which will be detailed in **Section 1.4.5.1.6**.[81]

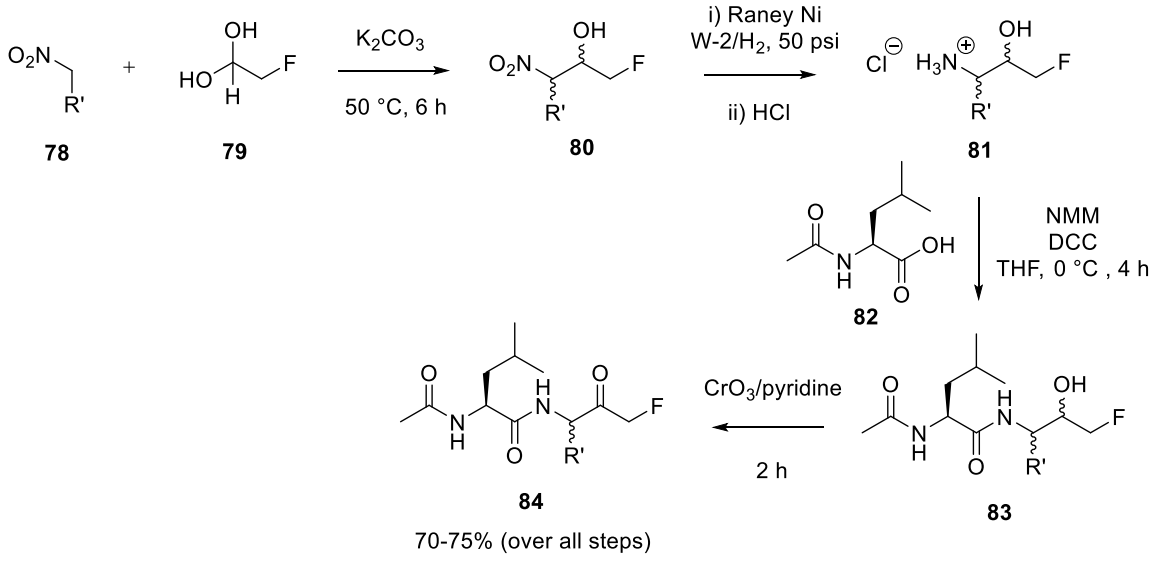

Scheme 1.8 - Isolation of peptidyl FMK **84** using a fluorinated hydrated aldehyde (**79**).[45]

The synthetic route presented by Cai *et al* in 2006 (**Scheme 1.9**) closely resembles the methodology already discussed (**Scheme 1.8**), with the key difference being the use of a fluorinated aldehyde instead of the hemiacetal (**79**).[88] Ester **85** was converted to amide **86** through the addition of dimethylamine. Further reaction with 2-fluoroacetaldehyde, which was accessed through Swern oxidation of the corresponding alcohol, enabled isolation of nitro-alcohol **87**. A subsequent hydrogenation step afforded **88** which could then be coupled to Cbz-Val-OH and finally oxidised to FMK **90**. Similar methodology was later employed by M. L. Forrest *et al* in 2012 for accessing an FMK with a fluorescent moiety attached for cellular imaging purposes.[47]

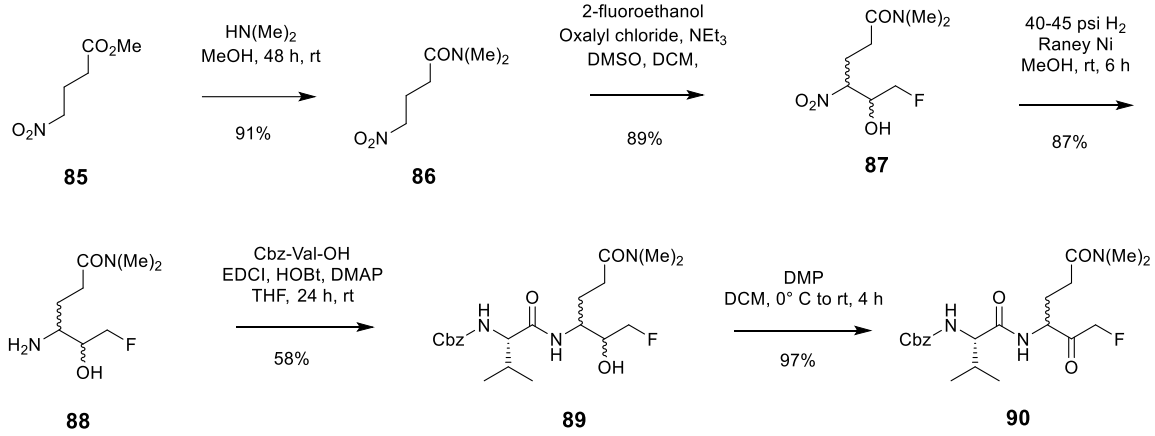

Scheme 1.9 - Synthetic route to peptidyl FMK **90** utilising a fluorinated aldehyde species.[88]

1.4.5.1.6 Synthetic Methodology Employing Silyl Enol Ether Fluorination

Chatterjee and co-workers described a novel approach for accessing peptidyl FMKs in 1997 (**Scheme 1.10**).[81] Starting from Cbz-Val-Phe-OH (**91**), conversion to the Weinreb amide (**92**) was achieved with unavoidable epimerisation at the P_1 position in the presence of *N,O*-dimethylhydroxylamine hydrochloride, triethylamine and BOP. Further reaction with MeMgBr led to the successful isolation of methyl ketone **93**. This could then be transformed into the corresponding silyl enol ether and subsequently fluorinated with F-TEDA-BF_4, affording dipeptide FMK **94**. It should; however, be noted that the fluorination step proceeded with a yield of just 10%, rendering the method rather inefficient.

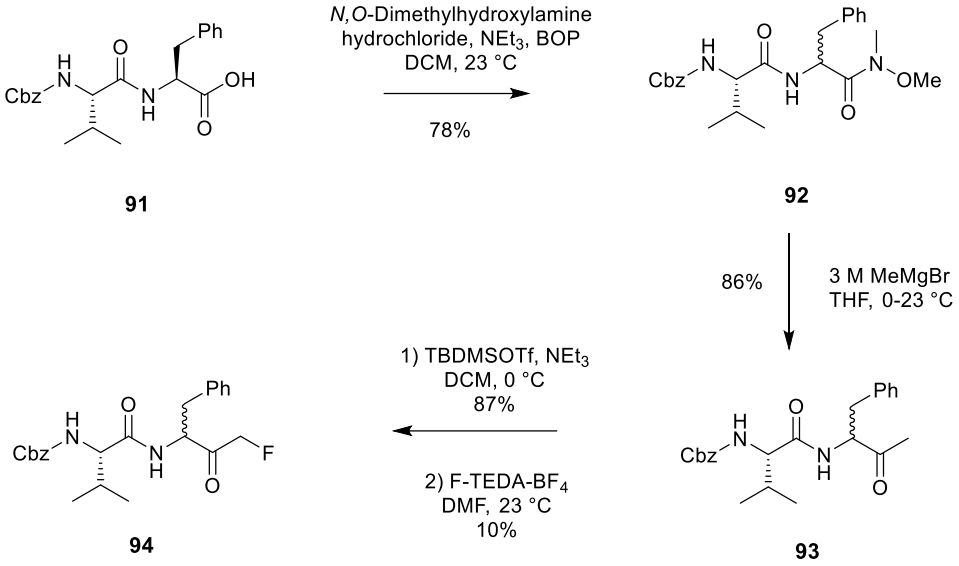

Scheme 1.10 - Isolation of dipeptide FMK **94** through silyl enol ether fluorination.[81]

1.4.5.1.7 Synthetic Pathway Involving 1-amino-3-fluoro-propan-2-ol hydrochloride (96)

A literature procedure for accessing peptidyl FMKs, which was reported by Tang *et al* in 2016 (**Scheme 1.11**),[57] involves the coupling of a Boc-protected amino acid (**95**) with 1-amino-3-fluoro-propan-2-ol hydrochloride (**96**), which was synthesised according to a two-step procedure (not shown). Amide bond formation between **95** and **96** proceeds through exposure to HATU under basic conditions (DIPEA). Subsequent Boc deprotection of **97** is achieved by treatment with HCl in ethyl acetate, allowing for the coupling of the following amino acid. The final step in the process involves the oxidation of alcohol **99** to FMK **100** in the presence of Dess–Martin periodinane (DMP). Whilst this procedure gave good yields throughout, the fluorinated amine shown also required initial synthesis, increasing the length of the synthetic procedure beyond what is shown in **Scheme 1.11**.

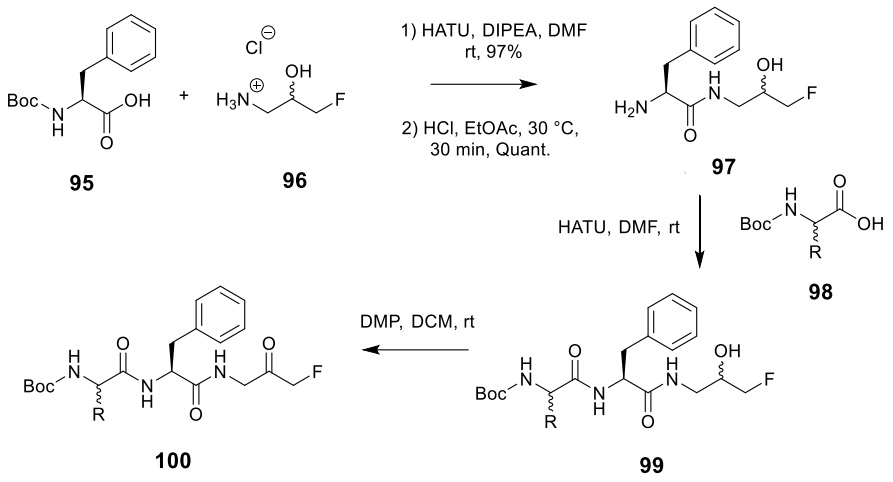

Scheme 1.11 - Formation of peptidyl FMK **100** from 1-amino-3-fluoro-propan-2-ol hydrochloride (**96**).[57]

1.4.5.1.8 Synthetic Approach Involving Employment of a Magnesium Fluoromalonate

In 1991, Palmer patented a novel approach to access peptidyl mono-FMKs through the use of magnesium fluoromalonate **104**.[181] This method was later employed by Vederas *et al* in 1997, as shown in **Scheme 1.12**.[97] After initial generation of magnesium benzyl fluoromalonate **104** from dimethyl fluoromalonate **101** (**Scheme 1.12a**), further reaction with Boc-*N,N*-dimethylglutamine (**105**) in the presence of 1,1'-carbonyldiimidazole (CDI) afforded **106** without racemisation at the P_1 position (**Scheme 1.12b**). Subsequent catalytic hydrogenation gave the desired FMK **107**.

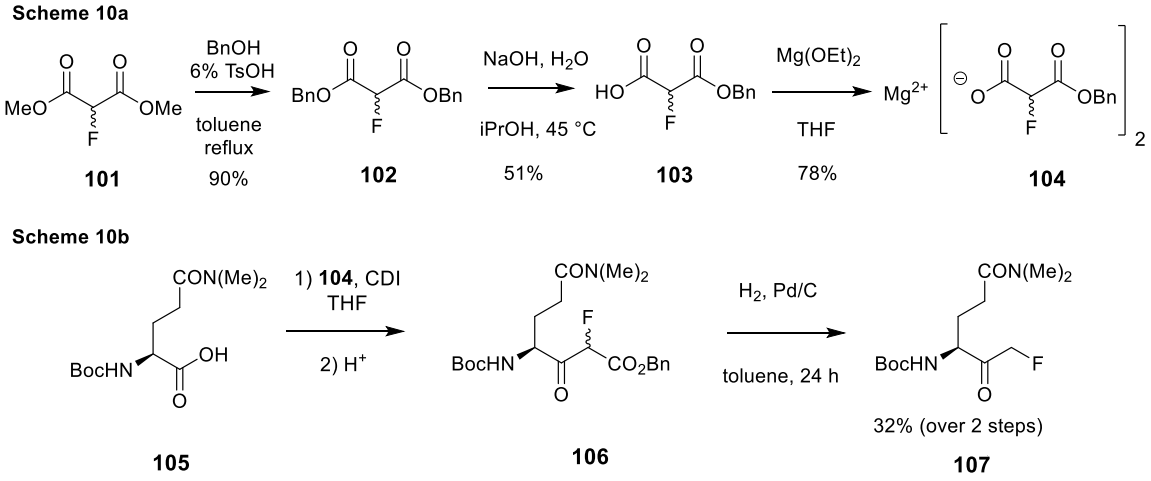

Scheme 1.12 - Synthesis of FMK **107** using magnesium benzyl fluoromalonate (**104**).[97]

Implementation of this methodology was later carried out by Scott and co-workers in their work to explore the use of peptidyl FMKs as covalent inhibitors of MALT1.[86] Magnesium benzyl fluoromalonate (**104**) was coupled to a Boc-arginine unit protected with a 2,2,5,7,8-pentamethylchroman (Pmc) sulfonyl group on the side chain (**108**) in the presence of CDI (**Scheme 1.13**). A one-pot benzyl ester deprotection and subsequent decarboxylation to the FMK was then achieved through the use of H_2 and Pd/C in ethanol. A final selective Boc deprotection step gave the desired protected arginine building block (**110**) which could then be coupled to other amino acid units as required. Unfortunately, partial racemisation of the arginine residue was observed during the formation of **109**.

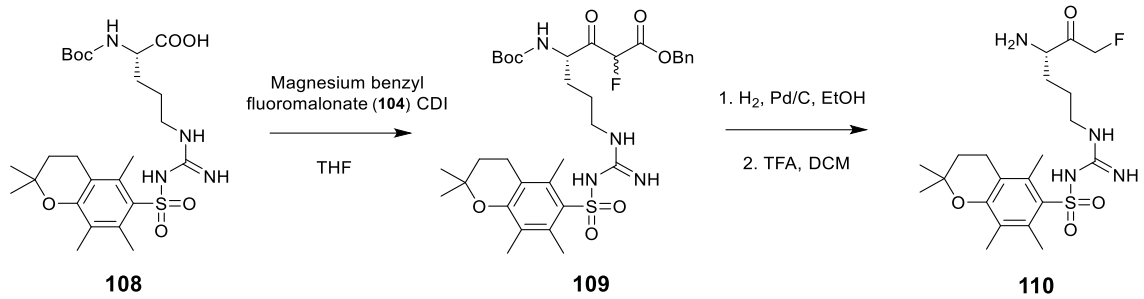

Scheme 1.13 - Synthesis of peptidyl FMK building block **110** using magnesium benzyl fluoromalonate (**104**).[86]

1.4.5.1.9 Synthetic Approach Involving Magnesium Monobenzyl Fluoromalonate Enolate 113

Witte *et al*[168] described an approach that made use of monobenzyl fluoromalonate magnesium enolate **113**. The procedure for accessing FMK **115** (**Scheme 1.14**) involves an adapted version of the patented methodology described by Palmer *et al*.[182] Initial sidechain methylation and subsequent debenzylation of **111** allowed isolation of acid **112**. Further reaction with CDI followed by addition of enolate **113** and subsequent hydrogenation gave FMK **43** in a yield of 68%. This was then Boc-deprotected under acidic conditions and coupled to fragment **114** in order to generate the FMK (**115**). In this case, the Boc group in **110** was removed and reacted with BODIPY TMR-OSu, which allowed for the preparation of a fluorescent probe for studying yeast peptide *N*-glycanase activity.

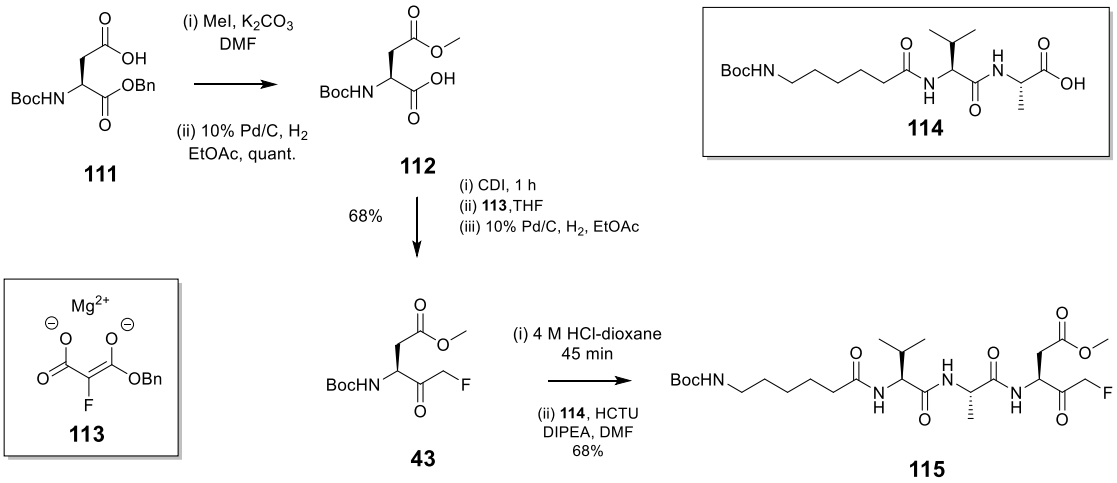

Scheme 1.14 - Synthetic route to peptidyl FMK **115** using fluorinated magnesium enolate **113**.[168]

1.4.5.2 Solid-Phase Synthetic Routes to Peptidyl-FMKs

At present, only two solid-phase peptide synthesis (SPPS) methods for accessing peptidyl mono-FMKs have been reported in the literature, with both requiring the use of a linker in some cases.[59,183] The first approach, which was developed by Roiban *et al* in 2012,[59] involves initial formation of the FMK moiety through utilisation of a halogen-exchange reaction in a similar manner to the work of Kolb *et al*[172] described earlier (**Scheme 1.4**). This is followed by attachment to the resin and peptide elongation. The first part of the process, involving construction of the FMK group from the amino acid building block Fmoc-Asp(O^{t}Bu)-OH (**116**), is shown in **Scheme 1.15**. Firstly, the formation of diazoketone derivative **117** is achieved via a two-step process involving diazomethane. **117** is converted to the bromomethyl ketone (**118**) with HBr and then subsequently transformed into the desired FMK (**119**) using TBAF as a fluoride source in the presence of *p*-toluenesulfonic acid (PTSA). Repeating these steps using Fmoc-Gly-OH to produce the corresponding FMK analogue resulted in purification difficulties. As a result, the diazoketone was instead converted to the FMK via the hydroxymethyl ketone instead of the bromomethyl ketone, as this proved more successful for this particular substrate (not shown in scheme).

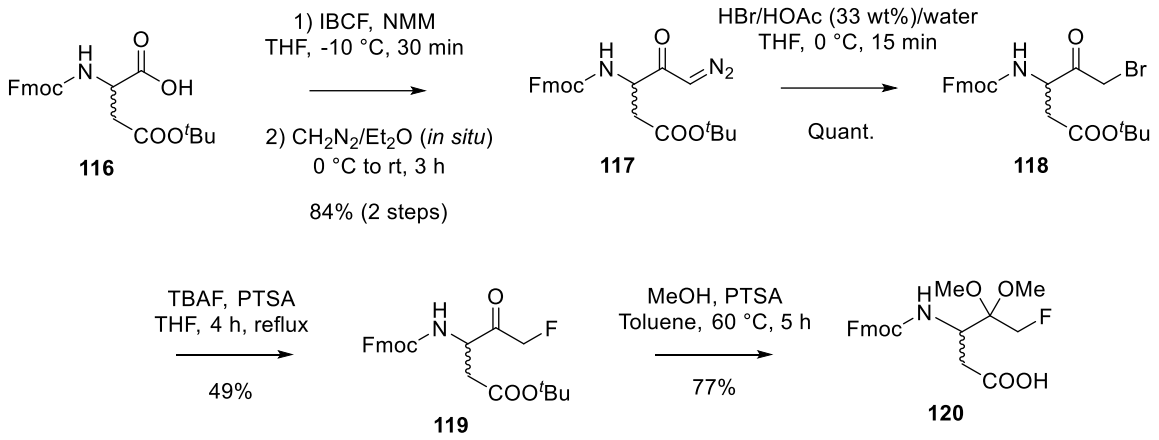

Scheme 1.15 - Generation of building block **120** from Fmoc-Asp(O^{t}Bu)-OH (**116**).[59]

In the case of the FMK (**119**) obtained from Fmoc-Asp(O^{t}Bu)-OH, because of the acid-derived sidechain, attachment to the resin could occur in a straightforward manner, allowing for subsequent growth of the peptide chain and standard acidolytic cleavage from the resin. For use in solid-phase synthesis, temporary protection of the FMK ketone functionality was required. Thus, FMK **119** was heated for 5 h with methanol in the presence of PTSA to give dimethylketal **120** with concomitant removal of the ^{t}Bu side-chain protection.

Given that not all amino acids possess a carboxylic acid functional group in their side chain, an alternative approach needed to be employed for amino acids such as Gly. This modified approach involved the synthesis of a linker which could be anchored to both the ketone of the FMK using a 1,3-diol and to the resin via a carboxy group. The linker was made in such a way that it was stable during SPPS, yet capable of being cleaved under acidic conditions. **Figure 1.25** shows the FMK moiety bound to the linker (**121**). However, multiple synthetic steps were required in order to access the linker in the first place, making it a rather inconvenient and long-winded procedure. It was later reported [183] that unwanted lactone formation was observed during attempts to protect the ketone functionality as the dimethylketal (**120**). Additionally, the harsh cleavage conditions required (37% HCl) render the method rather unattractive.

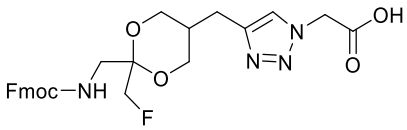

121

Figure 1.25 - FMK moiety bound to linker for solid-phase peptide synthesis (SPPS).[59]

A modified solid-phase method was subsequently reported by Joshi *et al* in 2021 (**Scheme 1.16**)[183] offering several improvements including milder cleavage conditions, although synthesis of a linker was still required. Fmoc-Asp(OMe)-FMK (**123**) was accessed through conversion of Fmoc-Asp(OMe)-OH to the bromomethyl ketone via the diazoketone, followed by reaction with a fluoride source in a similar manner to that described above in **Scheme 1.15**. Subsequent attachment to a solid support was achieved using linker **125** which then allowed a number of peptidyl FMKs to be synthesised (**Scheme 1.16**).

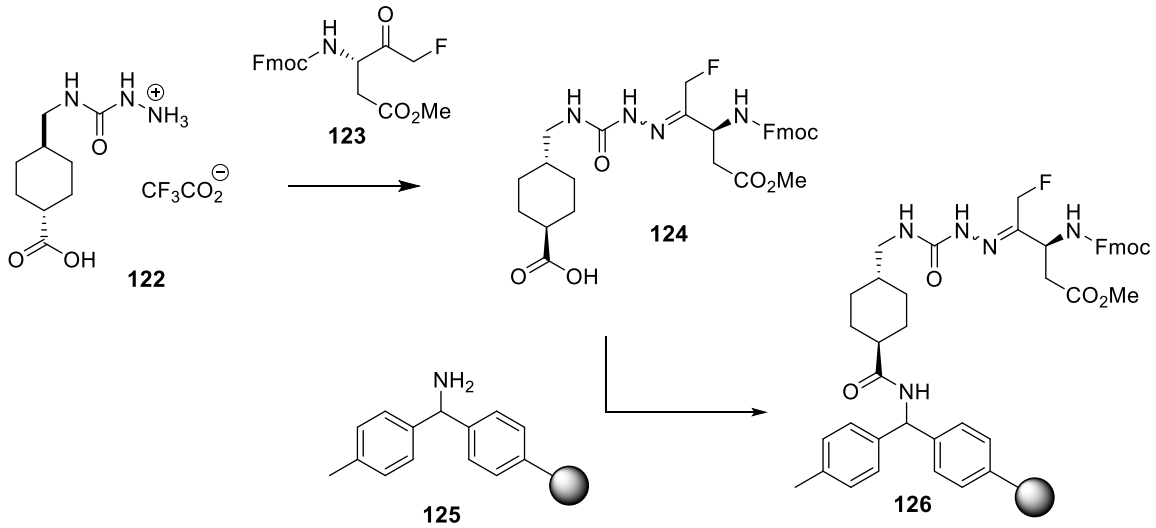

Scheme 1.16 – Solid-phase route to peptidyl FMKs.[183]

1.4.5.3 Summary of Current Synthetic Methods to FMKs & Their Applications

As highlighted, peptidyl mono-FMKs have been reported to exhibit promising therapeutic activity against a range of diseases including Rheumatoid arthritis, lymphoid malignancies, and the SARS-CoV viral pathogen. Furthermore, mFMKs can also be used as chemical probes for studying a range of cellular processes. The multifunctional nature of these biologically relevant FMK warheads, coupled with the fact that they are significantly more selective than the analogous chloromethyl-ketone-based inhibitors, makes them attractive moieties with potential utility in a wide range of applications including in vivo.

Given their applications in these aforementioned areas, a range of synthetic approaches have been developed to access mFMKs. The key synthetic solid- and solution-phase routes discussed for accessing peptidyl mono-fluoromethyl ketones (mFMKs) are summarised in **Figure 1.26.** These include halogen exchange methods (**Figure 1.26**, **i**),[97,176] diazomethyl ketone fluorination (**Figure 1.26**, **ii**),[50] a modified Dakin–West reaction (**Figure 1.26**, **iii**),[56] epoxide ring opening with a fluoride source (**Figure 1.26**, **iv**),[58,164] fluorination of silyl enol ethers (**Figure 1.26**, **v**),[81] utilisation of a fluorinated hemiacetal/aldehyde (**Figure 1.26**, **vi**),[45,47,88,141] and the use of magnesium fluoromalonates (**Figure 1.26**, **vii**).[86,97,168,182,184] Additionally, the use of a linker has been employed where appropriate for the synthesis of peptidyl FMKs by solid-phase peptide synthesis (**Figure 1.26**, **viii**).[59] With many of these approaches suffering from low overall yields, the use of hazardous materials, racemisation, and incompatibility with solid phase peptide synthesis (SPPS) methodology, there is clearly still scope for the future development of new synthetic routes in this area.

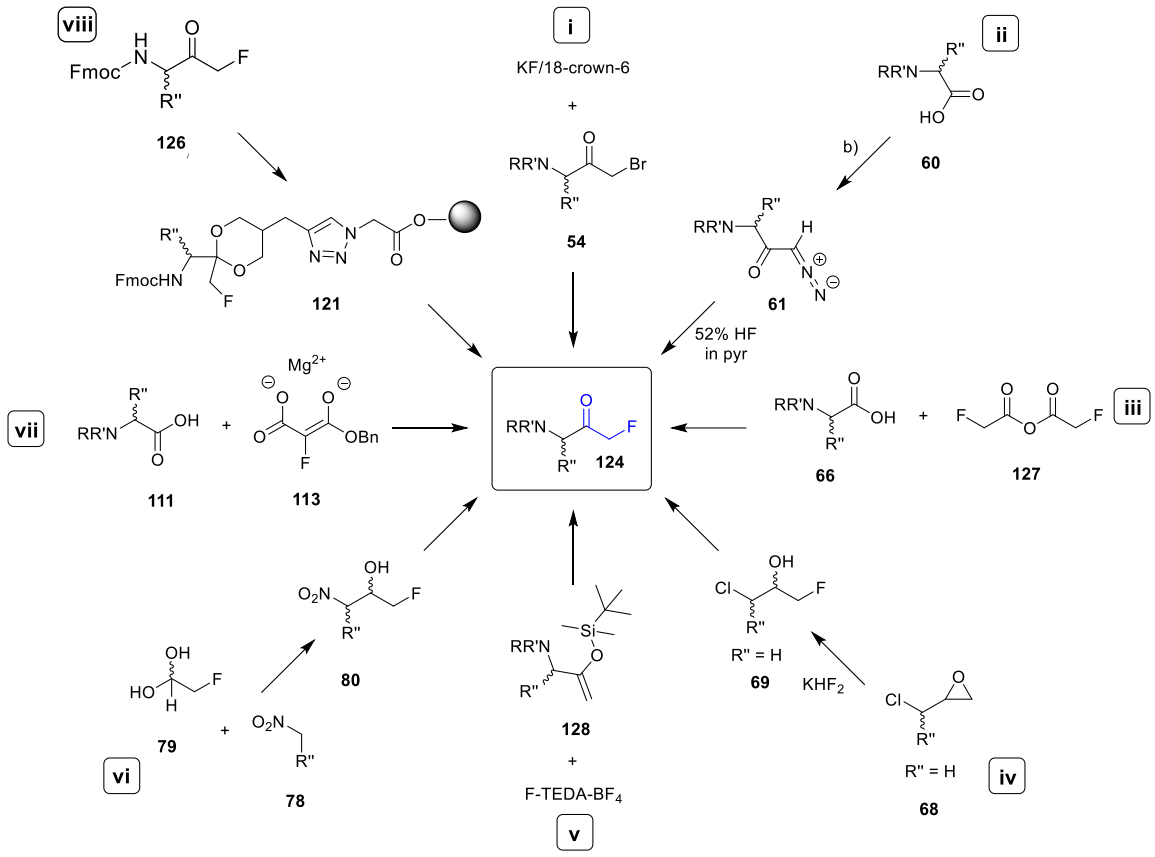

Figure 1.26 - Summary of current solid- and solution-phase synthetic routes for accessing peptidyl mono-fluoromethyl ketones (mFMKs).

1.5 Project Aims

Given their ability to act as irreversible cysteine protease inhibitors, peptidyl mono-fluoromethyl ketones (mFMKs) have shown potential as both therapeutic agents [46] and diagnostic tools for interrogating biological activity.[47] Despite this, these compounds remain highly expensive and the number of viable synthetic routes for accessing these types of compounds is limited, with many of them suffering from long-winded procedures, low-yielding steps, limited substrate scope, the use of hazardous materials and/or unwanted racemisation.[60] Furthermore, there are only currently two solid-phase routes for accessing mFMKs, with both requiring attachment via a linker.[60] Consequently, there is still scope for improved methodology to be developed.

The key aim of the project was therefore to develop new methodology for accessing stereoisomerically pure peptidyl mFMKs (**Figure 1.27**, **129**) via solution and/or

solid-phase techniques, providing convenient access to these biologically relevant molecules in few steps with minimal cost whilst avoiding highly toxic materials. Additionally, it was hoped that substrate scope could be expanded further to enable access to other biologically relevant peptide-based moieties, such as mono-chloromethyl ketones (mCMKs) (**Figure 1.27**, **130**) and trifluoromethyl ketones (tFMKs) (**Figure 1.27**, **131**), both known to act as serine inhibitors. Facilitating easier access to these promising compounds would contribute towards enabling further research into their potential use in chemical-biology and medicinal chemistry.

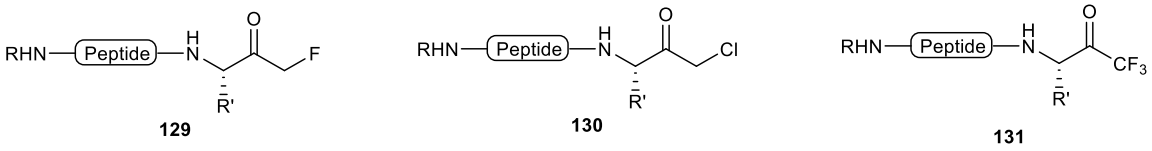

Figure 1.27 – General structures for target compounds peptidyl mFMK **129**, peptidyl mCMK **130** and peptidyl tFMK **131**. R = H, acetyl or protecting group. R' = amino acid sidechain of choice.

1.6 References for Chapter 1

1. Lau, J. L. & Dunn, M. K. Therapeutic peptides: Historical perspectives, current development trends, and future directions. *Bioorg. Med. Chem.* **26**, 2700–2707 (2018).

2. He, Y., Chen, D. & Zheng, W. An enhanced functional interrogation/manipulation of intracellular signaling pathways with the peptide 'stapling' technology. *Oncogene* **34**, 5685–5698 (2015).

3. de la Torre, B. G. & Albericio, F. Peptide Therapeutics 2.0. *Molecules* **25**, 2293 (2020).

4. Lien, S. & Lowman, H. B. Therapeutic peptides. *Trends Biotechnol.* **21**, 556–562 (2003).

5. Sorolla, A. *et al.* Precision medicine by designer interference peptides: applications in oncology and molecular therapeutics. *Oncogene* **39**, 1167–1184 (2020).

6. Fosgerau, K. & Hoffmann, T. Peptide therapeutics: current status and future directions. *Drug Discov. Today* **20**, 122–128 (2015).

7. Latham, P. W. Therapeutic peptides revisited. *Nat. Biotechnol.* **17**, 755–757 (1999).

8. Vilas Boas, L. C. P., Campos, M. L., Berlanda, R. L. A., de Carvalho Neves, N. & Franco, O. L. Antiviral peptides as promising therapeutic drugs. *Cell. Mol. Life Sci.* **76**, 3525–3542 (2019).

9. Davenport, A. P., Scully, C. C. G., de Graaf, C., Brown, A. J. H. & Maguire, J. J. Advances in therapeutic peptides targeting G protein-coupled receptors. *Nat. Rev. Drug Discov.* **19**, 389–413 (2020).

10. Mahlapuu, M., Björn, C. & Ekblom, J. Antimicrobial peptides as therapeutic agents: opportunities and challenges. *Crit. Rev. Biotechnol.* **40**, 978–992 (2020).

11. Vlieghe, P., Lisowski, V., Martinez, J. & Khrestchatisky, M. Synthetic therapeutic peptides: science and market. *Drug Discov. Today* **15**, 40–56 (2010).

12. Wang, Y. *et al.* Interrogating PP1 Activity in the MAPK Pathway with Optimized PP1-Disrupting Peptides. *Chembiochem.* **20**, 66–71 (2019).

13. Di, L. Strategic Approaches to Optimizing Peptide ADME Properties. *The AAPS J.* **17**, 134–143 (2015).

14. Ladner, R. C., Sato, A. K., Gorzelany, J. & de Souza, M. Phage display-derived peptides as therapeutic alternatives to antibodies. *Drug Discov. Today* **9**, 525–529 (2004).

15. Lee, S., Xie, J. & Chen, X. Peptide-Based Probes for Targeted Molecular Imaging. *Biochem.* **49**, 1364–1376 (2010).

16. Lee, A. C.-L., Harris, J. L., Khanna, K. K. & Hong, J.-H. A Comprehensive Review on Current Advances in Peptide Drug Development and Design. *Int J Mol Sci* **20**, 2383 (2019).

17. Marqus, S., Pirogova, E. & Piva, T. J. Evaluation of the use of therapeutic peptides for cancer treatment. *J. Biomed. Sci.* **24**, 21 (2017).

18. Otvos, L. & Wade, J. D. Current challenges in peptide-based drug discovery. *Front. Chem.* **2**, 8–11 (2014).

19. Haggag, Y. A. Peptides as Drug Candidates: Limitations and Recent Development Perspectives. *Biomed. J. Sci. Tech. Res.* **8**, 6659–6662 (2018).

20. Drucker, D. J. Advances in oral peptide therapeutics. *Nat. Rev. Drug Discov.* **19**, 277–289 (2020).

21. Usmani, S. S. *et al.* THPdb: Database of FDA-approved peptide and protein therapeutics. *PLoS One* **12**, e0181748 (2017).

22. Henninot, A., Collins, J. C. & Nuss, J. M. The Current State of Peptide Drug Discovery: Back to the Future? *J. Med. Chem.* **61**, 1382–1414 (2018).

23. deGruyter, J. N., Malins, L. R. & Baran, P. S. Residue-Specific Peptide Modification: A Chemist's Guide. *Biochem.* **56**, 3863–3873 (2017).

24. Sato, A. K., Viswanathan, M., Kent, R. B. & Wood, C. R. Therapeutic peptides: technological advances driving peptides into development. *Curr. Opin. Biotechnol.* **17**, 638–642 (2006).

25. McGregor, D. P. Discovering and improving novel peptide therapeutics. *Curr. Opin. Pharmacol.* **8**, 616–619 (2008).

26. Lee, A. C.-L., Harris, J. L., Khanna, K. K. & Hong, J.-H. A Comprehensive Review on Current Advances in Peptide Drug Development and Design. *Int. J. Mol. Sci.* **20**, 2383 (2019).

27. Cooper, B. M., Iegre, J., O' Donovan, D. H., Ölwegård Halvarsson, M. & Spring, D. R. Peptides as a platform for targeted therapeutics for cancer: peptide–drug conjugates (PDCs). *Chem. Soc. Rev.* **50**, 1480–1494 (2021).

28. Gehringer, M. & Laufer, S. A. Emerging and Re-Emerging Warheads for Targeted Covalent Inhibitors: Applications in Medicinal Chemistry and Chemical Biology. *J. Med. Chem.* **62**, 5673–5724 (2019).

29. Pan, Z. *et al.* Discovery of selective irreversible inhibitors for Bruton's tyrosine kinase. *ChemMedChem* **2**, 58–61 (2007).

30. Abbas, A., Xing, B. & Loh, T. P. Allenamides as Orthogonal Handles for Selective Modification of Cysteine in Peptides and Proteins. *Angew. Chem. Int. Ed.* **53**, 7491–7494 (2014).

31. Jaworski, M. & Thome, M. The paracaspase MALT1: Biological function and potential for therapeutic inhibition. *Cell. Mol. Life Sci.* **73**, 459–473 (2016).

32. Cullen, B. M., Halliday, I. M., Kay, G., Nelson, J. & Walker, B. The application of a novel biotinylated affinity label for the detection of a cathepsin B-like precursor produced by breast-tumour cells in culture. *Biochem. J.* **283**, 461–465 (1992).

33. Fahrney, D. E. & Gold, A. M. Sulfonyl Fluorides as Inhibitors of Esterases. I. Rates of Reaction with Acetylcholinesterase, α-Chymotrypsin, and Trypsin. *J. Am. Chem. Soc.* **85**, 997–1000 (1963).

34. Kore, A. R. & Shanmugasundaram, M. Efficient Synthesis of New Peptidyl Chloromethyl Ketones for the Application of Proteinase K Inhibitors. *Synth. Commun.* **42**, 40–45 (2012).

35. Kam, C. M., Abuelyaman, A. S., Li, Z., Hudig, D. & Powers, J. C. Biotinylated isocoumarins, new inhibitors and reagents for detection, localization, and isolation of serine proteases. *Bioconjug. Chem.* **4**, 560–567 (1993).

36. Imperiali, B. & Abeles, R. H. Inhibition of Serine Proteases by Peptidyl Fluoromethyl Ketones. *Biochem.* **25**, 3760–3767 (1986).

37. Green, G. D. J. The inactivation of one- and two-chain forms of tissue plasminogen activator by a series of peptidyl chloromethyl ketones. *Thromb. Res.* **44**, 175–183 (1986).

38. Godiksen, S. *et al.* Detection of Active Matriptase Using a Biotinylated Chloromethyl Ketone Peptide. *PLoS One* **8**, 1–10 (2013).

39. Mangold, M., Gütschow, M. & Stirnberg, M. A Short Peptide Inhibitor as an Activity-Based Probe for Matriptase-2. *Pharmaceuticals* **11**, 49 (2018).

40. Guyot, N. *et al.* Elafin, an Elastase-specific Inhibitor, Is Cleaved by Its Cognate Enzyme Neutrophil Elastase in Sputum from Individuals with Cystic Fibrosis. *J. Biol. Chem.* **283**, 32377–32385 (2008).

41. Chatterjee, S. *et al.* Synthesis and Biological Activity of a Series of Potent Fluoromethyl Ketone Inhibitors of Recombinant Human Calpain I. *J. Med. Chem.* **40**, 3820–3828 (1997).

42. Citarella, A. & Micale, N. Peptidyl Fluoromethyl Ketones and Their Applications in Medicinal Chemistry. *Molecules* **25**, 4031 (2020).

43. Veale, C. A. *et al.* Orally Active Trifluoromethyl Ketone Inhibitors of Human Leukocyte Elastase. *J. Med. Chem.* **40**, 3173–3181 (1997).

44. Kelly, C. B., Mercadante, M. A. & Leadbeater, N. E. Trifluoromethyl ketones: Properties, preparation, and application. *ChemComm.* **49**, 11133–11148 (2013).

45. Imperiali, B. & Abeles, R. H. A versatile synthesis of peptidyl fluoromethyl ketones. *Tetrahedron Lett.* **27**, 135–138 (1986).

46. Sani, M., Sinisi, R. & Viani, F. Peptidyl Fluoro-Ketones as Proteolytic Enzyme Inhibitors. *Curr. Top. Med. Chem.* **6**, 1545–1566 (2006).

47. Luan, Y. *et al.* A sensitive near-infrared fluorescent probe for caspase-mediated apoptosis: Synthesis and application in cell imaging. *Drug Discov Ther.* **5**, 220–226 (2011).

48. Angliker, H., Wikstrom, P., Rauber, P., Stone, S. & Shaw, E. Synthesis and properties of peptidyl derivatives of arginylfluoromethanes. *Biochem. J.* **256**, 481–486 (1988).

49. Yagel, S. *et al.* Suppression by cathepsin L inhibitors of the invasion of amnion membranes by murine cancer cells. *Cancer Res.* **49**, 3553–1557 (1989).

50. Rauber, P., Angliker, H., Walker, B. & Shaw, E. The synthesis of peptidylfluoromethanes and their properties inhibitors of serine proteinases and cysteine proteinases. *Biochem. J.* **239**, 633–640 (1986).

51. Sun, A., Shoji, M., Lu, Y. J., Liotta, D. C. & Snyder, J. P. Synthesis of EF24−Tripeptide Chloromethyl Ketone: A Novel Curcumin-Related Anticancer Drug Delivery System. *J. Med. Chem.* **49**, 3153–3158 (2006).

52. Hedstrom, L. Serine Protease Mechanism and Specificity. *Chem. Rev.* **102**, 4501–4524 (2002).

53. Tsuda, Y., Okada, Y., Nagamatsu, Y. & Okamoto, U. Synthesis of Peptide Chloromethyl Ketones and Examination of Their Inhibitory Effects on Human Spleen Fibrinolytic Proteinase (SFP) and Human Leukocyte Elastase (LE). *Chem. Pharm. Bull.* **35**, 3576–3584 (1987).

54. Shaw, E., Mares-Guia, M. & Cohen, W. Evidence for an Active-Center Histidine in Trypsin through Use of a Specific Reagent, 1-Chloro-3-tosylamido-7-amino-2-heptanone, the Chloromethyl Ketone Derived from Nα-Tosyl-L-lysine. *Biochem.* **4**, 2219–2224 (1965).

55. Hoffman, R. L. *et al.* Discovery of Ketone-Based Covalent Inhibitors of Coronavirus 3CL Proteases for the Potential Therapeutic Treatment of COVID-19. *J. Med. Chem.* **63**, 12725–12747 (2020).

56. Rasnick, D. Synthesis of Peptide Fluoromethyl Ketones and the inhibition of Human Cathepsin B. *Anal. Biochem.* **149**, 461–465 (1985).

57. Qiu, Z. *et al.* Discovery of Fluoromethylketone-Based Peptidomimetics as Covalent ATG4B (Autophagin-1) Inhibitors. *ACS Med. Chem. Lett.* **7**, 802–806 (2016).

58. Dobrotă, C. *et al.* Glycine Fluoromethylketones as SENP-Specific Activity Based Probes. *Chembiochem* **13**, 80–84 (2012).

59. Roiban, G. D., Matache, M., Hădade, N. D. & Funeriu, D. P. A general solid phase method for the synthesis of sequence independent peptidyl-fluoromethyl ketones. *Org. Biomol. Chem.* **10**, 4516–4523 (2012).

60. Lloyd, C. M., Colgin, N. & Cobb, S. L. Current Synthetic Routes to Peptidyl Mono-Fluoromethyl Ketones (FMKs) and Their Applications. *Molecules* **25**, 5601 (2020).

61. Ahmed, N. K. *et al.* Peptidyl fluoromethyl ketones as inhibitors of cathepsin B. *Biochem. Pharmacol.* **44**, 1201–1207 (2002).

62. la Manna, S., di Natale, C., Florio, D. & Marasco, D. Peptides as Therapeutic Agents for Inflammatory-Related Diseases. *Int. J. Mol. Sci.* **19**, 2714 (2018).

63. Eichhold, T. H., Hookfin, E. B., Taiwo, Y. O., De, B. & Wehmeyer, K. R. Isolation and quantification of fluoroacetate in rat tissues, following dosing of Z-Phe-Ala-CH2-F, a peptidyl fluoromethyl ketone protease inhibitor. *J. Pharm. Biomed. Anal.* **16**, 459–467 (1997).

64. Siklos, M., BenAissa, M. & Thatcher, G. R. J. Cysteine proteases as therapeutic targets: does selectivity matter? A systematic review of calpain and cathepsin inhibitors. *Acta Pharm. Sin. B* **5**, 506–519 (2015).

65. Danckwardt, S., Hentze, M. W. & Kulozik, A. E. Pathologies at the nexus of blood coagulation and inflammation: Thrombin in hemostasis, cancer, and beyond. *J. Mol. Med.* **91**, 1257–1271 (2013).

66. Laurens, N., Koolwijk, P. & de Maat, M. P. M. Fibrin structure and wound healing. *J. Thromb. Haemost.* **4**, 932–939 (2006).

67. Antalis, T. M., Shea-Donohue, T., Vogel, S. N., Sears, C. & Fasano, A. Mechanisms of disease: Protease functions in intestinal mucosal pathobiology. *Nat. Rev. Gastroenterol. Hepatol.* **4**, 393–402 (2007).

68. Swanstrom, R., Anderson, J., Schiffer, C. & Lee, S. K. Viral protease inhibitors. *Handb. Exp. Pharmacol.* **189**, 85–110 (2009).

69. Powers, J. C., Asgian, J. L., Ekici, Ö. D. & James, K. E. Irreversible Inhibitors of Serine, Cysteine, and Threonine Proteases. *Chem. Rev.* **102**, 4639–4750 (2002).

70. Angliker, H., Wikstrom, P., Rauber, P. & Shaw, E. The synthesis of lysylfluoromethanes and their properties inhibitors of trypsin, plasmin and cathepsin B. *Biochem. J.* **241**, 871–875 (1987).

71. Van Norden, C. J., Smith, R. E. & Rasnick, D. Cysteine proteinase activity in arthritic rat knee joints and the effects of a selective systemic inhibitor, Z-Phe-AlaCH2F. *J. Rheumatol.* **15**, 1525–1535 (1988).

72. Esser, R. *et al.* The effects of fluoromethyl ketone inhibitors of cathepsin B on adjuvant induced arthritis. *J. Rheumatol.* **20**, 1176–1183 (1993).

73. Hashimoto, Y. *et al.* Significance of Cathepsin B Accumulation in Synovial Fluid of Rheumatoid Arthritis. *Biochem. Biophys. Res. Commun.* **283**, 334–339 (2001).

74. Lawrence, C. P., Kadioglu, A., Yang, A. & William, R. The Cathepsin B Inhibitor , z-FA-FMK, Inhibits Human T Cell Proliferation In Vitro and Modulates Host Response to Pneumococcal Infection In Vivo. *J. Immunol.* **177**, 3827–3836 (2006).

75. Schotte, P., Schauvliege, R., Janssens, S. & Beyaert, R. The Cathepsin B Inhibitor z-FA.fmk Inhibits Cytokine Production in Macrophages Stimulated by Lipopolysaccharide. *J. Biol. Chem.* **276**, 21153–21157 (2001).

76. Jakoš, T., Pišlar, A., Jewett, A. & Kos, J. Cysteine Cathepsins in Tumor-Associated Immune Cells. *Front. Immunol.* **10**, 2037 (2019).

77. Tan, G.-J., Peng, Z.-K., Lu, J.-P. & Tang, F.-Q. Cathepsins mediate tumor metastasis. *World J. Biol. Chem.* **4**, 91 (2013).

78. Kam, C.-M. *et al.* Design and evaluation of inhibitors for dipeptidyl peptidase I (Cathepsin C). *Arch. Biochem. Biophys.* **427**, 123–134 (2004).

79. Cocchiaro, P. *et al.* The Multifaceted Role of the Lysosomal Protease Cathepsins in Kidney Disease. *Front. Cell Dev. Biol.* **5**, 114 (2017).

80. Rudzińska, M. *et al.* Cysteine Cathepsins Inhibition Affects Their Expression and Human Renal Cancer Cell Phenotype. *Cancers (Basel)* **12**, 1310 (2020).

81. Chatterjee, S. *et al.* Synthesis and Biological Activity of a Series of Potent Fluoromethyl Ketone Inhibitors of Recombinant Human Calpain I. *J. Med. Chem.* **40**, 3820–3828 (1997).

82. Chatterjee, S. *et al.* Potent fluoromethyl ketone inhibitors of recombinant human calpain I. *Bioorg. Med. Chem.* **6**, 1237–1240 (1996).

83. Sasakis, T., Kikuchi, T., Yumoto, N., Yoshimurag, N. & Murachi, T. Comparative Specificity and Kinetic Studies on Porcine Calpain I and Calpain II with Naturally Occurring Peptides and Synthetic Fluorogenic Substrates. *J. Biol. Chem.* **259**, 12489–12494 (1984).

84. Ono, Y. & Sorimachi, H. Calpains — An elaborate proteolytic system. *Biochim. Biophys. Acta* **1824**, 224–236 (2012).

85. Angliker, H., Anagli, J. & Shaw, E. Inactivation of calpain by peptidyl fluoromethyl ketones. *J. Med. Chem.* **35**, 216–220 (1992).

86. Hatcher, J. M. *et al.* Peptide-based covalent inhibitors of MALT1 paracaspase. *Bioorganic Med. Chem. Lett.* **29**, 1336–1339 (2019).

87. Peiris, J. S. M., Guan, Y. & Yuen, K. Y. Severe acute respiratory syndrome. *Nat. Med.* **10**, 88–97 (2004).

88. Zhang, H.-Z. *et al.* Design and Synthesis of Dipeptidyl Glutaminyl Fluoromethyl Ketones as Potent Severe Acute Respiratory Syndrome Coronovirus (SARS-CoV) Inhibitors. *J Med Chem* **49**, 1198–1201 (2006).

89. Hegyi, A. & Ziebuhr, J. Conservation of substrate specificities among coronavirus main proteases. *J. Gen. Virol.* **83**, 595–599 (2002).

90. Anand, K., Ziebuhr, J., Wadhwani, P., Mesters, J. R. & Hilgenfeld, R. Coronavirus Main Proteinase (3CL pro) Structure: Basis for Design of Anti-SARS Drugs. *Science (1979)* **300**, 1763–1767 (2003).

91. Jiang, S., Du, L. & Shi, Z. An emerging coronavirus causing pneumonia outbreak in Wuhan, China: calling for developing therapeutic and prophylactic strategies. *Emerg. Microbes Infect.* **9**, 275–277 (2020).

92. Lu, S. Timely development of vaccines against SARS-CoV-2. *Emerg. Microbes Infect.* **9**, 542–544 (2020).

93. Lee, J. T. *et al.* Genetic Surveillance of SARS-CoV-2 Mpro Reveals High Sequence and Structural Conservation Prior to the Introduction of Protease Inhibitor Paxlovid. *mBio* **13**, (2022).

94. Zaki, A. M. M., Ahmed, Y. M. & Abdelhafez, E.-S. M. N. Candidature of the Synthetic Caspase Inhibitors as New Anti-SARS-COV-2 Drug Discovery, In-Silico Molecular Docking. *Int. J. Pharm. Sci. Res.* **12**, 104–119 (2021).

95. Lu, M., Yang, H. T., Wang, Z. Y., Zhao, Y. & Xing, Y. F. *Crystal structure of the SARS-CoV-2 (COVID-19) main protease in complex with Z-VAD-FMK*. (2021) doi:10.2210/pdb7CUT/pdb.

96. Wang, Z. *et al.* Identification of proteasome and caspase inhibitors targeting SARS-CoV-2 Mpro. *Signal Transduct. Target. Ther.* **6**, (2021).

97. Morris, T. S. *et al.* In Vitro and Ex Vivo Inhibition of Hepatitis A Virus 3C Proteinase by a Peptidyl Monofluoromethyl Ketone. *Bioorg. Med. Chem.* **5**, 797–807 (1997).

98. LeMessurier, K., Hacker, H., Tuomanen, E. & Redecke, V. Inhibition of T Cells Provides Protection against Early Invasive Pneumococcal Disease. *Infect. Immun.* **78**, 5287–5294 (2010).

99. Falk, M. *et al.* Caspase Inhibition Blocks Human T Cell Proliferation by Suppressing Appropriate Regulation of IL-2, CD25, and Cell Cycle-Associated Proteins. *J. Immunol.* **173**, 5077–5085 (2004).

100. Alam, A., Cohen, L. Y., Aouad, S. & Sékaly, R.-P. Early Activation of Caspases during T Lymphocyte Stimulation Results in Selective Substrate Cleavage in Nonapoptotic Cells. *J. Exp. Med.* **190**, 1879–1890 (1999).

101. Kennedy, N. J., Kataoka, T., Tschopp, J. & Budd, R. C. Caspase Activation Is Required for T Cell Proliferation. *J. Exp. Med.* **190**, 1891–1896 (1999).

102. Mcilwain, D. R., Berger, T. & Mak, T. W. Caspase Functions in Cell Death and Disease. *Cold Spring Harb. Perspect. Biol.* **5**, 1–29 (2013).

103. Cohen, G. M. Caspases: the executioners of apoptosis. *Biochem. J.* **326**, 1–16 (1997).

104. Thornberry, N. A. Caspases: key mediators of apoptosis. *Chem. Biol.* **5**, R97–R103 (1998).

105. Garcia-Calvo, M. *et al.* Inhibition of Human Caspases by Peptide-based and Macromolecular Inhibitors. *J. Biol. Chem.* **273**, 32608–32613 (1998).

106. Citarella, A. & Micale, N. Peptidyl Fluoromethyl Ketones and Their Applications in Medicinal Chemistry. *Molecules* **25**, 4031 (2020).

107. Mackenzie, S. H., Schipper, J. L. & Clark, A. C. The potential for caspases in drug discovery. *Curr. Opin. Drug Discov. Dev.* **13**, 568–576 (2010).

108. Yang, W. *et al.* MX1013, a dipeptide caspase inhibitor with potent in vivo antiapoptotic activity. *Br. J. Pharmacol.* **140**, 402–412 (2003).

109. Deszcz, L., Cencic, R., Sousa, C., Kuechler, E. & Skern, T. An Antiviral Peptide Inhibitor That Is Active against Picornavirus 2A Proteinases but Not Cellular Caspases. *J. Virol.* **80**, 9619–9627 (2006).

110. Cheng, Y. *et al.* Caspase Inhibitor Affords Neuroprotection with Delayed Administration in a Rat Model of Neonatal Hypoxic-Ischemic Brain Injury. *J. Clin. Investig.* **101**, 1992–1999 (1998).

111. Allen, J. W., Knoblach, S. M. & Faden, A. I. Combined mechanical trauma and metabolic impairment in vitro induces NMDA receptor- dependent neuronal cell death and caspase-3-dependent apoptosis. *FASEB J.* **13**, 1875–1882 (1999).

112. Werth, J. L., Deshmukh, M., Cocabo, J., Johnson, E. M. & Rothman, S. M. Reversible Physiological Alterations in Sympathetic Neurons Deprived of NGF but Protected from Apoptosis by Caspase Inhibition or Bax Deletion. *Exp. Neurol.* **161**, 203–211 (2000).

113. Chan, Y.-M., Wu, W., Yip, H. K., So, K.-F. & Oppenheim, R. W. Caspase inhibitors promote the survival of avulsed spinal motoneurons in neonatal rats. *Neuroreport* **12**, 541–545 (2001).

114. Howe, P. H. & Basnett, K. Caspase inhibitor BD-fmk distinguishes transforming growth factor beta-induced apoptosis from growth inhibition. *Cell Growth Differ.* **9**, 869–875 (1998).

115. Cowburn, A. S., White, J. F., Deighton, J., Walmsley, S. R. & Chilvers, E. R. z-VAD-fmk augmentation of TNFα-stimulated neutrophil apoptosis is compound specific and does not involve the generation of reactive oxygen species. *Blood* **105**, 2970–2972 (2005).

116. Clark, R. S. B. *et al.* boc-Aspartyl (OMe)-fluoromethylketone attenuates mitochondrial release of cytochrome c and delays brain tissue loss after traumatic brain injury in rats. *J. Cereb. Blood Flow Metab.* **27**, 316–326 (2007).

117. Wang, Y. *et al.* Dipeptidyl aspartyl fluoromethylketones as potent caspase-3 inhibitors: SAR of the P2 amino acid. *Bioorg. Med. Chem. Lett.* **14**, 1269–1272 (2004).

118. Mittl, P. R. E. *et al.* Structure of Recombinant Human CPP32 in Complex with the Tetrapeptide Acetyl-Asp-Val-Ala-Asp Fluoromethyl Ketone. *J. Biol. Chem.* **272**, 6539–6547 (1997).

119. Wang, Y. *et al.* Dipeptidyl aspartyl fluoromethylketones as potent caspase inhibitors: peptidomimetic replacement of the P2 α-amino acid by a α-hydroxy acid. *Bioorg. Med. Chem. Lett.* **15**, 1379–1383 (2005).

120. Wang, Y., Jia, S., Tseng, B., Drewe, J. & Cai, S. X. Dipeptidyl aspartyl fluoromethylketones as potent caspase inhibitors: Peptidomimetic replacement of the P2 amino acid by 2-aminoaryl acids and other non-natural amino acids. *Bioorg. Med. Chem. Lett.* **17**, 6178–6182 (2007).

121. Hara, H. *et al.* Inhibition of interleukin 1β converting enzyme family proteases reduces ischemic and excitotoxic neuronal damage. *Proc. Natl. Acad. Sci. USA* **94**, 2007–2012 (1997).

122. Endres, M. *et al.* Attenuation of Delayed Neuronal Death After Mild Focal Ischemia in Mice by Inhibition of the Caspase Family. *J. Cereb. Blood Flow Metab.* **18**, 238–247 (1998).

123. Wiessner, C., Sauer, D., Alaimo, D. & Allegrini, P. Protective effect of a caspase inhibitor in models for cerebral ischemia in vitro and in vivo. *Cell Mol. Biol. (Noisy-Le-Grand)* **46**, 53–62 (2000).

124. Li, H., Colbourne, F., Sun, P., Zhao, Z. & Buchan, A. M. Caspase Inhibitors Reduce Neuronal Injury After Focal but Not Global Cerebral Ischemia in Rats. *Stroke* **31**, 176–182 (2000).

125. Yaoita, H., Ogawa, K., Maehara, K. & Maruyama, Y. Attenuation of Ischemia/Reperfusion Injury in Rats by a Caspase Inhibitor. *Circulation* **97**, 276–281 (1998).

126. Farber, A. *et al.* A specific inhibitor of apoptosis decreases tissue injury after intestinal ischemia-reperfusion in mice. *J. Vasc. Surg.* **30**, 752–760 (1999).

127. Iwata, A., Harlan, J. M., Vedder, N. B. & Winn, R. K. The caspase inhibitor z-VAD is more effective than CD18 adhesion blockade in reducing muscle ischemia-reperfusion injury: implication for clinical trials. *Blood* **100**, 2077–2080 (2002).

128. Daemen, M. A. R. C. *et al.* Inhibition of apoptosis induced by ischemia-reperfusion prevents inflammation. *J. Clin. Investig.* **104**, 541–549 (1999).

129. Rozman-Pungercar, J. *et al.* Inhibition of papain-like cysteine proteases and legumain by caspase-specific inhibitors: when reaction mechanism is more important than specificity. *Cell Death Differ.* **10**, 881–888 (2003).

130. Adrain, C., Creagh, E. M. & Martin, S. J. Apoptosis-associated release of Smac/DIABLO from mitochondria requires active caspases and is blocked by Bcl-2. *EMBO J.* **20**, 6627–6636 (2001).

131. Caserta, T. M., Smith, A. N., Gultice, A. D., Reedy, M. A. & Brown, T. L. Q-VD-OPh , a broad spectrum caspase inhibitor with potent antiapoptotic properties. *Apoptosis* **8**, 345–352 (2003).

132. Ma, J., Qiu, J., Hirt, L., Dalkara, T. & Moskowitz, M. A. Synergistic protective effect of caspase inhibitors and bFGF against brain injury induced by transient focal ischaemia. *Br. J. Pharm. 2001* **133**, 345–350 (2001).

133. Iwata, A. *et al.* A Broad-Spectrum Caspase Inhibitor Attenuates Allergic Airway Inflammation in Murine Asthma Model. *J. Immunol.* **170**, 3386–3391 (2003).

134. Kopalli, S. R., Kang, T.-B. & Koppula, S. Necroptosis inhibitors as therapeutic targets in inflammation mediated disorders - a review of the current literature and patents. *Expert Opin. Ther. Pat.* **26**, 1239–1256 (2016).

135. Li, X. *et al.* The Caspase Inhibitor Z-VAD-FMK Alleviates Endotoxic Shock via Inducing Macrophages Necroptosis and Promoting MDSCs-Mediated Inhibition of Macrophages Activation. *Front. Immunol.* **10**, 1824 (2019).

136. Liu, M. *et al.* Caspase inhibitor zVAD-fmk protects against acute pancreatitis-associated lung injury via inhibiting inflammation and apoptosis. *Pancreatology* **16**, 733–738 (2016).

137. Elena, M. E. *et al.* Theriogenology Inhibition of apoptosis by caspase inhibitor Z-VAD-FMK improves cryotolerance of in vitro derived bovine embryos. *Theriogenology* **108**, 127–135 (2018).

138. McCarthy, M. J., Rubin, L. L. & Philpott, K. L. Involvement of caspases in sympathetic neuron apoptosis. *J. Cell Sci.* **110**, 2165–2173 (1997).

139. Huang, J.-Q., Radinovic, S., Rezaiefar, P. & Black, S. C. In vivo myocardial infarct size reduction by a caspase inhibitor administered after the onset of ischemia. *Eur. J. Pharmacol.* **402**, 139–142 (2000).

140. Mocanu, M. M., Baxter, G. F. & Yellon, D. M. Caspase inhibition and limitation of myocardial infarct size: protection against lethal reperfusion injury. *Br. J. Pharmacol.* **130**, 197–200 (2000).

141. Revesz, L. *et al.* Synthesis of P1 aspartate-based peptide acyloxymethyl and fluoromethyl ketones as inhibitors of interleukin-1β-converting enzyme. *Tetrahedron Lett.* **35**, 9693–9696 (1994).

142. Shaalan, A., Carpenter, G. & Proctor, G. Caspases are key regulators of inflammatory and innate immune responses mediated by TLR3 in vivo. *Mol. Immunol.* **94**, 190–199 (2018).

143. Rodriguez, I., Matsuura, K., Ody, C., Nagata, S. & Vassalli, P. Systemic Injection of a Tripeptide Inhibits the Intracellular Activation of CPP32-1ike Proteases In Vivo and Fully Protects Mice against Fas-mediated Fulminant Liver Destruction and Death. *J. Exp. Med.* **184**, 2067–2072 (1996).

144. Chandler, J. M., Cohen, G. M. & Macfarlane, M. Different Subcellular Distribution of Caspase-3 and Caspase-7 following Fas-induced Apoptosis in Mouse Liver. *J. Biol. Chem.* **273**, 10815–10818 (1998).

145. Braun, J. S. *et al.* Neuroprotection by a caspase inhibitor in acute bacterial meningitis. *Nat. Med.* **5**, 298–302 (1999).

146. Okuda, Y., Sakoda, S., Fujimura, H. & Yanagihara, T. The Effect of Apoptosis Inhibitors on Experimental Autoimmune Encephalomyelitis: Apoptosis as a Regulatory Factor. *Biochem. Biophys. Res. Commun.* **267**, 826–830 (2000).

147. Rudel, T. Caspase Inhibitors in Prevention of Apoptosis. *Herz* **24**, 236–241 (1999).

148. Chen, J. *et al.* Induction of Caspase-3-Like Protease May Mediate Delayed Neuronal Death in the Hippocampus after Transient Cerebral Ischemia. *J. Neurosci.* **18**, 4914–4928 (1998).

149. Zhao, H., Yenari, M. A., Cheng, D., Sapolsky, R. M. & Steinberg, G. K. Biphasic cytochrome c release after transient global ischemia and its inhibition by hypothermia. *J. Cereb. Blood Flow Metab.* **25**, 1119–1129 (2005).

150. Kaul, S., Kanthasamy, A., Kitazawa, M., Anantharam, V. & Kanthasamy, A. G. Caspase-3 dependent proteolytic activation of protein kinase Cδ mediates and regulates 1-methyl-4-phenylpyridinium (MPP^+)-induced apoptotic cell death in dopaminergic cells: relevance to oxidative stress in dopaminergic degeneration. *Eur. J. Neurosci.* **18**, 1387–1401 (2003).

151. Zhan, R.-Z. *et al.* Both Caspase-Dependent and Caspase-Independent Pathways May Be Involved in Hippocampal CA1 Neuronal Death Because of Loss of Cytochrome c from Mitochondria in a Rat Forebrain Ischemia Model. *J. Cereb. Blood Flow Metab.* **21**, 529–540 (2001).

152. Kanthasamy, A. G. *et al.* A novel peptide inhibitor targeted to caspase-3 cleavage site ofa proapoptotic kinase protein kinase C delta (PKCδ) protects against dopaminergic neuronal degeneration in Parkinson's disease models. *Free Radic. Biol. Med.* **41**, 1578–1589 (2006).

153. Rosenthal, P. J., Wollish, W. S., Palmer, J. T. & Rasnick, D. Antimalarial effects of peptide inhibitors of a Plasmodium falciparum cysteine proteinase. *J. Clin. Investig.* **88**, 1467–1472 (1991).

154. Rosenthal, P. J., Lee, G. K. & Smith, R. E. Inhibition of a Plasmodium vinckei cysteine proteinase cures murine malaria. *J. Clin. Investig.* **91**, 1052–1056 (1993).

155. Ettari, R., Bova, F., Zappala, M., Grasso, S. & Micale, N. Falcipain-2 Inhibitors. *Med. Res. Rev.* **30**, 136–167 (2009).

156. Harth, G. *et al.* Peptide-fluoromethyl ketones arrest intracellular replication and intercellular transmission of Trypanosoma cruzi. *Mol. Biochem. Parasitol.* **58**, 17–24 (1993).

157. Gillmor, S. A. & Fletterick, R. J. *Cruzain Inhibited With Benzoyl-Arginine-Alanine-Fluoromethylketone*. (1997) doi:http://doi.org/10.2210/pdb2AIM/pdb.

158. Gillmor, S. A., Craik, C. S. & Fletterick, R. J. Structural determinants of specificity in the cysteine protease cruzain. *Protein Sci.* **6**, 1603–1611 (1997).

159. McGrath, M. E. *et al.* The Crystal Structure of Cruzain: A Therapeutic Target for Chagas' Disease. *J. Mol. Biol.* **247**, 251–259 (1995).

160. Reggiori, F. & Mauthe, M. At the Center of Autophagy: Autophagosomes. in *Encyclopedia of Cell Biology* vol. 2 243–247 (Elsevier, 2016).

161. Kobayashi, S. Choose Delicately and Reuse Adequately: The Newly Revealed Process of Autophagy. *Biol. Pharm. Bull.* **38**, 1098–1103 (2015).

162. Rubinsztein, D. C., Codogno, P. & Levine, B. Autophagy modulation as a potential therapeutic target for diverse diseases. *Nat. Rev. Drug Discov.* **11**, 709–730 (2012).

163. Chang, H. & Zou, Z. Targeting autophagy to overcome drug resistance: further developments. *J. Hematol. Oncol.* **13**, 159 (2020).

164. Coover, R. A. *et al.* Design, synthesis, and in vitro evaluation of a fluorescently labeled irreversible inhibitor of the catalytic subunit of cAMP-dependent protein kinase (PKACα). *Org. Biomol. Chem.* **14**, 4576–4581 (2016).

165. Misaghi, S., Korbel, G. A., Kessler, B., Spooner, E. & Ploegh, H. L. z-VAD-fmk inhibits peptide:N-glycanase and may result in ER stress. *Cell Death Differ.* **13**, 163–165 (2006).

166. Suzuki, T., Park, H. & Lennarz, W. J. Cytoplasmic peptide: N-glycanase (PNGase) in eukaryotic cells: occurrence, primary structure, and potential functions. *FASEB J.* **16**, 635–641 (2002).

167. Suzuki, T. *et al.* Site-specific Labeling of Cytoplasmic Peptide:N-Glycanase by N,N'-Diacetylchitobiose-related Compounds. *J. Biol. Chem.* **281**, 22152–22160 (2006).

168. Witte, M. D. *et al.* Bodipy-VAD-Fmk, a useful tool to study yeast peptide N-glycanase activity. *Org. Bio. Chem.* **5**, 3690 (2007).

169. Misaghi, S., Pacold, M. E., Blom, D., Ploegh, H. L. & Korbel, G. A. Using a Small Molecule Inhibitor of Peptide: N-Glycanase to Probe Its Role in Glycoprotein Turnover. *Chem. Biol.* **11**, 1677–1687 (2004).

170. Peet, N. P. *et al.* Synthesis of Peptidyl Fluoromethyl Ketones and Peptidyl a-Keto Esters as Inhibitors of Porcine Pancreatic Elastase, Human Neutrophil Elastase, and Rat and Human Neutrophil Cathepsin G. *J. Med. Chem.* **33**, 394–407 (1990).

171. Edwards, P. D. A method for the stereoselective synthesis of peptidyl trifluoromethyl ketones. *Tetrahedron Lett.* **33**, 4279–4282 (1992).

172. Kolb, M., Barth, J. & Neises, B. Synthesis of fluorinated α-amino ketones part I: α-benzamidoalkyl mono- di- and trifluoromethyl ketones. *Tetrahedron Lett.* **27**, 1579–1582 (1986).

173. Becker, H. *Organikum: organisch-chemisches Grundpraktikum*. (Deutscher Verl. d. Wissenschaften, 1968).

174. Penke, B., Czombos, J., Baláspiri, L., Petres, J. & Kovács, K. Synthese von Diazoketonen aus Acylaminosäuren unter Verwendung von gemischten Anhydriden bzw. N, N'-Dicyclohexyl-carbodiimid. *Helv. Chim. Acta* **53**, 1057–1061 (1970).

175. Mancuso, A. J., Huang, S.-L. & Swern, D. Oxidation of long-chain and related alcohols to carbonyls by dimethyl sulfoxide 'activated' by oxalyl chloride. *J. Org. Chem.* **43**, 2480–2482 (1978).

176. Kolb, M., Neises, B. & Gerhart, F. Synthesis of fluorinated α-amino ketones, III. Preparation of fluorinated ketone analogues of phenylalanine, lysine, and p-(Guanidino)phenylalanine. *Liebigs Ann. Chem.* **1990**, 1–6 (1990).

177. Smith, A. B. & Dieter, R. K. The Acid Promoted Decomposition of α-Diazo Ketones. *Tetrahedron* **37**, 2407–2439 (1981).

178. Olah, G. A., Shih, G. J. & Prakash, G. K. S. Fluorine-containing reagents in organic synthesis. *J. Fluor. Chem.* **33**, 377–396 (1986).

179. Vechia, L. D., Octavio, R., Alves, M., Soter, L. & Mariz, D. The Dakin-West reaction : Past, present and future. *Tetrahedron* **74**, 4359–4371 (2018).

180. Dalla Vechia, L., Octavio Mendonça Alves de Souza, R. & Soter de Mariz e Miranda, L. S. The Dakin-West reaction: Past, present and future. *Tetrahedron* **74**, 4359–4371 (2018).

181. Palmer, J. T. Reagents and Methods for Stereospecific Fluoromethylation. vol. 99 1–23 (1991).

182. Palmer, J. T. Magnesium Fluoromalonates. 1–12 (1992).

183. Joshi, D. *et al.* An improved method for the incorporation of fluoromethyl ketones into solid phase peptide synthesis techniques. *RSC Adv.* **11**, 20457–20464 (2021).

184. Palmer, J. T. Reagents and Methods for Stereospecific Fluoromethylation. 1–44 (1991).

2. Utilisation of Tri-Carbonyl Systems for Accessing Peptidyl Mono-Fluoromethyl Ketones

2.1 Organofluorine Chemistry

The introduction of fluorine into organic molecules through the formation of C-F bonds can lead to a drastic change in both chemical and physical properties.[1] This is in part due to the highly electronegative nature of the fluorine atom, which has a value of 4.0 on the Pauling scale. The implication of this is that the C-F bond is strongly polarised and thus possesses high ionic character, with profound effects on the acidity of nearby functional groups.[2] In some cases, the addition of fluorine to a drug molecule has been shown to lower the basicity of local moieties in such a way that lipophilicity is increased, and with it, cell-membrane permeability, leading to improved bioavailability.[3,4] The strong electrostatic attraction between $C^{\delta+}$ and $F^{\delta-}$ gives rise to an average bond dissociation energy of 485 kJ/mol, making it the strongest single bond to carbon.[2] This can add significant stability to the molecule, often meaning that fluorine can demonstrate better resistance towards displacement by nucleophiles compared to chloride and bromide which leave much more readily. Installation of fluorine groups at metabolically labile sites which are prone to oxidation by P450 enzymes[3] has been successfully employed to enhance the stability of drug molecules.[5] Furthermore, the inherently small size of fluorine enables the replacement of one or more hydrogen atoms with fluorine without major steric ramifications.[6] The addition of fluorine to a molecule may also increase target protein binding affinity through enhancing the reactivity of local functional groups by lowering their pK_a, or alternatively through direct interaction between fluorine atoms and the protein target.[7,8] Given their unique properties, organofluorine compounds have found use in a wide range of applications ranging from technological to pharmaceutical.[9,10] In fact, the incorporation of fluorine into biologically active compounds in order to improve their activity

is now commonplace,[11] with a large number of FDA-approved fluorinated drugs currently available on the market.[12] Examples include Atorvastatin (**132**) used in the treatment of cardiovascular conditions,[13,3] the chemotherapeutic agent 5-Fluorouracil (**133**)[14,15] and Ubrogepant (**134**) for the treatment of migraines[12,16,17] (**Figure 2.1**). Approximately 30% of all agrochemicals and 20% of all pharmaceuticals possess at least one fluorine atom in their structure.[18–20]

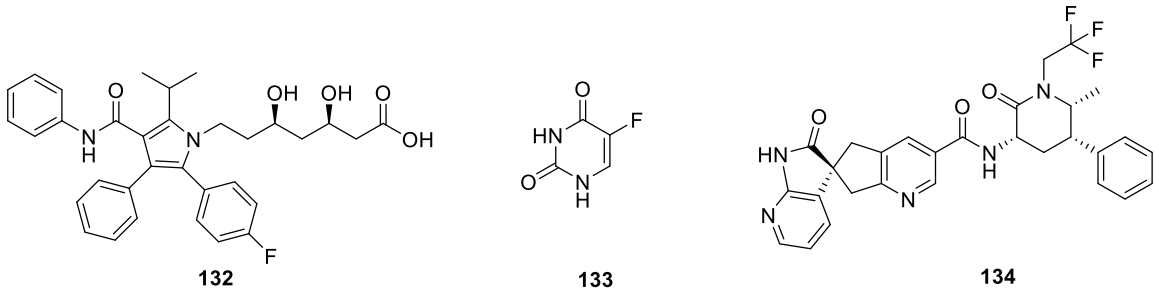

Figure 2.1 – Structures of Atorvastatin (**132**), 5-Fluorouracil (**133**) and Ubrogepant (**134**).

One of the key challenges in the successful isolation of fluorinated molecules such as peptidyl mono-fluoromethyl ketones (mFMKs) is the incorporation of fluorine into the system in a selective and efficient manner. Very few naturally occurring organofluorine compounds exist,[21–23] and thus the formation of carbon-fluorine containing compounds is almost entirely reliant on synthetic chemistry. A vast array of fluorinating agents has been developed, ranging from electrophilic to nucleophilic in nature. These are generally derived from the mining of the naturally occurring mineral fluorspar (CaF_2), which is subsequently converted to anhydrous hydrogen fluoride (aHF), the key building block for the synthesis of all fluorinated chemicals. A summary of the main sources of fluorine is provided in **Figure 2.2**[23] and some of these will be discussed in more detail in the following sections.

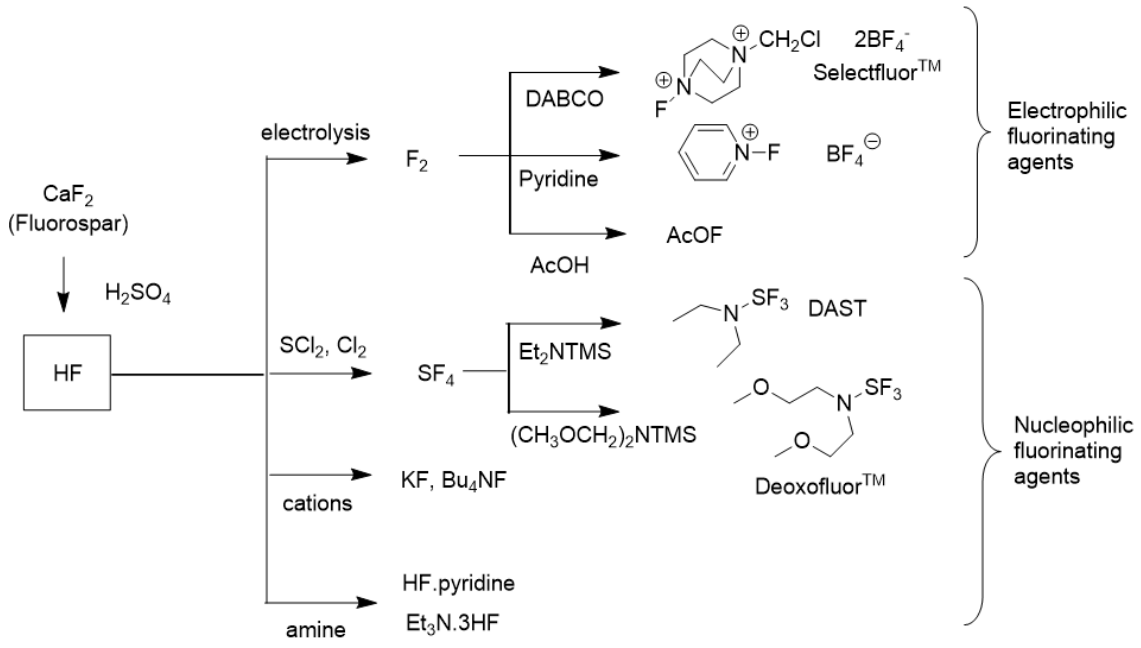

Figure 2.2 – Summary of common sources of fluorine.[23]

2.1.1 Nucleophilic Methods of C-F Bond Formation

Nucleophilic fluorination involves the attack of a fluoride source on an electrophile.[24] Several different reagents are capable of providing a source of F^{-} for this purpose,[25] including hydrogen fluoride (HF).[26] However, despite its use in industry, the highly corrosive and toxic nature of this compound renders it undesirable for use on a regular basis. Other alternatives include alkali metal fluorides such as KF and CsF. These tend to be readily available; however, suffer from poor solubility in organic solvents[27] and hygroscopicity[28] due to the ability for hydrogen bonding between the fluoride anion and any moisture present, resulting in a substantial decrease in reactivity. For this reason, non-hygroscopic nucleophilic fluorinating agents have been developed that are not easily quenched by moisture, such as tetrabutylammonium difluorotriphenylstannate (**135**) (**Figure 2.3**).[29] This fluorinating agent was demonstrated to fluorinate benzyl bromide (**136**) (**Scheme 2.1**) eighteen times faster than flame-dried caesium fluoride.[29]

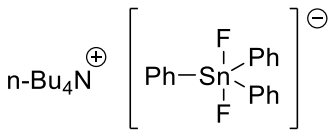

135

Figure 2.3 – Tetrabutylammonium difluorotriphenylstannate (**135**), a nucleophilic fluorinating agent.[29]

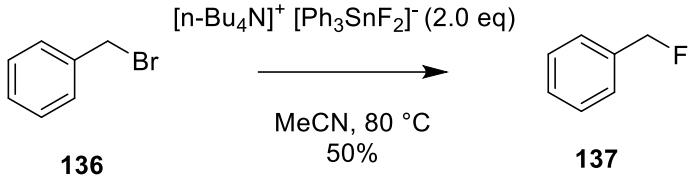

136 **137**

Scheme 2.1 – Nucleophilic fluorination of benzyl bromide (**136**) with tetrabutylammonium difluorotriphenylstannate.[29]

Deoxofluor™ (**139**)[30] and (Diethylamino)sulphur trifluoride (DAST)[31,32] (**142**) provide fluoride sources capable of converting aldehydes (**138**) and ketones to *gem*-difluorides[33] (e.g. **140**) as well as alcohols (**141**) to their corresponding alkyl fluorides through deoxyfluorination[34] (e.g. **143**), as illustrated in **Scheme 2.2**. Deoxofluor™ was shown to be the more thermally stable of the two reagents, likely due to enhanced conformational rigidity thanks to coordination of the methoxy groups with the electron-deficient sulphur atom of the trifluoride.[30]

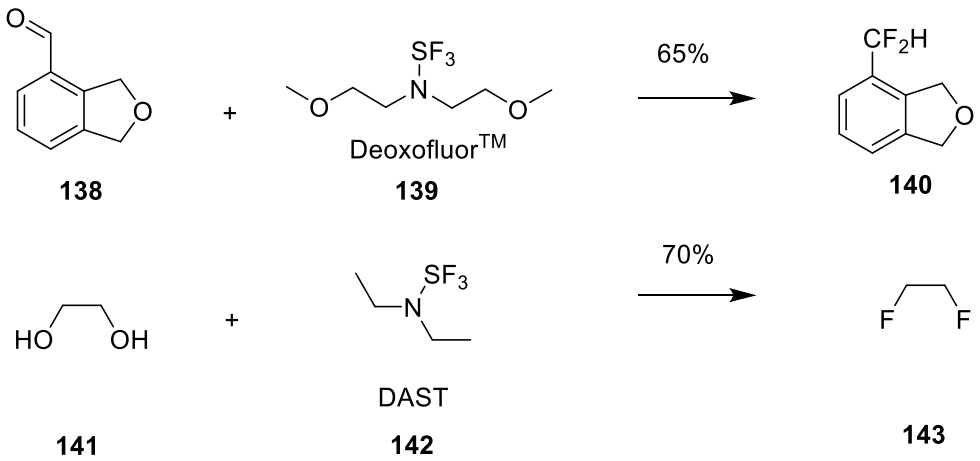

138 **139** **140**

141 **142** **143**

Scheme 2.2 – Examples of reactions involving Deoxofluor™ [33] and DAST[34] as nucleophilic fluorinating agents.

Tetra-*n*-butylammonium fluoride (TBAF)[35] (**Figure 2.4**, **145**) has also been utilised as a fluoride ion source. Despite its highly hygroscopic nature,[36] it has seen use in a range of settings including nucleophilic aromatic fluorination (**Scheme 2.3a**),[37] the synthesis of alkyl fluorides (**Scheme 2.3b**)[39] and as a means for accessing fluorovinyl compounds (**Scheme 2.3c**).[40]

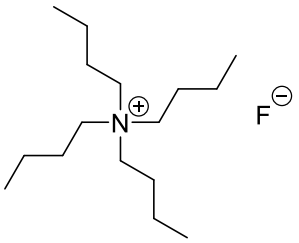

144

Figure 2.4 – Nucleophilic fluorinating agent tetra-*n*-butylammonium fluoride (TBAF).

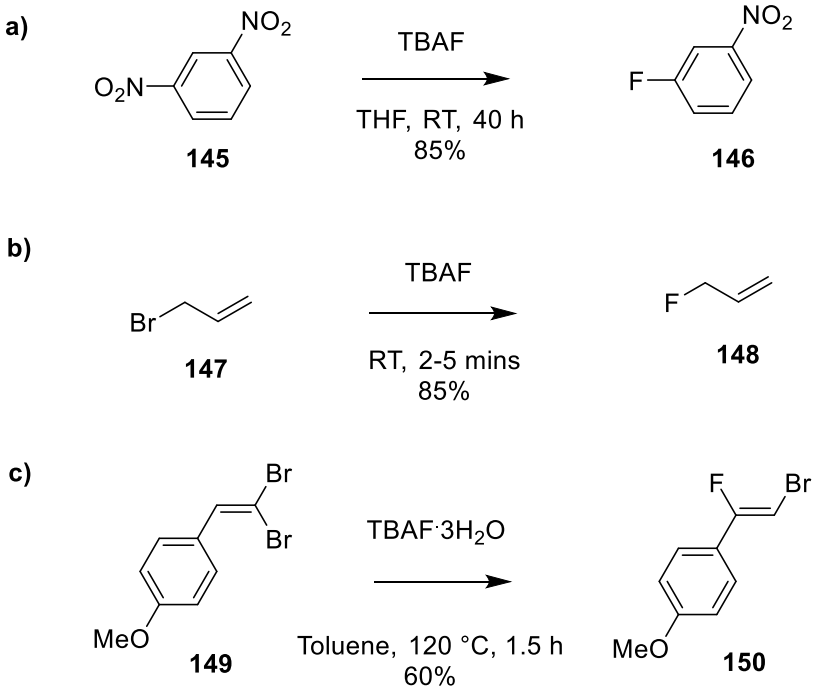

Scheme 2.3 – Examples of nucleophilic fluorination with TBAF.[38–40]

2.1.2 Electrophilic Methods of C-F Bond Formation

Electrophilic fluorination reagents[41,42] consist of a catalogue of *N*-fluoropyridinium salts[43,44] (such as **151** and **152**) which are capable of delivering fluorine to nucleophiles. The addition of electron-withdrawing or donating groups to the pyridine ring can greatly alter the fluorinating ability of the compound. Some examples of electrophilic fluorinating reagents are shown in **Figure 2.5**.

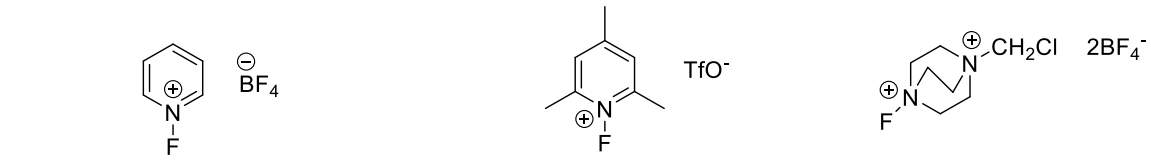

1-Fluoropyridinium tetrafluoroborate **151** | FP-T300 **152** | Selectfluor™ **153**

Figure 2.5 – Examples of electrophilic fluorinating agents.

In 2010, M. Beller and co-workers[45] demonstrated that 1-fluoropyridinium tetrafluoroborate (**151**) can be utilised as an electrophilic fluorinating agent[46] for the isolation of aryl fluorides from aryl Grignard reagents according to **Scheme 2.4**.[45]

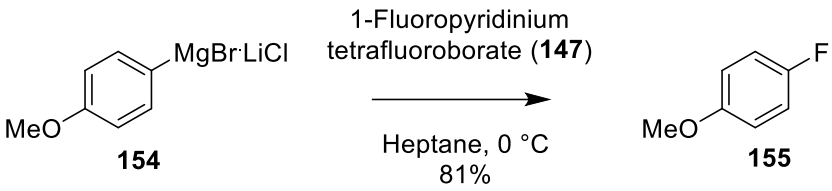

154 **155**

Scheme 2.4 – Electrophilic fluorination of aryl Grignard reagent with 1-Fluoropyridinium tetrafluoroborate.[45]

N-fluoro-2,4,6-trimethylpyridiniumtriflate (FP-T300) (**152**) is an electrophilic fluorinating agent which has been employed in fluorocylisation reactions, as shown in **Scheme 2.5**.[47,48]

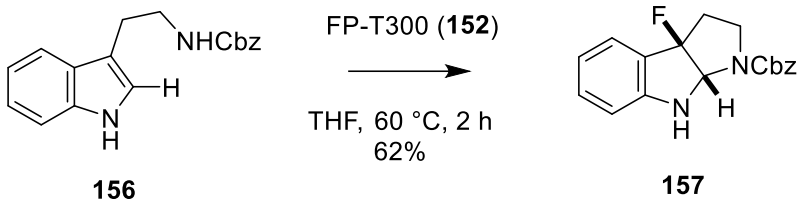

Scheme 2.5 – Fluorocyclisation with FP-T300.[47]

Selectfluor™ (**153**, **Figure 2.5**) benefits from being relatively inexpensive, safe to use and is often highly selective. As demonstrated by Y. Takeuchi *et al*, indoles can be successfully fluorinated in the presence of Selectfluor™ (**Scheme 2.6**).[49]

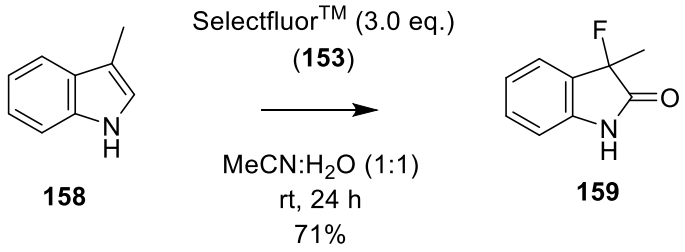

Scheme 2.6 – Electrophilic fluorination of indoles with Selectfluor™.[49]

Furthermore, Selectfluor™ (**149**) has proved to be effective as a fluorinating agent for enolizable multi-carbonyl systems, such as 1,3-dicarbonyl compounds.[50,51–54] In the example shown (**Scheme 2.7**), microwave irradiation was employed, and the conditions could be adapted to afford either the mono- (**160**) or di-fluorinated analogue (**162**) preferentially.[51]

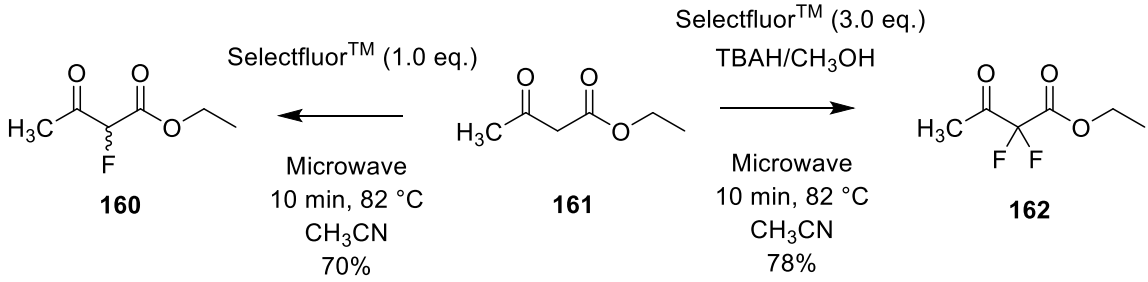

Scheme 2.7 – Mono and di-fluorination of a 1,3-dicarbonyl system with Selectfluor™.[51]

Selective mono-fluorination of *β*-ketoesters has also been reported using Selectfluor™ and $CpTiCl_3$ (**Scheme 2.8**)[55]. In the presence of this titanium catalyst, unwanted di-fluorination was kept to less than 5% for substrate **164**, as determined by ^{19}F NMR spectroscopy.

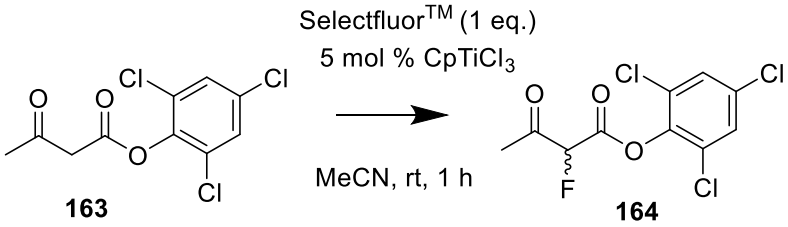

Scheme 2.8 – Mono-fluorination with F-TEDA in the presence of $CpTiCl_3$.[55]

The electrophilic fluorination[56] of highly reactive tri-carbonyl systems[57–59] has also been explored. In 2020, Sandford and co-workers reported the synthesis of a selection of α-fluorotricarbonyl compounds through reaction of Selectfluor™ with phen-acyl Meldrum's acid substrates such as **165** (**Scheme 2.9**).[56] Competing fluorination of the aromatic ring was not observed. These systems could be further functionalised through subsequent reaction with water, ethanol, Grignard and alkynyllithium reagents, leading to the isolation of the corresponding fluoro-acetophenone (**167**), fluoro–1,3-keto ester (**168**), fluoro–1,3-diketone (**169**) and fluoro-pyran-4-one (**170**) building blocks respectively (**Scheme 2.9**).

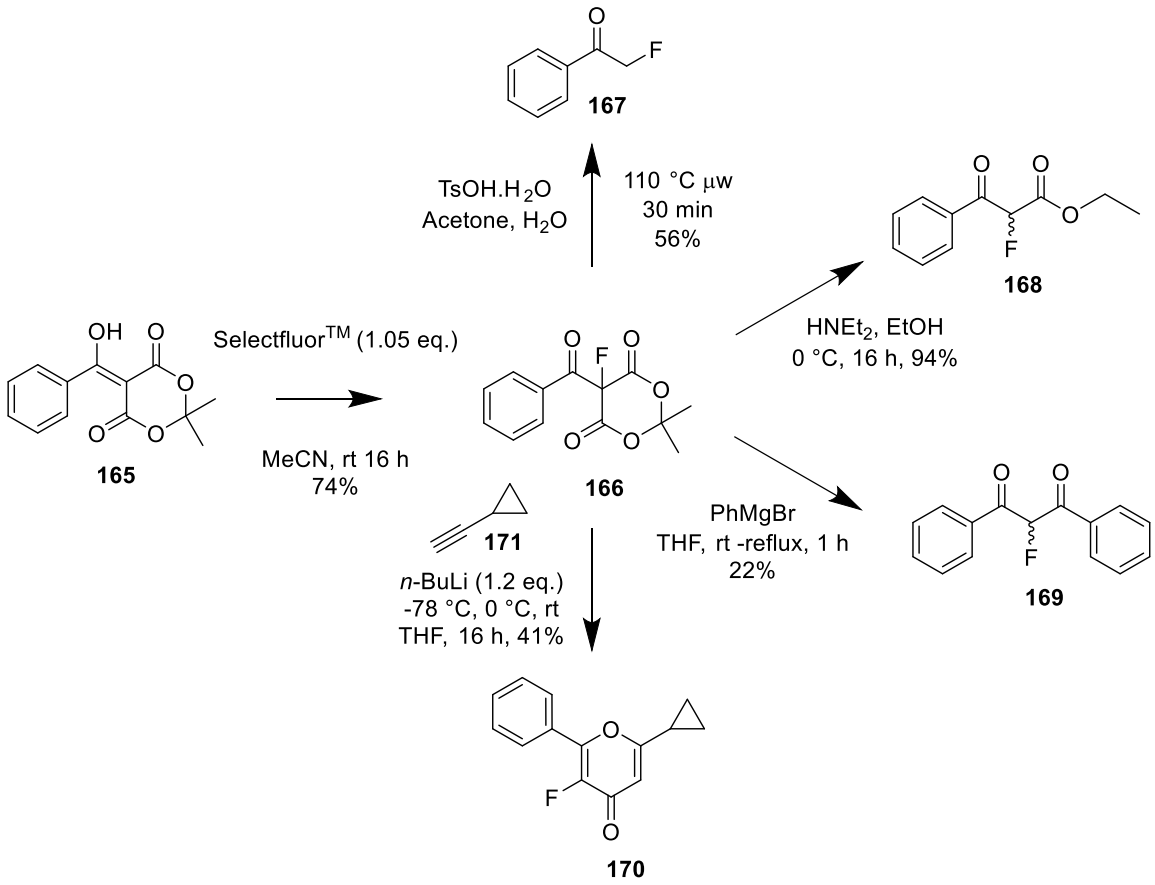

Scheme 2.9 – Electrophilic fluorination of 5-benzoyl-2,2-dimethyl-1,3-dioxane-4,6-dione (**165**) and subsequent reaction with various nucleophiles to give a selection of fluorinated building blocks (**167**, **168**, **169** and **170**).[56]

Inspired by this methodology and the ease at which tri-carbonyl systems can be α-fluorinated, along with the possibility for subsequent transformation into various building blocks, it was hypothesised that an adapted approach could be utilised to access peptidyl mFMKs. The fluoro-acetophenone (**167**) contains the key fluoromethyl ketone functionality required for making peptidyl mFMKs, and thus it was proposed that extending Sandford's chemistry beyond aromatic-containing fluorinated compounds to include a broader substrate scope could enable access to the desired targets.

2.2 The Synthesis of Boc-protected FMKs for Solution-Phase Peptide Coupling via a Tri-carbonyl System

In order to achieve the goal of accessing peptidyl mFMKs in a more efficient and reliable manner, a route was proposed that utilises methodology described by Sandford

and co-workers involving electrophilic α-fluorination of a tricarbonyl system.[56] Through adaptation of their approach, it was hypothesised that **Scheme 2.10** could be an effective means of accessing the targets. Starting from any Boc-protected amino acid of choice, assuming the R group is compatible with the conditions used, it was envisaged that generation of tri-carbonyl **174** would set up a system capable of undergoing electrophilic α-fluorination. **175** could then be further functionalised to FMK **176** which would be an ideal building block for solution-phase peptide synthesis.

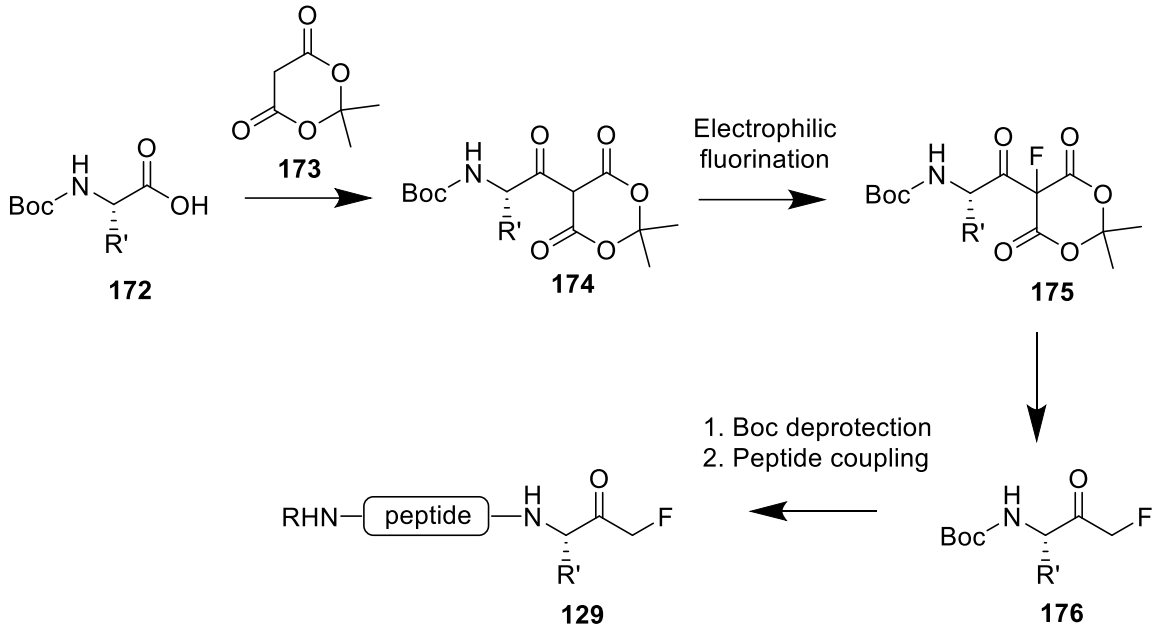

Scheme 2.10 – Proposed solution-phase route to peptidyl mFMKs (**129**) via Boc-protected FMK building block **176**.

2.2.1 Generation of a Tri-Carbonyl System

The first step in the process involved generation of the tri-carbonyl system through reaction of a Boc-protected amino acid; in this case *L*-Boc-alanine (**177**), with 2,2-dimethyl-1,3-dioxane-4,6-dione (**173**), otherwise known as Meldrum's acid.[56] It was proposed that this could be achieved through generation of acid chloride **178** *in situ*, followed by attack of Meldrum's acid (**173**) in a nucleophilic addition-elimination reaction (**Scheme 2.11**).

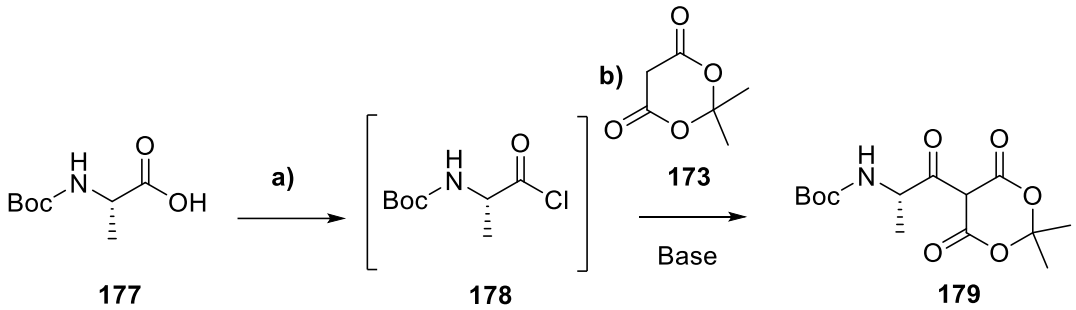

Scheme 2.11– Proposed formation of a tri-carbonyl system through the nucleophilic addition-elimination reaction of Meldrum's acid with an acid chloride generated *in situ*.

The second step (**b**) in **Scheme 2.11** involving generation of the tri-carbonyl system from an acid chloride was first attempted using phenylacetyl chloride (**180**) as a test reagent, for which the conditions employed[60,61] are shown in **Scheme 2.12**.

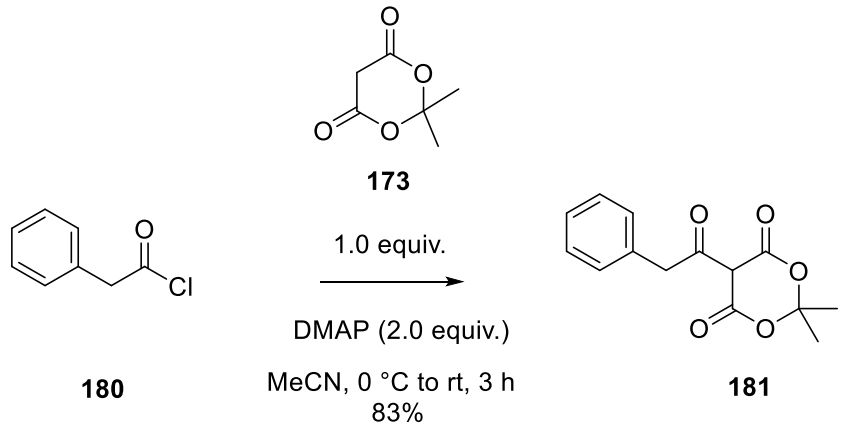

Scheme 2.12 – Nucleophilic addition-elimination reaction of Meldrum's acid with the test substrate, phenylacetyl chloride.

The reaction proceeded efficiently, giving tri-carbonyl **181** in a yield of 83% with excellent purity, as illustrated by the corresponding ^{1}H NMR spectrum (**Figure 2.6**). It was also evident that the product was isolated in the enol form due to the absence of a peak corresponding to the aliphatic C-H, and the presence of a broad OH peak at 15 ppm integrating to 1 (not shown). The enol tautomer is favoured over the keto form due to intramolecular hydrogen bonding between the OH and the nearby carbonyl oxygen atom.[56]

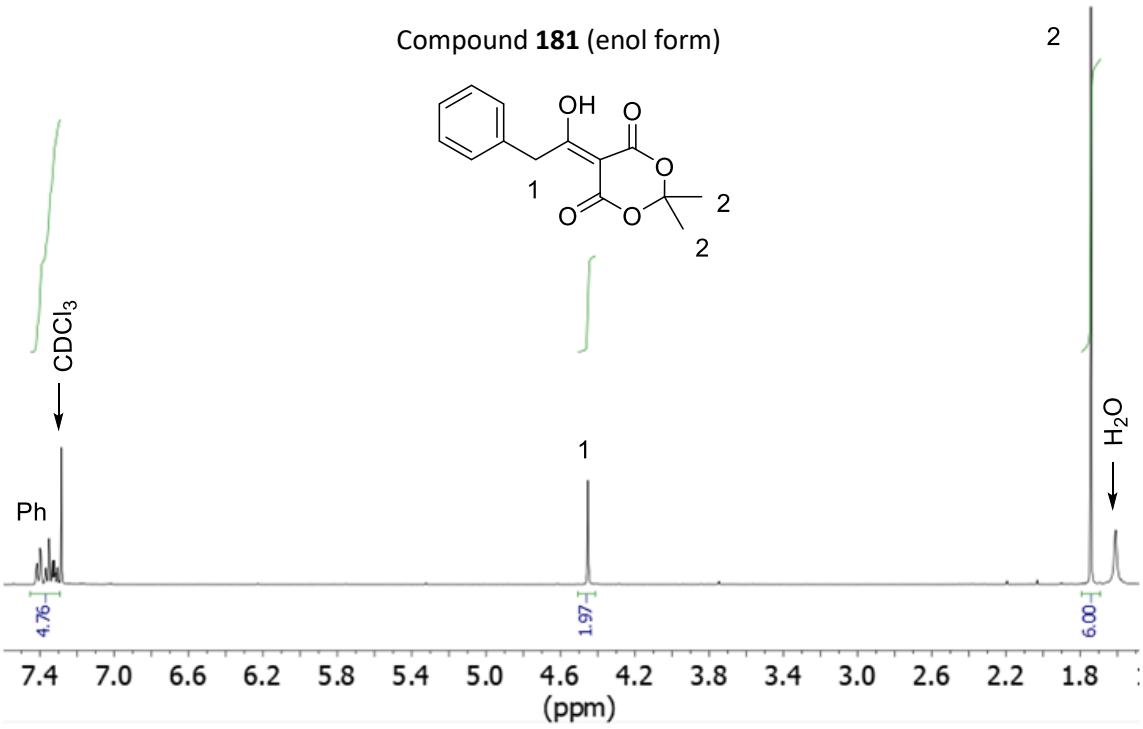

Figure 2.6 – ^{1}H NMR spectrum in $CDCl_3$ after nucleophilic addition-elimination reaction of Meldrum's acid (**173**) with test substrate phenylacetyl chloride (**180**) to give tri-carbonyl **181**.

Having successfully synthesised the tri-carbonyl system (**181**), the next step was to transfer these conditions to the substrate of choice (**177**), with the added requirement of first generating the acid chloride *in situ* (**Scheme 2.11**). An attempt to prepare the acid chloride (**178**) *in situ* using thionyl chloride at reflux and subsequently trap this with Meldrum's acid (**173**) did not produce the desired tri-carbonyl system (**179**). This was likely due to loss of the acid-sensitive Boc group as a result of HCl produced during the acid chloride formation step, and assisted by the acidic work-up employed to protonate the tri-carbonyl system generated under basic conditions. This would have led to the formation of the ammonium salt, which was likely lost to the aqueous phase during the work-up.

An attempt to use a modified literature procedure[62] involving *iso*-butylchloroformate in the presence of *N*-methylmorpholine for generation of mixed anhydride **184**, followed by reaction with Meldrum's acid (**173**) allowed generation of the desired tri-carbonyl (**179**, **Scheme 2.13**), as evidenced by a peak in the LCMS (+ve) trace corresponding to $[M+H]^+$

= 316 (**Figure 2.7**). However, an ^{1}H NMR spectrum revealed the presence of impurity peaks.

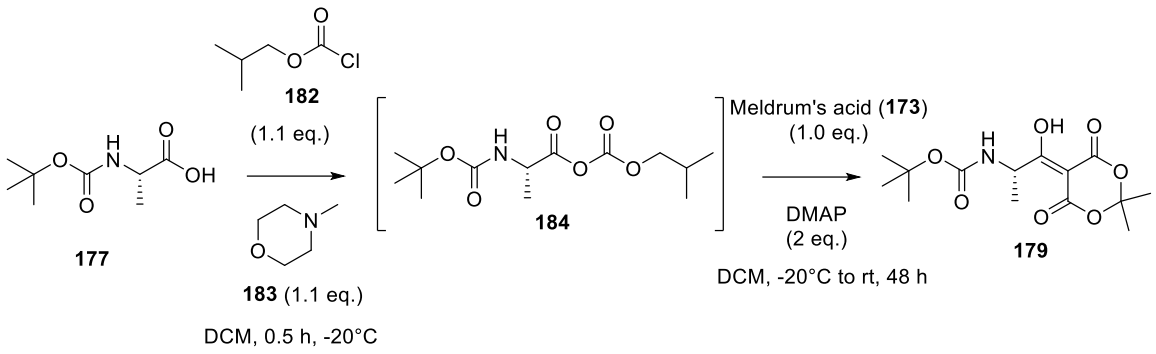

Scheme 2.13 – Attempted generation of tri-carbonyl **179** via mixed anhydride **184**.

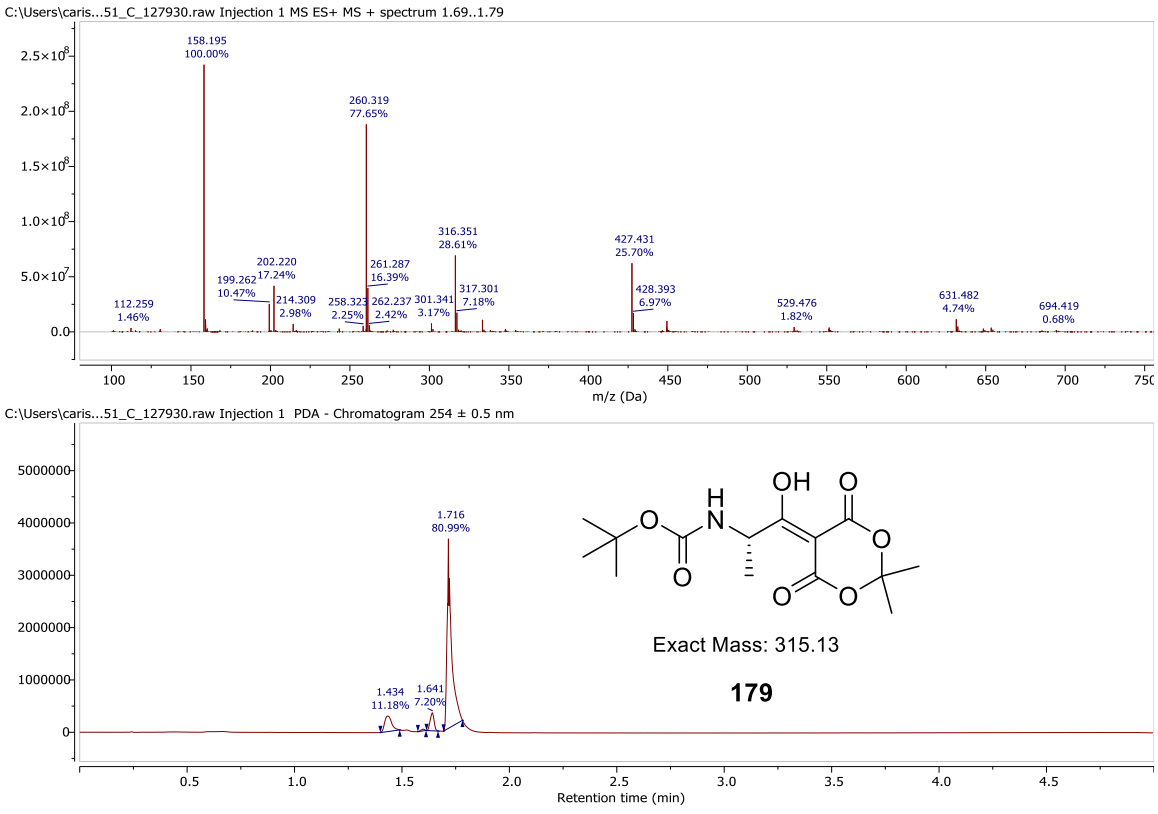

Figure 2.7 – LCMS data (+ve, λ = 254 nm) showing evidence for the formation of tri-carbonyl **179**.

Consequently, other approaches involving the use of coupling agents were pursued instead. **Scheme 2.14** illustrates two sets of conditions that were trialled from the literature.[63,64]

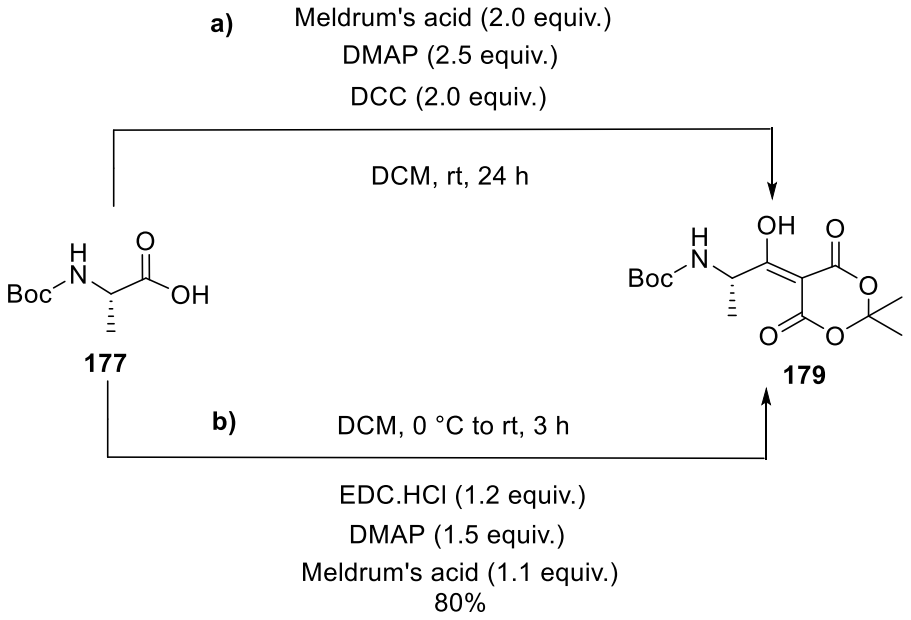

Scheme 2.14 – Conditions employed for the attempted coupling of Meldrum's acid (**173**) with L-Boc-alanine (**177**).[63,64]

Both methods seemed to generate product (**179**), as seen by LCMS (+ve); however, the use of DCC (**Scheme 2.14a**) did not allow for its clean isolation by ^{1}H NMR spectroscopy (even after purification by column chromatography), and therefore full characterisation was not possible. EDC.HCl proved to be much more successful as a coupling agent (**Scheme 2.14b**), allowing isolation of **179** in the enol form in a yield of 80%. The product obtained (**179**) was found to be relatively pure without purification by column chromatography (**Figure 2.8**), although the presence of some Meldrum's acid starting material could be identified in some cases. Despite this, it was decided that the product should be used directly in the next step without further purification, as the tri-carbonyl system, particularly the Boc-alanine derivative, was found to be incredibly unstable. This can be seen by the ^{1}H NMR spectra in **Figure 2.8**, which indicate isolation of the desired product (**179**) in the enol form after a 3-hour reaction period (**Figure 2.8a**) and the occurrence of degradation over longer periods of time (**Figure 2.8b**). For this reason, it was important that the reaction time for generating the Boc-alanine derived tri-carbonyl system was carefully controlled. Whilst the reaction for the formation of test substrate **181** could be left overnight with no ramifications, it appeared that the optimum

amount of time for the reaction involving Boc-alanine was about 3-4 hours. Any less than this and very little product was formed, but if left too long, degradation could be seen to occur.

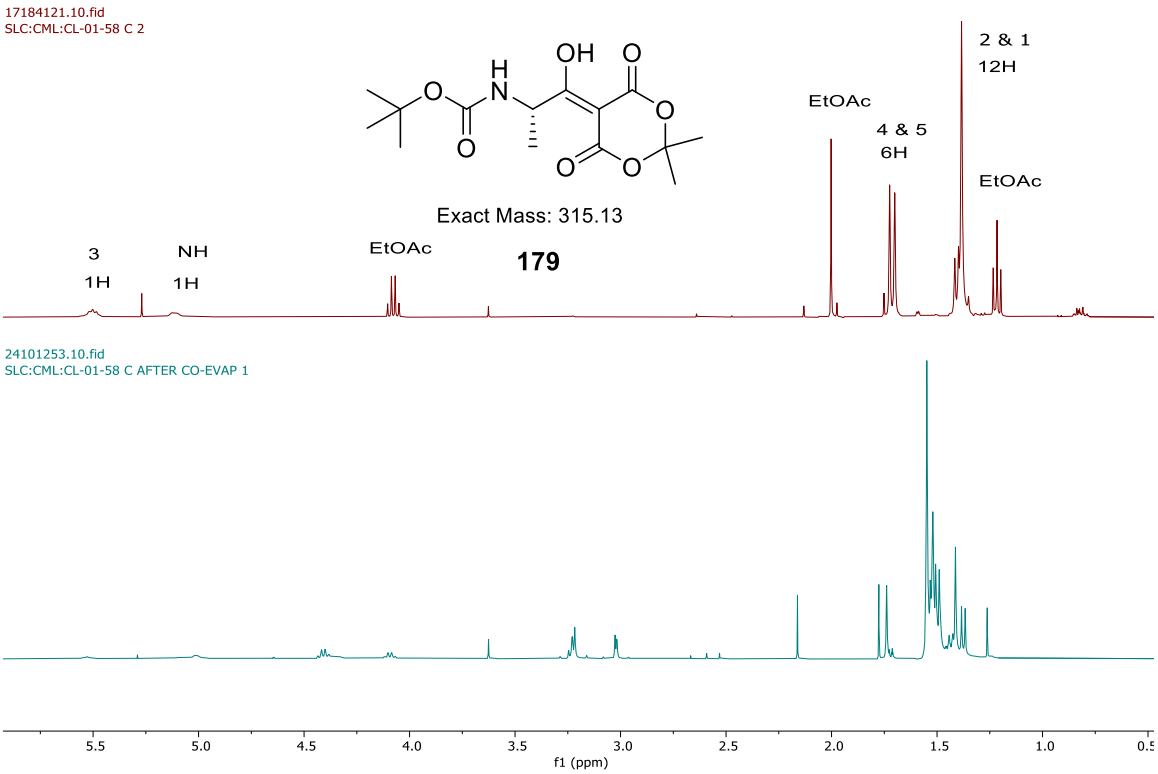

Figure 2.8 – ^{1}H NMR spectrum (**a**) in $CDCl_3$ shows isolation of the desired product (**179**) in the enol form after a reaction time of 3 h, with residual EtOAc present. ^{1}H NMR (**b**) in $CDCl_3$ shows degradation starting to occur over longer periods of time.

2.2.2 Electrophilic Fluorination of Meldrum's Acid Tri-Carbonyl System

After the successful synthesis of the tri-carbonyl system, the next step in the process was the generation of the C-F bond through electrophilic fluorination using Selectfluor™.[56] As before, this reaction[60] was first piloted on the phenylacetyl chloride (**186**) derived tri-carbonyl test substrate **181** (**Scheme 2.15**).

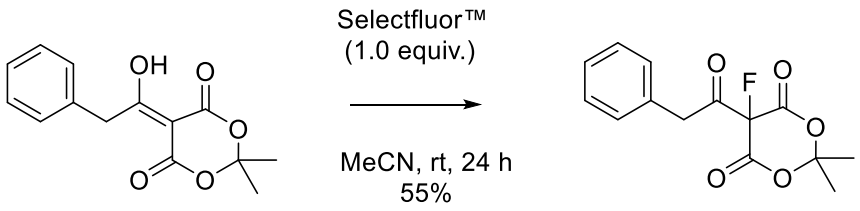

181 **185**

Scheme 2.15 – Electrophilic fluorination of a tri-carbonyl system (**181**) derived from phenylacetyl chloride (**186**) and Meldrum's acid (**173**).

As expected, assuming the reaction was set up fairly quickly to prevent unwanted degradation before the fluorination had time to proceed, successful fluorination was observed, encouraged by the high enol content of the substrate, the electron-withdrawing nature of the phenyl group and the ability for resonance stabilisation of electron density around three carbonyl groups. The pure product was isolated without the need for column chromatography. This can be seen by ^{1}H NMR spectrum (**Figure 2.9**), in which the benzylic protons which originally appeared as a singlet have now become a doublet (4.24 ppm) due to coupling with fluorine. Likewise, the ^{19}F NMR spectrum (**Figure 2.10**) shows the presence of a triplet at -165.89 ppm as a result of $^{4}J_{FH}$ bond coupling with the benzylic CH_2.

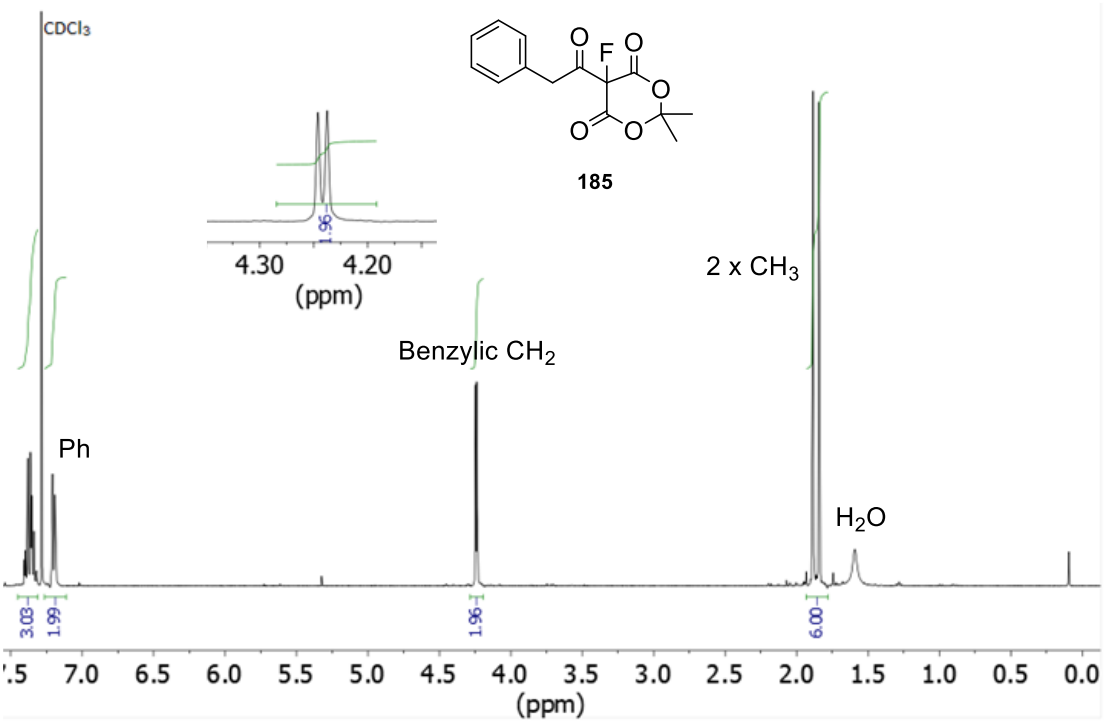

Figure 2.9 – ^{1}H NMR spectrum in $CDCl_3$ for fluorinated test compound **185**.

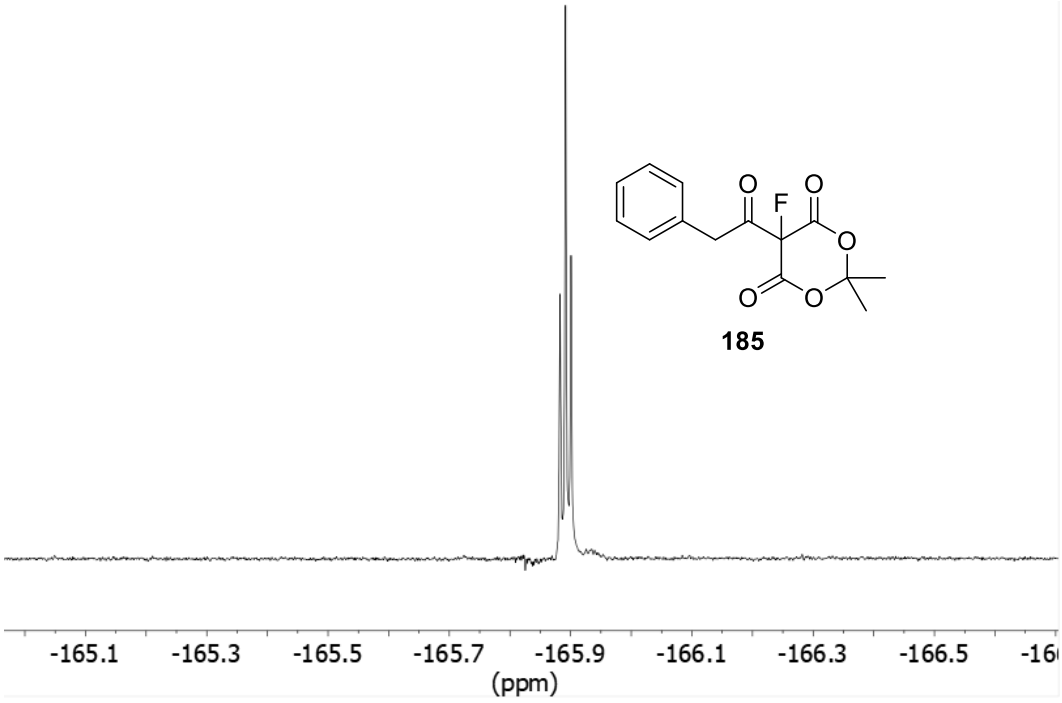

Figure 2.10 – ^{19}F NMR spectrum (^{1}H coupled) in $CDCl_3$ for fluorinated test compound **185** showing a clear triplet due to ^{4}J bond coupling with the benzylic CH_2.

It is interesting to note that the two CH_3 groups attached to the Meldrum's acid cyclic ring each exist in separate environments, as revealed by two singlet peaks at 1.84 and 1.88 ppm in the ^1H NMR spectrum with an integration of 1:1 relative to each other. This is likely due to the fact that these types of molecules tend to adopt a distorted-boat conformation, as has been shown by X-ray crystallography for the benzoyl analogue **167** in the literature (**Figure 2.11**).[56,60,65] This implies that one CH_3 is axial whilst the other is equatorial, thus leading to two distinct NMR environments.

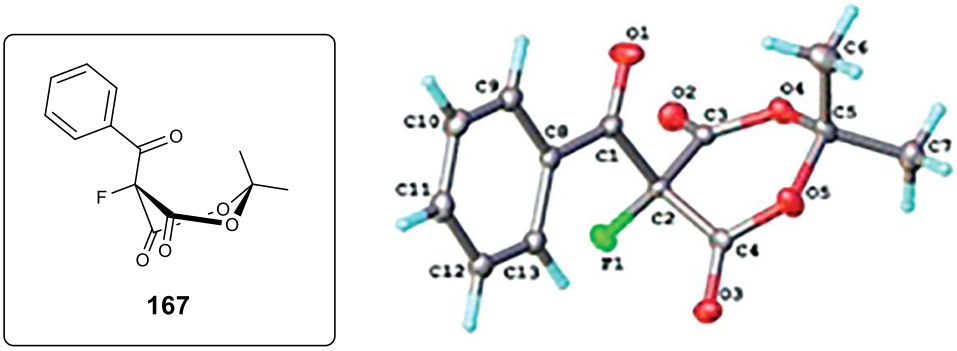

Figure 2.11 – Twisted boat conformation for the fluorinated Meldrum's acid analogue **167**.[56]

Again, it should be highlighted that the instability of these tri-carbonyl systems requires quick and efficient handling, along with the need to be stored in a cool, dry environment, avoiding contact with moisture. As shown in **Figure 2.12**, despite the successful isolation of the product (**185**) giving a clean ^{19}F NMR spectrum (**Figure 2.12a**), after being left in the fridge for 72 hours, the emergence of a new major peak in the ^{19}F NMR spectrum was observed around -206 ppm (**Figure 2.12b**). Comparison with a ^{19}F NMR spectrum for the mono- (**187**) and di-fluorination (**188**) of Meldrum's acid (**Figure 2.12c**) strongly suggests that mono-fluorinated Meldrum's acid (**187**) is a culprit in the contamination of the sample with time.

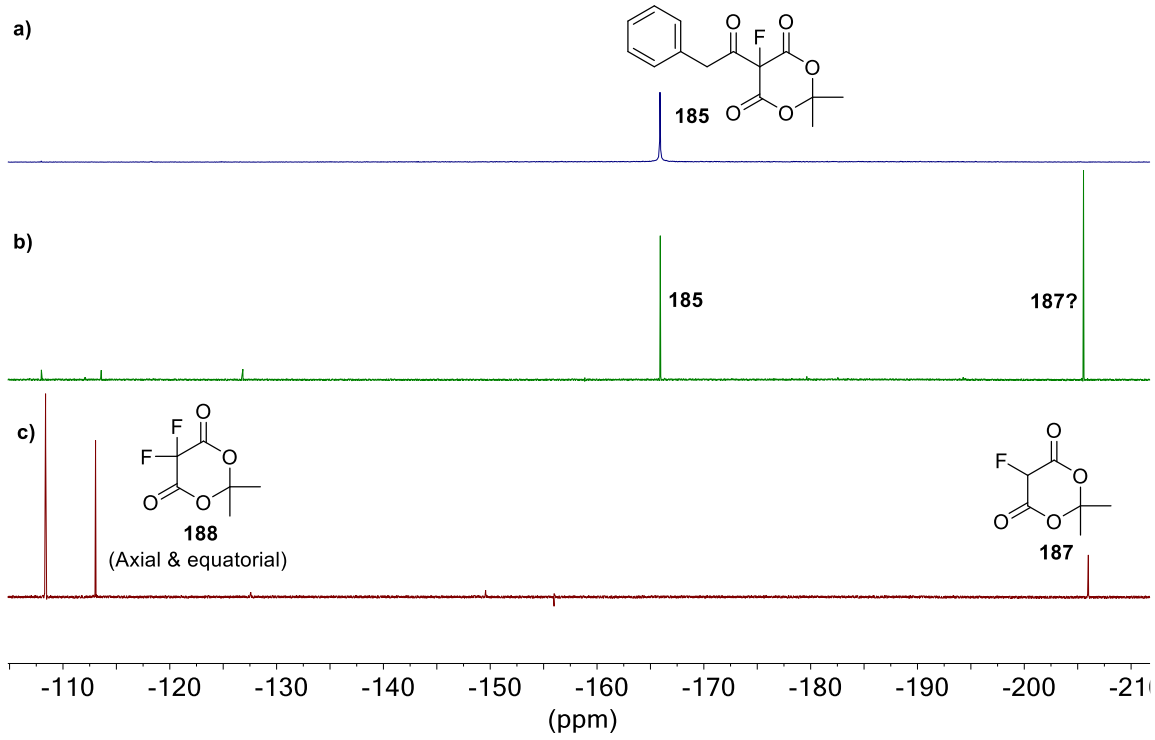

Figure 2.12 – ^{19}F NMR $\{^{1}H\}$ spectra in $CDCl_3$ for pure fluorinated test product **185** (**a**), product **185** after 72 h left in the fridge (**b**) and mono- (**187**) and di-fluorinated Meldrum's acid (**188**) (**c**).

The reason for the emergence of the new dominant fluorine peak at -206 ppm and the disappearance of the product peak at -166 ppm with time (**Figure 2.12b**) is likely to be due to the presence of a small amount of water which is apparent from **Figure 2.9**, along with possible further accumulation of moisture from exposure to air causing degradation.[60] Due to the sensitivity of the compound towards nucleophiles such as water, an aqueous work-up was not performed, but instead the purification process involved dissolution of the product in ethyl acetate and removal of insoluble Selectfluor™ impurities by filtration, followed by precipitation of product from DCM through the addition of hexane. Further to this, these reactive species were pushed through to the more stable ethanolysis products as quickly as possible in order to reduce chances of picking up moisture and limit unwanted hydrolysis as much as possible. A yield of 55% was achieved for the fluorination step; however, it is suspected that this could perhaps be improved by carrying out the reaction under inert conditions. A proposed mechanism for the unwanted degradation

process is shown in **Scheme 2.16**.[60] Nucleophilic attack of the water likely occurs primarily at the most electrophilic position i.e. the ketone, causing generation of the carboxylic acid along with mono-fluorinated Meldrum's acid, which starts to dominate the ^{19}F NMR spectrum (**Figure 2.12b**).

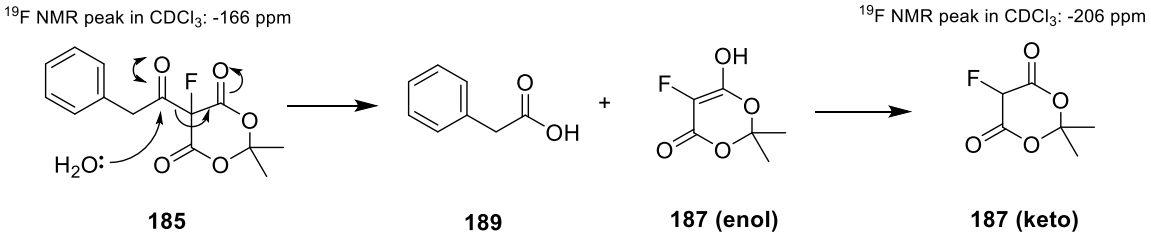

Scheme 2.16 – Possible mechanism for the degradation of product **185** in the presence of water.

As the electrophilic fluorination reaction proved to be successful when performed on test substrate **181**, the conditions were transferred to the desired substrate i.e. Boc-alanine derived tri-carbonyl system **179** (**Scheme 2.17**).

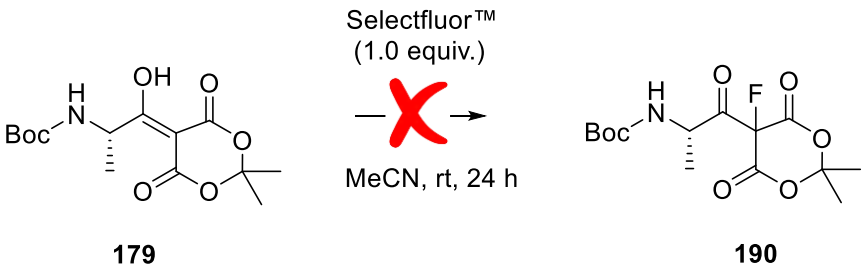

Scheme 2.17 – Attempted electrophilic fluorination of a tri-carbonyl system (**179**) derived from Boc-Ala-OH (**177**) and Meldrum's acid (**173**).

Unfortunately, carrying out the same procedure did not appear to result in the formation of **190** as the expected peaks were not visible in the ^{19}F NMR spectrum post-purification. This could be because of rapid hydrolysis caused by moisture in the air and in the solvents used, again giving the characteristic mono-fluorinated Meldrum's acid peak visible in the crude ^{19}F NMR spectrum, along with a host of other impurities. This is illustrated in **Figure 2.13**, which shows comparison of the crude ^{19}F NMR spectrum (**a**) with that of mono- and di-fluorinated Meldrum's acid (**b**). It should also be noted that a small amount of unreacted Meldrum's acid (**173**) was present in the starting material prior

to fluorination which would have also been susceptible to electrophiles and could have contributed a small amount towards the presence of the peak at -206 ppm.

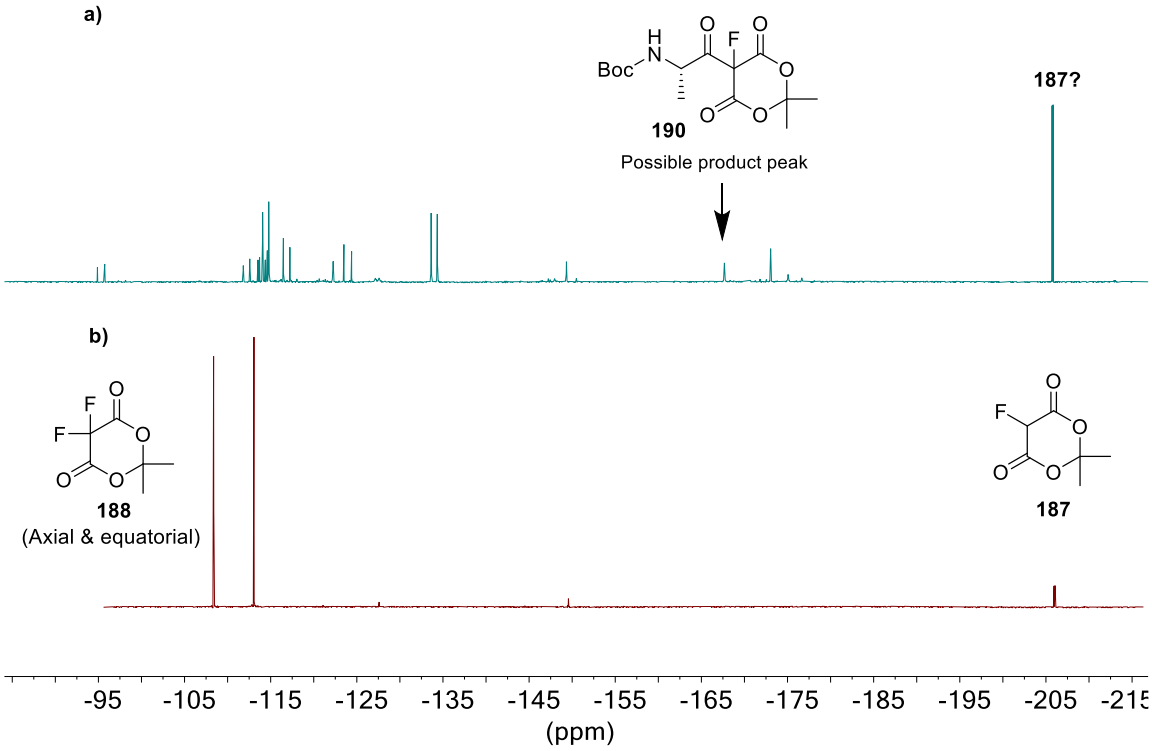

Figure 2.13– Comparison of ^{19}F NMR spectra (^{1}H coupled) recorded in $CDCl_3$ for (**a**) fluorinated Boc-Alanine derived compound **190** with (**b**) mono- (**187**) and di-fluorinated Meldrum's acid (**188**).

An attempt to convert the impure crude material (**190**) to the corresponding FMK (**191**) via reaction with *p*-toluenesulfonic acid monohydrate using microwave irradiation (**Scheme 2.18**)[56] did not give rise to a ^{19}F NMR peak in the expected FMK region (around -230 ppm). This is likely because, in reality, very little fluorinated tri-carbonyl starting material (**190**) was present in the crude reaction mixture due to prior degradation. Concomitant Boc removal would also be expected to occur under these acidic conditions; however, this would in effect be a desirable outcome since the amine functionality could then be coupled to a peptide in solution.

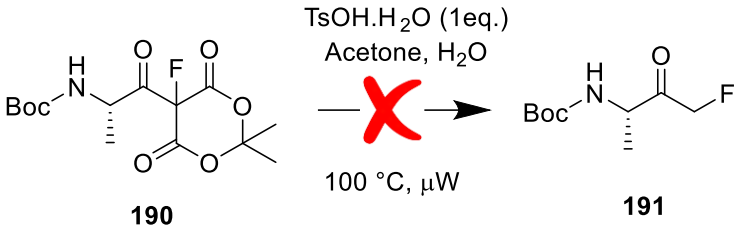

Scheme 2.18 – Unsuccessful attempt at conversion of tri-carbonyl **190** to the corresponding FMK (**191**). Conditions adapted from Sandford and co-workers.[56]

In an attempt to overcome the aforementioned issues, it was decided that fluorination of tri-carbonyl **179** should be repeated (**Scheme 2.17**), but this time the decision was made to push the resulting product (**190**) through to the next step rapidly, without any form of purification beforehand other than solvent removal under reduced pressure. Utilising conditions described by Graham and co-workers,[56] it was proposed that if access to the more stable 1,3-dicarbonyl system (**192**) could be achieved through ethanolysis (**Scheme 2.19a**), this would enable easier purification by column chromatography. The resulting product could then be transformed to the FMK through ester hydrolysis and subsequent decarboxylation (**Scheme 2.19b**). This would help to limit the time of exposure of tri-carbonyl **190** to moisture in the air by not having to leave the product to precipitate out overnight in the fridge. It would also ensure that product wasn't being lost during the precipitation step due to differences in solubility between the fluorinated Boc-Ala-OH derived tri-carbonyl (**190**) and the benzylic tri-carbonyl (**185**) used as a proof of concept. Furthermore, the added benefit of proceeding via the 1,3-dicarbonyl system rather than going directly to the FMK is that it provides the opportunity to explore the suitability of using a similar system for attachment to a solid support for possible solid-phase FMK synthesis; however, this will be discussed further in **Chapter 3**.

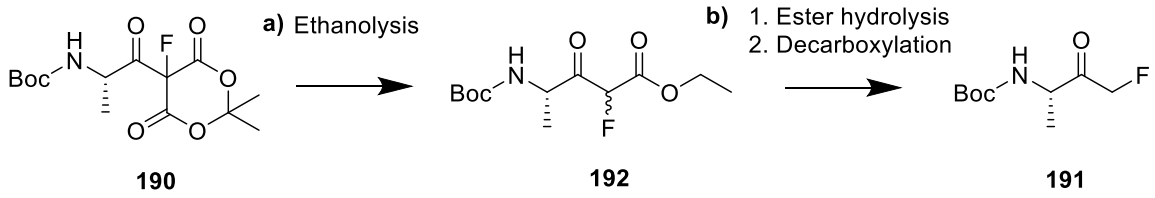

Scheme 2.19 – Proposed conversion of tri-carbonyl **190** to the corresponding FMK (**191**) via 1,3-dicarbonyl **192**, through adaptation of conditions described by Sandford and co-workers.[56]

This time, after more rapid handling and no purification as described above, the ^{19}F NMR spectrum seemed more promising for the fluorination of tri-carbonyl **179 (Figure 2.14**), with a peak that appeared to correspond to the desired fluorinated tri-carbonyl (**190**) at -167.54 ppm, although many other impurities were also present.

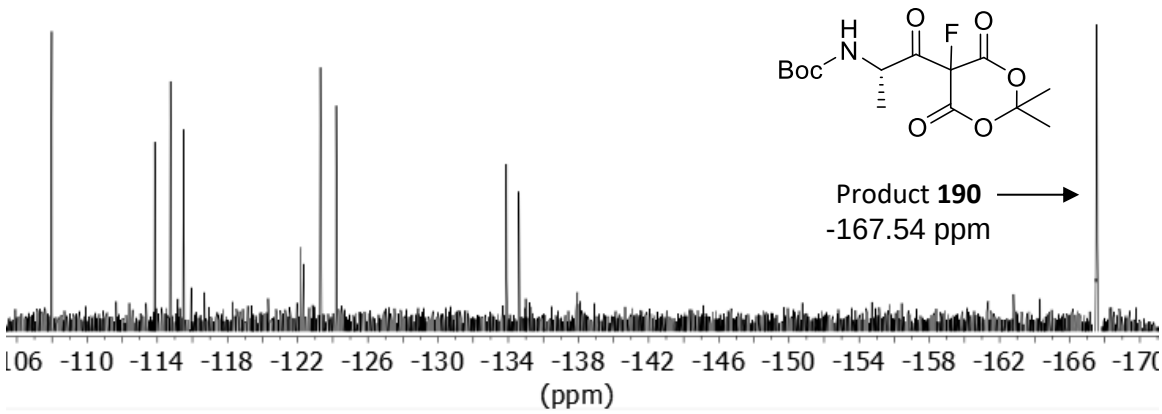

Figure 2.14 – Crude ^{19}F NMR spectrum (^{1}H coupled) in $CDCl_3$ for fluorinated Boc-alanine derived tri-carbonyl **190**.

The ^{1}H NMR spectrum was not entirely useful for identifying the desired product (**190**) as it proved too difficult to convincingly decipher due to the impurities present; however, ESI mass spectrometry (+ve) did seem to confirm the presence of the desired compound, with peaks corresponding to $[M+H]^+$ = 334, $[M+NH_4]^+$ = 351 and $[M+Na]^+$ = 356 identified (**Figure 2.15**).

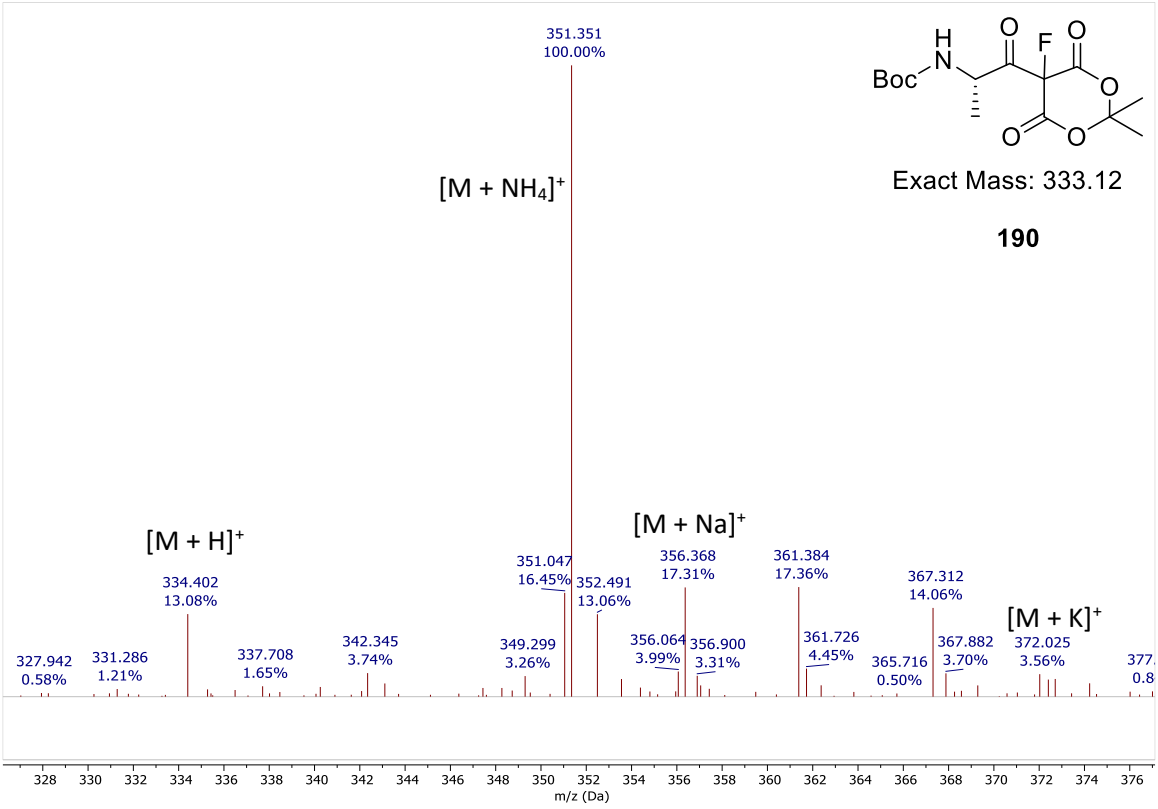

Figure 2.15 – ESI mass spectrum (+ve) for crude fluorinated tri-carbonyl **190**.

2.2.3 Ethanolysis of the Fluorinated Meldrum's Acid Tri-carbonyl Systems

Following on from the fluorination step, both the benzylic tri-carbonyl **185** and the Boc-alanine derived substrate **190** underwent an ethanolysis reaction[56,60,61] (**Scheme 2.20**), which was set up as quickly as possible so as to avoid unwanted hydrolysis. The latter of the two substrates was carried through in the crude form.

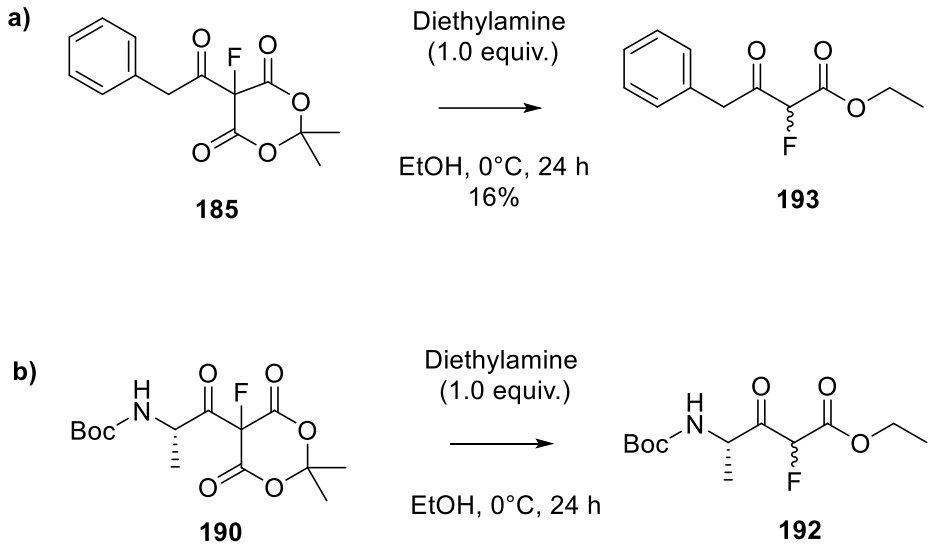

Scheme 2.20 – Ethanolysis of fluorinated Meldrum's acid test substrate **185** (**a**) and crude Boc-alanine derived analogue **190** (**b**).

These reactions involve nucleophilic attack of ethanol on the lactone under basic conditions (diethylamine), leading to the loss of carbon dioxide and acetone as by-products,[61] which drives the reaction forwards. Starting with the benzylic tri-carbonyl (**185**, **Scheme 2.20a**), the reaction proceeded smoothly, allowing for the successful isolation of the ethyl ester **193** after purification by column chromatography. The TLC spots were best viewed using a phosphomolybdic acid (PMA) stain as spots were sometimes difficult to identify under UV, especially when the collected fractions were dilute. The ^{1}H NMR spectrum in **Figure 2.16** provides evidence that the desired compound was in fact made, with a doublet observed at 5.3 ppm as a result of coupling to fluorine ($^{2}J_{HF}$ = 49 Hz); however, a very poor yield of 16% was observed.

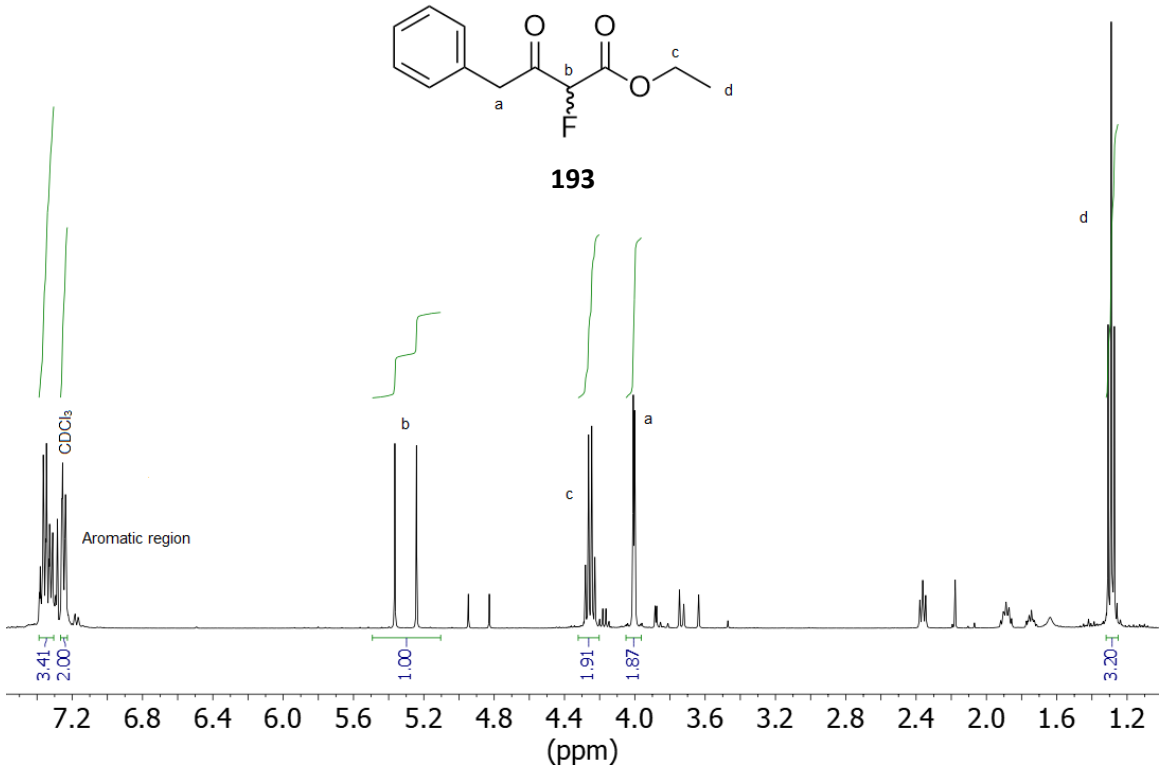

Figure 2.16 – ^{1}H NMR spectrum of *β*-ketoester **193** recorded in $CDCl_3$.

Despite the clear indication of product (**193**) formation, it is also evident that some of the ^{1}H NMR spectrum peaks appear to be doubling up (**Figure 2.16**). Whilst the ^{19}F NMR spectrum taken immediately after isolation of the product (**Figure 2.17** and **Figure 2.18a**) showed very few impurities and indicated a clear doublet of triplets at -194.30 ppm as expected ($^{2}J_{FH}$ = 49.2 Hz, $^{4}J_{FH}$ = 3.2 Hz), comparison with another ^{19}F NMR spectrum taken a few hours later (**Figure 2.18b**) revealed the increased emergence of a triplet of triplets at -227 ppm. This, along with the additional peaks observed in the ^{1}H NMR spectrum, suggested that the decarboxylated fluoromethyl ketone **194** was starting to form. This was likely due to some acquired moisture bringing about ester hydrolysis to the free carboxylic acid, allowing decarboxylation to occur, and has been reported previously during reactions of this kind.[61]

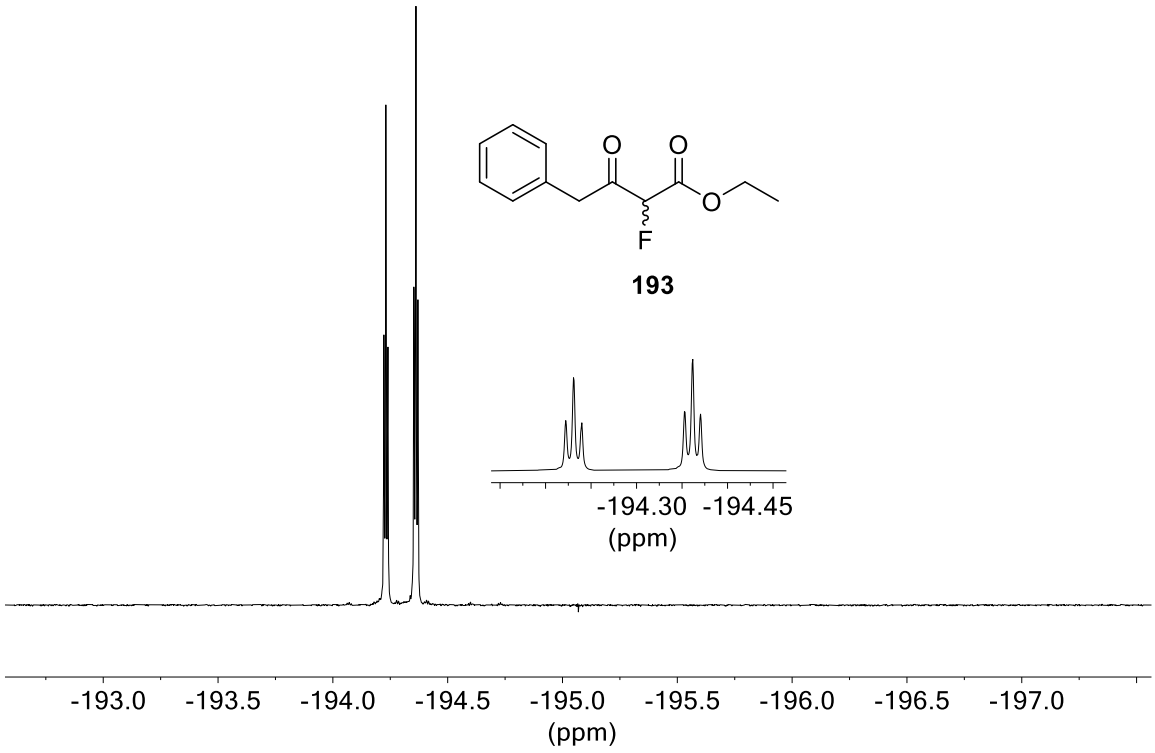

Figure 2.17 – ^{19}F NMR spectrum (^{1}H coupled) in $CDCl_3$ recorded immediately after column chromatography of *β*-ketoester **193**.

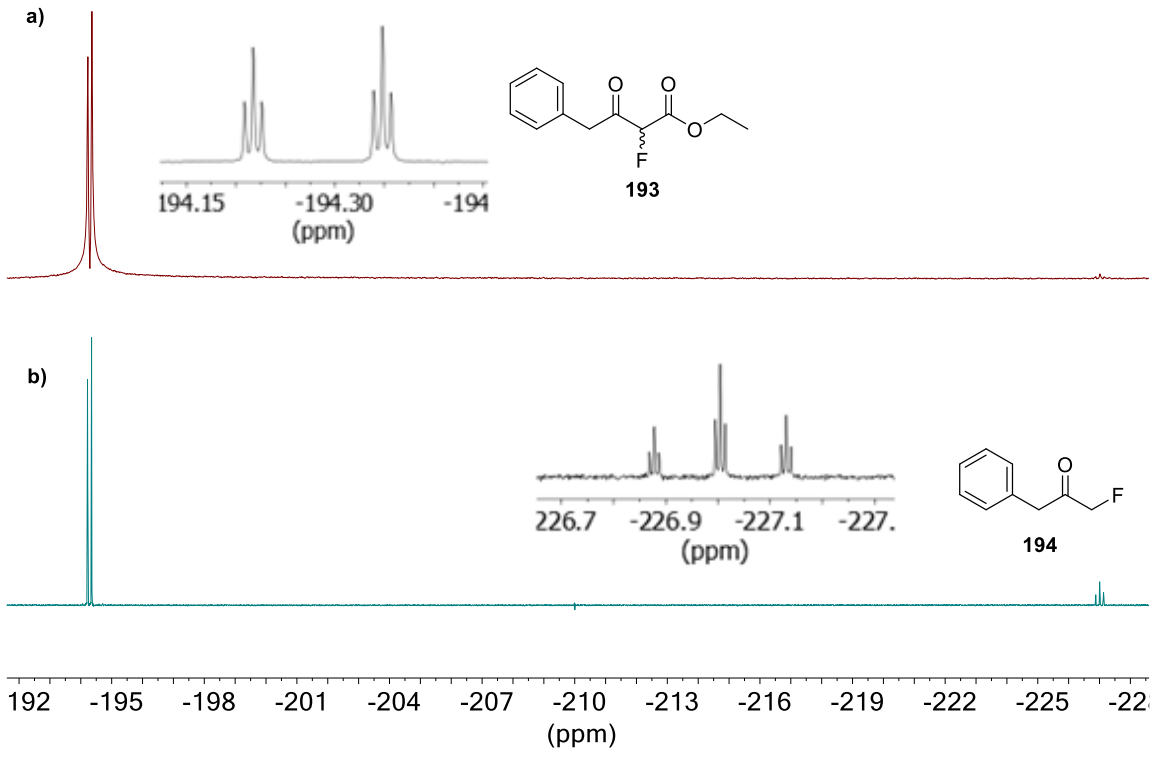

Figure 2.18 – ^{19}F NMR spectra (^{1}H coupled) in $CDCl_3$ recorded immediately after column chromatography for test compound **193** showing predominantly ethyl ester (**a**) and ^{19}F NMR showing emergence of FMK (**194**) peak a few hours later (**b**).

Evidence for the successful ethanolysis of the Boc-alanine derived substrate (**190**) according to **Scheme 2.20b** was less convincing; however, the peak in the post-column ^{19}F NMR spectrum (**Figure 2.19**) at around -198 ppm did seem to show promise, appearing as two doublets, likely due to diastereoisomers. Unfortunately, other inseparable impurities were also present, despite having undergone column chromatography. The presence of the product (**192**) was supported by ESI MS (+ve) (**Figure 2.20**) in which the molecular ion was identified; however, peak intensity was low in the UV trace.

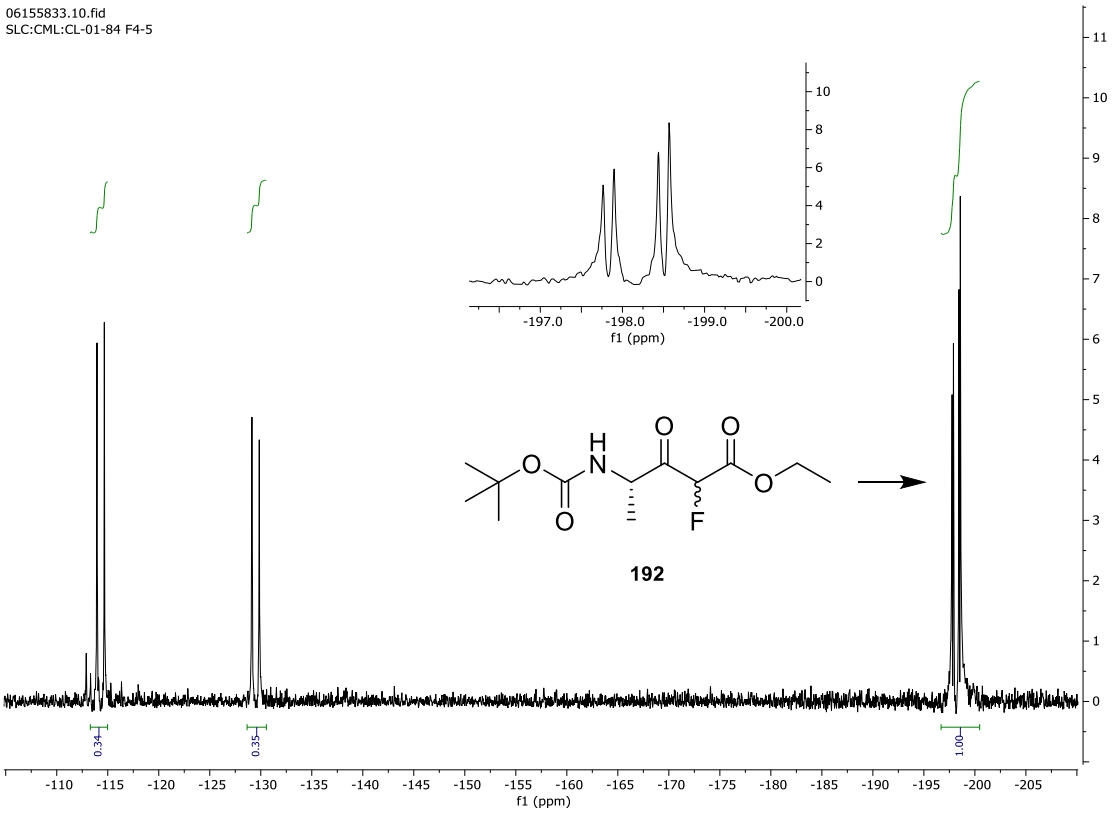

Figure 2.19 – ^{19}F NMR spectrum (^{1}H coupled) recorded in $CDCl_3$ showing possible isolation of *β*-ketoester **192** in the presence of impurities, post-column chromatography.

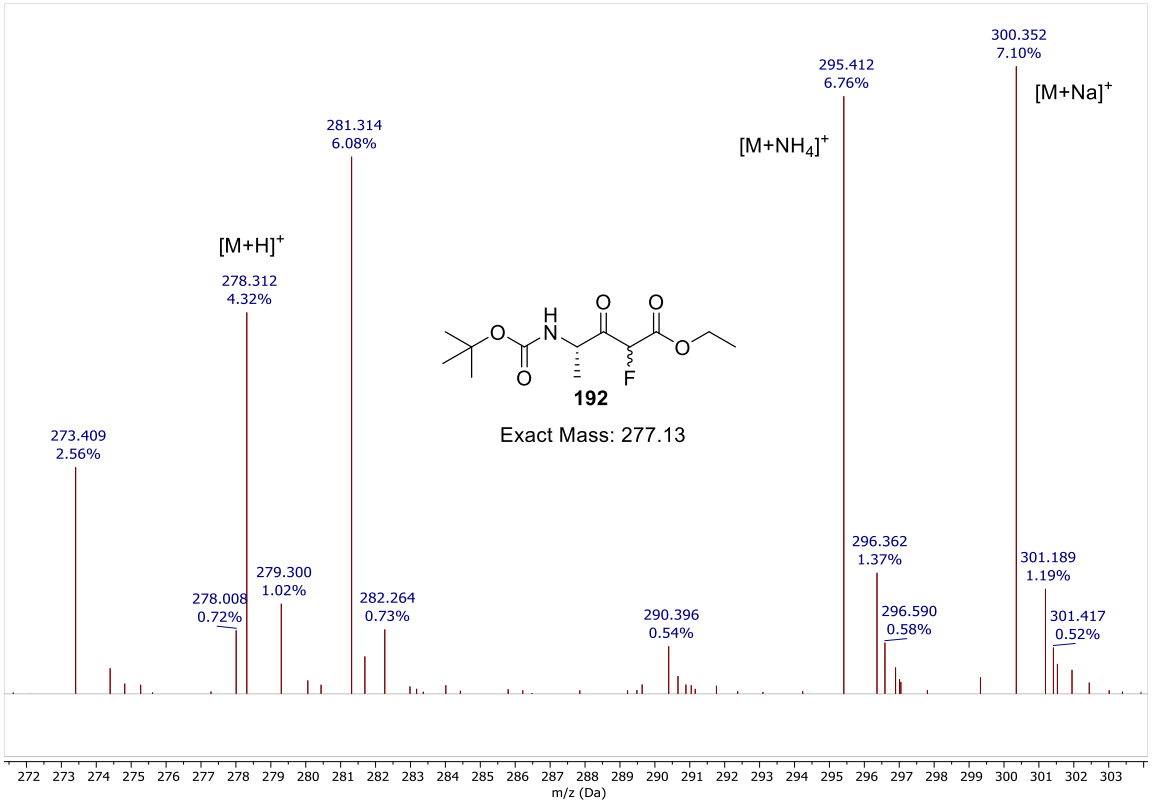

Figure 2.20 – ESI mass spectrum (+ve) identifying a small amount of 1,3-dicarbonyl **192**.

2.2.4 Carboxylic Acid formation and Decarboxylation to the FMK

The final step in order to generate the fluoromethyl ketone (FMK) moiety is decarboxylation via initial conversion of the ethyl ester to the carboxylic acid. This was first trialled on test substrate **193**, the conditions for which are shown in **Scheme 2.21**.

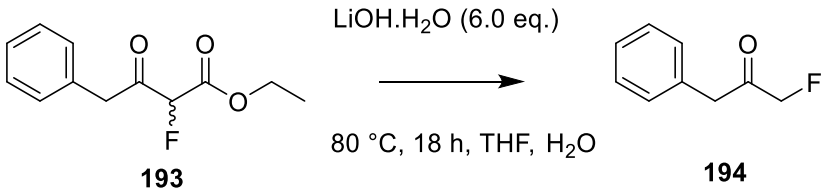

Scheme 2.21 – Deprotection and decarboxylation conditions for generation of FMK **194**.

It was anticipated that this reaction should proceed with ease due to the fact that decomposition to the FMK had already begun at room temperature; however, surprisingly no peaks were observed at all in the ^{19}F NMR spectrum. Whilst the cause of this was uncertain, it was initially reasoned that this molecule (**194**) may be volatile enough to be

removed with the solvent during rotary evaporation, although this was since deemed unlikely because, according to the literature, the substrate would only boil at 83-86 °C if the pressure was reduced to 5 Torr.[66] Alternatively, it was considered a possibility that the conditions employed brought about conversion to the hydroxy methyl ketone analogue (**Scheme 2.22**, **195**). Another consideration was whether an unwanted transformation could have occurred as a result of the presence of an α-proton in *β*-ketoester **193** which would be prone to deprotonation under basic conditions. Because of the challenges encountered at this stage, the use of these conditions on the actual substrate of interest was not pursued (**192**), but instead it was decided that Boc-alanine derived *β*-ketoester **192** would be left as a 1,3-dicarbonyl ethyl ester and an attempt would be made to couple it to an amino acid in solution to form a dipeptide, as will be described in **Section 2.2.5**. The goal would then be to saponify and decarboxylate to the desired FMK once peptide synthesis was complete. This would mean that the additional mass acquired after peptide coupling would prevent unwanted evaporation of the resulting product in case this was a contributing factor towards the problems encountered in **Scheme 2.21**.

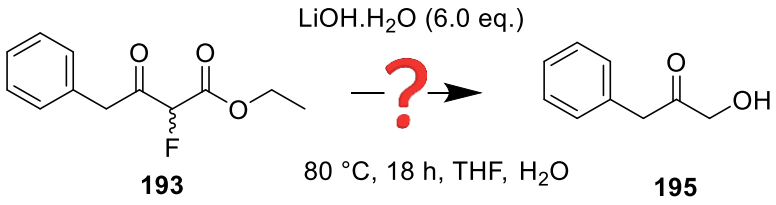

193 **195**

Scheme 2.22 – Possible unwanted conversion of **193** to hydroxy methyl ketone (HMK) **195**.

2.2.5 Boc Deprotection and Amino Acid Coupling

Boc deprotection was carried out on the Boc-alanine derived substrate **192**, as shown in **Scheme 2.23**, causing generation of the TFA salt under acidic conditions. A shift in the position of the peaks in the ^{19}F NMR spectrum (**Figure 2.21**) at -198 ppm corresponding to the starting material (**Figure 2.21a**) suggests product formation likely occurred; however, this can't be confirmed as the solvents employed for ^{19}F NMR spectroscopy before (**Figure 2.21a**) and after the reaction (**Figure 2.21b**) were different

($CDCl_3$ and DMSO-d_6 respectively). However, the reduction in peak complexity from two doublets to a single doublet could suggest that Boc removal has occurred with concomitant abolishment of rotamers. Unfortunately, the ^{1}H NMR spectrum proved challenging to decipher due to the presence of impurity peaks.

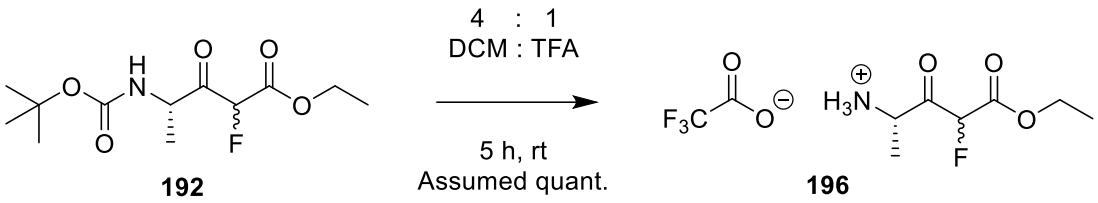

Scheme 2.23 – Conditions employed for Boc deprotection of **196**.

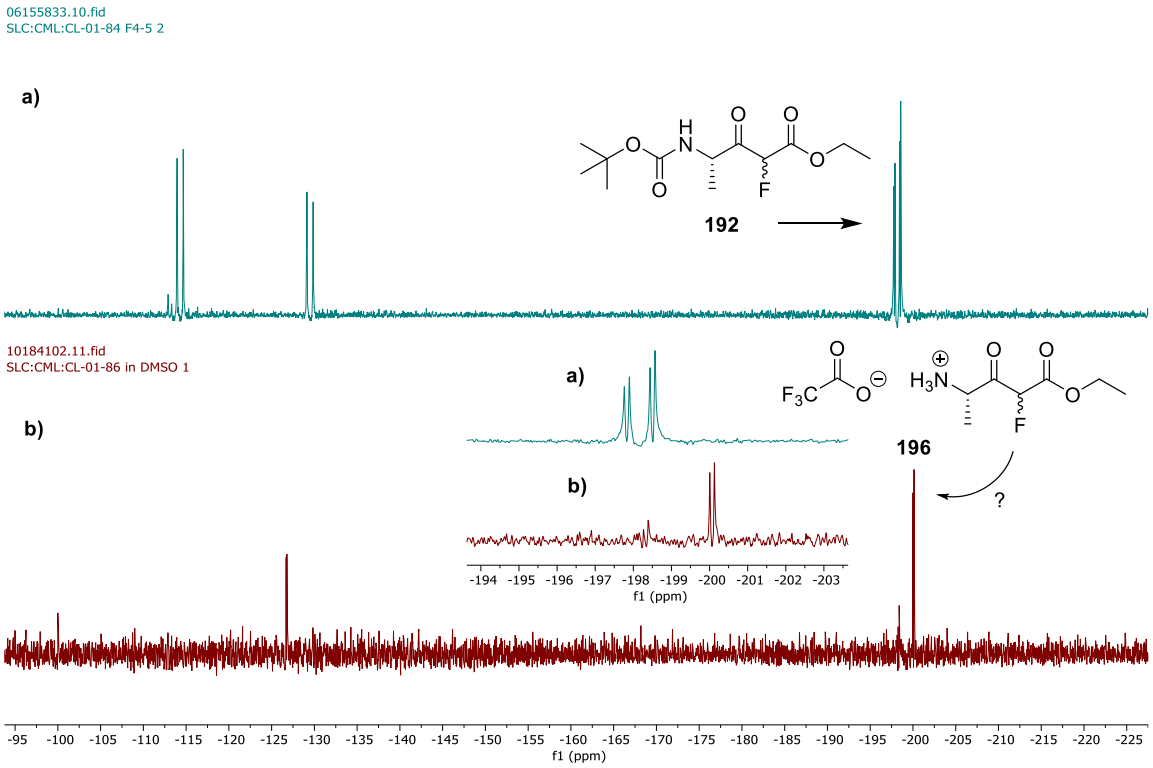

Figure 2.21 – ^{19}F NMR spectra before (**a**) and after (**b**) attempted Boc removal of **192**. (**a**) is recorded in $CDCl_3$, whilst (**b**) is recorded in DMSO-d_6.

Analysis by ESI (+ve) LCMS and accurate mass (+ve) confirmed that the desired product (**196**) had indeed been isolated, albeit a small amount. The yield was therefore assumed to be quantitative and the crude mixture was used in an attempted coupling reaction with Boc-phenylalanine (**197**). An extra equivalent of base was employed to

ensure initial deprotonation of the ammonium salt to generate the free amine and PyBOP was used as a coupling agent (**Scheme 2.24**).

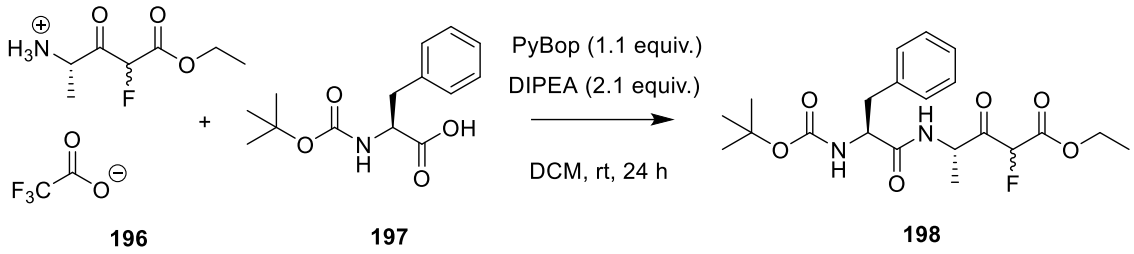

196 **197** **198**

Scheme 2.24 – Attempted coupling of **196** with Boc-Phe-OH (**197**).

Looking at the ^{19}F NMR spectrum of the crude reaction mixture, there did not seem to be a peak in the expected region (around -200 ppm) any longer; however, it was suspected that the signal was being swamped by a number of fluorine-containing impurities, as the molecular ion was successfully identified by ESI mass spectrometry (+ve) (**Figure 2.22**).

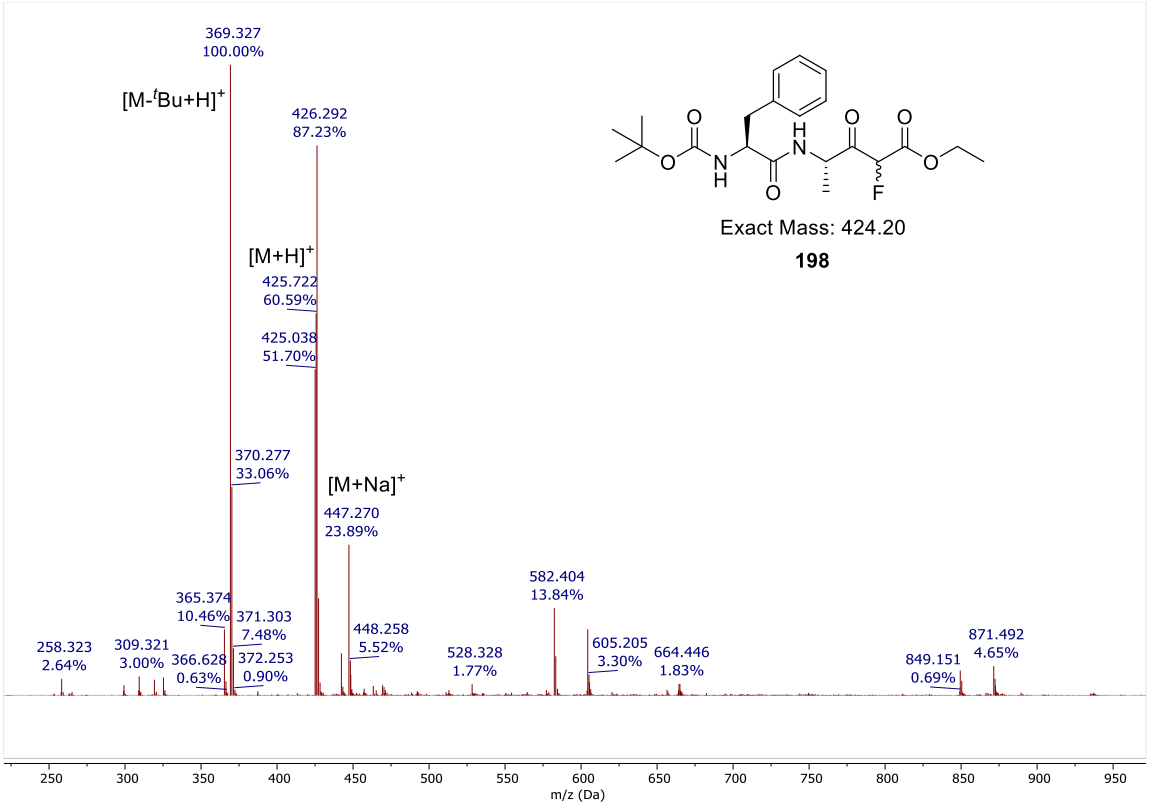

Figure 2.22 – ESI mass spectrum (+ve) indicating the presence of *β*-ketoester **198**.

Thus, it was concluded that the desired peptide-based *β*-ketoester (**198**) had likely been synthesised; however, only a very small amount was present, indicating the method did not proceed with great efficiency as had been hoped. For this reason, this route was not pursued further and alternative approaches were explored. These will be discussed in the following chapters.

2.3 Chapter Summary

In this chapter, solution-phase synthesis of peptidyl mono-fluoromethyl ketones via electrophilic fluorination of Boc-protected tri-carbonyl compounds and subsequent conversion to 1,3-dicarbonyl systems through ethanolysis was pursued. The intention was that this would then enable Boc deprotection, amide coupling with a peptide of choice, saponification to the free acid and decarboxylation to give the desired target peptidyl mono-fluoromethyl ketone (mFMK). Whilst successful fluorination of an aromatic-containing tri-carbonyl system (**Scheme 2.15**) was possible assuming quick and careful handling of the substrate to avoid unwanted hydrolysis, isolation of the fluorinated Boc-alanine derived tri-carbonyl analogue (**190**, **Scheme 2.17**) proved more challenging. Subsequent ethanolysis also revealed a disparity between the two systems, with the reaction involving the aromatic-containing substrate proceeding more convincingly (**Scheme 2.20a**), although evidence for the presence of some Boc-alanine derived product (**192**, **Scheme 2.20b**) was found. As a result, attempted Boc removal of *β*-ketoester **192** (**Scheme 2.23**) and subsequent solution-phase peptide coupling was performed (**Scheme 2.24**), with proof of the desired product (**198**) confirmed by LCMS. However, due to the problems encountered as a result of the high reactivity and instability of the Boc-alanine derived tri-carbonyl system making it difficult and inconvenient to handle, it was decided that a different approach would instead be considered.

2.4 References for Chapter 2

1. Gillis, E. P., Eastman, K. J., Hill, M. D., Donnelly, D. J. & Meanwell, N. A. Applications of Fluorine in Medicinal Chemistry. *J. Med. Chem.* **58**, 8315–8359 (2015).

2. O'Hagan, D. Understanding organofluorine chemistry. An introduction to the C–F bond. *Chem. Soc. Rev.* **37**, 308–319 (2008).

3. Böhm, H.-J. *et al.* Fluorine in Medicinal Chemistry. *ChemBioChem* **5**, 637–643 (2004).

4. Linclau, B. *et al.* Investigating the Influence of (Deoxy)fluorination on the Lipophilicity of Non-UV-Active Fluorinated Alkanols and Carbohydrates by a New log P Determination Method. *Angew. Chem. Int. Ed.* **128**, 684–688 (2016).

5. Bright, T. V, Dalton, F., Elder, V. L., Murphy, C. D. & Sandford, G. A convenient chemical-microbial method for developing fluorinated pharmaceuticals. *Org. Biomol. Chem.* **11**, 1135–1142 (2013).

6. Brittain, W. D. G., Lloyd, C. M. & Cobb, S. L. Synthesis of complex unnatural fluorine-containing amino acids. *J. Fluor. Chem.* **239**, 109630 (2020).

7. Mu, K. & Bo, H. Facilitating the Design of Fluorinated Drugs. *Chem. Bio.* **16**, 1130–1131 (2009).

8. Dalvit, C., Invernizzi, C. & Vulpetti, A. Fluorine as a Hydrogen-Bond Acceptor: Experimental Evidence and Computational Calculations. *Chem. Eur. J.* **20**, 11058–11068 (2014).

9. Wang, J. *et al.* Fluorine in Pharmaceutical Industry: Fluorine-Containing Drugs Introduced to the Market in the Last Decade (2001–2011). *Chem. Rev.* **114**, 2432–2506 (2014).

10. Zhou, Y. *et al.* Next Generation of Fluorine-Containing Pharmaceuticals, Compounds Currently in Phase II–III Clinical Trials of Major Pharmaceutical Companies: New Structural Trends and Therapeutic Areas. *Chem. Rev.* **116**, 422–518 (2016).

11. Purser, S., Moore, P. R. & Gouverneur, V. Fluorine in medicinal chemistry. *Chem. Soc. Rev.* **37**, 237–432 (2008).

12. Mei, H. *et al.* Fluorine-containing drugs approved by the FDA in 2019. *Chin Chem Lett* **31**, 2401–2413 (2020).

13. Ojima, I. Exploration of Fluorine Chemistry at the Multidisciplinary Interface of Chemistry and Biology. *J. Org. Chem.* **78**, 6358–6383 (2014).

14. Pardini, B. *et al.* 5-Fluorouracil-based chemotherapy for colorectal cancer and MTHFR/MTRR genotypes. *Br. J. Clin. Pharmacol.* **72**, 162–163 (2011).

15. Longley, D. B., Harkin, D. P. & Johnston, P. G. 5-Fluorouracil: mechanisms of action and clinical strategies. *Nat. Rev. Cancer* **3**, 330–338 (2003).

16. Dodick, D. W. *et al.* Ubrogepant, an Acute Treatment for Migraine, Improved Patient-Reported Functional Disability and Satisfaction in 2 Single-Attack Phase 3 Randomized Trials, ACHIEVE I and II. *Headache* **60**, 686–700 (2020).

17. Dodick, D. W. *et al.* Ubrogepant for the Treatment of Migraine. *N. Engl. J. Med.* **381**, 2230–2241 (2019).

18. Milner, L. M. *et al.* Access to novel fluorovinylidene ligands via exploitation of outer-sphere electrophilic fluorination: New insights into C-F bond formation and activation. *Dalton Trans.* **45**, 1717–1726 (2016).

19. Ogawa, Y., Tokunaga, E., Kobayashi, O., Hirai, K. & Shibata, N. Current Contributions of Organofluorine Compounds to the Agrochemical Industry. *iScience* **23**, 101467 (2020).

20. Inoue, M., Sumii, Y. & Shibata, N. Contribution of Organofluorine Compounds to Pharmaceuticals. *ACS Omega* **5**, 10633–10640 (2020).

21. O'Hagan, D., Schaffrath, C., Cobb, S. L., Hamilton, J. T. G. & Murphy, C. D. Biosynthesis of an organofluorine molecule. *Nature* **416**, 279 (2002).

22. Cheng, X. & Ma, L. Enzymatic synthesis of fluorinated compounds. *Appl. Microbiol. Biotechnol.* **105**, 8033–8058 (2021).

23. Harsanyi, A. & Sandford, G. Organofluorine chemistry: applications, sources and sustainability. *Green Chem.* **17**, 2081–2086 (2015).

24. Monsen, P. J. & Luzzio, F. A. Selective fluorination of natural products. *Arkivoc* **2017**, 117–147 (2017).

25. Wu, J. Review of recent advances in nucleophilic C–F bond-forming reactions at sp3 centers. *Tetrahedron Lett.* **55**, 4289–4294 (2014).

26. McBee, E. T., Bolt, R. O., Graham, P. J. & Tebbe, R. F. The Preparation of Certain Ethers of Trifluoromethyl-substituted Phenols. *J. Am. Chem. Soc.* **69**, 947–950 (1947).

27. Schimler, S. D., Ryan, S. J., Bland, D. C., Anderson, J. E. & Sanford, M. S. Anhydrous Tetramethylammonium Fluoride for Room-Temperature SNAr Fluorination. *J. Org. Chem.* **80**, 12137–12145 (2015).

28. Ishikawa, N., Kitazume, T., Yamazaki, T., Mochida, Y. & Tatsuno, T. Enhanced Effect Of Spray-Dried Potassium Fluoride On Fluorination. *Chem. Lett.* **10**, 761–764 (1981).

29. Gingras, M. Tetrabutylammonium difluorotripheylstannate as a new anhydrous synthetic equivalent to TBAF. *Tetrahedron Lett.* **32**, 7381–7384 (1991).

30. Lal, G. S., Pez, G. P., Pesaresi, R. J., Prozonic, F. M. & Cheng, H. Bis(2-methoxyethyl)aminosulfur Trifluoride: A New Broad-Spectrum Deoxofluorinating Agent with Enhanced Thermal Stability. *J. Org. Chem.* **64**, 7048–7054 (1999).

31. Middleton, W. J. New fluorinating reagents. Dialkylaminosulfur fluorides. *J. Org. Chem.* **40**, 574–578 (1975).

32. Baumann, M., Baxendale, I. R. & Ley, S. v. The use of diethylaminosulfur trifluoride (DAST) for fluorination in a continuous-flow microreactor. *Synlett* **14**, 2111–2114 (2008).

33. Singh, R. P., Chakraborty, D. & Shreeve, J. M. Nucleophilic trifluoromethylation and difluorination of substituted aromatic aldehydes with Ruppert's and Deoxofluor™ reagents. *J. Fluor. Chem.* **111**, 153–160 (2001).

34. Shellhamer, D. F. *et al.* Reaction of diethylaminosulfur trifluoride with diols. *J. Chem. Soc. Perkin Trans. 2* **2**, 861 (1995).

35. Sun, H. & Dimagno, S. G. Anhydrous Tetrabutylammonium Fluoride. *J. Am. Chem. Soc.* **127**, 2050–2051 (2005).

36. Sharma, R. K. & Fry, J. L. Instability of anhydrous tetra-n-alkylammonium fluorides. *J. Org. Chem.* **48**, 2112–2114 (1983).

37. Hu, Y. F., Luo, J. & Lü, C. X. A mild and efficient method for nucleophilic aromatic fluorination using tetrabutylammonium fluoride as fluorinating reagent. *Chin Chem Lett* **21**, 151–154 (2010).

38. Hu, Y. F., Luo, J. & Lu, C. X. A mild and efficient method for nucleophilic aromatic fluorination using tetrabutylammonium fluoride as fluorinating reagent. *Chinese Chemical Letters* **21**, 151–154 (2010).

39. Cox, D. P., Terpinski, J. & Lawrynowicz, W. 'Anhydrous' tetrabutylammonium fluoride: a mild but highly efficient source of nucleophilic fluoride ion. *J. Org. Chem.* **49**, 3216–3219 (1984).

40. Zhao, M., Ming, L., Tang, J. & Zhao, X. Regioselective fluorination of 1-(2,2-dibromovinyl)benzene derivatives with wet tetra-n-butylammonium fluoride: One-pot synthesis of (Z)-1-(2-bromo-1-fluorovinyl)benzenes. *Org. Lett.* **18**, 416–419 (2016).

41. Rozatian, N., Ashworth, I. W., Sandford, G. & Hodgson, D. R. W. A quantitative reactivity scale for electrophilic fluorinating reagents. *Chem. Sci.* **9**, 8692–8702 (2018).

42. Oliver, E. W. & Evans, D. H. Electrochemical studies of six N-F electrophilic fluorinating reagents. *J. Electroanal. Chem.* **474**, 1–8 (1999).

43. Lal, G. S., Pez, G. P. & Syvret, R. G. Electrophilic NF Fluorinating Agents. *Chem. Rev.* **96**, 1737–1756 (1996).

44. Kiselyov, A. S. Chemistry of N-fluoropyridinium salts. *Chem. Soc. Rev.* **34**, 1031–1037 (2005).

45. Anbarasan, P., Neumann, H. & Beller, M. Efficient Synthesis of Aryl Fluorides. *Angew. Chem. Int. Ed.* **49**, 2219–2222 (2010).

46. Said, M. S. *et al.* Regioselective One-Pot Synthesis of 3-Fluoro-Imidazo[1,2-a]pyridines from Styrene. *Asian J. Org. Chem.* **8**, 2143–2148 (2019).

47. Fujiwara, T., Seki, T., Yakura, T. & Takeuchi, Y. Useful procedures for fluorocyclization of tryptamine and tryptophol derivatives to 3a-fluoropyrrolo[2,3-b]indoles and 3a-fluorofuro[2,3-b]indoles. *J. Fluor. Chem.* **165**, 7–13 (2014).

48. Shibata, N., Tarui, T., Doi, Y. & Kirk, K. L. Synthesis of Fluorogypsetin and Fluorobrevianamide E by a Novel Fluorination - Cyclization of cyclo-L-Trp-L-AAs. *Angew. Chem. Int. Ed.* **40**, 4461–4463 (2001).

49. Takeuchi, Y., Tarui, T. & Shibata, N. A Novel and Efficient Synthesis of 3-Fluorooxindoles from Indoles Mediated by Selectfluor. *Org. Lett.* **2**, 639–642 (2000).

50. Nyffeler, P. T., Durón, S. G., Burkart, M. D., Vincent, S. P. & Wong, C. H. Selectfluor: Mechanistic Insight and Applications. *Angew. Chem. Int. Ed.* **44**, 192–212 (2005).

51. Xiao, J.-C. & Shreeve, J. M. Microwave-assisted rapid electrophilic fluorination of 1,3-dicarbonyl derivatives with Selectfluor®. *J. Fluor. Chem.* **126**, 473–476 (2005).

52. Tang, L. *et al.* Chemoselective Mono- And Difluorination of 1,3-Dicarbonyl Compounds. *J. Org. Chem.* **84**, 10449–10458 (2019).

53. Hintermann, L. & Togni, A. Catalytic Enantioselective Fluorination of β-Ketoesters. *Angew. Chem. Int. Ed.* **39**, 4359–4362 (2000).

54. Hintermann, L., Perseghini, M. & Togni, A. Development of the titanium-TADDOLate-catalyzed asymmetric fluorination of β-ketoesters. *Beilstein J. Org. Chem.* **7**, 1421–1435 (2011).

55. Frantz, R., Hintermann, L., Perseghini, M., Broggini, D. & Togni, A. Titanium-Catalyzed Stereoselective Geminal Heterodihalogenation of β-Ketoesters. *Org. Lett.* **5**, 1709–1712 (2003).

56. Harsanyi, A. *et al.* α-Fluorotricarbonyl Derivatives as Versatile Fluorinated Building Blocks: Synthesis of Fluoroacetophenone, Fluoroketo Ester and Fluoropyran-4-one Derivatives. *Eur. J. Chem.* **2020**, 3872–3878 (2020).

57. Oikawa, Y., Sugano, K. & Yonemitsu, O. Meldrum's acid in organic synthesis. 2. A general and versatile synthesis of ß-keto esters. *J. Org. Chem.* **43**, 2087–2088 (1978).

58. Janikowska, K., Rachoń, J. & Makowiec, S. Acyl Meldrum's acid derivatives: application in organic synthesis. *Russ. Chem. Rev.* **83**, 620–637 (2014).

59. Sørensen, U. S., Falch, E. & Krogsgaard-Larsen, P. A Novel Route to 5-Substituted 3-Isoxazolols. Cyclization of N,O-DiBoc β-Keto Hydroxamic Acids Synthesized via Acyl Meldrum's Acids. *J. Org. Chem.* **65**, 1003–1007 (2000).

60. Harsanyi, A. Elemental fluorine for the greener synthesis of life-science building blocks. (2016).

61. Tam, L. Biocatalytic Reactions of Fluorinated Dicarbonyl Systems. (Durham Unviersity, 2018).

62. Dowlatshahi, H. A. *et al.* 4-Hydroxy-3-quinolinecarboxamides with Antiarthritic and Analgesic Activities. *J. Med. Chem.* **27**, 1453–1462 (1988).

63. Yamamoto, S. *et al.* Design and synthesis of an orally active matrix metalloproteinase inhibitor. *Bioorg. Med. Chem.* **14**, 6383–6403 (2006).

64. Tanaka-Yanuma, A. *et al.* Synthesis of the polyketide moiety of the jamaicamides. *Tetrahedron Lett.* **56**, 6777–6781 (2015).

65. Nakamura, S., Hirao, H. & Ohwada, T. Rationale for the Acidity of Meldrum's Acid. Consistent Relation of C−H Acidities to the Properties of Localized Reactive Orbital. *J. Org. Chem.* **69**, 4309–4316 (2004).

66. Kitazume, T., Asai, M., Lin, J. T. & Yamazaki, T. The synthesis of optically active building blocks carrying a monofluoromethyl group. *J. Fluor. Chem.* **35**, 477–488 (1987).

3. Solid-Phase Synthesis of Peptidyl Mono-FMKs

3.1 Introduction

Solid-phase peptide synthesis involves the growth of a peptide chain through the attachment of the C-terminal end of the first amino acid to an insoluble polymeric resin (**Figure 3.1**).[1,2] Subsequent coupling of amino acid units allows extension of the peptide from the C to N terminus. Once the peptide is fully synthesised, removal from the resin can be achieved through various cleavage conditions, depending on the type of resin used. Orthogonal protection should be employed in such a way that the *N*-terminal end of the peptide being extended can easily be deprotected without affecting the sidechain protecting groups. Common orthogonal groups utilised include fluorenylmethyloxycarbonyl (Fmoc), a base sensitive group removed with piperidine, and *tert*-butoxycarbonyl (Boc) or *tert*-butyl ester (O^{t}Bu) which are cleaved in acid (TFA).

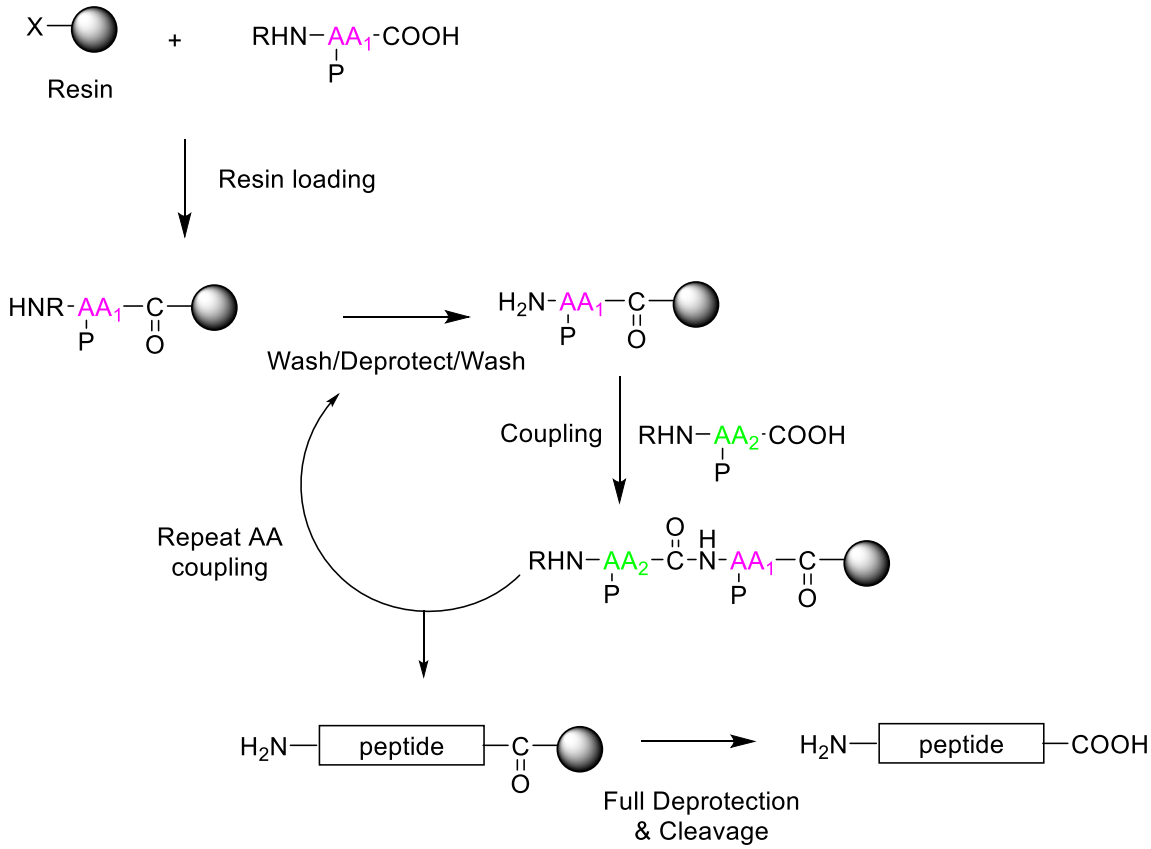

Figure 3.1 – General scheme for SPPS[1]. P = protecting group.

One significant advantage of SPPS over solution-phase synthesis is the ability to simply wash away impurities without removal of the product, which remains securely attached to the resin. This enables easier purification and significantly enhances the yield due to the ability to use a large excess of reagents with the knowledge that unreacted materials can be filtered off easily. Another hugely attractive feature is the simplicity of the process and the speed at which peptides can be assembled using this method, along with the possibility for automated peptide synthesis using equipment such as CEM's Liberty Blue peptide synthesiser. It also enables the construction of long, complex peptides that would otherwise be challenging in solution.

Given the benefits associated with SPPS and the simplicity of the process, the development of a novel solid-phase route for the synthesis of peptidyl mono-fluoromethyl ketones (mFMKs) was pursued. Furthermore, as highlighted in **Chapter 1** (**Section 1.4.5.2**), only two examples to achieve this have been described in the literature, with both requiring the synthesis and use of a linker in some examples, adding additional steps and complexity to the process.[3,4] For this reason, it was proposed that there was further scope for the development of a simplified general approach which allows for the direct use of a standard, commercially available solid support along with mild cleavage conditions, avoids the use of hazardous diazomethane, and is compatible with a wide range of amino acid substrates. It was therefore believed that an improved route for accessing FMK building blocks for solid-phase synthesis (with potential to be adapted for solution-phase applications) would prove useful in helping to fill a gap in the literature.

During attempts to access peptidyl mFMKs via a solution-phase approach through electrophilic fluorination of a tri-carbonyl system (**Chapter 2**), successful isolation of the corresponding mono-fluorinated 1,3-dicarbonyl derivative **199** through ethanolysis was achieved (**Scheme 3.1**). It was proposed that utilisation of an adapted system, such as Fmoc-protected *β*-ketoester **199** (**Scheme 3.2**) offers potential for solid-phase synthesis through deprotection to the *β*-ketoacid (**200**), as this provides a carboxylic acid handle for

resin attachment and can subsequently be decarboxylated to the FMK (**129**) once cleaved from the resin after peptide growth (**Scheme 3.2**).

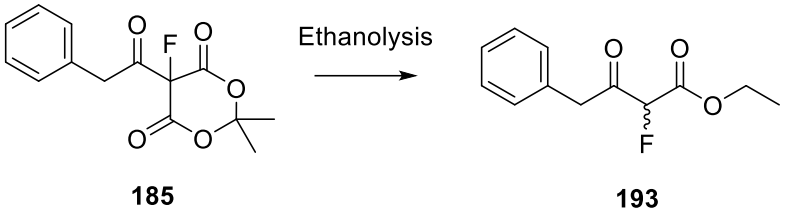

Scheme 3.1 – Ethanolysis of tricarbonyl **185** to 1,3-dicarbonyl **193**, as described in **Chapter 2**.

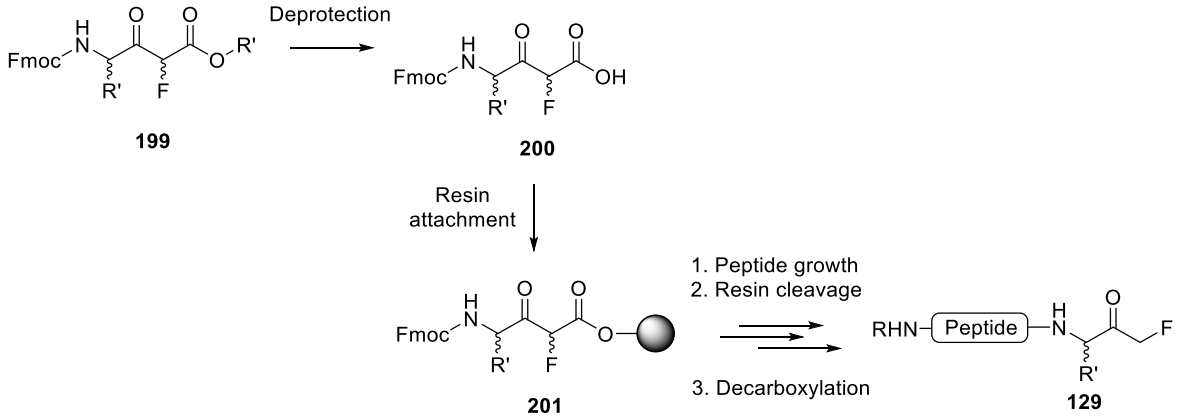

Scheme 3.2 – Proposed solid-phase route to peptidyl mFMKs (**129**), starting from *β*-ketoester building block **199**.

In light of the challenges associated with handling the Boc-protected hydrolysis-prone tri-carbonyls (**Chapter 2**), accessing Fmoc-protected *β*-ketoester **199** via this approach was not pursued. Instead, it was proposed that direct mono-fluorination of a 1,3-dicarbonyl system may be a viable alternative option. As alluded to in **Chapter 2** (**Section 2.1.2**), mono-fluorination of 1,3-dicarbonyls (**202**) has been reported in the literature, and a summary of some key examples is provided in **Figure 3.2**. This includes examples involving F-TEDA with microwave irradiation (**Figure 3.2**, **i**),[5] F-TEDA in MeCN/H_2O (**Figure 3.2**, **ii**),[6] F-TEDA in the presence of a titanium catalyst (**Figure 3.2**, **iii**),[7] fluoroiodane **197** in conjunction with $Et_3N{\cdot}3HF$ (**Figure 3.2**, **iv**),[8] fluorine gas (**Figure 3.2**, **v**),[9] mechanochemical techniques (**Figure 3.2**, **vi**),[10,11] aqueous HF with iodosylbenzene (**Figure 3.2**, **vii**)[12] and (diacetoxyiodo)benzene in the presence of $Et_3N{\cdot}3HF$ (**Figure 3.2**, **viii**).[13]

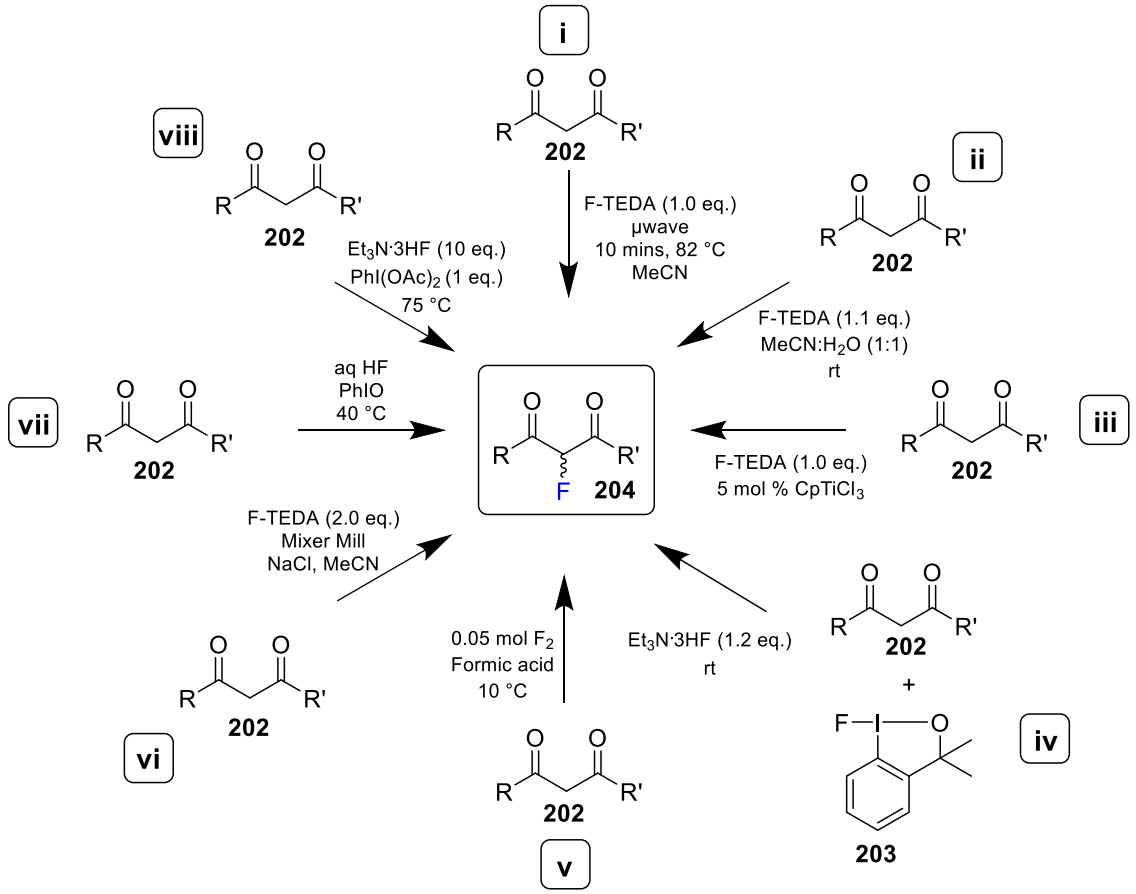

Figure 3.2 – Summary of some key examples of mono-fluorination of 1,3-dicarbonyl systems in the literature.

Considering these examples, it was envisioned that isolation of Fmoc-protected *β*-ketoacid building block **205** could be achieved through electrophilic fluorination of a 1,3-dicarbonyl system (**207**), accessed through oxidation of a fully protected *β*-hydroxyester (**208**), as shown in retrosynthetic **Scheme 3.3**. 4-amino-3-hydroxybutyric acid (**209**) is commercially available, and thus was the starting material of choice. The following sections will provide details of endeavours made to access building block **205** and subsequently utilise it for the solid-phase synthesis of peptidyl mFMKs according to **Scheme 3.2**.

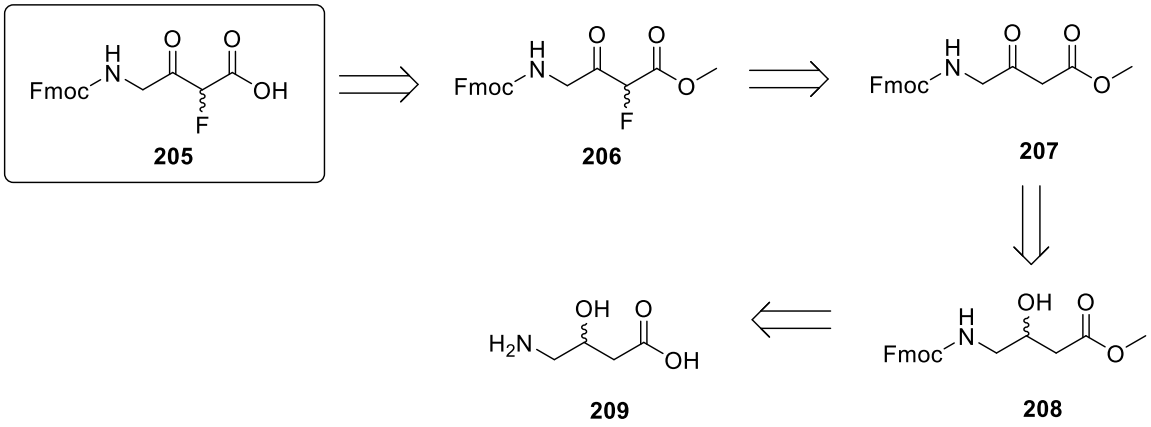

Scheme 3.3 – Proposed retrosynthetic scheme for accessing Fmoc-FMK building block **205** for SPPS of mFMKs.

3.2 Synthesis of Fmoc-protected *β*-ketoacid building block 205

3.2.1 Methyl Ester Protection

Starting from commercially available 4-amino-3-hydroxybutyric acid (**209**), it was deemed necessary to first fully protect the acid and amine functionalities in order to reduce the likelihood of unwanted side-reactions occurring during later transformations. A methyl ester was chosen to mask the carboxylic acid moiety, whilst Fmoc, a protecting group commonly employed in solid-phase peptide synthesis, was used for the amine. Methyl ester protection was achieved using thionyl chloride to generate the acid chloride *in situ*, followed by attack of methanol, the nucleophile (**Scheme 3.4**). This reaction step proceeded without incident, affording the target compound in a quantitative yield (**210**).

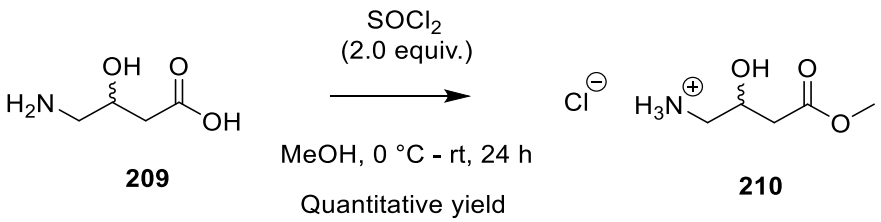

Scheme 3.4 – Methyl ester protection of carboxylic acid **209**.

3.2.2 Fmoc Protection of *β*-Hydroxyester 210

The second step in the process involved Fmoc protection of the free amine. As can be seen in **Table 3.1**, several conditions were screened before a satisfactory yield was obtained. In all cases, an excess of one equivalent of base was designated to ensuring initial deprotonation of the ammonium salt, which was generated due to the acidic environment in which methyl ester **210** was formed. Two reaction attempts involving a combination of H_2O and 1,4-dioxane as solvents[14] (**Table 3.1**, **Entries 1 & 2**) failed to produce any isolated product whatsoever, even when swapping $NaHCO_3$ for K_2CO_3, a stronger base. This could be due to poor solubility once deprotonation of the ammonium salt has occurred. A small amount of product (**208**) was observed by ^1H NMR spectroscopy when using the same solvent conditions in the presence of K_2CO_3, except with the addition of a 2-hour reflux period to encourage dissolution, a longer reaction time overall and the use of the more reactive Fmoc-Cl instead of Fmoc-OSu (**Table 3.1**, **Entry 3**). However, a yield of only 7% meant that the search for enhanced efficiency continued. A slightly improved yield of 22% was observed when the solvent was changed to DCM, Fmoc-Cl was used and the inorganic base swapped for pyridine (**Table 3.1**, **Entry 4**), as reported in the literature.[15] However, it was suspected that excess pyridine could be pulling some product into the aqueous layer during the work-up step, contributing to the poor overall yield. For this reason, the use of pyridine was abandoned and attention was instead returned to sodium bicarbonate due to easier purification, but with a different solvent system in the hope of enhancing solubility. The use of acetone and 1,4-dioxane along with aqueous $NaHCO_3$ was trialled and found to be effective, giving a good yield of 69% in only 4 hours (**Table 3.1**, **Entry 5**).

Table 3.1 – Conditions screened for Fmoc protection.

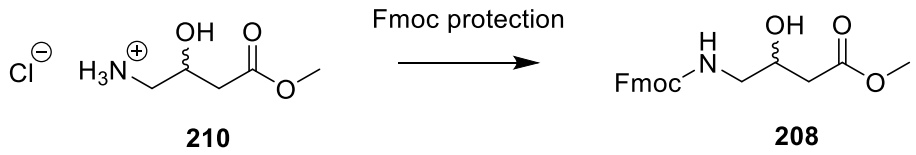

210 **208**

Entry	Reagents	Conditions	Isolated Yield
1	Fmoc-OSu (0.95 equiv.), $NaHCO_3$ (2.1 equiv.), H_2O, 1,4-dioxane	0 °C – rt 24 h	0%
2	Fmoc-OSu (0.95 equiv.), K_2CO_3 (2.1 equiv.), H_2O, 1,4-dioxane	0 °C – rt 24 h	0%
3	Fmoc-Cl (0.95 equiv.), 1,4-dioxane, H_2O, K_2CO_3 (2.6 equiv.)	0 °C – reflux 48 h	7%
4	Fmoc-Cl (0.90 equiv.), pyridine (2.2 equiv.), DCM	0 °C – rt 3 h	22%
5	Fmoc-OSu (1.2 equiv.), 0.8 M aq $NaHCO_3$ (3.5 equiv.), Acetone, 1,4-dioxane	rt 4 h	69%

3.2.3 Oxidation of Fmoc-Protected *β*-Hydroxyester 208

In order to allow electrophilic fluorination in the position of choice, it was necessary for oxidation of *β*-hydroxyester **208** to the *β*-ketoester derivative (**207**) in order to generate the desired 1,3-dicarbonyl system. Once again, various conditions were screened in order to obtain the best yield possible for the oxidation process (**Table 3.2**). A literature procedure involving Dess–Martin periodinane (DMP)[16] was initially attempted, with limited success on this particular substrate, giving a yield of only 10% (**Table 3.2**, **Entry 1**). Pyridinium chlorochromate (PCC)[17] was found to give **207** in a moderate yield of 57% (**Table 3.2**, **Entry 2**); however, the highly toxic nature of this heavy-metal required careful handling and disposal, rendering the reaction undesirable and inconvenient. Consequently, a better alternative was pursued. The use of 2-iodoxybenzoic acid (IBX) as

an oxidising agent has previously been overlooked due to its poor solubility in many organic solvents.[18] However, it has since been shown to operate effectively in a heterogeneous manner, as demonstrated in the literature.[19] In fact, the reaction was found to proceed very efficiently in ethyl acetate, giving an excellent yield of 80% after just 3 hours of refluxing (**Table 3.2**, **Entry 3**).

Table 3.2 – Conditions screened for the oxidation of *β*-hydroxyester **208** to 1,3-dicarbonyl **207**.

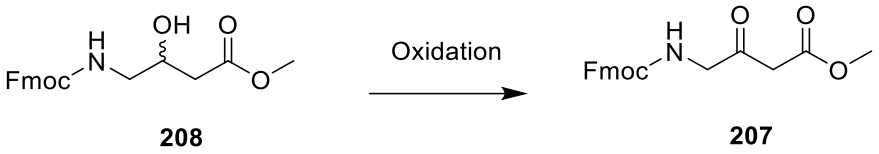

208 **207**

Entry	Reagents	Conditions	Isolated Yield
1	DMP (1.2 eq.)	DCM, rt 24 h	10%
2	PCC (3.0 eq.)	DCM, rt 4 h	57%
3	IBX (3.0 eq.)	EtOAc, reflux 3 h	80%

3.2.4 C-F Bond Formation

The electrophilic fluorinating agent of choice for installation of a fluorine atom into a *β*-ketoester (**211**) (**Scheme 3.5**) was Selectfluor (F-TEDA) due to its high reactivity, low toxicity, and the ease at which it can be handled.[20]

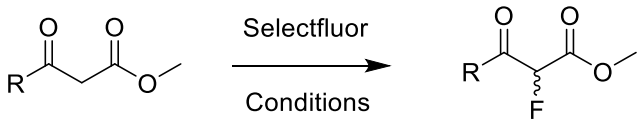

211 **212**

Scheme 3.5 – General scheme for mono-fluorination of *β*-ketoesters (**211**).

Although there has been speculation that electrophilic fluorination could proceed through either a single electron transfer (SET) event or an S_N2 process, based on kinetic

studies it is suspected that the latter of these two mechanisms is favoured.[21] This means that the enolate acts as a nucleophile, attacking the electrophilic source of fluorine and displacing the remainder of the fluorinating agent as a leaving group (**Scheme 3.6**).

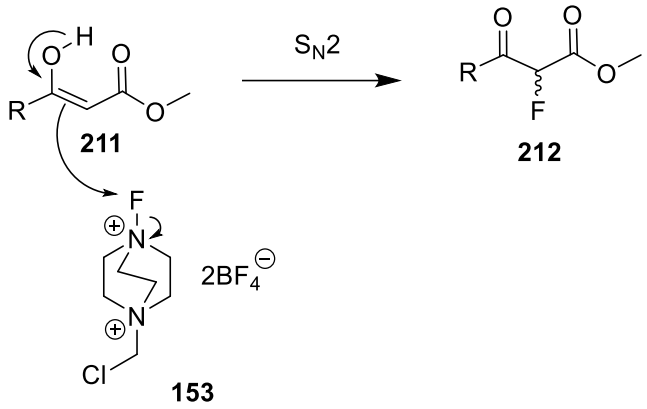

Scheme 3.6 – S_N2 mechanism for electrophilic fluorination of a 1,3-dicarbonyl (**211**) using Selectfluor.[21]

A range of fluorination conditions was screened on methyl acetoacetate (**213**), which was used as a test substrate in order to determine optimum conditions for electrophilic fluorination of 1,3-dicarbonyl systems (**Table 3.3**).

Table 3.3 - Conditions screened for electrophilic fluorination of methyl acetoacetate (**213**).

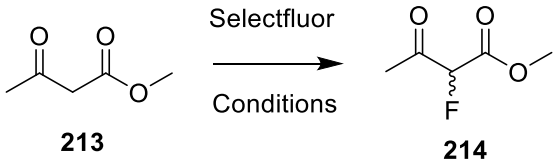

Entry	Reagents	Conditions	Comment
1	F-TEDA (1.0 eq.)	MeCN, rt 24 h	No isolated yield
2	F-TEDA (1.0 eq.), K_2CO_3 (1.0 eq.)	MeCN, rt 24 h	No isolated yield
3	F-TEDA (1.0 eq.), $CpTiCl_3$ (0.05 eq.)	MeCN, rt 24 h	43% isolated yield

An initial attempt involving the reaction of *β*-ketoester **213** with Selectfluor in the absence of a base, using MeCN as a solvent (**Table 3.3**, **entry 1**), failed to bring about complete conversion to the product (**214**). Whilst evidence for successful mono-fluorination (-193 ppm) along with an insignificant amount of di-fluorination (-113 ppm) was apparent by ^{19}F NMR spectroscopy (**Figure 3.3**), the ^{1}H NMR spectrum indicated only 56% conversion to **214** after 24 hours.

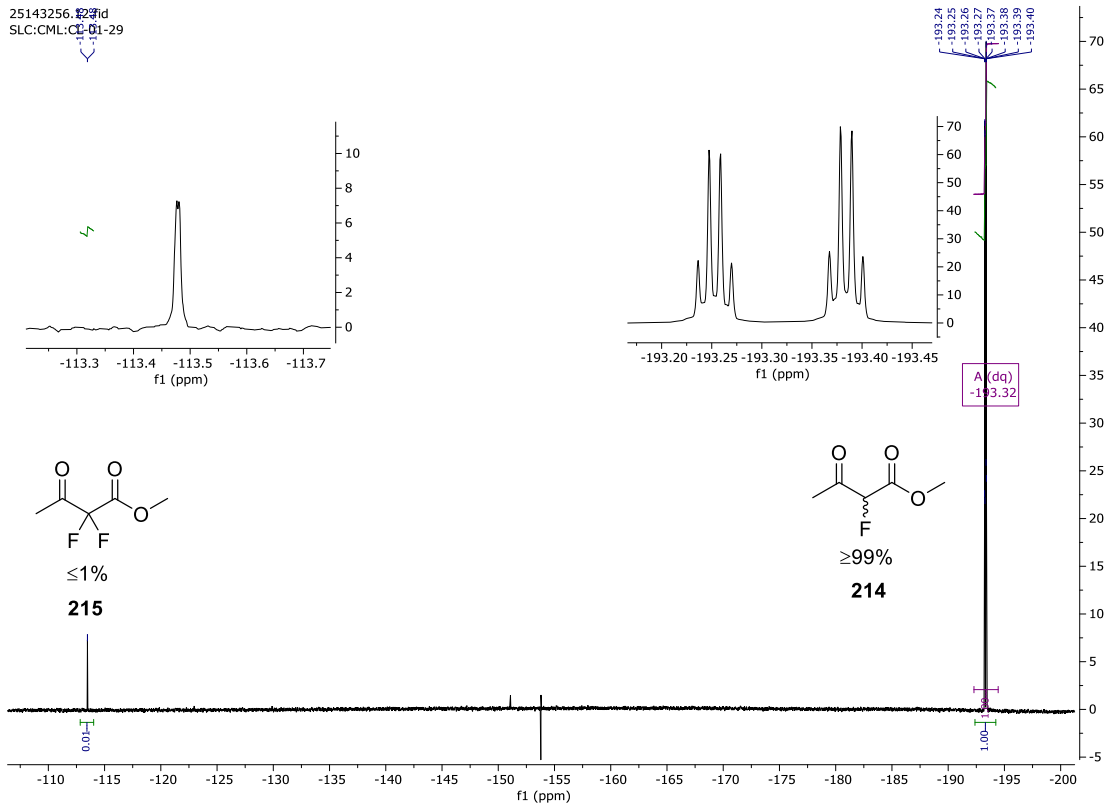

Figure 3.3 – Crude ^{19}F NMR (^{1}H coupled) spectrum ($CDCl_3$) after mono-fluorination of methyl acetoacetate (**213**) with F-TEDA. Percentage of mono-fluorination (**214**) relative to di-fluorination (**215**) is shown.

The introduction of 1.0 equivalent of base in the form of potassium carbonate (**Table 3.3**, **entry 2**) resulted in a significant increase in di-fluorination (**215**) relative to mono-fluorination (0.6 : 1.0), as can be seen by the crude ^{19}F NMR spectrum in **Figure 3.4a**. An attempt to separate the two by silica gel column chromatography proved unsuccessful due to very similar retention times. The transformation was therefore attempted without base, using F-TEDA in the presence of $CpTiCl_3$ (**Table 3.3**, **entry 3**), as

described by Togni and co-workers.[7] This enabled good conversion to product, and selectivity for mono- over di-fluorination in a ratio of 0.04 : 1.0 (**Figure 3.4b**).

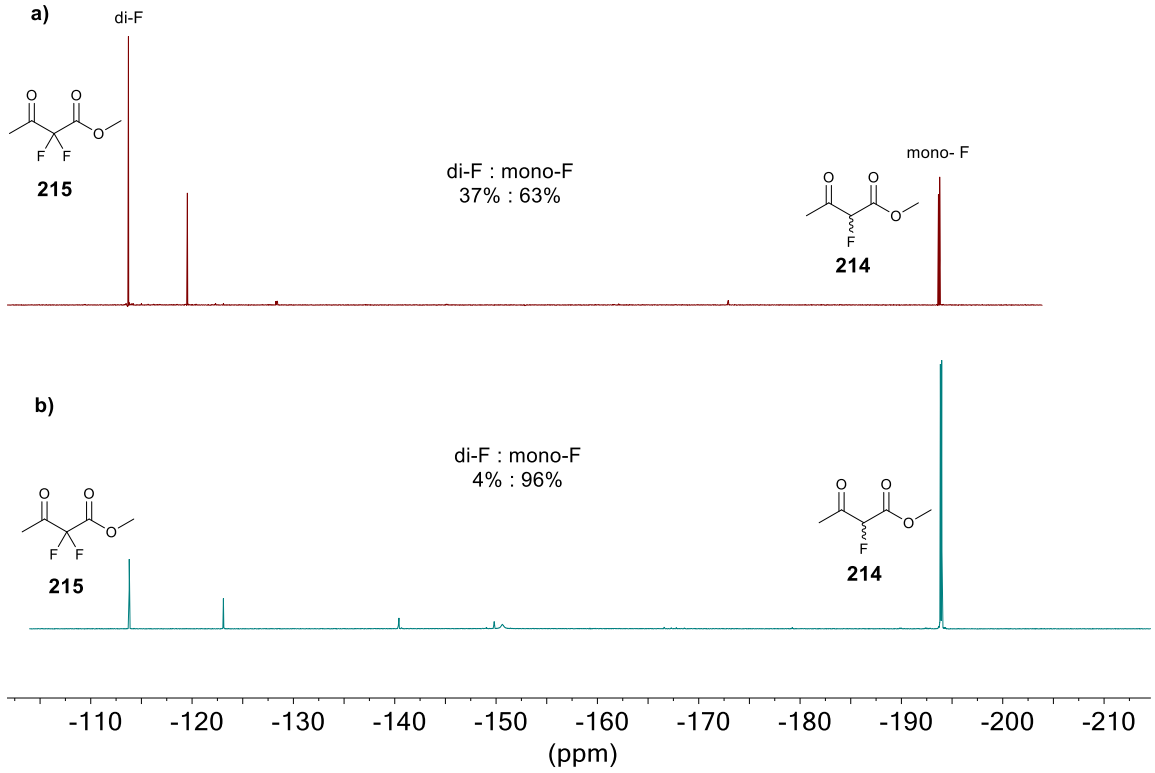

Figure 3.4 - Crude **19**F NMR (^{1}H coupled) spectra ($CDCl_3$) after electrophilic fluorination of methyl acetoacetate (**213**) with Selectfluor in the presence of either K_2CO_3 (**a**) or $CpTiCl_3$ (**b**).

These conditions, which utilised F-TEDA and $CpTiCl_3$, were successfully transferred to Fmoc-protected *β*-ketoester **207** (**Scheme 3.7**), allowing mono-fluorination to dominate (**Figure 3.5**, ^{19}F NMR signal at -200 ppm). Whilst it was not possible to fully eliminate the presence of a small amount of di-fluorinated material (~10%), as shown by a peak at -114 ppm in the post-column chromatography ^{19}F NMR spectrum (**Figure 3.5**), the relative amounts were generally kept low. Furthermore, once the resulting fluorinated building block had been coupled to a peptide of choice, it would likely be necessary to perform additional purification by reverse-phase HPLC anyway, helping to further enhance purity.

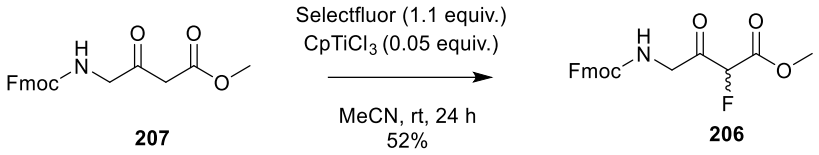

Scheme 3.7 - Conditions employed for electrophilic fluorination of *β*-ketoester **207**.

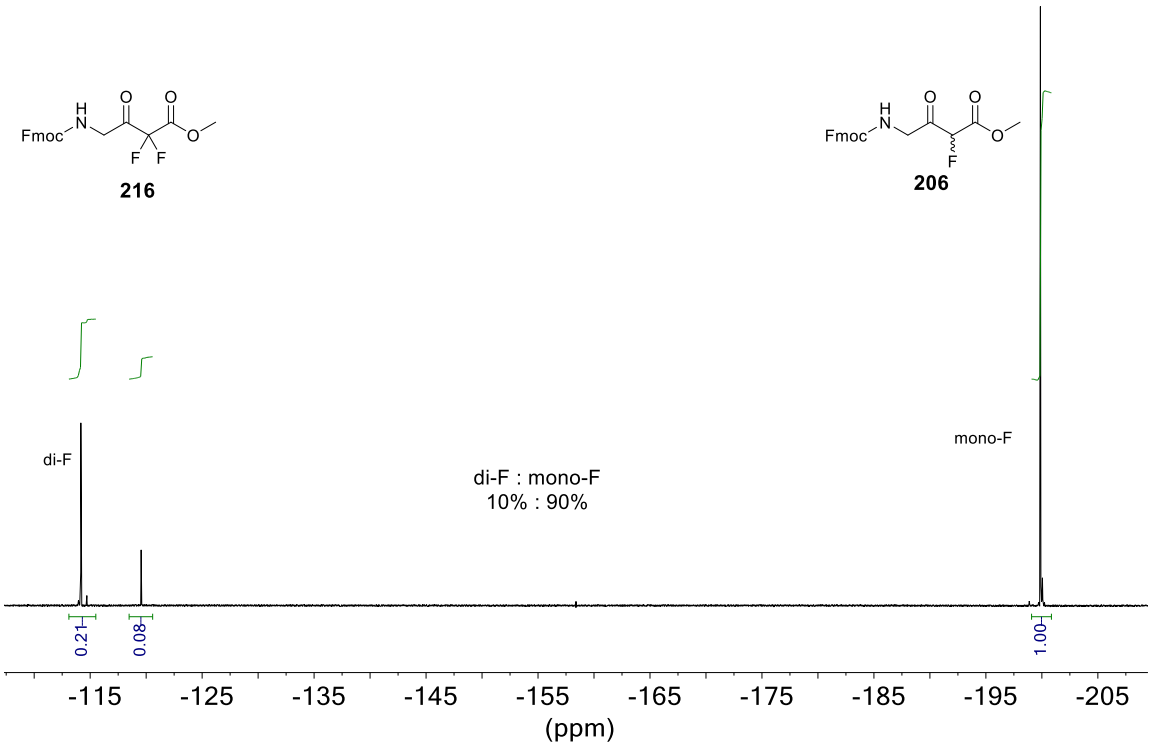

Figure 3.5 - Post-column chromatography ^{19}F NMR spectrum ($CDCl_3$) after electrophilic fluorination of *β*-ketoester **207**.

As with methyl acetoacetate (**213**), an attempt to bring about mono-fluorination in MeCN using F-TEDA in the absence of any additives brought about poor conversion to desired product (**206**). **Figure 3.6** indicates the presence of significantly more mono- (**206**) than di-fluorinated (**216**) material (98 : 11); however, LCMS data (**Figure 3.7**) suggests predominance of starting material (**207**) over fluorinated product. Thus, the titanium-catalysed method was utilised and carried forward in subsequent mono-fluorination reactions.

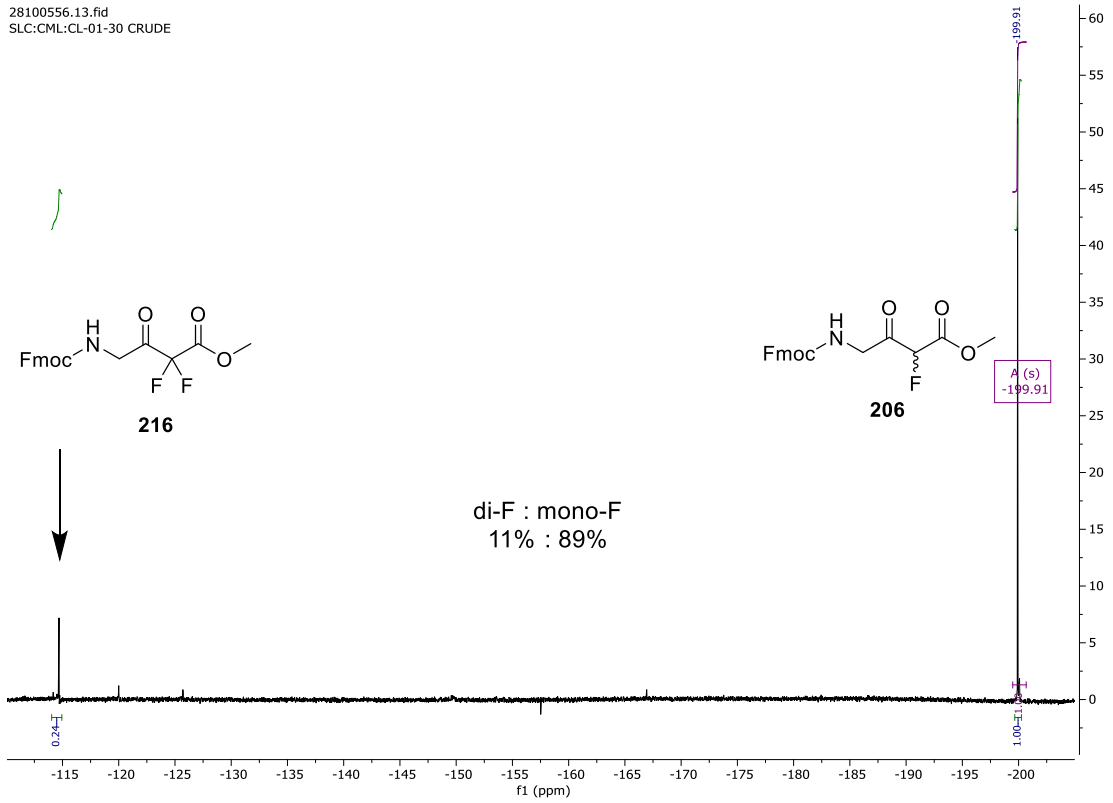

Figure 3.6 – Crude $^{19}F\{^{1}H\}$ NMR ($CDCl_3$) indicating the predominance of mono- over di-fluorination when *β*-ketoester **207** was reacted with F-TEDA in MeCN without base.

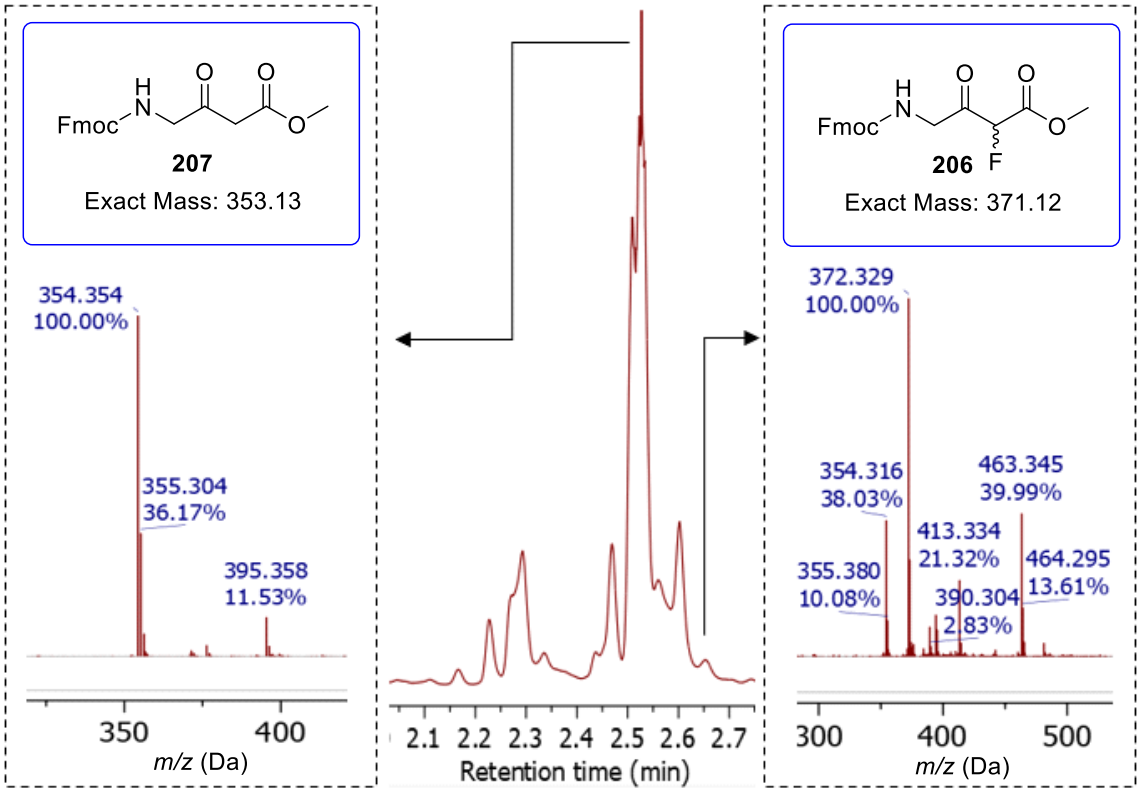

Figure 3.7 – Crude liquid chromatography UV trace viewed at λ = 254 nm (middle) and corresponding ESI MS peaks (+ve) for the starting material (left) and desired mono-fluorinated product (right).

3.2.5 Methyl Ester Deprotection

In order to enable attachment to a solid support for SPPS, a selection of conditions was trialled for the regeneration of the carboxylic acid (**205**) functionality from ester **206** (**Scheme 3.8**). Given the potential for unwanted simultaneous Fmoc removal under standard basic saponification conditions, an alternative approach described by R. Pascal and R. Sola, in which Fmoc preservation was reported, was first attempted.[22] This involved the use of NaOH in a 7 : 3 mix of isopropanol and water, along with the addition of $CaCl_2$ (**Scheme 3.8a**). The calcium salt is thought to act as a hydroxide trap, forming $Ca(OH)_2$ which exhibits only partial solubility, thus reducing the concentration of hydroxide in solution, limiting basicity and increasing Fmoc lifetime.[23]

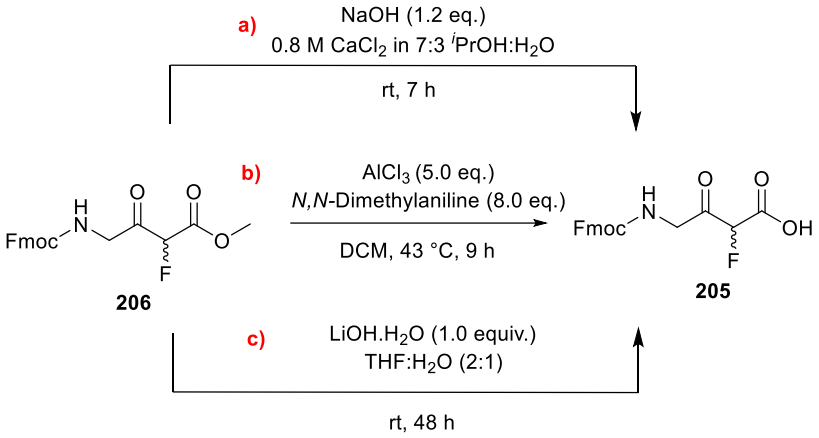

Scheme 3.8 - Conditions screened for saponification of *β*-ketoester **206**.

This method (**Scheme 3.8a**) did seem to bring about methyl ester removal without evidence for the characteristic by-product of Fmoc removal, dibenzofulvene, by ^{1}H NMR spectroscopy. However, the signal in the ^{19}F NMR spectrum (**Figure 3.8b**), which had shifted relative to the position of the starting material (**Figure 3.8a**) as expected, was weak, suggesting it was possible that very little fluorinated material was present. Furthermore, the resulting crude ^{1}H NMR spectrum (**Figure 3.9b**) appeared messy, and the distinctive doublet at 5.38 ppm corresponding to the CF-*H* functionality of the starting material (**Figure 3.9a**) was no longer apparent in the crude ^{1}H NMR spectrum after attempted

saponification (**Figure 3.9b**). This was in line with the observation that very little fluorinated material appeared to be present by ^{19}F NMR spectroscopy (**Figure 3.8b**) after the reaction was performed.

The work-up had involved acidification to pH 5, followed by dissolution in methanol and subsequent precipitation of product from water. To ensure that no deprotonated carboxylate was still sitting in the aqueous phase, accounting for the aforementioned poor recovery of fluorinated material, it was acidified again, this time to pH 3, before being extracted into DCM. Interestingly, after this second work-up, an unexpected shift was observed in the position of the ^{19}F NMR peak (**Figure 3.8c**), despite $CDCl_3$ being employed as the solvent of choice for all three NMR spectrums (**Figure 3.8**). Because of the confusion surrounding the reason for this, it was decided that alternative conditions would be pursued. Furthermore, an attempt to attach the crude material to 2-chlorotrityl chloride resin, Fmoc deprotect and couple on Fmoc-L-Phe-OH proved unsuccessful.

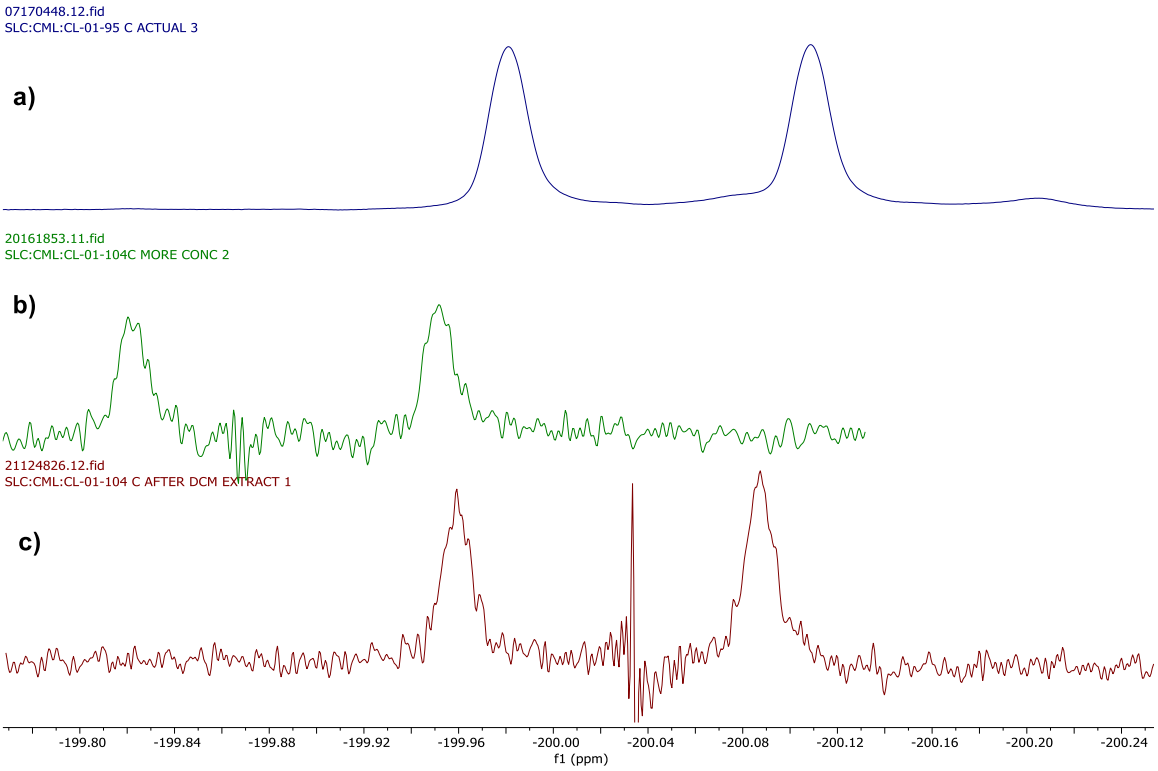

Figure 3.8 – ^{19}F NMR ($CDCl_3$) shifts for: starting material (**206**) prior to saponification attempt (**a**), obtained crude after first work-up of saponification reaction (**b**) and isolated crude after second work-up (**c**).

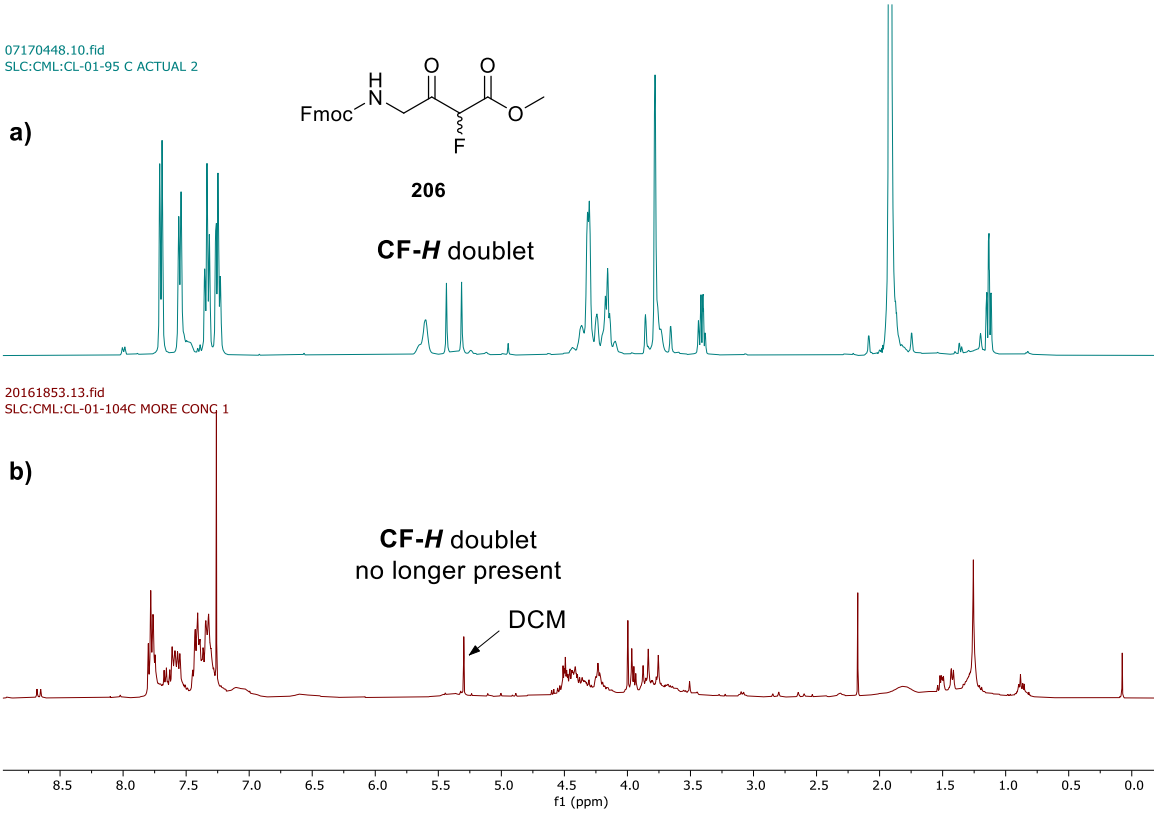

Figure 3.9 – ^{1}H NMR spectra ($CDCl_3$) for (**a**) starting material (**206**) prior to saponification attempt and (**b**) for crude material after first work-up of saponification reaction.

Given the problems encountered, it was decided that another approach would be trialled, this time using $AlCl_3$ in the presence of *N,N*-dimethylaniline at reflux (**Scheme 3.8b**).[24] Whilst evidence for the occurrence of methyl ester removal could be seen by ^{1}H NMR spectroscopy, and a shift in the position of the major fluorine signal was observed when compared with the starting material (**Figure 3.10**), several fluorine-containing impurities were also present after the reaction (**Figure 3.11**), rendering it rather inefficient.

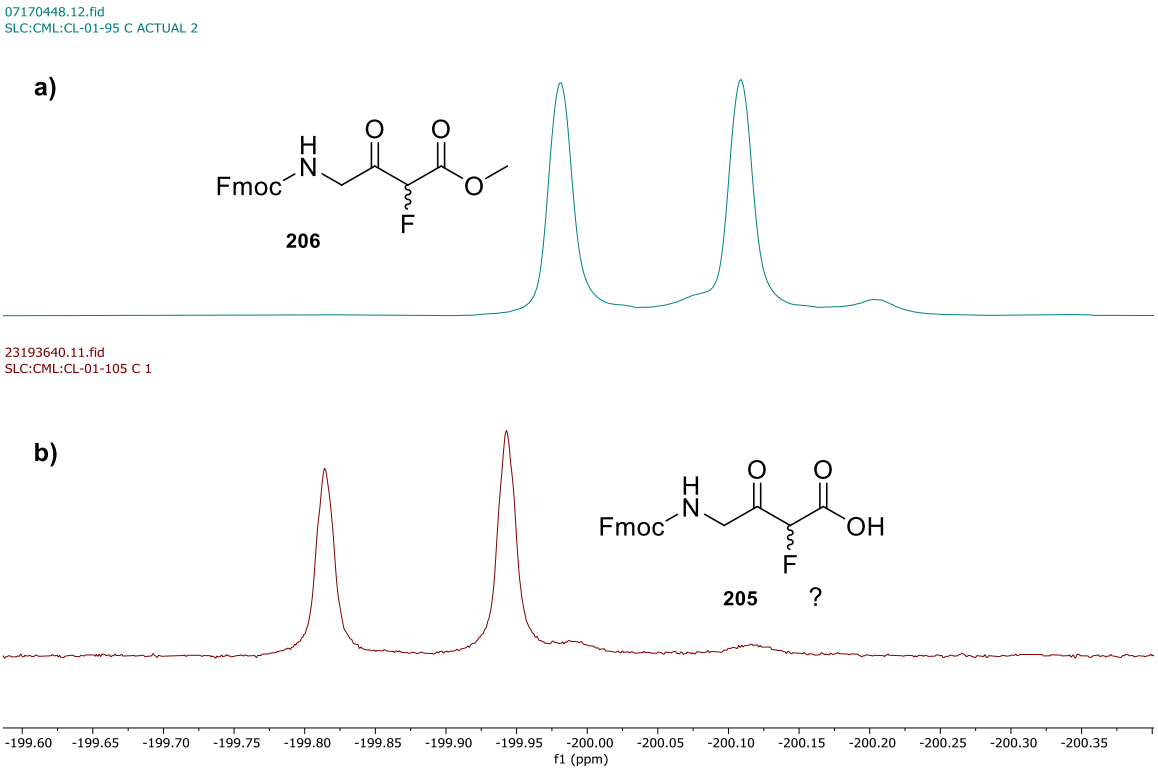

Figure 3.10 – Close-up of the main ^{19}F NMR shifts before (**a**) and after (**b**) saponification attempted with $AlCl_3$ and *N,N*-dimethylaniline. Both spectra were recorded in $CDCl_3$.

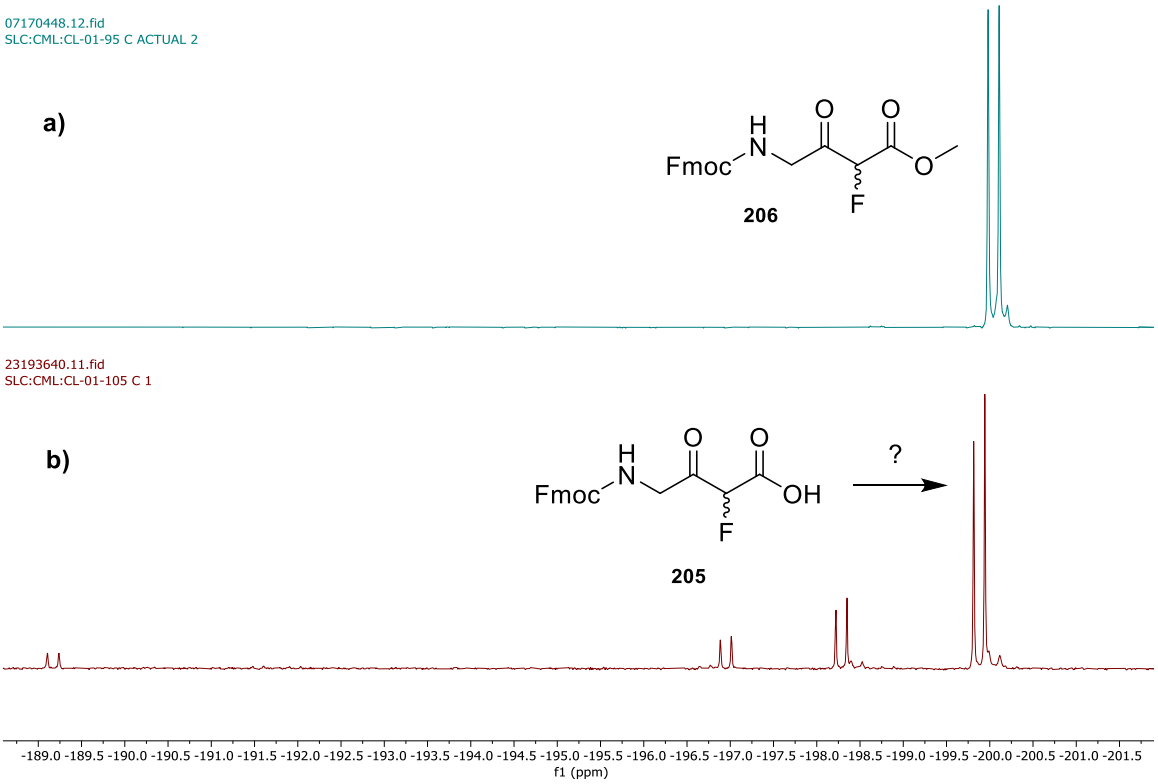

Figure 3.11 – ^{19}F NMR spectra ($CDCl_3$) for (**a**) *β*-ketoester **206** and (**b**) for the crude material after attempted saponification of **206** with $AlCl_3$ and *N,N*-dimethylaniline.

In order to confirm that standard saponification conditions would not be suitable for substrate **206**, the reaction was also attempted using LiOH.H_2O according to **Scheme 3.8c**. Despite concerns surrounding unwanted Fmoc removal, the key problem came in relation to the C-F bond, whilst the Fmoc group remained mostly intact. When using 1.0 equivalent of LiOH.H_2O, comparison of the ^{19}F NMR spectra before (**Figure 3.12a**) and after (**Figure 3.12b**) attempted saponification revealed an unexpected apparent increase in di-fluorinated product (**217**) relative to mono-fluorinated material (**205**) (**Figure 3.12**), leaving very little, if any, of the desired mono-fluorinated product (**205**). In addition to this, it was evident that fluoromethyl ketone **218** had started to form, likely due to heat being applied during rotary evaporation, bringing about premature decarboxylation.

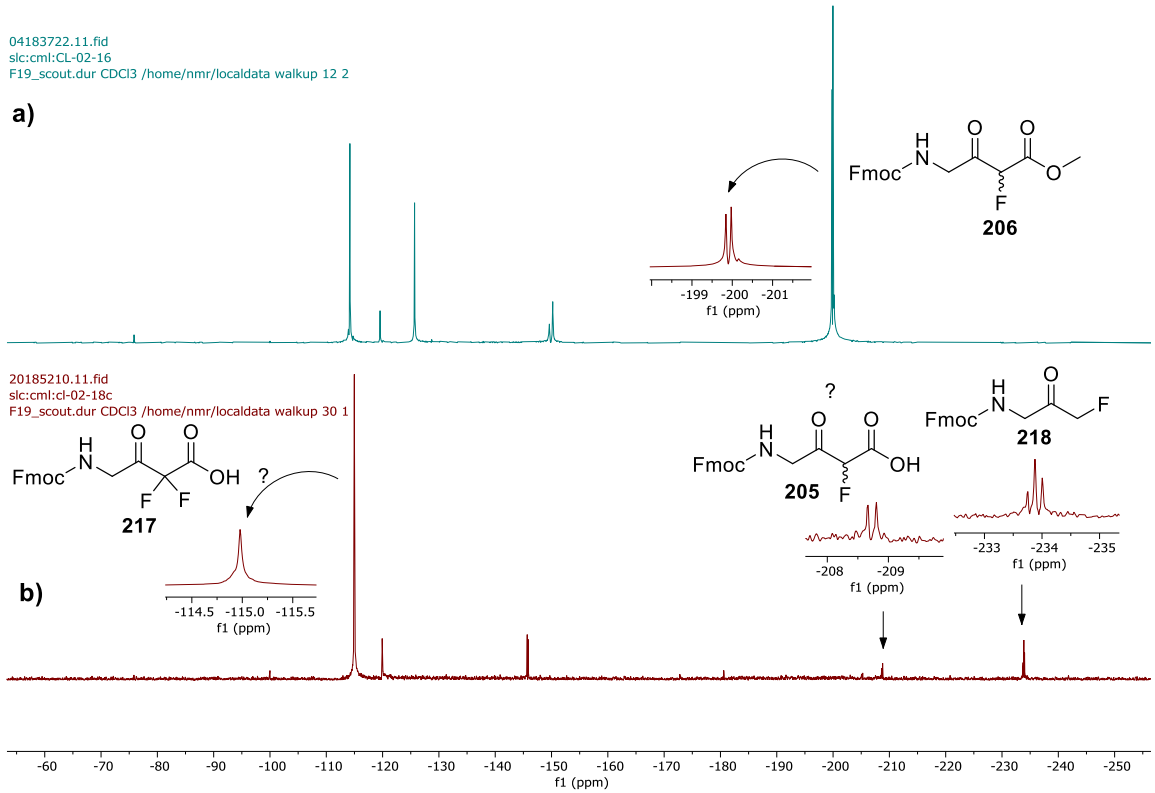

Figure 3.12 - Crude ^{19}F NMR (^1H coupled) spectrum ($CDCl_3$) before (**a**) and after (**b**) saponification of **206** with LiOH.H_2O.

In order to further probe what was causing this unexpected increase in di-fluorinated material, the same saponification conditions were applied to 2-fluoro-3-oxobutyric acid methyl ester (**214**), the test substrate (**Scheme 3.9**). This would help

determine if the Fmoc group or some other component of molecule **206** was playing a role. Interestingly, it was discovered that a similar ^{19}F NMR profile was observed when the test substrate (**214**) was saponified using $LiOH.H_2O$, again revealing an apparent increase in the proportion of di-fluorinated material (**Figure 2.13b**) in conjunction with methyl ester removal (**Figure 3.13**). A proposed mechanism for the significant increase in di-fluorinated product observed during attempted saponification of fluorinated *β*-ketoesters is given in **Scheme 3.10**.

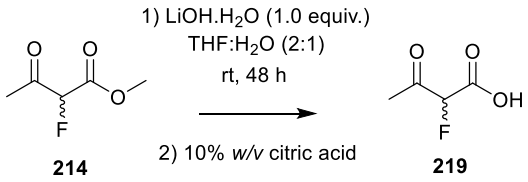

Scheme 3.9 – Conditions employed for attempted saponification of *β*-ketoester **214**.

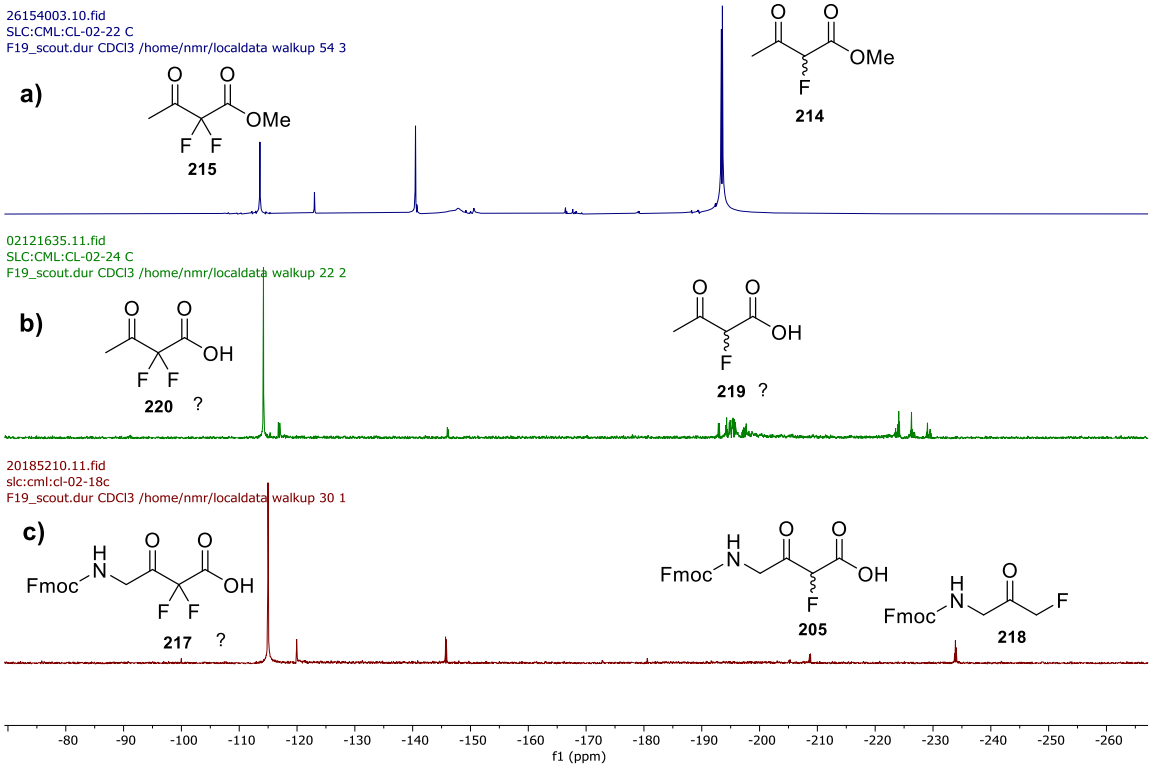

Figure 3.13 - Crude ^{19}F NMR spectrum ($CDCl_3$) after fluorination of **213** (**a**), saponification of **208** (**b**) and saponification of **206** (**c**), included for comparison.

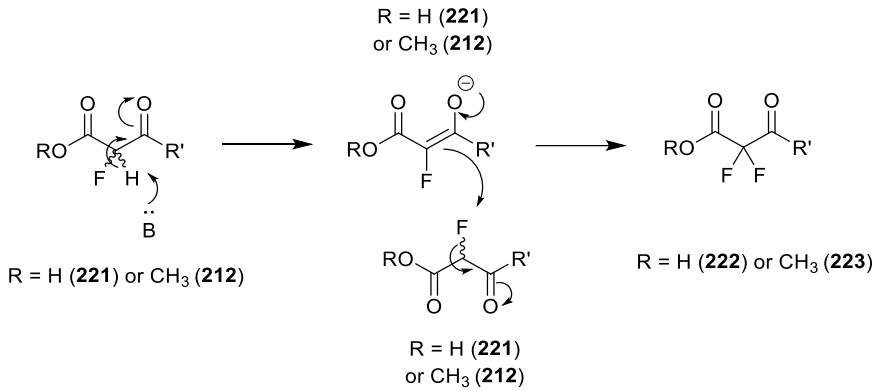

Scheme 3.10 - Proposed mechanism for the increase in di-fluorinated material observed during attempted saponification of mono-fluorinated *β*-ketoesters with $LiOH.H_2O$.

With the intention of gaining further insight into this phenomenon and to determine whether issues were exclusively observed only when fluorine was present, saponification of non-fluorinated *β*-ketoester **207** was attempted, again using $LiOH.H_2O$ (**Scheme 3.11**). This time, after the addition of 1.0 equivalent of base, although some methyl ester removal had occurred within 48 hours, as indicated by a reduction in the methyl ester peak integral, the major component was still starting material (**207**), as seen by comparing the ^1H NMR spectrum of the starting material (**Figure 3.14a**) against that obtained after attempted saponification (**Figure 3.14b**). This was likely because the acidic alpha proton had simply been deprotonated by the base and re-protonated during the acidic workup. Re-addition of base; 2.0 equivalents this time, and an additional 24-hour reaction period brought about Fmoc removal, as confirmed by the presence of dibenzofulvene (**225**, **Figure 3.14c**). It was therefore concluded that the presence of the acidic alpha protons in the Fmoc-protected *β*-ketoester complicates saponification under standard basic conditions due the potential for deprotonation in the presence of 1.0 equivalent of base and Fmoc removal when an excess of base is employed. Furthermore, it was also hypothesised that when a fluorine atom is present in the alpha position, there is potential for defluorination by another 1,3-dicarbonyl molecule in its enolate form under basic conditions, resulting in an overall increase in di-fluorinated material relative to mono-fluorinated product.

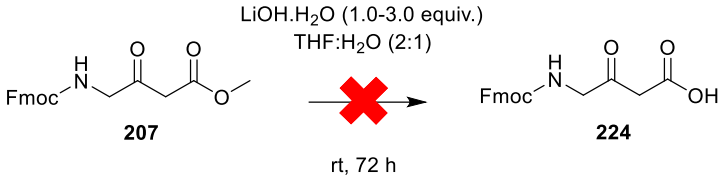

Scheme 3.11 - Conditions employed for attempted saponification of non-fluorinated *β*-ketoester **207** using $LiOH.H_2O$.

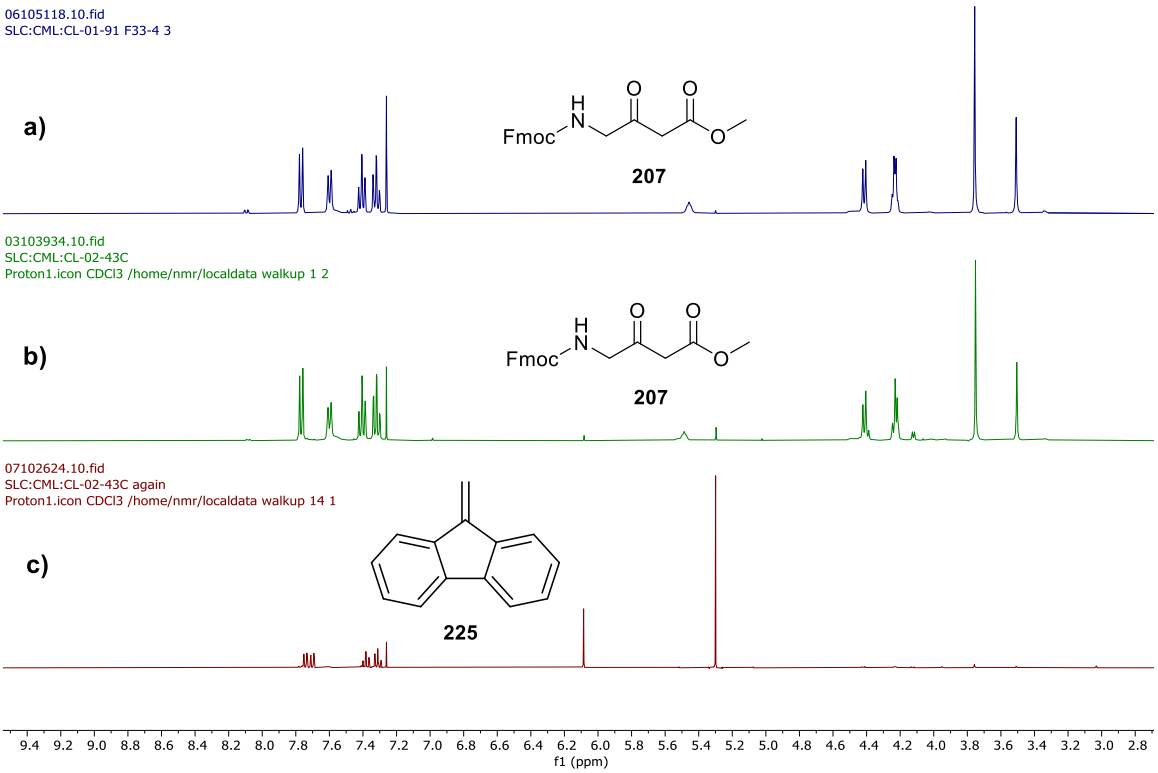

Figure 3.14 - Crude ^1H NMR spectra ($CDCl_3$) prior to saponification of **207** (**a**) and after attempted saponification with 1.0 eq. (**b**) and 2.0 eq. (**c**) of $LiOH.H_2O$.

3.3 Alternative route to Fmoc-protected *β*-ketoacid building block 205

Given the challenges encountered during methyl ester deprotection, an alternative strategy was sought. Thus, the option of by-passing protection of the acid altogether was considered; however, it first needed to be established whether oxidation and subsequent fluorination could be achieved efficiently in the absence of a protecting group on the acid. If found to be possible, this would conveniently allow direct attachment to a solid support without the need for deprotection to the acid (**205**), as shown in **Scheme 3.12**.

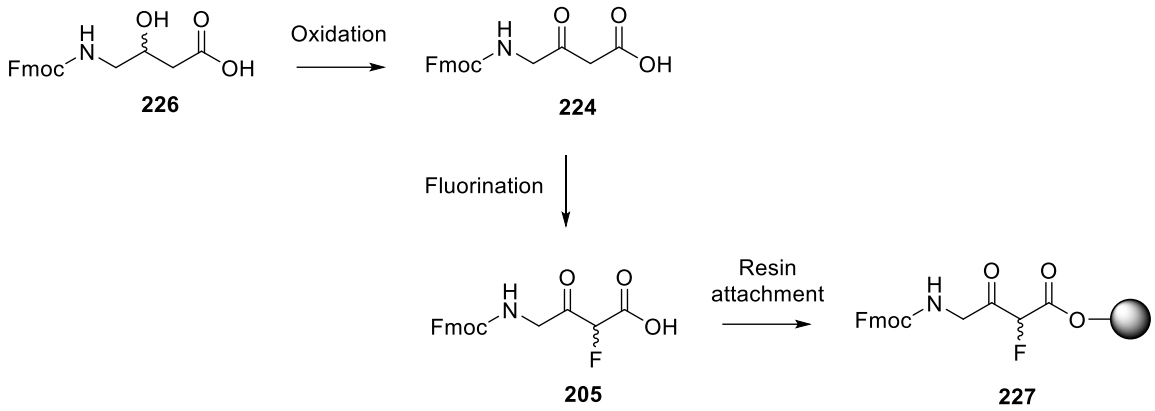

Scheme 3.12 – Proposed route to building block **205** for SPPS applications.

Starting from commercially available 4-amino-3-hydroxybutyric acid (**209**), the first step involved Fmoc protection (**Scheme 3.13**). This was initially attempted through reaction with Fmoc succinimide in a solution of aqueous $NaHCO_3$, acetone and dioxane for 4.5 hours (**Scheme 3.13a**). After acidification, the product was extracted into ethyl acetate and purified further by column chromatography; however, a poor yield of only 10% was achieved. It was thought this could in part be explained by a loss of some product (**226**) to the aqueous layer during the work-up. Repeating this step with a longer reaction time of 24 hours, acidifying, and purifying by column chromatography whilst excluding the extraction step seemed to improve the yield to 79% (**Scheme 3.13b**), although some impurity peaks were present by ^1H NMR analysis, including a peak at 2.7 ppm associated with the Fmoc succinimide starting material.

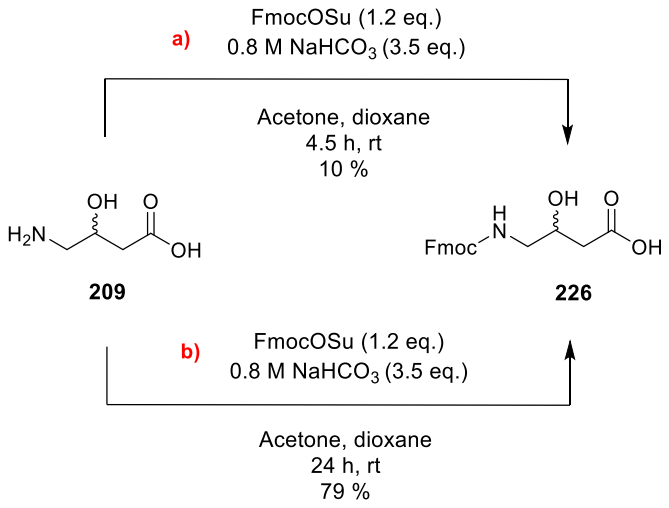

Scheme 3.13 Conditions screened for Fmoc protection of **209**.

After Fmoc protection of 4-amino-3-hydroxybutyric acid (**209**) to give **226**, oxidation to *β*-ketoacid **224** was attempted, initially using 3.0 equivalents of IBX in ethyl acetate at reflux overnight. However, after a 24-hour period, starting material (**226**) was still apparent in the crude material by ^{1}H NMR analysis. After re-addition of a further 3.0 equivalents of IBX and another 24 hours at reflux (**Scheme 3.14a**), neither product (**224**) nor starting material (**226**) was convincingly evident from the crude ^{1}H NMR spectrum, with a predominance of IBX aromatic peaks visible. It seems likely that the application of heat could have led to decarboxylation of the oxidised substrate; however, the ^{1}H NMR spectrum was found to be difficult to decipher, so this was not confirmed. The use of DMP at room temperature overnight was therefore trialled as an alternative approach (**Scheme 3.14b**). However, the presence of starting material (**226**), among other impurities, was confirmed by ^{1}H NMR spectroscopy, and no product (**224**) was isolated after column chromatography.

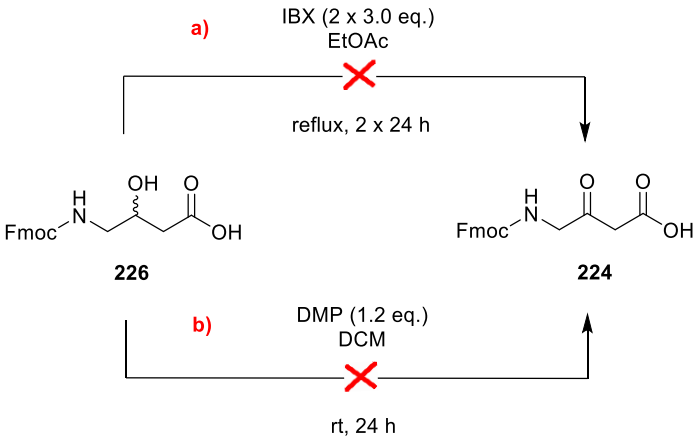

Scheme 3.14 – Conditions employed during unsuccessful attempted oxidation of **226** to **224**.

3.4 On-Resin Oxidation and Fluorination

Whilst oxidation and fluorination reactions are more typically utilised in solution-phase chemistry than on resin, it was of interest to determine whether these conditions could be applied to substrate **226** on a solid-support (**Scheme 3.15**). This would eliminate the need for carboxylic acid protection and deprotection prior to resin loading, as the resin itself would act as a temporary protecting group.

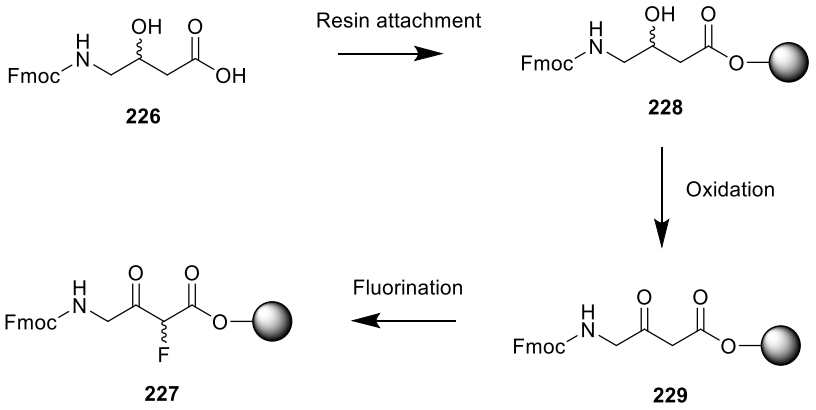

Scheme 3.15 – Proposed on-resin oxidation and electrophilic fluorination to give **227**.

Starting from Fmoc-protected *β*-hydroxyacid **226**, 2-chlorotrityl chloride resin attachment was achieved through standard loading procedures, similar to that described in **Chapter 7** (**Section 7.3.1.1**). The *β*-hydroxyacid (**226**) was added in 5:2 (7 ml) DCM:DMF to ensure complete dissolution during this step. Oxidation was then attempted

using 3.0 equivalents of DMP in DCM at room temperature for 2.5 hours. Evidence for successful oxidation to **224** on resin was identified by LCMS (**Figure 3.15**); however, a significant amount of hydroxy starting material **226** was also visible (**Figure 3.15a**). Repeating the oxidation in DMF instead of DCM resulted in a significant increase in conversion to oxidised product (**224**, **Figure 3.15b**).

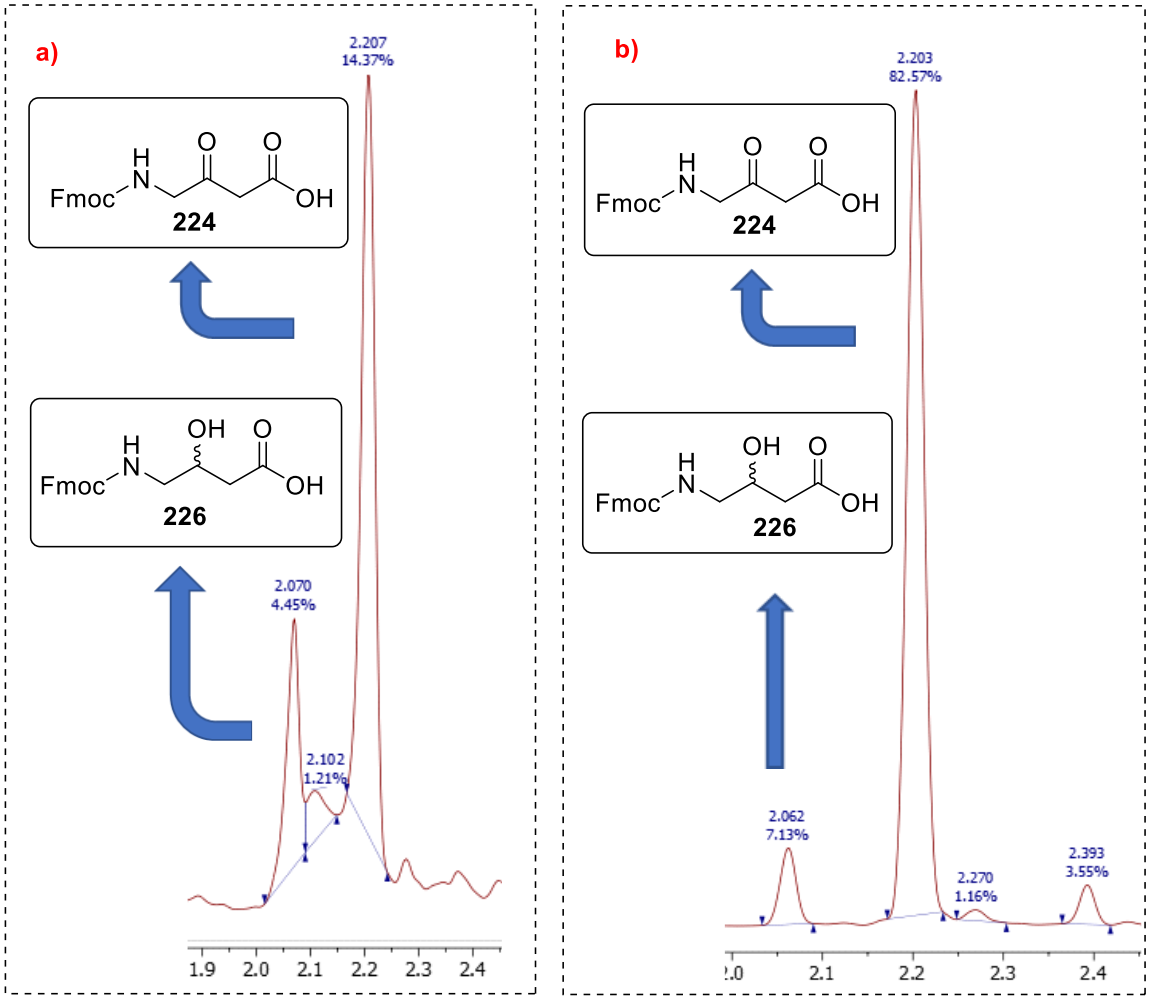

Figure 3.15 – LC UV trace for on-resin oxidation of **226** in DCM (**a**) and in DMF (**b**).

On-resin fluorination was attempted using conditions similar to that previously described (**Table 3.3**, **entry 3**). This involved the resin being treated with 1.1 equivalent of Selectfluor and 0.05 equivalents of $CpTiCl_3$ at room temperature overnight. However, instead of using acetonitrile, the reaction was instead performed in DMF initially; a more commonly used solvent for solid-phase synthesis. Unfortunately, evidence for successful

formation of the target (**205**) was not convincing by LCMS, and no product was identified by ^{19}F NMR spectroscopy. Thus, the reaction was repeated, this time with 10 equivalents of Selectfluor and 1.0 equivalent of $CpTiCl_3$. Again, there did not appear to be a significant amount of product formation, if any at all, seen by LCMS. The reaction was then attempted again using 10 equivalents of Selectfluor and 1.0 equivalent of $CpTiCl_3$ overnight, but this time utilising a 5:3 MeCN:DMF solvent mixture. However, no improvement was observed, so the method was not pursued further.

3.5 Alternative Protecting Group Strategy

In the wake of the challenges encountered during methyl ester deprotection in **Section 3.2.5**, the lack of success when attempting oxidation in the absence of a protecting group on the carboxylic acid (**Section 3.3**) and the inability to efficiently fluorinate on resin (**Section 3.4**), it was suggested that modifying the approach described in **Section 3.1** by changing the protecting group strategy from Fmoc/OMe to Fmoc/O^{t}Bu may be a more feasible approach (**Scheme 3.16**). This would allow deprotection to the free carboxylic acid under acidic rather than basic conditions, thus avoiding the unwanted ^{19}F NMR peak shifts observed in base and eliminating the risk of Fmoc removal. Care would have to be taken to ensure that premature decarboxylation to the FMK does not occur during ^{t}Bu ester removal as this would disable resin attachment. However, it was proposed that with careful handling, the desired target (**205**) could be isolated. A retrosynthetic scheme depicting the modified route is shown in **Scheme 3.16**.

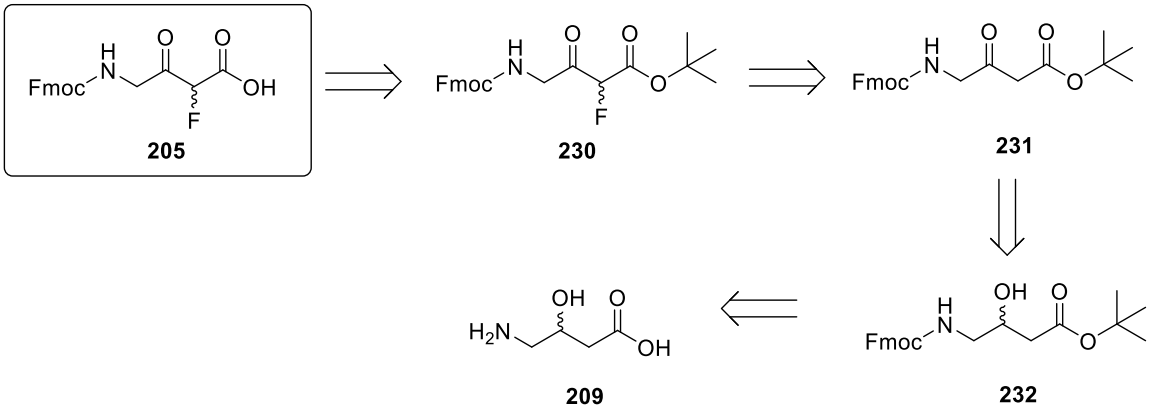

Scheme 3.16 – Proposed retrosynthetic scheme for accessing Fmoc-FMK building block **205** for SPPS.

3.5.1 Fmoc and ^{t}Bu Ester Protection of 4-Amino-3-Hydroxybutyric Acid 209

Starting from commercially available 4-amino-3-hydroxybutyric acid (**209**), the first step involved Fmoc protection, which was carried out according to **Scheme 3.17a**, as first described in **Section 3.3**. Protection of the carboxylic acid (**226**) as the *tert*-butyl ester (**232**) was then accomplished through reaction with 2.0 equivalents of *tert*-butyl 2,2,2-trichloroacetimidate (TBTA) in ethyl acetate (**Scheme 3.17b**). Additional formation of di-protected material, in which ^{t}Bu was added to both the acid and the hydroxy functionality, contributed towards a low yield. An attempt to run the reaction with just 1.0 equivalent of TBTA over a shorter reaction period of 24 hours didn't seem to improve the yield significantly. Because of the inefficiency of the ^{t}Bu protection step and evidence for competing di-protection, an alternative route was pursued for accessing *β*-ketoacid **205** (described in **Section 3.6**).

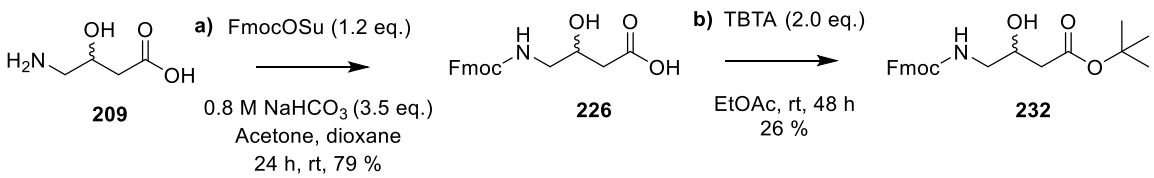

Scheme 3.17 – Conditions used for Fmoc protection of **209** followed by ^{t}Bu ester protection.

3.6 Alternative Route to Fmoc-Protected *β*-Ketoacid Building Block 205

Inspired by the work reported by E. Haug and co-workers in which a 1,3-dicarbonyl system was constructed from an Fmoc-protected amino acid using enolate chemistry (**Scheme 3.18**),[25] a new route was proposed utilising these conditions (**Scheme 3.19**). Not only does it reduce the number of steps through eliminating the need for Fmoc protection, ^{t}Bu ester formation and oxidation, but it also benefits from an expanded substrate scope. This is because, assuming the sidechain is compatible under strongly basic conditions, any amino acid of choice could be used as a building block, allowing for a wide selection of sidechain moieties at the C-terminal end of the peptide. The presence of the Asp(OMe) sidechain at the C-terminal end of peptidyl FMKs is particularly pertinent for caspase inhibition, with multiple examples reported in the literature.[26–31] Thus, this was considered a better approach for accessing more biologically relevant targets.

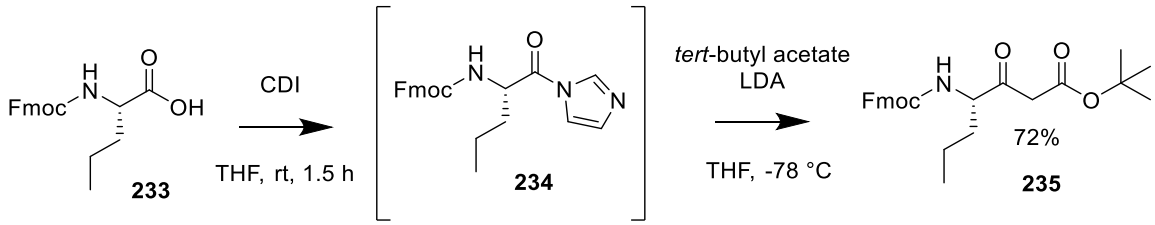

Scheme 3.18 – Enolate chemistry described by E. Haug and co-workers for accessing *β*-ketoester **230** from Fmoc-L-Norvaline (**233**) using CDI, LDA and *tert*-butyl acetate.[25]

As illustrated by retrosynthetic **Scheme 3.19**, the utilisation of the aforementioned enolate chemistry would in theory allow access to *β*-ketoester **237** in just one-step. This could then be fluorinated and the ^{t}Bu ester deprotected to give *β*-ketoacid **200** for use in SPPS. Thus, the hope was that this would provide a quick and efficient means of acquiring a catalogue of peptidyl-FMK building blocks with a selection of different R groups in the sidechain.

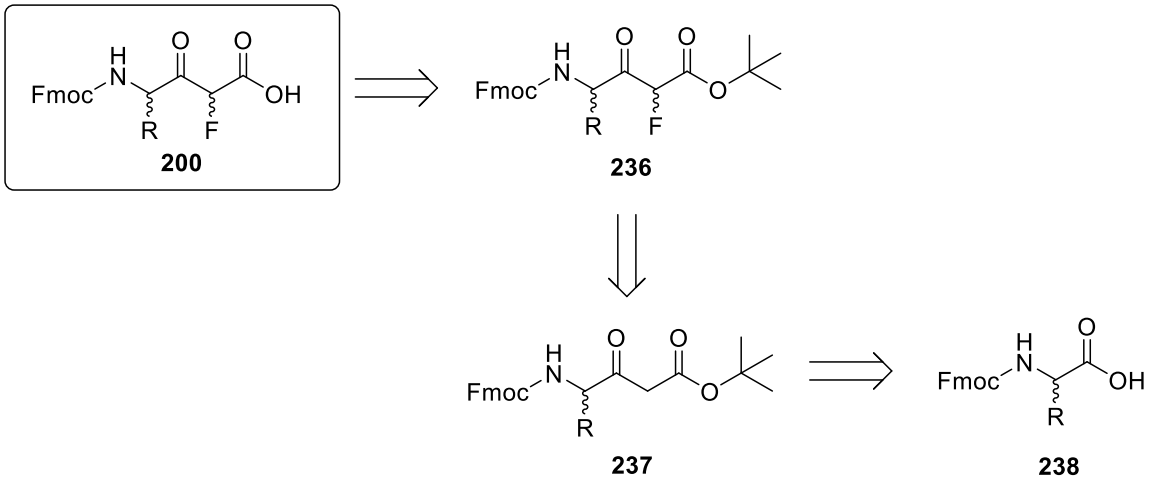

Scheme 3.19 – Proposed retrosynthetic scheme for accessing Fmoc-FMK building block **200** for SPPS. R = an amino acid sidechain group compatible under strongly basic conditions.

3.6.1 Formation of *β*-Ketoesters via Enolate Chemistry

Starting from an Fmoc-protected amino acid of choice (**239**), activation with 1,1'-carbonyldiimidazole (CDI) in dry THF for 1.5 hours allowed *in situ* formation of intermediate **240** (**Scheme 3.20**). This was then reacted with the enolate of *tert*-butyl acetate at -78 °C under an inert atmosphere for around 1-3 hours, which had been formed in the presence of lithium diisopropylamide (LDA) for 20 minutes, to give the corresponding *β*-ketoester, which was isolated after acidification with 1 M HCl, extraction into ethyl acetate and column chromatography. A selection of compounds was accessed, as shown in **Scheme 3.20**. The isolated yields tended to be relatively low, with evidence in some cases for the formation of dibenzofulvene due to the occurrence of Fmoc removal seen by ^{1}H NMR spectroscopy and LCMS, suggesting enolate formation had not gone to completion prior to reaction with the activated amino acid (**240**), leaving unreacted LDA available for Fmoc removal. Additionally, starting material was identified in some cases. Leaving the reaction between activated amino acid **240** and the solution containing the enolate of *tert*-butyl acetate beyond 1.5 hours did not seem to seem to improve the yield. However, this wasn't considered to be a major concern since the reaction was replacing a multi-step process involving Fmoc protection, ^{t}Bu ester formation and oxidation, combining it into one single step.

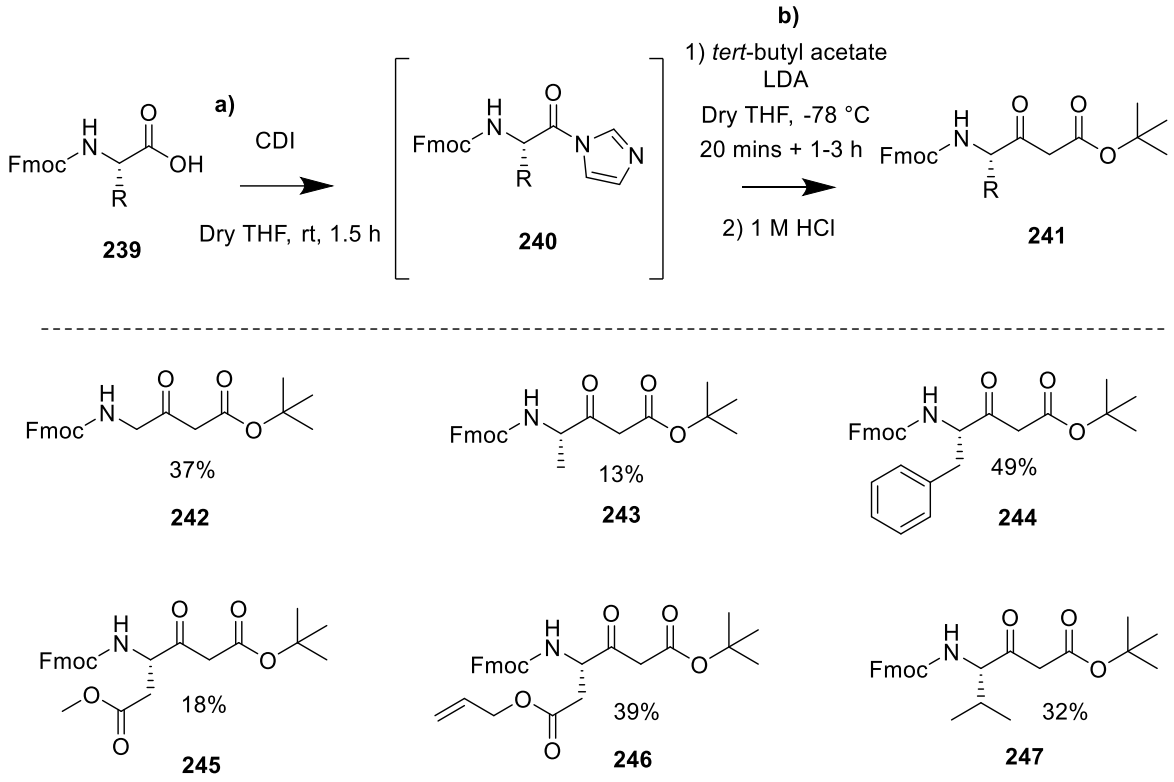

Scheme 3.20 – A selection of *β*-ketoesters synthesised using CDI, LDA and *tert*-butyl acetate.

3.6.2 Fluorination of *β*-Ketoesters

Mono-fluorination of the *β*-ketoesters shown in **Scheme 3.21** was achieved using Selectfluor in conjunction with a catalytic amount of $CpTiCl_3$ in MeCN, as described in **Section 3.2.4**. This allowed access to a selection of fluorinated building blocks (**Scheme 3.21**), with isolated yields ranging from 52-71% including a smaller proportion of di-fluorinated material which did not prove completely separable by column chromatography. In most cases, competing di-fluorination was kept to a minimum after purification (less than 12%); however; for the Fmoc-phenylalanine derived substrate (**244**), di-fluorination did seem more prominent (around 22%). The relative percentages of mono- to di-fluorinated material after column chromatography, as determined by ^{19}F NMR spectroscopy, are given in **Scheme 3.21**. Post-column chromatography ^{19}F NMR spectra are provided for fluorinated *β*-ketoesters **250** and **252** in **Figure 3.16** and **Figure 3.17** respectively.

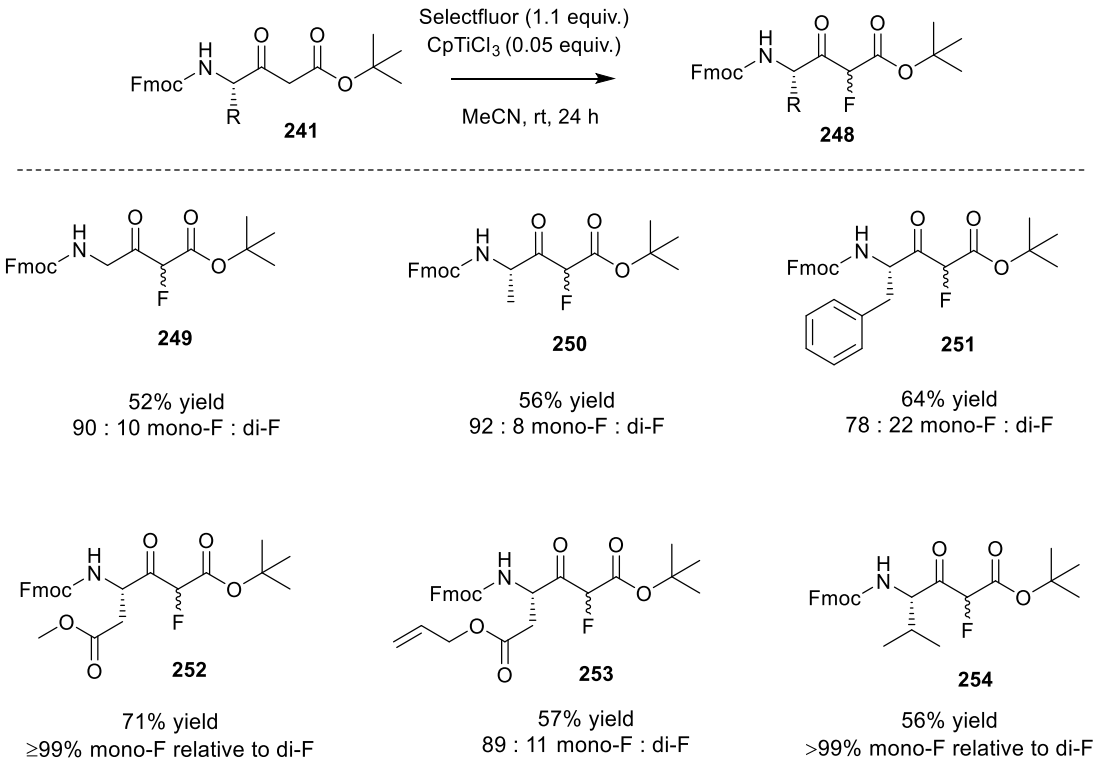

Scheme 3.21 – A selection of fluorinated *β*-ketoesters synthesised using F-TEDA and $CpTiCl_3$. Isolated yields are given, along with the ratio of mono-fluorinated material relative to di-fluorinated material after column chromatography, as determined by ^{19}F NMR spectroscopy.

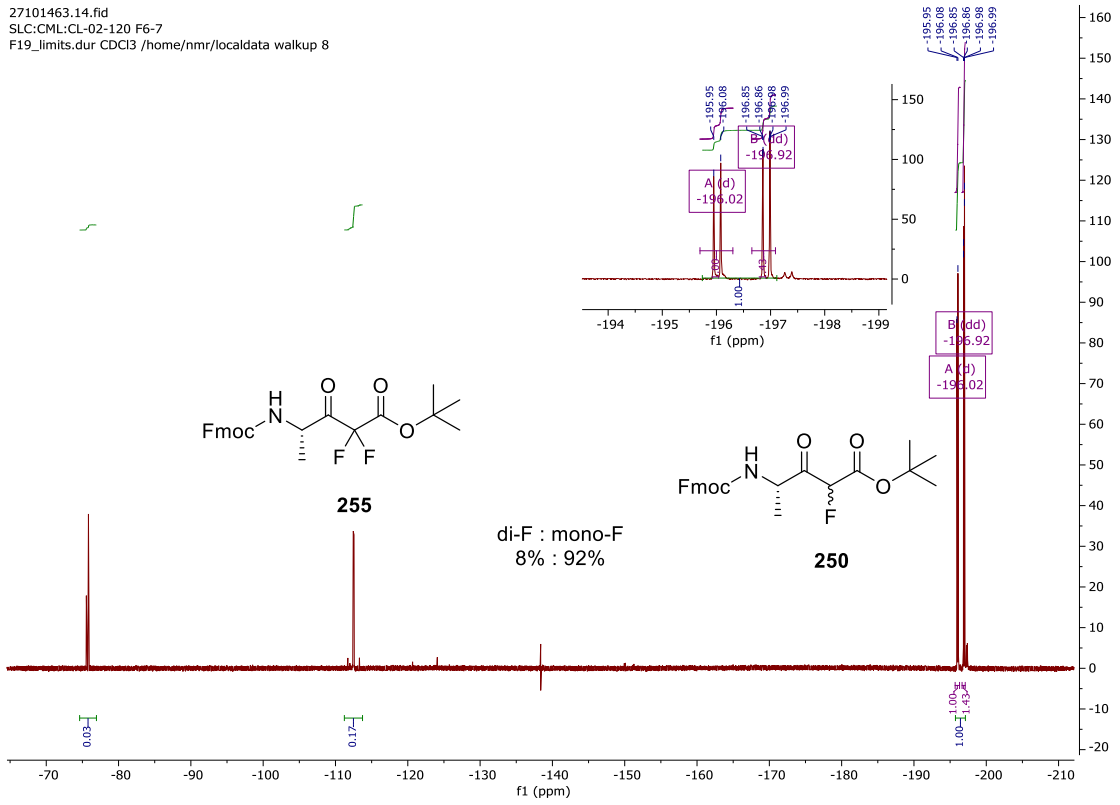

Figure 3.16 – Post-column chromatography ^{19}F NMR (^{1}H coupled) spectrum ($CDCl_3$) of *β*-ketoester **250** along with a small amount of di-fluorinated material (**255**) and other impurities.

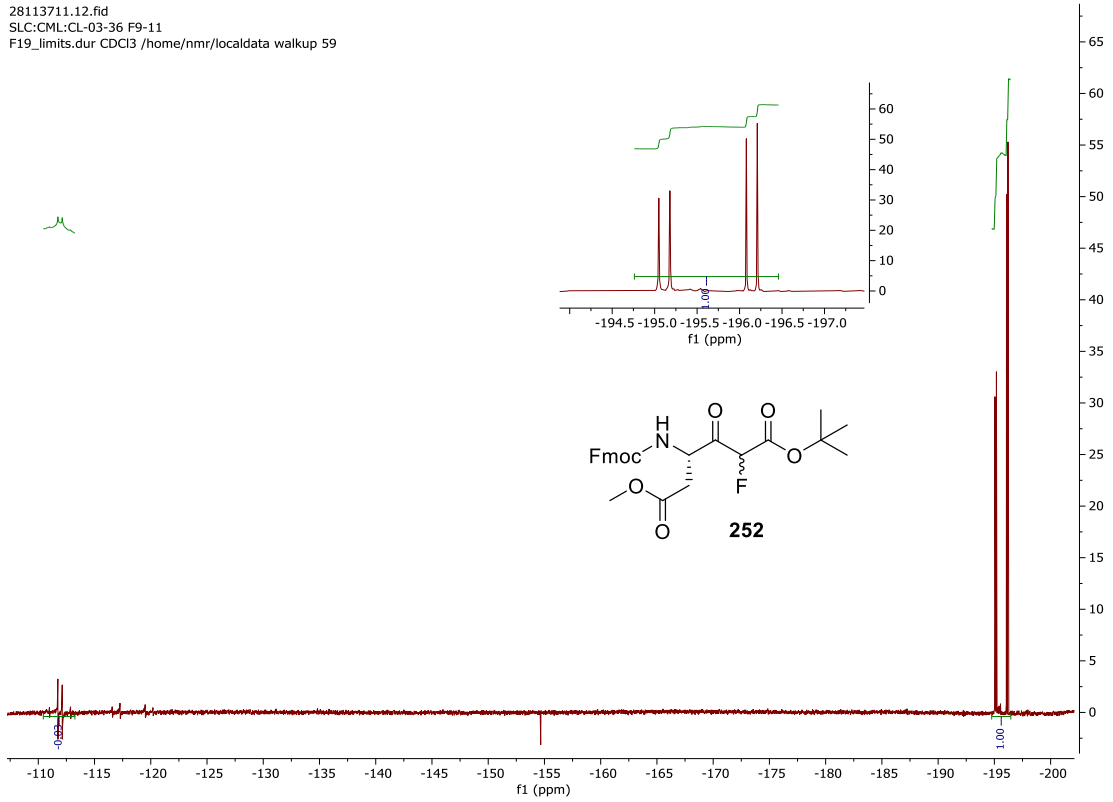

Figure 3.17 – Post-column chromatography ^{19}F NMR (^{1}H coupled) spectrum ($CDCl_3$) of *β*-ketoester **252**.

3.6.3 *tert*-Butyl Ester Deprotection of Fluorinated *β*-Ketoesters

With the fluorinated building blocks in hand, it was desirable to access the corresponding free carboxylic acids by removal of the *tert*-butyl ester in order to enable attachment to a solid support. As previously mentioned, it was envisioned that the challenge would be successfully deprotecting whilst avoiding premature decarboxylation, as the carboxylic acid handle is necessary for resin loading. The transformation was first trialled using Fmoc-Gly-OH derived *β*-ketoester **249** (**Scheme 3.22**) before transferring these conditions to other similar compounds possessing variable sidechains. Addition of 30% TFA in DCM to **249** for a period of 1 hour at room temperature (**Scheme 3.22a**) resulted in a 3 : 1 ratio of deprotected to protected material (as determined by ^{19}F NMR spectroscopy), with negligible FMK formation. An extended reaction time of 2.5 hours (**Scheme 3.22b**) resulted in complete conversion, with a small amount of decarboxylation observed. **Figure 3.18** illustrates a shift in the position of the ^{19}F NMR peak due to ^{t}Bu

ester removal by showing a close-up of the ^{19}F NMR spectra for the starting material (**a**), partially deprotected material after 1 hour (**b**) and fully deprotected product (**205**) after 2.5 hours (**c**), whilst **Figure 3.19a-c** shows a wider-angle view of the same spectra, proving that FMK formation was kept to a minimum.

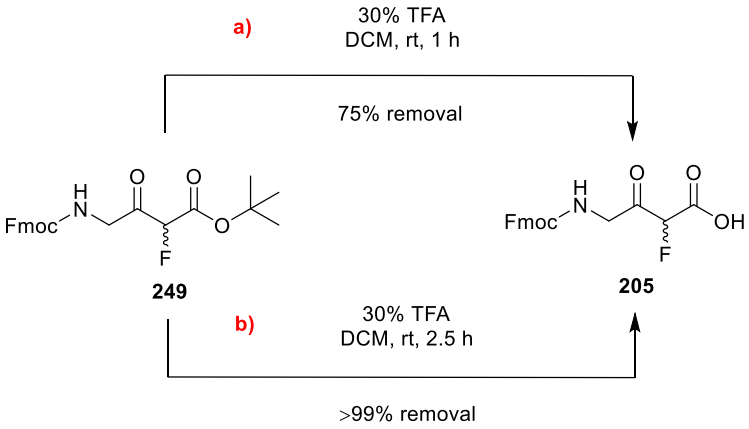

Scheme 3.22 – Conditions employed for ^{t}Bu ester deprotection over 1 h (**a**) and 2.5 h (**b**) periods.

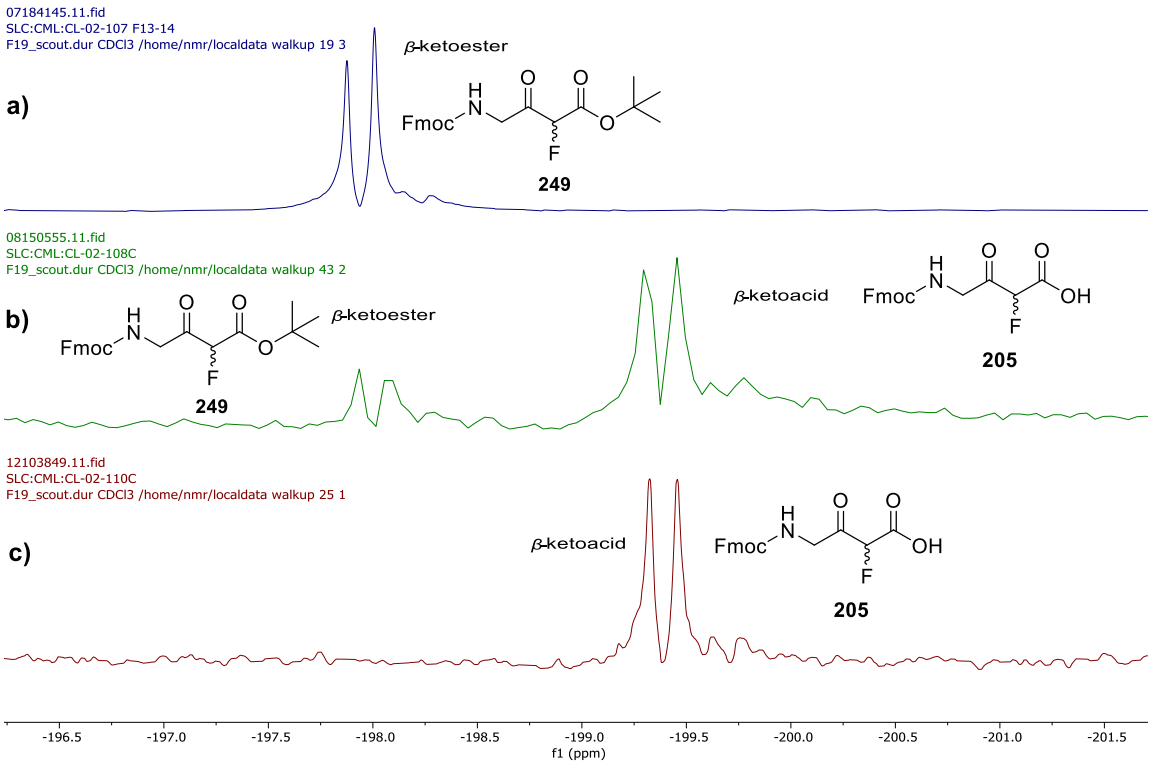

Figure 3.18 – Close-up view of the ^{19}F NMR (^{1}H coupled) spectra ($CDCl_3$) for starting material **249** (**a**), partially deprotected material after 1 h (**b**) and fully deprotected product (**205**) after 2.5 h (**c**).

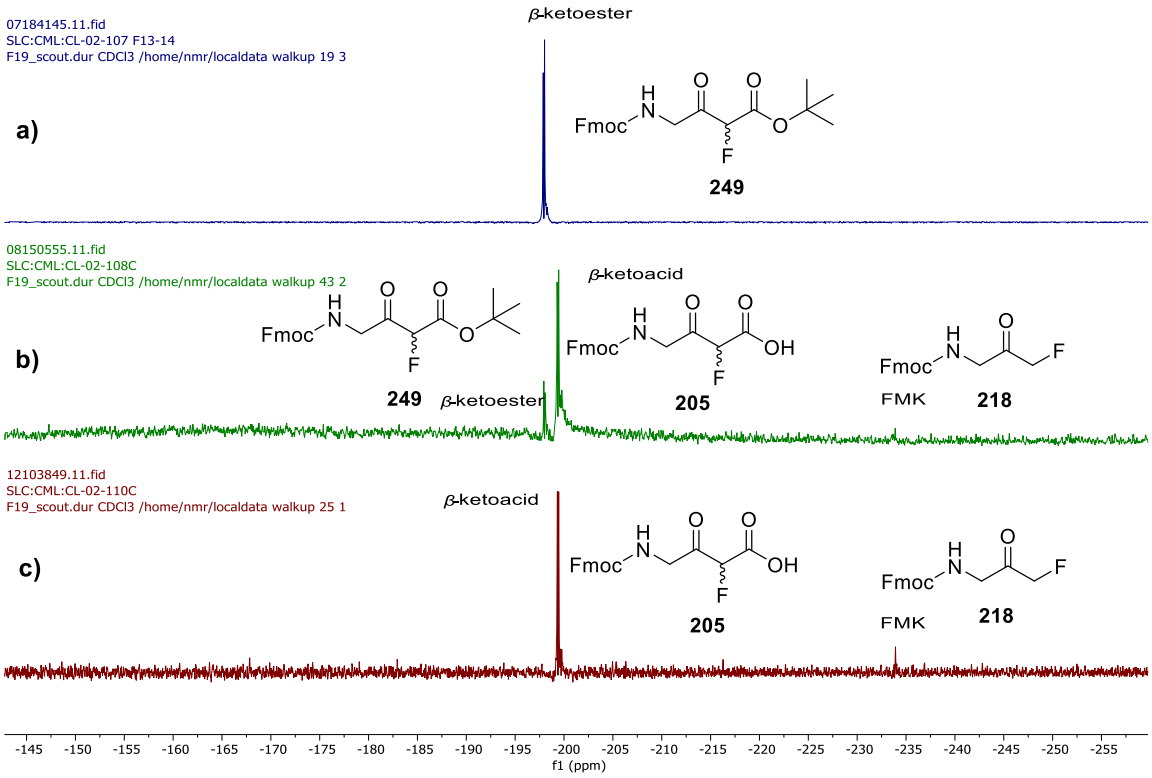

Figure 3.19 – ^{19}F NMR (^{1}H coupled) spectra ($CDCl_3$) showing regions typical of mono-fluorination and FMK formation for (**a**) the starting material, (**b**) partially deprotected material after 1 h and (**c**) fully deprotected product after 2.5 h (**c**).

Interestingly, in some cases of ^{t}Bu ester removal, there did appear to be a noticeable increase in di-fluorinated material (-115 ppm) relative to mono-fluorinated (-199 ppm), as can be seen by comparing the ^{19}F NMR spectrum for *β*-ketoester **249** (**Figure 3.20a**) with that taken after *tert*-butyl ester removal (**Figure 3.20b**). Integration of the peaks revealed that difluorinated material increased from 10% in the starting material to around 22% in the crude product relative to mono-fluorinated product.

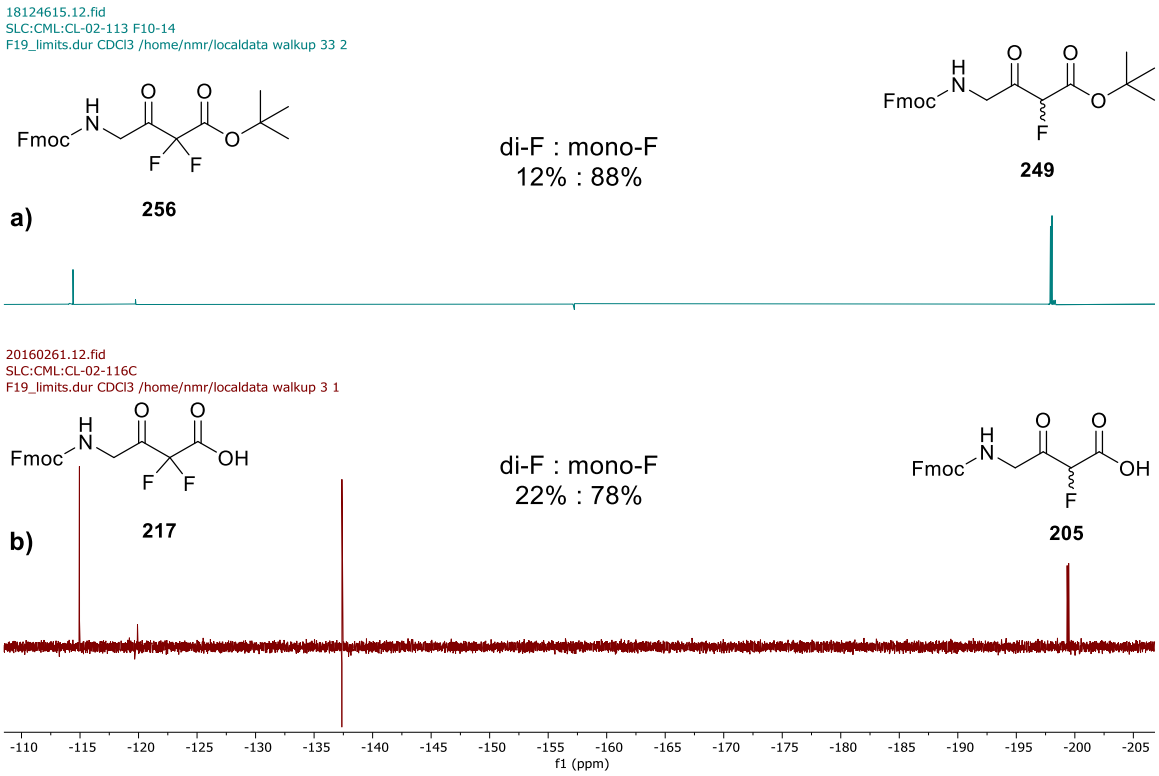

Figure 3.20 – ^{19}F NMR (^{1}H coupled) spectra ($CDCl_3$) showing regions of mono- (-199 ppm) and di-fluorination (-115 ppm) before (**a**) and after (**b**) ^{t}Bu ester removal of *β*-ketoester **249**.

In general, during these deprotections, unwanted FMK formation (^{19}F NMR resonance, around -234 ppm) was kept to a minimum through quick and careful handling. Excess TFA removal was assisted through co-evaporation with diethyl ether under reduced pressure as rapidly as possible, with the water bath kept low at around 40 °C. Lyophilisation was then employed in an attempt to remove residual TFA without the application of heat, and the resulting *β*-ketoacid used rapidly for resin loading or stored in the freezer. On one occasion, when the deprotected material was left exposed to air over the weekend to enable complete evaporation of residual TFA, the FMK became the major component. This was somewhat encouraging, as it re-affirmed the belief that decarboxylation would occur with relative ease under acidic conditions,[25] and thus should occur in conjunction with resin cleavage after SPPS, allowing generation of the final peptidyl FMKs. In order to put this to the test in a more controlled manner prior to resin loading, a one-pot ^{t}Bu ester deprotection and decarboxylation[25] of Fmoc-Asp(OMe)-OH

derived *β*-ketoester **252** (**Scheme 3.23**) was attempted. When this was first attempted using 10% TFA at room temperature overnight, a significant amount of starting material was still present (**252**). Re-addition of reagents, this time 50% TFA in DCM at room temperature for a further 24-hour period, brought about complete conversion, giving the pure product (**257**) after column chromatography, characterised by a triplet in the ^{19}F NMR spectrum (**Figure 3.21**).

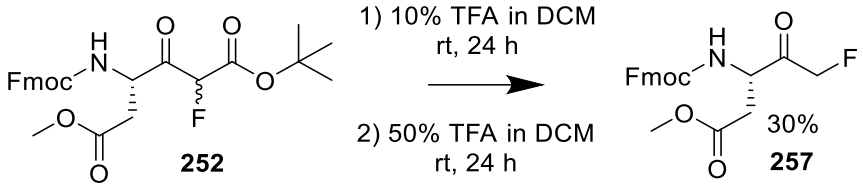

Scheme 3.23 – Conditions employed for a one-pot ^{t}Bu ester deprotection and decarboxylation.

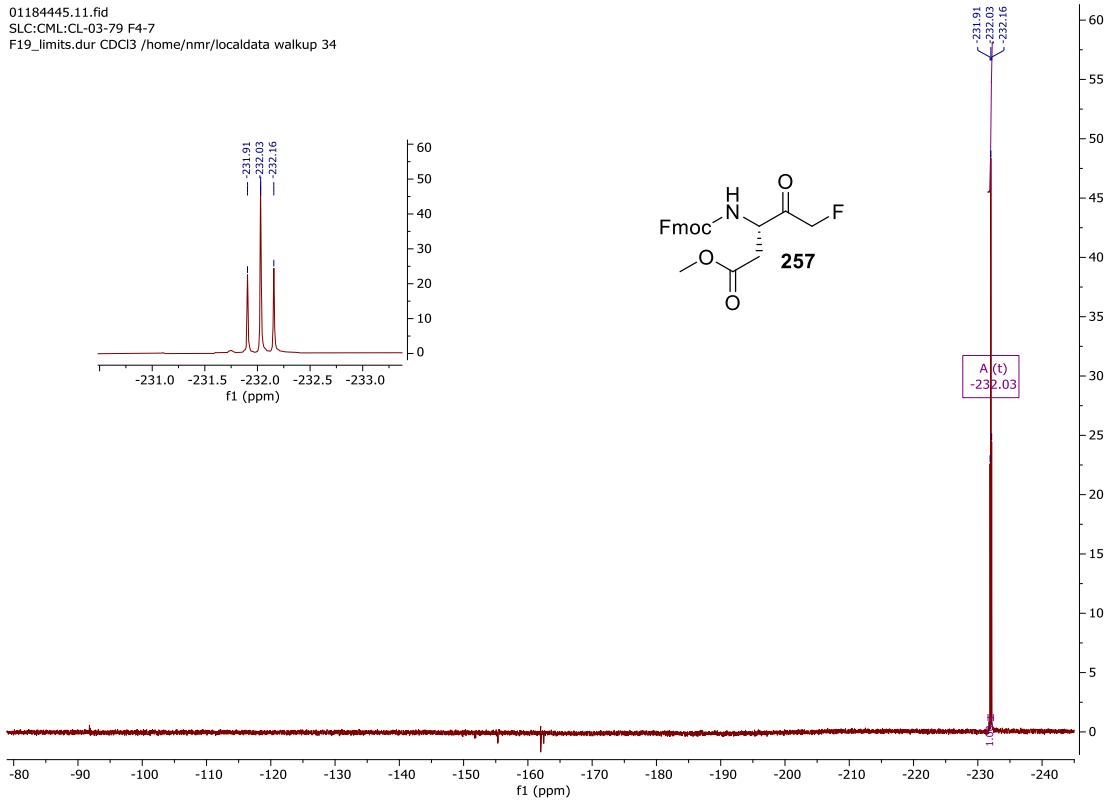

Figure 3.21 – ^{19}F NMR (^{1}H coupled) spectrum ($CDCl_3$) of FMK **257**.

Equipped with the means to deprotect *β*-ketoesters to *β*-ketoacids whilst avoiding a significant amount of FMK formation, along with the ability to decarboxylate when required in the presence of acid, loading of the free carboxylic acids to a solid-support for SPPS was attempted, as will be reported in **Section 3.6.4**.

3.6.4 Resin Loading of Fluorinated *β*-Ketoacids

When selecting a resin to be loaded for SPPS, several factors need to be considered, including the desired C-terminal peptide functionality, the ease at which loading is achieved and the conditions under which resin cleavage is triggered. In this case, the requirement to regenerate the carboxylic acid C-terminal functionality to allow decarboxylation to the FMK ruled out the use of rink amide resin (**Figure 3.22**, **259**). Thus, the resins of choice became Wang (**Figure 3.22**, **258**) and 2-Chlorotrityl chloride (**Figure 3.22**, **260**).

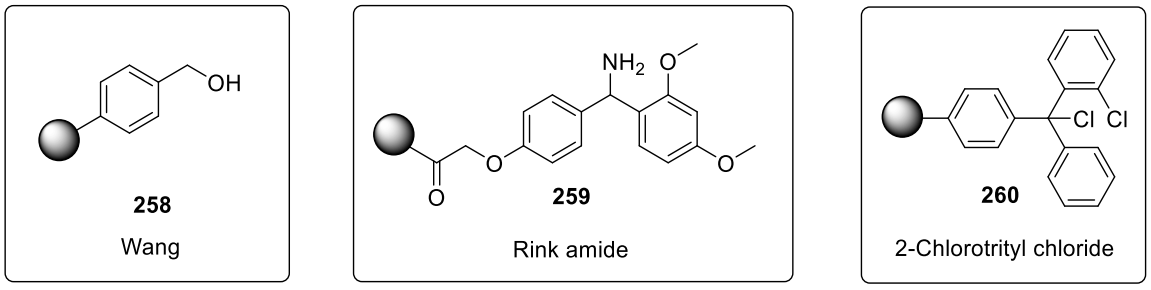

Figure 3.22 – Linkers of Wang (**258**), Rink amide (**259**) and 2-Chlorotrityl chloride (**260**) resins.

One commonly employed method for loading amino acids to Wang resin[32] involves the formation of the symmetrical anhydride of the Fmoc-protected amino acid of choice.[33] Utilising this approach, loading of *β*-ketoacid **261**, which was synthesised using the conditions described in **Scheme 3.22b** (although admittedly some impurities, including the corresponding mFMK, were present in the material carried forward), was attempted through its reaction with DIC (in a 2 : 1 ratio) in the presence of HOBt.H_2O and DMAP to generate the corresponding symmetrical anhydride which was then added to Wang resin (**Scheme 3.24**) before being left to agitate at room temperature overnight.

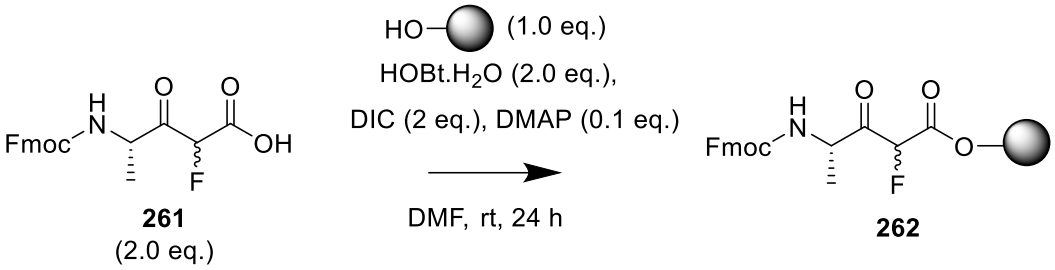

Scheme 3.24 – Wang resin loading conditions employed using the symmetrical anhydride approach.

A test cleave of the resulting resin was performed and an LCMS recorded, but no convincing evidence for the presence of the desired product (**261**), or corresponding mFMK, was found. In order to check the authenticity of the resin, loading was repeated using Fmoc-Phe-OH and found to proceed without issue, confirming that degradation of the resin was not the problem. A different approach[32] was therefore trialled involving formation of Wang chloride resin (**263**) through reaction of Wang resin **258** with thionyl chloride before subsequent addition of the carboxylic acid along (**264**) with KI and DIPEA (**Scheme 3.25**). Again, this approach was successful when loading Fmoc-Phe-OH (**266**), as evidenced by LCMS (**Figure 3.23**), but did not work when the loading of *β*-ketoacid **264**, which was synthesised using the conditions described in **Scheme 3.22b** (although impurities were present), was attempted (**Scheme 3.25**).

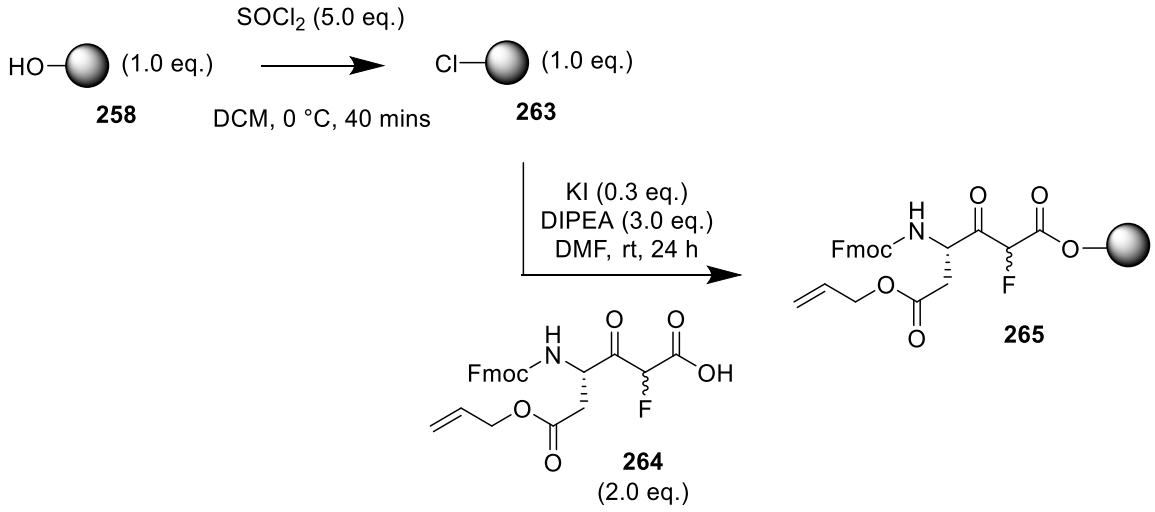

Scheme 3.25 – Wang resin loading conditions employed via Wang Chloride resin.

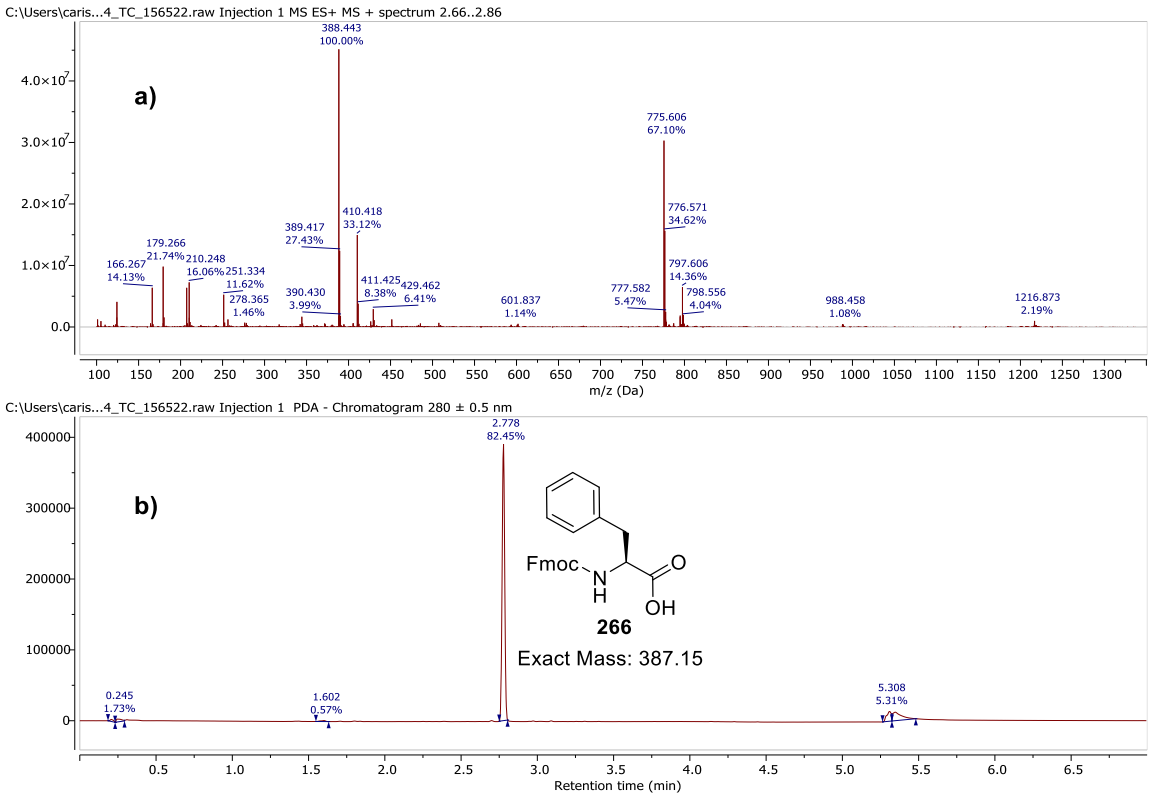

Figure 3.23 – (**a**) Mass spectrum (+ve) and (**b**) LC trace (λ = 280 nm) after loading Fmoc-Phe-OH (**261**) to Wang resin.

As a consequence of the problems encountered, loading of **205** to 2-chlorotrityl chloride resin (**260**) was instead attempted, using standard conditions according to **Scheme 3.26**. After a test cleave, the presence of $[M+H]^+$ = 358, $[M+Na]^+$ = 380 and $[M+K]^+$ = 396 in the LCMS (highlighted in yellow, **Figure 3.24**) suggests loading did occur. However, as can be seen from the UV trace, the intensity of the peak corresponding to those masses (retention time = 2.1 mins) was relatively weak for a compound which would be expected to exhibit strong UV activity at 280 nm, suggesting that loading was highly inefficient.

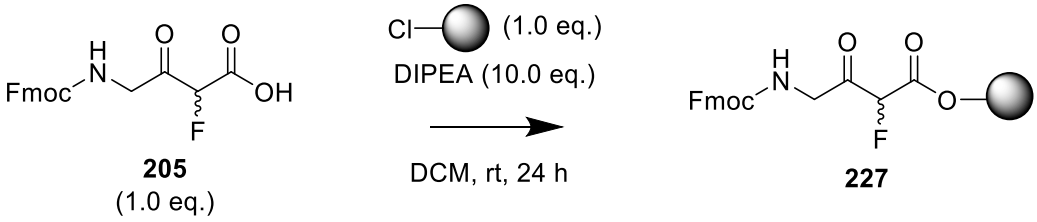

Scheme 3.26 – 2-Chlorotrityl chloride resin loading conditions employed.

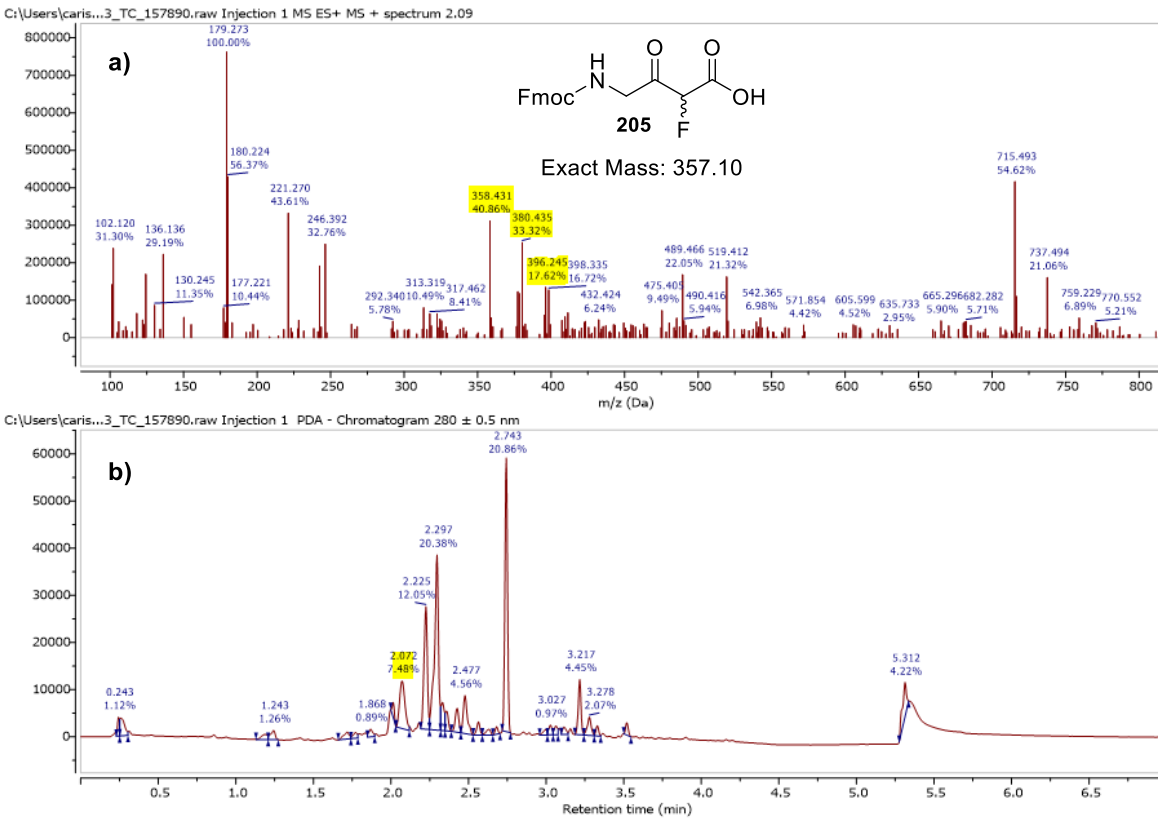

Figure 3.24 – (**a**) Mass spectrum (+ve) and (**b**) LC trace (λ = 280 nm) after attempted loading of **205** to 2-Chlorotrityl chloride resin.

It was considered possible that the challenges encountered during 2-chlorotrityl chloride resin loading are exacerbated by the installation of the fluorine atom reducing the nucleophilicity of the carboxylate through its electron-withdrawing properties. In order to explore this claim, ^{t}Bu ester deprotection of non-fluorinated *β*–ketoester **231** was accomplished using 30% TFA in DCM (**Scheme 3.27a**), followed by attempted loading of non-fluorinated *β*-ketoacid **224** to the resin (**Scheme 3.27b**). Interestingly, after a test cleave, the molecular ion ($[M+H]^+$ = 340) of the expected material (**224**) was identifiable by LCMS (highlighted in yellow, **Figure 3.25**), appearing as a significant peak in the UV trace at 280 nm (retention time = 2.2 mins), suggesting that 2-chlorotrityl chloride resin loading was indeed somewhat hampered by the presence of the fluorine atom.

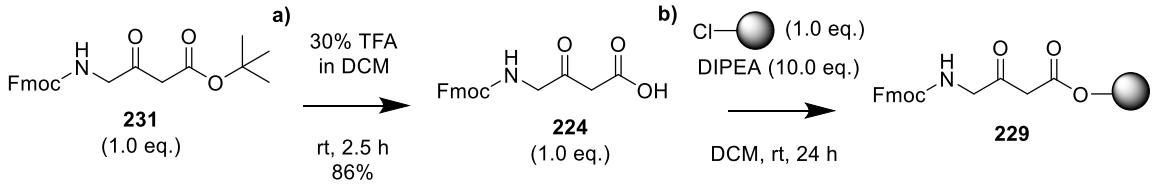

Scheme 3.27 – Conditions employed for (**a**) ^{t}Bu removal of **231** and (**b**) 2-Chlorotrityl chloride resin loading.

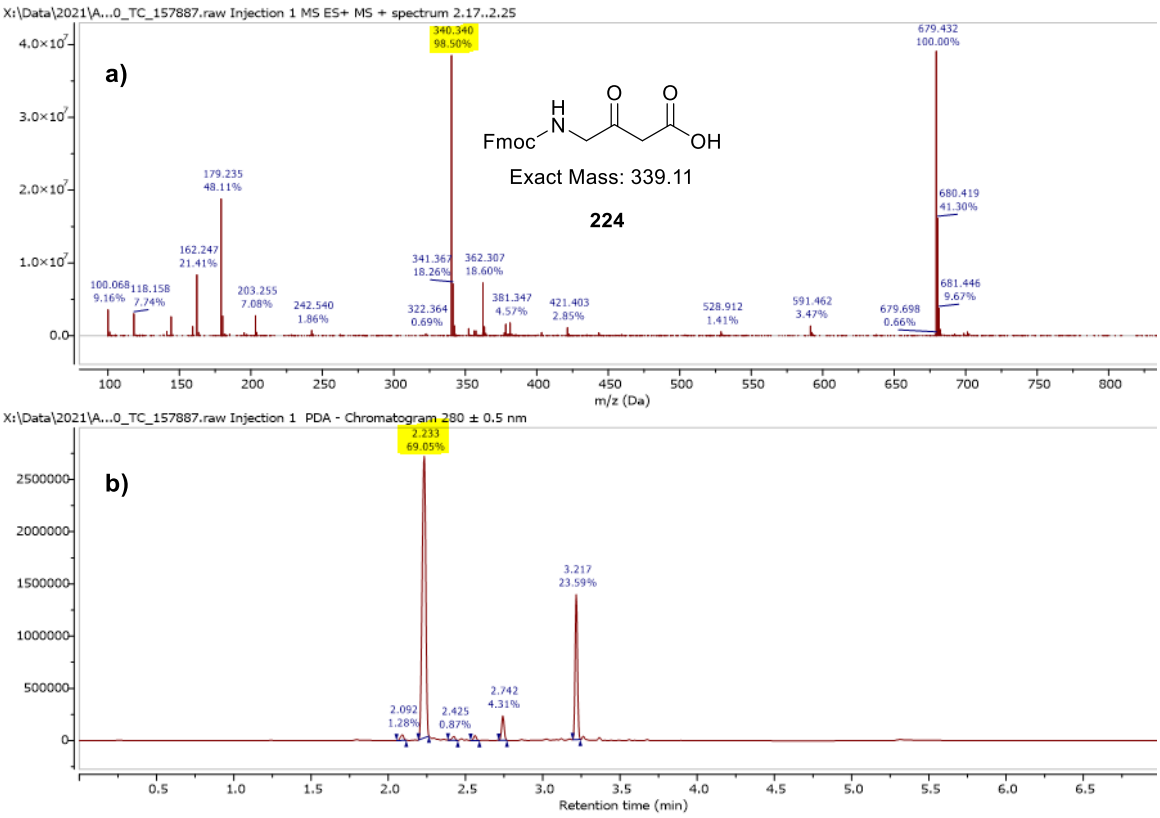

Figure 3.25 – (**a**) Mass spectrum (+ve) and (**b**) LC trace (λ = 280 nm) after loading of **224** to 2-Chlorotrityl chloride resin.

Another potential contribution towards the problems encountered during resin loading is the tendency for the substrates to decarboxylate to FMKs prematurely. If this occurs, no carboxylic acid handle is available for resin attachment. In order to investigate whether this is a contributing factor despite careful handling and storage, 2-chlorotrityl chloride resin loading was attempted with substrate **267** (**Scheme 3.28**), but this time the drainage solution was collected after the loading step and analysed by LCMS. This revealed the presence of a large peak in the UV trace at 280 nm corresponding to the FMK (**269**) (**Figure 3.26**).

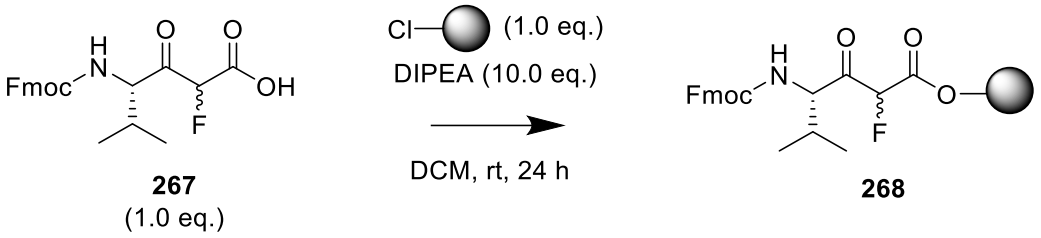

Scheme 3.28 – 2-Chlorotrityl chloride resin loading conditions employed.

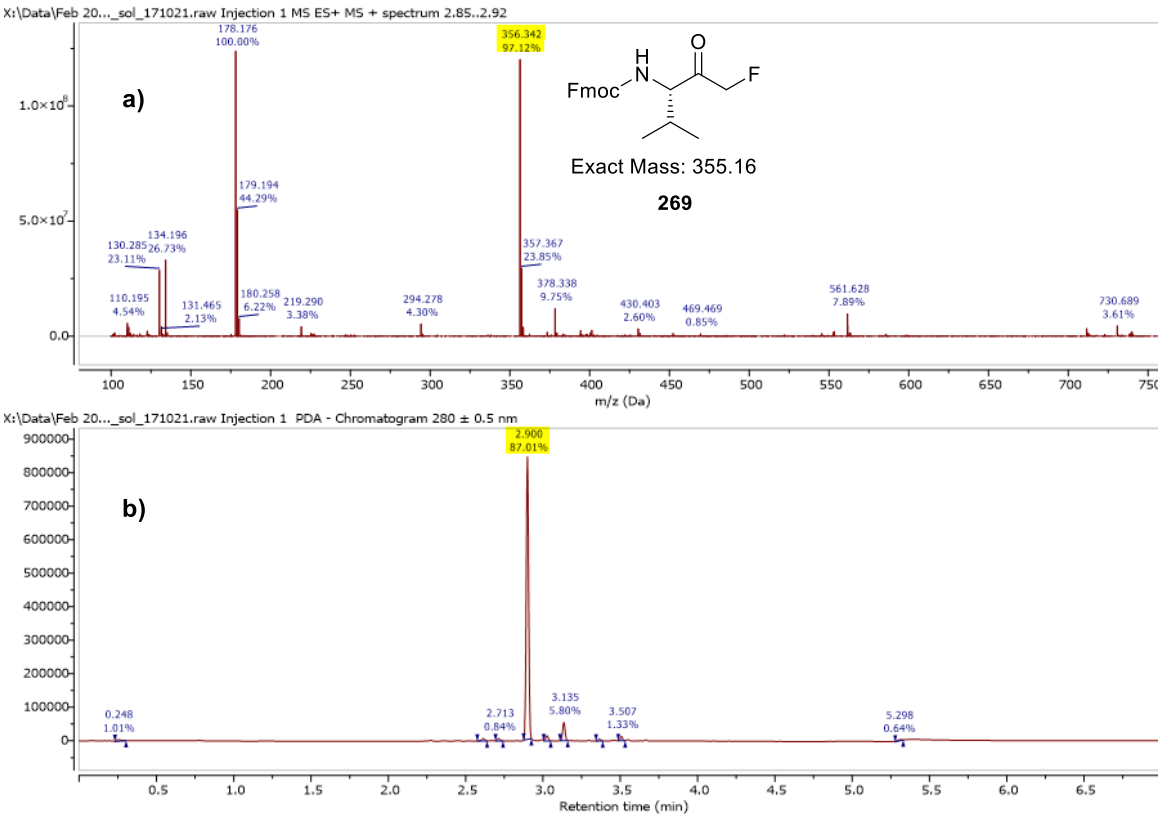

Figure 3.26 – (**a**) Mass spectrum (+ve) and (**b**) LC trace (λ = 280 nm) after attempted loading of **267** to 2-Chlorotrityl chloride resin.

In order to confirm that decarboxylation was not just occurring as a result of the mass spectrometry process, an ^{19}F NMR-tracked solution-phase experiment was carried out involving the reaction of *β*-ketoacid **267**, which was isolated through utilisation of similar conditions to that described in **Scheme 3.22b**, with benzyl chloride (**270**) (**Scheme 3.29**). Whilst a small amount of FMK **269** was present prior to the reaction along with starting material **267** (**Figure 3.27a**), after 2 hours, complete conversion to the FMK (**269**) was observed by ^{19}F NMR spectroscopy (**Figure 3.27b**) despite the use of an excess of

base to neutralise residual TFA still present after ^{t}Bu ester deprotection, rotary evaporation and freeze-drying. This suggests that preference for decarboxylation over ester bond formation was hindering the desired reaction.

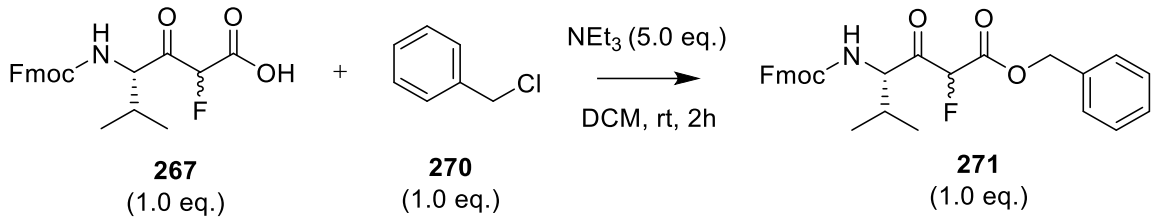

267 (1.0 eq.) **270** (1.0 eq.) **271** (1.0 eq.)

Scheme 3.29 – Nucleophilic substitution conditions employed.

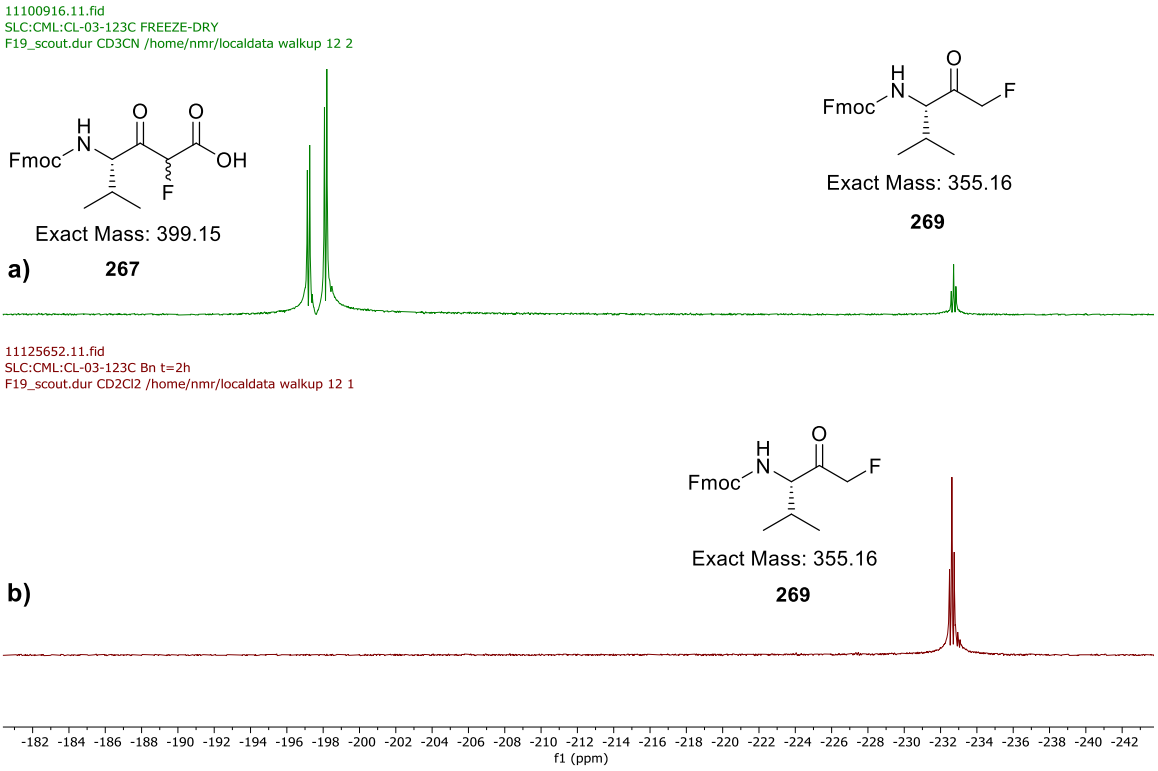

Figure 3.27 – ^{19}F NMR spectra for *β*-ketoacid **267** before (**a**) (CD_3CN) and after (**b**) 2 h reaction with benzyl chloride and triethylamine (CD_2Cl_2).

As a potential solution to this problem, resin loading via a sidechain functional group was instead considered. That way, if decarboxylation of the 1,3-dicarbonyl did occur, attachment to the resin would still be possible. Of course, this does reduce substrate scope significantly due to the requirement for a nucleophilic group in the sidechain. However, as Asp(OMe) is commonly installed at the C-terminal position of

peptidyl FMKs in the literature,[26–31] it was proposed that attachment via the acid side-chain of Fmoc-Asp-OH-derived sidechain carboxylic acid **272** (**Scheme 3.30**), followed by peptide growth and eventual resin cleavage along with concomitant methylation, as has been reported in the literature,[34] would allow access to a selection of biologically relevant FMKs. In order to ensure orthogonal protection between the 1,3-dicarbonyl carboxylic acid and the Asp sidechain protecting group, the *tert*-butyl ester and allyl ester were utilised respectively (**253**, **Scheme 3.30**). However, during attempted allyl ester deprotection with tetrakis(triphenylphosphine)palladium(0) under an inert atmosphere (**Scheme 3.30**),[35] the appearance of additional fluorine peaks in the ^{19}F NMR spectrum of the crude reaction material (**Figure 3.28b**) compared to that of the starting material (**Figure 3.28a**) suggested the conditions were incompatible with substrate **253**. Specifically, the diminishment of the mono-fluorinated 1,3-dicarbonyl peaks (-195 ppm) and the emergence of multiple unidentified peaks around -170 ppm was observed, meaning these conditions were not pursued further.

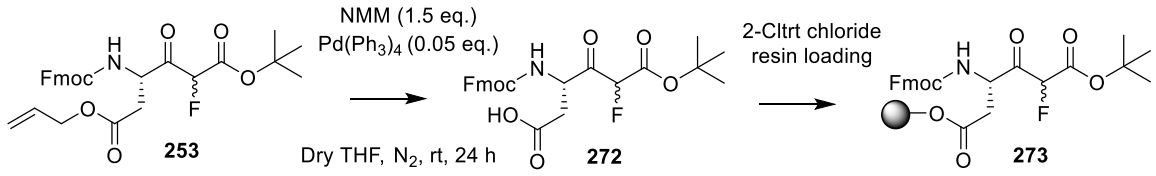

Scheme 3.30 – Conditions for attempted allyl ester deprotection[35] to allow for subsequent sidechain resin attachment.

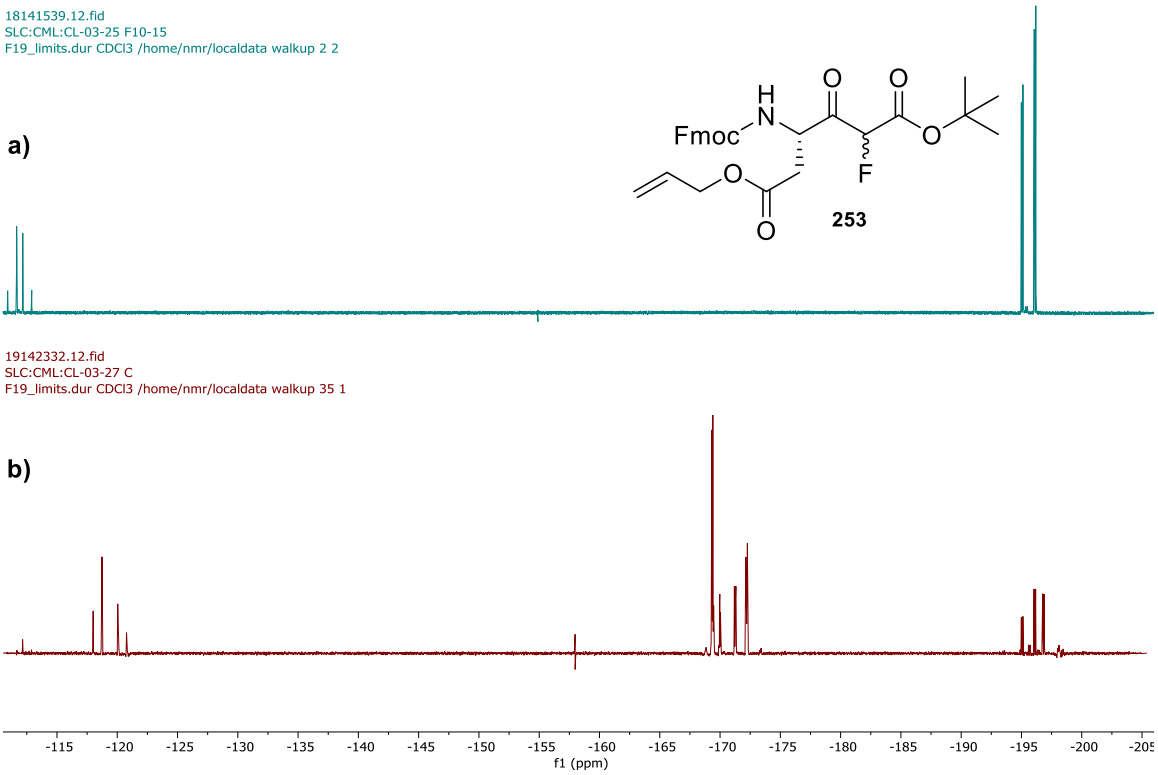

Figure 3.28 – ^{19}F NMR (^{1}H coupled) spectra ($CDCl_3$) for *β*-ketoacid **253** before (**a**) and after (**b**) attempted allyl ester deprotection.

Despite exploring different resins, loading methods and attachment sites, it became clear that loading fluorinated 1,3-dicarbonyl systems was not straightforward, with multiple problems encountered along the way. However, in spite of the struggles encountered during attempted solid-phase peptidyl FMK synthesis, it was proposed that the methods utilised throughout this section, including electrophilic fluorination and decarboxylation, could be modified and redeployed for accessing peptidyl FMKs via a solution-phase approach instead. This will be described in **Chapter 4**.

3.7 Chapter Summary

During this chapter, methodology for building mono-fluorinated *β*-ketoacid building blocks possessing a carboxylic acid handle to be attached to a solid support and used for solid-phase synthesis of peptidyl mono-fluoromethyl ketones (mFMKs) through initial peptide growth (SPPS) and eventual resin cleavage with concomitant decarboxylation to

the desired FMK was pursued. In order to do this, construction of an Fmoc-protected *β*-ketoester was initially achieved through oxidation of an Fmoc protected *β*-hydroxyester (**Table 3.2**, **entry 3**); however, in order to expand substrate scope and reduce steps, enolate chemistry was employed to enable *β*-ketoester formation from an Fmoc-protected amino acid of choice in a single step (**Scheme 3.20**). Subsequently, successful electrophilic mono-fluorination was achieved (**Scheme 3.21**) utilising conditions described by Togni and co-workers,[7] before careful *tert*-butyl ester deprotection, without significant amounts of unwanted decarboxylation, was accomplished (**Scheme 3.22b**). Resin loading then proved challenging, despite trialling different conditions and resins, with both Wang and 2-chlorotrityl chloride failing to provide convincing evidence for successful loading, despite success when loading a standard Fmoc-protected amino acid (Fmoc-Phe-OH). Furthermore, collection of the drainage solution after attempted loading revealed FMK formation by LCMS (**Figure 3.26**), suggesting that the strongly electron-withdrawing nature of the fluorine may be reducing nucleophilicity of the carboxylate and favouring decarboxylation to the FMK rather than resin loading. Despite these problems, it was somewhat encouraging that decarboxylation to the FMK was found to occur in a straightforward manner. Furthermore, the ability to successfully access a selection of fluorinated amino acid derived *β*-ketoesters (**Figure 3.22**) was demonstrated, and thus it was believed that adjusting the protecting group strategy would allow redeployment of this approach for use in solution-phase synthesis of peptidyl FMKs, as will be described in **Chapter 4**.

3.8 References for Chapter 3

1. Palomo, J. M. Solid-phase peptide synthesis: an overview focused on the preparation of biologically relevant peptides. *RSC Adv.* **4**, 32658–32672 (2014).

2. Coin, I., Beyermann, M. & Bienert, M. Solid-phase peptide synthesis: from standard procedures to the synthesis of difficult sequences. *Nat. Protoc.* **2**, 3247–3256 (2007).

3. Roiban, G. D., Matache, M., Hădade, N. D. & Funeriu, D. P. A general solid phase method for the synthesis of sequence independent peptidyl-fluoromethyl ketones. *Org. Biomol. Chem.* **10**, 4516–4523 (2012).

4. Joshi, D. *et al.* An improved method for the incorporation of fluoromethyl ketones into solid phase peptide synthesis techniques. *RSC Adv.* **11**, 20457–20464 (2021).

5. Xiao, J.-C. & Shreeve, J. M. Microwave-assisted rapid electrophilic fluorination of 1,3-dicarbonyl derivatives with Selectfluor®. *J. Fluor. Chem.* **126**, 473–476 (2005).

6. Tang, L. *et al.* Chemoselective Mono- And Difluorination of 1,3-Dicarbonyl Compounds. *J. Org. Chem.* **84**, 10449–10458 (2019).

7. Frantz, R., Hintermann, L., Perseghini, M., Broggini, D. & Togni, A. Titanium-Catalyzed Stereoselective Geminal Heterodihalogenation of β-Ketoesters. *Org. Lett.* **5**, 1709–1712 (2003).

8. Geary, G. C., Hope, E. G., Singh, K. & Stuart, A. M. Electrophilic fluorination using a hypervalent iodine reagent derived from fluoride. *Chem. Commun.* **49**, 9263–9265 (2013).

9. Chambers, R. D., Hutchinson, J. & Sandford, G. Recent studies at Durham on direct fluorination. *J. Fluor. Chem.* **100**, 63–73 (199AD).

10. Howard, J. L., Sagatov, Y. & Browne, D. L. Mechanochemical electrophilic fluorination of liquid beta-ketoesters. *Tetrahedron* **74**, 3118–3123 (2018).

11. Howard, J. L., Sagatov, Y., Repusseau, L., Schotten, C. & Browne, D. L. Controlling reactivity through liquid assisted grinding: The curious case of mechanochemical fluorination. *Green Chem.* **19**, 2798–2802 (2017).

12. Kitamura, T., Kuriki, S., Morshed, M. H. & Hori, Y. A Practical and Convenient Fluorination of 1,3-Dicarbonyl Compounds Using Aqueous HF in the Presence of Iodosylbenzene. *Org. Lett.* **13**, 2392–2394 (2011).

13. Nash, T. J. & Pattison, G. Apparent Electrophilic Fluorination of 1,3-Dicarbonyl Compounds Using Nucleophilic Fluoride Mediated by PhI(OAc)2. *Eur. J. Org. Chem.* **2015**, 3779–3786 (2015).

14. Popovici-Muller, J. *et al.* Therapeutically active compounds and their methods of use. 1–67 (2015).

15. Crich, D. & Sana, K. Solid-Phase Synthesis of Peptidyl Thioacids Employing a 9-Fluorenylmethyl Thioester-Based Linker in Conjunction with Boc Chemistry. *J.Org.Chem.* **74**, 7383–7388 (2009).

16. Qiu, Z. *et al.* Discovery of Fluoromethylketone-Based Peptidomimetics as Covalent ATG4B (Autophagin-1) Inhibitors. *ACS Med. Chem. Lett.* **7**, 802–806 (2016).

17. Shao, J. & Panek, J. S. Total synthesis of cystothiazoles A and B. *Org. Lett.* **6**, 3083–3085 (2004).

18. Sharma, P., Kaur, N., Pareek, A. & Kishore, D. An insight in to general features of IBX (2-iodoxybenzoic acid). *Sci. Revs. Chem. Commun.* **3**, 16–42 (2013).

19. More, J. D. & Finney, N. S. A Simple and Advantageous Protocol for the Oxidation of Alcohols with o-Iodoxybenzoic Acid (IBX). *Org. Lett.* **4**, 3001–3003 (2002).

20. Nyffeler, P. T., Durón, S. G., Burkart, M. D., Vincent, S. P. & Wong, C. H. Selectfluor: Mechanistic Insight and Applications. *Angew. Chem. Int. Ed.* **44**, 192–212 (2005).

21. Differding, E. & Wehrli, M. Nucleophilic substitution versus electron transfer: 2. SN2 at flouride and electron transfer are competing and different pathways in electrophilic flourinations. *Tetrahedron Lett.* **32**, 3819–3822 (1991).

22. Pascal, R. & Sola, R. Preservation of the Fmoc protective group under alkaline conditions by using CaCl2. Applications in peptide synthesis. *Tetrahedron Lett.* **39**, 5031–5034 (1998).

23. Binette, R., Desgagné, M., Theaud, C. & Boudreault, P. L. Efficient Fmoc-Protected Amino Ester Hydrolysis Using Green Calcium (II) Iodide as a Protective Agent. *Molecules* **27**, 2788 (2022).

24. Di Gioia, M. L. *et al.* Alternative and Chemoselective Deprotection of the α-Amino and Carboxy Functions of N-Fmoc-Amino Acid and N-Fmoc-Dipeptide Methyl Esters by Modulation of the Molar Ratio in the AlCl3/N,N-Dimethylaniline Reagent System. *Eur. J. Org. Chem.* **2004**, 4437–4441 (2004).

25. Budnjo, A. *et al.* Reversible Ketomethylene-Based Inhibitors of Human Neutrophil Proteinase 3. *J. Med. Chem.* **57**, 9396–9408 (2014).

26. Deszcz, L., Cencic, R., Sousa, C., Kuechler, E. & Skern, T. An Antiviral Peptide Inhibitor That Is Active against Picornavirus 2A Proteinases but Not Cellular Caspases. *J. Virol.* **80**, 9619–9627 (2006).

27. Cheng, Y. *et al.* Caspase inhibitor affords neuroprotection with delayed administration in a rat model of neonatal hypoxic-ischemic brain injury. *J. Clin. Investig.* **101**, 1992–1999 (1998).

28. Kudelova, J., Fleischmannova, J., Adamova, E. & Matalova, E. Pharmacological caspase inhibitors: research towards therapeutic perspectives. *J. Physiol. Pharmacol.* **66**, 473–82 (2015).

29. Knoblach, S. M. *et al.* Caspase Inhibitor z-DEVD-fmk Attenuates Calpain and Necrotic Cell Death in Vitro and after Traumatic Brain Injury. *J. Cereb. Blood Flow Metab.* **24**, 1119–1132 (2004).

30. Li, L. *et al.* Photodynamic therapy induces human esophageal carcinoma cell pyroptosis by targeting the PKM2/caspase-8/caspase-3/GSDME axis. *Cancer Lett.* **520**, 143–159 (2021).

31. Citarella, A. & Micale, N. Peptidyl Fluoromethyl Ketones and Their Applications in Medicinal Chemistry. *Molecules* **25**, 4031 (2020).

32. Sandhya, K. & Ravindranath, B. A protocol for racemization-free loading of Fmoc-amino acids to Wang resin. *Tetrahedron Lett.* **49**, 2435–2437 (2008).

33. Atherton, E., Logan, C. J. & Sheppard, R. C. Peptide synthesis. Part 2. Procedures for Solid-phase Synthesis using Nα-Fluorenylmethoxycarbonylamino-acids on Polyamide Supports. Synthesis of substance P and of Acyl Carrier Protein 65–74 Decapeptide. *J. Chem. Soc., Perkin Trans. 1* 538–546 (1981) doi:10.1039/P19810000538.

34. Turner, R. A., Weber, R. J. & Lokey, R. S. Direct Conversion of Resin-Bound Peptides to C-Terminal Esters. *Org. Lett.* **12**, 1852–1855 (2010).

35. Vonnussbaum, F. von *et al.* Freezing the Bioactive Conformation to Boost Potency: The Identification of BAY85-8501, a Selective and Potent Inhibitor of Human Neutrophil Elastase for Pulmonary Diseases. *ChemMedChem* **10**, 1163–1173 (2015).

4. Solution-Phase Synthesis of Peptidyl Mono-FMKs

4.1 Introduction

Whilst several solution-phase routes have been reported in the literature for accessing peptidyl mono-FMKs,[1] many of them suffer from low yielding steps, racemisation, long-winded procedures and the use of hazardous materials. For example, diazomethane, a highly toxic and potentially explosive gas, is used in some examples.[2,3] For these reasons, a new and improved route for accessing these compounds in solution was pursued, as it was clear there was still scope for further improvement. During attempts to develop a solid-phase approach in **Chapter 3**, successful construction of mono-fluorinated 1,3-dicarbonyl systems which could then be decarboxylated to the corresponding FMKs was possible. This was demonstrated through deprotection and decarboxylation of *β*–ketoester **252** to the corresponding FMK (**257**) (**Scheme 4.1**), as well as through unintentional decarboxylation observed during resin loading attempts.

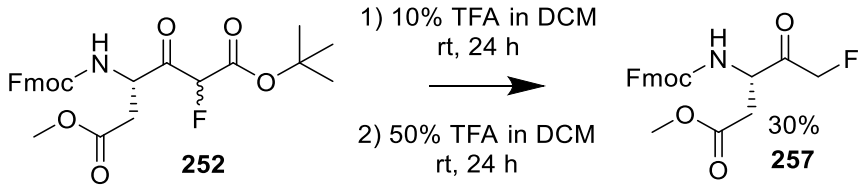

Scheme 4.1 – Conditions employed for a one-pot *t*Bu ester deprotection and decarboxylation.

It was proposed that these types of mono-fluorinated 1,3-dicarbonyl systems could be redeployed for solution-phase applications. This would involve coupling the peptide of choice (**275**), which could either have been synthesised in solution or on resin, with a fluorinated 1,3-dicarbonyl building block (**274**) in solution to generate the desired peptidyl FMK (**129**) after deprotection and decarboxylation, as illustrated by retrosynthetic **Scheme 4.2**.

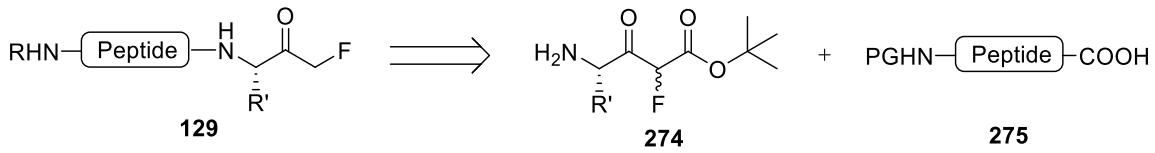

Scheme 4.2 – Proposed solution phase-route to peptidyl mono-FMKs. R = H, protecting group or acetyl group. R' = amino acid sidechain moiety. PG = protecting group.

In order to access building block **274** (**Scheme 4.2**), it was envisioned that similar chemistry to that described in **Chapter 3** (**Scheme 3.20**) could be utilised, with the key difference being the need to access the free amine for solution-phase coupling rather than the carboxylic acid for resin attachment. This would involve constructing the *β*-ketoester (**237**) using enolate chemistry and carrying out selective mono-fluorination before deprotecting to the free amine (**Scheme 4.3**). In **Chapter 3**, an orthogonal Fmoc/O^{t}Bu ester protecting group strategy was employed for the amine and carboxylic acid functionalities respectively. Given that Fmoc removal in solution is notoriously inconvenient, rendering the use of Fmoc-protected building block **236** for accessing mFMKs via solution-phase methods undesirable (**Scheme 4.3**), employment of an alternative orthogonal system (**276**) was sought after. This led to a literature procedure in which selective Boc removal in the presence of a *tert*-butyl ester[4] (**Scheme 4.4**) was achieved. A Boc/O^{t}Bu ester protecting group strategy was therefore utilised instead (starting from **278**, **Scheme 4.3**), for which methodological details will be presented in the following sections.

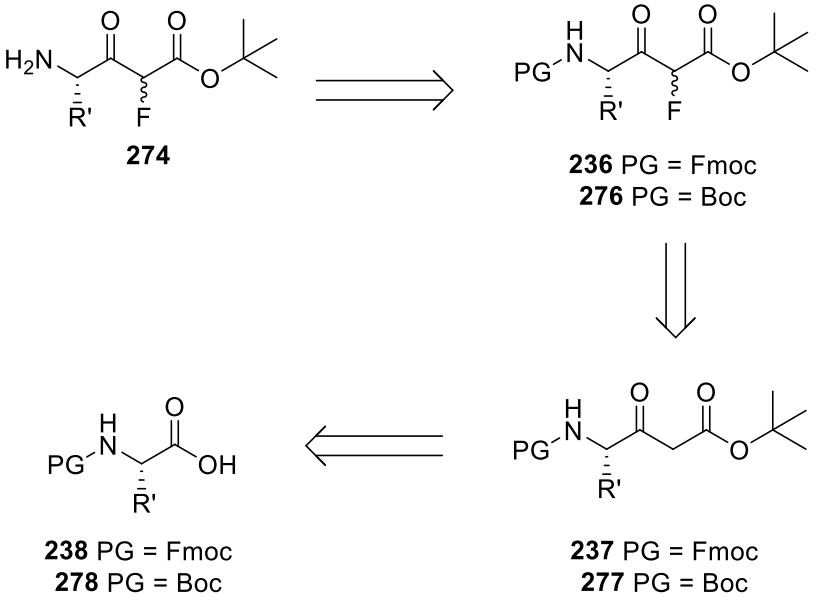

Scheme 4.3 – Retrosynthetic scheme for 2**74**. PG = protecting group.

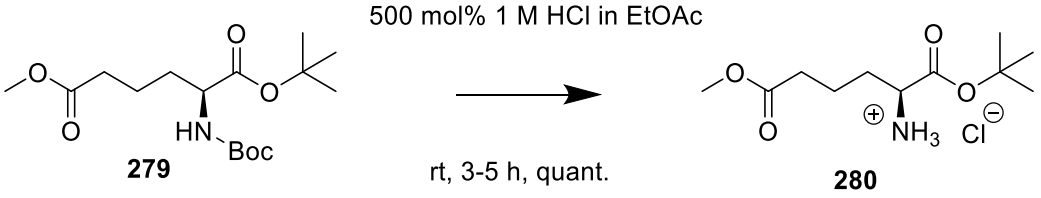

Scheme 4.4 – Selective Boc removal in the presence of a *tert*-butyl ester.[4]

4.2 Synthesis of Mono-Fluorinated *β*-Ketoester Building Block 274

4.2.1 *β*-Ketoester Construction

Generation of a selection of Boc-protected *β*-ketoesters was achieved through activation of a Boc-protected amino acid of choice with 1,1'-carbonyldiimidazole (CDI) followed by reaction with the enolate of *tert*-butyl acetate, which had been formed using LDA (**Scheme 4.5**).[5] This procedure was similar to that described in **Chapter 3**, **Section 3.6.1**, but with the key difference being that the work-up was carried out using 10% *w/v* citric acid rather than 1 M HCl to avoid unwanted Boc removal. Again, the yields were found to be relatively low, with evidence by ^{1}H NMR spectroscopy for a substantial amount of starting material still present in the crude material. Extending the reaction time between

activated amino acid **281** (R = Asp(OMe)) and the solution containing the enolate of *tert*-butyl acetate from 1 to 4 hours did not appear to improve the yield. In **Chapter 3.6.1**, some Fmoc removal was observed during construction of Fmoc-protected *β*-ketoesters (**Scheme 3.21**), which suggested that enolate formation of *tert*-butyl acetate hadn't gone to completion before being added to the activated amino acid. Poor conversion to the enolate could again be a contributing factor towards the disappointing yields observed for the Boc-derived species shown in **Scheme 4.5**, as incomplete enolate formation could result in the presence of unreacted activated amino acid **281**, which would then revert to the starting amino acid (**278**) during the aqueous work-up. However, this was not considered to be a major concern as the procedure allows construction of *β*-ketoesters in just one step, and in future the yield could potentially be improved by using an excess of LDA relative to *tert*-butyl acetate to drive enolate formation to completion.

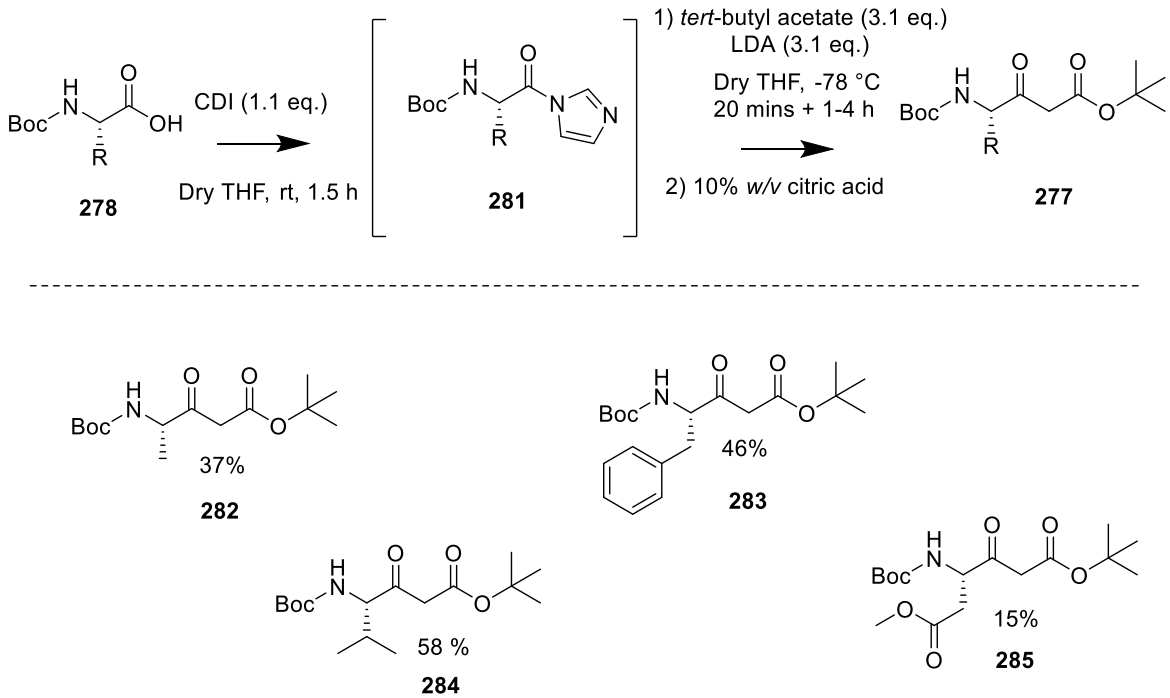

Scheme 4.5 – A selection of *β*-ketoesters synthesised using CDI, LDA and *tert*-butyl acetate.

4.2.2 Electrophilic Fluorination

As in **Chapter 3.6.2**, selective mono-fluorination of the Boc/O^{t}Bu protected *β*-ketoesters was found to proceed without issue using Selectfluor in the presence of $CpTiCl_3$ (**Scheme 4.6**).[6] Whilst some di-fluorination was evident even after column chromatography, the major isolated material was the mono-fluorinated product, with difluorination kept to only 2% after column chromatography for substrates **286** and **287**, whilst 7% di-fluorination was observed for substrate **288**. The isolated yields along with the relative ratios of mono- to di-fluorinated material after purification, as determined by ^{19}F NMR spectroscopy, are given in **Scheme 4.6**. Additionally, the ^{19}F NMR spectrum is shown for Boc-Asp(OMe)-OH derived fluorinated *β*-ketoester **287** (**Figure 4.1**).

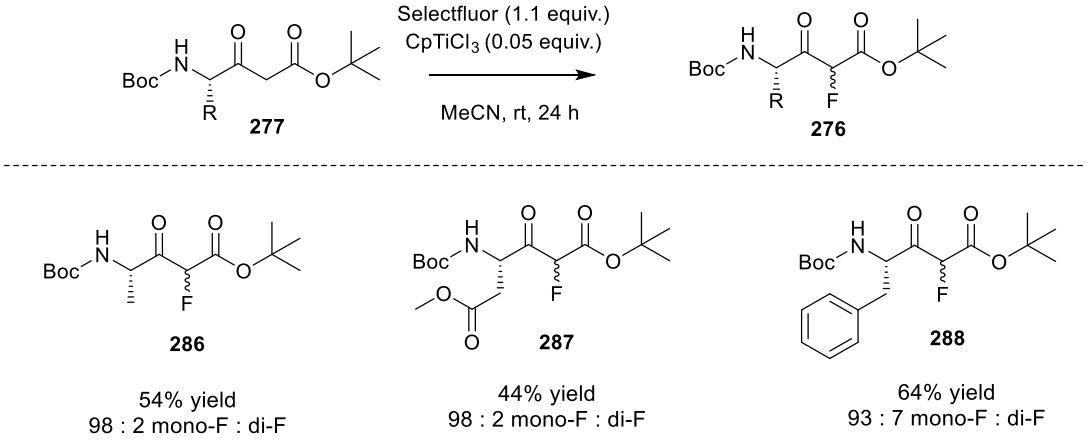

Scheme 4.6 – A selection of fluorinated *β*-ketoesters synthesised using F-TEDA and $CpTiCl_3$. Isolated yields are given, along with the ratio of mono-fluorinated material relative to di-fluorinated material after column chromatography, as determined by ^{19}F NMR spectroscopy.

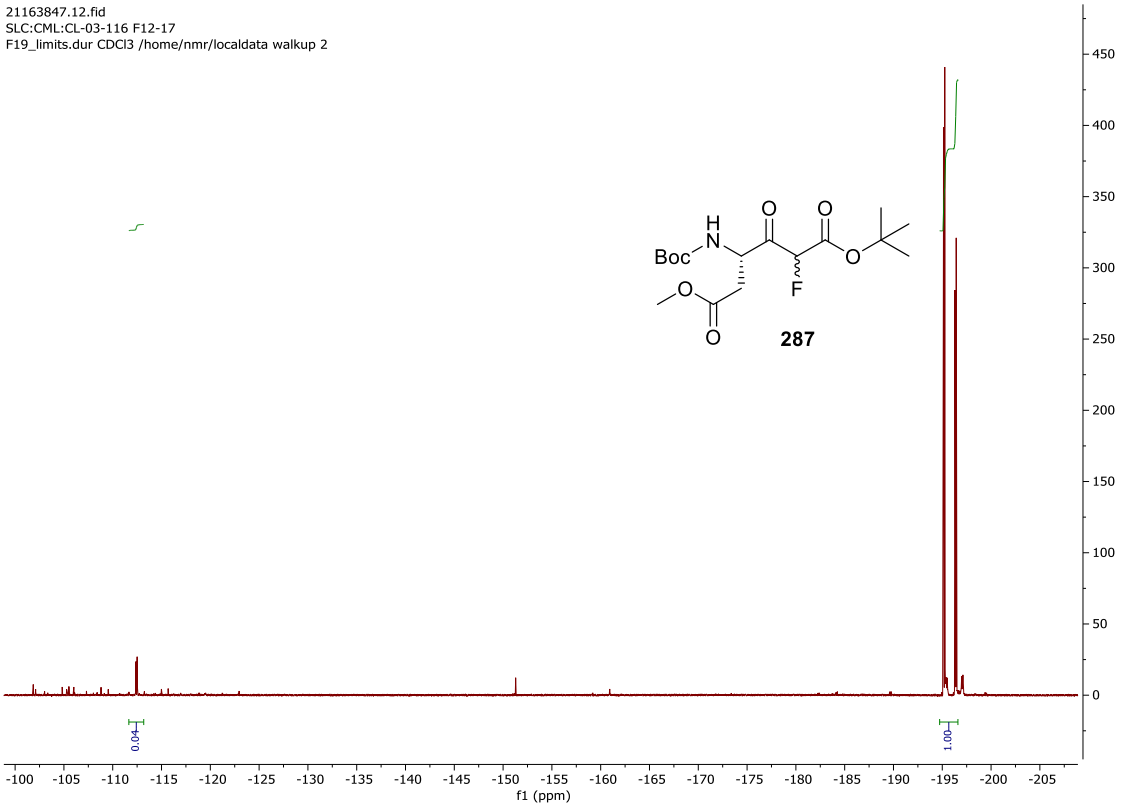

Figure 4.1 – ^{19}F NMR spectrum ($CDCl_3$) for fluorinated *β*-ketoester **287**.

4.2.3 Selective Boc Deprotection

As already highlighted, Rapoport and co-workers were able to successfully carry out Boc deprotection whilst avoiding concomitant *tert*-butyl ester removal.[4] This was achieved using 500 mol% 1 M HCl in EtOAc at room temperature, typically over a period of 3-5 hours. Utilising a similar procedure, selective Boc deprotection of substrate **288** was attempted (**Scheme 4.7**). Initially, this was performed at room temperature as the paper had described; however, it became apparent that the reaction was not occurring very rapidly. In fact, after 24, 48 and 72 hours, conversion to the product (**289**) had only reached around 16%, 25% and 30% respectively, as determined by ^{19}F NMR spectroscopy (**Figure 4.2a-d**).

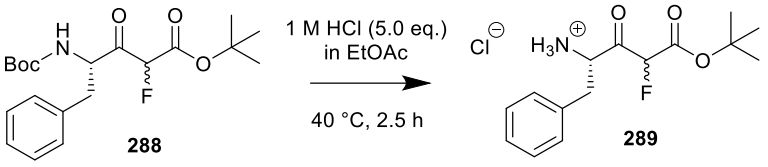

Scheme 4.7 – Conditions employed for selective Boc removal of **288**.

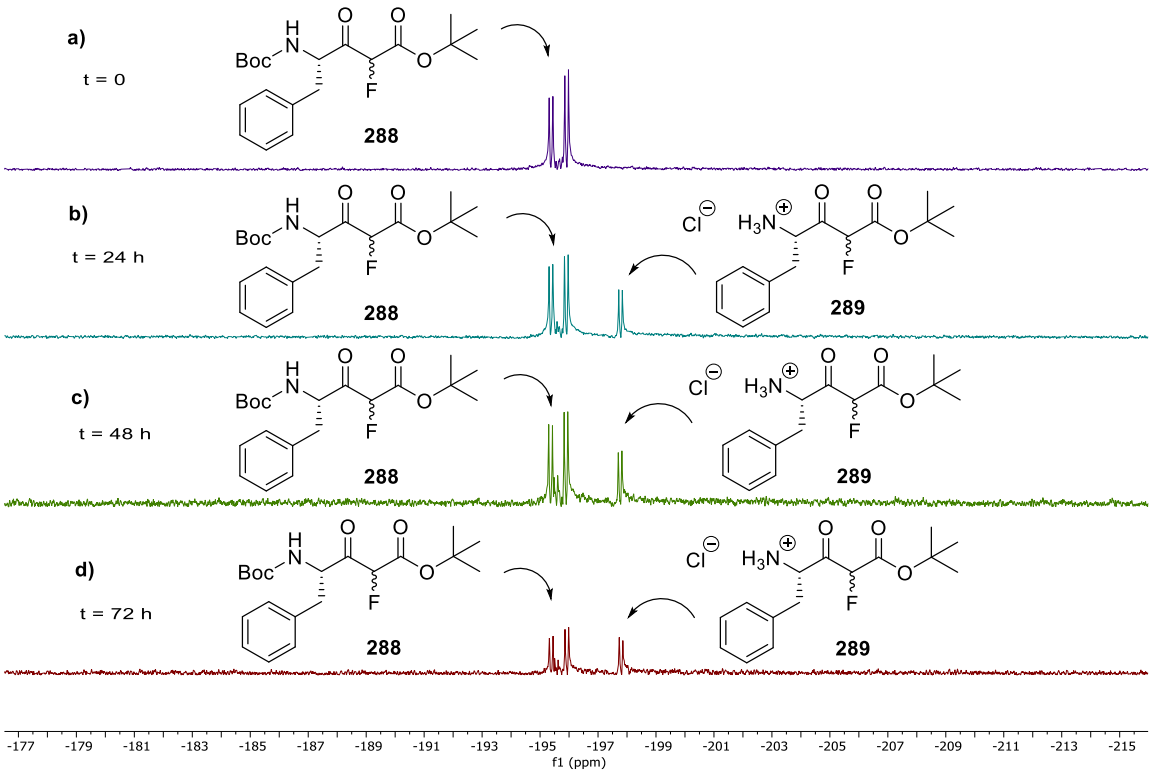

Figure 4.2 – ^{19}F NMR spectra (DMSO-d_6) at regular time intervals (t = 0 h (**a**), 24 h (**b**), 48 h (**c**) and (**d**) 72 h) during selective Boc deprotection of **288**.

Repeating the reaction at 40 °C offered significant improvement, with conversion reaching around 72% after just 2.5 hours (**Figure 4.3a**-**b**). However, subsequently leaving the same reaction mixture stirring overnight at room temperature to encourage complete conversion to product resulted in an increase in impurity peaks in the ^{19}F NMR spectrum, highlighting the importance of tracking progress and not leaving it for extended periods unnecessarily. During the reaction, the fluorine peaks changed from existing as two doublets to a single doublet after Boc removal. This is due to the fact that rotamers are no longer present in the absence of Boc and is also evidenced by ^{1}H NMR spectroscopy which indicates a decrease in the Boc peak and a merging of the ^{t}Bu ester peak from 2 peaks (**Figure 4.4a**) into 1 shifted peak as rotamers are no longer present (**Figure 4.4b**).

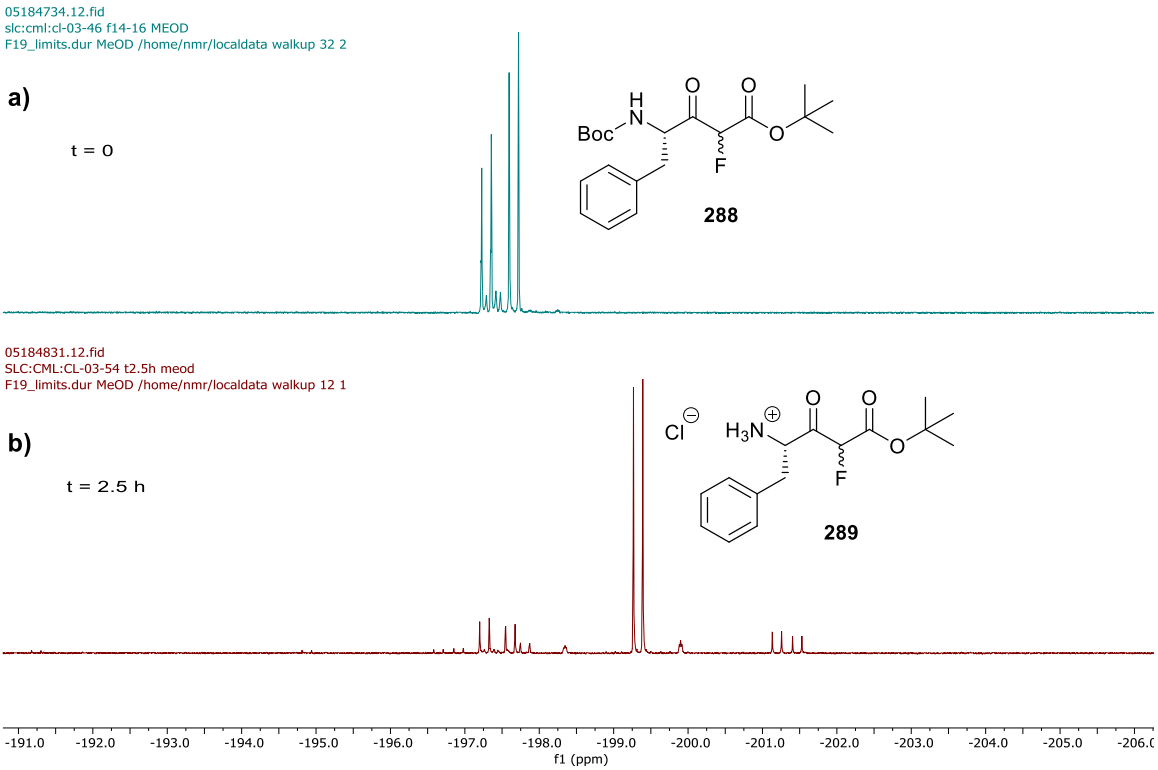

Figure 4.3 – ^{19}F NMR spectra recorded in MeOD at t = 0 h (**a**) and t = 2.5 h (**b**) during selective Boc deprotection at 40 °C.

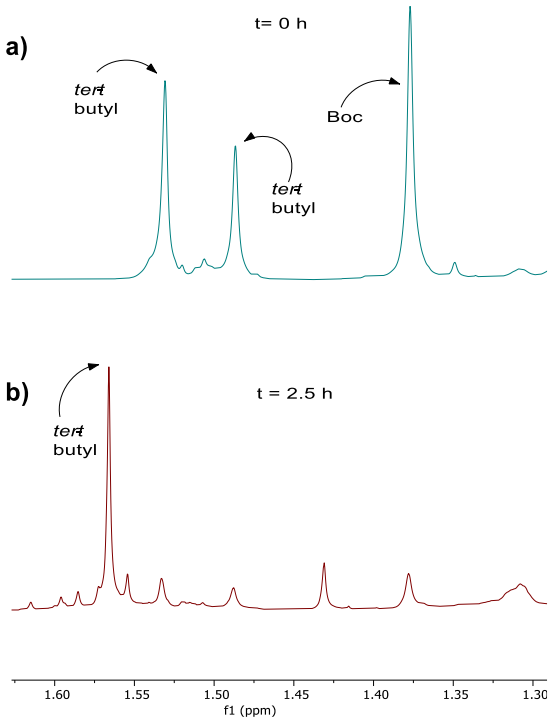

Figure 4.4 – Close-up of ^{1}H NMR spectra (CD_3OD) at t = 0 h (**a**) and t = 2.5 h (**b**) during selective Boc deprotection at 40 °C.

Similar conditions were also applied to substrate **287** (**Scheme 4.8**) in order to access Boc-deprotected 1,3-dicarbonyl **290** (derived from of Boc-Asp(OMe)-OH). This substrate was of particular interest because it is commonly positioned at the C-terminal end of peptidyl mono-FMKs in the literature.[7–12] The methyl ester-protected sidechain is employed to aid cell permeability and subsequently demethylated via endogenous esterases.[7]

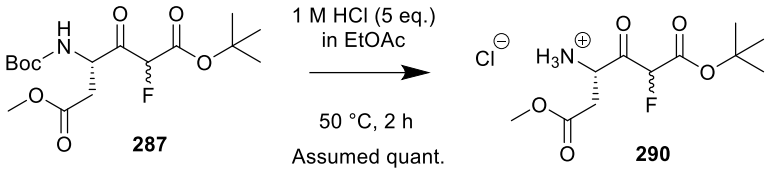

Scheme 4.8 – Conditions employed for selective Boc removal of **287**.

In addition to selective removal of Boc in the presence of a *tert*-butyl ester, the option of simply using harsher conditions to bring about simultaneous Boc removal, *tert*-butyl ester deprotection and decarboxylation to the FMK was also considered. Whilst the former method would prove more desirable if there was a *tert*-butyl ester protected sidechain that needed to be kept intact for subsequent reactions (until the final deprotection and decarboxylation step), it was thought that the latter method may otherwise prove more convenient. The resulting FMK substrate could then be coupled to a peptide of choice in solution. In order to achieve this, *β*-ketoester **287** was exposed to 50% TFA in DCM at room temperature overnight and concentrated under reduced pressure (**Scheme 4.9a**). Both the ^{t}Bu ester and Boc peaks disappeared from the ^{1}H NMR spectrum whilst the ^{19}F NMR spectrum showed the appearance of a triplet peak around -215 ppm (**Figure 4.5**). In order to speed up the process, the reaction was also carried out using 50% TFA in DCM at 40 °C for 1 hour (**Scheme 4.9b**). However, after this period of time, by comparison with the ^{19}F NMR spectrum of the starting material (**Figure 4.6a**), it appeared that some 1,3-dicarbonyl, possibly the corresponding Boc-deprotected *β*-ketoacid (as no significant Boc or *tert*-butyl ester peaks were observed by ^{1}H NMR

spectroscopy), was still present at -198 ppm in the crude material, in addition to the emergence of a triplet at -233 ppm (**Figure 4.6b**). After lyophilisation, the signal at -198 ppm disappeared, but the triplet at -233 ppm was found to have mostly been replaced by another triplet at -215 ppm (**Figure 4.6c**). Comparison of the ^{1}H NMR spectrum for the *β*-ketoester starting material (**287**) (**Figure 4.7a**) with that of the crude material after the 1-hour reaction period (**Figure 4.7b**) revealed a shift in the position of the doublet corresponding to the CH_2 adjacent to the fluorine atom from 5.35 ppm to 5.09 ppm. Interestingly, a further shift was observed to 5.53 ppm after lyophilisation (**Figure 4.7c**), in keeping with the change seen by ^{19}F NMR spectroscopy. A close-up view of the ^{1}H NMR spectra portraying these changes is given in **Figure 4.8a-c**. Whilst the reason for the shifts observed is uncertain, it was suggested that the initial change in the ^{19}F NMR spectrum to a triplet at -233 ppm in combination with the ^{1}H NMR shift to 5.09 ppm could represent *tert*-butyl ester deprotection and decarboxylation to the FMK, with only partial Boc removal to the carboxylic acid (**293**). This would be consistent with the fact that no significant *tert*-butyl or Boc peaks were present by ^{1}H NMR spectroscopy (**Figure 4.7b**). Furthermore, it could explain why the peaks in the ^{19}F and ^{1}H NMR spectra shifted again to -215 ppm and 5.53 ppm respectively after lyophilisation, as this could have facilitated further Boc removal. Given that a small amount of the doublet at 5.09 ppm was still identifiable by ^{1}H NMR spectroscopy after lyophilisation (**Figure 4.7c**), the reaction was also carried out at 40 °C for 2.5 hours followed by lyophilisation (**Scheme 4.9c**), which brought about the emergence of a triplet at -215 ppm in conjunction with what appeared to be complete Boc removal, as suggested by ^{1}H NMR spectroscopy, and the absence of a peak at -233 ppm in the ^{19}F NMR spectrum (**Figure 4.9**).

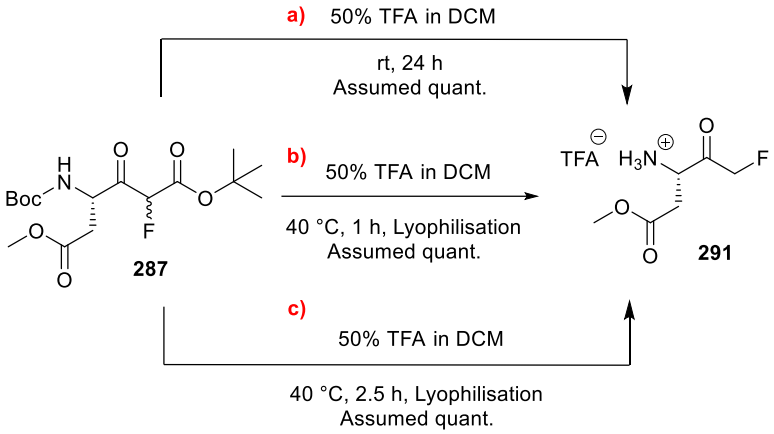

Scheme 4.9a-c – Conditions employed for concomitant Boc deprotection, *tert*-butyl ester removal and decarboxylation of **287** to **291**.

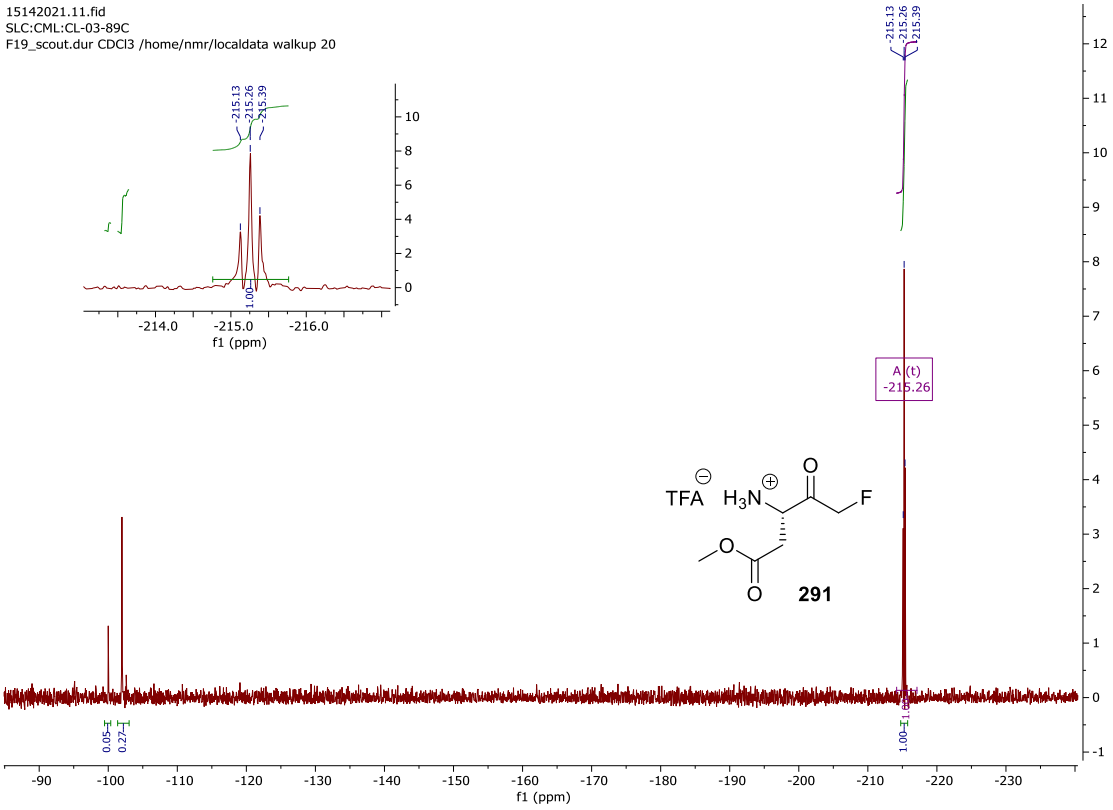

Figure 4.5 – ^{19}F NMR spectrum ($CDCl_3$) recorded after deprotection and decarboxylation of *β*-ketoester **287** to FMK **291** using 50% TFA in DCM at rt for 24 h.

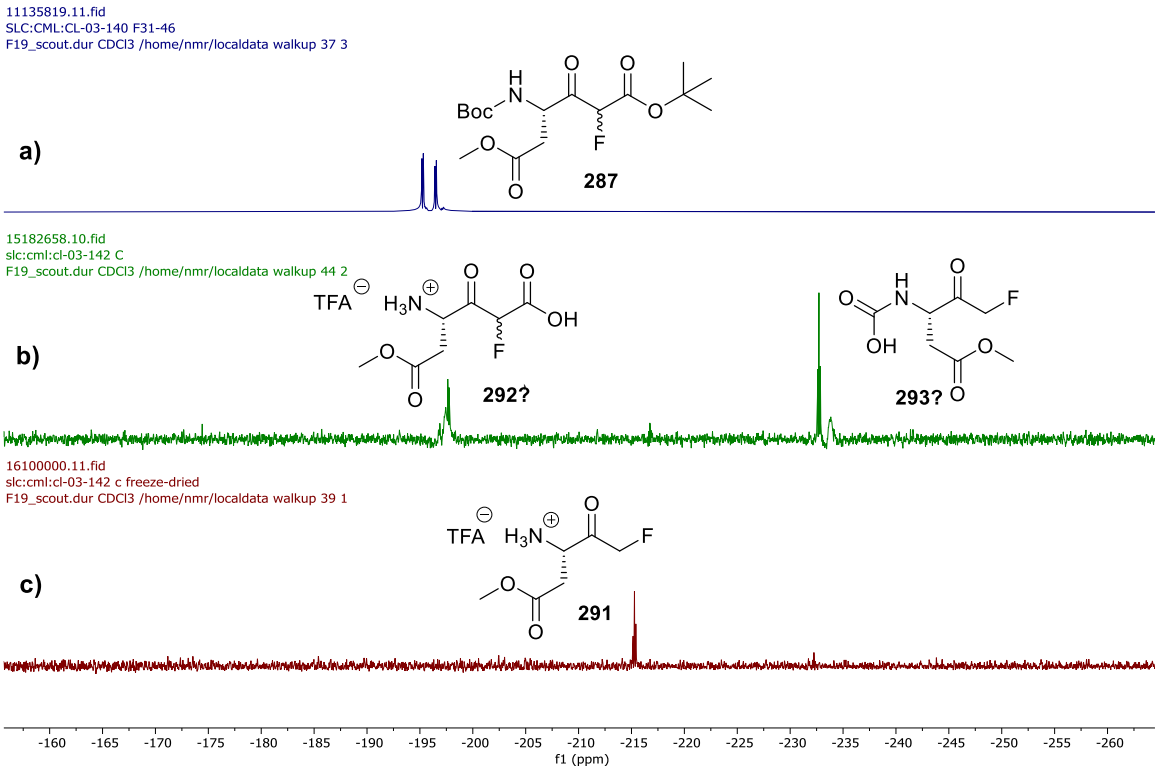

Figure 4.6 – ^{19}F NMR spectra ($CDCl_3$) for *β*-ketoester **287** (**a**), the crude material after reaction of **287** with 50% TFA at 40 °C for 1 hour (**b**) and after subsequent lyophilisation (**c**).

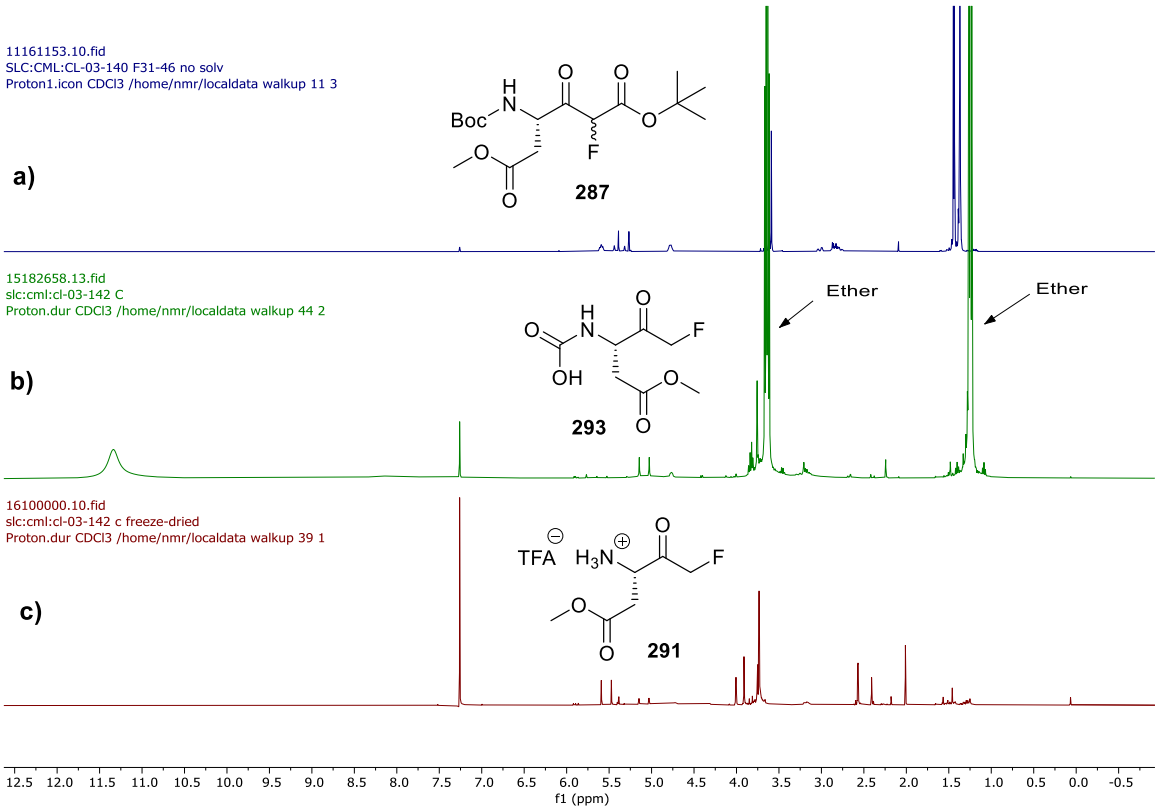

Figure 4.7 – ^{1}H NMR spectra ($CDCl_3$) for *β*-ketoester **287** (**a**), the crude material after reaction of **280** with 50% TFA at 40 °C for 1 hour (**b**) and after subsequent lyophilisation (**c**).

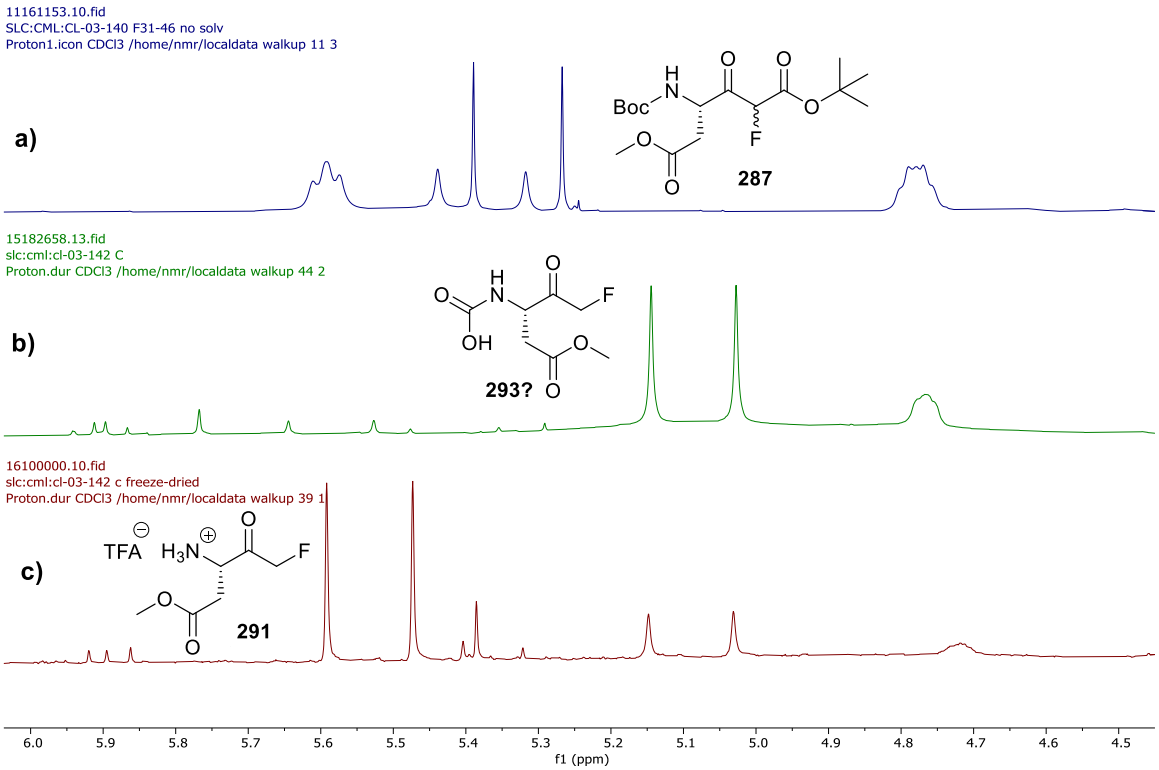

Figure 4.8 – Close-up ^{1}H NMR spectra ($CDCl_3$) for *β*-ketoester **287** (**a**), the crude material after reaction of **287** with 50% TFA at 40 °C for 1 hour (**b**) and after subsequent lyophilisation (**c**).

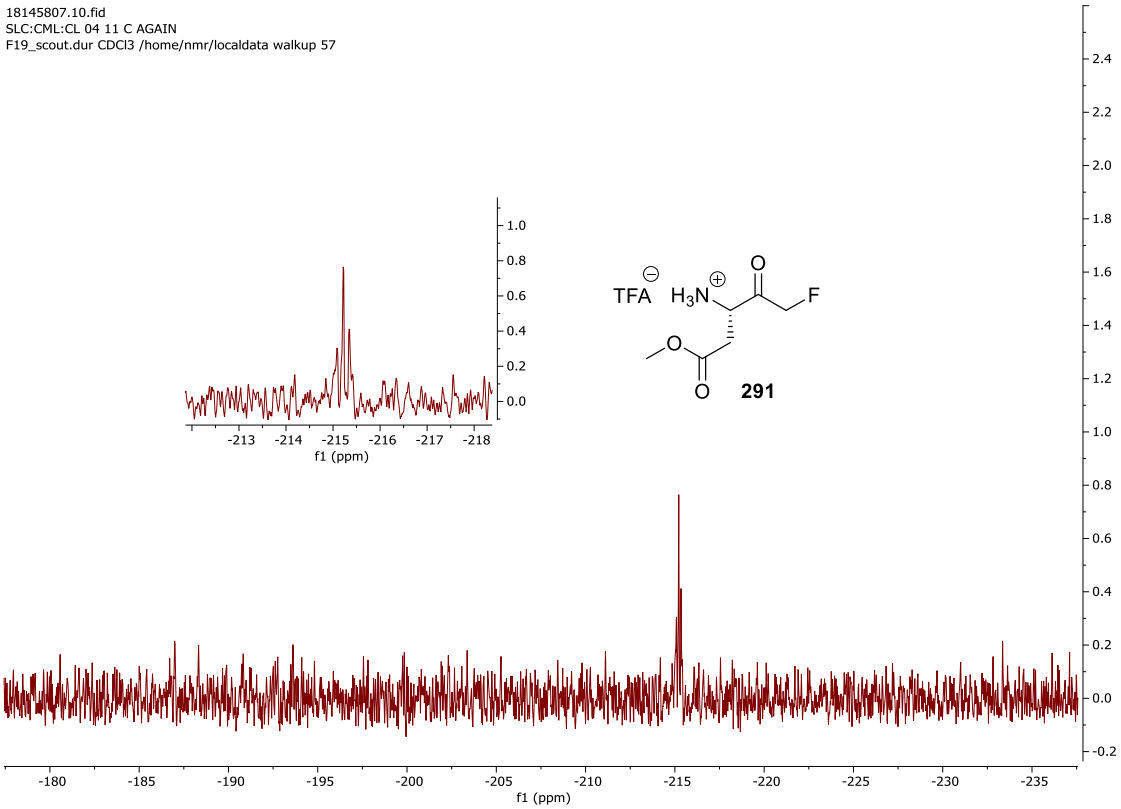

Figure 4.9 – ^{19}F NMR (^{1}H coupled) spectrum ($CDCl_3$) recorded after deprotection and decarboxylation of *β*-ketoester **287** to give FMK **291** using 50% TFA in DCM at 40 °C for 2.5 hours followed by lyophilisation.

Interestingly, after reaction of *β*–ketoester **287** with 50% TFA in DCM at 40 °C for 2.5 hours and subsequent lyophilisation (**Scheme 4.9c**), whilst the expected mass for FMK **291** (164 Da) was identified by mass spectrometry (+ve) (**Figure 4.10**), a clear peak with a mass corresponding to **291** minus two Daltons could also be seen (162 Da) at the same retention time (rt = 0.25 mins). A small amount of this material was also evident after reaction of *β*–ketoester **287** with 50% TFA in DCM for 1 hour and subsequent lyophilisation (**Scheme 4.9b**). It was reasoned that the mass difference could be explained by the replacement of a fluorine atom with a hydroxyl group, possibly during the acidic deprotection and decarboxylation step if moisture had accumulated in the TFA or solvent, or during lyophilisation when acid and water were likely present. Furthermore, the corresponding (**Scheme 4.9c**) crude ^{1}H NMR spectrum did appear to be messy (**Figure 4.11**), with the doublet at 5.53 ppm (corresponding to the CH_2 coupled to the fluorine atom) not appearing to integrate to two protons as would be expected for FMK **291**. Additionally, it was thought that the singlet at 3.9 ppm could represent the CH_2 adjacent to the hydroxyl group of the hydroxymethyl ketone (**294**), as it would be less deshielded than if it was next to the fluorine atom. Nonetheless, HPLC purification would ultimately be performed after the peptide coupling had been completed, and the building block was carried forward to the next step regardless, with varying amounts of hydroxymethyl ketone detected in different batches.

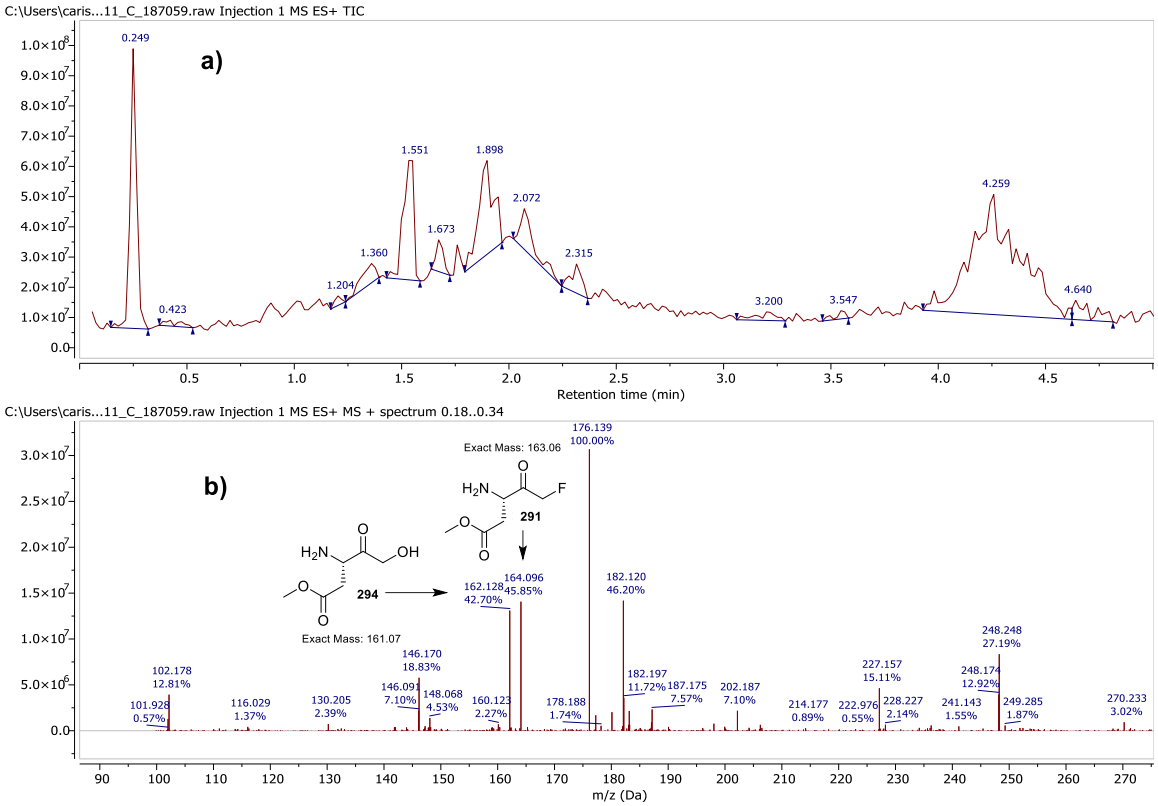

Figure 4.10 – (**a**) TIC (total ion chromatogram) and (**b**) mass spectrometry data (+ve) after formation of FMK **291**, showing evidence for the presence of hydroxymethyl ketone **294**.

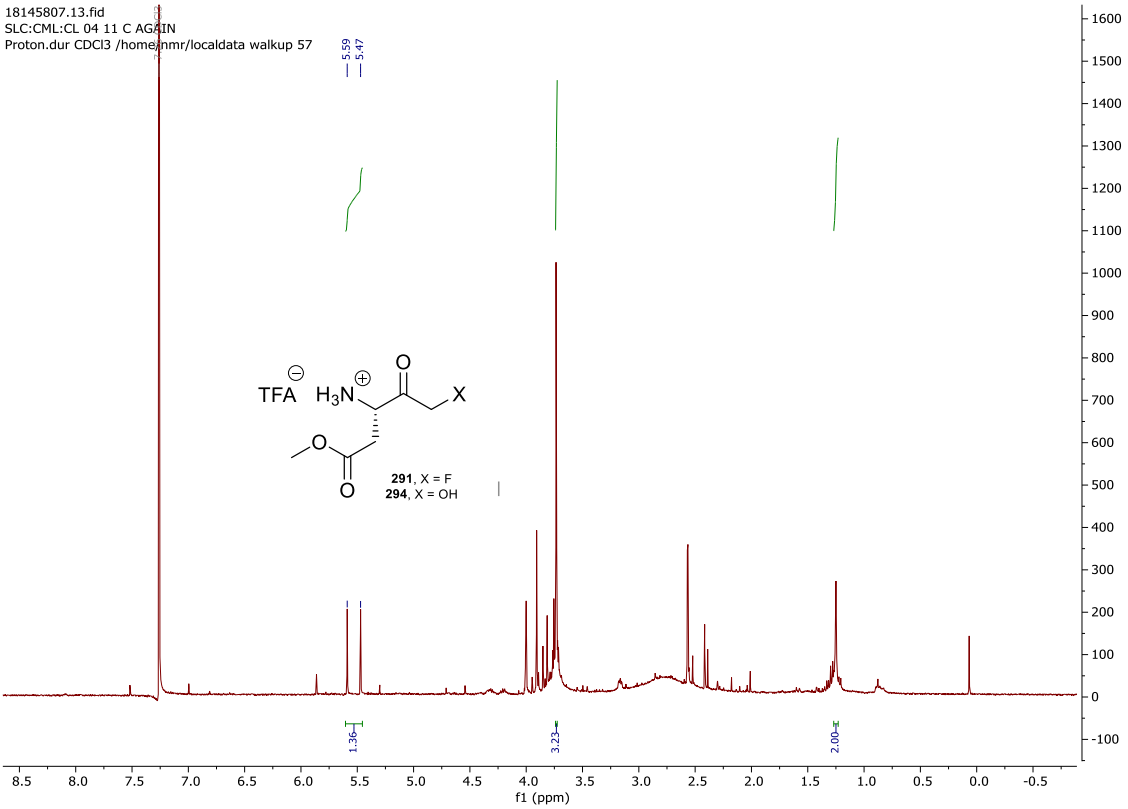

Figure 4.11 – ^{1}H NMR spectrum ($CDCl_3$) after deprotection and decarboxylation of *β*-ketoester **287** to FMK **291** (with suspected formation of hydroxymethyl ketone **294**) using 50% TFA in DCM at 40 °C for 2.5 hours followed by lyophilisation.

With both the 1,3-dicarbonyl and FMK deprotected building blocks in hand (**289**, **290** and **291**), the next step in the process involved coupling them to peptides in solution. In all cases, the product yield for deprotection of the fluorinated building blocks was assumed to be quantitative, and the materials were carried through to the next step in crude form.

4.3 Peptidyl mono-FMK Synthesis

4.3.1 Peptidyl mono-FMK Targets for Synthesis

In order to access peptidyl mono-FMKs of biological relevance, the literature was scoured to find a selection of sequences of interest to synthesise, along with consulting industrial partner, CRB (Cambridge Research Biochemicals). A list of desirable targets was therefore decided upon and is summarised in **Table 4.1**. Their full structures are given in **Figure 4.12**, along with a price and the corresponding supplier for those that are commercially available. As can be seen, these types of compounds are often expensive. Z-VAF-FMK **295** was used as a proof of principle substrate in order to first establish the synthetic methodology, whilst the other FMKs listed all possess known inhibitory characteristics. Z-YVAD(OMe)-FMK **296** reportedly inhibits caspase-1 irreversibly,[13] demonstrating anti-inflammatory and anti-tumour activities.[14] Z-VD(OMe)VAD(OMe)-FMK **297** and Z-D(OMe)E(OMe)VD(OMe)-FMK **46** are known to be caspase-2 and caspase-3 inhibitors respectively, both showing potential against cerebral vasospasm after subarachnoid haemorrhage (SAH).[15] Z-VE(OMe)ID(OMe)-FMK **298** is an inhibitor of caspase-6[16,17] whilst Z-IE(OMe)TD(OMe)-FMK **299** inhibits caspase-8, with the latter showing inhibition of influenza virus-induced apoptosis.[18] Boc-Asp(OMe)-FMK **43** and Z-VAD(OMe)-FMK **40** are both pan-caspase inhibitors, with the former being reported to delay brain tissue loss after traumatic brain injury in rats[19] and the latter showing evidence for endotoxic shock alleviation.[20] Z-FA-FMK **41** is often employed as a negative control[21] as it is unable to inhibit caspase-mediated apoptosis due to the absence of an Asp

sidechain residue in the P_1 position.[22] As a result, it is only able to inhibit cysteine proteases in which this is not a requirement, such as Cathepsin B.[23]

Table 4.1 – Selection of target mono-FMKs for synthesis.

FMK	Application	Sequence
295	Proof of principle	Z-VAF-FMK
296	Caspase-1 inhibitor	Z-YVAD(OMe)-FMK
297	Caspase-2 inhibitor	Z-VD(OMe)VAD(OMe)-FMK
46	Caspase-3 inhibitor	Z-D(OMe)E(OMe)VD(OMe)-FMK
298	Caspase-6 inhibitor	Z-VE(OMe)ID(OMe)-FMK
299	Caspase-8 inhibitor	Z-IE(OMe)TD(OMe)-FMK
43	Caspase Family inhibitor	Boc-Asp(OMe)-FMK
40	Caspase Family inhibitor	Z-VAD(OMe)-FMK
41	Negative Control inhibitor	Z-FA-FMK

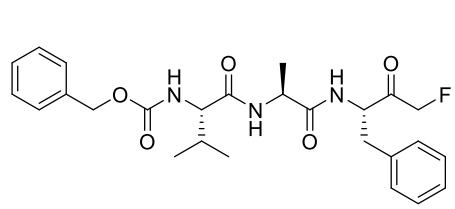

Cbz-Val-Ala-Phe-FMK **295**
Not commercially available

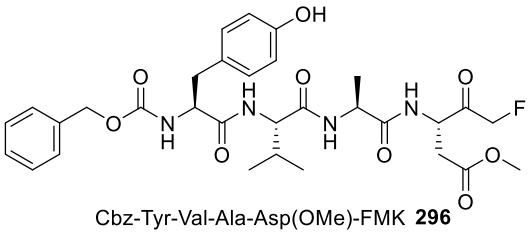

Cbz-Tyr-Val-Ala-Asp(OMe)-FMK **296**
1 mg = £225 (Cambridge Bioscience)

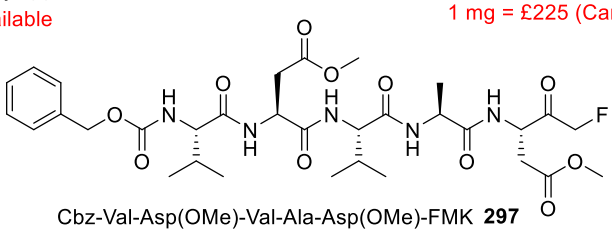

Cbz-Val-Asp(OMe)-Val-Ala-Asp(OMe)-FMK **297**
1 mg = £539 (Sigma-Aldrich)

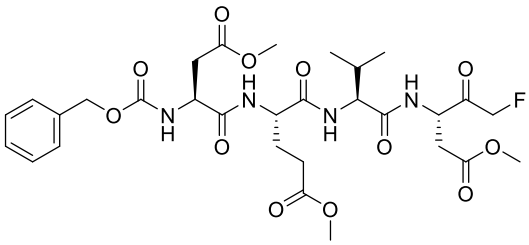

Cbz-Asp(OMe)-Glu(OMe)-Val-Asp(OMe)-FMK **46**
1 mg = £309 (Fisher Scientific)

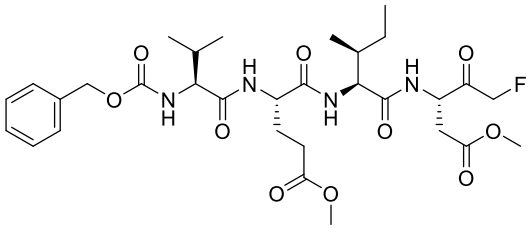

Cbz-Val-Glu(OMe)-Ile-Asp(OMe)-FMK **298**
1 mg = £218 (R&D Systems)

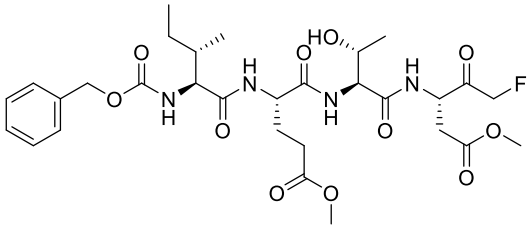

Cbz-Ile-Glu(OMe)-Thr-Asp(OMe)-FMK **299**
1 mg = £118 (AmBeed)

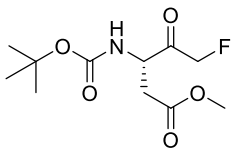

Boc-Asp(OMe)-FMK **43**
1 mg = £105 (Abcam)

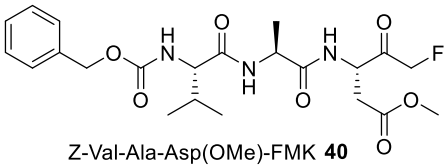

Z-Val-Ala-Asp(OMe)-FMK **40**
1 mg = £219 (Sigma-Aldrich)

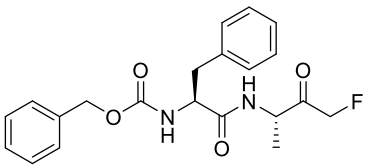

Z-Phe-Ala-FMK **41**
1 mg = £103 (Santa Cruz Biotechnology)

Figure 4.12 – Selection of target mono-FMKs for synthesis. A price and the corresponding supplier are given for those that are commercially available (correct as of November 2022).

The peptide-portion, excluding the C-terminal residue, of the FMKs shown above in **Table 4.1** and **Figure 4.12** (except for **43** and **41** which utilised a slightly different approach as will be described in later sections) were first acquired via either solid or solution-phase methods before being coupled to fluorinated building blocks **289**, **290**, or **291** in solution, as will be detailed below.

4.3.2 Peptide synthesis

The dipeptide needed for accessing Z-VAF-FMK **295** and Z-VAD(OMe)-FMK **296**, namely Z-VA-OH (**304**), was synthesised using standard solution-phase techniques due to its short length (**Scheme 4.10**). Starting from alanine (**300**), methyl ester protection was achieved using thionyl chloride in methanol (**Scheme 4.10a**). Subsequent coupling to Z-Val-OH (**302**) with PyBOP gave access to methyl ester-protected peptide **303** after column chromatography (**Scheme 4.10b**), for which an X-ray crystal structure was attained (**Figure 4.13**). Further reaction with $LiOH.H_2O$ allowed saponification to dipeptide **304** in a yield of 82% (**Scheme 4.10c**).

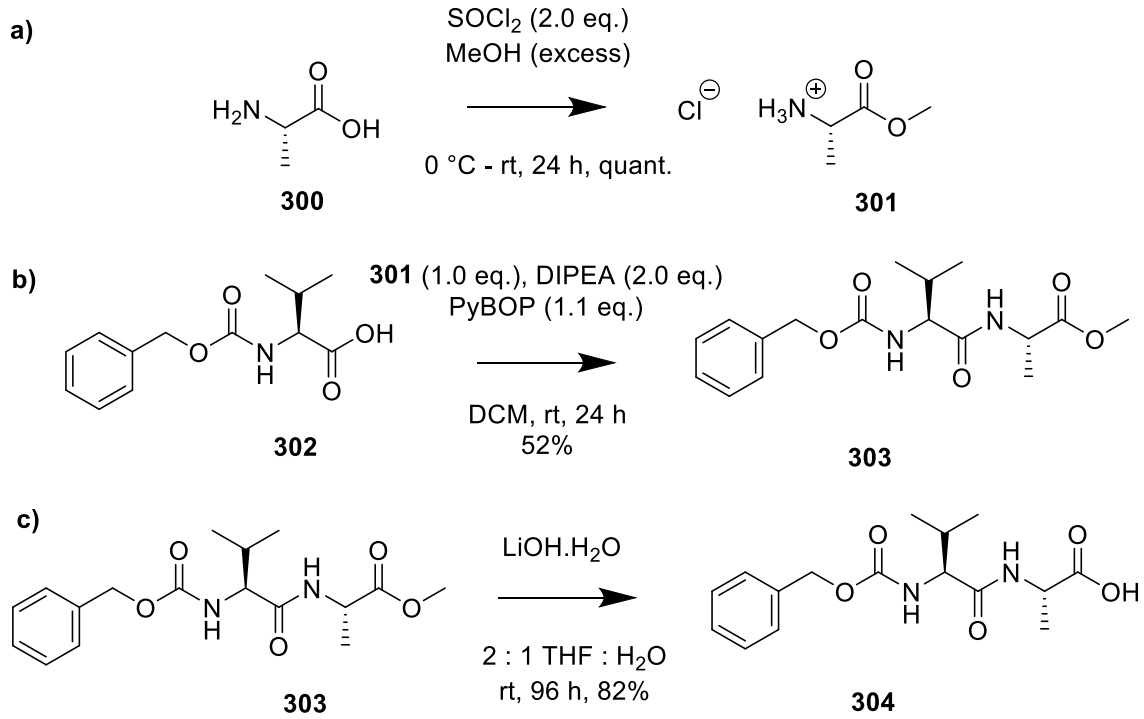

Scheme 4.10 – (**a**) Conditions for methyl ester protection of alanine (**300**). (**b**) Conditions for coupling of *L*-alanine methyl ester hydrochloride (**301**) to Z-Val-OH (**302**) in solution to give **303**. (**c**) Conditions employed for saponification to dipeptide **304**.

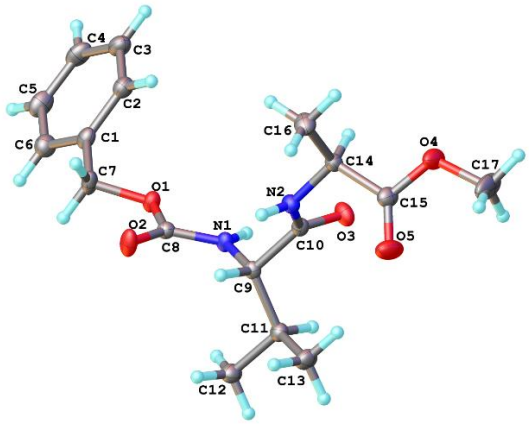

Figure 4.13 – X-ray crystal structure of Cbz-Val-Ala-OMe (**303**), reported with a 50% thermal ellipsoid probability.

The peptides needed for accessing Z-YVAD(OMe)-FMK **296**, Z-VD(OMe)VAD(OMe)-FMK **297**, Z-D(OMe)E(OMe)VD(OMe)-FMK **46**, Z-VE(OMe)ID(OMe)-FMK **298** and Z-IE(OMe)TD(OMe)-FMK **299** were Z-YVA-OH (**305**), Z-VD(OMe)VA-OH (**306**), Z-D(OMe)E(OMe)V-OH (**307**), Z-VE(OMe)I-OH (**308**) and Z-IE(OMe)T-OH (**309**) respectively (**Figure 4.14**). These sequences were all synthesised through standard solid-phase methods, utilising HATU as the coupling agent in the presence of DIPEA. The pre-loaded resin of choice was either Wang or 2-chlorotrityl chloride to ensure an acid C-terminus could be regenerated for further coupling in solution. The latter was employed when acid-sensitive sidechain protecting groups were present, to ensure mild resin cleavage could be achieved whilst leaving the sidechain protecting groups intact for the subsequent solution-phase coupling step to a fluorinated building block. Apart from Z-D(OMe)E(OMe)V-OH (**307**) and Z-Val-Glu(OMe)-Ile-OH (**308**), which were first purified using reverse-phase HPLC by Cambridge Research Biochemicals (CRB), all peptides were carried through to the next step in their crude forms. Analytical traces for each peptide are provided in **Figure 4.15a-f**, whilst mass spectrometry (+ve) data in **Figure 4.16** confirms the identity of peptides **305**, **306**, **307**, **308** and **309**. Notably, the observed peak shape of the analytical trace associated with peptide **308** was found to vary when recorded on two different analytical HPLC setups (**Figure 4.15d** relates to analytical HPLC protocol **7.3.8.4**, whilst **Figure 4.15e** relates to analytical HPLC protocol **7.3.8.5**), which could be associated with the variation in column and gradient used between the two systems. Both analytical traces for peptide **308** are given in **Figure 5.15** (**d** and **e**) for comparison.

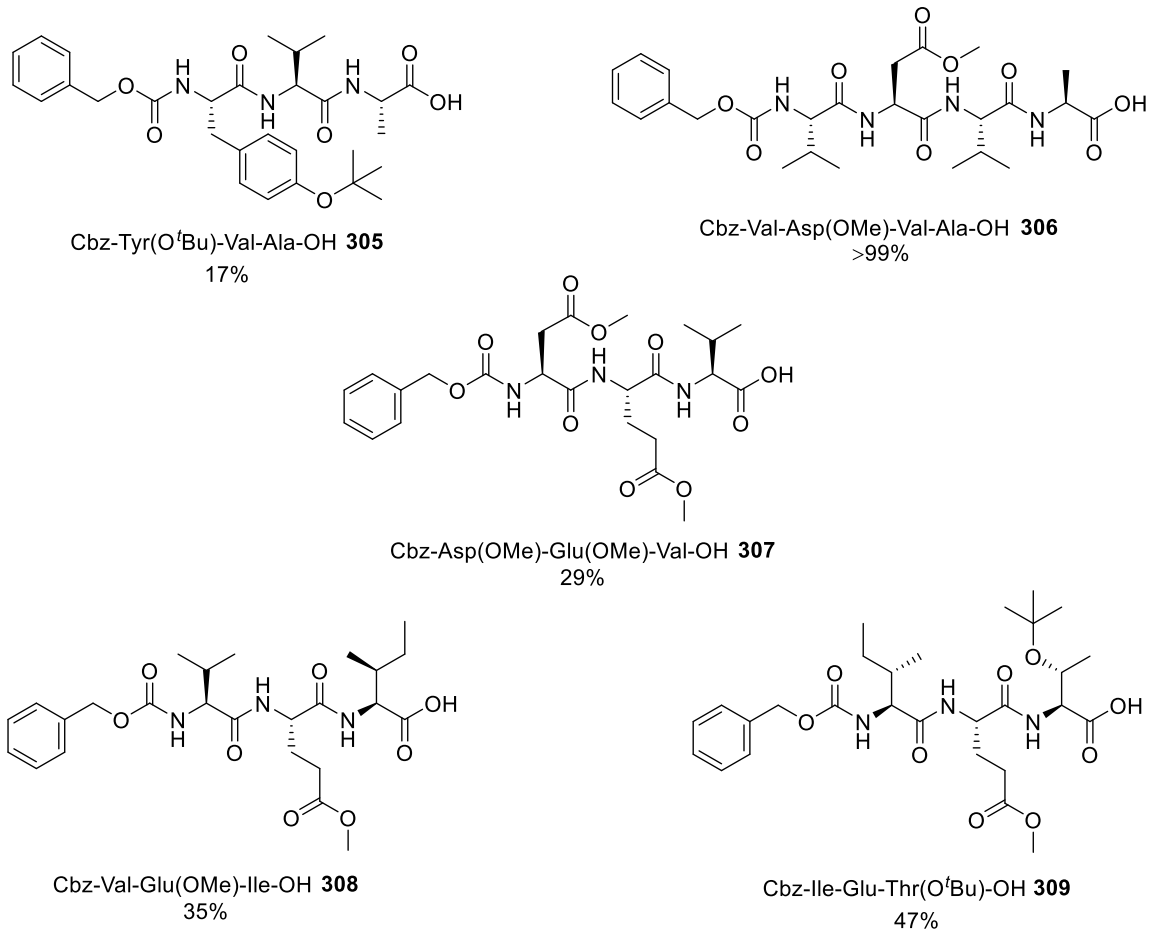

Figure 4.14 – Peptide targets **305**, **306**, **307**, **308** and **309** made for use in the synthesis of peptidyl FMKs **296**, **297**, **46**, **298** and **299** respectively. Crude yields are given for all, except **300** and **301** for which the HPLC-purified yield is provided.

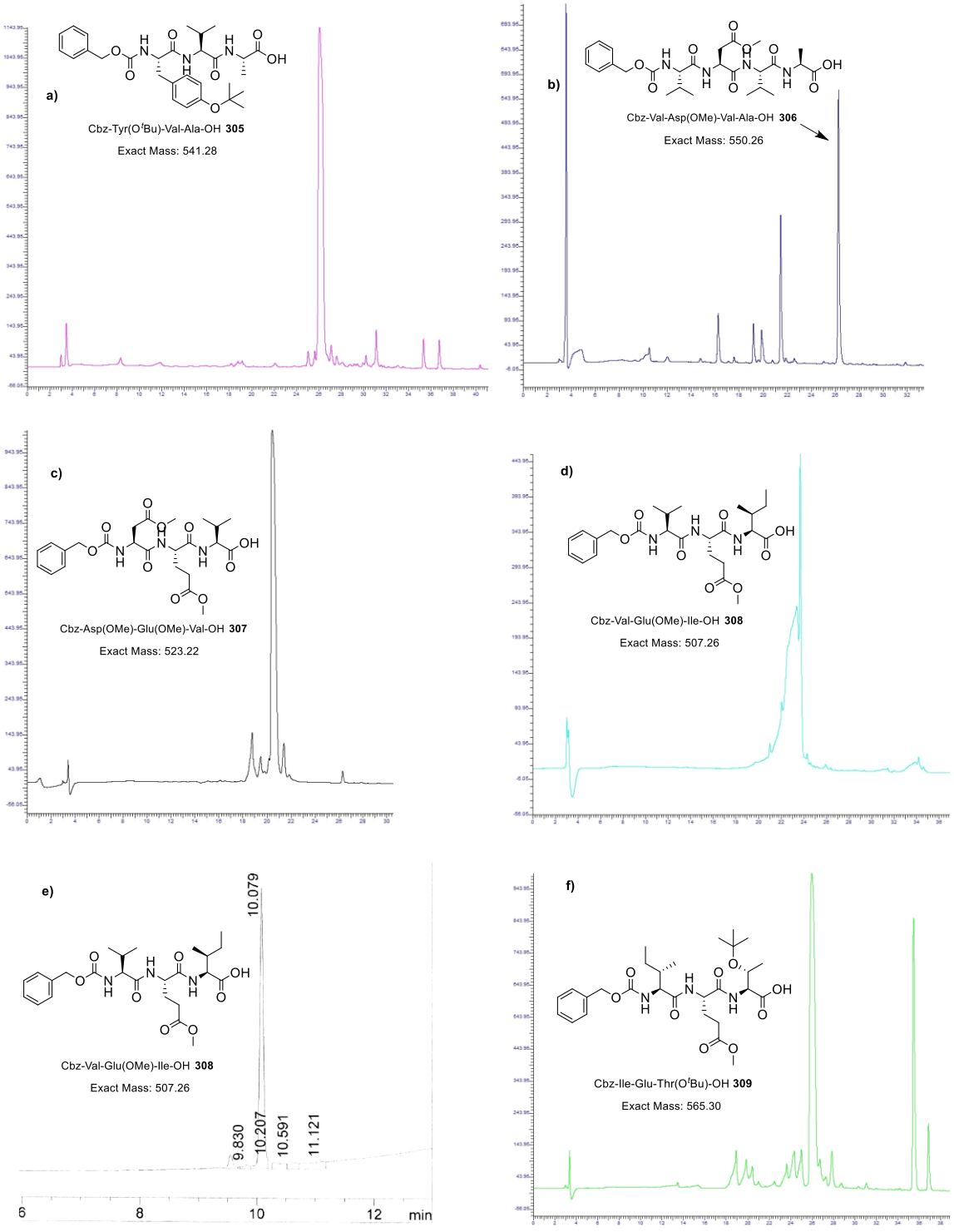

Figure 4.15 – Crude analytical HPLC traces (λ = 220-230 nm) for peptides **305** (**a**), **306** (**b**), **307** (**c**) and **309** (**f**), along with post-prep analytical HPLC traces for peptide **308** (**d** and **e**) recorded on two different machines. X-axes represent the retention times in minutes.

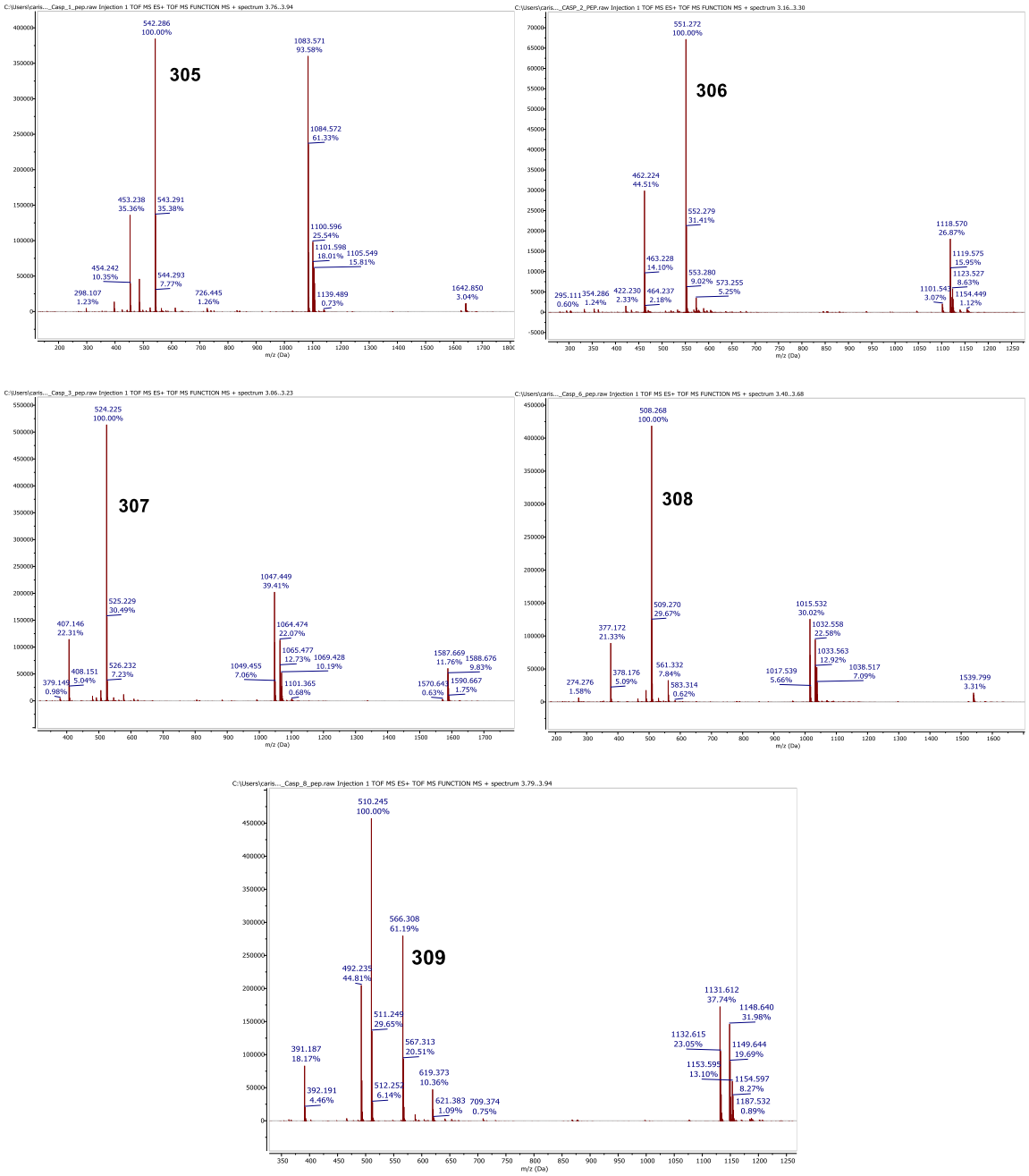

Figure 4.16 – Mass spectrometry (+ve) data for peptides **305**, **306**, **307**, **308** and **309**.

4.3.3 Mono-FMK Formation in Solution

Now that the necessary fluorinated building blocks and peptide sequences had been acquired, the next step was to couple them together in solution. This was initially trialled by coupling Z-VA-OH (**304**) to phenylalanine-derived fluorinated 1,3-dicarbonyl **289** using PyBOP and *N*-methylmorpholine (NMM) (**Scheme 4.11a**). After column chromatography, **310** was successfully isolated in a yield of 36%, although a very small amount of suspected di-fluorinated material was also apparent by ^{19}F NMR spectroscopy (**Figure 4.17a**, -112 ppm). These conditions were then transferred to Z-VA-OH (**304**) and aspartic acid-derived fluorinated 1,3-dicarbonyl **290**, affording **311** in a yield of 22% (**Scheme 4.11b**). The ^{19}F NMR spectra for both products display peaks in the region of -196 ppm as expected (**Figure 4.17**). Isolated yields were found to be low in both cases despite extended reaction times, which could be due to the electron-withdrawing nature of the fluorine atom reducing the nucleophilicity of the amine, as was likely a contributing factor towards the problems encountered during resin loading attempts in **Chapter 3**. Furthermore, there were concerns that the use of NMM could be leading to unwanted epimerisation at the C-terminal amino acid sidechain (alanine), evidenced by the complexity of the ^{19}F NMR peaks beyond what would be expected due to the presence of diastereoisomers (**Figure 4.18**), although it is also plausible that rotamers were responsible. Thus, moving forwards from here, all couplings of peptides to the fluorinated building blocks in solution were instead performed using the sterically hindered base, 2,4,6-collidine (2,4,6-trimethylpyridine), to help reduce this.[24]

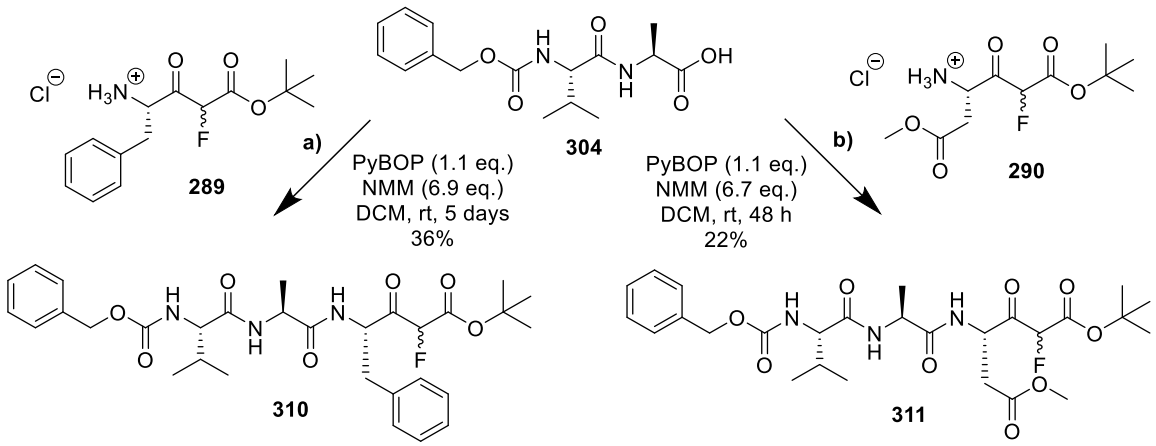

Scheme 4.11 – Conditions for coupling dipeptide **304** to fluorinated building blocks **289** (**a**) and **290** (**b**).

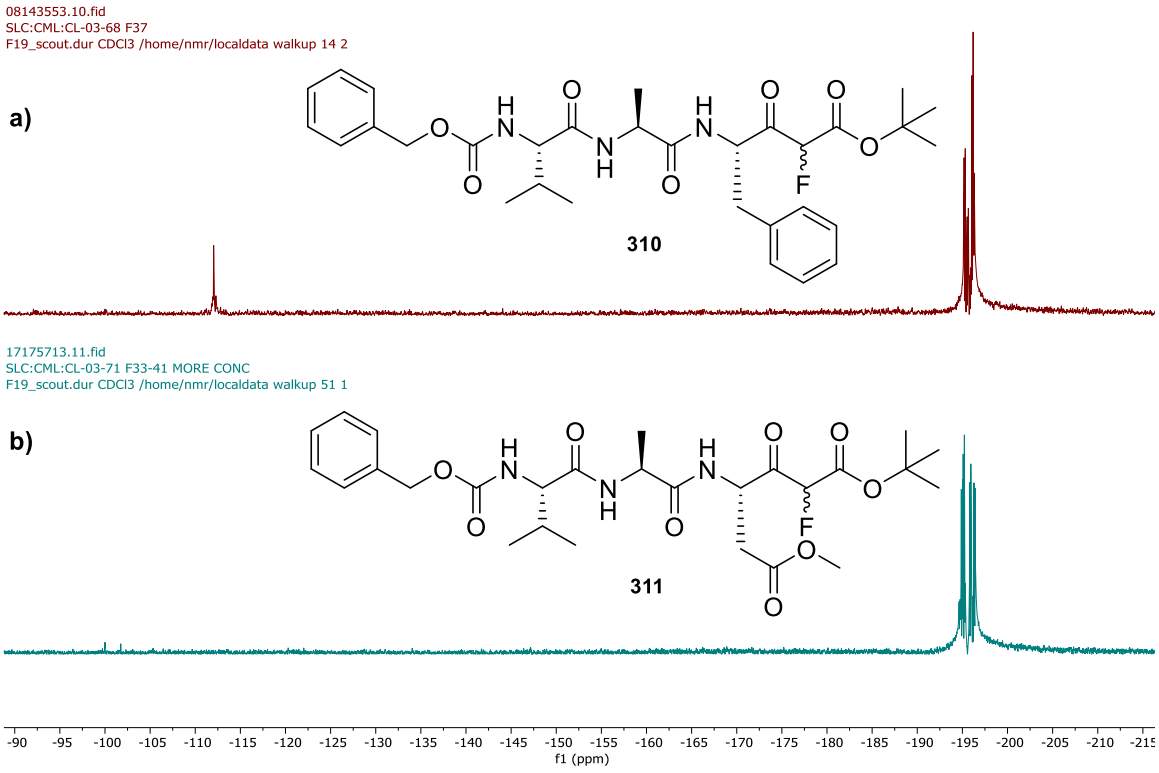

Figure 4.17 – ^{19}F NMR (^{1}H coupled) spectra ($CDCl_3$) for **310** (**a**) and **311** (**b**).

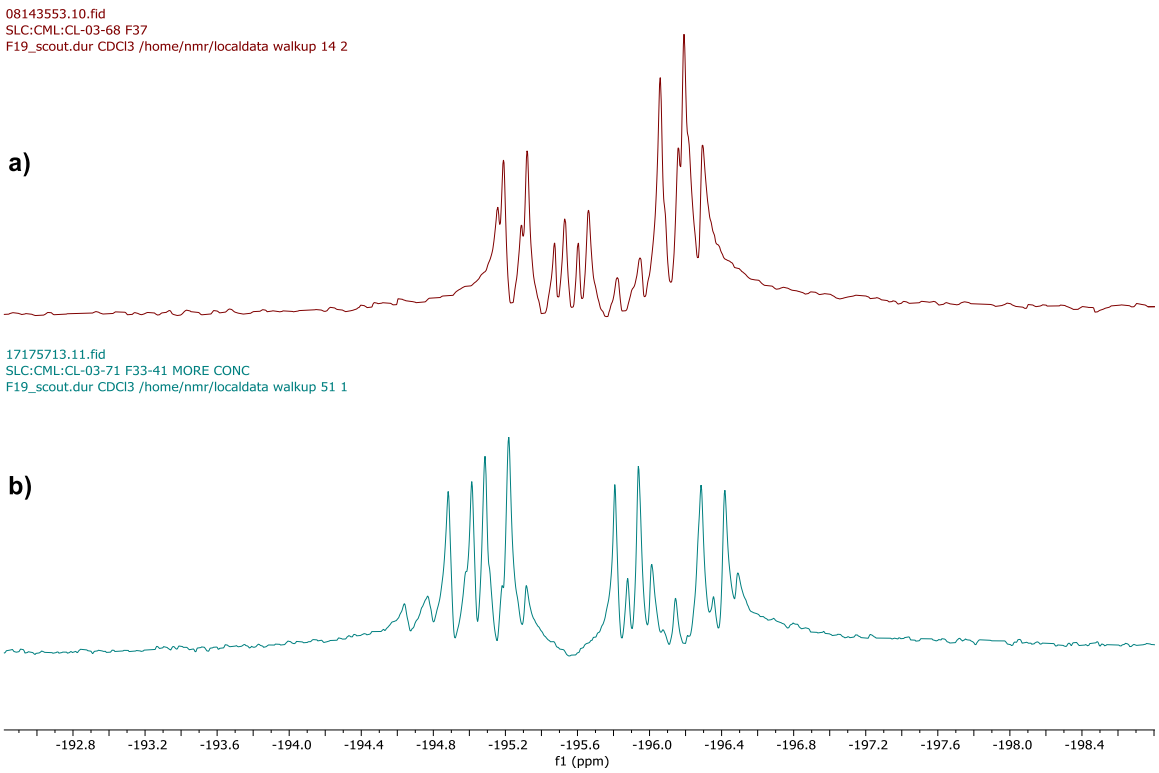

Figure 4.18 – Close-up view of ^{19}F NMR (^{1}H coupled) spectra ($CDCl_3$) for **310** (**a**) and **311** (**b**).

With fluorinated peptides **310** and **311** in hand, *tert*-butyl ester deprotection and decarboxylation were the final steps needed to reach the desired FMK targets. As a similar transformation had already successfully been performed in **Section 3.6.3**, the same one-pot conditions were employed here. 13% TFA in DCM was added at room temperature overnight to substrates **310** and **311**, affording the corresponding FMKs **295** and **40** in isolated yields of 62% and 25% respectively after column chromatography (**Scheme 4.12**). For the formation of FMK **295**, a shift in the ^{19}F NMR spectrum was observed from –195.7 ppm, which is typical of mono-fluorinated di-carbonyls, to around -230.5 ppm, characteristic of mono-FMKs (**Figure 4.19**). Likewise, the peak at -195.6 ppm was replaced by a peak at -231.7 ppm during the synthesis of FMK **40** (**Figure 4.20**). Whilst the peaks would each be expected to appear as a triplet, the added complexity of the splitting patterns, in which multiple triplet peaks seem to be present, could be attributed to potential racemisation during the earlier solution-phase coupling step, leading to diastereoisomers. Alternatively, the presence of rotamers could also be a plausible explanation. The identity of the FMKs was verified further via ^{1}H NMR spectroscopy, ^{13}C NMR spectroscopy and high-resolution mass spectrometry (HRMS).

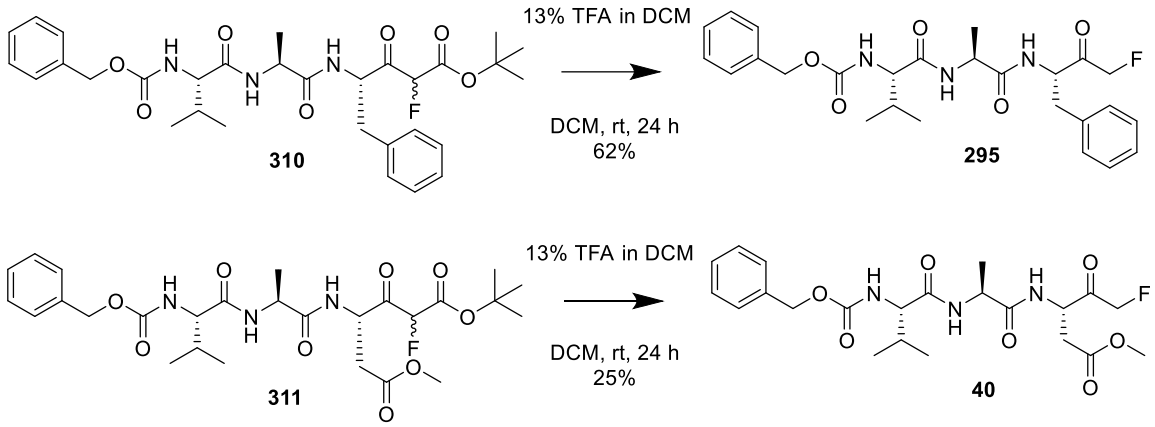

Scheme 4.12 – Conditions for decarboxylation of **310** and **311** to FMKs **295** and **40** respectively.

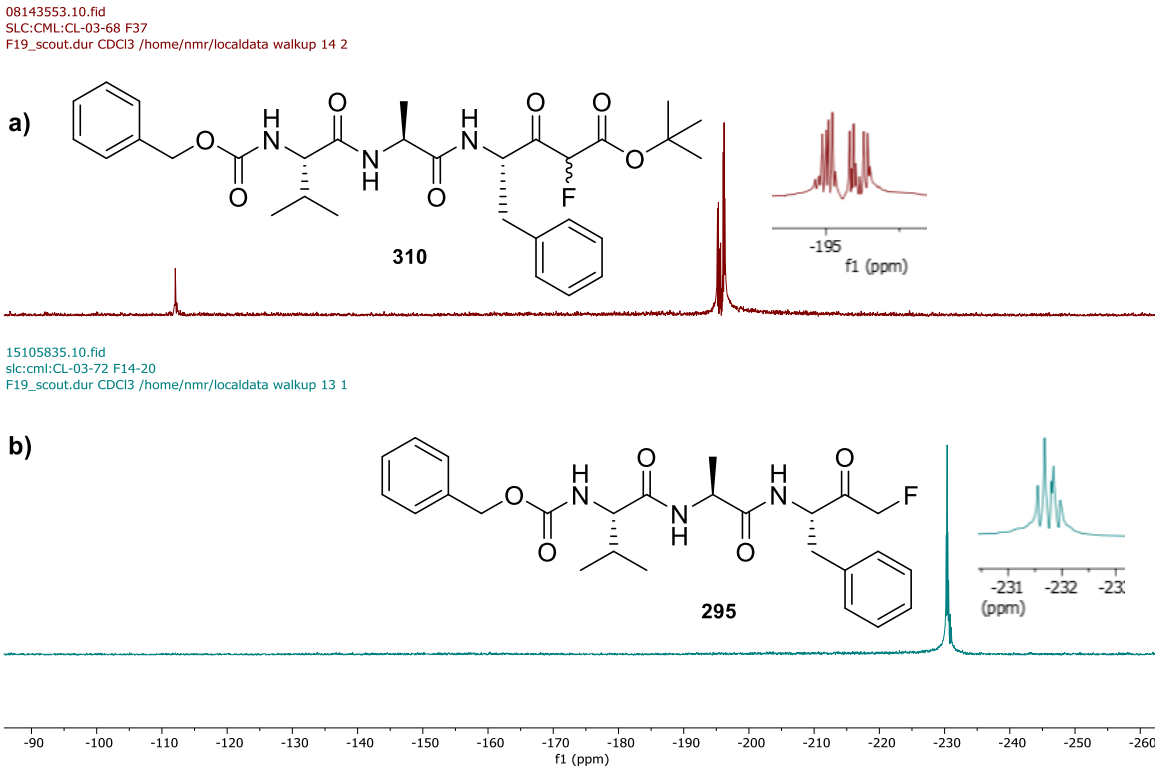

Figure 4.19 – ^{19}F NMR (^{1}H coupled) spectra ($CDCl_3$) for fluorinated di-carbonyl **310** (**a**) and FMK **295** (**b**).

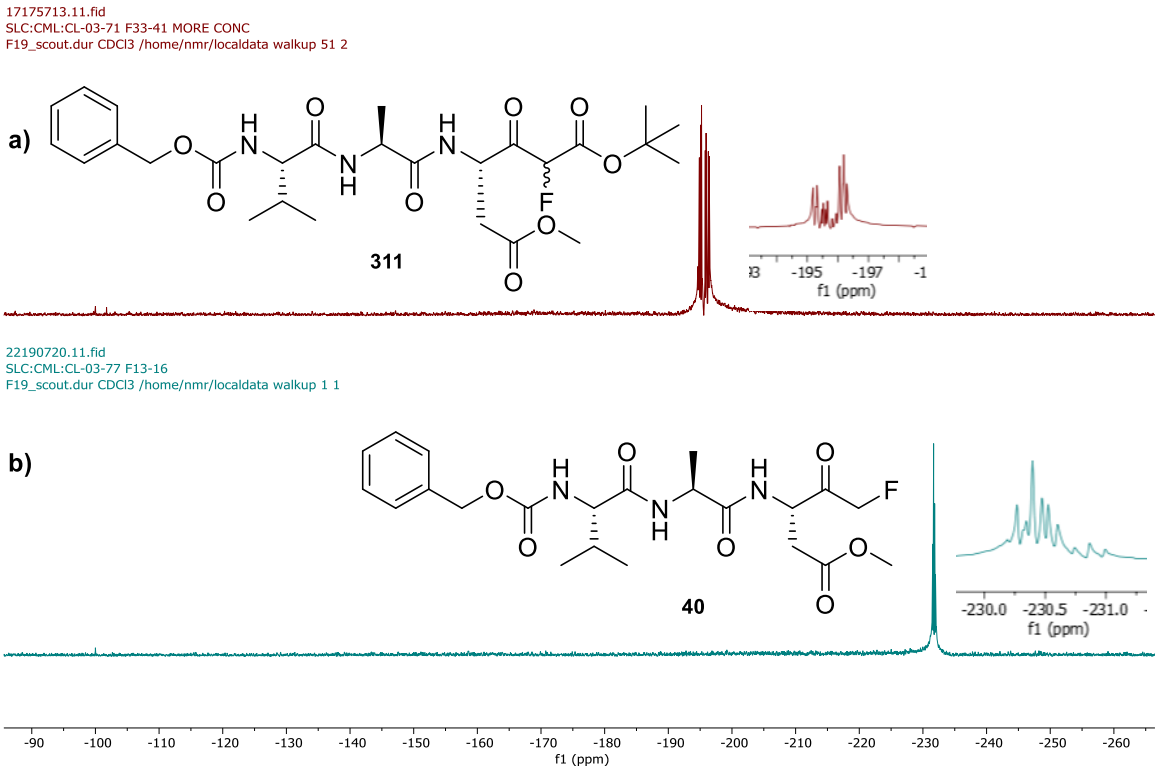

Figure 4.20 – ^{19}F NMR (^{1}H coupled) spectra ($CDCl_3$) for fluorinated di-carbonyl **311** (**a**) and FMK **40** (**b**).

Now that a route had been established for successfully isolating peptidyl mono-fluoromethyl ketones, similar methodology (with some changes) was employed to provide access to the remaining FMKs shown in **Figure 4.12** (*Note* - synthesis of **43** and **41** utilised adapted approaches, as will be described later). Modifications to the coupling method involved the use of 2,4,6-collidine in the place of NMM to reduce racemisation (as described above), the employment of HATU as a coupling agent instead of PyBOP due to its enhanced reactivity, and the coupling of peptides directly to FMK building block **291** rather than the corresponding *β*–ketoester (**290**) to avoid the necessity for selective Boc deprotection, as shown in **Scheme 4.13, step 1**. Global deprotection was then performed using 2.5% H_2O in TFA for accessing compounds **296** and **299**, as these possessed acid-sensitive sidechain protecting groups (**Scheme 4.13**, **step 2**). This allowed access to peptidyl FMKs **296**, **297**, **46**, **298** and **299**; however, impurities were present, as determined by LCMS (+ve). Purification by reverse-phase HPLC offered significant improvements; however, unwanted peaks were still identifiable by LCMS (+ve) and

analytical HPLC, including the presence of what appeared to be the hydroxymethyl ketone analogue in the case of FMKs **46** and **298**, likely having been carried through from the previous step as described above (**Section 4.2.3**). Furthermore, the target purity of ≥95% had not been reached. Consequently, the peptidyl FMKs were re-purified by HPLC in an attempt to attain enhanced purity. The resulting analytical traces (λ = 220 nm) and corresponding mass spectra (+ve) are provided for FMKs **296**, **46**, **298** and **299** in **Figures 4.21**, **4.23**, **4.24** and **4.25** respectively. The LCMS trace for FMK **297** is shown in **Figure 4.22**. As can be seen for Caspase 3 inhibitor **46** (**Figure 4.23**) and Caspase 6 inhibitor **298** (**Figure 4.24**), identification of masses corresponding to two Daltons less than those expected (667.4 and 651.5 Da respectively) in addition to the target FMK masses (669.4 and 653.4 Da respectively) suggested the presence of the hydroxymethyl ketone analogues (**312** and **313** respectively) in addition to the FMKs (**46** and **298** respectively). Other unassigned impurity masses were also observed alongside those expected for FMKs **296**, **298** and **299**. Additionally, the isolated yields acquired were very low (**Figure 4.13**), especially after repeated purification attempts, with very little material being recovered in some cases. A ^{19}F NMR spectrum recorded for FMK **298** revealed the presence of a triplet peak, as expected, at -216.89 ppm (**Figure 4.26**). Interestingly, the ^{19}F NMR spectrum corresponding to FMK **46** possessed multiple triplet signals (**Figure 4.27**), which were each reduced to singlets in the ^{1}H decoupled ^{19}F NMR spectrum, suggesting four different species. Whilst the reason for this is uncertain, it was suggested that epimerisation could have occurred during the coupling of peptide **307** to FMK building block **291**, resulting in diastereoisomers due to a lack of stereospecificity a the P_2 position of FMK **46**. Thus, the extra signals observed could in part be due to diastereoisomers and/or rotamers.

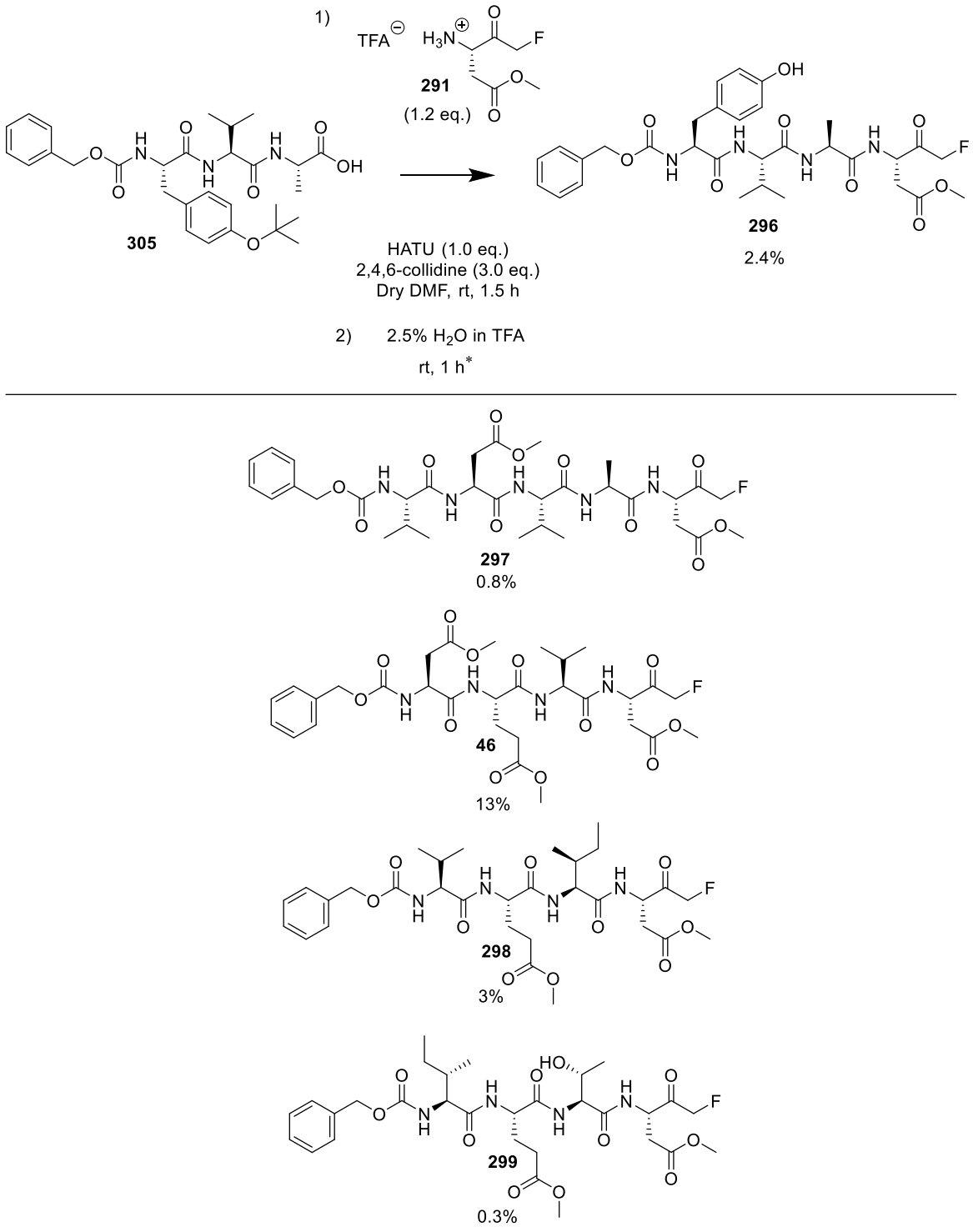

Scheme 4.13 – Conditions employed for accessing peptidyl FMKs **296**, **297**, **46**, **298** and **299** via solution-phase coupling and sidechain deprotection where necessary. *Only FMKs **296** and **299** required step 2 i.e. 2.5% H_2O in TFA at rt for 1 h. Yields given refer to isolated yields, including any impurities that were still present.

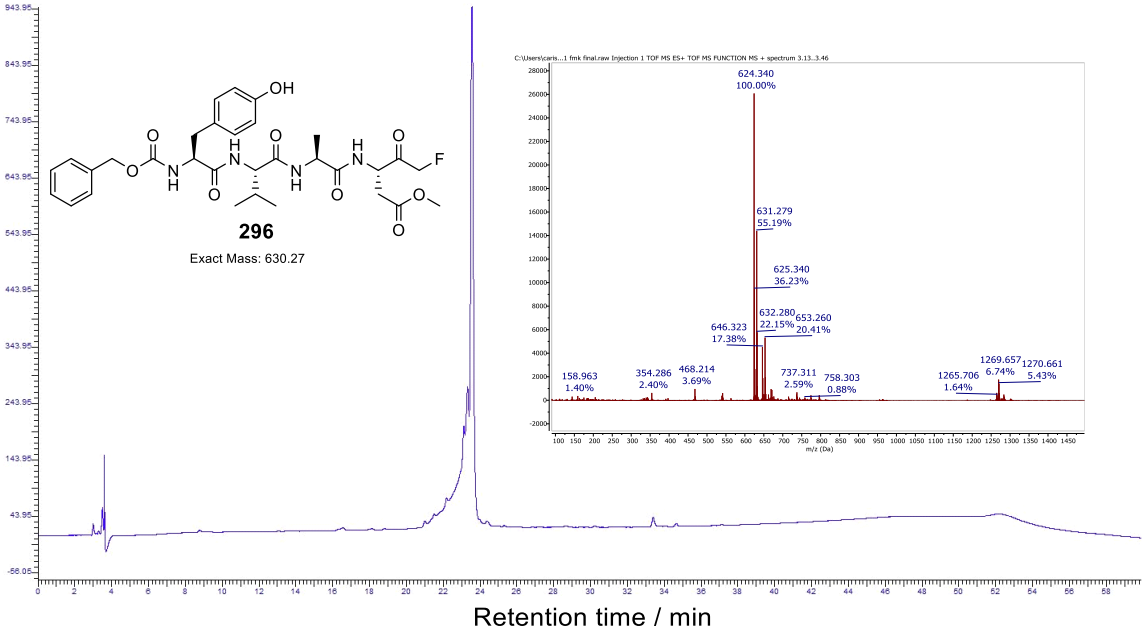

Figure 4.21 – Analytical trace (λ = 220 nm) and mass spectrometry data (+ve) for Caspase 1 inhibitor **296**.

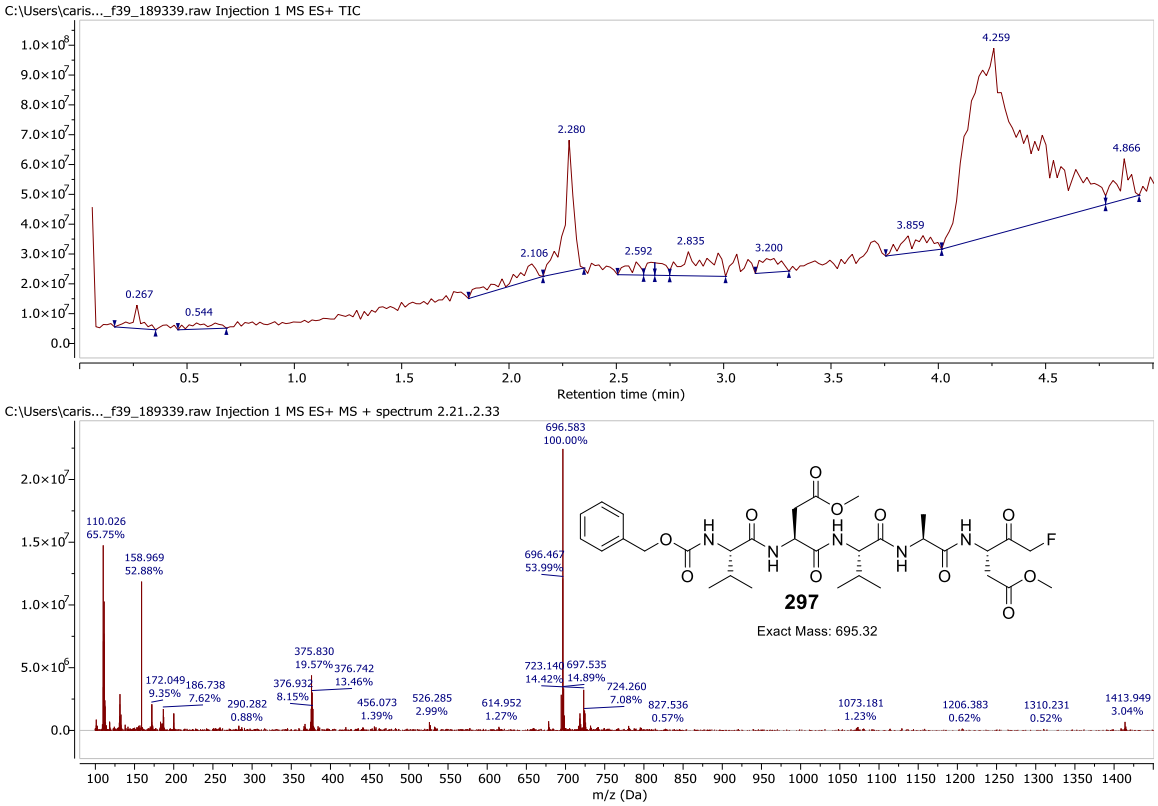

Figure 4.22 – LCMS data (λ = 220 nm) (+ve) for Caspase 2 inhibitor **297**.

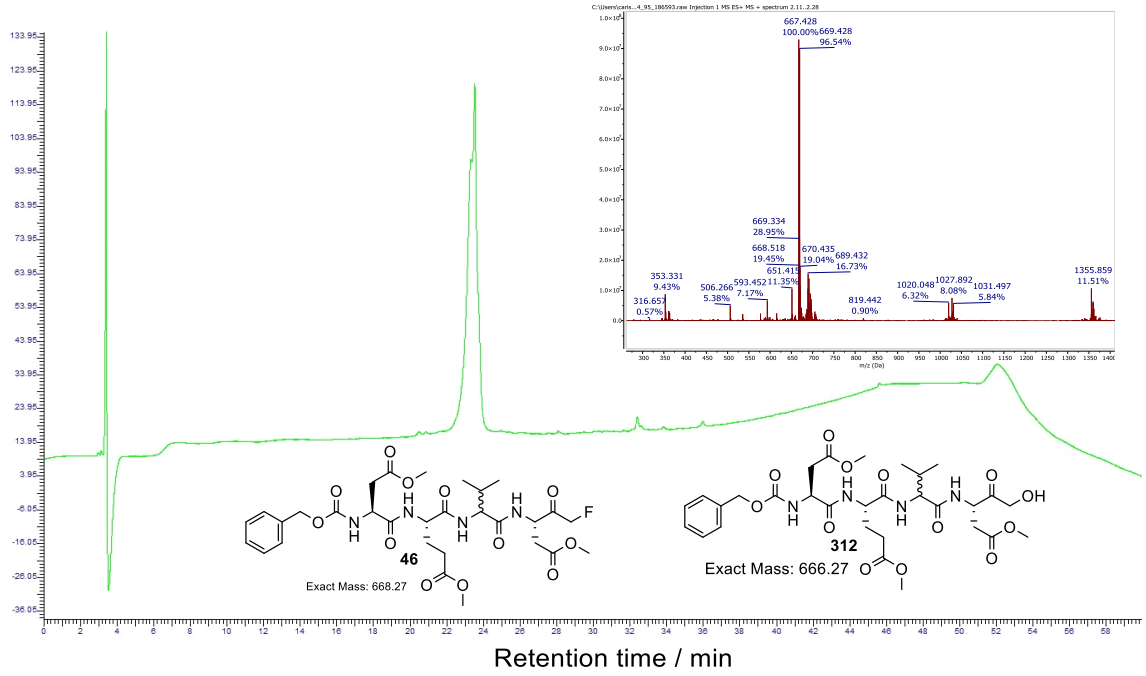

Figure 4.23 – Analytical trace (λ = 220 nm) and mass spectrometry data (+ve) for Caspase 3 inhibitor **46**, with the possibility of hydroxymethyl ketone **312** being present too.

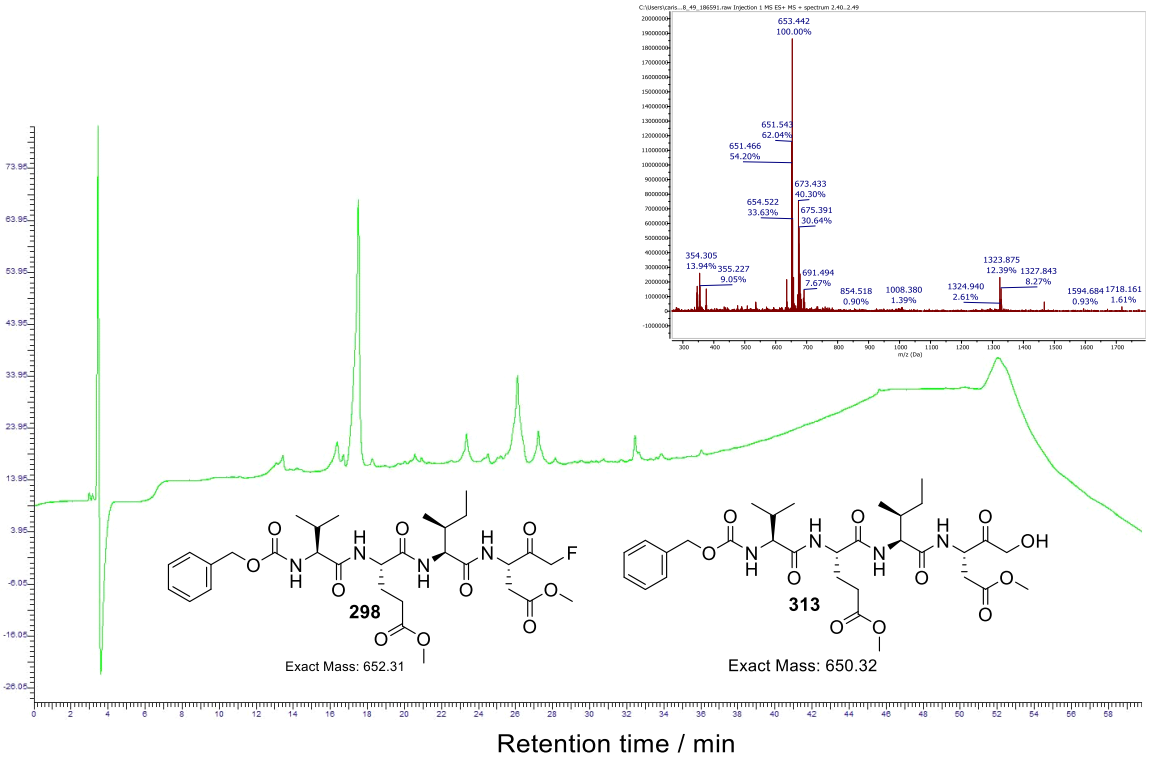

Figure 4.24 – Analytical trace (λ = 220 nm) and mass spectrometry data (+ve) for Caspase 6 inhibitor **298,** with the possibility of hydroxymethyl ketone **313** being present too.

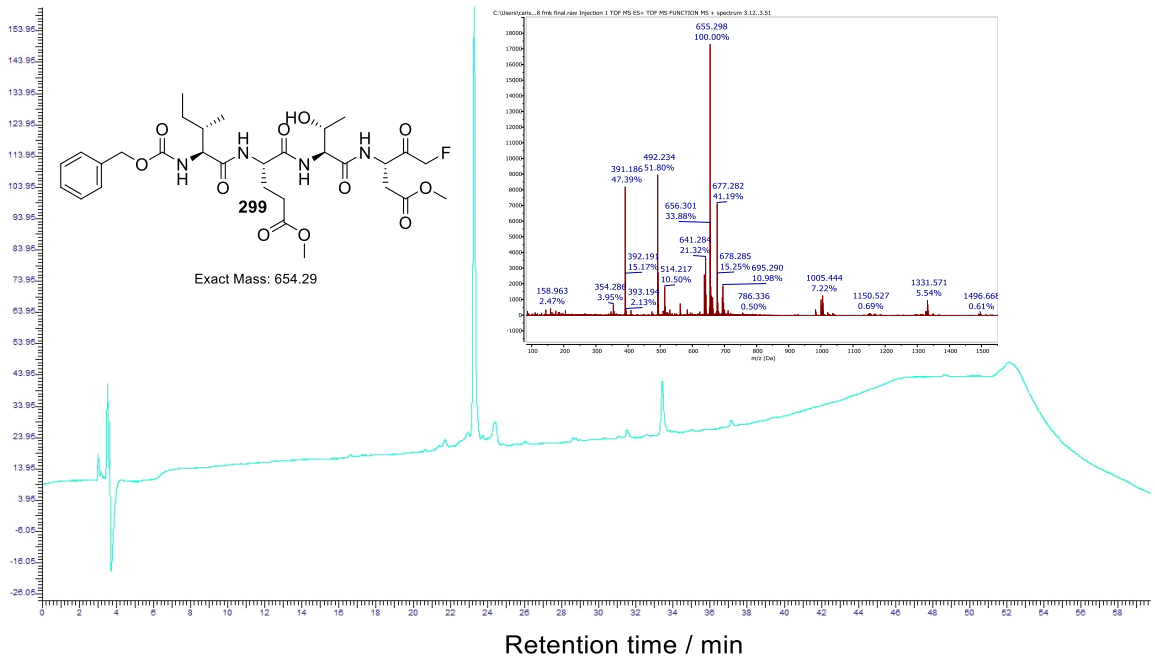

Figure 4.25 – Analytical trace (λ = 220 nm) and mass spectrometry data (+ve) for Caspase 8 inhibitor **299**.

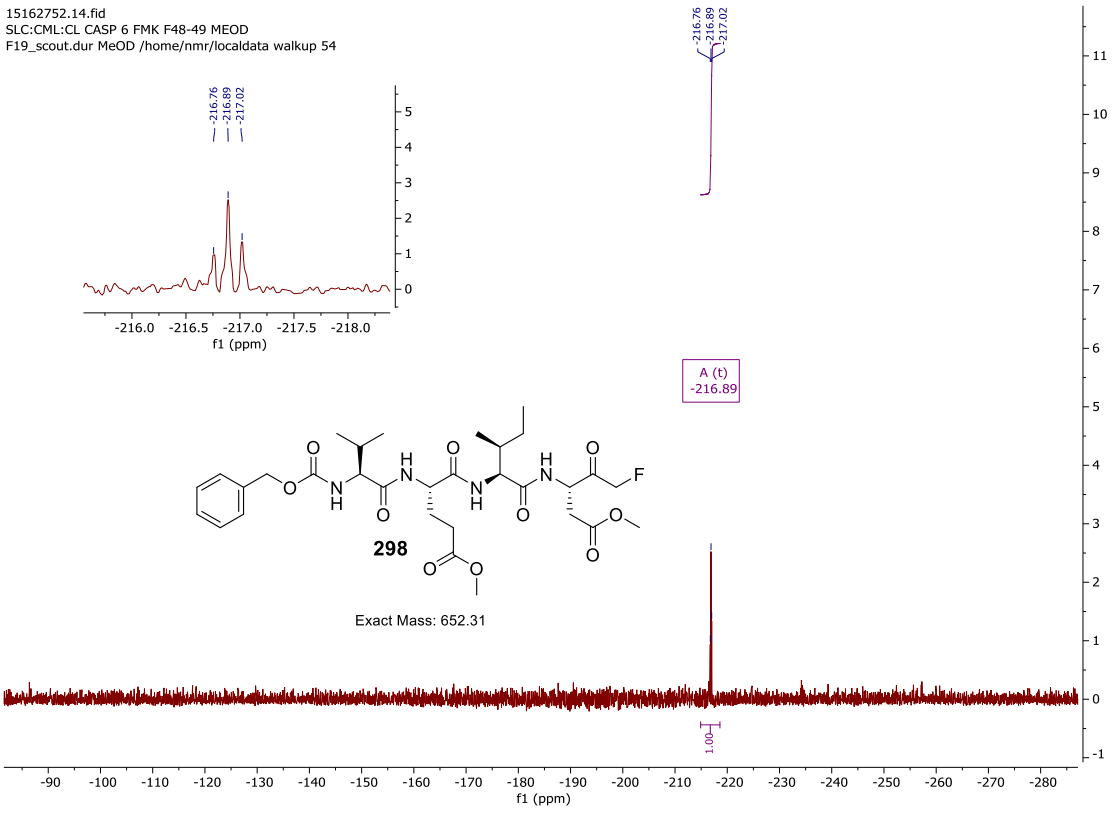

Figure 4.26 – ^{19}F NMR (^{1}H coupled) spectrum (CD_3OD) for Caspase 6 inhibitor FMK **298**.

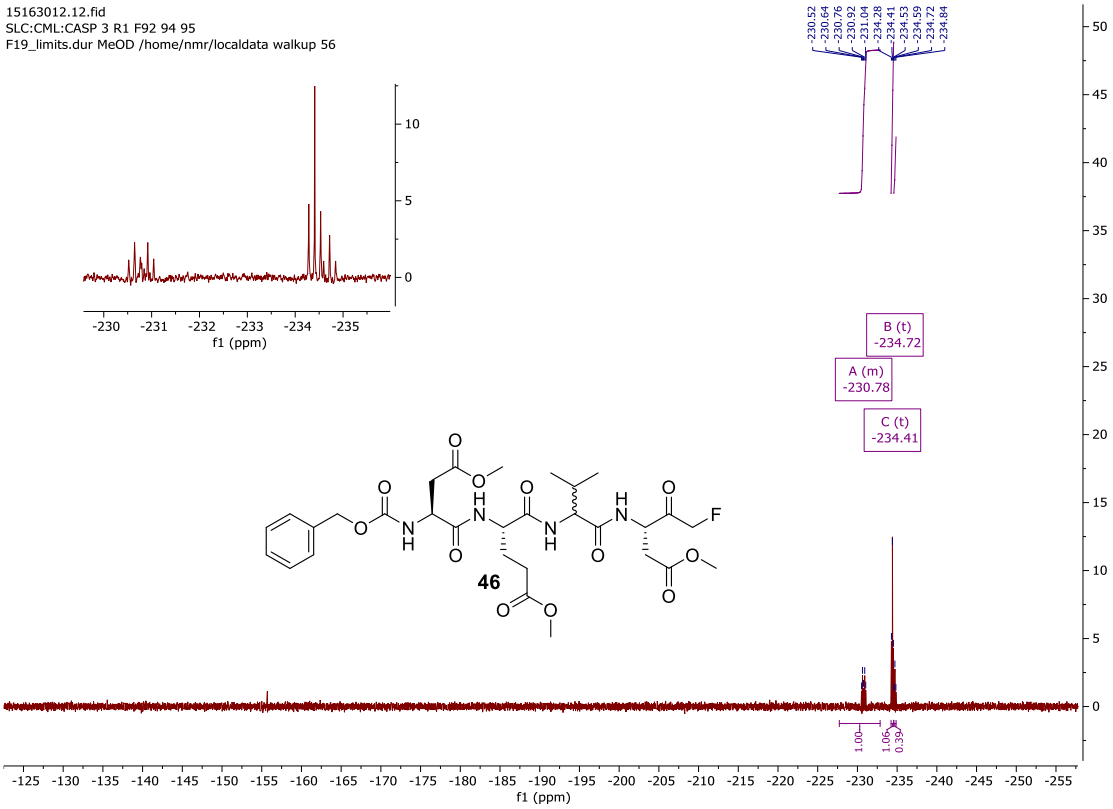

Figure 4.27 – ^{19}F NMR (^{1}H coupled) spectrum (CD_3OD) after attempted synthesis of Caspase 3 inhibitor FMK **46**, with possible epimerisation having occurred at the P_2 position during coupling.

Whilst access to peptidyl FMKs was achieved through the coupling of peptides with FMK building block **291** (**Scheme 4.13**), the challenges associated with this procedure, namely poor yields and the purification difficulties encountered made the procedure rather inefficient. It was therefore concluded that coupling the fluorinated *β*-ketoester (**290**) as a masked FMK (**Scheme 4.2**) and then decarboxylating at a later stage proved more effective, with scope for further improvements to be made with regards to the stereoselectivity of the reaction through the employment of sterically hindered base, 2,4,6-collidine (2,4,6-trimethylpyridine),[24] instead of NMM. The developed methodology (**Scheme 4.2**) allowed access to peptidyl mFMKs (**295** and **40**) in only 5 steps through the use of thermally stable and easy to handle Selectfluor™,[25] whilst avoiding the use of toxic diazomethane, as has previously been employed.[2]

4.3.4 Solution-phase synthesis of Z-Phe-Ala-FMK (41) and Boc-Asp(OMe)-FMK (43)

Equipped with a method for accessing peptidyl mono-FMKs in solution within relatively few steps, albeit low yielding, attention was then turned towards the two remaining FMK targets **41** and **43** shown in **Figure 4.12** and depicted again in **Figure 4.28**.

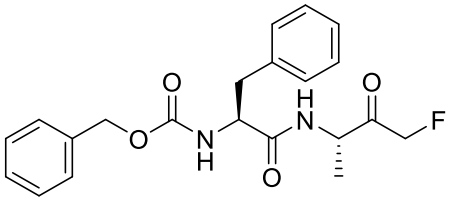

Cbz-Phe-Ala-FMK **41**

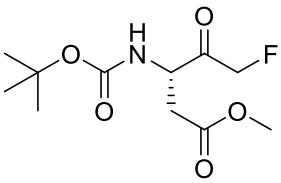

Boc-Asp(OMe)-FMK **43**

Figure 4.28 – Structures of FMK targets **41** and **43**.

4.3.4.1 Synthesis of Z-Phe-Ala-FMK (41)

As Z-Phe-Ala-FMK **41** is only a dipeptide, and therefore shorter in length than the FMKs synthesised thus far, it was envisioned that it could be acquired using a modified approach with fewer steps. Given that Z-Phe-Ala-OH (**316**) is commercially available, it was proposed that FMK **41** could be accessed through generation of the corresponding *β*-ketoester of the dipeptide directly (**315**), avoiding having to first form fluorinated alanine building block **286** (**Scheme 4.6**) and subsequently couple it to Z-Phe-OH. The *β*-ketoester of the dipeptide (**315**) could then be fluorinated and deprotected to afford FMK **41** in just 3 steps, as illustrated by retrosynthetic **Scheme 4.14**.

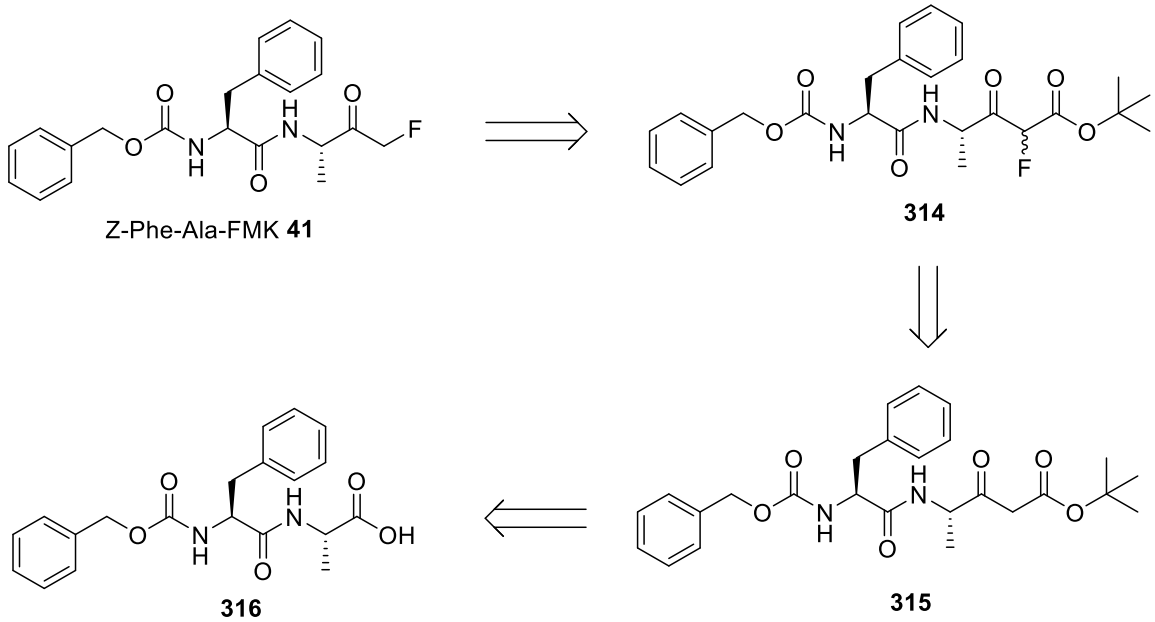

Scheme 4.14 – Retrosynthetic route for accessing FMK **41** from Z-Phe-Ala-OH (**316**).

Starting from commercially available Z-Phe-Ala-OH (**316**), formation of the corresponding *β*-ketoester (**315**) was achieved with CDI, *tert*-butyl acetate and LDA under an inert atmosphere (**Scheme 4.15**) using a similar procedure to that detailed in **Section 4.2.1**; however, the isolated yield was found to be particularly low (7%) and it appeared by TLC that a significant amount of starting material was present. Again, as highlighted in **Section 3.6.1** and **Chapter 4.2.1**, it was reasoned that this could be due to poor conversion to the enolate of *tert*-butyl acetate, meaning any excess activated amino acid leftover as a result would have reverted back to the starting material when quenched with water. Product identity (**315**) was confirmed by ^{1}H NMR spectroscopy (**Figure 4.29**), with several peaks doubling up, likely due to rotamers caused by restricted rotation around the Cbz group.

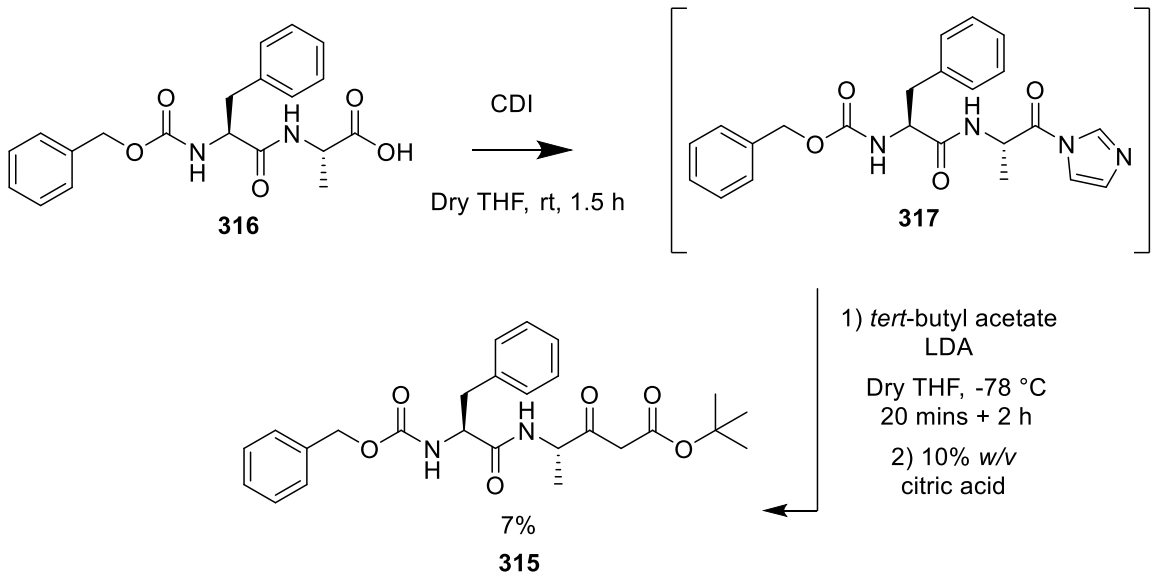

Scheme 4.15 – Conditions employed for synthesis of *β*-ketoester dipeptide **315**.

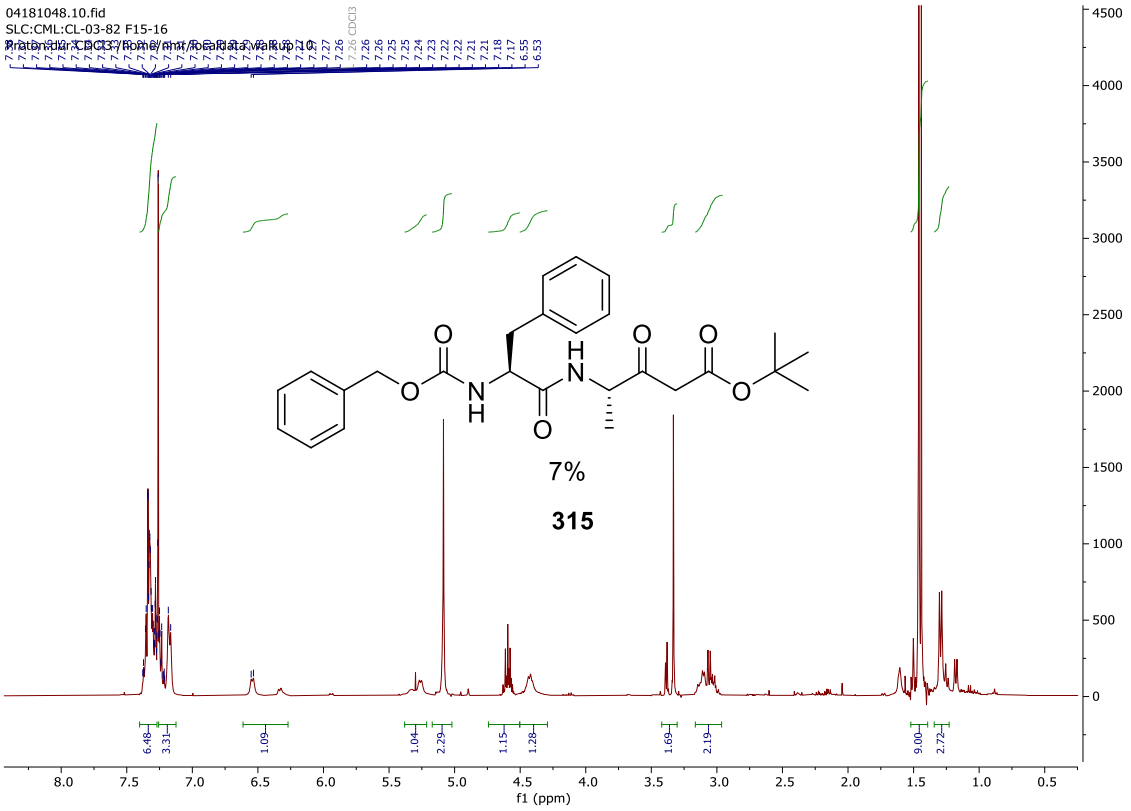

Figure 4.29 – ^{1}H NMR spectrum ($CDCl_3$) for isolation of fluorinated *β*-ketoester dipeptide **315**.

Electrophilic mono-fluorination was then achieved using Selectfluor and $CpTiCl_3$ (**Scheme 4.16**), in a similar manner to that described in **Section 4.2.2**. Isolation of **314** after flash silica gel column chromatography was confirmed via ^{19}F NMR spectroscopy (**Figure 4.30**), with two doublets at –196.0 ppm and -196.9 in a ratio of 0.8 : 1.0

respectively, likely due to diastereoisomers, or alternatively because of rotamers (if the ^{19}F NMR signals for both diastereoisomers are too similar to distinguish).

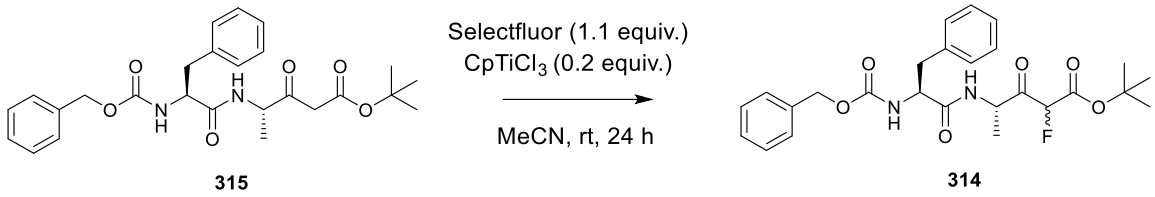

Scheme 4.16 – Conditions employed for mono-fluorination of **315**.

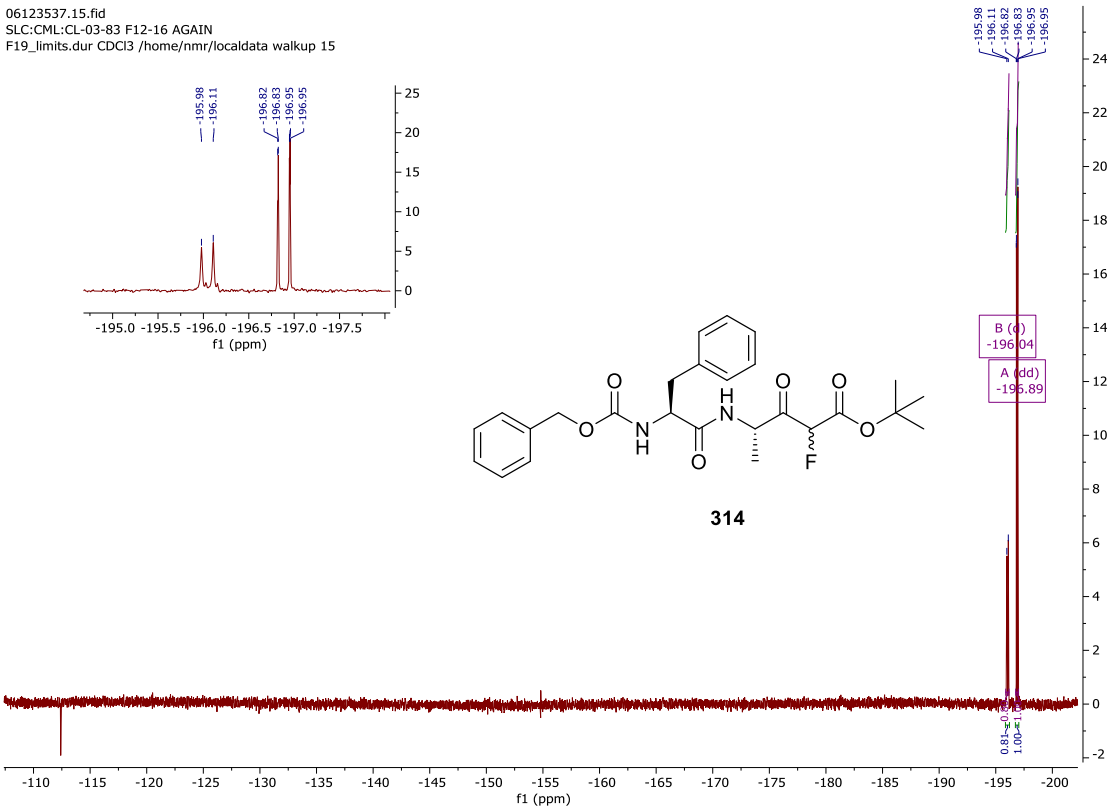

Figure 4.30 – ^{19}F NMR (^{1}H coupled) spectrum ($CDCl_3$) with evidence for isolation of fluorinated *β*-ketoester dipeptide **314**.

The final step involved simultaneous *tert*-butyl ester removal and decarboxylation to the FMK (**41**), as presented in **Section 4.3.3**. This was accomplished through subjection to 50% TFA in DCM at 40 °C (**Scheme 4.17**), with complete conversion to product observed by ^{19}F NMR after 2 hours, as evidenced by the appearance of a triplet at -231.6 ppm (**Figure 4.31**) and the disappearance of the signals at -196 and -197 ppm (**Figure**

4.30). Subsequent purification proved challenging, with isolation of impure product, as confirmed by ^{1}H NMR spectroscopy in **Figure 4.32**, despite attempted prep TLC purification. Nonetheless, despite a relatively low yield of 43% and subpar purity, the desired FMK (**41**) was acquired.

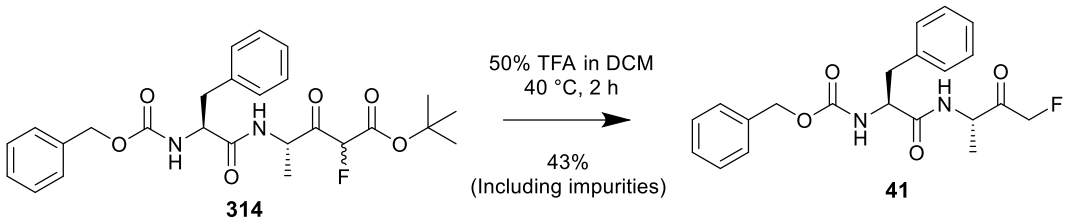

Scheme 4.17 – Conditions employed for decarboxylation of **314** to FMK **41**.

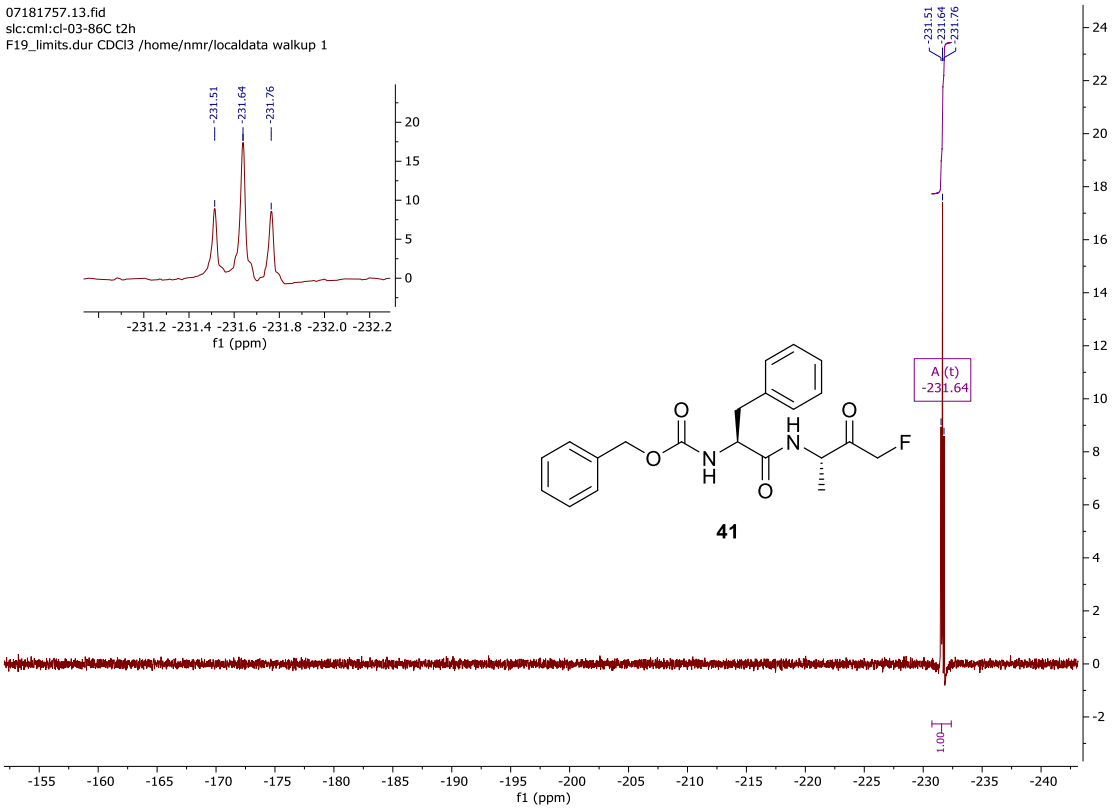

Figure 4.31 – Zoomed in crude ^{19}F NMR (^{1}H coupled) spectrum ($CDCl_3$) after decarboxylation to FMK **41**.

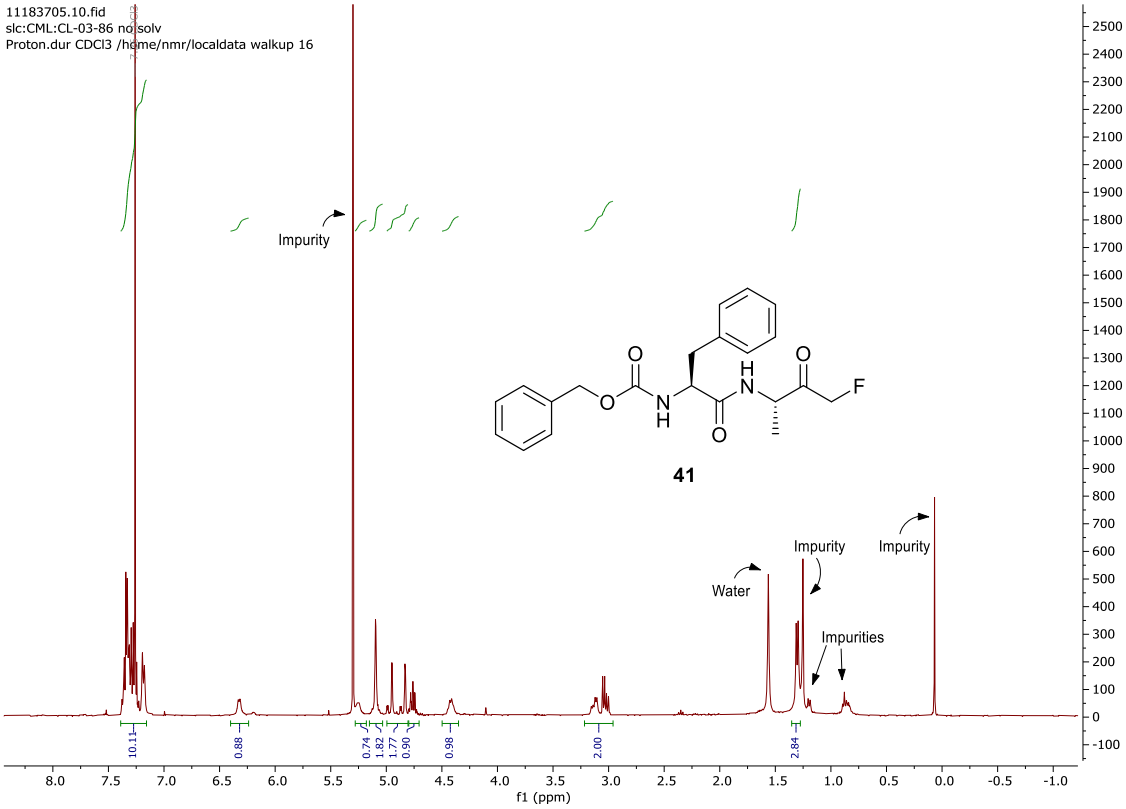

Figure 4.32 – ^{1}H NMR spectrum ($CDCl_3$) for FMK **41** with impurity peaks highlighted.

4.3.4.2 Synthesis of Boc-Asp(OMe)-FMK (43)

It was initially proposed that conversion of Boc-Asp(OMe)-OH (**318**) to the corresponding mono-fluorinated *β*-ketoester (**287**, **Scheme 4.18**), as previously described in **Section 4.21** and **Section 4.22**, followed by decarboxylation, would be a feasible approach for accessing Boc-Asp(OMe)-FMK **43** (**Scheme 4.18**), although it was recognised that a final protection step would be required to reinstate the Boc group, which would inevitably be removed as a result of the acidic conditions utilised for decarboxylation (**Scheme 4.19**).

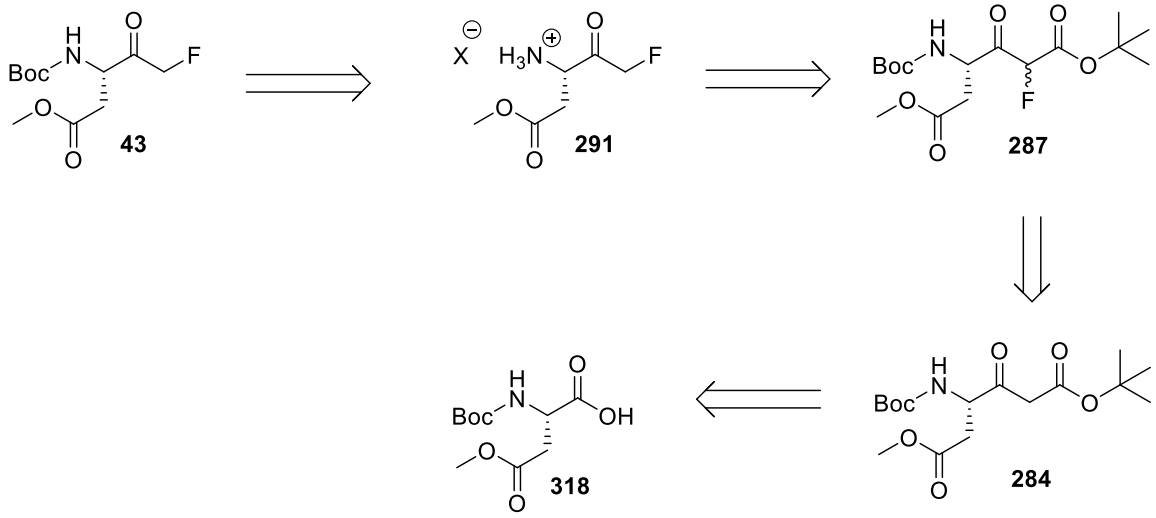

Scheme 4.18 – Retrosynthetic scheme to Boc-Asp(OMe)-FMK **43**.

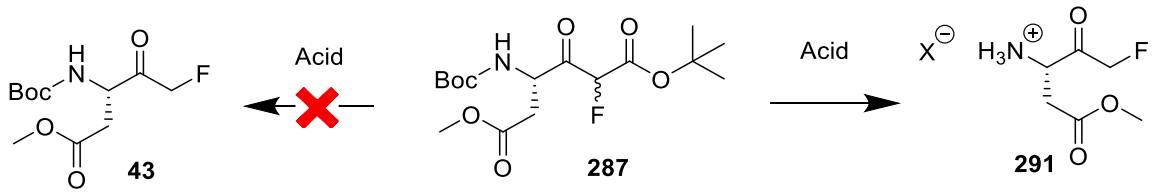

Scheme 4.19 – Illustration of the inability to convert *β*-ketoester **287** to Boc-protected FMK **43** in acid without concomitant Boc removal giving **291**.

Treatment of *β*-ketoester **287** with 50% TFA in DCM at room temperature overnight, as previously shown in **Scheme 4.9a**, resulted in the disappearance of the ^{t}Bu ester and Boc peaks in the corresponding ^{1}H NMR spectrum, along with a shift in the ^{19}F NMR spectrum from two doublets at -196 and -195 ppm (**Figure 4.33a**) to a triplet at -215 ppm (**Figure 4.33b**), suggesting FMK TFA salt **291** had formed.

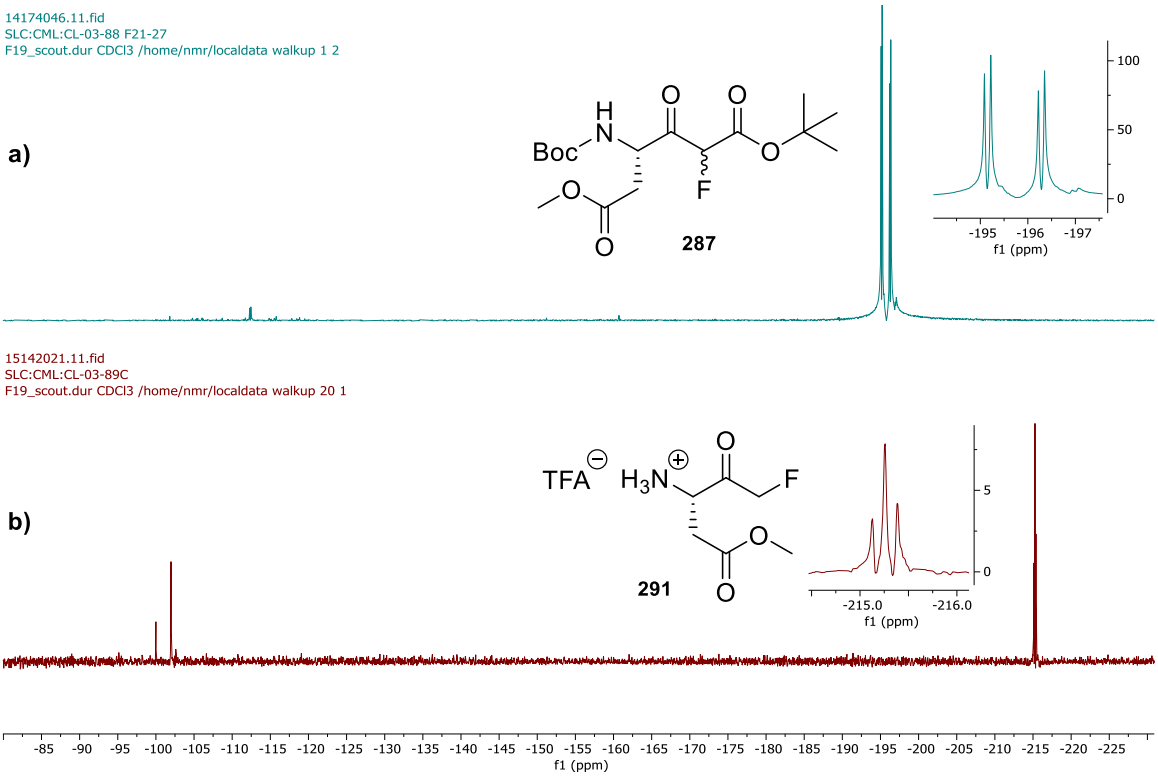

Figure 4.33 – ^{19}F NMR ($CDCl_3$) spectra (^{1}H coupled) for (**a**) *β*-ketoester **287** and (**b**) FMK **291** after deprotection and decarboxylation of **287**.

Subsequent Boc-protection was attempted using Boc anhydride in the presence of triethylamine (**Scheme 4.20**). However, after a 72-hour reaction period (as the reaction was left over the weekend), a crude mass spectrum (+ve) (**Figure 4.34**) did not show the expected product mass (**43**, 263 Da), but instead revealed the presence of $[M\text{-Boc}+H]^+$ = 162 Da and $[M+Na]^+$ = 284 Da, which appeared to correlate to hydroxymethyl ketone **319**. Isolation of hydroxymethyl ketone **319** after column chromatography was confirmed by ^{1}H NMR spectroscopy, whilst no FMK **43** was isolated post-purification, suggesting it had all been converted to the hydroxy analogue (**319**). It is thought that a shorter reaction time may have allowed access to the desired FMK (**43**); however, because of the problems encountered, coupled with the necessity for Boc regeneration rendering **Scheme 4.18** rather inefficient and unattractive anyway, a different protecting group strategy was pursued.

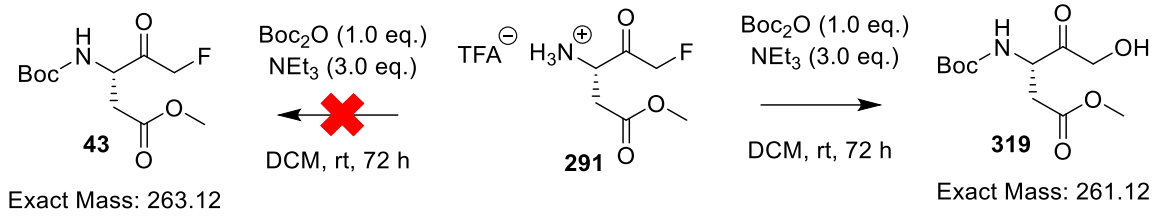

Scheme 4.20 – Attempted Boc protection of FMK **291** led to hydroxymethyl ketone **319** formation instead of isolation of FMK **43**.

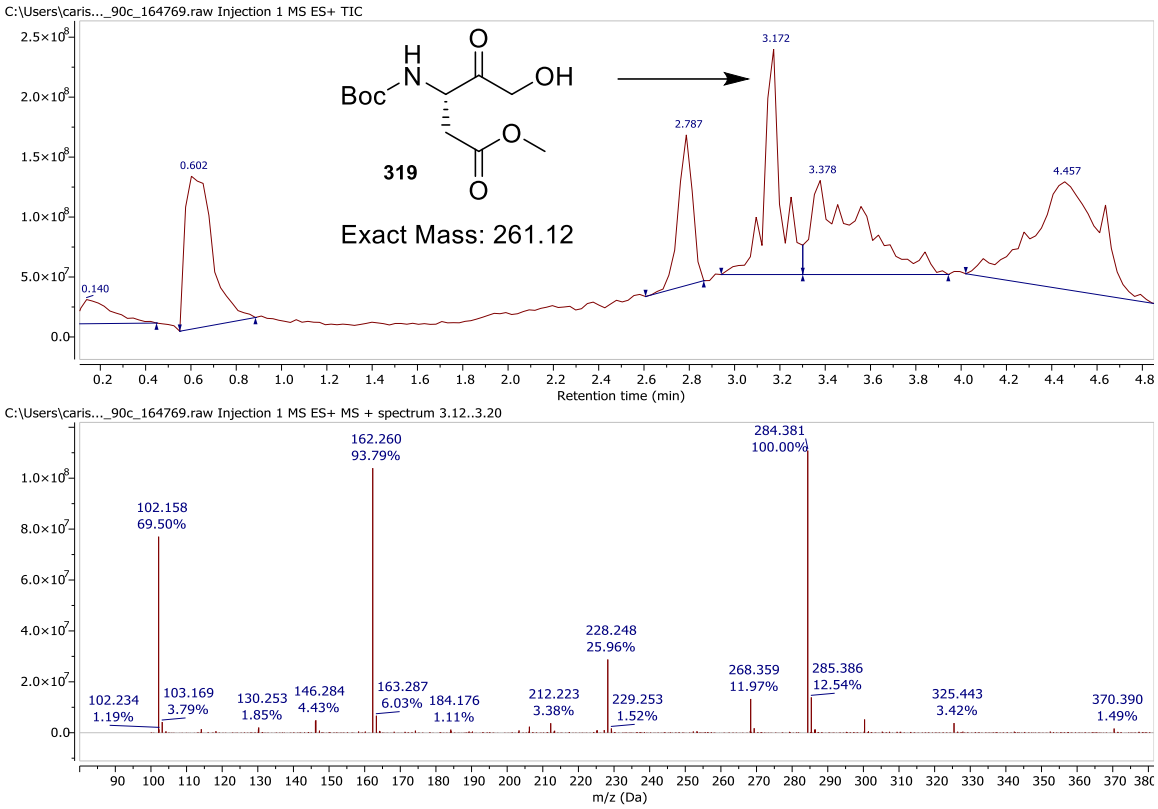

Figure 4.34 – Crude TIC and mass spectrometry data (+ve) revealing the presence of hydroxymethyl ketone **319**.

Instead of utilising the *tert*-butyl ester (**287**), it was envisioned that this could be replaced by the benzyl ester to give *β*–ketoester **321** (**Scheme 4.21**). This would then allow for subsequent fluorination of *β*-ketoester **321** followed by removal of the ester via hydrogenation without the need for acid, thus leaving the Boc group in place (**43**). Furthermore, conditions employed for hydrogenation have been reported to bring about simultaneous decarboxylation,[26] potentially allowing for a one-pot final step to generate

the FMK (**43**). A proposed retrosynthetic route outlining these transformations is given in **Scheme 4.21**.

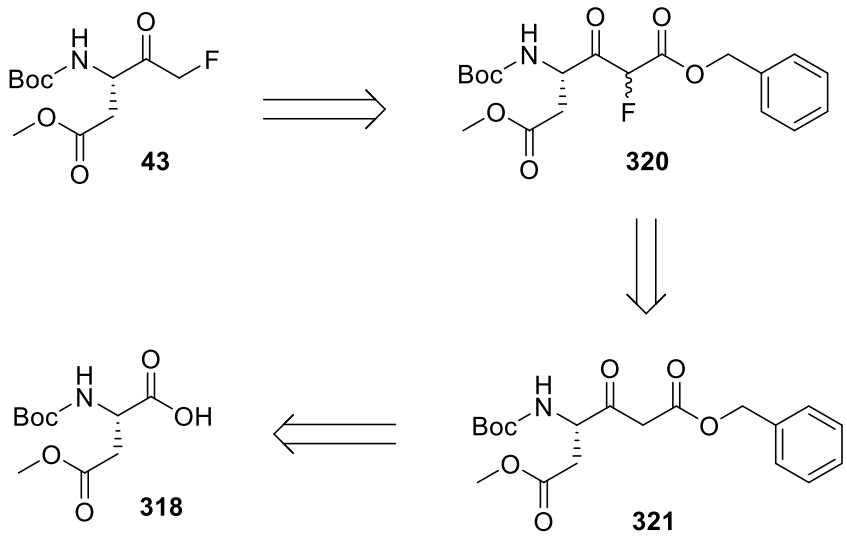

Scheme 4.21 – Retrosynthetic scheme for accessing Boc-Asp(OMe)-FMK **43**.

Starting from commercially available Boc-Asp(OMe)-OH (**318**), conversion to the corresponding *β*-keto-benzyl-ester (**321**) was achieved in a similar manner to that described in **Section 4.21** using CDI and LDA, with the key difference being the replacement of *tert*-butyl acetate with benzyl acetate (**Scheme 4.22**). This allowed access to **3121**; however, the isolated yield was found to be very low (4%), possibly due to inefficient enolate formation, as already highlighted as a potential issue for these types of reactions (**Chapter 3.6.1** and **Chapter 4.2.1**).

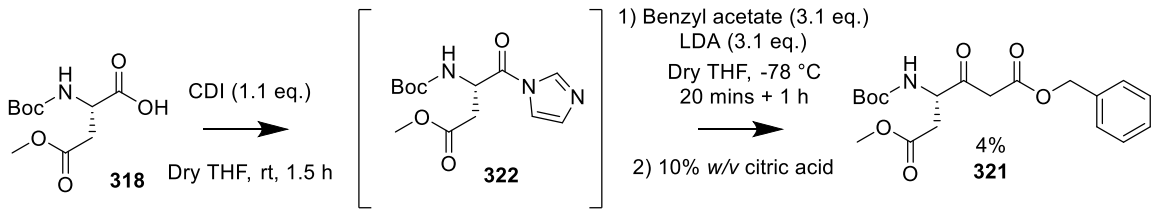

Scheme 4.22 – Conditions employed for synthesis of *β*-ketoester **321**.

Subsequent electrophilic fluorination using Selectfluor and $CpTiCl_3$ (as in **Section 4.22**) allowed access to mono-fluorinated *β*–ketoester **320** (**Scheme 4.23**) after column chromatography, as confirmed by ^{19}F NMR spectroscopy (**Figure 4.35**), which shows two

doublets at -196.7 and -197.9 ppm in a ratio of 1.0 : 0.9 respectively, likely due to diastereoisomers.

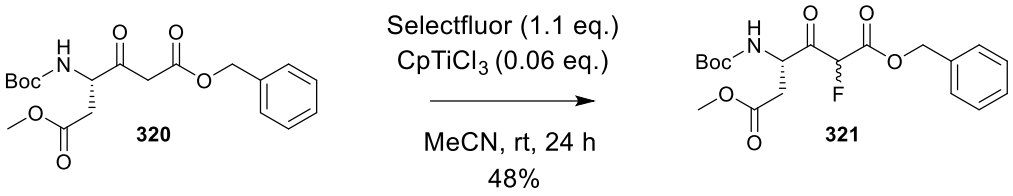

Scheme 4.23 – Conditions employed for fluorination of *β*-ketoester **321** to **330**.

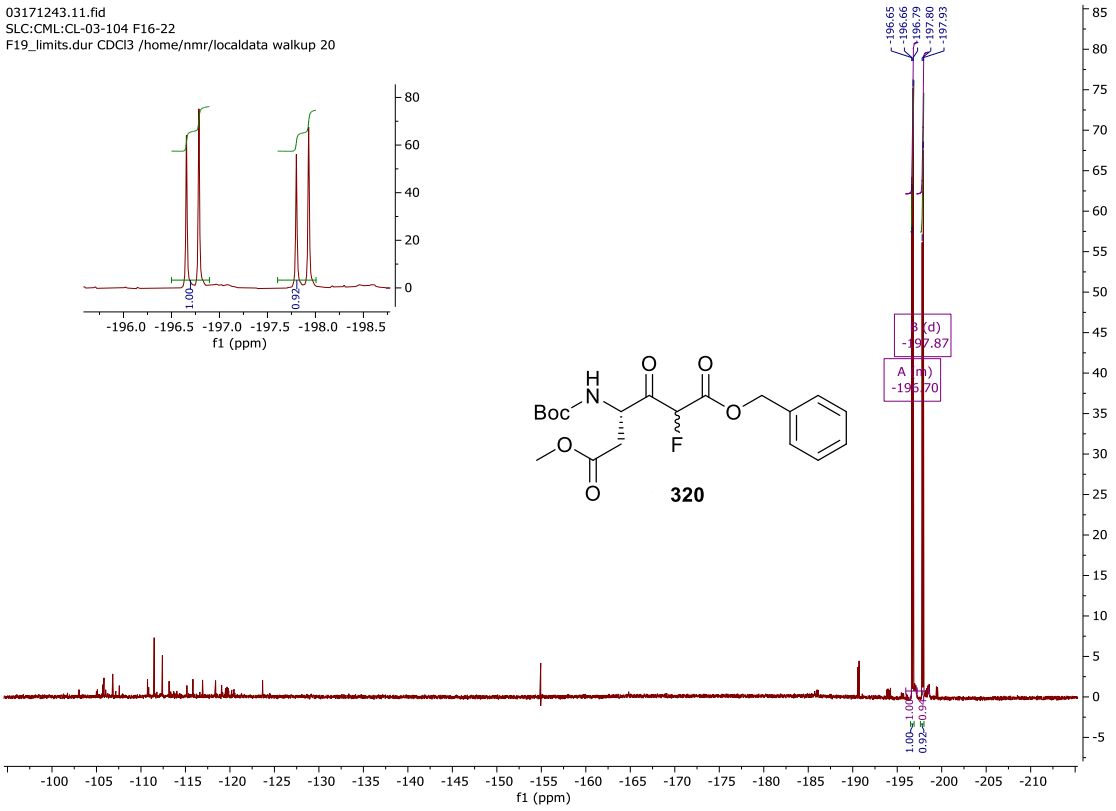

Figure 4.35 – ^{19}F NMR (^{1}H coupled) spectrum ($CDCl_3$) for *β*-ketoester **320**.

Interestingly, the corresponding ^{1}H NMR spectrum appeared to once again reveal a mixture of product (**320**) and hydroxymethyl ketone (**319**), which was further confirmed by mass spectrometry (+ve), as shown in **Figure 4.36**.

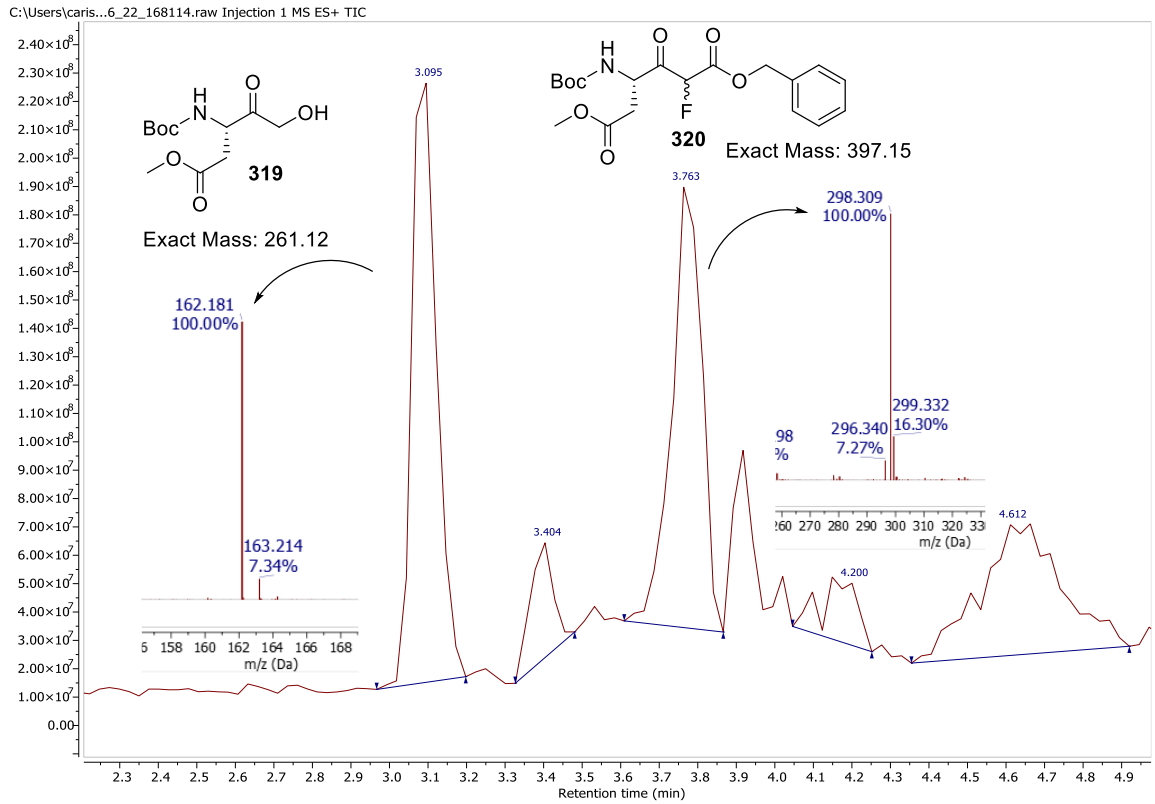

Figure 4.36 – TIC and mass spectrometry data (+ve) revealing the presence of desired *β*-ketoester **320** at rt = 3.76 mins, along with hydroxymethyl ketone **319** at rt = 3.10 mins.

In order to access the desired FMK (**43**), a one-pot hydrogenation and decarboxylation step was attempted, utilising similar conditions to that already described in the literature.[26] Starting from fluorinated *β*-ketoester **320**, reaction with 21% *w/w* of 10% Pd/C in absolute ethanol at room temperature was found to bring about benzyl ester removal after 1 hour (**Scheme 4.24**); however, no evidence of decarboxylation to the FMK was observed. The material was therefore heated at 40 °C overnight in air to encourage complete conversion to product (**Scheme 4.24**). Purification proved challenging, with the hydroxymethyl ketone analogue of **43** present in the crude ^{1}H NMR spectrum (**319**), likely having been carried through from the previous step. However, after flash column chromatography and two subsequent prep TLC purifications, a small amount of product was obtained, albeit impure, as seen by ^{1}H NMR spectroscopy (**Figure 4.37**). Peaks were seen to double-up in some cases, perhaps due to restricted rotation around the carbamate

C-N bond, inducing rotamers. Product identity was further confirmed through the presence of a triplet signal at -232.2 ppm in the ^{19}F NMR spectrum (**Figure 4.37**, **top left of image**).

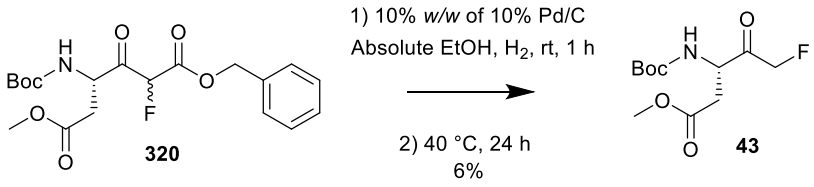

Scheme 4.24 – Conditions employed for accessing Boc-Asp(OMe)-FMK **43** from **320**.

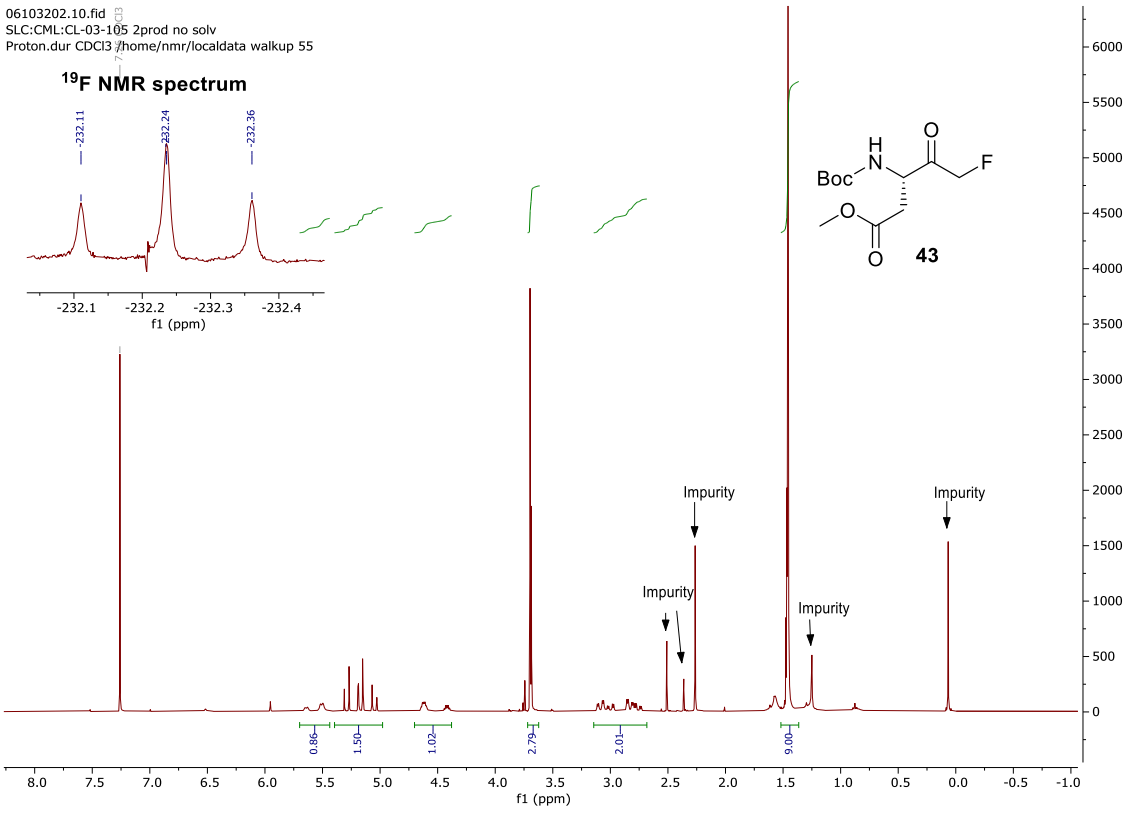

Figure 4.37 – ^{1}H and ^{19}F NMR (**top left of image**) in $CDCl_3$ after isolation of impure Boc-Asp(OMe)-FMK **43**, with impurities still present.

4.4 Chapter Summary

The successful acquisition of peptidyl mono-fluoromethyl ketones (mFMKs) was achieved in solution through selective electrophilic mono-fluorination of a selection of *β*–ketoesters derived from the corresponding *N*-Boc protected amino acids of choice. Selective Boc removal and subsequent coupling of the resulting *β*–ketoesters to peptides in solution, followed by concomitant global deprotection and decarboxylation led to the

isolation of the desired peptidyl mFMKs in only 5 steps. It appeared that epimerisation did occur during the coupling step, resulting in diastereoisomers; however, it is thought that the use of a bulkier base such as 2,4,6-collidine should reduce this.

A similar approach for accessing peptidyl FMKs was also trialled in which mono-fluorinated *β*–ketoesters were constructed as before, but instead of selectively removing the Boc group, complete deprotection and decarboxylation to the FMK in acid was performed prior to the solution-phase peptide coupling step. Whilst peptidyl mFMKs were isolated, challenges were encountered with regards to inseparable impurities, including the presence of hydroxymethyl ketones analogues of the FMKs in some cases. Furthermore, low yielding steps contributed towards the overall small amounts of compound obtained. Therefore, it was concluded that coupling the *β*–ketoesters (**Scheme 4.11**, **289** and **290**) as masked FMKs proved more effective than forming and coupling the FMK building block (**Figure 4.13**, **291**) to peptides themselves.

Cbz-Phe-Ala-FMK (**41**) was isolated through a slightly modified approach. This involved construction of the *β*–ketoester (**315**) derived from dipeptide Cbz-Phe-Ala-OH (**316**), followed by subsequent mono-fluorination. A final one-pot deprotection and decarboxylation step generated the Cbz-Phe-Ala-FMK (**41**) as desired, albeit with some other impurities still present after purification.

Boc-Asp(OMe)-FMK (**43**) also required an adapted approach due to the requirement for the acid-sensitive Boc group to remain intact. This was achieved through the formation of the *N*-Boc *β*-keto-benzyl-ester (**321**) derived from Boc-Asp(OMe)-OH (**318**) followed by mono-fluorination and a one-pot hydrogenation and decarboxylation step. Again, purification proved difficult; however, a small amount of product was obtained, although impurities were still present and further optimisation of the reaction conditions is required.

In summary, a route was developed which enabled access to peptidyl mono-FMKs through coupling mono-fluorinated *β*–ketoesters to peptides in solution and then decarboxylating. The method allowed isolation of mFMKs in only 5 steps, whilst avoiding the use of hazardous diazomethane. Additionally, there is still scope for improving the stereospecificity of the coupling step and enhancing the yields. Thus, it is believed that this route provides a beneficial pathway for accessing these highly expensive and desirable warheads in relatively few steps.

4.5 References for Chapter 4

1. Lloyd, C. M., Colgin, N. & Cobb, S. L. Current Synthetic Routes to Peptidyl Mono-Fluoromethyl Ketones (FMKs) and Their Applications. *Molecules* **25**, 5601 (2020).

2. Rauber, P., Angliker, H., Walker, B. & Shaw, E. The synthesis of peptidylfluoromethanes and their properties inhibitors of serine proteinases and cysteine proteinases. *Biochem. J.* **239**, 633–640 (1986).

3. Roiban, G. D., Matache, M., Hădade, N. D. & Funeriu, D. P. A general solid phase method for the synthesis of sequence independent peptidyl-fluoromethyl ketones. *Org. Biomol. Chem.* **10**, 4516–4523 (2012).

4. Gibson, F. S., Bergmeier, S. C. & Rapoport, H. Selective Removal of an N-BOC Protecting Group in the Presence of a tert-Butyl Ester and Other Acid-Sensitive Groups. *J. Org. Chem.* **59**, 3216–3218 (1994).

5. Preciado, A. & Williams, P. G. A Simple Microscale Method for Determining the Relative Stereochemistry of Statine Units. *J. Org. Chem.* **73**, 9228–9234 (2008).

6. Frantz, R., Hintermann, L., Perseghini, M., Broggini, D. & Togni, A. Titanium-Catalyzed Stereoselective Geminal Heterodihalogenation of β-Ketoesters. *Org. Lett.* **5**, 1709–1712 (2003).

7. Deszcz, L., Cencic, R., Sousa, C., Kuechler, E. & Skern, T. An Antiviral Peptide Inhibitor That Is Active against Picornavirus 2A Proteinases but Not Cellular Caspases. *J. Virol.* **80**, 9619–9627 (2006).

8. Cheng, Y. *et al.* Caspase inhibitor affords neuroprotection with delayed administration in a rat model of neonatal hypoxic-ischemic brain injury. *J. Clin. Investig.* **101**, 1992–1999 (1998).

9. Kudelova, J., Fleischmannova, J., Adamova, E. & Matalova, E. Pharmacological caspase inhibitors: research towards therapeutic perspectives. *J. Physiol. Pharmacol.* **66**, 473–82 (2015).

10. Knoblach, S. M. *et al.* Caspase Inhibitor z-DEVD-fmk Attenuates Calpain and Necrotic Cell Death in Vitro and after Traumatic Brain Injury. *J. Cereb. Blood Flow Metab.* **24**, 1119–1132 (2004).

11. Li, L. *et al.* Photodynamic therapy induces human esophageal carcinoma cell pyroptosis by targeting the PKM2/caspase-8/caspase-3/GSDME axis. *Cancer Lett.* **520**, 143–159 (2021).

12. Citarella, A. & Micale, N. Peptidyl Fluoromethyl Ketones and Their Applications in Medicinal Chemistry. *Molecules* **25**, 4031 (2020).

13. Pereira, F. v *et al.* Metformin exerts antitumor activity via induction of multiple death pathways in tumor cells and activation of a protective immune response. *Oncotarget* **9**, 25808–25825 (2018).

14. Li, R. *et al.* ATP/P2X7-NLRP3 axis of dendritic cells participates in the regulation of airway inflammation and hyper-responsiveness in asthma by mediating HMGB1 expression and secretion. *Exp. Cell Res.* **366**, 1–15 (2018).

15. Meguro, T., Chen, B., Parent, A. D. & Zhang, J. H. Caspase Inhibitors Attenuate Oxyhemoglobin-Induced Apoptosis in Endothelial Cells. *Stroke* **32**, 561–566 (2001).

16. Yao, Y. *et al.* Identification of Caspase-6 as a New Regulator of Alternatively Activated Macrophages. *J. Biol. Chem.* **291**, 17450–17466 (2016).

17. Mañas, A., Chen, W., Nelson, A., Yao, Q. & Xiang, J. BaxΔ2 sensitizes colorectal cancer cells to proteasome inhibitor-induced cell death. *Biochem. Biophys. Res. Commun.* **496**, 18–24 (2018).

18. Takizawa, T., Tatematsu, C., Ohashi, K. & Nakanishi, Y. Recruitment of Apoptotic Cysteine Proteases (Caspases) in Influenza Virus-Induced Cell Death. *Microbiol. Immunol.* **43**, 245–252 (1999).

19. Clark, R. S. B. *et al.* boc-Aspartyl(OMe)-fluoromethylketone attenuates mitochondrial release of cytochrome c and delays brain tissue loss after traumatic brain injury in rats. *J. Cereb. Blood Flow Metab.* **27**, 316–326 (2007).

20. Li, X. *et al.* The Caspase Inhibitor Z-VAD-FMK Alleviates Endotoxic Shock via Inducing Macrophages Necroptosis and Promoting MDSCs-Mediated Inhibition of Macrophages Activation. *Front. Immunol.* **10**, 1824 (2019).

21. Koike, S. *et al.* Advanced Glycation End-Products Induce Apoptosis of Vascular Smooth Muscle Cells: A Mechanism for Vascular Calcification. *Int. J. Mol. Sci.* **17**, (2016).

22. Mackenzie, S. H., Schipper, J. L. & Clark, A. C. The potential for caspases in drug discovery. *Curr. Opin. Drug Discov. Dev.* **13**, 568–576 (2010).

23. Lawrence, C. P., Kadioglu, A., Yang, A.-L., Coward, W. R. & Chow, S. C. The Cathepsin B Inhibitor, z-FA-FMK, Inhibits Human T Cell Proliferation In Vitro and Modulates Host Response to Pneumococcal Infection In Vivo. *J. Immunol.* **177**, 3827–3836 (2006).

24. Carpino, L. A. & El-Faham, A. Effect of Tertiary Bases on O-Benzotriazolyluronium Salt-Induced Peptide Segment Coupling. *J. Org. Chem.* **59**, 695–698 (1994).

25. Stavber, S. Recent Advances in the Application of SelectfluorTM F-TEDA-BF4 as a Versatile Mediator or Catalyst in Organic Synthesis. *Molecules* **16**, 6432–6464 (2011).

26. Krabill, A. D. *et al.* Optimization and Anti-Cancer Properties of Fluoromethylketones as Covalent Inhibitors for Ubiquitin C-Terminal Hydrolase L1. *Molecules* **26**, 1227 (2021).

5. Synthesis of C-Terminal Modified Peptides

5.1 Introduction

Having developed a route for successfully accessing peptidyl mono-fluoromethyl ketones (mFMKs) capable of cysteine inhibition, it was envisioned that the methodology could be applied to the synthesis of a selection of peptides containing other biologically relevant C-terminal modifications, thus expanding substrate scope beyond that of fluorine. Two targets of interest were peptidyl trifluoromethyl ketones (tFMKs)[1] and mono-chloromethyl ketones (mCMKs), which have been shown to act as serine protease inhibitors. For example, CO_2CH_3-Val-Pro-Val-CF_3 (**16**) and Ac-Ala-Tyr-Leu-Val-CH_2Cl (**323**) were found to inhibit human leukocyte elastase (HLE),[2,3] a serine protease enzyme involved in inflammation and tissue degradation (**Figure 5.1**).[4]

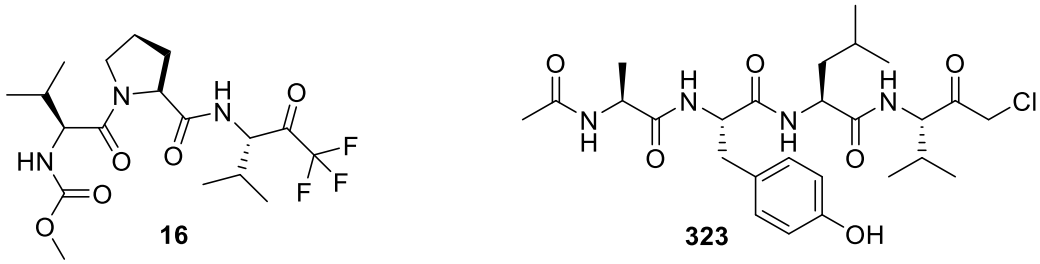

Figure 5.1 – Structures of CO_2CH_3-Val-Pro-Val-CF_3 (**16**) and Ac-Ala-Tyr-Leu-Val-CH_2Cl (**323**).

In order to access mCMKs such as **323**, it was proposed that a similar solution-phase approach to that already described in **Chapter 4** (**Scheme 4.3**, starting from **278**) for accessing peptidyl mFMKs could be utilised, with the key difference being the installation of chlorine instead of fluorine at the α-carbon of the 1,3-dicarbonyl. Whilst it is not possible to access trifluoromethyl ketones such as **16** utilising the same approach, it was envisioned that trifluoroethyl ketones (tFEKs) (**324**) could be accessed in this way. Although tFEKs have not been reported in the literature to date, it was thought that they could be of interest due to the fact that tFMKs can undergo reversible inhibition according to **Scheme 1.2b** and **c** in **Chapter 1**, with the possibility that tFEKs could operate in a similar manner. A retrosynthetic scheme depicting a possible pathway to tFEK **324** and

CMK **326** is shown in **Scheme 5.1**. This would involve starting from a Boc-protected amino acid of choice (**278**), converting it to the corresponding *β*-ketoester (**277**), trifluoromethylating or chlorinating as required and finally *tert*-butyl ester deprotecting and decarboxylating to **324** or **326**. The resulting building blocks (**324** and **326**) could then be coupled to a peptide of choice in solution, allowing access to peptidyl tFEKs and CMKs respectively (**Scheme 5.2**) in a similar manner to that previously described for the synthesis of peptidyl mFMKs in **Chapter 4**.

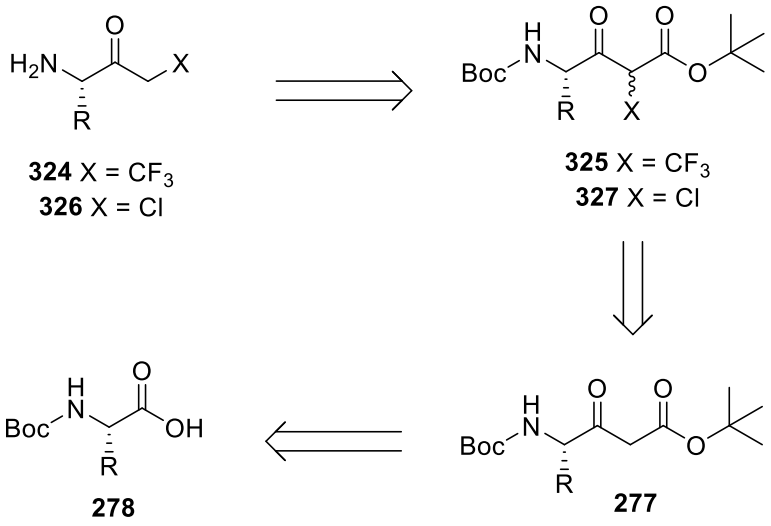

Scheme 5.1 – Retrosynthetic scheme for accessing tFEK and CMK building blocks **324** and **326** respectively from Boc-protected amino acid **278**, where R = an amino acid sidechain of choice.

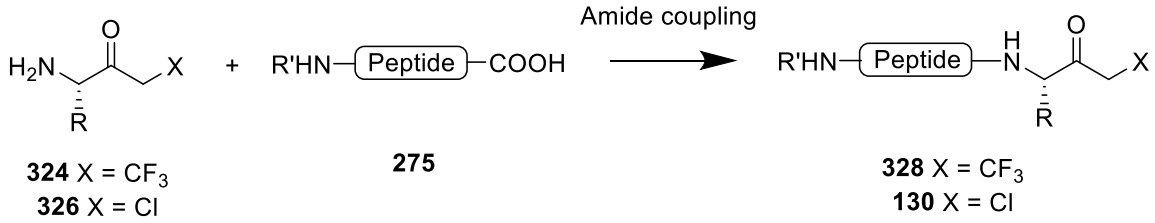

Scheme 5.2 – Proposed route for accessing peptidyl tFEKs (**328**) and CMKs (**130**) through coupling peptide **275** (where R' = H, acetyl or a protecting group) with building blocks **324** and **326** respectively (where R = an amino acid sidechain of choice).

5.2 Synthesis of Peptidyl Trifluoroethyl Ketones (tFEKs)

A number of synthetic routes to peptidyl trifluoromethyl ketones (tFMKs) have been reported in the literature (**Figure 5.2**). Kolb *et al* disclosed a modified Dakin-West

procedure (**Figure 5.2**, **i**) for accessing trifluoromethyl ketones derived from the corresponding amino acids through their reaction with trifluoroacetic anhydride (TFAA);[5–7] however, the protocol only tolerated the synthesis of benzoyl nitrogen-substituted tFMKs, making their use in peptide synthesis undesirable. An alternative approach involves a Henry reaction between fluoral and a nitro alkane (**Figure 5.2**, **ii**),[8] whilst Patel *et al* adopted conditions involving condensation of fluoral with the dianion of substituted acetic acids and a subsequent Curtius rearrangement (**Figure 5.2**, **iii**).[9] Katzenellenbogen and co-workers[10] described the synthesis of peptidyl tFMKs through generation of 4-trifluoromethyl-substituted Δ^3-imidazolines from Fmoc-protected amino acid fluorides which could then be incorporated into a peptide sequence and subsequently hydrolysed in mild acid to give the desired peptidyl tFMK (**Figure 5.2**, **iv**). The presence of readily oxidisable residues such as methionine was found to be compatible under these conditions, however; the paper only reported examples in which glycine or an epimerised phenylglycine residue was stationed at the P_1 position, meaning substrate scope was limited. Additionally, *N*-substituted tripeptidyl tFMKs were synthesised in several steps by Skiles *et al* in a method involving the reaction of TMS-CF_3 with amino aldehydes (**Figure 5.2**, **v**, TMS-CF_3).[11,12] However, in all these examples, the chiral centre at the P_1 position existed as a racemic mixture, which may be undesirable depending on the intended application of the material prepared.

In 1992, Philip D. Edwards[13] developed methodology (**Figure 5.2**, **v**, CF_3I) to address this issue, achieving ≥99% isomeric purity through reaction of trifluoromethyl zinc iodide with a peptidyl aldehyde, followed by oxidation. Nonetheless, trifluoroiodomethane (CF_3I) is a toxic and potentially explosive gas, rendering it undesirable to handle. Conditions have also been reported for accessing stereoisomerically pure peptidyl tFMKs in which the absolute configuration was unknown (**Figure 5.2**, **vi**).[14] This was achieved through condensation of a homochiral *syn* (*RS* or *SR*) trifluoromethyl amino alcohol (**342**), which had been synthesised from the corresponding epoxy ether (**341**) via an azide,[15] with

an amino acid of choice. The resulting dipeptide, which had been separated from its diastereoisomer by column chromatography, was then oxidised to the desired peptidyl tFMK, whilst retaining either *D* or *L* configuration at the P_1 position, using Dess-Martin Periodinane (DMP). However, the fact that this procedure is fairly long-winded (as the epoxy ether itself needs to be synthesised[16] prior to use), absolute stereochemistry is unknown at the P_1 position, and toxic sodium azide is used, limits its utility. In 1995, Walter *et al*[17] presented a means for accessing optically pure *N*-substituted α-amino-trifluoromethyl ketones through reaction of α-amino acid-derived oxazolidin-5-ones with TMS-CF_3 followed by acidic hydrolysis with Amberlite® IR-120 (**Figure 5.2**, **vii**), a highly acidic ion exchange resin. A similar, yet slightly modified approach was also described by the same group in 1997,[18] along with a new method allowing access to α-amido trifluoromethyl ketones through initial generation of *N*-protected α-amino aldehydes via reduction of Weinreb-amide intermediates derived from the corresponding Boc or Cbz-protected amino acids of choice. Purification of the resulting α-amino aldehydes was avoided due to their tendency to epimerise in the process of silica gel flash column chromatography. The aldehydes were then reacted with TMS-CF_3 in a similar manner to that described by Skiles *et al* (**Figure 5.2**, **v**, TMS-CF_3), and ultimately oxidised to product using DMP.

A solid-phase route has also been reported (**Figure 5.2**, **viii**)[19] in which Boc-protected trifluoromethyl ketone building block **345** was first synthesised in a similar manner to that described by Imperiali and Abeles[8] via a Henry reaction (**Figure 5.2**, **ii**). **345** was then attached to a linker through an acid-catalysed condensation, which was subsequently coupled to a polystyrene BHA resin. After SPPS, resin cleavage was performed through refluxing aqueous HCl and acetic acid in THF at 65 °C for 4 h; however, this had to be repeated 3 times in order to maximise peptide recovery. Furthermore, the product (**347**) was obtained as a racemate at the P_1 position, in an overall yield of only 28%.

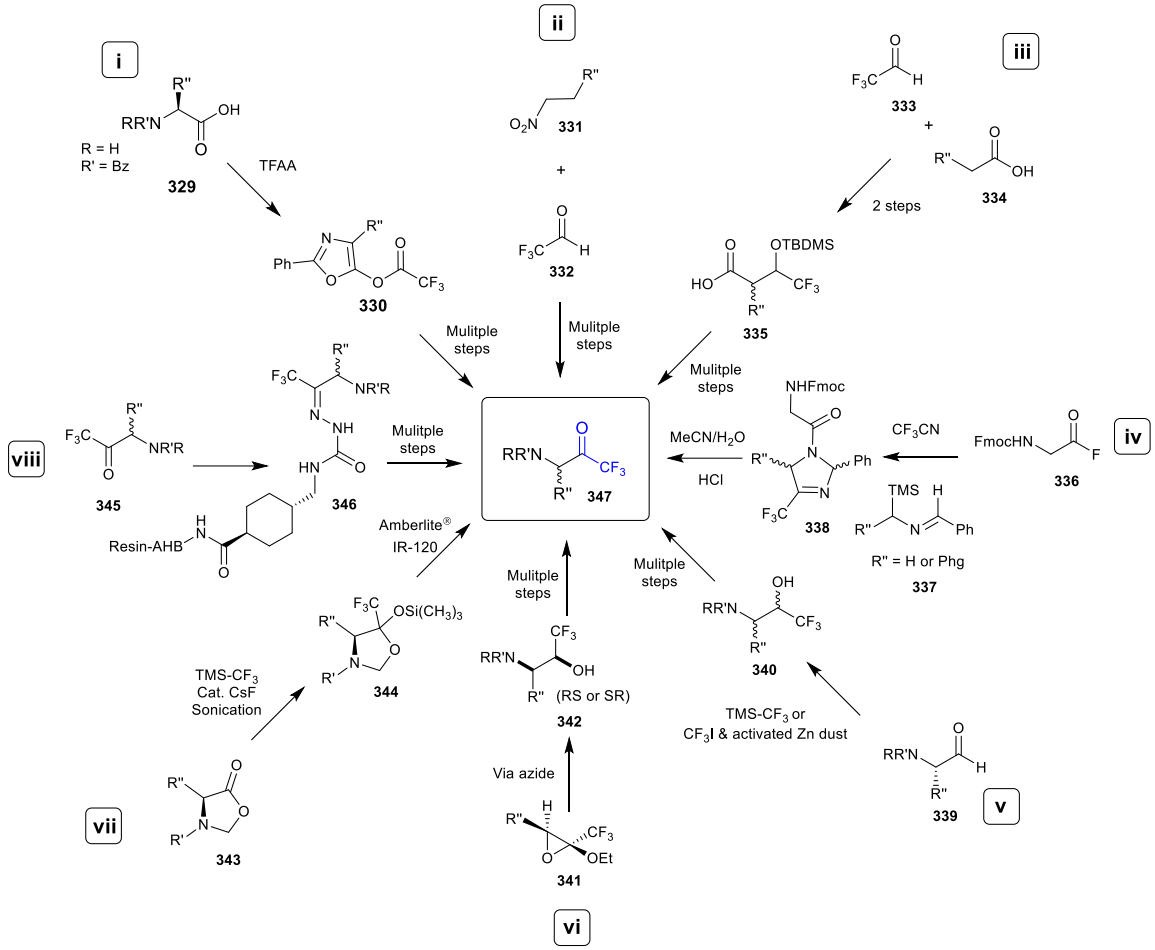

Figure 5.2 - Summary of current solid- and solution-phase synthetic routes for accessing peptidyl trifluoromethyl ketones (tFMKs).

Additionally, in 2018, Olsen and Moreno-Yruela[20] exploited the tendency for tFMKs to undergo hydration to geminal diols in aqueous media to incorporate 1,3-dioxane protected amino acid **352**, which had been synthesised in several steps from diethyl acetamidomalonate (**348**), 6-bromohexanoic acid (**349**) and trifluoroacetic anhydride (TFAA) (**350**), into a peptide sequence via SPPS (**Scheme 5.3**). This allowed enantiomerically pure installation of a tFMK moiety into the sidechain of a peptide.

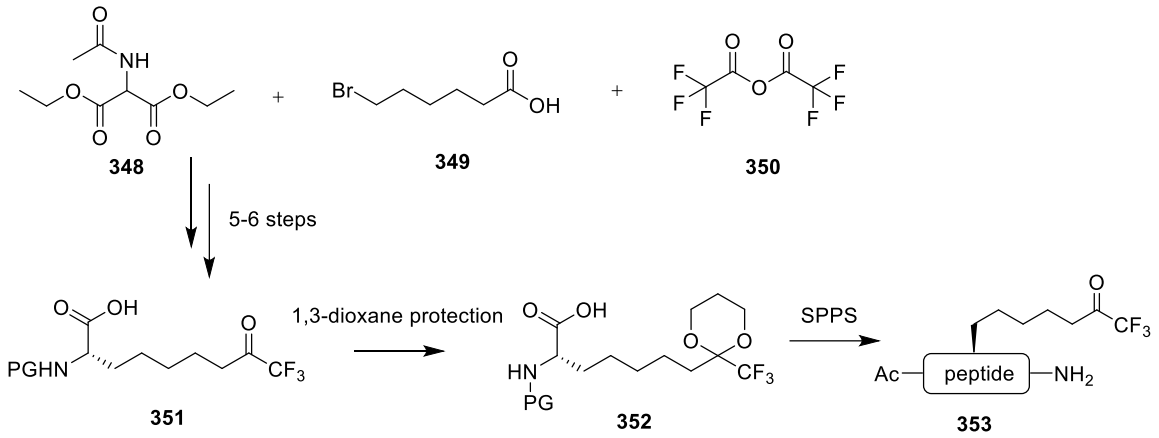

Scheme 5.3 – Route to peptidyl tFMK **353**.[20]

However, despite the fact that methodology does exist for accessing peptidyl tFMKs, the drawbacks associated with many of these approaches, including the use of hazardous materials and the lack of stereospecificity in some cases, the presence of low-yielding steps and the need for a final oxidation step limiting substrate scope in some examples, it was believed that there was still scope for the development of new methodology in this area.

In order to adapt the approach reported in **Chapter 4** (**Scheme 4.3**, starting from **273**) to enable installation of a CF_3 functionality at the α-position of a *β*-ketoester, a source of electrophilic CF_3 needed to be employed. Whilst this wouldn't allow access to tFMKs, it could enable isolation of tFEKs, which may also be of interest for use as serine protease inhibitors, as already highlighted. Two commonly utilised classes of electrophilic CF_3 reagents include Umemoto's[21] such as **354** or **355** (**Figure 5.3**) and Togni's such as **356** (**Figure 5.3**); however, whilst the former is known for its thermal stability, the latter is notoriously explosive, making Umemoto's reagents the more attractive candidates.[22,23] For this reason, attention was turned to Umemoto's reagents 5-(trifluoromethyl)dibenzothiophenium tetrafluoroborate (**354**, **Figure 5.3**) and 5-(trifluoromethyl)dibenzothiophenium trifluoromethanesulfonate (**355**, **Figure 5.3**), which have previously been utilised as agents for trifluoromethylation of a selection of 1,3-

dicarbonyl systems, although in some instances, only aromatic or cyclic examples are described.

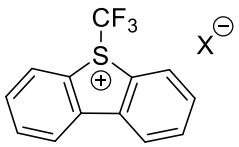

Umemoto's reagent
354, X = BF_4
355, X = OTf

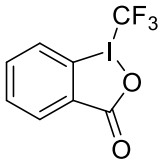

Togni reagent II (**356**)

Figure 5.3 – Structures of Umemoto's reagent **354** and **355**, along with Togni reagent II (**356**).

In 1993, Umemoto and Ishihara reported the trifluoromethylation of the sodium salt of a diester (**357**, **Scheme 5.4a**) through employment of Umemoto's reagent **355** as a source of CF_3 in a yield of 38%.[24] Subsequently, Gade and co-workers described the enantioselective copper-catalysed trifluoromethylation of *β*-ketoester **359** utilising a chiral pincer ligand (**350**) in addition to Umemoto's reagent **354** (**Scheme 5.4b**).[25] However, the method was found to be incompatible with acyclic substrates as no reactivity was observed.[25] An alternative approach involved chiral non-racemic guanidines as Brønsted bases for generation of guanidinium enolates, allowing subsequent trifluoromethylation of *β*-ketoesters such as **362**. In this example, the product (**364**) was isolated with 62% *ee* (**Scheme 5.4c**).[26] However, once again, all example substrates presented in the paper possessed a cycle or an aromatic moiety. In 2002, Ma and Cahard described conditions for trifluoromethylation of cyclic and acyclic *β*-ketoesters through the use of Umemoto's reagent **354** in conjunction with the phase-transfer catalyst, tetrabutylammonium iodide (TBAI). This allowed access to **367** in a yield of 28% (**Scheme 5.4d**).[27]

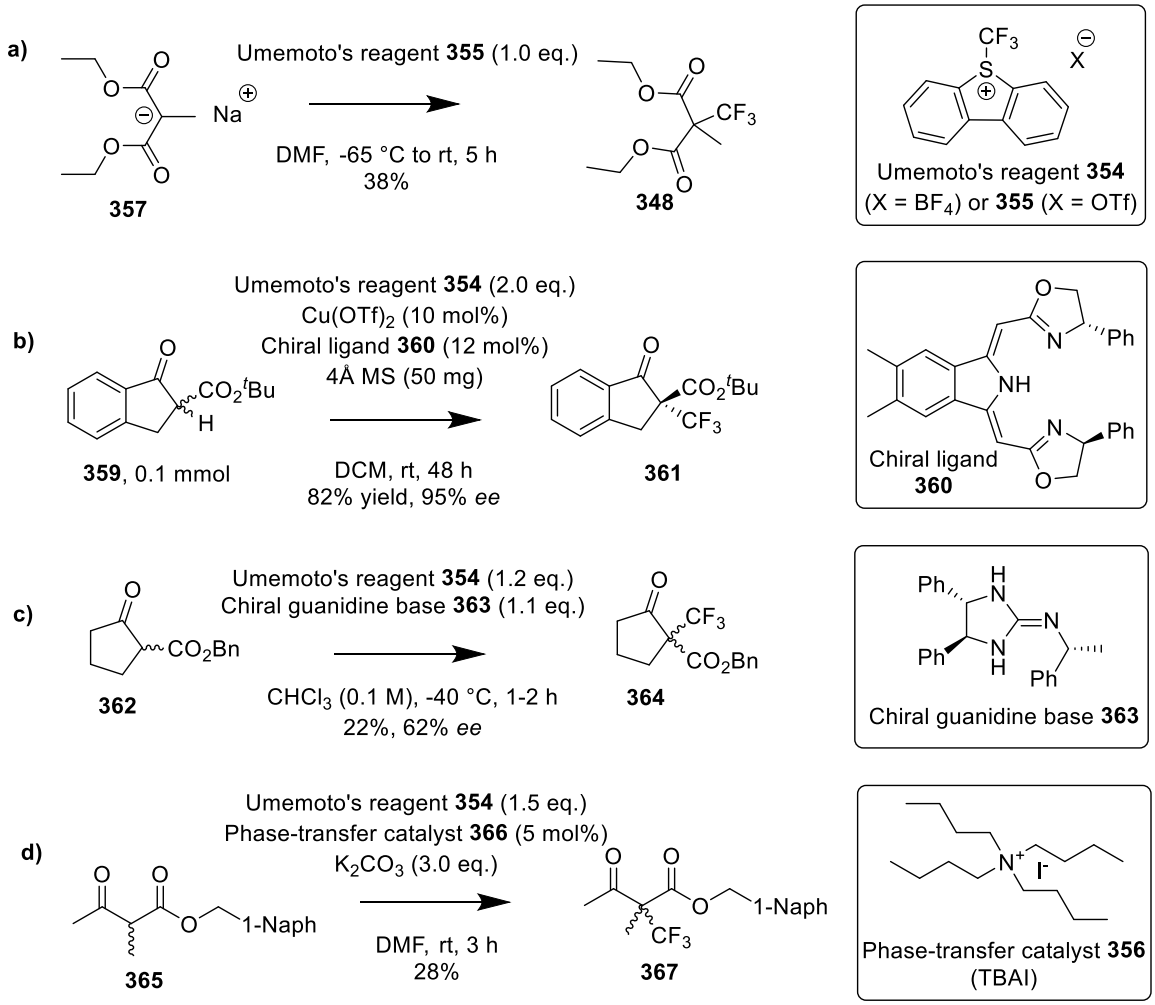

Scheme 5.4 – Conditions for trifluoromethylation of **357** to **358** (**a**),[24] **359** to **361** (**b**),[25] **362** to **364** (**c**)[26] and **365** to **367** (**d**).[27]

Due to the fact that stereospecific trifluoromethylation of 1,3-dicabonyl systems is not required for the synthesis of peptidyl tFEKs as the chiral centre will eventually be eliminated anyway due to decarboxylation, methods inconveniently requiring the synthesis or purchase of special chiral ligands or bases to ensure stereospecificity were avoided (**Scheme 5.4 b** and **c**). Instead, it was initially considered a possibility that the conditions employed in **Chapter 3.2.4** (**Scheme 3.8**) for mono-fluorination of 1,3-dicarbonyls could be adapted for trifluoromethylation. In order to investigate this hypothesis, the reaction of methyl acetoacetate (**213**), a commercially available 1,3-dicarbonyl system, with Umemoto's reagent **355** in the presence of $CpTiCl_3$ was trialled (**Scheme 5.5a**). Unfortunately, little evidence of product formation was observed by ^{19}F NMR

spectroscopy, even after a 72-hour period. Repeating the reaction in the presence of a base offered no significant improvements (**Scheme 5.5b**). It was therefore concluded that these conditions were not suitable for this purpose.

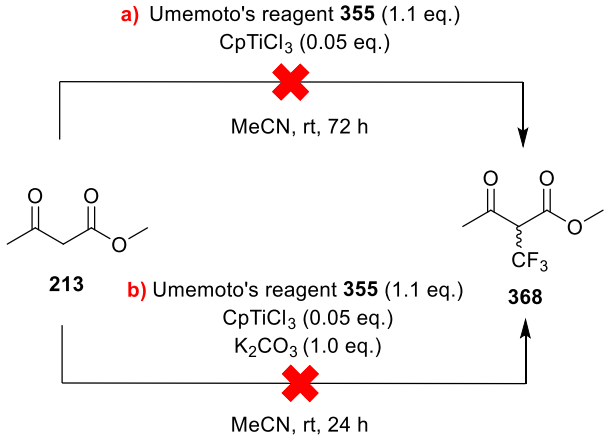

Scheme 5.5 – Conditions employed for attempted trifluoromethylation of methyl acetoacetate (**213**) with (**a**) and without (**b**) a base.

Consequently, the literature procedures summarised in **Scheme 5.4** were evaluated in search of a viable method. Given the harsh conditions used to generate sodium salts such as **357** with sodium hydride (**Scheme 5.4a**), this approach was shelved along with those requiring chiral reagents (**Scheme 5.4b** and **c**). Thus, attention turned towards the conditions described by Ma and Cahard,[27] which utilises Umemoto's reagent **354** in the presence of TBAI (**Scheme 5.4d**), due to their operational simplicity and relatively low toxicity. Adapting these conditions, methyl acetoacetate (**213**) was reacted with Umemoto's reagent (**355**) in the presence of TBAI along with K_2CO_3 and tracked by ^{19}F NMR spectroscopy in both DCM-d_2 and DMF (**Scheme 5.6**).

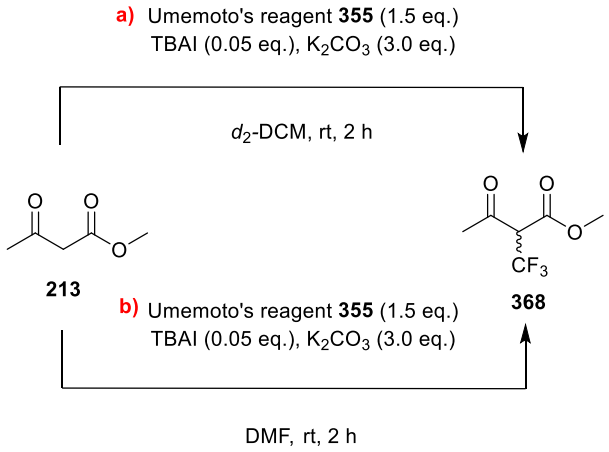

Scheme 5.6 – Conditions employed for attempted trifluoromethylation of methyl acetoacetate (**213**) in DCM-d_2 (**a**) and DMF (**b**).

The ^{19}F NMR spectrum recorded after two hours (**Figure 5.4b**) of attempted trifluoromethylation of **213** in DCM-d_2 (**Scheme 5.6a**) showed little change compared to the spectrum corresponding to Umemoto's reagent (**355**) itself (**Figure 5.4a**), although a few smaller peaks could be seen around -62 ppm, which is in the region reported in the literature for similar trifluoromethylated compounds.[28]

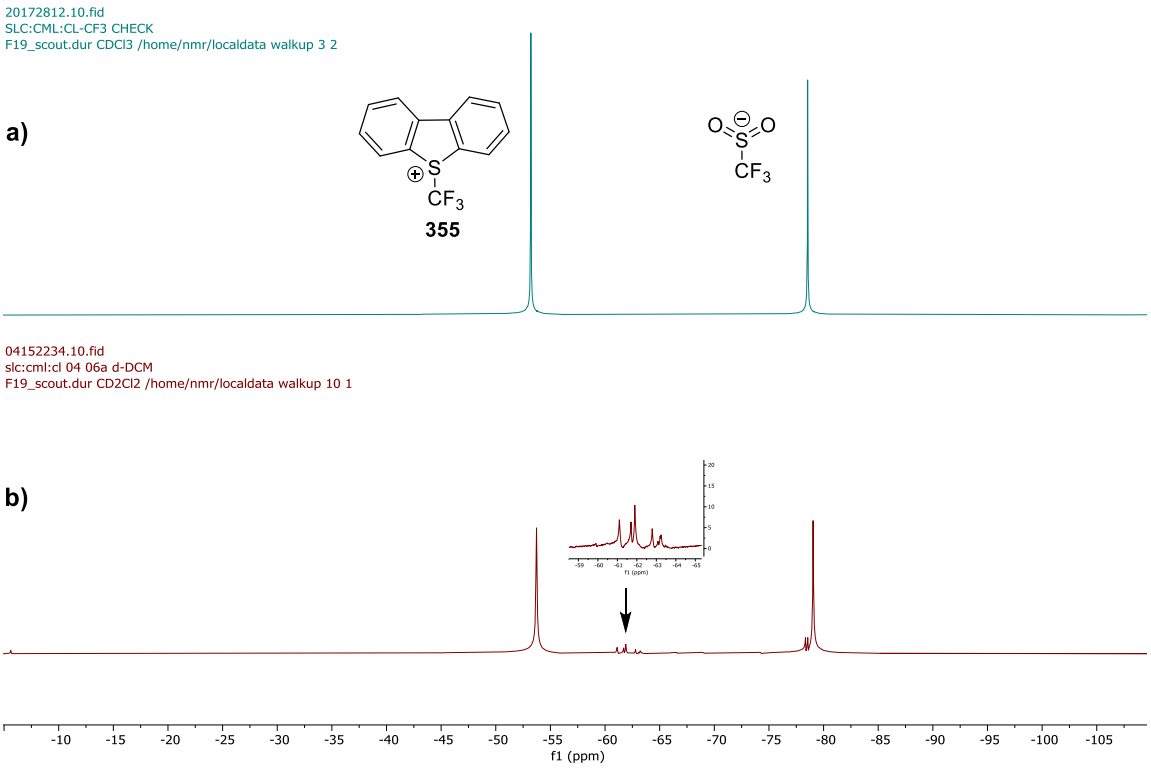

Figure 5.4 – ^{19}F NMR spectra for Umemoto's reagent **355** recorded in $CDCl_3$ (**a**) and after attempted trifluoromethylation of methyl acetoacetate, recorded in CD_2Cl_2 (**b**).

On the contrary, when the reaction was performed in DMF (**Scheme 5.6b**), the resulting ^{19}F NMR spectrum (**Figure 5.5b**) revealed the disappearance of the peak corresponding to the CF_3 group from Umemoto's reagent **355** (-54.3 ppm) (**Figure 5.5a**), suggesting a transformation had occurred. Again, the appearance of new peaks was apparent, including in the region of -62 ppm; however, they were extremely small. An LCMS spectrum of the crude material post-workup did not support the presence of product (**368**); however, GCMS did reveal a peak corresponding to the correct mass of 184 (**Figure 5.6**). Unfortunately, the mass of a potential by-product (**369**) possesses the same exact mass value, further adding to the uncertainty. Admittedly, the isotopic distribution of the mass spectrum (**Figure 5.6**) did seem to suggest that the by-product (**369**) was likely responsible.

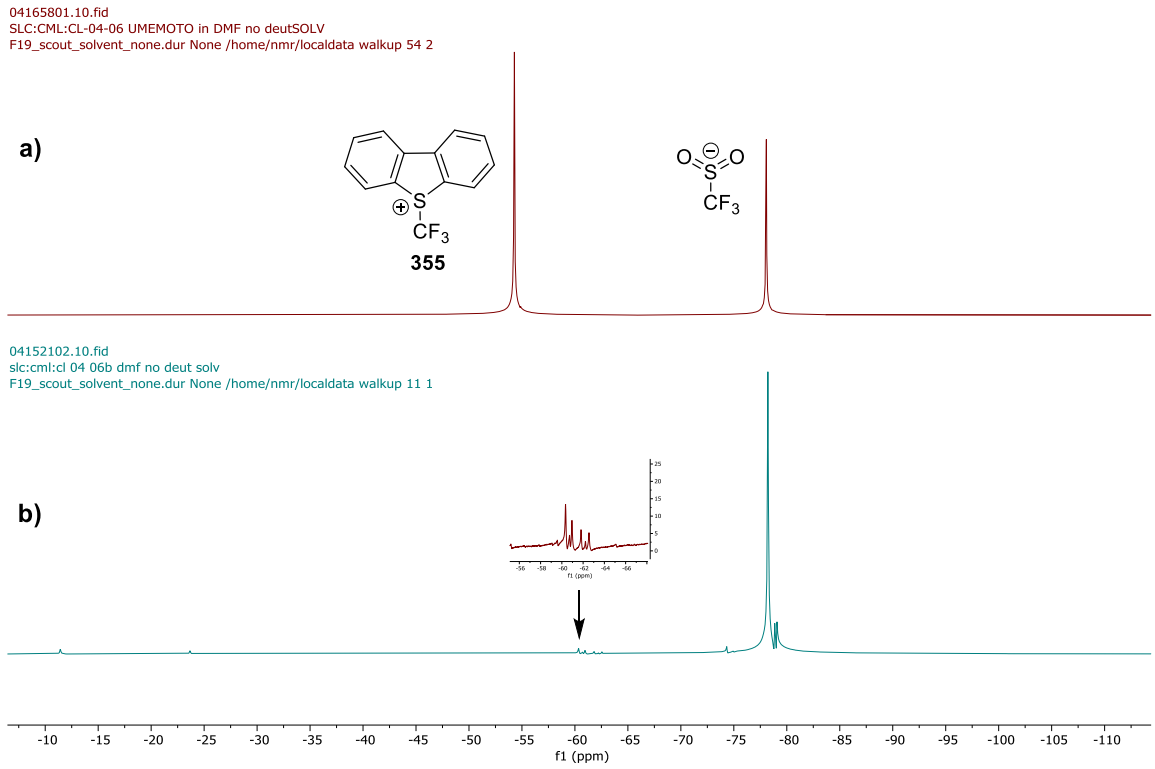

Figure 5.5 – ^{19}F NMR spectra for Umemoto's reagent **345** (**a**) and after attempted trifluoromethylation of methyl acetoacetate (**213**) in DMF (**b**). Both spectra were recorded in the absence of deuterated solvent.

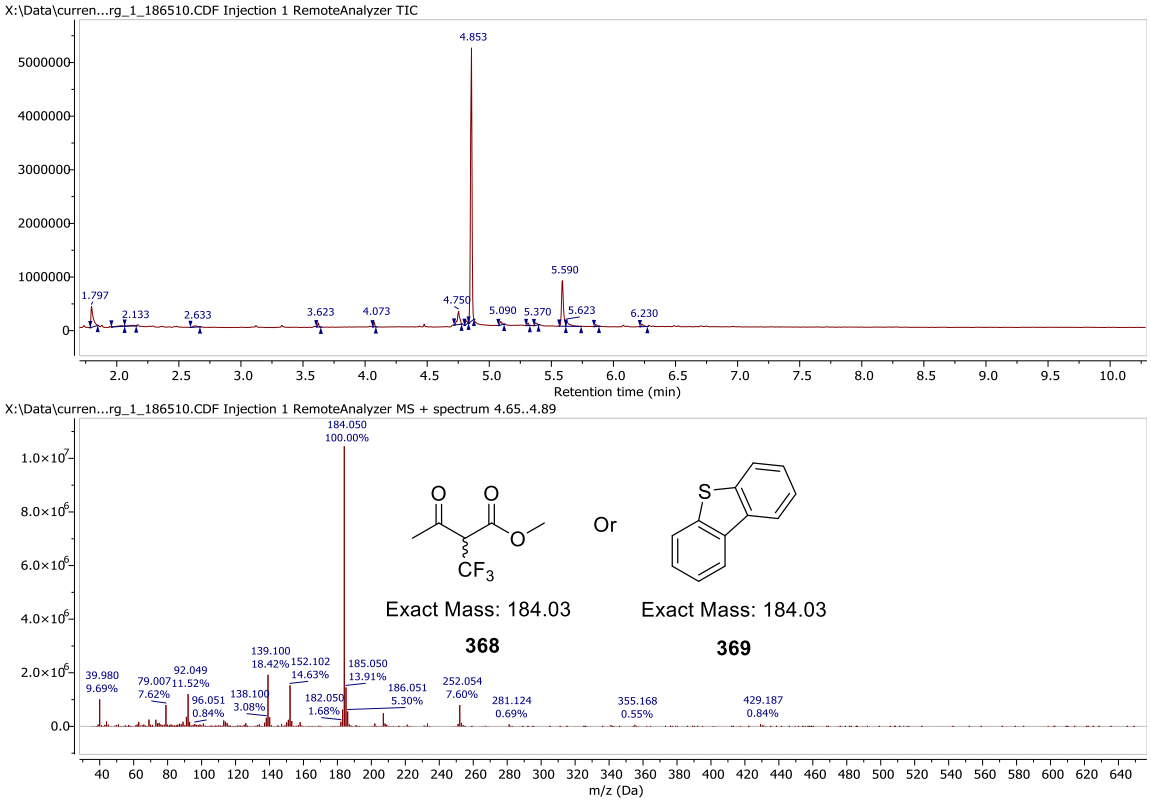

Figure 5.6 – GCMS spectrum of crude material after attempted trifluoromethylation of methyl acetoacetate **213**.

Purification of the crude material obtained from the attempted trifluoromethylation of methyl acetoacetate (**213**) in DMF (**Scheme 5.6b**) via prep TLC allowed a closer look at the material relating to the mass of 184 Daltons. Multiple peaks could be seen by ^{19}F NMR spectroscopy (**Figure 5.7a**) in the region of –62 ppm, which surprisingly did not significantly reduce in complexity when proton decoupled (**Figure 5.7b**), suggesting they did not relate to product **368** as a doublet peak would be expected when ^{1}H coupled and a singlet when ^{1}H decoupled. Furthermore, the ^{1}H NMR spectrum revealed the presence of aromatic peaks, suggesting they may instead relate to Umemoto's reagent. It was therefore concluded that this approach was not suitable for the substrate of interest (**213**), especially as none of the examples in the paper being followed[27] possessed two α-protons prior to trifluoromethylation.

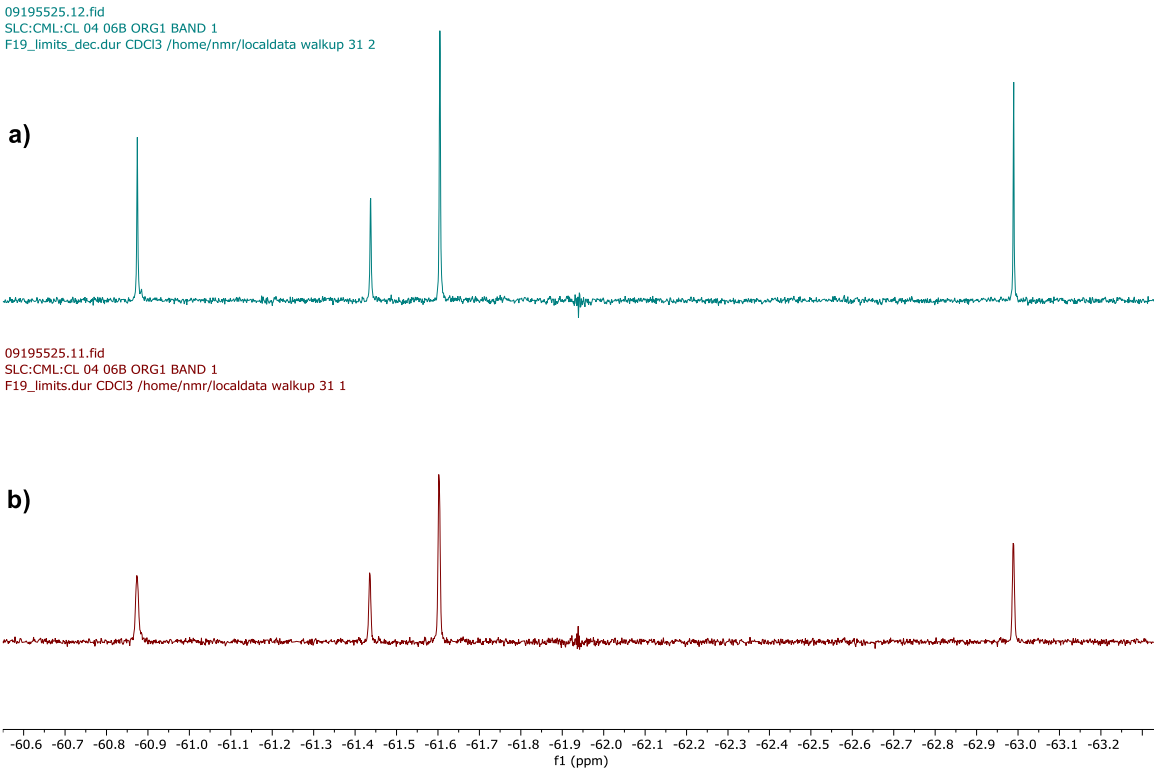

Figure 5.7 – ^{1}H coupled (**a**) and ^{1}H decoupled (**b**) ^{19}F NMR spectrum of material acquired from attempted trifluoromethylation via prep TLC.

A paper was found reporting the mono-trifluoromethylation of *β*-ketoesters with two α-protons present (**Scheme 5.7**);[28] however, the method involved the use of CF_3I in the form of a Ritter trifluoroiodomethane-DMSO adduct, an expensive reagent to buy (5 mL = £221 from Sigma Aldrich, correct as of March 2023). The use of CF_3I gas directly would be undesirable due to its associated toxicity and potential to explode if heated. Thus, it was decided that the work would be shelved, and attention turned instead towards the synthesis of peptidyl mono-chloromethyl ketones (mCMKs) (**Section 5.3**).

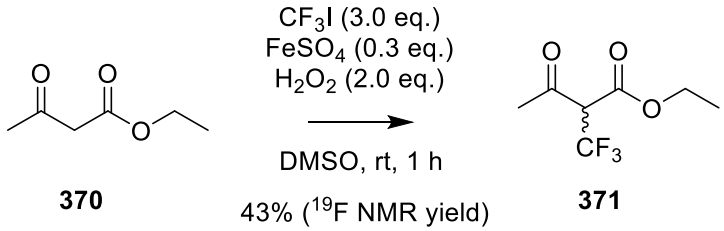

Scheme 5.7 – Conditions reported for trifluoromethylation of **370**.[28]

5.3 Synthesis of Peptidyl mono-Chloromethyl Ketones (mCMKs)

5.3.1 Solution-Phase Approach

In order to adapt and redeploy the previously described route to peptidyl mFMKs (**Scheme 4.3**, starting from **278**) for accessing peptidyl CMKs, employment of an electrophilic source of chlorine was pursued so as to enable its installation at the α-position of a *β*-ketoester. A similar approach has in fact been reported in the literature for accessing amino acid-based CMK building blocks through electrophilic chlorination of a *β*-ketoester followed by subsequent decarboxylation.[29,30] However, the conditions they employed were different and their amine protecting group strategy involved Cbz rather than Boc or Fmoc. Furthermore, they did not demonstrate the ability to incorporate the CMK into a peptide sequence.

In 2003, along with publishing methodology for mono-fluorination of *β*-ketoesters, which was utilised in **Chapter 4** (**Scheme 4.6**) for accessing mFMKs, Togni and co-workers also disclosed a means for electrophilic mono-chlorination using *N*-chlorosuccinimide (NCS) in the presence of a catalytic amount of $CpTiCl_3$.[31] Thus, these conditions were initially trialled on methyl acetoacetate **213** (**Scheme 5.8**), which was employed as a test substrate for proof of principle, and found to give the desired product in a keto-enol ratio of around 1 : 1 after column chromatography, as confirmed by ^{1}H NMR spectroscopy (**Figure 5.8**). As can be seen, a couple of impurity peaks are present even after purification, likely due to the presence of a small amount of di-chlorinated material.

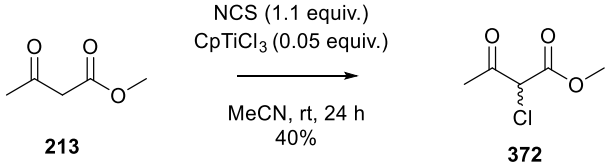

213 **372**

Scheme 5.8 - Conditions for electrophilic mono-chlorination of 1,3-dicarbonyl **213**.

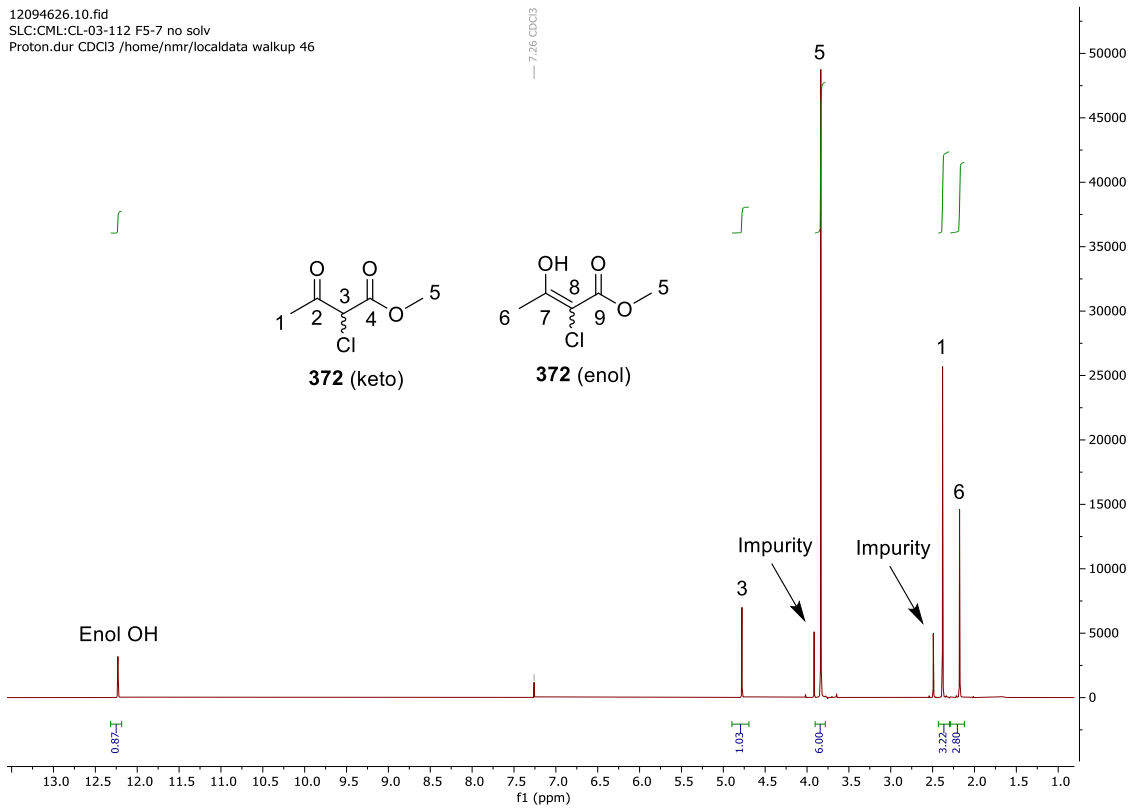

Figure 5.8 – ^{1}H NMR spectrum ($CDCl_3$) showing evidence for the presence of mono-chlorinated keto (**372**) and enol (**372**) substrates.

With this success behind us, the conditions were then transferred to the substrate of interest. In light of their ability to inhibit serine protease enzymes, peptidyl CMKs often possess a valine monomer in the C-terminal position. Therefore, it was decided that chlorination of a *β*-ketoester derived from Boc-Val-OH would be pursued. This *β*-ketoester (**284**) was first constructed as described in **Chapter 4** (**Scheme 4.5**), using CDI, LDA and *tert*-butyl acetate, allowing access to the desired target (**284**, **Scheme 5.9**). Electrophilic chlorination was then performed using NCS and $CpTiCl_3$ (**Scheme 5.9**), affording the desired product (**373**) as a mixture of keto and enol tautomers in a ratio of 4 : 1 (as determined by ^{1}H NMR spectroscopy), predominantly in the keto-form with an isolated yield of 55%. Diastereoisomers also appeared to be present in a ratio of 2 : 3. The identity of the desired product (**373**) was confirmed by ^{1}H NMR spectroscopy (**Figure 5.9**) and LCMS (+ve) (**Figure 5.10**).

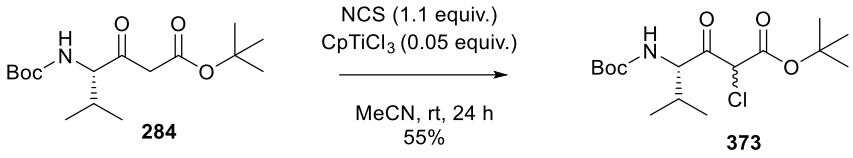

Scheme 5.9 - Conditions for electrophilic mono-chlorination of 1,3-dicarbonyl **284**.

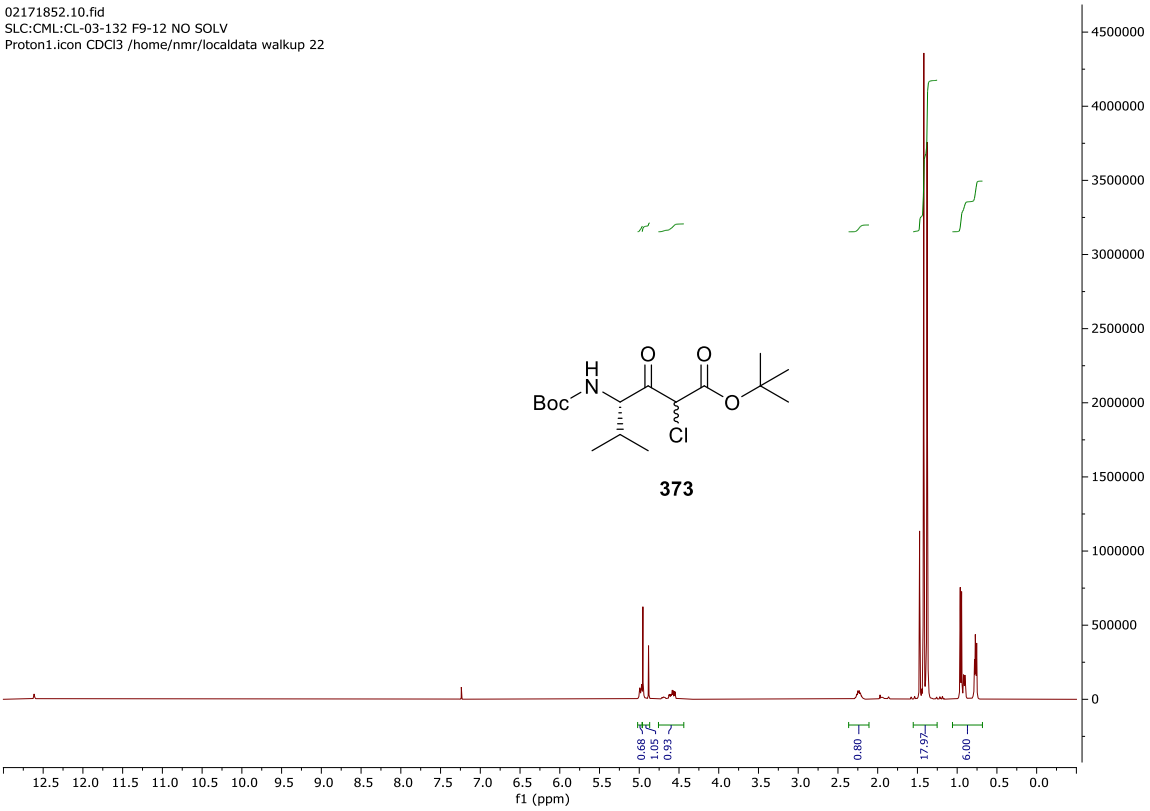

Figure 5.9 – ^{1}H NMR spectrum ($CDCl_3$) recorded after electrophilic chlorination of *β*-ketoester **284** to give **373**.

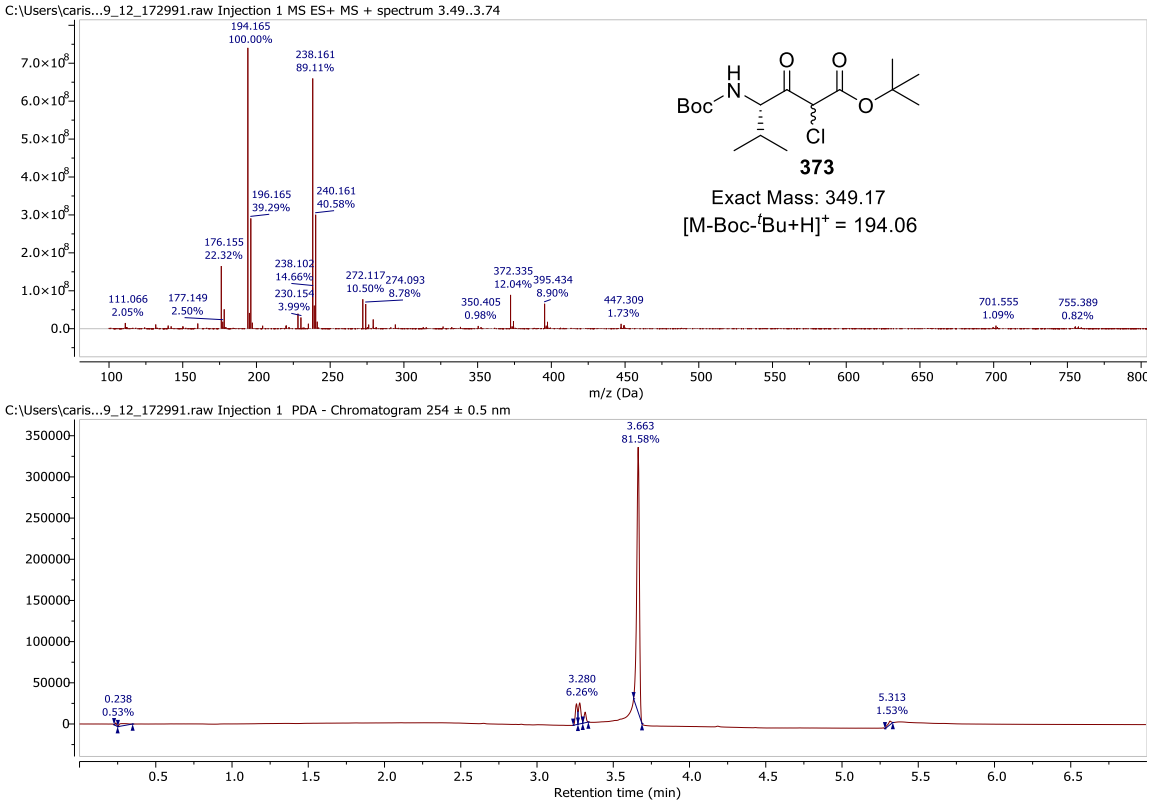

Figure 5.10 – LCMS spectrum (+ve, λ = 254 nm) showing evidence for the presence of **373**.

Moving forward from here, deprotection of the Boc group and *tert*-butyl ester with concomitant decarboxylation to CMK building block **374** (**Scheme 5.10**) was achieved in a similar manner to that utilised for FMK formation (**Chapter 4**, **Scheme 4.9**), with product identity confirmed via HRMS (+ve) (**Figure 5.11**).

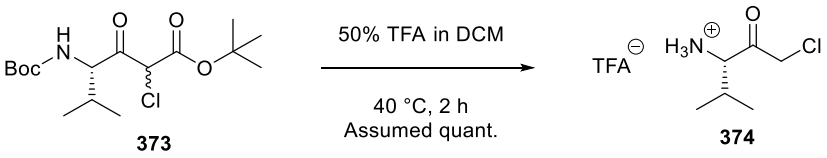

Scheme 5.10 - Conditions for deprotection and decarboxylation of **373** to CMK building block **374**.

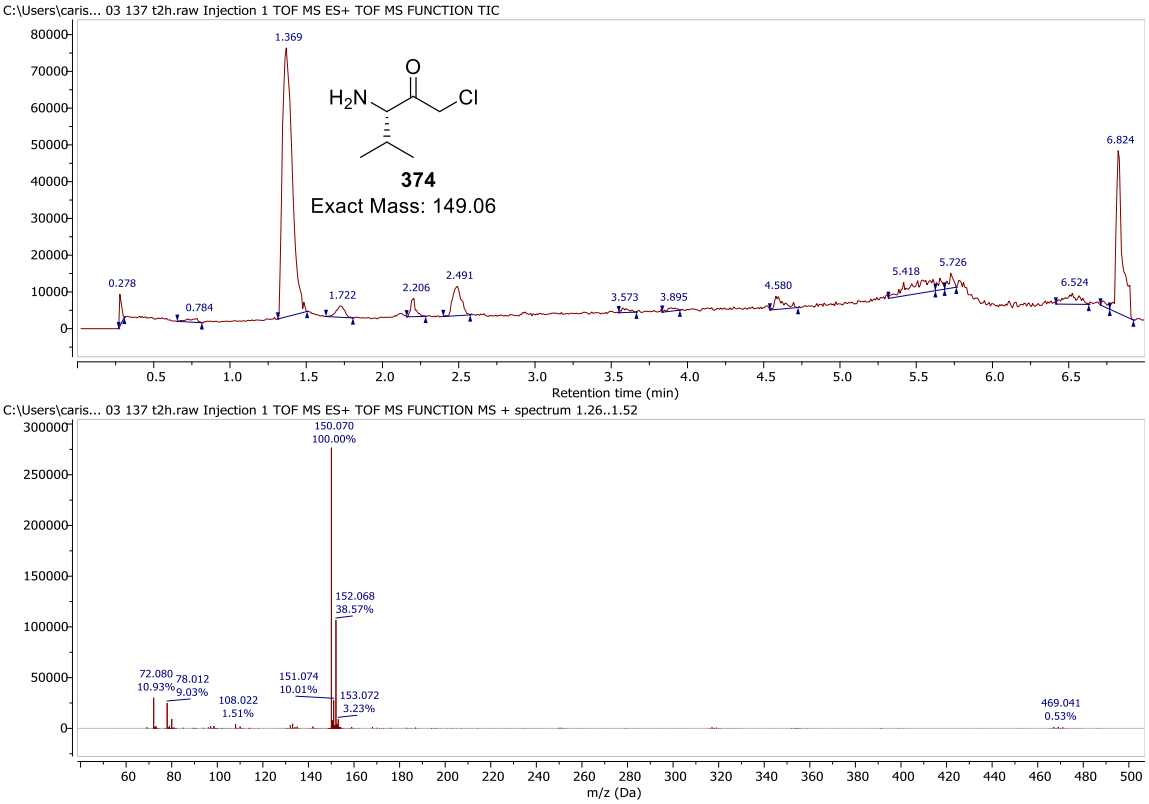

Figure 5.11 – TIC and mass spectrometry data (+ve) showing evidence for the presence of CMK building block **374**.

The resulting CMK building block (**374**) was assumed to have been acquired in a quantitative yield and carried forward in crude form to be coupled in solution with the peptide of choice, Ac-Ala-Tyr-Leu-OH (**375**), with the goal of ultimately accessing Ac-Ala-Tyr-Leu-Val-CH_2Cl (**323**, **Figure 5.1**), a known inhibitor of HLE.[2] The peptide component (**365**) was synthesised on 2-chlorotrityl chloride resin via standard protocols and mild cleaved using 2,2,2-trifluoroethanol (TFE) in order to keep the sidechain protecting group on tyrosine intact for the subsequent coupling reaction. The crude protected-peptide, obtained in a purity of 86% as determined by analytical HPLC and identifiable by mass spectrometry (**Figure 5.12**) and ^{1}H NMR spectroscopy (**Figure 5.13**), was carried forward and coupled to CMK building block **374** through reaction with HATU in the presence of 2,4,6-collidine (**Scheme 5.11**). This allowed access to protected peptidyl CMK **376** in a yield of 75% after purification via column chromatography, as confirmed by HRMS (+ve) (**Figure 5.14**) and ^{1}H NMR spectroscopy (**Figure 5.15**). Notably, product peaks in the ^{1}H

NMR spectrum (**Figure 5.15**) did appear to double up in a ratio of approximately 2.5 : 1.0. It was thought that this could be an indication of epimerisation having occurred during the coupling step, leading to the presence of diastereoisomers, but it could also be rationalised if rotamers were present. Clarification of this could be achieved by carrying out high-temperature NMR analysis, but it was not possible to do so at this time.

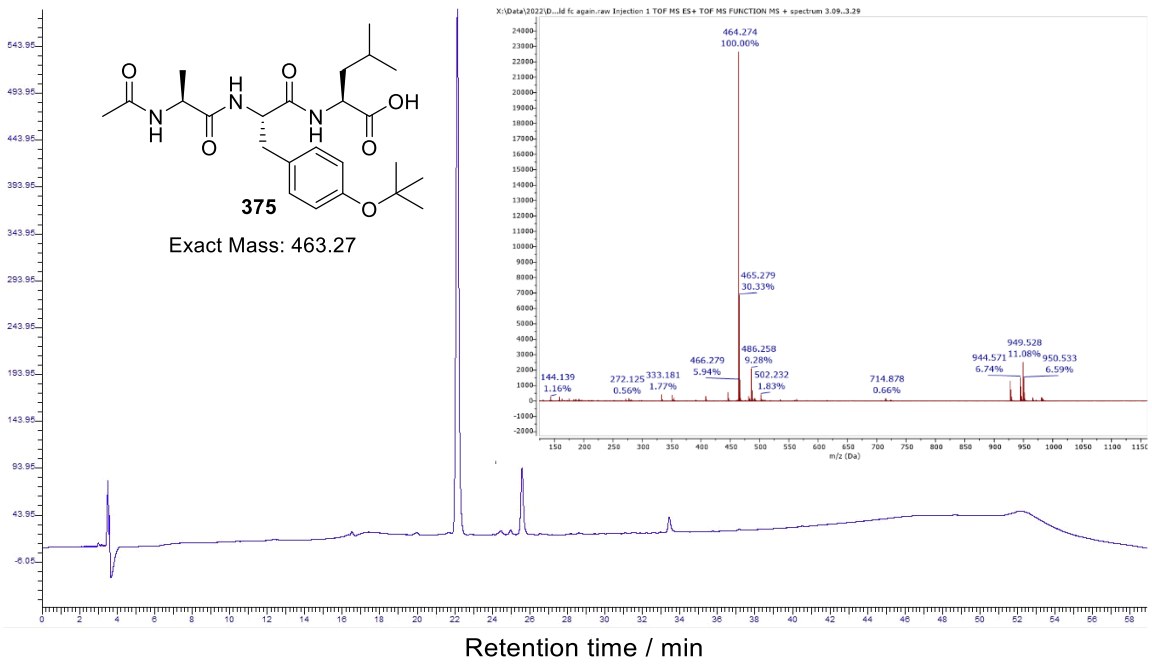

Figure 5.12 – Analytical HPLC trace (λ = 220 nm) and mass spectrum (+ve) for crude protected-peptide **375**.

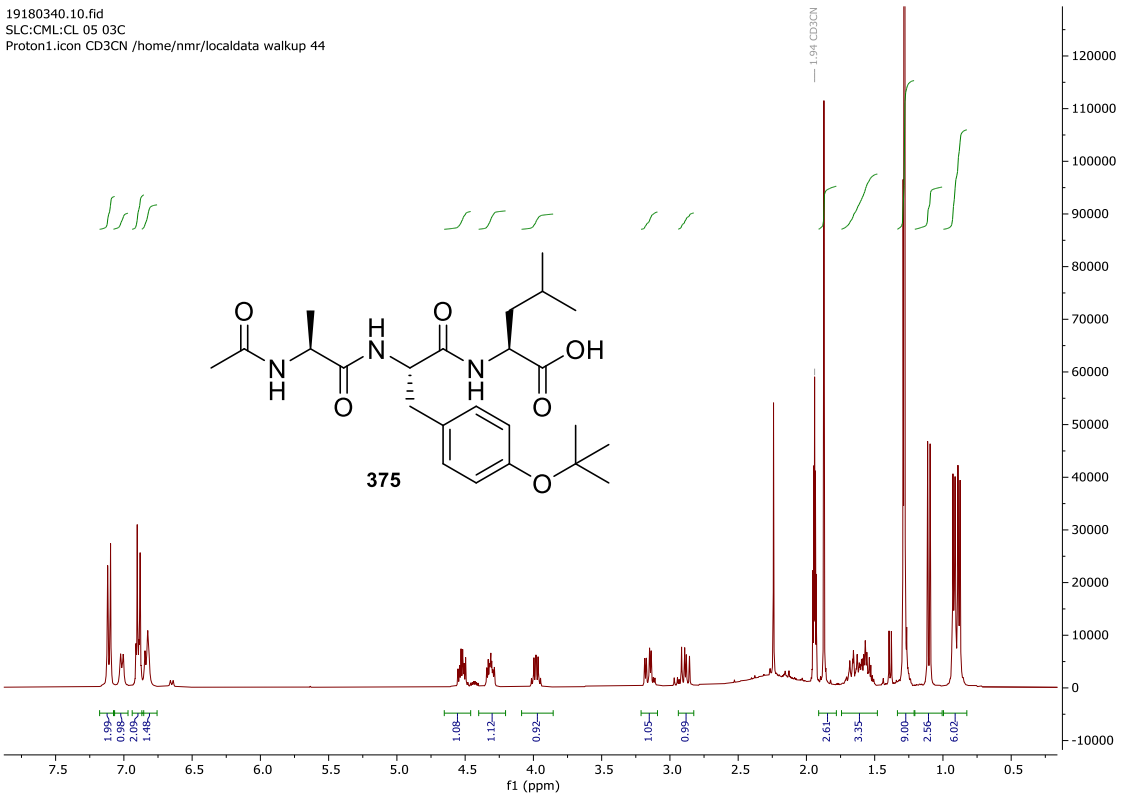

Figure 5.13 – ^{1}H NMR spectrum (CD_3CN) of crude peptide Ac-Ala-Tyr-Leu-OH (**375**).

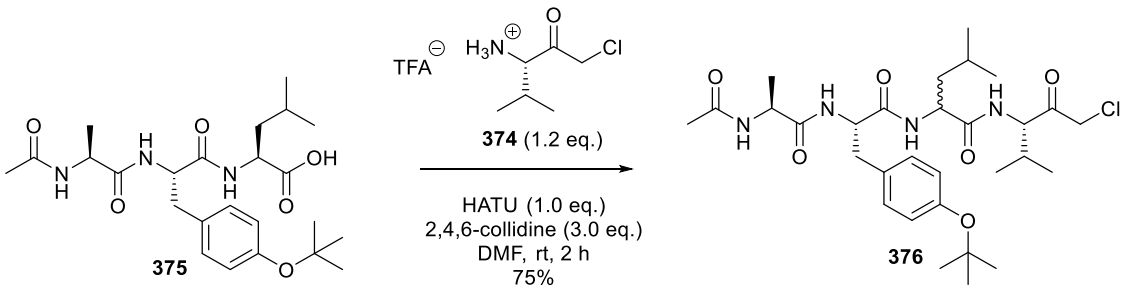

Scheme 5.11 - Conditions for solution-phase coupling of peptide **375** to CMK building block **374**.

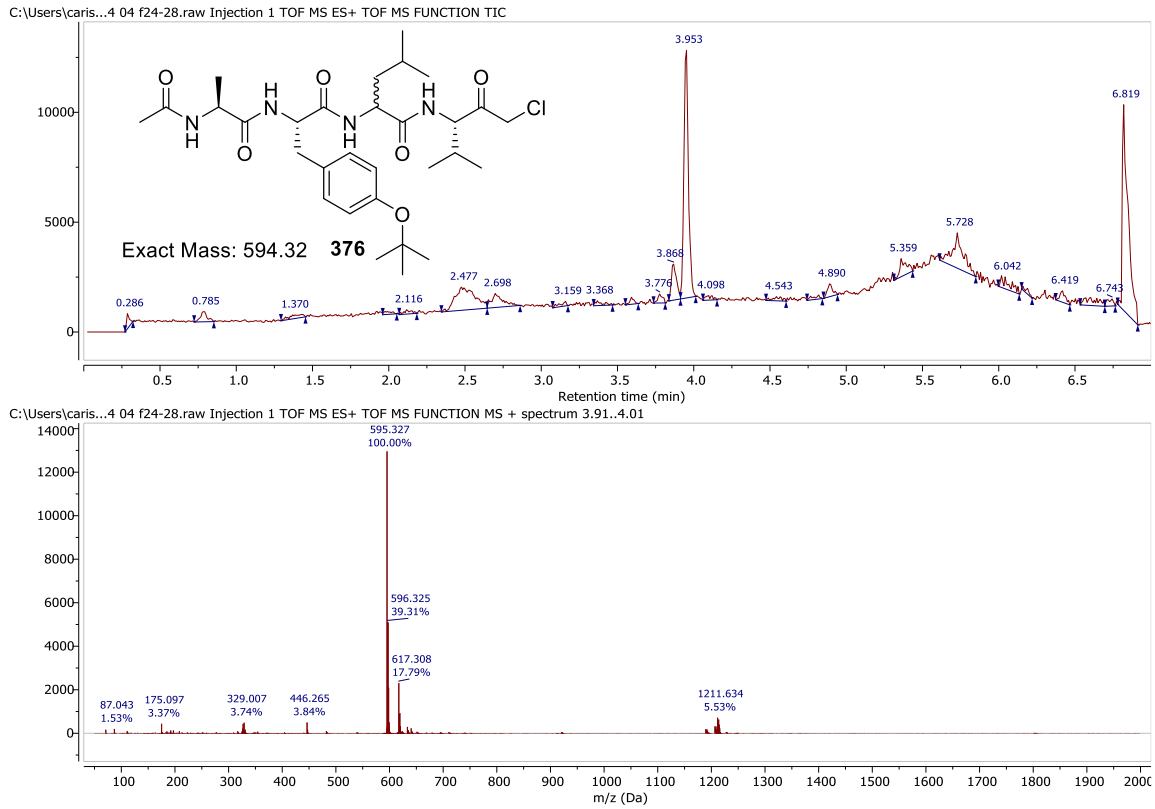

Figure 5.14 – TIC and mass spectrometry data (+ve) of protected peptidyl CMK **376**.

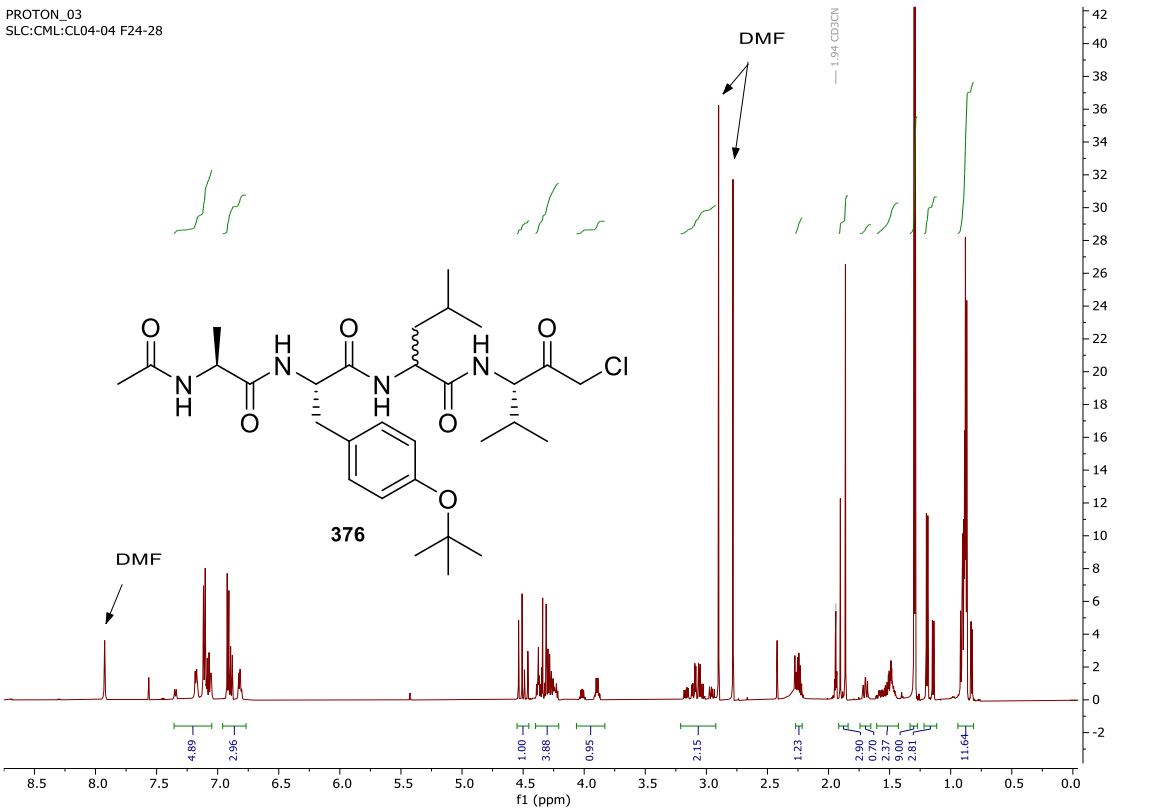

Figure 5.15 – ^{1}H NMR spectrum (CD_3CN) of protected peptidyl CMK **376**.

Finally, sidechain ^{t}Bu ester deprotection of **376** with 2.5% H_2O in TFA for 1.5 hours at room temperature afforded target peptidyl CMK **323** in a yield of 96% (**Scheme 5.12**). Product identity was confirmed by HRMS (+ve) (**Figure 5.16**); however, the associated analytical HPLC trace (λ = 220 nm) (**Figure 5.16**) appeared to suggest a combination of two peaks of the same mass in a ratio of 3.1 : 1.0. Furthermore, the ^{1}H NMR spectrum (**Figure 5.17**) again revealed several signals doubling up in a ratio of approximately 2.7 : 1.0. The consistent doubling of peaks in the NMR spectrum led to the assumption that the stereo centre of the Leu had in part epimerised and that target CMK **323** was isolated as a diastereoisomeric mixture.

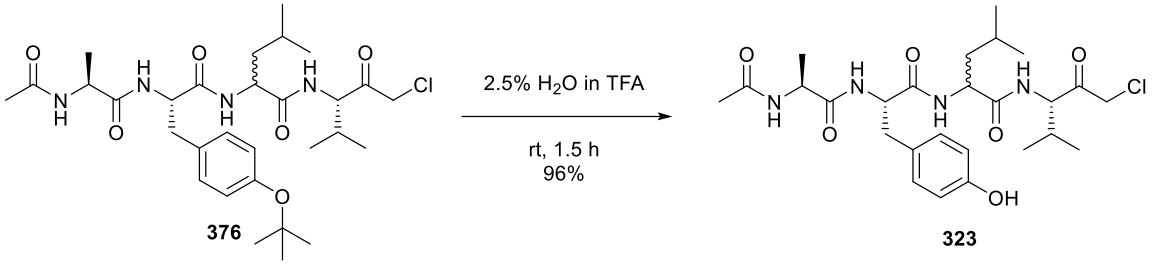

Scheme 5.12 - Conditions for *tert*-butyl ester deprotection of **376** to give peptidyl CMK **323**.

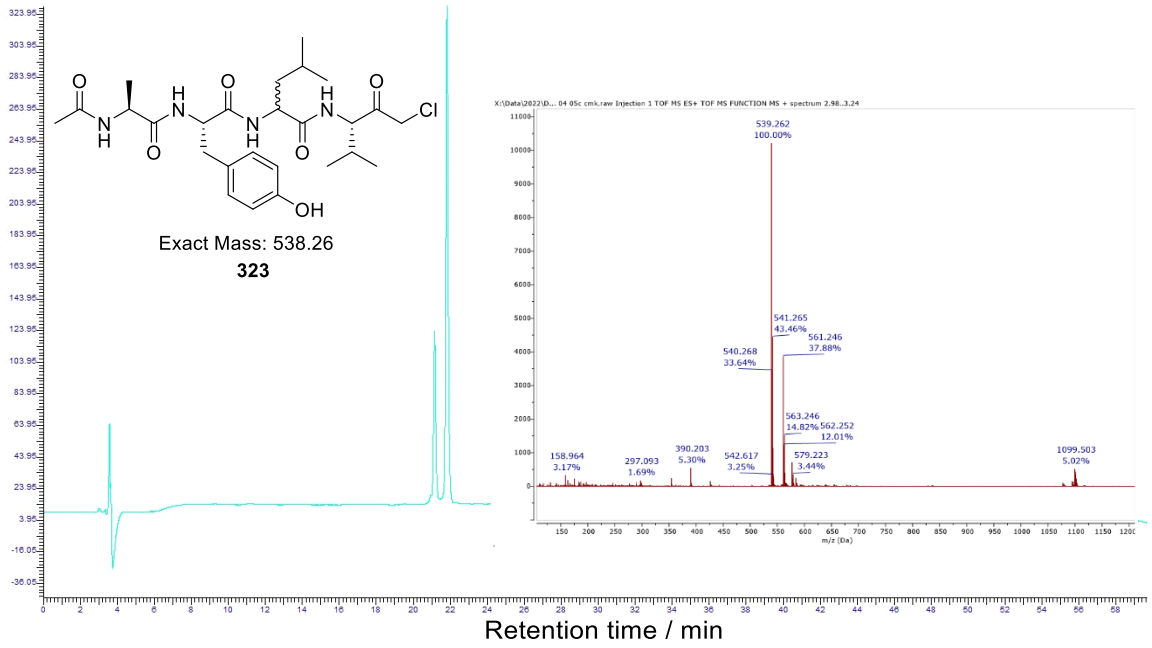

Figure 5.16 – Analytical HPLC trace (λ = 220 nm) and mass spectrum (+ve) for peptidyl CMK **323**.

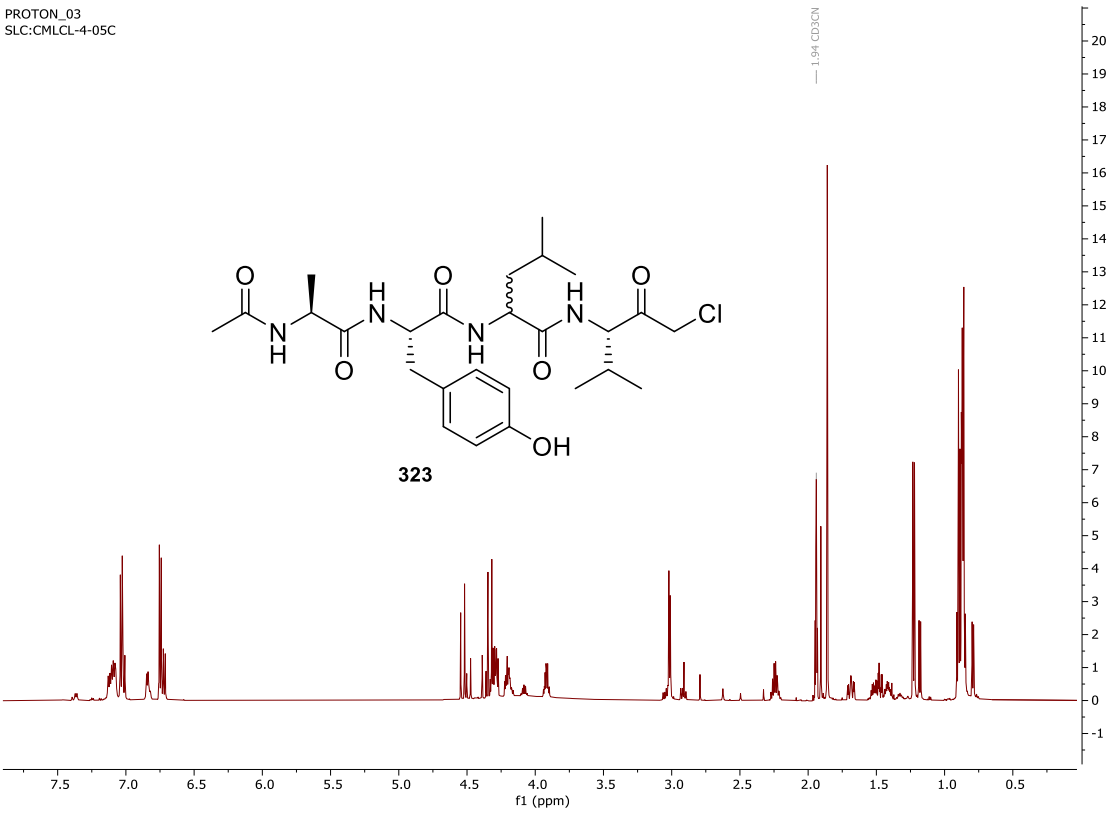

Figure 5.17 – ^{1}H NMR spectrum (CD_3CN) showing evidence for the formation of peptidyl CMK **323**. [A mix of diastereoisomers is likely present].

As a result of the two peaks in the analytical trace (**Figure 5.16**) both possessing the mass corresponding to peptidyl CMK **323**, and the proposed hypothesis, based on the NMR analysis, that epimerisation had occurred to some degree, resulting in the presence of diastereoisomers (**323a** and **323b**), the crude material containing peptidyl CMK **323** was therefore purified by prep HPLC (**Chapter 7.3.8.2**). Separation proved more successful for one suspected diastereoisomer (**323a**) (**Figure 5.18a**) than the other (**323b**) (**Figure 5.18b**), with the former occurring as one major peak (**peak a**) whilst the latter still appeared to be a combination of two peaks by analytical HPLC (**peak b**) post-purification. An ^{1}H NMR spectrum recorded of **peak a** (**Figure 5.19**) confirmed it was indeed peptidyl CMK **323**. Comparison of this ^{1}H NMR spectrum (**Figure 5.20a**) with that recorded for **peak b** (**Figure 5.20b**) revealed the presence of a small amount of **peak a** (as expected based on the analytical trace), likely representing the same diastereoisomer of peptidyl CMK **323**

seen in **peak a**, plus another major species which was suspected to be the other diastereoisomer (**323b**).

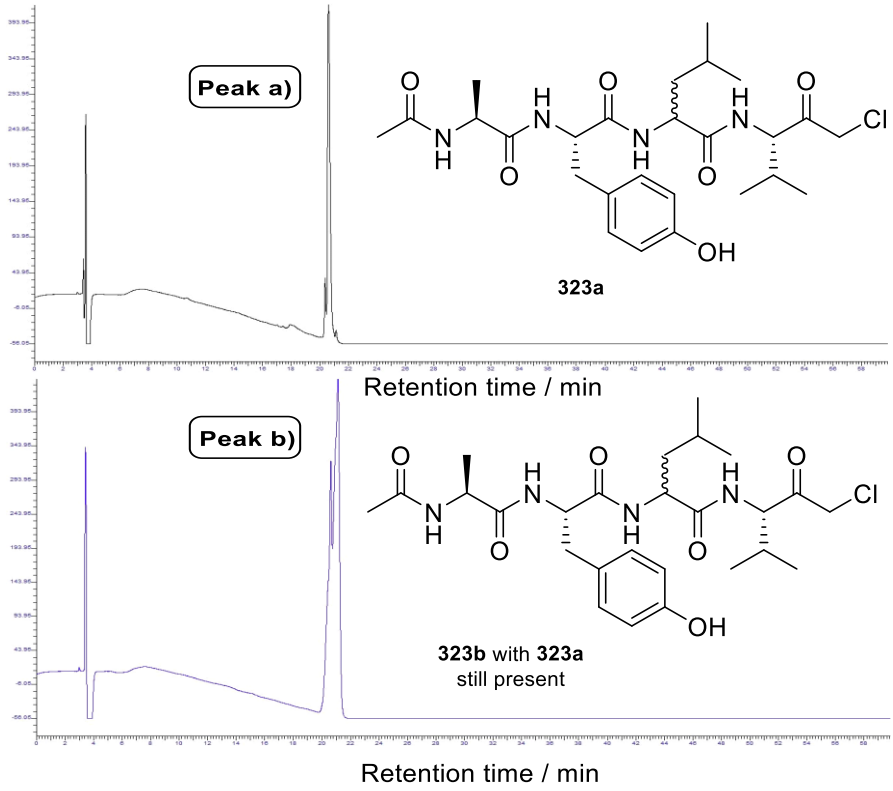

Figure 5.18 – Analytical HPLC traces (λ = 220 nm) after attempted separation of suspected diastereoisomers of CMK **323**.

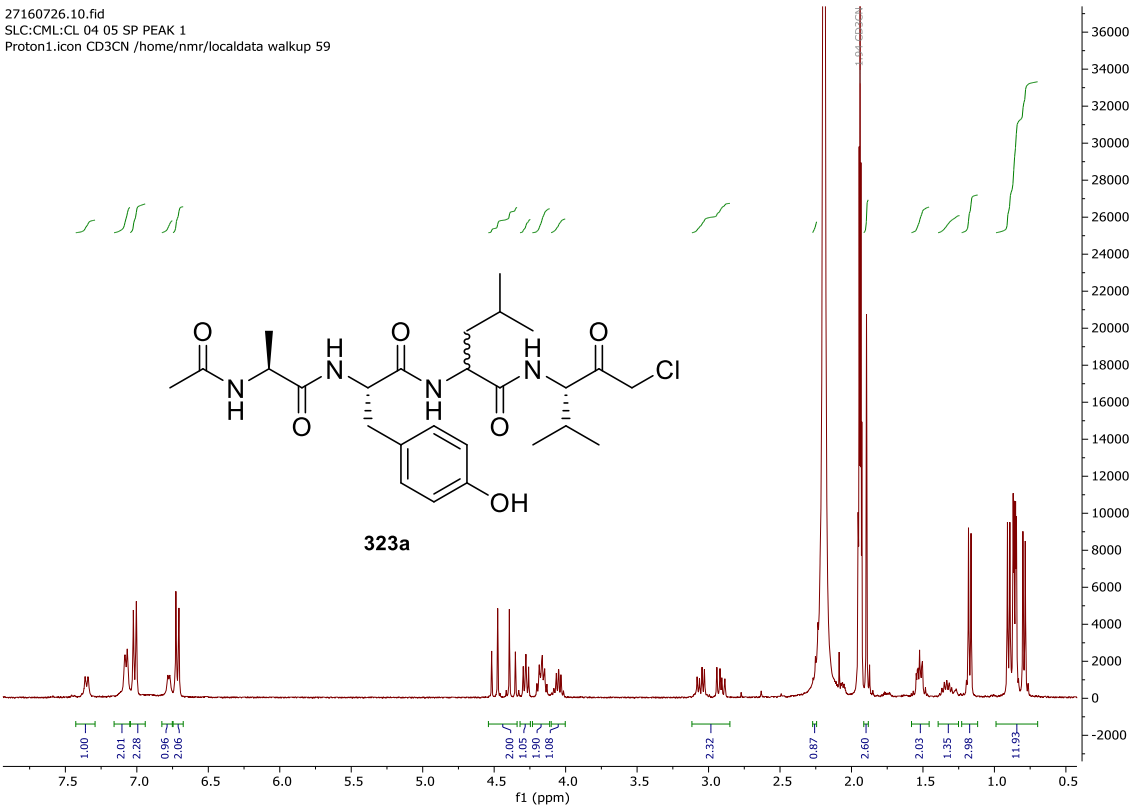

Figure 5.19 – ^{1}H NMR spectrum (CD_3CN) of a suspected single diastereoisomer of CMK **323a**.

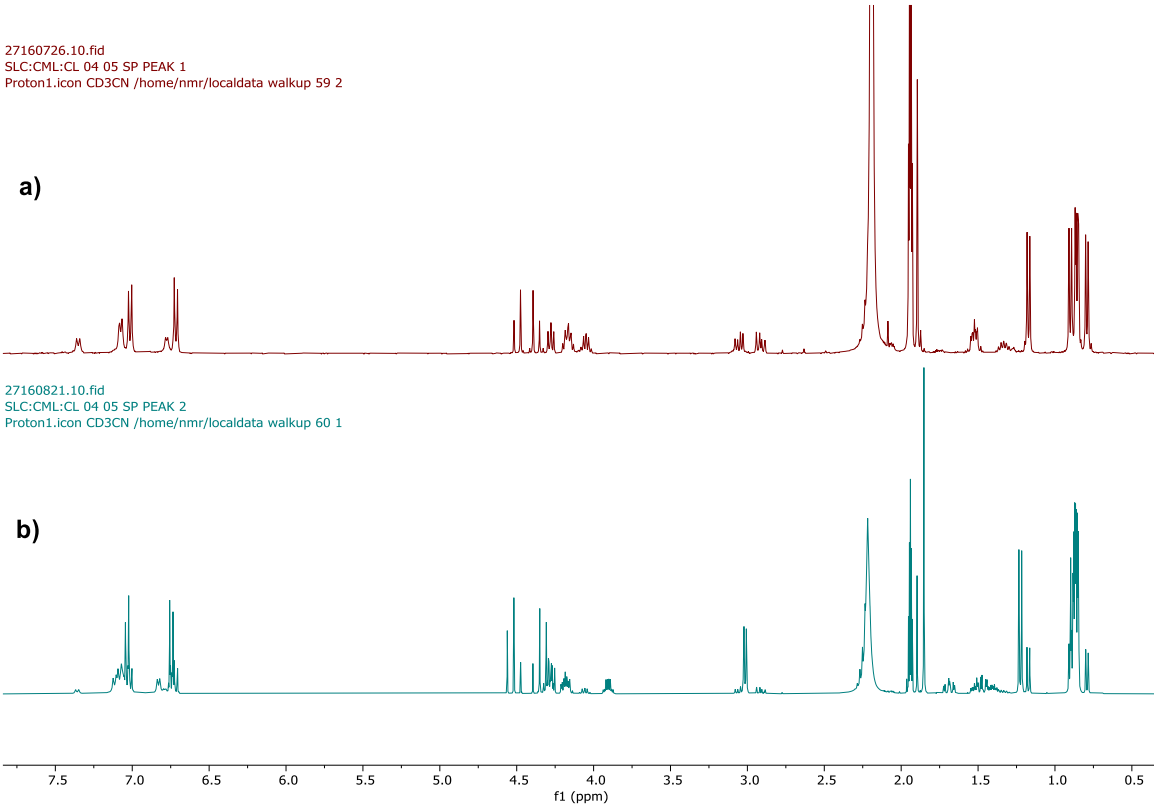

Figure 5.20 – Comparison of ^{1}H NMR spectra (CD_3CN) for **peak a** (**a**) and **peak b** (**b**).

Despite the fact that epimerisation was likely observed to some degree during the synthesis, peptidyl CMK formation was successfully achieved in relatively few steps, with potential for further improving the stereoselectivity of the coupling reaction.

5.3.2 Solid-Phase Approach

An Fmoc-protected analogue (**247**) was also made of the Boc-protected *β*-ketoester (**284**), this time derived from Fmoc-Val-OH, using CDI, *tert*-butyl acetate and LDA as described in **Chapter 3.6.1** (**Scheme 3.21**)**,** with the intention of chlorinating and attempting on-resin synthesis of peptidyl CMKs through careful *tert*-butyl ester deprotection of **377** to *β*-ketoacid **378** and subsequent resin attachment. This would then allow SPPS and ultimately decarboxylation to the desired peptidyl CMK (**380**) (**Scheme 5.13**). Whilst this approach did not prove viable for accessing peptidyl mFMKs via solid-phase methods, it was believed that because the replacement of fluorine with chlorine would not invoke such extreme electron-withdrawing effects, resin loading could be more favourable due to improved nucleophilicity of the carboxylate. After construction of Fmoc-protected *β*-ketoester **247**, electrophilic chlorination was achieved using NCS and $CpTiCl_3$, giving **377** in a yield of 55% (**Scheme 5.14**), as confirmed by ^1H NMR spectroscopy and HRMS (**Figure 5.21**).

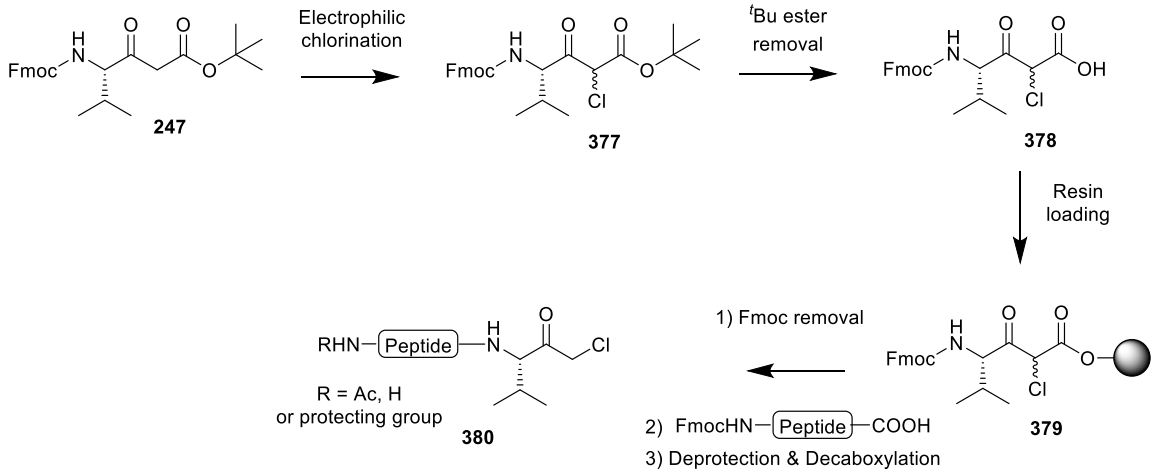

Scheme 5.13 – Proposed route to peptidyl CMK **380** through SPPS.

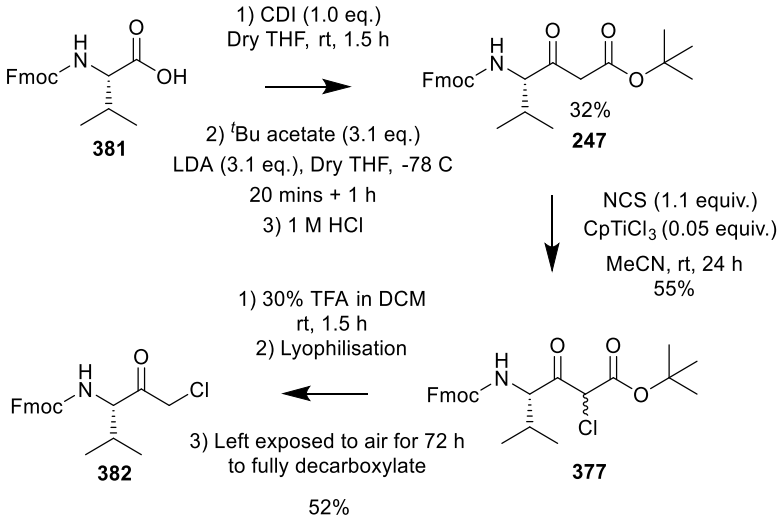

Scheme 5.14 - Conditions employed for accessing Fmoc-Val-CMK **382**.

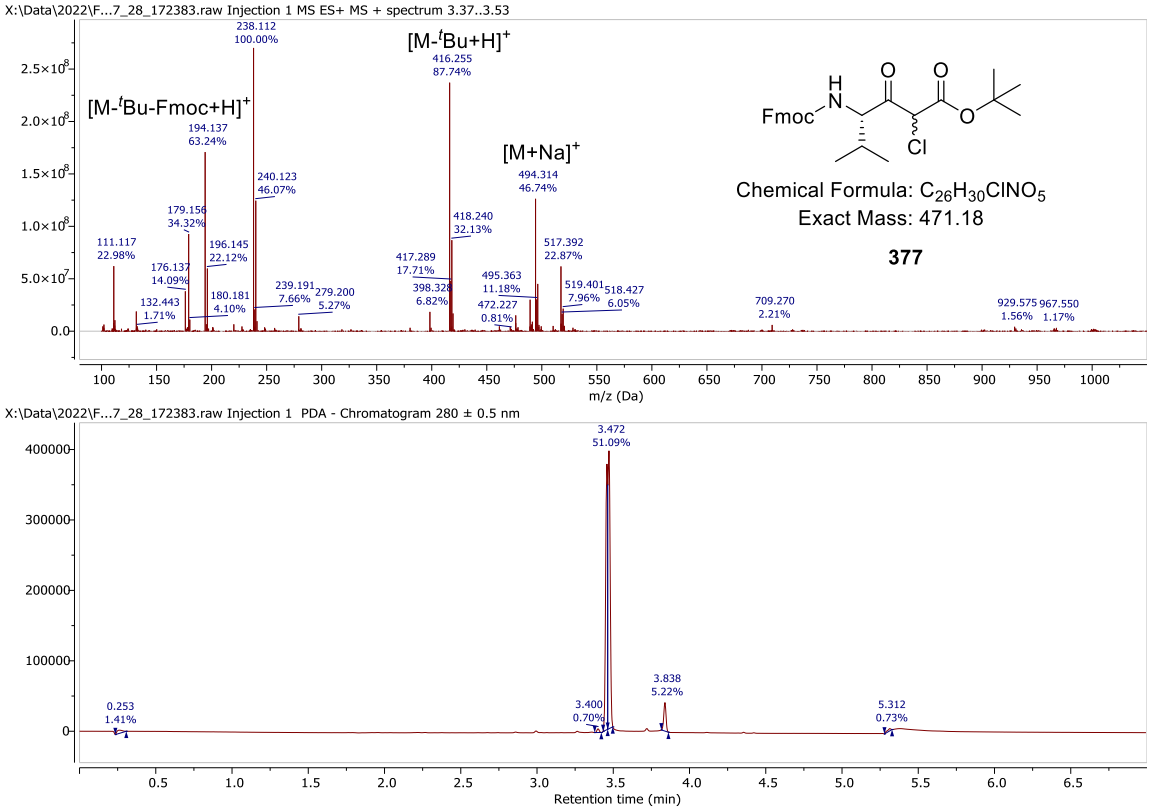

Figure 5.21 – LCMS data (+ve, λ = 280 nm) confirming successful isolation of *β*-ketoester **377**.

*t*Butyl ester deprotection to carboxylic acid **378** was then attempted through exposure of **377** to 30% TFA in DCM for 1.5 h (**Scheme 5.14**) followed by lyophilisation in a similar manner to that reported in **Chapter 3.6.3** (**Scheme 3.23**). However, it was evident by both ^{1}H NMR spectroscopy and LCMS that CMK **382** was the dominant species. As

very little of the desired *β*-ketoacid (**378**) was present due to decarboxylation dominating, it was decided that resin loading would be abandoned and the sample would be left exposed to air over a 72-hour period in order to encourage complete decarboxylation. This allowed access to Fmoc-Val-CMK **382** in a yield of 52%, as confirmed by ^{1}H NMR (**Figure 5.22**) spectroscopy and LCMS (**Figure 5.23**). Whilst deprotection of Fmoc in solution is less preferable than Boc which possesses by-products which are volatile and therefore easily removed, it has been described in the literature.[32] Thus, mono-chlorinated *β*-ketoester **377** and CMK **382** may represent useful building blocks for solution-phase coupling to a peptide of choice in order to access peptidyl CMKs. Furthermore, the use of *N*-Fmoc for analogues of *β*-ketoester **377** derived from amino acids possessing sidechains with acid-sensitive protecting groups may prove particularly useful as it can be removed in base whilst leaving the protecting groups intact during the remaining solution-phase peptide coupling steps. A final acidolysis step would enable global deprotection and decarboxylation to the desired peptidyl CMK.

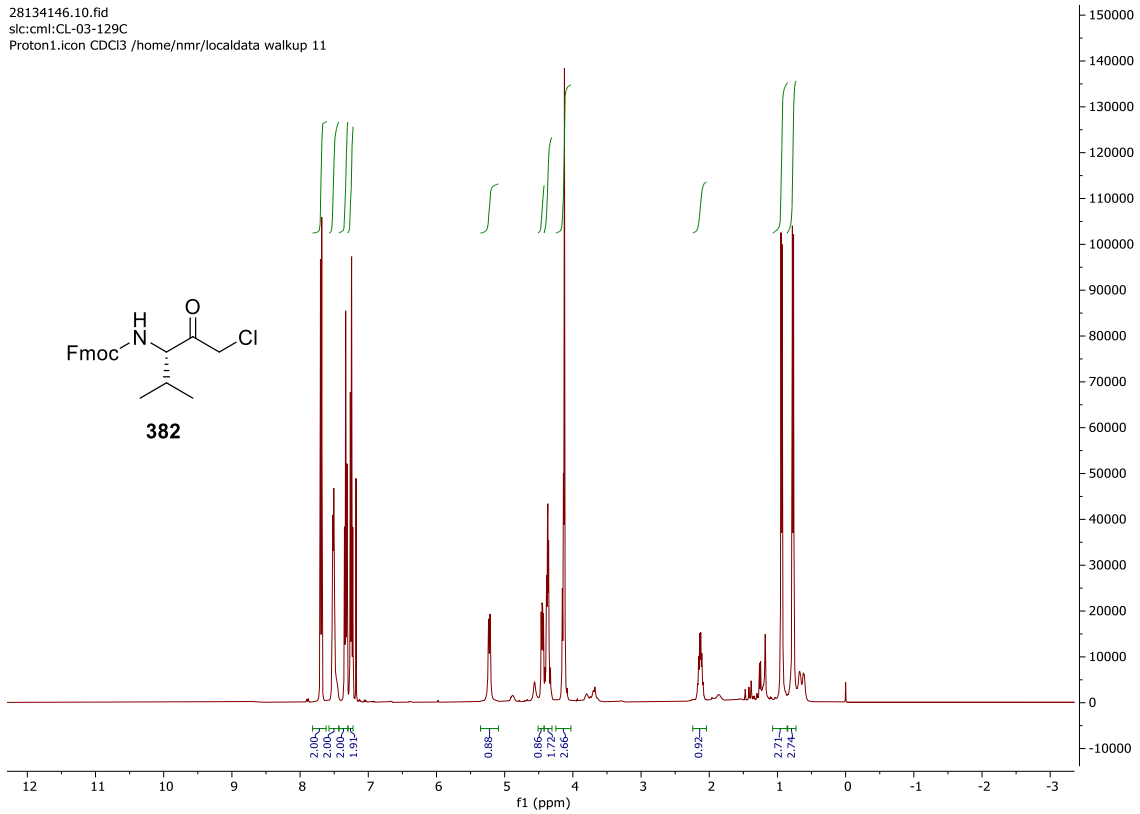

Figure 5.22 – ^{1}H NMR spectrum ($CDCl_3$) for Fmoc-Val-CMK **382**.

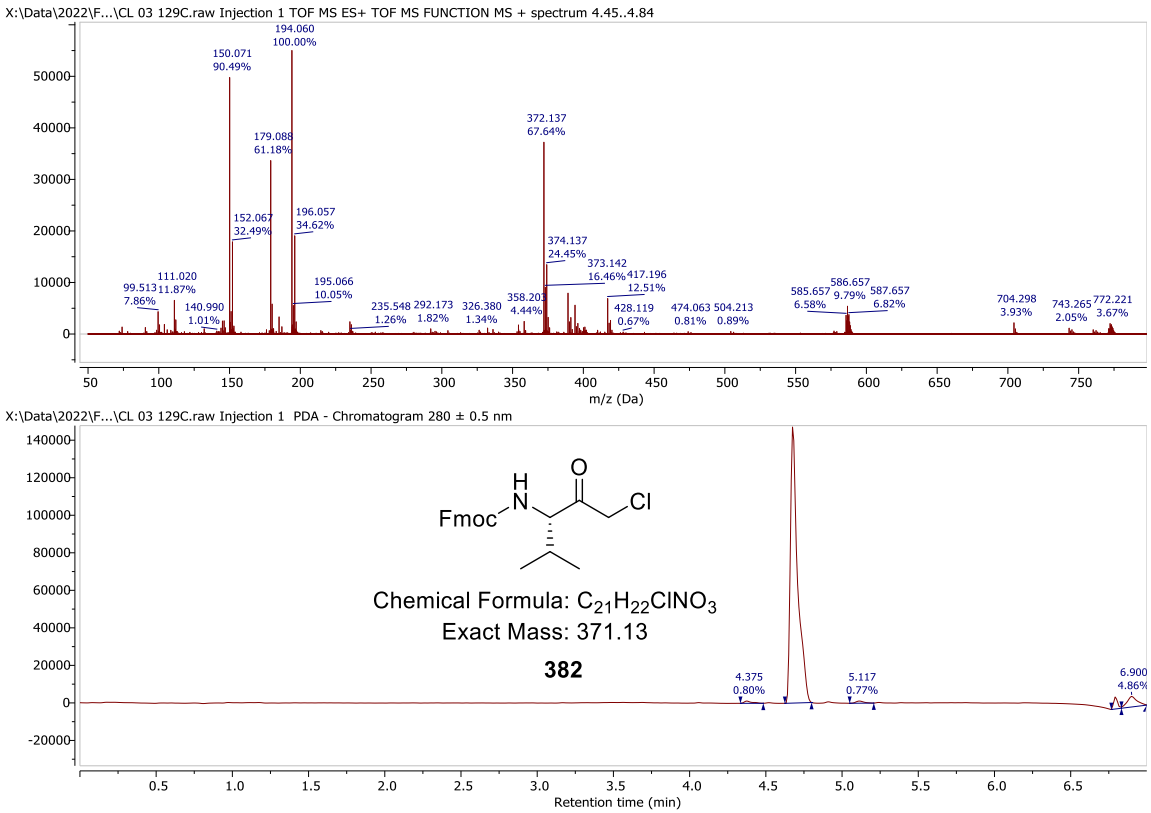

Figure 5.23 – LCMS data (+ve, λ = 280 nm) confirming successful isolation of Fmoc-Val-CMK **382**.

5.4 Chapter Summary

This chapter sought to adapt and redeploy the conditions employed in **Chapter 4** (**Scheme 4.3**, starting from **278**) for accessing peptidyl mono-fluoroethyl ketones (mFEKs) via solution-phase techniques in order to allow isolation of other C-terminal halogenated peptide-based warheads, namely trifluoroethyl ketones (tFEKS), which have not been reported in the literature to date, but may offer potential as serine protease inhibitors in a similar manner to peptidyl trifluoromethyl ketones (tFMKs), and mono-chloromethyl ketones (mCMKs) which are known to inhibit serine proteases. It was thought that this could be achieved through the construction of a *β*-ketoester followed by attempted electrophilic trifluoromethylation or chlorination and subsequent decarboxylation. A selection of conditions was trialled using Umemoto's reagent as an electrophilic source of CF_3 in order to trifluoromethylate methyl acetoacetate; however, all attempts failed to

produce convincing evidence for successful product formation. Moving forwards, the use of CF_3I in the form of a Ritter trifluoroiodomethane-DMSO adduct, as described in the literature,[28] could instead be piloted. Selective installation of a chlorine atom to a Boc-protected *β*-ketoester derived from Boc-Val-OH was successfully achieved according to conditions described by Togni and co-workers[31] using *N*-chlorosuccinimide (NCS) in the presence of $CpTiCl_3$. Concomitant Boc-removal, *tert*-butyl ester deprotection and decarboxylation generated a CMK building block (**374**) which could then be coupled in-solution to a peptide sequence, allowing access to a biologically relevant peptidyl CMK (**323**) known to act as an inhibitor of HLE, although some epimerisation did appear to have occurred. Furthermore, a mono-chlorinated Fmoc-protected *β*-ketoester analogue (**377**) was also developed, derived from Fmoc-Val-OH, for application in SPPS. Whilst attempted resin loading was not possible due to premature decarboxylation to the CMK during *tert*-butyl ester removal, the resulting Fmoc-protected CMK substrate (**382**) may prove useful for solution-phase peptide coupling after Fmoc-removal. Additionally, the Fmoc-protected mono-chlorinated *β*-ketoester (**377**) may also be beneficial after Fmoc removal as a masked CMK for solution-phase coupling, especially if the sidechain of the residue to be installed in the P_1 position of the peptidyl CMK possesses an acid-sensitive sidechain protecting group which needs to remain intact until the end of the synthesis. After peptide coupling, a final global deprotection and decarboxylation step would then readily generate the desired peptidyl CMK.

In the future, it is believed that the methodology described in this chapter for accessing peptidyl chloromethyl ketones could be further optimised to reduce racemisation through the utilisation of milder coupling agents such as EDC or DCC in conjunction with HOBt or HOAt. Alternatively, a mixed anhydride approach involving isobutyl chloroformate (IBCF) may also prove effective. Furthermore, it is believed that adaptation of the reported conditions could also enable solution-phase access to other C-terminally modified peptide-based warheads, such as biologically relevant peptidyl difluoromethyl ketones (dFMKs), known to inhibit serine protease enzyme α-

chymotrypsin.[33] Finally, alternative milder conditions could be trialled in order to allow careful *tert*-butyl ester deprotection to the corresponding mono-chlorinated Fmoc-protected *β*-ketoacid for the purpose of attempting to load to a solid support for SPPS.

5.5 References for Chapter 5

1. Citarella, A. & Micale, N. Peptidyl Fluoromethyl Ketones and Their Applications in Medicinal Chemistry. *Molecules* **25**, 4031 (2020).

2. Tsuda, Y., Okada, Y., Nagamatsu, Y. & Okamoto, U. Synthesis of Peptide Chloromethyl Ketones and Examination of Their Inhibitory Effects on Human Spleen Fibrinolytic Proteinase (SFP) and Human Leukocyte Elastase (LE). *Chem. Pharm. Bull.* **35**, 3576–3584 (1987).

3. Veale, C. A. *et al.* Orally Active Trifluoromethyl Ketone Inhibitors of Human Leukocyte Elastase. *J. Med. Chem.* **40**, 3173–3181 (1997).

4. Rondeau, J.-M. & Schreuder, H. Protein Crystallography And Drug Discovery. in *The Practice of Medicinal Chemistry* vol. 2 417–443 (Elsevier, 2003).

5. Kolb, M., Neises, B. & Gerhart, F. Synthesis of fluorinated α-amino ketones, III. Preparation of fluorinated ketone analogues of phenylalanine, lysine, and p-(Guanidino)phenylalanine. *Liebigs Ann. Chem.* **1990**, 1–6 (1990).

6. Kolb, M., Barth, J. & Neises, B. Synthesis of fluorinated α-amino ketones part I: α-benzamidoalkyl mono- di- and trifluoromethyl ketones. *Tetrahedron Lett.* **27**, 1579–1582 (1986).

7. Peet, N. P. *et al.* Synthesis of Peptidyl Fluoromethyl Ketones and Peptidyl a-Keto Esters as Inhibitors of Porcine Pancreatic Elastase, Human Neutrophil Elastase, and Rat and Human Neutrophil Cathepsin G. *J. Med. Chem.* **33**, 394–407 (1990).

8. Imperiali, B. & Abeles, R. H. A versatile synthesis of peptidyl fluoromethyl ketones. *Tetrahedron Lett.* **27**, 135–138 (1986).

9. Patel, D. v., Rielly-Gauvin, K. & Ryono, D. E. Peptidic trifluoromethyl alcohols and ketones a general synthesis and application as renin inhibitors. *Tetrahedron Lett.* **29**, 4665–4668 (1988).

10. Derstine, C. W., Smith, D. N. & Katzenellenbogen, J. A. Trifluoromethyl-Substituted Imidazolines: Novel Precursors of Trifluoromethyl Ketones Amenable to Peptide Synthesis. *J. Am. Chem. Soc.* **118**, 8485–8486 (1996).

11. Skiles, J. W. *et al.* Inhibition of human leukocyte elastase (HLE) by N-substituted peptidyl trifluoromethyl ketones. *J. Med. Chem.* **35**, 641–662 (1992).

12. Krishnamurti, R., Bellew, D. R. & Prakash, G. K. S. Preparation of trifluoromethyl and other perfluoroalkyl compounds with (perfluoroalkyl)trimethylsilanes. *J. Org. Chem.* **56**, 984–989 (1991).

13. Edwards, P. D. A method for the stereoselective synthesis of peptidyl trifluoromethyl ketones. *Tetrahedron Lett.* **33**, 4279–4282 (1992).

14. Amour, A. *et al.* Stereoselective Synthesis of Peptidyl Trifluoromethyl Alcohols and Ketones: Inhibitory Potency Against Human Leucocyte Elastase, Cathepsin G, Porcine Pancreatic Elastase and HIV-1 Protease. *J. Pharm. Pharmacol.* **50**, 593–600 (2011).

15. Bégué, J.-P., Bonnet-Delpon, D., Fischer-Durand, N., Amour, A. & Reboud-Ravaux, M. Stereoselective synthesis and inhibitor properties towards human leucocyte elastase of chiral β-peptidyl trifluoromethyl alcohols. *Tetrahedron Asymmetry* **5**, 1099–1110 (1994).

16. Benayoud, F., Bégué, J.-P., Bonnet-Delpon, D., Fischer-Durand, N. & Sdassi, H. A New and Efficient Synthesis of α-Bromoalkyl Perfluoroalkyl Ketones via Opening of Epoxides. *Synthesis (Stuttg)* **1993**, 1083–1085 (1993).

17. Walter, M. W., Adlington, R. M., Baldwin, J. E., Chuhan, J. & Schofield, C. J. Reaction of ruppert's reagent (TMS-CF3) with Oxazolidinones: Synthesis of protected α-amino trifluoromethylketones. *Tetrahedron Lett.* **36**, 7761–7764 (1995).

18. Walter, M. W., Adlington, R. M., Baldwin, J. E. & Schofield, C. J. Synthesis of metallo-β-lactamase inhibitors. *Tetrahedron* **53**, 7275–7290 (1997).

19. Poupart, M.-A., Fazal, G., Goulet, S. & Mar, L. T. Solid-Phase Synthesis of Peptidyl Trifluoromethyl Ketones. *J. Org. Chem.* **64**, 1356–1361 (1999).

20. Moreno-Yruela, C. & Olsen, C. Synthesis of Trifluoromethyl Ketone Containing Amino Acid Building Blocks for the Preparation of Peptide-Based Histone Deacetylase (HDAC) Inhibitors. *Synthesis (Stuttg)* **50**, 4037–4046 (2018).

21. Umemoto, T. & Ishihara, S. Power-variable trifluoromethylating agents, (trifluoromethyl)dibenzothio- and -selenophenium salt system. *Tetrahedron Lett.* **31**, 3579–3582 (1990).

22. Umemoto, T. *et al.* Powerful, Thermally Stable, One-Pot-Preparable, and Recyclable Electrophilic Trifluoromethylating Agents: 2,8-Difluoro- and 2,3,7,8-Tetrafluoro-S-(trifluoromethyl)dibenzothiophenium Salts. *J. Org. Chem.* **82**, 7708–7719 (2017).

23. Ma, J.-A. & Cahard, D. Copper(II) triflate-bis(oxazoline)-catalysed enantioselective electrophilic fluorination of β-ketoesters. *Tetrahedron Asymmetry* **15**, 1007–1011 (2004).

24. Umemoto, T. & Ishihara, S. Power-Variable Electrophilic Trifluoromethylating Agents. S-, Se-, and Te-(Trifluoromethyl)dibenzothio-, -seleno-, and -tellurophenium Salt System. *J. Am. Chem. Soc.* **115**, 2156–2164 (1993).

25. Deng, Q. H., Wadepohl, H. & Gade, L. H. Highly enantioselective copper-catalyzed electrophilic trifluoromethylation of β-ketoesters. *J. Am. Chem.Soc.* **134**, 10769–10772 (2012).

26. Noritake, S. *et al.* Enantioselective electrophilic trifluoromethylation of β-keto esters with Umemoto reagents induced by chiral nonracemic guanidines. *Org. Biomol. Chem.* **7**, 3599–3604 (2009).

27. Ma, J. A. & Cahard, D. Mild Electrophilic Trifluoromethylation of β-Ketoesters and Silyl Enol Ethers with 5-Trifluoro Methyldibenzothiophenium Tetrafluoroborate. *J. Org. Chem.* **68**, 8726–8729 (2003).

28. Ohtsuka, Y., Uraguchi, D., Yamamoto, K., Tokuhisa, K. & Yamakawa, T. Syntheses of 2-(trifluoromethyl)-1,3-dicarbonyl compounds through direct trifluoromethylation with CF3I and their application to fluorinated pyrazoles syntheses. *Tetrahedron* **68**, 2636–2649 (2012).

29. Honda, Y., Katayama, S., Kojima, M., Suzuki, T. & Izawa, K. Synthesis of Optically Active α-Aminoalkyl α'-Halomethyl Ketone: A Cross-Claisen Condensation Approach. *Org. Lett.* **4**, 447–449 (2002).

30. Honda, Y. *et al.* New approaches to the industrial synthesis of HIV protease inhibitors. *Org. Biomol. Chem.* **2**, 2061 (2004).

31. Frantz, R., Hintermann, L., Perseghini, M., Broggini, D. & Togni, A. Titanium-Catalyzed Stereoselective Geminal Heterodihalogenation of β-Ketoesters. *Org. Lett.* **5**, 1709–1712 (2003).

32. Kutty, S. K., Lutz, J. A., Felder, S., Hahn, P. & Taylor, C. M. Thioether macrocycles of the microbisporicins via reductive desulfurization. *Tetrahedron* **74**, 4247–4258 (2018).

33. Imperiali, B. & Abeles, R. H. Inhibition of Serine Proteases by Peptidyl Fluoromethyl Ketones. *Biochem.* **25**, 3760–3767 (1986).

6. Conclusions and Future Work

This thesis describes the development of a novel approach for accessing a selection of biologically relevant peptidyl mono-fluoromethyl ketones (mFMKs) known to act as caspase inhibitors. A number of approaches were trialled and eventually, a solution-phase approach was deemed the most effective (**Scheme 6.1c**).

In order to reach these desired targets, it was initially envisioned that this could be achieved through adaptation of methodology described by Sandford and co-workers[1] for the electrophilic fluorination of tri-carbonyl systems and subsequent functionalisation to mFMKs (**129**). Whilst their work centred around substrates possessing aromatic moieties in the absence of an amine functionality, the latter meaning incorporation into a peptide sequence was not possible, it was hypothesised that adaptation of this methodology could enable access to substrates derived from a Boc-protected amino acid of choice, capable of being used for peptide coupling in-solution after Boc-removal (**Scheme 6.1a**). However, whilst it was found to be possible for fluorination of a tri-carbonyl system derived from phenylacetyl chloride (**180**), the Boc-Ala-OH derived analogue (**190**) proved much less stable and more difficult to handle, likely due to unwanted degradation in the presence of moisture.

Thus, an alternative approach (**Scheme 6.1b**) offering improved stability was sought, inspired by Togni and co-workers'[2] ability to selectively mono-fluorinate *β*-ketoesters using Selectfluor in the presence of a catalytic amount of titanium catalyst. After construction of the desired *β*-ketoester (**241**) consisting of an Fmoc-protected amine and either a methyl or *tert*-butyl ester protected acid functionality, redeployment of these conditions enabled installation of a fluorine atom in the α-position (**384** and **237**). Given the ability for *β*-ketoesters to be readily transformed to *β*-ketoacids, which could subsequently undergo rapid decarboxylation, as described by Budnjo *et al*,[3] the fluorinated *β*-ketoesters (**384** and **237**) could essentially act as masked mFMKs (**129**). Thus, the hope

was that careful liberation of the ester to the free carboxylic acid functionality, whilst avoiding premature decarboxylation, would afford a *β*-ketoacid with a handle for resin attachment (**385**). Subsequent peptide growth followed by resin cleavage, deprotection and decarboxylation would allow access to the desired peptidyl mFMK (**129**, **Scheme 6.1b**).

However, because of challenges encountered during attempted methyl ester saponification of Fmoc-protected *β*-ketoester **206**, partly due to the presence of a second labile proton at the α-carbon position capable of being deprotonated in base, along with the ability for Fmoc removal when an excess is used, attention instead turned towards the use of the *tert*-butyl ester (**237**) which is orthogonal to Fmoc (**Scheme 6.1b**). Prudent removal of the ester group with limited decarboxylation was achieved using 30% TFA in DCM for 2.5 hours. However, subsequent attempts to load the resulting *β*-ketoacid on to a solid-support (resin) resulted in disappointment, despite employing a range of different resins and loading conditions. It is believed that the challenges associated with loading to the resin occurred as a result of the reduced nucleophilicity of the carboxylate, which arises due to the presence of the highly electronegative fluorine atom. Furthermore, evidence was found for conversion to the FMK (**269**) during the attempted loading step, suggesting this transformation is favoured over resin-loading. With the intention of instead loading via a sidechain acid functionality of a *tert*-butyl ester protected *β*-ketoester derived from Fmoc-Asp(OAll)-OH (**253**), standard conditions for allyl ester deprotection were employed; however, an unexpected shift in fluorine peaks was observed by ^{19}F NMR spectroscopy. Moving forwards, alternative conditions and/or protecting groups could still be trialled in order to establish suitable conditions for sidechain deprotection and attempted resin attachment via this position.

In light of the problems surrounding attempted SPPS of peptidyl mFMKs (**129**), this approach was shelved, and attention turned towards adapting the protecting group strategy to be compatible with a solution-phase approach instead (**Scheme 6.1c**). Thus,

β-ketoesters possessing Boc-protected amines and *tert*-butyl ester protected acids (**277**) were synthesised from the corresponding Boc-protected amino acids in a similar manner to that described by Preciado and Williams.[4] Subsequent mono-fluorination and deprotection were carried out, either with 1 M HCl to enable selective Boc-deprotection to **386**,[5] or with 50% TFA in DCM at 40 °C for 2 hours to bring about complete Boc and *tert*-butyl removal as well as decarboxylation to the FMK (**387**). The resulting building blocks could then be coupled in-solution to peptide sequences of choice and finally deprotected (and decarboxylated if not done so already), allowing generation of the target peptidyl mFMKs (**129**) in relatively few steps (**Scheme 6.1c**). Admittedly, some transformations in the protocol did prove rather low yielding, with the presence of inseparable impurity peaks found in some cases. It was also concluded that coupling the Boc-deprotected fluorinated *β*-ketoesters (**386**) as opposed to the FMK building block (**387**) to peptides in solution appeared to give cleaner products, although epimerisation was observed (**Figure 4.19** and **Figure 4.20**). Nonetheless, it is believed that stereoselectivity could be improved by utilising a bulkier base such as 2,4,6-collidine when coupling the *β*-ketoesters, conveniently allowing isolation of peptidyl FMKs in relatively few steps, whilst avoiding toxic diazomethane.

In addition to accessing peptidyl mFMKs (**129**) via **Scheme 6.2a**, whilst isolation of trifluoroethyl ketones (tFEKs) by a similar approach proved unsuccessful, perhaps due to the added steric bulk, the developed solution-phase protocol to peptidyl mFMKs involving the coupling of the FMK building block to the peptide (**Scheme 6.2a**) was modified and successfully applied to the synthesis of a peptidyl mono-chloromethyl ketone (**130**, **Scheme 6.2b**). Furthermore, it is believed that there is potential scope for further expansion to reach other peptide-based C-terminal modified warheads of interest such as di-fluoromethyl ketones (dFMKs) (**18**, **Scheme 6.2c**) and mono-bromomethyl ketones (mBMKs) (**397**, **Scheme 6.2d**).

In summary, the goal of accessing peptidyl mFMKs (**129**) was successfully achieved using solution-phase techniques in only 4 or 5 steps (**Scheme 6.2a**), with scope for further optimisation of yields and purity levels. Thus, it is believed that this methodology could contribute towards facilitation of further research into peptidyl mFMKs as promising therapeutic agents and diagnostic tools. Furthermore, it represents a general approach applicable to a wide range of biologically relevant peptidyl mFMK substrates (**129**), which can also be adapted, through utilisation of an electrophilic chlorinating agent,[2] to enable isolation of peptidyl mono-chloromethyl ketones (mCMKs) (**130**, **Scheme 6.2b**) and to potentially bring about other desirable C-terminal modifications (**Scheme 6.2c** and **d**).

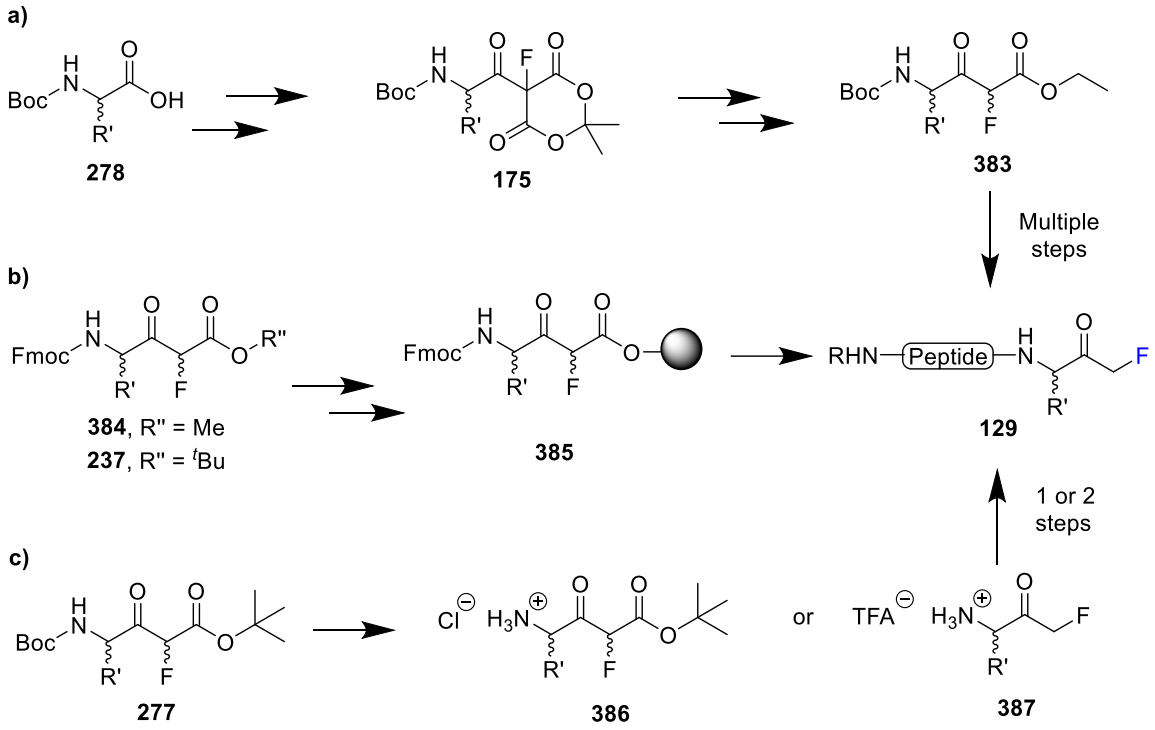

Scheme 6.1 – Summary of work pursued in **Chapters 2** (**a**), **3** (**b**) and **4** (**c**) for accessing peptidyl mFMKs (**129**) via solid (**b**) or solution-phase (**a** and **c**) methods. Although some pathways did not provide the desired outcome and were therefore abandoned, route (**c**) was found to be the most successful approach. R' = amino acid sidechain of choice.

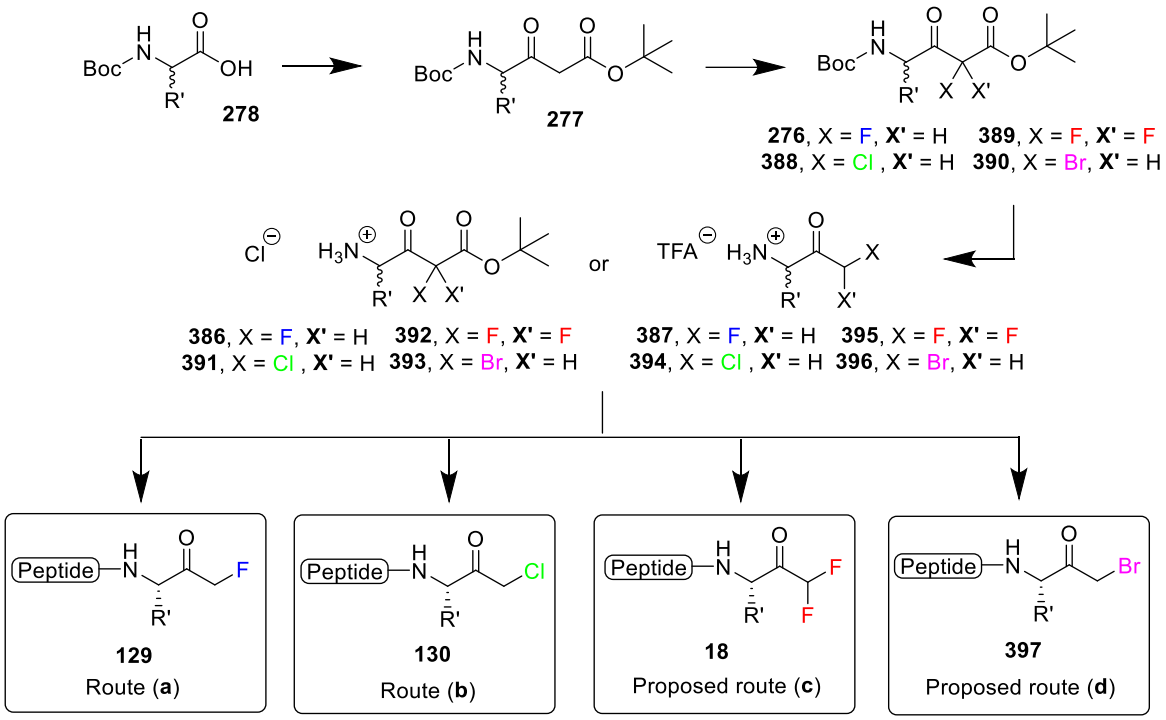

Scheme 6.2 – Summary of developed general solution-phase pathway to peptidyl mFMKs (**129**, route **a**) and peptidyl mCMKs (**130**, route **b**) along with proposed routes to peptidyl dFMKs (**18**, route **c**) and peptidyl mBMKs (**397**, route **d**). R' = amino acid sidechain of choice.

6.1 References for Chapter 6

1. Harsanyi, A. *et al.* α-Fluorotricarbonyl Derivatives as Versatile Fluorinated Building Blocks: Synthesis of Fluoroacetophenone, Fluoroketo Ester and Fluoropyran-4-one Derivatives. *Eur. J. Chem.* **2020**, 3872–3878 (2020).

2. Frantz, R., Hintermann, L., Perseghini, M., Broggini, D. & Togni, A. Titanium-Catalyzed Stereoselective Geminal Heterodihalogenation of β-Ketoesters. *Org. Lett.* **5**, 1709–1712 (2003).

3. Budnjo, A. *et al.* Reversible Ketomethylene-Based Inhibitors of Human Neutrophil Proteinase 3. *J. Med. Chem.* **57**, 9396–9408 (2014).

4. Preciado, A. & Williams, P. G. A Simple Microscale Method for Determining the Relative Stereochemistry of Statine Units. *J. Org. Chem.* **73**, 9228–9234 (2008).

5. Gibson, F. S., Bergmeier, S. C. & Rapoport, H. Selective Removal of an N-BOC Protecting Group in the Presence of a tert-Butyl Ester and Other Acid-Sensitive Groups. *J. Org. Chem.* **59**, 3216–3218 (1994).

7. Experimental

7.1 General

All starting materials and reagents were bought from commercial sources and used as received. All reactions, apart from where noted, were carried out in air using non-dried solvents or reagents. All flash column chromatography was carried out using silica purchased from Sigma Aldrich or Fluorochem using the solvent system noted. Solvent removal was accomplished under reduced pressure using a Büchi Rotavapor R11 or R100. Aqueous solutions were lyophilised using either a Christ Alpha 1-2 LD Plus freeze-drier or a Thermo Scientific ModulyoD system. ^{1}H NMR spectra were recorded at 400 MHz, 600 MHz or 700 MHz using Bruker Avance III, Varian VNMRS-600 or Varian VNMRS-700 spectrometers respectively. ^{13}C NMR spectra were recorded at 101, 151 or 176 MHz using Bruker Avance III, Varian VNMRS-600 or Varian VNMRS-700 spectrometers respectively. All coupling constants are reported in Hertz (Hz). In cases where it was required, 2D NMR techniques were used to confirm compound identity. Chemical shifts are reported in parts per million (δ ppm) and are referenced to residual solvent peaks; $CHCl_3$ (^{1}H 7.26 ppm, ^{13}C 77.0 ppm), CH_2Cl_2 (^{1}H 5.32 ppm, ^{13}C 53.8 ppm), DMSO (^{1}H 2.50 ppm, ^{13}C 39.52 ppm), H_2O (^{1}H 4.79 ppm), CH_3OH (^{1}H 3.31 ppm, ^{13}C 49.0 ppm) and CH_3CN (^{1}H 1.96 ppm, ^{13}C 118.3 ppm). Multiplicities are abbreviated as follows: s = singlet, d =doublet, dd = doublet of doublets, ddd = doublet of doublet of doublets, dt = doublet of triplets, m = multiplet, t = triplet, q = quartet, quint = quintet, br s = broad singlet, br m = broad multiplet. Where deemed necessary, baseline smoothing/correction was applied to NMR and mass spectra using MestReNova.

7.1.1 Mass Spectrometry at Durham University

Low resolution mass spectra were collected using either ESI-LCMS or GCMS. ESI-LCMS spectra were collected using a Waters SQD mass spectrometer with an Acquity UPLC BEH C18 1.7 µm (2.1 mm x 50 mm) column using a flow rate of 0.6 mL min^{-1} and

a linear gradient of 5–95 % of solvent B in solvent A over 3.8 min (A = 0.1 % formic acid in H_2O, B = acetonitrile).

GCMS experiments were carried out on a Shimadzu QP2010-Ultra with a Rxi-5Sil MS (0.15 µm x 10 m x 0.15 mm) column. Helium was employed as the carrier gas (0.41 mL/min). EI was carried out at 70 ev and the working mass range is 35 – 650 u for all GCMS experiments.

High-resolution mass spectra were recorded using an Acquity ultra-performance liquid chromatography system (Waters Ltd, UK) coupled to a QToF Premier mass spectrometer (Waters, UK) via an electrospray probe (+ve or -ve ion mode). Samples were injected (3 µL) on to an Acquity UPLC BEH C18 column (1.7 µm, 2.1 mm x 100 mm, Waters, UK) at a flow rate of 0.6 mL min^{-1} and a linear gradient of 0–99 % of solvent B in solvent A over 5 min (A = 0.1 % formic acid in H_2O, B = acetonitrile).

7.1.2 Mass Spectrometry at Cambridge Research Biochemicals (CRB)

LCMS data recorded at Cambridge Research Biochemicals (CRB) was collected using either Micromass LCT ToF with Waters Alliance 2695 or Agilent 6230 ToF LC/MS with Agilent 1260 Infinity II.

7.2 Peptide Synthesis - General

All reagents used in this project were purchased from commercial sources and used without further purification unless stated otherwise. HPLC grade DMF and MeCN were purchased from Fisher Scientific and amino acid derivatives were purchased from Fluorochem, Sigma Aldrich, CEM, Novabiochem (Merck) or AGTC. The general procedure for Fmoc SPPS synthesis is detailed in the following sections. All peptide coupling reactions were carried out in DMF (unless stated otherwise) using either doubly fritted polypropylene reaction vessels or larger fritted syringes for larger scale synthesis. The amino acids were protected in the following manner unless stated otherwise: Fmoc-

Tyr(O^{t}Bu)-OH, Fmoc-Asp(OMe)-OH or Cbz-Asp(OMe)-OH, Cbz-Val-OH or Fmoc-Val-OH, Fmoc-Glu(OMe)-OH, Cbz-Ile-OH, Cbz-Phe-OH, Fmoc-Ala-OH, Fmoc-Leu-OH. The following centrifuges were used: an Eppendorf centrifuge 5415D (for 1.5 mL tubes), a Fisherbrand GT 1 (for 15 mL or 50 mL tubes) or a Baird and Tatlock Mark IV refrigerated centrifuge. A Barnstead STEM Reacto-Station RS6000 shaker or Thermo Denley Spiramix tube roller mixer was used to agitate solutions containing resin where indicated.

Abbreviations for common reagents and protecting groups are as follows: tertbutoxycarbonyl (Boc); 9-fluorenylmethoxylcarbonyl (Fmoc); triphenylmethyl or trityl (Trt); trifluoroacetic acid (TFA); triisopropylsilyl (TIPS); *N,N*-dimethylformamide (DMF); *N,N*-diisopropylcarbodiimide (DIC); dimethylsulphoxide (DMSO); dichloromethane (DCM).

7.3 Manual Solid-Phase Peptide Synthesis (SPPS)

7.3.1 Resin Loading Procedures

7.3.1.1 2-Chlorotrityl Chloride Resin

2-Chlorotrityl chloride was swollen in DCM (10 minutes at room temperature). The resin was washed with DCM (x3) and treated with the Fmoc-protected amino acid of choice (2.5-5.0 equivalents with respect to the resin) and DIPEA (10 equivalents with respect to the resin) in the minimum amount of DCM (with a small amount of DMF added if necessary for complete dissolution) for 30 minutes at room temperature on a shaker at 400 rpm. The resin was then washed with DCM (x5) and often capped twice (2 x 10 minutes) with 17:2:1 solutions of DCM:MeOH:DIPEA on the shaker, or alternatively treated twice (2 x 10 minutes) with 2:1 solutions of DCM:MeOH on the shaker. Peptide synthesis then proceeded as detailed in **Section 7.3.2** or **7.3.3**.

7.3.2 Peptide Synthesis using HATU

Resin was first swollen through agitation at room temperature in DCM or DMF for 10-30 minutes. Peptide synthesis was then either carried out directly on to commercially available pre-loaded resin, on to non-pre-loaded resin which had undergone an amino acid loading procedure according to **Section 7.3.1**, or on to a linear peptide sequence already attached to the resin. Single couplings were carried out through treatment of the resin with 5 equivalents of amino acid (with respect to the resin), 4.5 equivalents of HATU (with respect to the resin) and 10 equivalents of DIPEA (with respect to the resin) in the minimum amount of DMF under agitation for 1.5 hours at room temperature. The reaction mixture was then drained, and the resin washed with 5 portions of DMF. If required, double couplings were performed through repeating the described addition of the amino acid/HATU/DIPEA/DMF solution. Removal of the Fmoc group was then carried out using a solution of 20% piperidine in DMF for 5 minutes under agitation, before being drained, re-added and agitated for a further 10 minutes. The piperidine solution was then drained, and the resin rinsed using 5 portions of DMF. Further amino acid couplings and Fmoc-deprotection steps were made as necessary, along with any additionally required modifications. The peptide was then cleaved from the resin as described in **Section 7.3.1**, analysed by analytical HPLC (**Section 7.3.8.2**) and LCMS (**Section 7.1.1** or **7.1.2**), and subsequently purified by reverse-phase HPLC where necessary (**Section 7.3.8.1**). Peptides were generally stored in the fridge or freezer.

7.3.3 Peptide Synthesis using PyBOP

Resin was first swollen through agitation at room temperature in DCM or DMF for 10-30 minutes. Peptide synthesis was then either carried out directly on to commercially available pre-loaded resin, on to non-pre-loaded resin which had undergone an amino acid loading procedure according to **Section 7.3.1**, or on to a linear peptide sequence already attached to the resin. Single couplings were carried out through treatment of the

resin with 5.0 equivalents of amino acid (with respect to the resin), 5.0 equivalents of PyBOP (with respect to the resin), 5.0 equivalents of DIPEA (with respect to the resin) in the minimum amount of DMF under agitation for 1.5 hours at room temperature. The reaction mixture was then drained, and the resin washed with 5 portions of DMF. If required, double couplings were performed through repeating the described addition of the amino acid/PyBOP/DIPEA/DMF solution. Removal of the Fmoc group was then carried out using a solution of 20% piperidine in DMF for 5 minutes under agitation, before being drained, re-added and agitated for a further 10 minutes. The piperidine solution was then drained, and the resin rinsed using 5 portions of DMF. Further amino acid couplings and Fmoc-deprotection steps were made as necessary, along with any additionally required modifications. The peptide was then cleaved from the resin as described in **Section 7.3.7**, analysed by analytical HPLC (**Section 7.3.8.4** or **7.3.8.5**) and LCMS (**Section 7.1**), and subsequently purified by reverse-phase HPLC where necessary (**Section 7.3.8.1**, **7.3.8.2** or **7.3.8.3**). Peptides were generally stored in the fridge or freezer.

7.3.4 On-Resin Cbz Protection

The swollen resin, consisting of a free amine at the *N*-terminus of the peptide sequence, was treated with a solution of 5.0 equivalents of benzyl chloroformate (with respect to the resin) and 5.0 equivalents of DIPEA (with respect to the resin) in the minimum amount of DCM. The mixture was agitated at room temperature for 1 hour before being drained and washed with DCM x 5.

7.3.5 On-Resin acetylation

The swollen resin, consisting of a free amine at the *N*-terminus of the peptide sequence, was treated with a solution of 10.0 equivalents of DIPEA (with respect to the resin) and 5.0 equivalents of acetyl chloride (with respect to the resin) in the minimum amount of DCM. The mixture was agitated at room temperature for 30 minutes before being drained and washed with DCM x 5.

7.3.6 On-Resin Primary Amine TNBS Test

In some cases, during peptide synthesis, a primary amine test was performed on resin in order to confirm successful amino acid coupling, Cbz protection or Fmoc removal. To do this, 5 drops of 10% DIPEA in DMF was added to a small sample of resin, followed by 3 drops of 2% picrylsulfonic acid in DMF and left for 15-20 seconds before being diluted with DMF. After shaking, red beads revealed the presence of a primary amine whilst white beads indicated no primary amine was present.

7.3.7 Resin Cleavage

7.3.7.1 TFA Test Cleavage

When necessary, a test cleavage was performed by placing a small amount of resin (which had been shrunk in diethyl ether) in a vial and treating it with 200 µL of the cleavage cocktail (95% TFA, 2.5% deionized water and 2.5% TIPS). After about 15-30 minutes (depending on the resin type and protecting groups present), the beads were allowed to settle on the bottom of the vial and 20-60 µL of the supernatant was diluted with deionised H_2O/MeCN and analysed by LC-MS spectrometry.

7.3.7.2 TFA Full Cleavage

In examples in which complete removal of acid-sensitive sidechain protecting groups was also required, the peptide resin was shrunk in diethyl ether and subsequently treated with a cleavage cocktail consisting of 95% TFA, 2.5% deionized water and 2.5% TIPS (as a scavenger) for 2-6 hours at room temperature with occasional swirling. The resin was eliminated by filtration and the solvent removed from the filtrate under reduced pressure before precipitation using diethyl ether and decanting of the liquid (followed by subsequent ether washes). The resulting solid peptide was dissolved in deionized water/acetonitrile and lyophilized.

7.3.7.3 Mild TFE Cleavage

In examples in which the acid-sensitive sidechain protecting groups were required to be left in place during the resin cleavage step, highly acid-sensitive resin (such as 2-chlorotrityl) was used and treated with 20% 2,2,2-trifluoroethanol (TFE) in DCM. The resulting mixture was agitated at room temperature for 1-3 hours. The resin was eliminated by filtration and the solvent removed from the filtrate under reduced pressure before being dissolved in deionized water/acetonitrile and lyophilized.

7.3.8 Peptide Purification and Analysis by HPLC

7.3.8.1 Preparative High Pressure Liquid Chromatography (Prep HPLC) at Durham University – Supelco/Perkin Elmer System

Samples to be purified were dissolved in a mix of deionised H_2O/MeCN (ratio dependent on solubility), centrifuged or filtered (if necessary) and injected onto a Supelco Analytical Discovery B10 Wide Pore C18-5 column (25 cm x 10 mm, 5 µm) using a semi-preparative Perkin Elmer Series 200 LC pump and 785A UV/Vis detector. A gradient of 0-100% solvent B in solvent A (solvent A = 95% H_2O, 5% MeCN, 0.1% TFA, solvent B = 95% MeCN, 5% H_2O, 0.1% TFA) over 40-60 minutes with a flow rate of 2.0 mL/min was used and absorbance data collected at 220 nm. Fractions were analysed by LCMS (according to **Section 7.1.1** or **7.1.2**) and analytical HPLC (**Section 7.3.8.4** or **7.3.8.5**) and the fractions containing desired product were lyophilised.

7.3.8.2 Preparative High Pressure Liquid Chromatography (Prep HPLC) at Durham University – InterChim PuriFlash System

The sample was purified using an InterChim PuriFlash 450 system equipped with a diode array detector monitor from 220 to 400 nm. Separation occurred on a Waters XBridge or SunFire C18 column (19 x 100 mm, 5 µm) with a gradient elution of 90% A (A = 0.1% formic acid in water) to 95% B (B = MeCN) over a 10-minute period at a flow rate of 17 mL/min. Absorbance data was collected at a wavelength of 220 nm.

7.3.8.3 Preparative High Pressure Liquid Chromatography (Prep HPLC) at Cambridge Research Biochemicals (CRB)

Samples to be purified were injected on to an ACE 10 µm C18-300 Å 250 x 21.2 mm column using a Gilson prep-HPLC system with an eluent consisting of solvent 1 (0.1% TFA in water) and solvent 2 (0.1% TFA in MeCN).

7.3.8.4 Analytical High Pressure Liquid Chromatography (Analytical HPLC) at Durham University

Samples were dissolved in a mix of deionised H_2O/MeCN (ratio dependent on solubility) and 10-150 µl injected onto a Phenomenex Luna C18 LC column (25 cm x 4.6 mm, 5 µm, 100 Å) or an SB Analytical ODS-H optimal column (25 cm x 4.6 mm, 5 µm) using a Perkin Elmer Series 200 Autosampler and Perkin Elmer Series 200 LC Pump. Detection was achieved using a Series 200 UV/Vis detector. A gradient of 0-100% solvent B in solvent A (solvent A = 95% H_2O, 5% MeCN, 0.05% TFA, solvent B = 95% MeCN, 5% H_2O, 0.03% TFA) over 40 minutes with a flow rate of 1.0 mL/min was used. Absorbance data was collected at 220 nm and processed using TotalChem software.

7.3.8.5 Analytical High Pressure Liquid Chromatography (Analytical HPLC) at Cambridge Research Biochemicals (CRB)

Samples were injected on to an ACE 3 µm C18-300 Å 150 x 2.1 mm column using an Agilent 1100 system with VWD. A gradient of 2-100% solvent 2 in solvent 1 (solvent 1 = 0.1% TFA in water, solvent 2 = 0.1% TFA in MeCN) over 13 minutes with a flow rate of 1.0 mL/min was used. Absorbance data was collected at 230 nm.

7.4 Experimental for Chapter 2

Synthesis of 181[1]

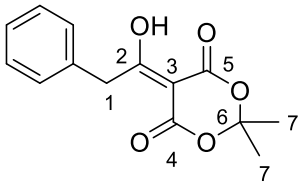

181

To a stirred solution of Meldrum's acid (**173**) (1.40 g, 9.71 mmol) and DMAP (2.37 g, 19.4 mmol) in MeCN was added phenylacetyl chloride (1.28 mL, 9.71 mmol) dropwise over a period of 15 minutes at 0 °C. Reaction mixture was allowed to return to room temperature before being left to stir for 24 hours. 1 M HCl (20 ml) was added, and the mixture stirred for a further 5 minutes until a clear solution was observed before being concentrated to about 15 mL *in vacuo*. The precipitated product was filtered and washed with water before being re-dissolved in DCM (30 ml). Water was added (10 ml) and the product extracted into the DCM. The organic layer was dried with anhydrous $MgSO_4$, filtered and concentrated *in vacuo* to yield the pure product as a pale-yellow solid (2.12 g, 8.08 mmol, 83%). ^{1}H NMR ($CDCl_3$, 400 MHz): δ (ppm) 15.32 (1H, br s, O-*H*), 7.33 (5H, m, Ph-*H*), 4.43 (2H, s, C**1**-*H*), 1.72 (6H, s, C**7**-*H*). ^{13}C NMR ($CDCl_3$, 101 MHz): δ (ppm) 194.8 (C**2**), 170.7 & 160.5 (C**4** & C**5**), 134.2 (C-**Ph**), 129.8 (C-**Ph**), 128.9 (C-**Ph**), 127.7 (C-**Ph**), 105.1 (C**6**), 91.6 (C**3**), 41.0 (C**1**), 27.0 (C**7**). HRMS (ESI) *m/z* calculated for $[M+H]^+$ $C_{14}H_{15}O_5^+$ 263.0919, found 263.0934. Characterisation data was found to be consistent with the literature.[1]

Synthesis of 179

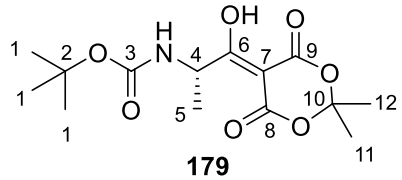

179

To a solution of L-Boc-alanine (**177**) (0.48g, 2.54 mmol), Meldrum's acid (**173**) (0.40 g, 2.79 mmol) and DMAP (0.46 g, 3.81 mmol) in DCM (15 ml) was added EDC.HCl (0.58g, 3.04 mmol) at 0 °C. Solution was allowed to return to room temperature and left to stir for 3 hours before being cooled to 0 °C, diluted with cold ethyl acetate (50 ml) and quenched with cold brine (25 ml). The organic layer was then washed with cold 5% $KHSO_4$ (3 x 75 ml) and cold brine (75 ml), dried with anhydrous $MgSO_4$ and concentrated *in vacuo* to afford the product as a yellow oil (0.64 g, 2.03 mmol, 80%). ^{1}H NMR ($CDCl_3$, 400 MHz): δ (ppm) 15.54 (1H, br s, O-*H*), 5.54 (1H, m, C**4**-*H*), 5.04 (1H, br s, N-*H*), 1.72-1.77 (6H, 2 s, C**11**-*H* & C**12**-*H*), 1.43 (12 H, m, C**1**-*H* & C**5**-*H*). ^{13}C NMR ($CDCl_3$, 101 MHz): δ (ppm) 196.8 (C**6**), 170.9 & 159.6 (C**8** & C**9**), 155.0 (C**3**), 105.6 (C**10**), 90.7 (C**7**), 80.2 (C**2**), 49.2 (C**4**), 28.3 (C**1**), 27.0 & 26.8 (C**11** & C**12**), 18.5 (C**5**). HRMS (ESI) *m/z* calculated for $[M+H]^+$ $C_{14}H_{22}NO_7^+$ 316.1396, found 316.1382.

Synthesis of 185

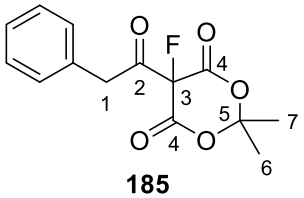

185

Compound **181** (1.71 g, 6.52 mmol) was dissolved in MeCN (20 ml) along with Selectfluor™ (2.38 g, 6.72 mmol) and left to stir at room temperature for 24 hours, after which the reaction mixture was evaporated to dryness under vacuum. The resulting residue was suspended in EtOAc, filtered with washings of EtOAc and the filtrate concentrated *in vacuo*. The residue was dissolved in DCM (5 ml) and hexane was added (15 ml). The solution underwent gentle heating at atmospheric pressure until solids started to appear, at which point the product was allowed to further precipitate in the refrigerator overnight. The pure product **185** was isolated as a pale yellow solid via filtration and subsequent drying *in vacuo* (1.01 g, 3.60 mmol, 55%). ^{1}H NMR ($CDCl_3$, 400 MHz): δ (ppm) 7.34 (3H, m, Ph), 7.17 (2H, m, Ph), 4.22 (2H, d, $^{4}J_{HF}$ = 3.4, C**1**-*H*), 1.86 & 1.82 (6H, 2 s, C**6**-*H* & C**7**-*H*).^{19}F NMR ($CDCl_3$, 376 MHz): δ (ppm) -165.89 (dt, $^{4}J_{FH}$ = 3.4, C**3**-*F*). LCMS (ESI) *m/z* calculated for $[M-C_5H_4O_4-H]^-$ $C_9H_8FO^-$ 151.1, found 151.2.

Synthesis of 193[2]

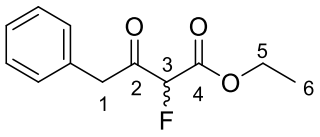

193

Compound **185** (0.78g, 2.78 mmol) was dissolved in excess ethanol (20 ml) and the solution cooled to 0 °C. Diethylamine (0.29 mL, 2.78 mmol) was added and the solution left to stir at 0 °C for 24 hours. The solvent was removed *in vacuo* and the resulting residue dissolved in DCM (60 ml). The organic layer was washed with sat. $NaHCO_3$ (20 ml) and brine (20 ml), dried with anhydrous $MgSO_4$ and concentrated *in vacuo*. The crude product was purified by silica gel column chromatography (hexane : ethyl acetate, 1 : 1) to afford the pure product **193** as a pale-yellow oil (0.10 g, 0.45 mmol, 16%).^{1}H NMR ($CDCl_3$, 400 MHz): δ (ppm) 7.32 (3H, m, Ph), 7.22 (2H, m, Ph), 5.28 (1H, d, $^{2}J_{HF}$ = 49.2, C**3**-*H*), 4.23 (2H, q, $^{3}J_{HH}$ = 7.1, C**5**-*H*), 3.98 (2H, d, $^{4}J_{HF}$ = 3.2, C**1**-*H*), 1.27 (3H, t, $^{3}J_{HH}$ = 7.1, C**6**-*H*). ^{13}C NMR ($CDCl_3$, 101 MHz): δ (ppm) 198.6 (d, $^{2}J_{CF}$ = 23.1, C**2**), 164.1 (d, $^{2}J_{CF}$ = 24.0, C**4**), 131.8 (Ph), 129.9 (Ph), 129.0 (Ph), 127.7 (Ph), 90.9 (d, $^{1}J_{CF}$ = 198.8, C**3**), 62.9 (C**5**), 45.5 (C**1**), 14.1 (C**6**). ^{19}F NMR ($CDCl_3$, 376 MHz): δ (ppm) -194.30 (dt, $^{2}J_{FH}$ = 49.2, $^{4}J_{FH}$ = 3.2, C**3**-F). HRMS (ESI) *m/z* calculated for $[M+H]^+$ $C_{12}H_{14}FO_3^+$ 225.0927, found 225.0926. Characterisation data was found to be consistent with the literature.[2]

7.5 Experimental for Chapter 3

Synthesis of methyl 4-amino-3-hydroxybutyrate hydrochloride (210)[3]

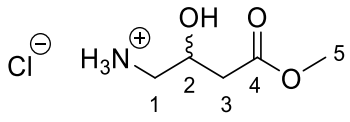

210

To a stirred solution of 4-amino-3-hydroxybutyric acid (0.50 g, 4.20 mmol) in methanol (60 ml) was added $SOCl_2$ (0.31 mL, 4.20 mmol) dropwise at 0˚C. The resulting mixture was allowed to warm to room temperature before being left to stir for 24 h. The mixture was concentrated under reduced pressure to yield **210** as a pale-yellow oil in a quantitative yield (0.71 g, 4.20 mmol, >99%), which was used without further purification. ^{1}H NMR (DMSO-d_6, 400 MHz): δ (ppm) 7.95 (3H, br s, N-*H*$_3$), 5.59 (1H, d, $^3J_{HH}$ = 5.5, O-*H*), 4.09 (1H, m, C**2**-*H*), 3.62 (3H, s, C**5**-*H*), 2.92 (1H, dd, $^2J_{HH}$ = 12.8, $^3J_{HH}$ = 3.4, C**1**-*H*), 2.73 (1H, dd, $^2J_{HH}$ = 12.8, $^3J_{HH}$ = 8.7, C**1**-*H*), 2.59 (1H, dd, $^2J_{HH}$ = 15.5, $^3J_{HH}$ = 4.8, C**3**-*H*), 2.44 (1H, dd, $^2J_{HH}$ = 15.6, $^3J_{HH}$ = 8.0, C**3**-*H*); ^{13}C NMR (DMSO-d_6, 101 MHz): δ (ppm) 171.0 (C**4**), 64.2 (C**2**), 51.5 (C**5**), 43.8 (C**1**), 39.4 (C**3**). HRMS (ESI) *m/z* calculated for $[M+H]^+$ $C_5H_{12}NO_3^+$ 134.0817, found 134.0814. Characterisation data was found to be consistent with the literature.[3]

Synthesis of 208

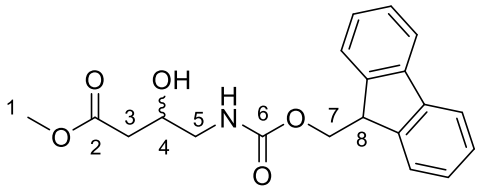

208

Compound **210** (0.70 g, 4.13 mmol) was suspended in 1,4-dioxane (40 ml) and acetone (30 ml). Subsequently, 0.8 M aqueous $NaHCO_3$ was added (18 mL, 14.5 mmol), followed by Fmoc-OSu (1.67 g, 4.96 mmol) added portion-wise over a period of 10 minutes. The reaction mixture was left to stir at room temperature for 4 hours before being extracted with diethyl ether. The organic phase was dried over anhydrous $MgSO_4$, filtered and concentrated *in vacuo*. The obtained residue was purified by silica gel column chromatography (hexane : ethyl acetate, 1 : 1) to afford *β*-hydroxyester **208** as a white solid (1.01 g, 2.85 mmol, 69%). ^{1}H NMR ($CDCl_3$, 400 MHz): δ (ppm) 7.76 (2H, d, $^3J_{HH}$ = 7.6, Ar-*H*), 7.59 (2H, d, $^3J_{HH}$ = 7.3, Ar-*H*), 7.40 (2H, m, Ar-*H*), 7.32 (2H, m, Ar-*H*), 5.23 (1H, br s, N-*H*), 4.42 (2H, d, $^3J_{HH}$ = 6.9, C**7**-*H*), 4.21 (1H, t, $^3J_{HH}$ = 6.9, C**8**-*H*), 4.13 (1H, m, C**4**-*H*), 3.72 (3H, s, C**1**-*H*), 3.41 (1H, m, C**5**-*H*), 3.19 (1H, m, C**5**-*H*), 2.51 (2H, m, C**3**-*H*). ^{13}C NMR ($CDCl_3$, 101 MHz): δ (ppm) 173.1 (C**2**), 157.1 (C**6**), 144.0 (Ar), 141.5 (Ar), 127.8 (Ar), 127.2 (Ar), 125.2 (Ar), 120.1 (Ar), 67.5 (C**4**), 67.0 (C**7**), 52.1 (C**1**), 47.4 (C**8**), 45.9 (C**5**), 38.3 (C**3**). HRMS (ESI) *m/z* calculated for $[M+H]^+$ $C_{20}H_{22}NO_5^+$ 356.1498, found 356.1488.

Synthesis of 207[4]

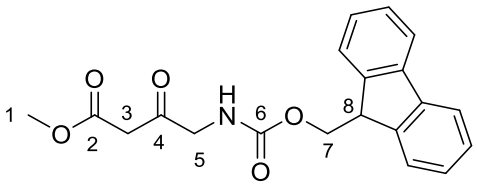

207

To a stirred solution of *β*-hydroxyester **208** (1.70 g, 4.78 mmol) in ethyl acetate was added IBX (4.02 g, 14.34 mmol). Mixture was left to stir under reflux overnight before being filtered. The filtrate was concentrated under reduced pressure and the resulting residue purified by silica gel column chromatography (hexane : ethyl acetate, 1 : 1), yielding an off-white solid as the pure product (1.11 g, 3.14 mmol, 66%). ^{1}H NMR ($CDCl_3$, 400 MHz): δ (ppm) 7.77 (2H, d, $^{3}J_{HH}$ = 7.6, Ar-*H*), 7.60 (2H, d, $^{3}J_{HH}$ = 7.5, Ar-*H*), 7.41 (2H, m, Ar-*H*), 7.32 (2H, m, Ar-*H*), 5.46 (1H, br s, N-*H*), 4.41 (2H, d, $^{3}J_{HH}$ = 7.0, C**7**-*H*), 4.23 (3H, m, C**8**-*H* & C**5**-*H*), 3.76 (3H, s, C**1**-*H*), 3.51 (2H, s, C**3**-*H*). ^{13}C NMR ($CDCl_3$, 101 MHz): δ (ppm) 198.1 (C**4**), 167.0 (C**2**), 156.3 (C**6**), 143.9 (Ar), 141.4 (Ar), 127.9 (Ar), 127.2 (Ar), 125.2 (Ar), 120.2 (Ar), 67.4 (C**7**), 52.8 (C**1**), 51.0 (C**5**), 47.2 (C**8**), 46.4 (C**3**). HRMS (ESI) *m/z* calculated for $[M+H]^+$ $C_{20}H_{20}NO_5^+$ 354.1341, found 354.1342. Characterisation data was found to be consistent with the literature.[4]

Synthesis of 214

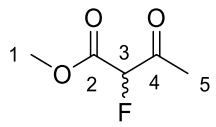

214

To a solution of methyl acetoacetate (**213**) (0.46 mL, 4.26 mmol) and 5 mol % $CpTiCl_3$ (47.0 mg, 0.21 mmol) in MeCN (50 ml) was added F-TEDA (1.71 g, 4.83 mmol). The reaction mixture was left to stir at room temperature overnight before diethyl ether was added. The resulting mixture was filtered, and the liquid phase concentrated under reduced pressure, affording the product as an orange oil (0.25 g, 1.84 mmol, 43%). ^{1}H NMR ($CDCl_3$, 400 MHz): δ (ppm) 5.17 (1H, d, $^{2}J_{HF}$ = 48.9, C**3**-*H*), 3.71 (3H, s, C**1**-*H*), 2.20 (2H, d, $^{4}J_{HF}$ = 3.9, C**5**-*H*). ^{13}C NMR ($CDCl_3$, 101 MHz): δ (ppm) 198.5 (d, $^{2}J_{CF}$ = 22.9, C**4**), 164.26 (d, C**2**, $^{2}J_{CF}$ = 24.0), 91.1 (d, C**3**, $^{1}J_{CF}$ = 197.2), 52.9 (C**1**), 25.8 (C**5**). ^{19}F NMR ($CDCl_3$, 376 MHz): δ (ppm) -194.05 (dd, $^{2}J_{FH}$ = 48.9, $^{4}J_{FH}$ = 3.8, C**3**-*F*). HRMS (ESI) *m/z* calculated for $[M+H]^+$ $C_5H_8O_3F^+$ 135.0457, found 135.0468.

Synthesis of 206

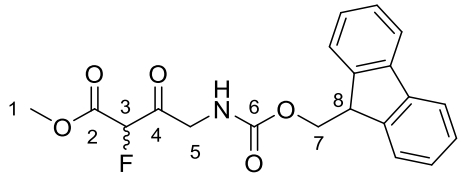

206

To a solution of *β*-ketoester **207** (0.20 g, 0.57 mmol) and 5 mol % $CpTiCl_3$ (6.2 mg, 28.3 µmol) in MeCN (7 ml) was added F-TEDA (0.22 g, 0.62 mmol). The reaction mixture was left to stir at room temperature overnight before diethyl ether was added. The resulting mixture was filtered, and the liquid phase concentrated under reduced pressure, affording the product as an orange oil (0.11 g, 0.30 mmol, 52%). ^{1}H NMR ($CDCl_3$, 400 MHz): δ (ppm) 7.70 (2H, d, $^{3}J_{HH}$ = 7.6, Ar), 7.55 (2H, d, $^{3}J_{HH}$ = 7.5, Ar), 7.33 (2H, m, Ar), 7.24 (2H, m, Ar), 5.60 (1H, br s, N-*H*), 5.38 (1H, d, $^{2}J_{HF}$ = 48.1, C**3**-*H*), 4.46-4.06 (2H, m, C**5**-*H*), 4.31 (2H, d, $^{3}J_{HH}$ = 5.8, C**7**-*H*), 4.16 (1H, t, $^{3}J_{HH}$ = 7.2, C**8**-*H*), 3.78 (3H, s, C**1**-*H*). ^{13}C NMR ($CDCl_3$, 101 MHz): δ (ppm) 196.7 (C**4**), 163.9 (d, C**2**, $^{2}J_{CF}$ = 23.7), 156.2 (C**6**), 143.8 (Ar), 141.5 (Ar), 127.9 (Ar), 127.2 (Ar), 125.2 (Ar), 120.2 (Ar), 90.7 (d, C**3**, $^{1}J_{CF}$ = 197.9), 67.5 (C**7**), 53.7 (C**1**), 48.2 (C**5**), 47.2 (C**8**). ^{19}F NMR ($CDCl_3$, 376 MHz): δ (ppm) -200.04 (d, $^{2}J_{FH}$ = 48.0, C**3**-*F*). HRMS (ESI) *m/z* calculated for $[M+H]^+$ $C_{20}H_{19}NO_5F^+$ 372.1247, found 372.1266.

Synthesis of 226

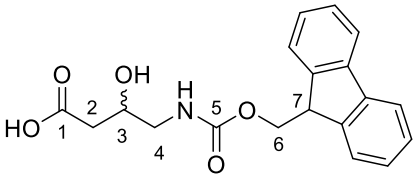

226

4-amino-3-hydroxybutyric acid (0.30 g, 2.52 mmol) was suspended in 1,4-dioxane (8.0 ml) and acetone (6.0 ml). Subsequently, 0.8 M aqueous $NaHCO_3$ was added (11 mL, 8.80 mmol), followed by Fmoc-OSu (1.00 g, 2.96 mmol) added portion-wise over a period of 10 min. The reaction mixture was left to stir at room temperature for 24 h before being acidified to pH 1 with 37% aqueous HCl and concentrated *in vacuo*. The crude material was purified by silica gel column chromatography (MeOH : DCM, 5 : 95) to afford *β*-ketoacid **220** as a yellow oily residue (0.68 g, 1.99 mmol, 79%). ^{1}H NMR ($CDCl_3$, 400 MHz): δ (ppm) 7.75 (2H, d, $^3J_{HH}$ = 7.5, Ar-*H*), 7.58 (2H, d, $^3J_{HH}$ = 7.5, Ar-*H*), 7.39 (2H, m, Ar-*H*), 7.31 (2H, m, Ar-*H*), 5.38 (1H, t, $^3J_{HH}$ = 6.0, N-*H*), 4.42 (2H, d, $^3J_{HH}$ = 6.8, C**6**-*H*), 4.20 (1H, t, $^3J_{HH}$ = 6.8, C**7**-*H*), 4.13 (1H, br m, C**3**-*H*), 3.39 (1H, m, C**4**-*H*), 3.21 (1H, m, C**4**-*H*), 2.51 (2H, m, C**2**-*H*). ^{13}C NMR ($CDCl_3$, 101 MHz): δ (ppm) 171.9 (C**1**), 157.5 (C**5**), 143.9 (Ar), 141.5 (Ar), 127.9 (Ar), 127.2 (Ar), 125.2 (Ar), 120.2 (Ar), 67.6 (C**3**), 67.1 (C**6**), 47.3 (C**7**), 45.9 (C**4**), 38.4 (C**2**). HRMS (ESI) *m/z* calculated for $[M+H]^+$ $C_{19}H_{20}NO_5^+$ 342.1341, found 342.1339.

Synthesis of 232

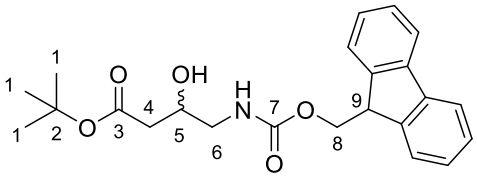

232

To a solution of *β*-hydroxy acid **226** (90.0 mg, 0.26 mmol) in EtOAc (10 ml) was added *tert*-butyl 2,2,2-trichloroacetimidate (0.13 g, 0.59 mmol) in EtOAc (5 ml). The reaction mixture was left to stir at room temperature for 48 h before being concentrated under reduced pressure and subsequently purified by silica gel column chromatography (hexane :EtOAc, 1 : 1), affording the product as an off-white solid residue (27.0 mg, 68.0 µmol, 26%). ^{1}H NMR ($CDCl_3$, 400 MHz): δ (ppm) 7.76 (2H, d, $^{3}J_{HH}$ = 7.7, Ar-*H*), 7.60 (2H, d, $^{3}J_{HH}$ = 7.5, Ar-*H*), 7.40 (2H, m, Ar-*H*), 7.32 (2H, m, Ar-*H*), 5.26 (1H, br m, N-*H*), 4.41 (2H, d, $^{3}J_{HH}$ = 7.0, C**8**-*H*), 4.21 (1H, t, $^{3}J_{HH}$ = 7.0, C**9**-*H*), 4.10 (1H, br m, C**5**-*H*), 3.40 (1H, ddd, $^{2}J_{HH}$ = 13.9, $^{3}J_{HH}$ = 6.6, $^{3}J_{HH}$ = 3.5, C**6**-*H*), 3.16 (1H, ddd, $^{2}J_{HH}$ = 13.4, $^{3}J_{HH}$ = 7.2, $^{3}J_{HH}$ = 5.6, C**6**-*H*), 2.40 (2H, m, C**4**-*H*), 1.47 (9H, s, C**1**-*H*). ^{13}C NMR ($CDCl_3$, 101 MHz): δ (ppm) 172.3 (C**3**), 157.0 (C**7**), 144.0 (Ar), 144.0 (Ar), 141.4 (Ar), 127.8 (Ar), 127.2 (Ar), 125.2 (Ar), 120.1 (Ar), 81.9 (C**2**), 67.6 (C**5**), 66.9 (C**8**), 47.4 (C**9**), 45.9 (C**6**), 39.5 (C**4**), 28.2 (C**1**). HRMS (ESI) *m/z* calculated for $[M+H]^+$ $C_{23}H_{28}NO_5^+$ 398.1967, found 398.1942.

Synthesis of 242 – General Procedure for the synthesis of Fmoc-protected *t*-butyl *β*-ketoesters (242-247)

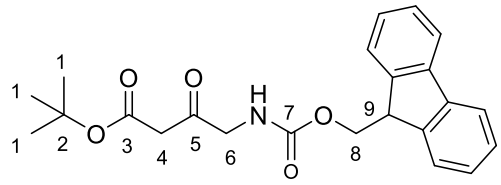

242

To a solution of Fmoc-Gly-OH (1.00 g, 3.36 mmol) in dry THF (6 ml) was added 1,1′-carbonyldiimidazole (0.55 g, 3.39 mmol) under an atmosphere of nitrogen. The reaction mixture was left to stir at room temperature for 1-3 h (generally 1.5 h) in order to generate the corresponding acyl imidazole *in situ*. Simultaneously, a solution of *tert*-butyl acetate (1.4 mL, 10.4 mmol) in dry THF (3 ml) was added dropwise under nitrogen to a solution of 2 M (unless stated otherwise) lithium diisopropylamide in dry THF (5.0 mL, 10.0 mmol) which had been cooled to -78 °C. The resulting solution was left to stir at -78 °C for 20 min before the addition of the acyl imidazole-containing solution at -78 °C. The reaction mixture was stirred at -78 °C under inert conditions for a further 45 min before being quenched with 1 M aqueous HCl (30 ml) and extracted with EtOAc (3 x 15 ml). The combined organic phases were dried over anhydrous $MgSO_4$, filtered and concentrated *in vacuo*. Subsequent purification by silica gel flash column chromatography (hexane : ethyl acetate, 1 : 0 to 7 : 3) gave the pure product as a yellow oil (0.49 g, 1.24 mmol, 37%). ^{1}H NMR ($CDCl_3$, 400 MHz): δ (ppm) 7.77 (2H, d, $^3J_{HH}$ = 7.6, Ar), 7.60 (2H, d, $^3J_{HH}$ = 7.4, Ar), 7.39 (2H, m, Ar), 7.32 (2H, m, Ar), 5.49 (1H, br s, N-*H*), 4.41 (2H, d, $^3J_{HH}$ = 7.1, C**8**-*H*), 4.23 (3H, m, C**9**-*H* & C**6**-*H*), 3.41 (2H, s, C**4**-*H*), 1.48 (9H, s, C**1**-*H*). ^{13}C NMR ($CDCl_3$, 101 MHz): δ (ppm) 198.7 (C**5**), 165.8 (C**3**), 156.2 (C**7**), 143.9 (Ar), 141.4 (Ar), 127.9 (Ar), 127.2 (Ar), 125.1 (Ar), 120.1 (Ar), 82.8 (C**2**), 67.3 (C**8**), 51.0 (C**6**), 48.0 (C**4**), 47.2 (C**9**), 28.1 (C**1**). HRMS (ESI) *m/z* calculated for $[M\text{-}^t Bu+H]^+$ $C_{19}H_{18}NO_5^+$ 340.1185, found 340.1164.

Synthesis of 243

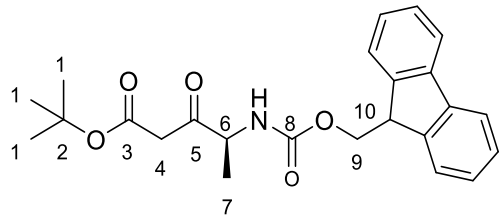

243

According to the general procedure Fmoc-Ala-OH (1.00 g, 3.21 mmol) and 1,1′-carbonyldiimidazole (0.52 g, 3.21 mmol) in dry THF (6 ml) were reacted under nitrogen and the resulting acyl imidazole added to a solution in which *tert*-butyl acetate (1.3 mL, 9.69 mmol) in dry THF (3 ml) and 2 M lithium diisopropylamide in dry THF (5 mL, 10.0 mmol) had been reacted together. The isolated crude material was purified by silica gel flash column chromatography (hexane : ethyl acetate, 1 : 0 to 7 : 3) to give the pure product as a yellow oil (0.18 g, 0.43 mmol, 13%). ^{1}H NMR ($CDCl_3$, 400 MHz): δ (ppm) 7.77 (2H, d, $^{3}J_{HH}$ = 7.5, Ar), 7.60 (2H, d, $^{3}J_{HH}$ = 7.3, Ar), 7.40 (2H, m, Ar), 7.32 (2H, m, Ar), 5.54 (1H, br s, N-*H*), 4.54-4.38 (3H, m, C**6**-*H* & C**9**-*H*), 4.22 (1H, t, $^{3}J_{HH}$ = 6.9, C**10**-*H*), 3.48 & 3.44 (2H, ABq, $^{2}J_{AB}$ = 16.0, C**4**-*H*), 1.47 (9H, s, C**1**-*H*), 1.40 (3H, d, $^{3}J_{HH}$ = 7.2, C**7**-*H*). ^{13}C NMR ($CDCl_3$, 101 MHz): δ (ppm) 202.3 (C**5**), 166.0 (C**3**), 155.8 (C**8**), 143.9 (Ar), 141.4 (Ar), 127.9 (Ar), 127.2 (Ar), 125.2 (Ar), 120.1 (Ar), 82.6 (C**2**), 67.1 (C**9**), 55.9 (C**6**), 47.3 (C**10**), 47.2 (C**4**) 28.1 (C**1**), 17.4 (C**7**). HRMS (ESI) *m/z* calculated for $[M+H]^+$ $C_{24}H_{28}NO_5^+$ 410.1967, found 410.1964.

Synthesis of 244

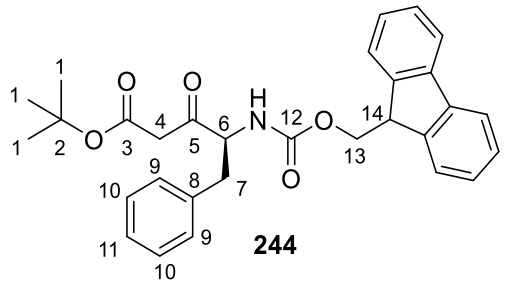

244

According to the general procedure, Fmoc-Phe-OH (1.00 g, 2.58 mmol) and 1,1′-carbonyldiimidazole (0.42 g, 2.59 mmol) in dry THF (6 ml) were reacted under nitrogen and the resulting acyl imidazole added to a solution in which *tert*-butyl acetate (1.1 mL, 8.20 mmol) in dry THF (3 ml) and 2 M lithium diisopropylamide in dry THF (4 mL, 8.00 mmol) had been reacted together. The isolated crude material was purified by silica gel flash column chromatography (hexane : ethyl acetate, 1 : 0 to 4 : 1) to give the pure product as a yellow oil (0.62 g, 1.27 mmol, 49%). ^{1}H NMR ($CDCl_3$, 400 MHz): δ (ppm) 7.78 (2H, d, $^{3}J_{HH}$ = 7.5, Fmoc Ar), 7.55 (2H, t, $^{3}J_{HH}$ = 8.2, Fmoc Ar), 7.42 (2H, t, $^{3}J_{HH}$ = 7.4, Fmoc Ar), 7.31 (5H, m, Ph), 7.17 (2H, d, $^{3}J_{HH}$ = 7.0, Fmoc Ar), 5.48 (1H, br s, N-*H*), 4.71 (1H, m, C**6**-*H*), 4.45 (1H, dd, $^{3}J_{HH}$ = 7.0, $^{2}J_{HH}$ = 10.7, C**13**-*H*), 4.37 (1H, dd, $^{3}J_{HH}$ = 6.9, $^{2}J_{HH}$ = 10.7, C**13**-*H*), 4.19 (1H, t $^{3}J_{HH}$ = 6.9, C**14**-*H*), 3.43 & 3.40 (2H, ABq, $^{2}J_{AB}$ = 16.0, C**4**-*H*), 3.21 (1H, dd, $^{3}J_{HH}$ = 6.0, $^{2}J_{HH}$ = 14.1, C**7**-*H*), 3.02 (1H, dd, $^{3}J_{HH}$ = 7.1, $^{2}J_{HH}$ = 14.1, C**7**-*H*), 1.49 (9H, s, C**1**-*H*). ^{13}C NMR ($CDCl_3$, 101 MHz): δ (ppm) 201.8 (C**5**), 166.0 (C**3**), 155.7 (C**12**), 143.7 (C-*Fmoc Ar*), 141.3 (C-*Fmoc Ar*), 135.9 (C-*Phe*) 129.4 (C-*Phe*), 128.8 (C-*Phe*), 127.8 (C-*Fmoc Ar*), 127.2 (C-*Ar*), 127.1 (C-*Ar*), 125.1 (C-*Fmoc Ar*), 120.1 (C-*Fmoc Ar*), 82.4 (C**2**), 66.9 (C**13**), 60.8 (C**6**), 48.1 (C**4**), 47.2 (C**14**), 37.0 (C**7**), 28.0 (C**1**). HRMS (ESI) *m/z* calculated for $[M+H]^+$ $C_{30}H_{32}NO_5^+$ 486.2280, found 486.2282. Characterisation data was found to be consistent with the literature[5].

Synthesis of 245

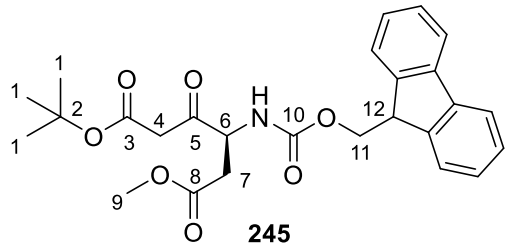

245

According to the general procedure, Fmoc-Asp(OMe)-OH (1.00 g, 2.71 mmol) and 1,1′-carbonyldiimidazole (0.44 g, 2.71 mmol) in dry THF (6 ml) were reacted under nitrogen and the resulting acyl imidazole added to a solution in which *tert*-butyl acetate (1.1 mL, 8.20 mmol) in dry THF (3 ml) and 2 M lithium diisopropylamide in dry THF (4.0 mL, 8.00 mmol) had been reacted together. The isolated crude material was purified by silica gel flash column chromatography (hexane : ethyl acetate, 1 : 0 to 7 : 3) to give the pure product as a yellow oil (0.23 g, 0.49 mmol, 18%). ^{1}H NMR ($CDCl_3$, 400 MHz): δ (ppm) 7.76 (2H, d, $^{3}J_{HH}$ = 7.6, Ar-*H*), 7.59 (2H, d, $^{3}J_{HH}$ = 7.5, Ar-*H*), 7.40 (2H, m, Ar-*H*), 7.32 (2H, m, Ar-*H*), 5.96 (1H, br d, $^{3}J_{HH}$ = 9.0, N-*H*), 4.64 (1H, m, C**6**-*H*), 4.51 (1H, dd, $^{3}J_{HH}$ = 6.9, $^{2}J_{HH}$ = 10.7, C**11**-*H*), 4.44 (1H, dd, $^{3}J_{HH}$ = 6.7, $^{2}J_{HH}$ = 10.7, C**11**-*H*), 4.22 (1H, t $^{3}J_{HH}$ = 6.8, C**12**-*H*), 3.69 (3H, s, C**9**-*H*), 3.49 & 3.49 (2H, ABq $^{2}J_{AB}$ = 16.0, C**4**-*H*), 3.00 (1H, dd, $^{3}J_{HH}$ = 4.9, $^{2}J_{HH}$ = 17.3, C**7**-*H*), 2.80 (1H, dd, $^{3}J_{HH}$ = 4.7, $^{2}J_{HH}$ = 17.3, C**7**-*H*), 1.46 (9H, s, C**1**-*H*). ^{13}C NMR ($CDCl_3$, 101 MHz): δ (ppm) 201.2 (C**5**), 171.8 (C**8**), 166.1 (C**3**), 156.1 (C**10**), 143.7 (Ar), 141.4 (Ar), 127.9 (Ar), 127.2 (Ar), 125.1 (Ar), 120.1 (Ar), 82.4 (C**2**), 67.2 (C**11**), 56.6 (C**6**), 52.2 (C**9**), 47.3 (C**12**), 47.1 (C**4**), 35.2 (C**7**), 28.0 (C**1**). HRMS (ESI) *m/z* calculated for $[M+H]^+$ $C_{26}H_{30}NO_7^+$ 468.2022, found 468.2025.

Synthesis of 246

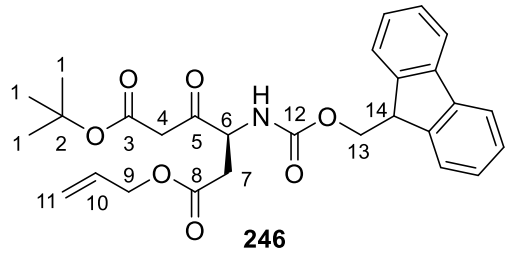

246

According to the general procedure, Fmoc-Asp(OAll)-OH (2.00 g, 5.06 mmol) and 1,1′-carbonyldiimidazole (0.82 g, 5.06 mmol) in dry THF (12 ml) were reacted under nitrogen and the resulting acyl imidazole added to a solution in which *tert*-butyl acetate (2.1 mL, 15.7 mmol) in dry THF (6 ml) and 2 M lithium diisopropylamide in dry THF (8 mL, 16.0 mmol) had been reacted together. The isolated crude material was purified by silica gel flash column chromatography (hexane : ethyl acetate, 1 : 0 to 4 : 1) to give the pure product as a yellow oil (0.97 g, 1.97 mmol, 39%). ^{1}H NMR ($CDCl_3$, 400 MHz): δ (ppm) 7.76 (2H, d, $^{3}J_{HH}$ = 7.4, Ar-*H*), 7.59 (2H, d, $^{3}J_{HH}$ = 7.5, Ar-*H*), 7.40 (2H, m, Ar-*H*), 7.32 (2H, m Ar-*H*), 5.98-5.83 (2H, m, N-*H* & C**10**-*H*), 5.32 (1H, m, C**11**-*H*), 5.25 (1H, m, C**11**-*H*), 4.64 (1H, m, C**6**-*H*), 4.58 (2H, m, C**9**-*H*), 4.49 (1H, dd, $^{3}J_{HH}$ = 6.9, $^{2}J_{HH}$ = 10.7, C**13**-*H*), 4.43 (1H, dd, $^{3}J_{HH}$ = 6.8, $^{2}J_{HH}$ = 10.7, C**13**-*H*), 4.21 (1H, t, $^{3}J_{HH}$ = 6.8, C**14**-*H*), 3.48 & 3.48 (2H, ABq, $^{2}J_{AB}$ = 16.0, C**4**-*H*), 3.03 (1H, dd, $^{3}J_{HH}$ = 4.9, $^{2}J_{HH}$ = 17.3, C**7**-*H*), 2.82 (1H, dd, $^{3}J_{HH}$ = 4.7, $^{2}J_{HH}$ = 17.3, C**7**-*H*), 1.48 (9H, s, C**1**-*H*). ^{13}C NMR ($CDCl_3$, 101 MHz): δ (ppm) 201.1 (C**5**), 171.1 (C**8**), 166.1 (C**3**), 156.1 (C**12**), 143.7 (Ar), 141.5 (Ar), 131.7 (C**10**), 127.9 (Ar), 127.2 (Ar), 125.1 (Ar), 120.2, (Ar), 119.0 (C**11**), 82.5 (C**2**), 67.3 (C**13**), 66.0 (C**9**), 56.7 (C**6**), 47.4 (C1**4**), 47.2 (C**4**), 35.4 (C**7**) 28.1 (C**1**). HRMS (ESI) *m/z* calculated for $[M+H]^+$ $C_{28}H_{32}NO_7^+$ 494.2179, found 494.2178.

Synthesis of 247

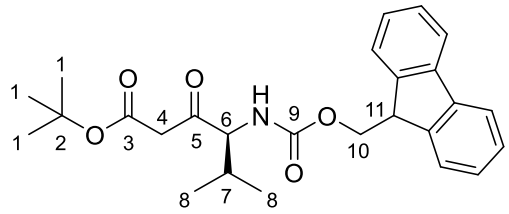

247

According to the general procedure, Fmoc-Val-OH (1.00 g, 2.95 mmol) and 1,1′-carbonyldiimidazole (0.48 g, 2.96 mmol) in dry THF (6 ml) were reacted under nitrogen and the resulting acyl imidazole added to a solution in which *tert*-butyl acetate (1.2 mL, 8.95 mmol) in dry THF (3 ml) and 1 M lithium diisopropylamide in dry THF (9.0 mL, 9.0 mmol) had been reacted together. The resulting reaction mixture was left at -78 ºC for a further 2 h. The isolated crude material was purified by silica gel flash column chromatography (hexane : ethyl acetate, 1 : 0 to 7 : 3) to give the pure product as a yellow oil (0.41 g, 0.94 mmol, 32%). ^{1}H NMR ($CDCl_3$, 400 MHz): δ (ppm) 7.79 (2H, d, $^{3}J_{HH}$ = 7.6, Ar-*H*), 7.63 (2H, d, $^{3}J_{HH}$ = 7.5, Ar-*H*), 7.42 (2H, m, Ar-*H*), 7.34 (2H, m Ar-*H*), 5.5 (1H, d, $^{3}J_{HH}$ = 9.0, N-*H*), 4.50 (1H, dd, $^{3}J_{HH}$ = 8.9, $^{3}J_{HH}$ =4.0, C**6**-*H*), 4.44 (2H, m, C**10**-*H*), 4.25 (1H, t, $^{3}J_{HH}$ = 7.0, C**11**-*H*), 3.47 (2H, apps, C**4**-*H*), 2.32 (1H, m, C**7**-*H*), 1.50 (9H, s, C**1**-*H*), 1.06 (3H, d, $^{3}J_{HH}$ = 6.8, C**8**-*H*), 0.85 (3H, d, $^{3}J_{HH}$ = 6.8, C**8**-*H*). ^{13}C NMR ($CDCl_3$, 101 MHz): δ (ppm) 202.1 (C**5**), 165.8 (C**3**), 156.5 (C**9**), 143.9 (Ar), 143.8 (Ar), 141.4 (Ar), 127.9 (Ar), 127.2 (Ar), 125.2 (Ar), 120.1, (Ar), 82.5 (C**2**), 67.1 (C**10**), 64.8 (C**6**), 48.5 (C**4**), 47.4 (C**11**), 29.8 (C**7**), 28.1 (C**1**), 20.0 (C**8**), 16.7 (C**8**). HRMS (ESI) *m/z* calculated for $[M+H]^+$ $C_{26}H_{32}NO_5^+$ 438.2280, found 438.2275.

Synthesis of 249

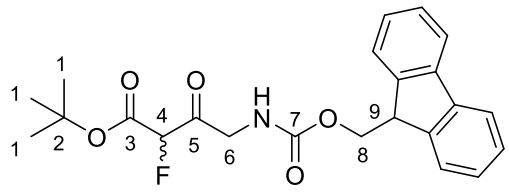

249

To a solution of *β*-ketoester **242** (0.22 g, 0.56 mmol) and 5 mol % $CpTiCl_3$ (6.0 mg, 27.4 μmol) in MeCN (20 ml) was added F-TEDA (0.22 g, 0.62 mmol). The reaction mixture was left to stir at room temperature overnight and subsequently concentrated under reduced pressure. The resulting crude material was purified by silica gel flash column chromatography (hexane : ethyl acetate, 1 : 0 to 8 : 2) to give the product (including 10% di-fluorinated material relative to mono-fluorinated) as a clear oil (0.12 g, 0.29 mmol, 52%). ^{1}H NMR ($CDCl_3$, 400 MHz): δ (ppm) 7.77 (2H, d, $^{3}J_{HH}$ = 7.6, Ar-*H*), 7.60 (2H, d, $^{3}J_{HH}$ = 7.5, Ar-*H*), 7.41 (2H, m, Ar-*H*), 7.32 (2H, m, Ar-*H*), 5.38 (1H, br s, N-*H*), 5.24 (1H, d, $^{2}J_{HF}$ = 48.9, C**4**-*H*), 4.51-4.25 (4H, m, C**6**-*H* & C**8**-*H*), 4.23 (1H, t, $^{3}J_{HH}$ = 7.0, C**9**-*H*), 1.52 (9H, s, C**1**-*H*). ^{13}C NMR ($CDCl_3$, 101 MHz): δ (ppm) 197.2 (d, C**5**, $^{2}J_{CF}$ = 23.8), 162.3 (d, C**3**, $^{2}J_{CF}$ = 23.5), 156.2 (C**7**), 143.8 (Ar), 141.4 (Ar), 127.9 (Ar), 127.2 (Ar), 125.2 (Ar), 120.1 (Ar), 90.9 (d, C**4**, $^{1}J_{CF}$ = 197.1), 85.4 (C**2**), 67.4 (C**8**), 48.1 (C**6**), 47.2 (C**9**), 28.0 (C**1**). ^{19}F NMR ($CDCl_3$, 376 MHz): δ (ppm) -197.99 (d, $^{2}J_{FH}$ = 48.9, C**4**-*F*). HRMS (ESI) *m/z* calculated for $[M\text{-}^{t}Bu+H]^{+}$ $C_{19}H_{17}NO_5F^{+}$ 358.1091, found 358.1081.

Synthesis of 250 (reported as a mixture of diastereoisomers)

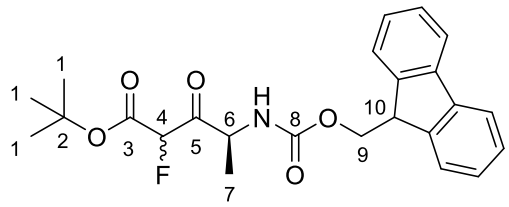

250

To a solution of *β*-ketoester **243** (48.0 mg, 0.12 mmol) and 5 mol % $CpTiCl_3$ (2.2 mg, 10 µmol) in MeCN (5 ml) was added F-TEDA (46.5 mg, 0.13 mmol). The reaction mixture was left to stir at room temperature overnight and subsequently concentrated under reduced pressure. The resulting crude material was purified by silica gel flash column chromatography (hexane : ethyl acetate, 1 : 0 to 7 : 3) to give the product (including 8% di-fluorinated material relative to mono-fluorinated) as a clear oil (28.0 mg, 65.5 µmol, 56%). Reported as a mixture of diastereoisomers (dr ~ 50:50), as determined by ^{19}F NMR spectroscopy. ^{1}H NMR ($CDCl_3$, 400 MHz): δ (ppm) 7.77 (2H, d, $^{3}J_{HH}$ = 7.5, Ar-*H*), 7.59 (2H, m, Ar-*H*), 7.41 (2H, t, $^{3}J_{HH}$ = 7.4, Ar-*H*), 7.32 (2H, m, Ar-*H*), 5.48 (0.5H, br d, $^{3}J_{HH}$ = 7.9, N-*H*), 5.34 (0.5H, br d, $^{3}J_{HH}$ = 7.7, N-*H*), 5.32 (0.5H, d, $^{2}J_{HF}$ = 48.8, C**4**-*H*), 5.30 (0.5H, d, $^{2}J_{HF}$ = 48.8, C**4**-*H*), 4.83 (1H, m, C**6**-*H*), 4.41 (2H, m, C**9**-*H*), 4.21 (1H, m, C**10**-*H*), 1.51 (9H, s, C**1**-*H*), 1.41 (3H, m, C**7**-*H*). ^{13}C NMR ($CDCl_3$, 101 MHz): δ (ppm) 200.7 (m, C**5**), 162.6 (d, C**3**, $^{2}J_{CF}$ = 23.5), 162.5 (d, C**3**, $^{2}J_{CF}$ = 23.7), 155.6 (C**8**), 143.8 (Ar), 141.4 (Ar), 127.9 (Ar), 127.2 (Ar), 125.2 (Ar), 120.1 (Ar), 90.5 (d, C**4**, $^{1}J_{CF}$ = 199.3), 85.2 (C**2**), 85.0 (C**2**), 67.2 (C**9**), 53.4 (C**6**), 52.7 (C**6**), 47.3 (C**10**), 28.0 (C**1**), 28.0 (C**1**), 17.4 (C**7**), 17.2 (C**7**). ^{19}F NMR ($CDCl_3$, 376 MHz): δ (ppm) -196.02 (d, $^{2}J_{FH}$ = 48.4, C**4**-*F*), -196.92 (d, $^{2}J_{FH}$ = 48.9, C**4**-*F*). HRMS (ESI) *m/z* calculated for $[M+H]^+$ $C_{24}H_{27}NO_5F^+$ 428.1873, found 428.1874.

Synthesis of 252 (reported as a mixture of diastereoisomers)

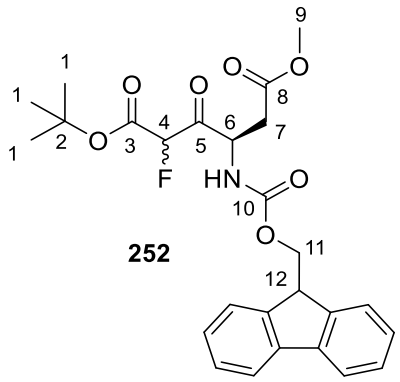

252

To a solution of *β*-ketoester **245** (0.11 g, 0.24 mmol) and 5 mol % $CpTiCl_3$ (2.5 mg, 11.4 μmol) in MeCN (10 ml) was added F-TEDA (90.0 mg, 0.25 mmol). The reaction mixture was left to stir at room temperature overnight and subsequently concentrated under reduced pressure. The resulting crude material was purified by silica gel flash column chromatography (hexane : ethyl acetate, 1 : 0 to 7 : 3) to give the product (including <1% di-fluorinated material relative to mono-fluorinated) as a clear oil (81.0 mg, 0.17 mmol, 71%). Reported as a mixture of diastereoisomers (dr ~ 50:50), as determined by ^{1}H NMR spectroscopy. ^{1}H NMR ($CDCl_3$, 400 MHz): δ (ppm) 7.77 (2H, d, $^3J_{HH}$ = 7.8, Ar-*H*), 7.59 (2H, d, $^3J_{HH}$ = 7.4, Ar-*H*), 7.43 (2H, m, Ar-*H*), 7.32 (2H, m, Ar-*H*), 5.90 (0.5H, br d, $^3J_{HH}$ = 8.5, N-*H*), 5.81 (0.5H, br d, $^3J_{HH}$ = 8.4, N-*H*), 5.37 (0.5H, d, $^2J_{HF}$ = 48.7, C**4**-*H*), 5.35 (0.5H, d, $^2J_{HF}$ = 49.1, C**4**-*H*), 4.89 (1H, m, C**6**-*H*), 4.43 (2H, m, C**11**-*H*), 4.22 (1H, t, $^3J_{HH}$ = 7.1, C**12**-*H*), 3.71 (1.5H, s, C**9**-*H*), 3.68 (1.5H, s, C**9**-*H*), 3.01 (2H, m, C**7**-*H*), 1.51 (9, s, C**1**-*H*). ^{13}C NMR ($CDCl_3$, 101 MHz): δ (ppm) 197.9 (d, $^2J_{CF}$ = 21.9, C**5**), 197.6 (d, $^2J_{CF}$ = 23.0, C**5**), 171.6 (C**8**), 171.2 (C**8**), 162.6 (d, C**3**, $^2J_{CF}$ = 23.7), 162.4 (d, C**3**, $^2J_{CF}$ = 24.0), 155.8 (C**10**), 143.7 (Ar), 141.4 (Ar), 127.9 (Ar), 127.2 (Ar), 125.2 (Ar), 120.1 (Ar), 90.6 (d, C**4**, $^1J_{CF}$ = 196.9), 89.9 (d, C**4**, $^1J_{CF}$ = 196.7), 85.2 (C**2**), 85.0 (C**2**), 67.4 (C**11**), 67.4 (C**11**), 54.9 (C**6**), 54.3 (C**6**), 52.3 (C**9**), 52.3 (C**9**), 47.2 (C**12**), 47.2 (C**12**), 35.5 (C**7**), 35.1 (C**7**), 27.9 (C**1**), 27.9 (C**1**). ^{19}F NMR ($CDCl_3$, 376 MHz): δ (ppm) -195.09 (d, $^2J_{FH}$ = 49.1, C**4**-*F*), -196.13 (d, $^2J_{FH}$ = 48.6, C**4**-*F*). HRMS (ESI) *m/z* calculated for $[M+H]^+$ $C_{26}H_{29}NO_7F^+$ 486.1928, found 486.1951.

Synthesis of 253 (reported as a mixture of diastereoisomers)

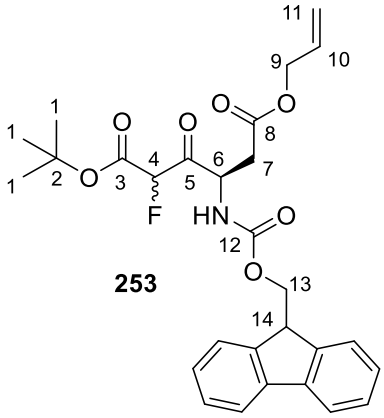

253

To a solution of *β*-ketoester **246** (0.87 g, 1.76 mmol) and 5 mol % $CpTiCl_3$ (18.7 mg, 85 μmol) in MeCN (20 ml) was added F-TEDA (0.70 g, 1.98 mmol). The reaction mixture was left to stir at room temperature overnight and subsequently concentrated under reduced pressure. The resulting crude material was purified by silica gel flash column chromatography (hexane : ethyl acetate, 1 : 0 to 4 : 1) to give the product (including 11% di-fluorinated material relative to mono-fluorinated) as a clear oil (0.51 g, 1.00 mmol, 57%). Reported as a mixture of diastereoisomers (dr ~ 50:50), as determined by ^{19}F NMR spectroscopy. ^{1}H NMR ($CDCl_3$, 400 MHz): δ (ppm) 7.76 (2H, d, $^{3}J_{HH}$ = 7.6, Ar-*H*), 7.59 (2H, d, $^{3}J_{HH}$ = 7.5, Ar-*H*), 7.41 (2H, t, $^{3}J_{HH}$ = 7.5, Ar-*H*), 7.32 (2H, m, Ar-*H*), 5.99-5.77 (2H, m, N-*H* & C**10**-*H*), 5.49-5.19 (3H, m, C**4**-*H* & C**11**-*H*), 4.91 (1H, br m, C**6**-*H*), 4.59 (2H, m, C**9**-*H*), 4.44 (2H, m, C**13**-*H*), 4.22 (1H, t, $^{3}J_{HH}$ = 6.7, C**14**-*H*), 3.04 (2H, m, C**7**-*H*) 1.51 (4.5H, s, C**1**-*H*), 1.50 (4.5H, s, C**1**-*H*). ^{13}C NMR ($CDCl_3$, 101 MHz): δ (ppm) 197.9 (d, $^{2}J_{CF}$ = 22.1, C**5**), 197.6 (d, $^{2}J_{CF}$ = 23.0, C**5**), 170.8 (C**8**), 170.5 (C**8**), 162.6 (d, C**3**, $^{2}J_{CF}$ = 23.6), 162.4 (d, C**3**, $^{2}J_{CF}$ = 23.8), 155.8 (C**12**), 143.7 (m, Ar), 141.5 (Ar), 131.6 (C**10**),127.9 (Ar), 127.2 (Ar), 125.2 (Ar), 120.2 (Ar), 119.1 (C**11**), 90.6 (d, C**4**, $^{1}J_{CF}$ = 196.9), 90.0 (d, C**4**, $^{1}J_{CF}$ = 196.6), 85.3 (C**2**), 85.0 (C**2**), 67.5 (C**13**), 67.4 (C**13**), 66.1 (C**9**), 66.0 (C**9**), 55.0 (C**6**), 54.4 (C**6**), 47.3 (C**14**), 47.2 (C**14**), 35.7 (C**7**), 35.3 (C**7**), 28.0 (C**1**). ^{19}F NMR ($CDCl_3$, 376 MHz): δ (ppm) -195.09 (d, $^{2}J_{FH}$ = 49.1, C**4**-*F*), -196.13 (d, $^{2}J_{FH}$ = 48.6, C**4**-*F*). HRMS (ESI) *m/z* calculated for $[M+H]^+$ $C_{28}H_{31}NO_7F^+$ 512.2085, found 512.2075.

Synthesis of 254 (reported as a mixture of diastereoisomers)

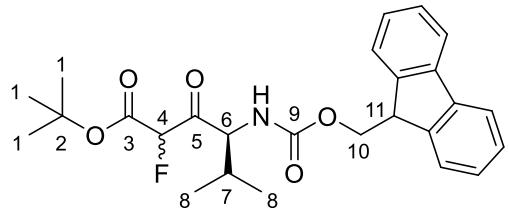

254

To a solution of *β*-ketoester **247** (0.32 g, 0.73 mmol) and 5 mol % $CpTiCl_3$ (8.9 mg, 40 µmol) in MeCN (40 ml) was added F-TEDA (0.54 g, 4.04 mmol). The reaction mixture was left to stir at room temperature overnight and subsequently concentrated under reduced pressure. The resulting crude material was purified by silica gel flash column chromatography (hexane : ethyl acetate, 1 : 0 to 9 : 1) to give the product (including <1% di-fluorinated material relative to mono-fluorinated) as a clear oil (0.19 g, 0.41 mmol, 56%). Reported as a mixture of diastereoisomers (dr ~ 40 : 60), as determined by ^{19}F NMR spectroscopy. ^{1}H NMR ($CDCl_3$, 400 MHz): δ (ppm) 7.77 (2H, d, $^{3}J_{HH}$ = 7.6, Ar-*H*), 7.60 (2H, m, Ar-*H*), 7.41 (2H, m, Ar-*H*), 7.32 (2H, m Ar-*H*), 5.52-5.09 (2H, m, N-*H* & C**4**-*H*), 4.89 (0.6H, m, C**6**-*H*), 4.77 (0.4H, m, C**6**-*H*), 4.42 (2H, m, C**10**-*H*), 4.23 (1H, t, $^{3}J_{HH}$ = 7.1, C**11**-*H*), 2.36 (0.6H, m, C**7**-*H*), 2.26 (0.4H, m, C**7**-*H*), 1.52-1.50 (9H, 2 x s, C**1**-*H*), 1.15-0.73 (6H, m, C**8**-*H*). ^{13}C NMR ($CDCl_3$, 101 MHz): δ (ppm) 200.5 (d, $^{2}J_{CF}$ = 22.1, C**5**), 200.3 (d, $^{2}J_{CF}$ = 23.1, C**5**), 162.6 (d, $^{2}J_{CF}$ = 23.6, C**3**), 162.3 (d, $^{2}J_{CF}$ = 24.0, C**3**), 156.4 (C**9**), 156.2 (C**9**), 143.9 (Ar), 143.8 (Ar), 141.4 (Ar), 141.4 (Ar), 127.9 (Ar), 127.9 (Ar), 127.2 (Ar), 127.2 (Ar), 125.2 (Ar), 125.1 (Ar), 120.1, (Ar), 120.1, (Ar), 90.8 (d, $^{1}J_{CF}$ = 198.5, C**4**), 90.6 (d, $^{1}J_{CF}$ = 197.5, C**4**), 85.2 (C**2**), 84.9 (C**2**), 67.2 (C**10**), 67.2 (C**10**), 62.2 (C**6**), 61.6 (C**6**), 47.3 (C**11**), 47.3 (C**11**), 29.5 (C**7**), 29.4 (C**7**), 28.0 (C**1**), 27.9 (C**1**), 20.0 (C**8**), 19.9 (C**8**), 16.8 (C**8**), 16.3 (C**8**). ^{19}F NMR ($CDCl_3$, 376 MHz): δ (ppm) -194.97 (d, $^{2}J_{FH}$ = 48.9, C**4**-*F*), -196.39 (d, $^{2}J_{FH}$ = 49.0, C**4**-*F*). LCMS (ESI) *m/z* calculated for $[M+Na]^+$ $C_{26}H_{31}FNO_5^+$ 478.2, found 478.4.

Synthesis of 205

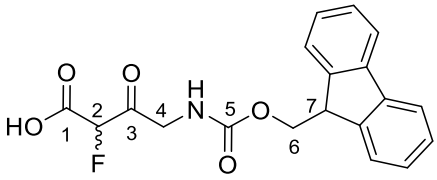

205

β-ketoester **249** (0.13 g, 0.31 mmol) was dissolved in 30% TFA in DCM (16 ml) and left to stir at room temperature for 2.5 h before being concentrated under reduced pressure and subsequently lyophilised to afford the crude product as a yellow-brown powder in what was assumed to be a quantitative yield, although around 22% of the fluorinated crude material was di-fluorinated, as determined by ^{19}F NMR spectroscopy. It was then used without further purification. ^{1}H NMR ($CDCl_3$, 400 MHz): δ (ppm) 7.76 (2H, d, Ar-*H*), 7.59 (2H, m, Ar-*H*), 7.40 (2H, m, Ar-*H*), 7.32 (2H, m, Ar-*H*), 6.07 (1H, br s, N-*H*), 4.95 (1H, d, $^{2}J_{HF}$ = 47.1, C**2**-*H*), 4.33 (5H, m, C**4**-*H*, C**6**-*H* & C**7**-*H*). ^{19}F NMR ($CDCl_3$, 376 MHz): δ (ppm) -199.41 (d, $^{2}J_{FH}$ = 48.7, C**2**-*F*). HRMS (ESI) *m/z* calculated for $[M+H]^+$ $C_{19}H_{17}NO_5F^+$ 358.1091, found 358.1092.

Synthesis of 257[5]

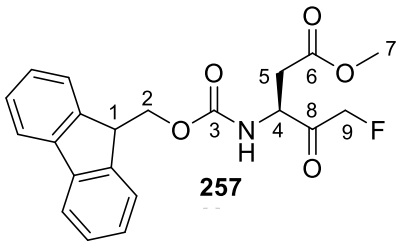

257

β-ketoester **252** (79.0 mg, 0.16 mmol) was dissolved in 13% TFA in DCM (3.9 mL, 6.53 mmol). The resulting solution was left to stir at room temperature overnight before being concentrated *in vacuo*. Due to reaction incompleteness, 50% TFA in DCM (2 mL, 13.1 mmol) was added and the solution left to stir at room temperature before being concentrated under reduce pressure. Subsequent purification by silica gel flash column chromatography (hexane : ethyl acetate, 1 : 0 to 1 : 1) afforded the product as a clear oil (19.0 mg, 49.3 µmol, 31%). ^{1}H NMR ($CDCl_3$, 700 MHz): δ (ppm) 7.78 (2H, d, $^{3}J_{HH}$ = 7.6, Ar-*H*), 7.58 (2H, m, Ar-*H*), 7.42 (2H, t, $^{3}J_{HH}$ = 7.4, Ar-*H*), 7.33 (2H, m, Ar-*H*), 5.71 (1H, d, $^{3}J_{HH}$ = 8.6, N-*H*), 5.10 (1H, dd, $^{2}J_{HF}$ = 47.0, $^{2}J_{HH}$ = 16.5, C**9**-*H*), 4.99 (1H, dd, $^{2}J_{HF}$ = 47.2, $^{2}J_{HH}$ = 16.4, C**9**-*H*), 4.67 (1H, m, C**4**-*H*), 4.56 (1H, dd, $^{2}J_{HH}$ = 10.8, $^{3}J_{HH}$ = 6.7, C**2**-*H*), 4.45 (1H, dd, $^{2}J_{HH}$ = 10.8, $^{3}J_{HH}$ = 6.6, C**2**-*H*), 4.22 (1H, t, $^{3}J_{HH}$ = 6.6, C**1**-*H*), 3.70 (3H, s, C**7**-*H*), 3.09 (1H, dd, $^{2}J_{HH}$ = 17.3, $^{3}J_{HH}$ = 4.5, C**5**-*H*), 2.86 (1H, dd, $^{2}J_{HH}$ = 17.4, $^{3}J_{HH}$ = 4.9, C**5**-*H*). ^{13}C NMR ($CDCl_3$, 101 MHz): δ (ppm) 202.8 (d, C**8**), 171.7 (C**6**), 156.0 (C**3**), 143.7 (Ar),143.6 (Ar), 141.6 (Ar), 141.5 (Ar), 128.0 (Ar), 128.0 (Ar), 127.3 (Ar), 127.3 (Ar), 125.1 (Ar), 125.0 (Ar), 120.2 (Ar), 120.2 (Ar), 84.3 (d, C**9**, $^{1}J_{CF}$ = 183.6), 67.2 (C**2**) 54.2 (C**4**), 52.5 (C**7**), 47.4 (C**1**), 35.5 (C**5**). ^{19}F NMR ($CDCl_3$, 376 MHz): δ (ppm) -232.03 (t, $^{2}J_{FH}$ = 47.1, C**9**-*F*). HRMS (ESI) *m/z* calculated for $[M+H]^+$ $C_{21}H_{21}NO_5F^+$ 386.1404, found 386.1402. Characterisation data was found to be consistent with the literature.[5]

Synthesis of 261 (reported as a suspected mixture of diastereoisomers)

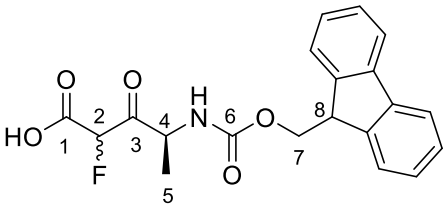

261

β-ketoester **250** (24.0 mg, 56.1 µmol) was dissolved in 30% TFA in DCM (3 ml) and left to stir at room temperature for 2.5 h before being concentrated under reduced pressure and subsequently lyophilised to afford the crude product as an off-white solid which was assumed to have been acquired in a quantitative yield, although impurity peaks were also present by ^{1}H NMR spectroscopy. It was then used without further purification. Reported as a mixture of suspected diastereoisomers (dr ~ 50 : 50). ^{1}H NMR (CD_3CN, 400 MHz): δ (ppm) 7.84 (2H, d, $^{3}J_{HH}$ = 7.6, Ar-*H*), 7.67 (2H, d, $^{3}J_{HH}$ = 7.2, Ar-*H*), 7.43 (2H, m, Ar-*H*), 7.34 (2H, m Ar-*H*), 6.12 (1H, m, N-*H*), 5.59 (1H, d, $^{2}J_{HF}$ = 47.9, C**2**-*H*), 4.65 (0.5H, m, C**4**-*H*), 4.52 (0.5H, m, C**4**-*H*), 4.35 (2H, m, C**7**-*H*), 4.23 (1H, t, $^{3}J_{HH}$ = 6.9, C**8**-*H*). HRMS (ESI) *m/z* calculated for $[M+H]^+$ $C_{20}H_{19}NO_5F^+$ 372.1272, found 372.1243.

Synthesis of 264 (reported as a suspected mixture of diastereoisomers)

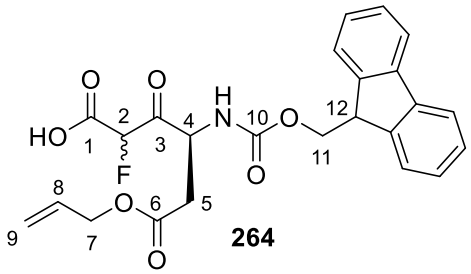

264

β-ketoester **253** (0.19 g, 0.37 mmol) was dissolved in 30% TFA in DCM (16 ml) and left to stir at room temperature for 2.5 h before being concentrated under reduced pressure and subsequently lyophilised to afford the crude product as an off-white solid which was assumed to have been acquired in a quantitative yield, although impurity peaks were also present by ^{1}H NMR spectroscopy. It was then used without further purification. Reported as a mixture of suspected diastereoisomers (dr ~ 44 : 56). ^{1}H NMR (CD_3CN, 599 MHz): δ (ppm) 7.83 (2H, d, $^{3}J_{HH}$ = 7.6, Ar-*H*), 7.65 (2H, d, $^{3}J_{HH}$ = 7.4, Ar-*H*), 7.42 (2H, m, Ar-*H*), 7.34 (2H, m Ar-*H*), 5.91 (1H, m, C**8**-*H*), 5.64 (0.6H, d, $^{2}J_{HF}$ = 47.7, C**2**-*H*), 5.62 (0.4H, d, $^{2}J_{HF}$ = 47.4, C**2**-*H*), 5.29 (2H, m, C**9**-*H*), 4.88 (1H, m, C**4**-*H*), 4.39 (2H, m, C**11**-*H*), 4.24 (1H, t, $^{3}J_{HH}$ = 6.8, C**12**-*H*), 2.83 (2H, m, C**5**-*H*). ^{19}F NMR (CD_3CN, 376 MHz): δ (ppm) -197.34 (d, $^{2}J_{FH}$ = 47.4, C**2**-*F*), -198.54 (d, $^{2}J_{FH}$ = 47.8, C**2**-*F*). LCMS (ESI) *m/z* calculated for $[M+H]^+$ $C_{24}H_{23}NO_7F^+$ 456.2, found 456.4.

Synthesis of 224

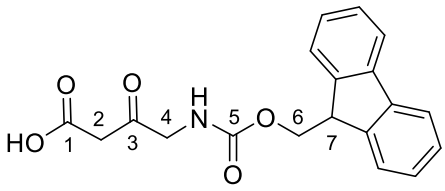

224

β-ketoester **231** (0.20 g, 0.51 mmol) was dissolved in 30% TFA in DCM (26 ml) and left to stir at room temperature for 2.5 h. The reaction mixture was then cautiously concentrated under reduced pressure at 40 ºC through co-evaporation with ether until the product was obtained as a yellow-brown solid (0.15 g, 0.44 mmol, 86%). ^{1}H NMR (CD_3CN, 400 MHz): δ (ppm) 7.84 (2H, d, $^{3}J_{HH}$ = 7.5, Ar-*H*), 7.67 (2H, d, $^{3}J_{HH}$ = 7.4, Ar-*H*), 7.42 (2H, m, Ar-*H*), 7.34 (2H, m, Ar-*H*), 5.97 (1H, br s, N-*H*), 4.36 (2H, d, C**6**-*H*, $^{3}J_{HH}$ = 6.9), 4.25 (1H, t, C**7**-*H*, $^{3}J_{HH}$ = 7.0), 4.02 (2H, d, C**4**-*H*, $^{3}J_{HH}$ = 5.9), 3.46 (2H, s, C**2**-*H*). ^{13}C NMR (CD_3CN, 101 MHz): δ (ppm) 201.1 (C**3**), 168.4 (C**1**), 157.4 (C**5**), 145.0 (Ar), 142.1 (Ar), 128.6 (Ar), 128.1 (Ar), 126.1 (Ar), 120.9 (Ar), 67.3 (C**6**), 51.1 (C**4**), 47.9 (C**7**), 46.4 (C**2**). HRMS (ESI) *m/z* calculated for $[M+H]^+$ $C_{19}H_{18}NO_5$ 340.1185, found 340.1182.

Synthesis of 267 (reported as a suspected mixture of diastereoisomers)

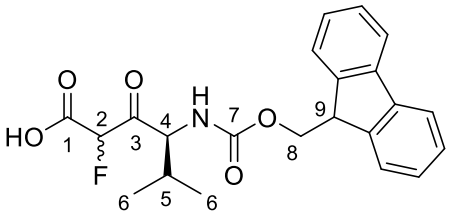

267

β-ketoester **254** (0.15 g, 0.33 mmol) was dissolved in 30% TFA in DCM (5 ml) and left to stir at room temperature for 2 h before being concentrated under reduced pressure and subsequently lyophilised to afford the crude product in what was assumed to be a quantitative yield, although impurity peaks were also present by ^{19}F NMR spectroscopy. It was then used without further purification. Reported as a mixture of suspected diastereoisomers (dr ~ 50 : 50). ^{1}H NMR (CD_3CN, 400 MHz): δ (ppm) 7.84 (2H, d, $^{3}J_{HH}$ = 7.5, Ar-*H*), 7.68 (2H, m, Ar-*H*), 7.42 (2H, m, Ar-*H*), 7.34 (2H, m Ar-*H*), 6.07 (1H, m, N-*H*), 5.57 (0.5H, d, $^{2}J_{HF}$ = 47.9, C**2**-*H*), 5.53 (0.5H, d, $^{2}J_{HF}$ = 48.0, C**2**-*H*), 4.67 (0.5H, m, C**4**-*H*), 4.46 (0.5H, m, C**4**-*H*), 4.35 (2H, m, C**8**-*H*), 4.24 (1H, t, $^{3}J_{HH}$ = 6.8, C**9**-*H*), 2.29 (0.5H, m, C**5**-*H*), 2.18 (0.5H, m, C**5**-*H*), 0.95 (3H, m, C**6**-*H*), 0.84 (3H, m, C**6**-*H*). ^{19}F NMR (CD_3CN, 376 MHz): δ (ppm) -196.84 (d, $^{2}J_{FH}$ = 48.1, C**2**-*F*), -197.74 (d, $^{2}J_{FH}$ = 47.9, C**2**-*F*). HRMS (ESI) *m/z* calculated for $[M+H]^+$ $C_{22}H_{23}NO_5F^+$ 400.1560, found 400.1544.

7.7 Experimental for Chapter 4

Synthesis of 282[6] – General Procedure for the Synthesis of Boc-protected *tert*-Butyl *β*-Ketoesters (282-285)

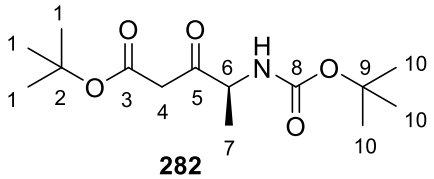

282

To a solution of Boc-Ala-OH (1.00 g, 5.29 mmol) in dry THF (6 ml) was added 1,1′-carbonyldiimidazole (0.86 g, 5.30 mmol) under an atmosphere of nitrogen. The reaction mixture was left to stir at room temperature for 1.5 h in order to generate the corresponding acyl imidazole *in situ*. Simultaneously a solution of *tert*-butyl acetate (2.2 mL, 16.4 mmol) in dry THF (3 ml) was added dropwise under nitrogen to a solution of 2 M (unless stated otherwise) lithium diisopropylamide in dry THF (8.2 mL, 16.4 mmol) which had been cooled to -78 °C. The resulting solution was left to stir at -78 °C for 20 min before the addition of the acyl imidazole-containing solution at -78 °C. The reaction mixture was stirred at -78 °C under inert conditions for a further 45 min (unless stated otherwise) before being quenched with 10% *w/v* citric acid (30 ml), extracted into EtOAc (3-4 x 15 ml) and washed with sat. $NaHCO_3$ (2 x 20 ml) and brine (1 x 20 ml). The combined organic phases were concentrated *in vacuo* and subsequent purification by silica gel flash column chromatography (hexane : ethyl acetate, 1 : 0 to 7 : 3) gave the pure product as a yellow oil (0.49 g, 1.24 mmol, 37%). ^{1}H NMR ($CDCl_3$, 400 MHz): δ (ppm) 5.17 (1H, br s, N-*H*), 4.36 (1H, m, C**6**-*H*), 3.47 & 3.42 (2H, ABq, $^2J_{AB}$ = 16.0, C**4**-*H*), 1.45 (9H, s, C**1**-*H*), 1.42 (9H, s, C**10**-*H*), 1.33 (3H, d, C**7**-*H*, $^3J_{HH}$ = 7.2). ^{13}C NMR ($CDCl_3$, 101 MHz): δ (ppm) 203.0 (C**5**), 166.3 (C**3**), 155.3 (C**8**), 82.4 (C**2**), 80.1 (C**9**), 55.5 (C**6**), 47.3 (C**4**), 28.4 (C**10**), 28.0 (C**1**), 17.3 (C**7**). HRMS (ESI) *m/z* calculated for $[M+H]^+$ $C_{14}H_{26}NO_5^+$ 288.1811, found 288.1805. Characterisation data was found to be consistent with the literature.[6]

Synthesis of 283[7]

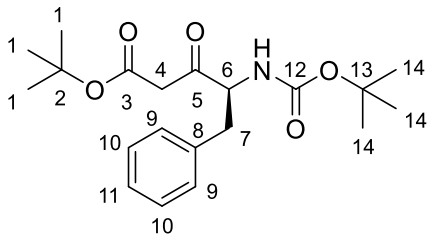

283

According to the general procedure, Boc-Phe-OH (3.00 g, 11.3 mmol) and 1,1′-carbonyldiimidazole (1.83 g, 11.3 mmol) in dry THF (18 mL) were reacted under nitrogen and the resulting acyl imidazole added to a solution in which *tert*-butyl acetate (4.7 mL, 35.0 mmol) in dry THF (9 ml) and 2 M lithium diisopropylamide in dry THF (17.5 mL, 35.0 mmol) had been reacted together. The isolated crude material was purified by silica gel flash column chromatography (hexane : ethyl acetate, 1 : 0 to 8 : 2) to give the pure product as a yellow oil (1.88 g, 5.17 mmol, 46%). ^{1}H NMR ($CDCl_3$, 400 MHz): δ (ppm) 7.24 (5H, m, Ph-*H*), 5.04 (1H, d, $^{3}J_{HH}$ = 7.9, N-*H*), 4.57 (1H, q, $^{3}J_{HH}$ = 7.4, C**6**-*H*), 3.41 & 3.36 (2H, ABq, $^{2}J_{AB}$ = 14.0, C**4**-*H*), 3.15 (1H, dd, $^{2}J_{HH}$ = 14.1, $^{3}J_{HH}$ = 6.1, C**7**-*H*), 2.97 (1H, dd, $^{2}J_{HH}$ = 14.1, $^{3}J_{HH}$ = 7.3, C**7**-*H*), 1.45 (9H, s, C**1**-*H*), 1.39 (9H, s, C**14**-*H*). ^{13}C NMR ($CDCl_3$, 101 MHz): δ (ppm) 202.4 (C**5**), 166.2 (C**3**), 155.3 (C**12**), 136.4 (Ar), 129.4 (Ar), 128.8 (Ar), 127.1 (Ar), 82.4 (C**2**), 80.2 (C**13**), 60.6 (C**6**), 48.3 (C**4**), 37.2 (C**7**), 28.4 (C**14**), 28.1 (C**1**). HRMS (ESI) *m/z* calculated for $[M+H]^+$ $C_{20}H_{30}NO_5^+$ 364.2124, found 364.2106. Characterisation data was found to be consistent with the literature.[7]

Synthesis of 284

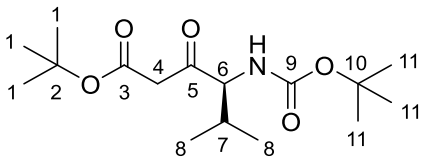

284

According to the general procedure, Boc-Val-OH (2.00 g, 9.21 mmol) and 1,1′-carbonyldiimidazole (1.49 g, 9.19 mmol) in dry THF (12 ml) were reacted under nitrogen and the resulting acyl imidazole added to a solution in which *tert*-butyl acetate (3.8 mL, 28.3 mmol) in dry THF (6 ml) and 1 M lithium diisopropylamide in dry THF (29 mL, 29.0 mmol) had been reacted together. The isolated crude material was purified by silica gel flash column chromatography (hexane : ethyl acetate, 1 : 0 to 4 : 1) to give the pure product as a yellow oil (1.68 g, 5.33 mmol, 58%). ^{1}H NMR ($CDCl_3$, 400 MHz): δ (ppm) 5.18 (1H, d, $^{3}J_{HH}$ = 8.9, N-*H*), 4.18 (1H, dd, $^{3}J_{HH}$ = 9.0, $^{3}J_{HH}$ = 4.3, C**6**-*H*), 3.30 & 3.30 (2H, ABq, $^{2}J_{AB}$ = 16.0, C**4**-*H*), 2.09 (1H, m, C**7**-*H*), 1.30 (9H, s, C**1**-*H*), 1.28 (9H, s, C**11**-*H*), 0.84 (3H, d, $^{3}J_{HH}$ = 6.8, C**8**-*H*) 0.65 (3H, d, $^{3}J_{HH}$ = 6.8, C**8**-*H*). ^{13}C NMR ($CDCl_3$, 101 MHz): δ (ppm) 202.4 (C**5**), 165.8 (C**3**), 155.7 (C**9**), 81.8 (C**2**), 79.4 (C**10**), 64.1 (C**6**), 48.1 (C**4**), 29.2 (C**7**), 28.1 (C**11**), 27.7 (C**1**), 19.6 (C**8**), 16.5 (C**8**). HRMS (ESI) *m/z* calculated for $[M\text{-}Boc+H]^+$ $C_{16}H_{30}NO_5^+$ 316.2124, found 316.2125.

Synthesis of 285

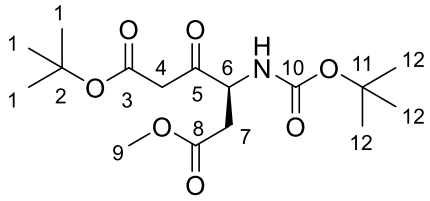

285

According to the general procedure (with scaled up volumes of solvent), Boc-Asp(OMe)-OH (3.00 g, 12.1 mmol) and 1,1′-carbonyldiimidazole (2.00 g, 12.3 mmol) in dry THF (18 ml) were reacted under nitrogen and the resulting acyl imidazole added to a solution in which *tert*-butyl acetate (5.1 mL, 38.0 mmol) in dry THF (9 ml) and 2 M lithium diisopropylamide in dry THF (18.8 mL, 37.6 mmol) had been reacted together. Resulting reaction mixture was left to stir at -78 ºC for 4 h. The isolated crude material was purified by silica gel flash column chromatography (hexane : ethyl acetate, 1 : 0 to 8 : 2) to give the product as a yellow oil (0.61 g, 1.77 mmol, 15%). ^{1}H NMR ($CDCl_3$, 400 MHz): δ (ppm) 5.66 (1H, d, $^{3}J_{HH}$ = 9.1, N-*H*), 4.53 (1H, dt, $^{3}J_{HH}$ = 9.4, $^{3}J_{HH}$ = 4.9, C**6**-*H*), 3.53 & 3.50 (2H, ABq, $^{2}J_{AB}$ = 16.0, C**4**-*H*), 2.92 (1H, dd, $^{2}J_{HH}$ = 17.1, $^{3}J_{HH}$ = 5.1, C**7**-*H*), 2.73 (1H, dd, $^{2}J_{HH}$ = 17.2, $^{3}J_{HH}$ = 4.7, C**7**-*H*), 1.42 (9H, s, C**1**-*H*), 1.41 (9H, s, C**12**-*H*). ^{13}C NMR ($CDCl_3$, 101 MHz): δ (ppm) 201.8 (C**5**), 171.9 (C**8**), 166.2 (C**3**), 155.4 (C**10**), 82.2 (C**2**), 80.5 (C**11**), 56.1 (C**6**) 52.1 (C**9**), 47.2 (C**4**) 35.2 (C**7**), 28.3 (C**12**), 28.0 (C**1**). HRMS (ESI) *m/z* calculated for $[M+H]^+$ $C_{16}H_{28}NO_7^+$ 346.1866, found 346.1855.

Synthesis of 286 (reported as a mixture of diastereoisomers)

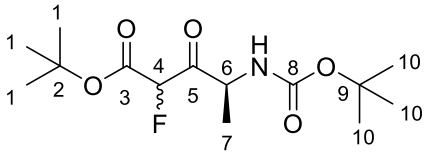

286

To a solution of *β*-ketoester **282** (0.57 g, 1.98 mmol) and 5 mol % $CpTiCl_3$ (22 mg, 0.10 mmol) in MeCN (20 ml) was added F-TEDA (0.78 g, 2.20 mmol). The reaction mixture was left to stir at room temperature overnight and subsequently concentrated under reduced pressure. The resulting crude material was purified by silica gel flash column chromatography (hexane : ethyl acetate, 1 : 0 to 7 : 3) to give the product as a yellow oil (0.33 g, 1.08 mmol, 54%). Reported as a mixture of diastereoisomers (dr ~ 80 : 20), as determined by ^{19}F NMR spectroscopy. ^{1}H NMR ($CDCl_3$, 400 MHz): δ (ppm) 5.32 (0.8H, d, $^{2}J_{HF}$ = 49.0, C**4**-*H*), 5.28 (0.2H, d, $^{2}J_{HF}$ = 48.9, C**4**-*H*), 5.12 (1H, br m, N-*H*), 4.70 (1H, br m, C**6**-*H*), 1.48 (9H, m, C**1**-*H*), 1.40 (9H, s, C**10**-*H*), 1.32 (3H, m, C**7**-*H*). ^{13}C NMR ($CDCl_3$, 101 MHz): δ (ppm) 201.1 (d, $^{2}J_{CF}$ = 21.6, C**5**), 162.7 (d, $^{2}J_{CF}$ = 23.7, C**3**), 155.0 (C**8**), 90.5 (d, C**4**, $^{1}J_{CF}$ = 196.9), 84.9 (C**2**), 84.8 (C**2**), 80.3 (C**9**), 80.2 (C**9**), 52.9 (C**6**), 52.1 (C**6**), 28.3 (C**10**), 27.9 (C**1**), 27.9 (C**1**), 17.1 (C**7**), 16.9 (C**7**). ^{19}F NMR ($CDCl_3$, 376 MHz): δ (ppm) -196.17 (d, $^{2}J_{FH}$ = 48.8, C**4**-*F*), -197.03 (d, $^{2}J_{FH}$ = 48.9, C**4**-*F*). HRMS (ESI) *m/z* calculated for $[M+H]^+$ $C_{14}H_{25}NO_5F^+$ 306.1717, found 306.1713.

Synthesis of 287 (reported as a mixture of diastereoisomers)

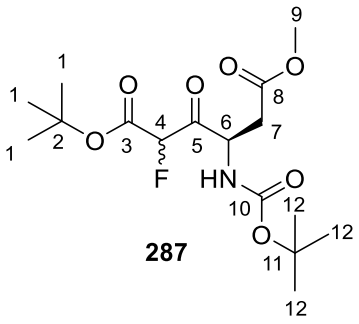

287

To a solution of *β*-ketoester **285** (1.07 g, 3.10 mmol) and 5 mol % $CpTiCl_3$ (34 mg, 0.16 mmol) in MeCN (50 ml) was added F-TEDA (1.15 g, 3.25 mmol). The reaction mixture was left to stir at room temperature overnight and subsequently concentrated under reduced pressure. The resulting crude material was purified by silica gel flash column chromatography (hexane : ethyl acetate, 1 : 0 to 8 : 2) to give the pure product as a clear oil (0.50 g, 1.36 mmol, 44%). Reported as a mixture of diastereoisomers (dr ~ 50 : 50), as determined by ^{19}F NMR spectroscopy. ^{1}H NMR ($CDCl_3$, 400 MHz): δ (ppm) 5.58 (1H, br d, $^{3}J_{HH}$ = 8.6, N-*H*), 5.39 (0.5H, d, $^{2}J_{HF}$ = 48.6, C**4**-*H*), 5.35 (0.5H, d, $^{2}J_{HF}$ = 49.0, C**4**-*H*), 4.81 (1H, br m, C**6**-*H*), 3.65 (1.5H, m, C**9**-*H*), 3.62 (1.5H, m, C**9**-*H*), 3.05 (1H, dd, $^{2}J_{HH}$ = 17.2, $^{3}J_{HH}$ = 4.9, C**7**-*H*), 2.84 (1H, m, C**7**-*H*), 1.46 (9H, m, C**1**-*H*), 1.39 (9H, br s, C**12**-*H*). ^{13}C NMR ($CDCl_3$, 101 MHz): δ (ppm) 198.3 (d, $^{2}J_{CF}$ = 20.8, C**5**), 198.0 (d, $^{2}J_{CF}$ = 22.5, C**5**), 171.6 (C**8**), 171.2 (C**8**), 162.6 (d, $^{2}J_{CF}$ = 23.8, C**3**), 162.5 (d, $^{2}J_{CF}$ = 23.8, C**3**), 155.2 (C**10**), 155.0 (C**10**), 90.6 (d, C**4**, $^{1}J_{CF}$ = 196.4), 89.7 (d, C**4**, $^{1}J_{CF}$ = 196.5), 84.9 (C**2**), 84.8 (C**2**), 80.7 (C**11**), 80.5 (C**11**), 54.3 (C**6**), 53.6 (C**6**), 52.2 (C**9**), 52.2 (C**9**), 35.5 (C**7**), 35.1 (C**7**), 28.3 (C**12**), 27.9 (C**1**), 27.8 (C**1**). ^{19}F NMR ($CDCl_3$, 376 MHz): δ (ppm) -195.16 (d, $^{2}J_{FH}$ = 49.0, C**4**-*F*), -196.30 (d, $^{2}J_{FH}$ = 48.9, C**4**-*F*). HRMS (ESI) *m/z* calculated for $[M\text{-}^{t}Bu\text{-}Boc+H]^{+}$ $C_7H_{11}NO_5F^{+}$ 208.0621, found 208.0637.

Synthesis of 288 (reported as a mixture of diastereoisomers)

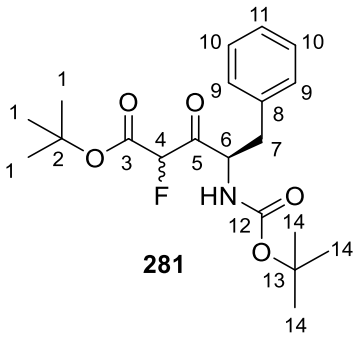

281

To a solution of *β*-ketoester **283** (0.34 g, 0.94 mmol) and 5 mol % $CpTiCl_3$ (9.7 mg, 44 µmol) in MeCN (20 ml) was added F-TEDA (0.37 g, 1.04 mmol). The reaction mixture was left to stir at room temperature overnight and subsequently concentrated under reduced pressure. The resulting crude material was purified by silica gel flash column chromatography (hexane : ethyl acetate, 1 : 0 to 8 : 2) to give the pure product as a clear oil (0.23 g, 0.60 mmol, 64%). Reported as a mixture of diastereoisomers (dr ~ 50 : 50), as determined by ^{1}H NMR spectroscopy. ^{1}H NMR ($CDCl_3$, 400 MHz): δ (ppm) 7.25 (5H, m, Ph-*H*), 5.30 (0.5H, d, $^2J_{HH}$ = 48.9), 5.19 (0.5H, d, $^2J_{HH}$ = 48.5), 4.97 (1H, m, N-*H* & C**6**-*H*), 3.18 (1H, m, C**7**-*H*), 2.88 (1H, m, C**7**-*H*), 1.50 (4.5H, s, C**1**-*H*), 1.48 (4.5H, s, C**1**-*H*), 1.37 (9H, s, C**14**-*H*). ^{13}C NMR ($CDCl_3$, 101 MHz): δ (ppm) 200.0 (m, C**5**), 162.6 (d, $^2J_{CF}$ = 23.5, C**3**), 155.1 (C**12**), 135.8 (Ar), 135.6 (Ar), 129.5 (Ar), 128.9 (Ar), 128.8 (Ar), 127.3 (Ar), 127.2 (Ar), 90.8 (d, C**4**, $^1J_{CF}$ = 198.0), 85.1 (C**2**), 84.9 (C**2**), 80.5 (C**11**), 80.3 (C**11**), 58.0 (C**6**), 57.3 (C**6**), 37.3 (C**7**), 36.6 (C**7**), 28.3 (C**14**), 28.0 (C**1**). ^{19}F NMR ($CDCl_3$, 376 MHz): δ (ppm) -195.61 (d, $^2J_{FH}$ = 48.9, C**4**-*F*), -196.30 (d, $^2J_{FH}$ = 48.6, C**4**-*F*). HRMS (ESI) *m/z* calculated for $[M\text{-}^t\text{Bu-Boc+H}]^+$ $C_{11}H_{13}NO_3F^+$ 226.0879, found 226.0864.

Synthesis of 289

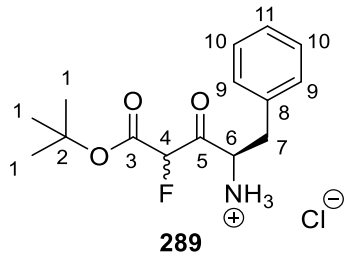

289

β-ketoester **288** (0.33 g, 0.87 mmol) was dissolved in 1 M HCl in EtOAc (4.3 mL, 4.33 mmol) and left to stir at 40 ºC for 2.5 h. Careful concentration under reduced pressure at 40-50 ºC gave the crude material (including product **289** and impurities) in what was assumed to be a quantitative yield. It was then rapidly used without further purification. ^{19}F NMR (CD_3OD, 376 MHz): δ (ppm) -199.42 (d, $^2J_{FH}$ = 47.2, C**4**-*F*). HRMS (ESI) *m/z* calculated for $[M\text{-}^tBu+H]^+$ $C_{11}H_{13}NO_3F^+$ 226.0879, found 226.0877.

Synthesis of 290

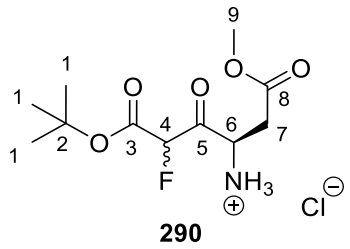

290

β-ketoester **287** (59.0 mg, 0.16 mmol) was dissolved in 1 M HCl in EtOAc (0.97 mL, 0.97 mmol) and left to stir at 50 ºC for 3.5 h. Careful concentration under reduced pressure at 40-50 ºC gave the crude material (including product **290** and impurities) in what was assumed to be a quantitative yield. It was then rapidly used without further purification. ^{1}H NMR (CD_3OD, 400 MHz): δ (ppm) 5.78 (1H, d, $^2J_{HH}$ = 48.9, C**4**-*H*), 4.73 (1H, m, C**6**-*H*), 3.73 (3H, m, C**9**-*H*), 3.20 (2H, m, C**7**-*H*), 1.53 (9H, m, C**1**-*H*). ^{19}F NMR (CD_3OD, 376 MHz): δ (ppm) -199.61 (d, $^2J_{FH}$ = 47.3, C**4**-*F*). HRMS (ESI) *m/z* calculated for $[M+H]^+$ $C_{11}H_{19}NO_5F^+$ 264.1247, found 264.1245.

Synthesis of FMK 291 in crude form

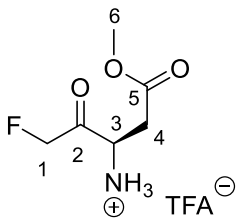

291

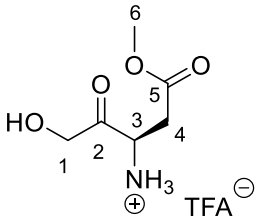

294

β-ketoester **287** (70.0 mg, 0.19 mmol) was dissolved in 50% TFA in DCM (6 ml) and left to stir at 40 ºC for 2.5 h. Concentration under reduced pressure and subsequent lyophilisation gave the crude material (including product **291** and hydroxymethyl ketone analogue **294**) in what was assumed to be a quantitative yield. It was then rapidly used without further purification. ^{19}F NMR ($CDCl_3$, 376 MHz): δ (ppm) -215.26 (t, $^2J_{HH}$ = 48.9, C**1**-*F*). LCMS (ESI) *m/z* calculated for **284**: $[M+H]^+$ $C_6H_{11}FNO_3^+$ 164.1, found 164.1. Evidence for the hydroxymethyl ketone analogue (**294**) was also found: LCMS (ESI) *m/z* calculated for $[M+H]^+$ $C_6H_{12}NO_4^+$ 162.1, found 162.1.

Synthesis of *L*-Alanine Methyl Ester Hydrochloride (301)[8]

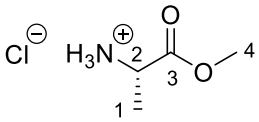

301

A solution of *L*-alanine (5.03 g, 56.5 mmol) in MeOH (50 ml) was cooled to 0 ºC before $SOCl_2$ (8.2 mL, 0.11 mol) was added dropwise and left to stir at room temperature overnight. The reaction mixture was concentrated *in vacuo* to yield the product as a white solid (7.88 g, 56.5 mmol, >99%). ^{1}H NMR (CD_3CN, 599 MHz): δ (ppm) 4.79 (3H, br s, N-*H*$_3$), 4.11 (1H, q, C**2**-*H*, $^3J_{HH}$ = 7.3), 3.81 (3H, s, C**4**-*H*), 1.53 (3H, d, C**1**-*H*, $^3J_{HH}$ = 7.3). ^{13}C NMR (CD_3CN, 151 MHz): δ (ppm) 171.4 (C**3**), 53.7 (C**4**), 49.9 (C**2**), 16.2 (C**1**). HRMS (ESI) *m/z* calculated for $[M+H]^+$ $C_4H_{10}NO_2^+$ 104.0712, found 104.0687 Characterisation data was found to be consistent with the literature.[8]

Synthesis of Benzyloxycarbonyl-*L*-valyl-*L*-alanine Methyl Ester (303)[9]

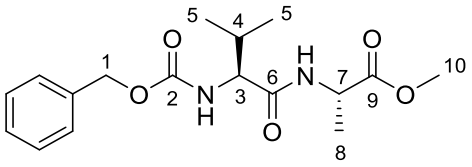

303

A solution of *L*-alanine methyl ester hydrochloride (**302**) (0.47 g, 3.37 mmol) and DIPEA (1.2 mL, 6.89 mmol) in DCM (20 ml) was stirred for 5 min followed by subsequent addition of Cbz-Val-OH (0.85 g, 3.38 mmol) and PyBop (1.94 g, 3.73 mmol). The reaction mixture was left to stir at room temperature overnight before being concentrated under reduced pressure. The resulting crude material was purified by silica gel flash column chromatography (hexane : ethyl acetate, 1 : 0 to 3 : 7) to give the pure product as a white solid (0.59 g, 1.75 mmol, 52%). ^{1}H NMR ($CDCl_3$, 400 MHz): δ (ppm) 7.32 (5H, m, Ph-*H*), 6.69 (1H, m, N-*H*), 5.55 (1H, m, N-*H*), 5.11 & 5.08 (2H, ABq, $^{2}J_{AB}$ = 12.0, C**1**-*H*), 4.57 (1H, m, C**7**-*H*), 4.07 (1H, m, C**3**-*H*), 3.73 (3H, s, C**10**-*H*), 2.09 (1H, m, C**4**-*H*), 1.38 (3H, d C**8**-*H*, $^{3}J_{HH}$ = 7.5), 0.97 (3H, d, C**5**-*H*, $^{3}J_{HH}$ = 6.8), 0.93 (3H, d, C**5**-*H,* $^{3}J_{HH}$ = 6.8). ^{13}C NMR ($CDCl_3$, 101 MHz): δ (ppm) 173.3 (C**9**), 171.0 (C**6**), 156.5 (C**2**), 136.3 (Ph), 128.6 (Ph), 128.3 (Ph), 128.1 (Ph), 67.1 (C**1**), 60.3 (C**3**), 52.6 (C**10**), 48.1 (C**7**), 31.5 (C**4**), 19.2 (C**5**), 18.2 (C**8**), 17.9 (C**5**). HRMS (ESI) m/z calculated for $[M+H]^+$ $C_{17}H_{25}N_2O_5^+$ 337.1763, found 337.1750. Compound identity was also confirmed by single crystal X-ray crystallography (**Appendix A1.2**). Characterisation data was found to be consistent with the literature.[9,10]

Synthesis of Cbz-Val-Ala-OH (304)[11]

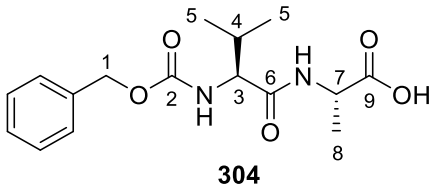

304

To a solution of benzyloxycarbonyl-*L*-valyl-*L*-alanine methyl ester **303** (0.47, 1.40 mmol) in 2 : 1 THF : H_2O (30 ml) was added LiOH.H_2O (58.0 mg, 1.38 mmol). The reaction mixture was left to stir at room temperature for 96 h followed by THF removal *in vacuo*. Subsequent acidification to p*H* 4 with 10% *w/v* citric acid followed by extraction with ethyl acetate (3 x 15 ml), drying of the combined organic phases over anhydrous $MgSO_4$, filtration and solvent removal *in vacuo* gave the product as a white solid (0.37 g, 1.15 mmol, 82%). ^{1}H NMR (CD_3OD, 400 MHz): δ (ppm) 7.33 (5H, m, Ph-*H*), 5.09 & 5.09 (2H, ABq, $^2J_{AB}$ = 12.0, C**1**-*H*), 4.39 (1H, q, C**7**-*H*, $^3J_{HH}$ = 7.3), 3.97 (1H, m, C**3**-*H*), 2.06 (1H, m, C**4**-*H*), 1.40 (3H, d C**8**-*H*, $^3J_{HH}$ = 7.3), 0.99 (3H, d, C**5**-*H*, $^3J_{HH}$ = 6.8), 0.94 (3H, d, C**5**-*H,* $^3J_{HH}$ = 6.8). ^{13}C NMR (CD_3OD, 101 MHz): δ (ppm) 175.7 (C**9**), 173.9 (C**6**), 158.6 (C**2**), 138.2 (Ph), 129.5 (Ph), 129.0 (Ph), 128.8 (Ph), 67.7 (C**1**), 61.8 (C**3**), 49.3 (C**7**), 32.2 (C**4**), 19.7 (C**5**), 18.4 (C**5**), 17.7 (C**8**). HRMS (ESI) m/z calculated for $[M+H]^+$ $C_{16}H_{22}N_2O_5^+$ 323.1607, found 323.1600. Characterisation data was found to be consistent with the literature.[11]

Synthesis of Cbz-Tyr(O^{t}Bu)-Val-Ala-OH (305)

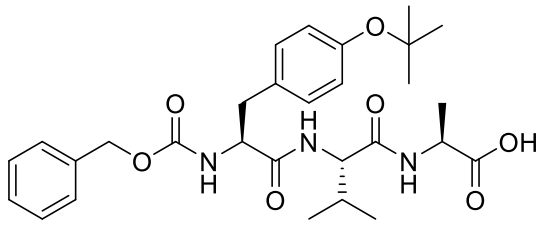

305

According to the general procedure described in **Section 7.3.2**, the linear peptide was synthesised via manual Fmoc SPPS at room temperature on a 1.50 mmol scale using pre-loaded H-Ala-2-Cltrt resin (0.72 mmol/g loading). All couplings were single couplings, and a final Cbz protection step was carried out as described in **Section 7.3.4**. Mild TFE cleavage of the resin was achieved according to **Section 7.3.7.3**, affording the desired peptide, with a purity of 79% as determined by analytical HPLC (**Section 7.3.8.4**), as a white solid (0.14 g, 0.26 mmol, 17%) which was used without further purification. HRMS (ESI) m/z calculated for $[M+H]^+$ $C_{29}H_{40}N_3O_7^+$ 542.2866, found 542.2858.

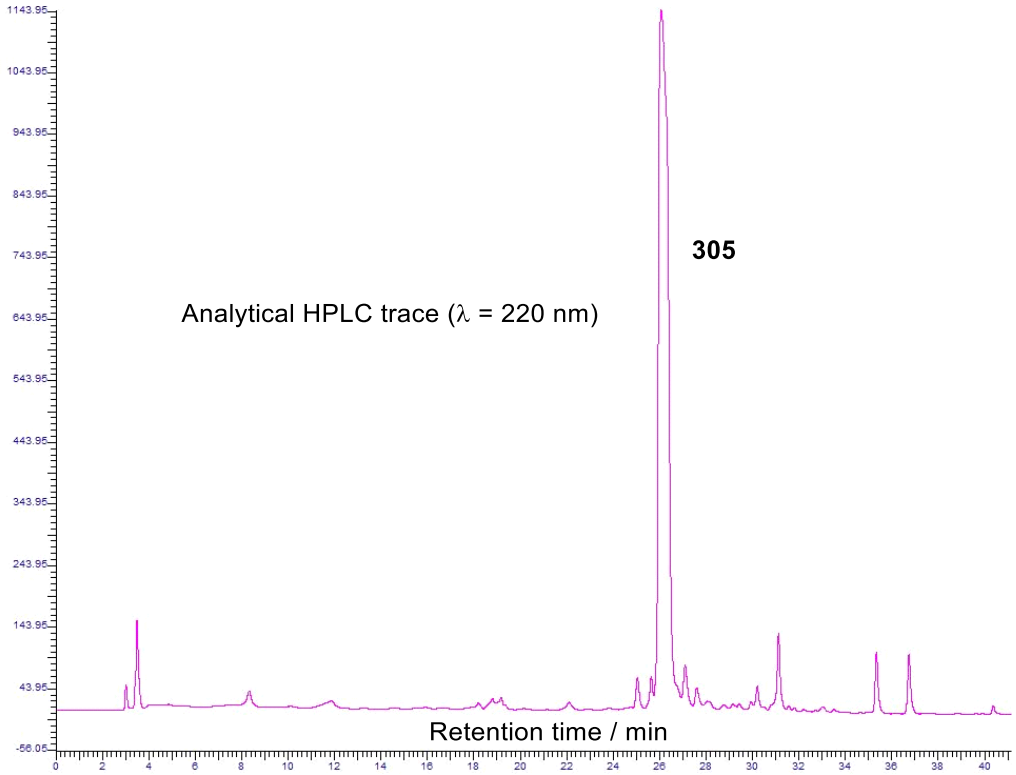

Synthesis of Cbz-Val-Asp(OMe)-Val-Ala-OH (306)

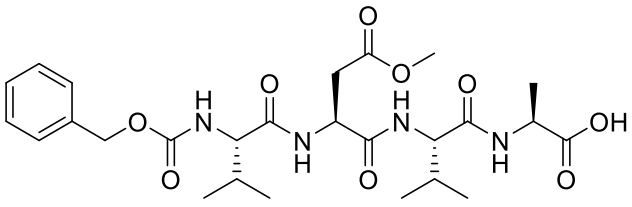

306

According to the general procedure described in **Section 7.3.2**, the linear peptide was synthesised via manual Fmoc SPPS at room temperature on a 1.70 mmol scale using pre-loaded Fmoc-Ala-Wang resin (0.68 mmol/g loading). All couplings were single couplings, with the final monomer being coupled as the Cbz-protected amino acid (Cbz-Val-OH). Full TFA cleavage of the resin was achieved according to **Section 7.3.7.2**, affording the desired peptide, with a purity of 42% as determined by analytical HPLC (**Section 7.3.8.4**), as an off-white solid (0.97 g, 1.76 mmol, assume quantitative) which was used without further purification. HRMS (ESI) m/z calculated for $[M+H]^+$ $C_{26}H_{39}N_4O_9^+$ 551.2717, found 551.2725.

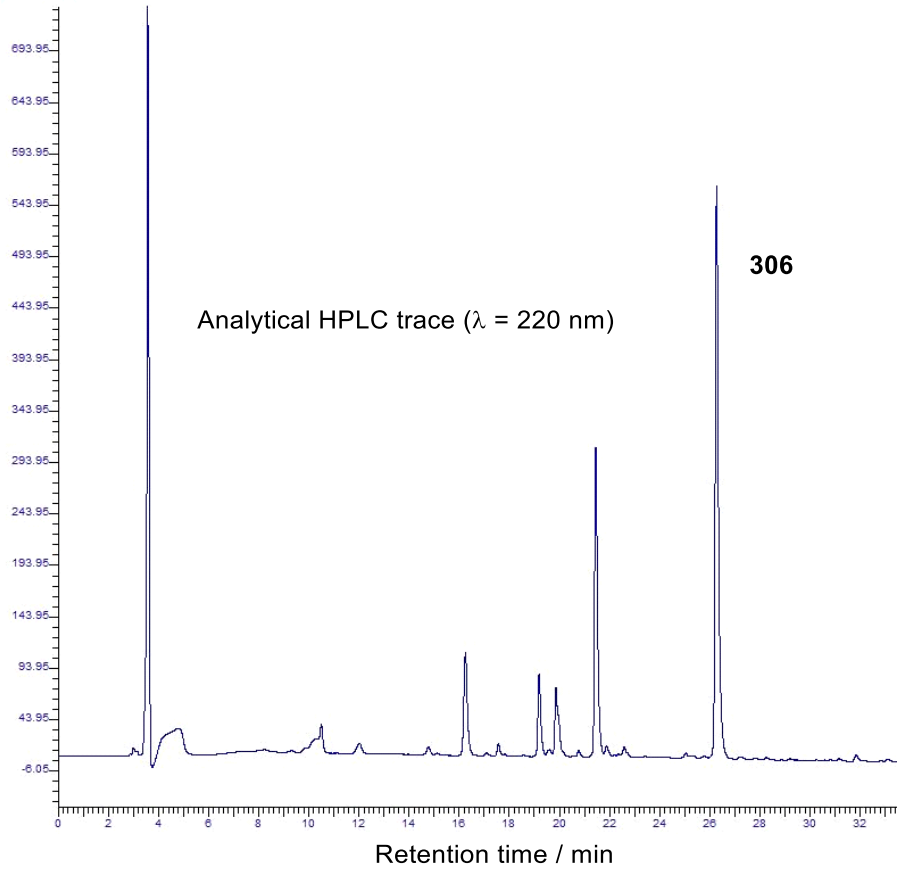

Synthesis of Cbz-Asp(OMe)-Glu(OMe)-Val-OH (307)

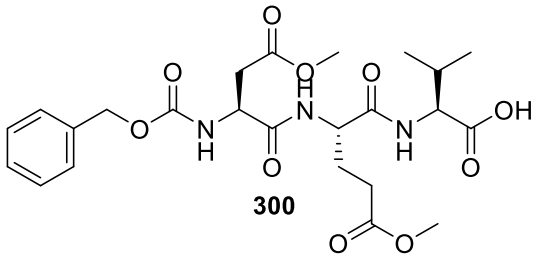

300

According to the general procedure described in **Section 7.3.2**, the linear peptide was synthesised via manual Fmoc SPPS at room temperature on a 1.70 mmol scale using pre-loaded Fmoc-Val-Wang resin (0.69 mmol/g loading). All couplings were single couplings, with the final monomer being coupled as the Cbz-protected amino acid (Cbz-Asp(OMe)-OH). Full TFA cleavage of the resin was achieved according to **Section 7.3.7.2**, affording the desired peptide, with a purity of 77% as determined by analytical HPLC (**Section 7.3.8.4**), as a white solid (0.26 g, 0.50 mmol, 29%) after HPLC purification (by Neil Colgin at CRB) (**Section 7.3.8.3**). HRMS (ESI) m/z calculated for $[M+H]^+$ $C_{24}H_{34}N_3O_{10}^+$ 524.2244, found 524.2240.

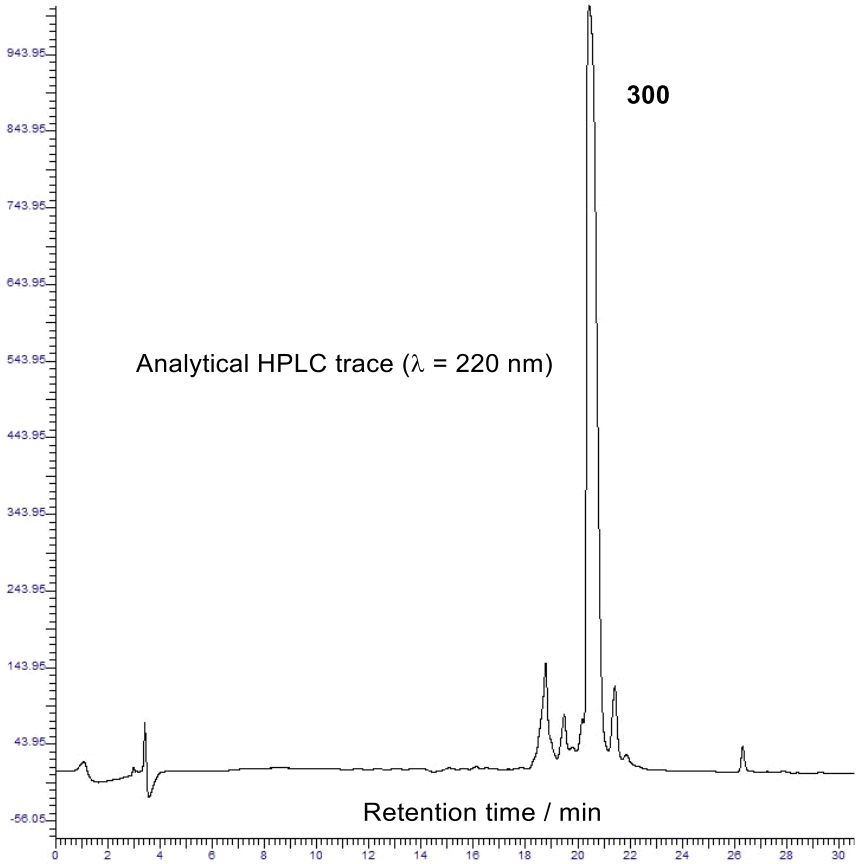

Synthesis of Cbz-Val-Glu(OMe)-Ile-OH (308)

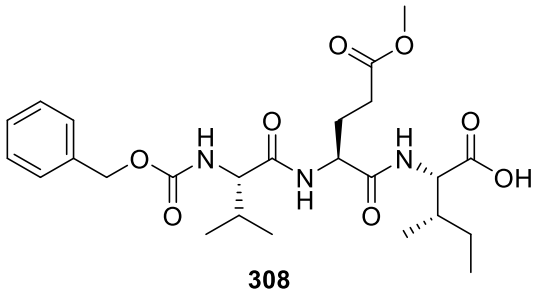

308

According to the general procedure described in **Section 7.3.2**, the linear peptide was synthesised via manual Fmoc SPPS at room temperature on a 0.92 mmol scale using pre-loaded Fmoc-Ile-Wang resin (0.69 mmol/g loading). All couplings were single couplings, with the final monomer being coupled as the Cbz-protected amino acid (Cbz-Val-OH). Full TFA cleavage of the resin was achieved according to **Section 7.3.7.2**, affording the desired peptide, with a purity of 72%, as determined by analytical HPLC (**Section 7.3.8.5**), as a white solid (0.16 g, 0.32 mmol, 35%) after HPLC purification (by Neil Colgin at CRB) (**Section 7.3.8.3**). HRMS (ESI) m/z calculated for $[M+H]^+$ $C_{25}H_{38}N_3O_8^+$ 508.2659, found 508.2667.

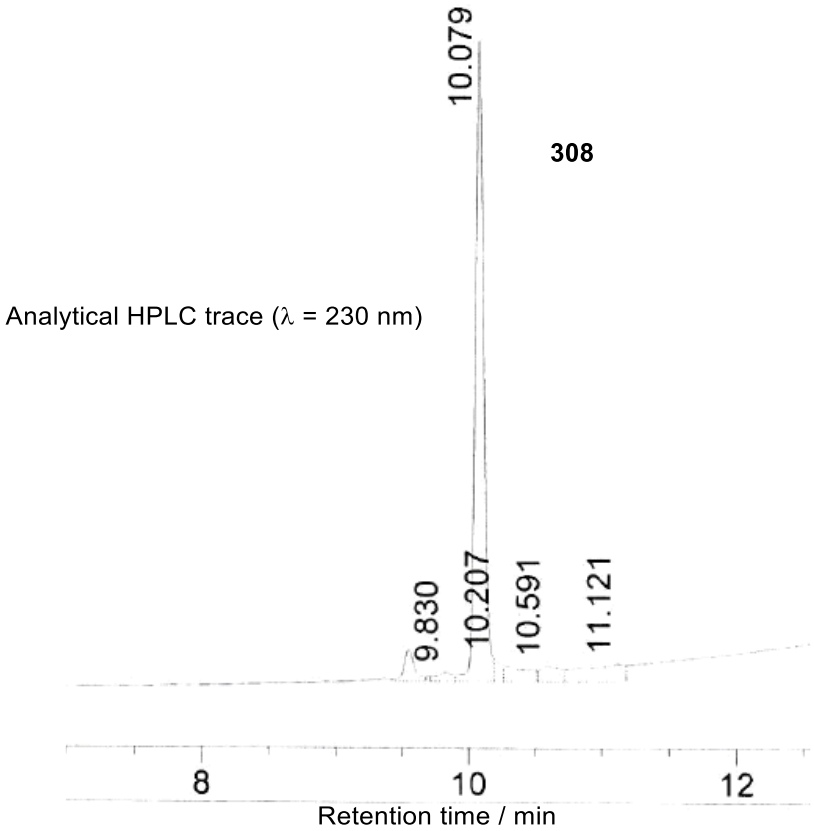

Synthesis of Cbz-Ile-Glu(OMe)-Thr-OH (309)

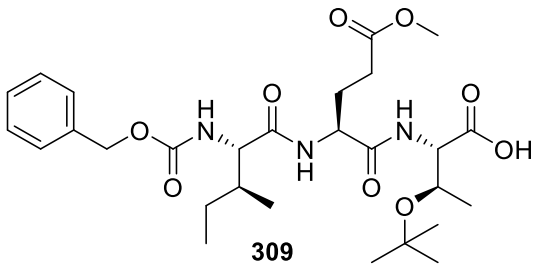

309

According to the general procedure described in **Section 7.3.2**, the linear peptide was synthesised via manual Fmoc SPPS at room temperature on a 1.44 mmol scale using pre-loaded H-L-Thr(^{t}Bu)-2-Cltrt resin (0.63 mmol/g loading). All couplings were single couplings, with the final monomer being coupled as the Cbz-protected amino acid (Cbz-Ile-OH). Mild TFE cleavage of the resin was achieved according to **Section 7.3.7.3**, affording the desired peptide, with a purity of 51% as determined by analytical HPLC (**Section 7.3.8.4**) as an off-white solid (0.38 g, 0.67 mmol, 47%) which was used without further purification. HRMS (ESI) m/z calculated for $[M+H]^+$ $C_{28}H_{44}N_3O_9^+$ 566.3078, found 566.3083.

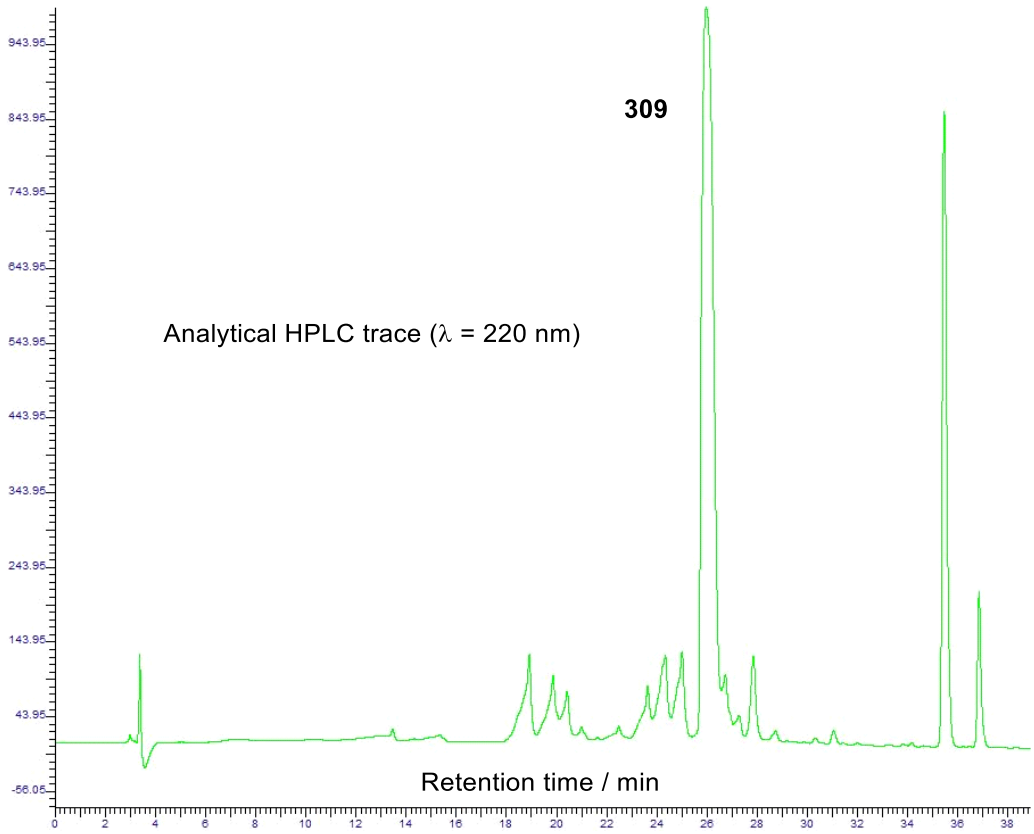

Synthesis of 310

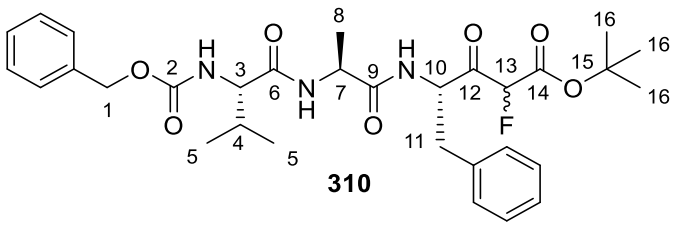

310

To a solution of **289** (0.28 g, 0.88 mmol) and *N*-methylmorpholine (0.67 mL, 6.09 mmol) in DCM was added Cbz-Val-Ala-OH (**304**) (0.28 g, 0.87 mmol) and PyBop (0.50 g, 0.96 mmol). The resulting solution was left to stir at room temperature for 5 days before being concentrated *in vacuo*. Subsequent purification by silica gel flash column chromatography (hexane : ethyl acetate, 1 : 0 to 1 : 1) afforded the product as a clear oil (0.19 g, 0.32 mmol, 36%). ^{1}H NMR ($CDCl_3$, 400 MHz): δ (ppm)‡ 7.23 (10H, m, Ph-*H*), 7.04 (1H, m, N-*H*), 6.87 (1H, m, N-*H*), 5.63 (1H, m, N-*H*), 5.47-4.94 (4H, m, C**13**-*H* & C**10**-*H* & C**1**-*H*), 4.48 (1H, m, C**7**-*H*), 4.03 (1H, m, C**3**-*H*), 3.02 (2H, m, C**11**-*H*), 2.06 (1H, m, C**4**-*H*), 1.48 (9H, m, C**16**-*H*), 1.25 (3H, m, C**8**-*H*), 0.89 (6H, m, C**5**-*H*). ^{19}F NMR ($CDCl_3$, 376 MHz): δ (ppm)* -195.22 (d, $^{2}J_{FH}$ = 48.5, C**13**-*F*), -195.52 (d, $^{2}J_{FH}$ = 48.7, C**13**-*F*), -196.03 (d, $^{2}J_{FH}$ = 48.6, C**13**-*F*), -196.10 (d, $^{2}J_{FH}$ = 48.4, C**13**-*F*). HRMS (ESI) *m/z* calculated for $[M+H]^+$ $C_{31}H_{41}N_3O_7F^+$ 586.2929, found 586.2939. *Note* – Exists as an inseparable mixture of diastereoisomers. ‡ ^{1}H NMR data suggests the presence of rotamers. * ^{19}F NMR data suggests the presence of rotamers.

Synthesis of 311

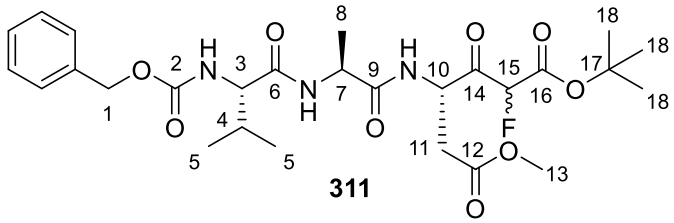

311

To a solution of **290** (0.15 g, 0.50 mmol) and *N*-methylmorpholine (0.37 mL, 3.37 mmol) in DCM was added Cbz-Val-Ala-OH (**304**) (0.15 g, 0.50 mmol) and PyBop (0.28 g, 0.54 mmol). The resulting solution was left to stir at room temperature for 48 h before being concentrated *in vacuo*. Subsequent purification by silica gel flash column chromatography (hexane : ethyl acetate, 1 : 0 to 1 : 1) afforded the product as a clear oil (60.0 mg, 0.11 mmol, 22%). ^{1}H NMR ($CDCl_3$, 599 MHz): δ (ppm)‡ 7.33 (6H, m, N-*H* & Ph-*H*), 6.66 (1H, m, Ni-*H*), 5.57-5.25 (2H, m, N-*H* & C**15**-*H*), 5.20-4.94 (3H, m, C**1**-*H*, C**10**-*H*), 4.54 (1H, m, C**7**-*H*), 4.00 (1H, m, C**3**-*H*), 3.65 (3H, m, C**13**-*H*), 2.96 (1H, m, C**11**-*H*), 2.11 (1H, m, C**4**-*H*), 1.47 (9H, m, C**16**-*H*), 1.37 (3H, m, C**8**-*H*), 0.96 (3H, m, C**5**-*H*), 0.91 (3H, m, C**5**-*H*). ^{13}C NMR ($CDCl_3$, 101 MHz): δ (ppm) 197.4 (m, C**14**), 172.18 (m, C**9**), 171.80-170.80 (m, C**6** & C**12**), 162.8 (d, $^{2}J_{CF}$ = 24.2, C**16**), 156.8 (m, C**2**), 136.3 (m, Ar), 128.7 (m, Ar), 128.3 (m, Ar), 128.2 (m, Ar), 90.84 (d, $^{1}J_{CF}$ = 197.6, C**15**), 90.2 (d, C**15**), 85.2 (**17**), 85.1 (C**17**), 67.3 (m, C**1**), 60.5 (m, C**3**), 53.0 (d, $^{3}J_{CF}$ = 12.3, C**10**), 48.9 (m, C**7**), 34.8 (C**11**), 31.1 (C**4**), 28.0 (m, C**18**), 19.4 (m, C**5**), 18.2 (m, C**8** & C**5**). ^{19}F NMR ($CDCl_3$, 376 MHz): δ (ppm)* -194.90 (d, $^{2}J_{FH}$ = 49.0, C**15**-*F*), -195.15 (d, $^{2}J_{FH}$ = 49.3, C**13**-*F*), -195.80 (d, $^{2}J_{FH}$ = 48.6, C**13**-*F*), -196.30 (d, $^{2}J_{FH}$ = 48.7, C**13**-*F*). HRMS (ESI) *m/z* calculated for $[M+H]^+$ $C_{27}H_{39}N_3O_9F^+$ 568.2670, found 568.2674. *Note* – Exists as an inseparable mixture of diastereoisomers. ‡ ^{1}H NMR data suggests the presence of rotamers. * ^{19}F NMR data suggests the presence of rotamers.

Synthesis of 295

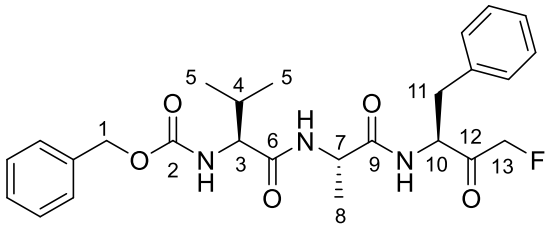

295

Compound **310** (0.15 g, 0.26 mmol) was dissolved in 13% TFA in DCM (3.9 mL, 6.53 mmol). The resulting solution was left to stir at room temperature overnight before being concentrated *in vacuo*. Subsequent purification by silica gel flash column chromatography (hexane : ethyl acetate, 1 : 0 to 1 : 1) afforded the product as a clear oil (76.0 mg, 0.16 mmol, 62%). ^{1}H NMR ($CDCl_3$, 400 MHz): δ (ppm)‡ 7.24 (11H, m, Ph-*H* & N-*H*), 6.72 (1H, m, N-*H*), 5.52 (1H, m, N-*H*), 5.20-4.63 (5H, m, C**1**-*H* & C**10**-*H* & C**13**-*H*), 4.48 (1H, m, C**7**-*H*), 4.02 (1H, m, C**3**-*H*), 3.15 (1H, m, C**11**-*H*), 2.95 (1H, m, C**11**-*H*), 2.08 (1H, m, C**4**-*H*), 1.26 (3H, m, C**8**-*H*), 0.92 (6H, m, C**5**-*H*). ^{13}C NMR ($CDCl_3$, 101 MHz): δ (ppm) 204.0 (d, $^{2}J_{CF}$ = 17.8, C**12**), 172.08 (C**9**), 171.48 (C**6**), 171.40 (C**6**), 156.8 (C**2**), 136.2 (Ar), 135.1 (Ar), 135.5 (Ar), 129.3 (Ar), 129.3 (Ar), 129.0 (Ar), 128.9 (Ar), 128.7 (Ar), 128.4 (Ar), 128.3 (Ar), 128.2 (Ar), 127.5 (Ar), 127.5 (Ar), 84.6 (d, C**13**, $^{1}J_{CF}$ = 185.2), 67.4 (C**1**), 60.7 (C**3**), 56.2 (C**10**), 48.8 (C**7**), 36.7 (C**11**), 31.1 (C**4**), 19.4 (C**5**), 18.3-17.7 (C**8** & C**5**). ^{19}F NMR ($CDCl_3$, 376 MHz): δ (ppm)* -230.43 (m, C**13**-*F*). HRMS (ESI) *m/z* calculated for $[M+H]^+$ $C_{26}H_{33}N_3O_5F^+$ 486.2404, found 486.2409. ‡ ^{1}H NMR data suggests the presence of rotamers. * ^{19}F NMR data suggests the presence of rotamers.

Synthesis of 40

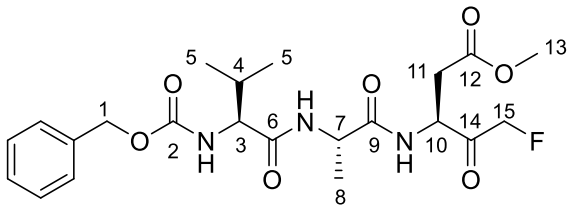

40

Compound **311** (27.0 mg, 47.6 µmol) was dissolved in 13% TFA in DCM (3.9 mL, 6.53 mmol). The resulting solution was left to stir at room temperature overnight before being concentrated *in vacuo*. Subsequent purification by silica gel flash column chromatography (hexane : ethyl acetate, 1 : 0 to 3 : 7) afforded the product as a white solid (5.6 mg, 12.0 µmol, 25%). ^{1}H NMR ($CDCl_3$, 599 MHz): δ (ppm) ‡ 7.34 (6H, m, Ph-*H* & N-*H*), 6.59 (1H, br m, N-*H*), 5.42 (1H, m, N-*H*), 5.25-4.95 (4H, m, C**1**-*H* & C**15**-*H*), 4.89 (1H, m, C**10**-*H*), 4.50 (1H, m, C**7**-*H*), 3.99 (1H, m, C**3**-*H*), 3.67 (3H, s, C**13**-*H*), 2.98 (1H, m, C**11**-*H*), 2.87 (1H, m, C**11**-*H*), 2.12 (1H, m, C**4**-*H*), 1.38 (3H, m, C**8**-*H*), 0.97 (3H, m, C**5**-*H*), 0.93 (3H, m, C**5**-*H*). ^{13}C NMR ($CDCl_3$, 151 MHz): δ (ppm) 202.4 (d, $^{2}J_{CF}$ = 17.8, C**12**), 172.3 (C**9**), 171.7-171.3 (C**6** & C**12**), 156.9 (C**2**), 136.2 (Ar), 136.1 (Ar), 128.8 (Ar), 128.7 (Ar), 128.5 (Ar), 128.5 (Ar), 128.3 (Ar), 128.3 (Ar), 84.4 (d, C**15**, $^{1}J_{CF}$ = 183.4), 84.3 (d, C**15**, $^{1}J_{CF}$ = 183.7), 67.5 (C**1**), 67.5 (C**1**), 60.8 (C**3**), 52.4 (C**10**), 52.4 (C**10**), 49.1 (C**7**), 35.0 (C**11**), 31.0 (C**4**), 19.4 (C**5**), 18.0 (C**8** & C**5**). ^{19}F NMR ($CDCl_3$, 376 MHz): δ (ppm) * -231.78 (m, C**15**-*F*). HRMS (ESI) *m/z* calculated for $[M+H]^+$ $C_{22}H_{31}N_3O_7F^+$ 468.2146, found 468.2159. ‡ ^{1}H NMR data suggests the presence of rotamers. * ^{19}F NMR data suggests the presence of rotamers.

Synthesis of Caspase 1 Inhibitor 296

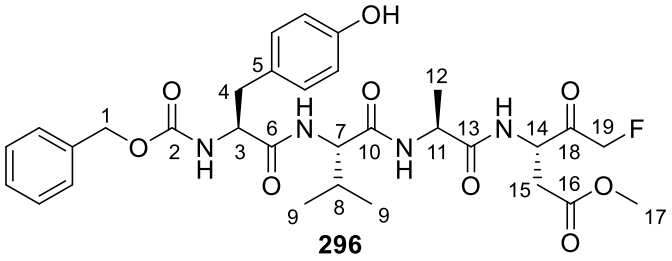

296

To a solution of Cbz-Tyr-Val-Ala-OH (**305**) (0.14 g, 0.25 mmol) and HATU (96.9 mg, 0.25 mmol) in DMF (1 ml) was added 2,4,6-trimethylpyridine (0.10 mL, 0.76 mmol). The mixture was left to pre-activate for about 1 minute before addition of ammonium salt **291** (0.31 mmol) in DMF (1.2 ml). The solution was then stirred at room temperature for 1.5 hours whilst being tracked by LCMS. Water was then added (25 ml) and the product extracted into ethyl acetate (8 x 15 ml). The organic phases were combined and concentrated under reduced pressure. Global deprotection was achieved through the addition of a solution of 2.5% H_2O in TFA (50 ml) for 1 hour. Subsequent concentration under reduced pressure afforded the crude product, which was purified by HPLC x 2 according to **Section 7.3.8.3** giving the product (along with impurity) as a brown solid (3.8 mg, 6.03 µmol, 2.4%). HRMS (ESI) *m/z* calculated for $[M+H]^+$ $C_{31}H_{40}N_4O_9F^+$ 631.2789, found 631.2779.

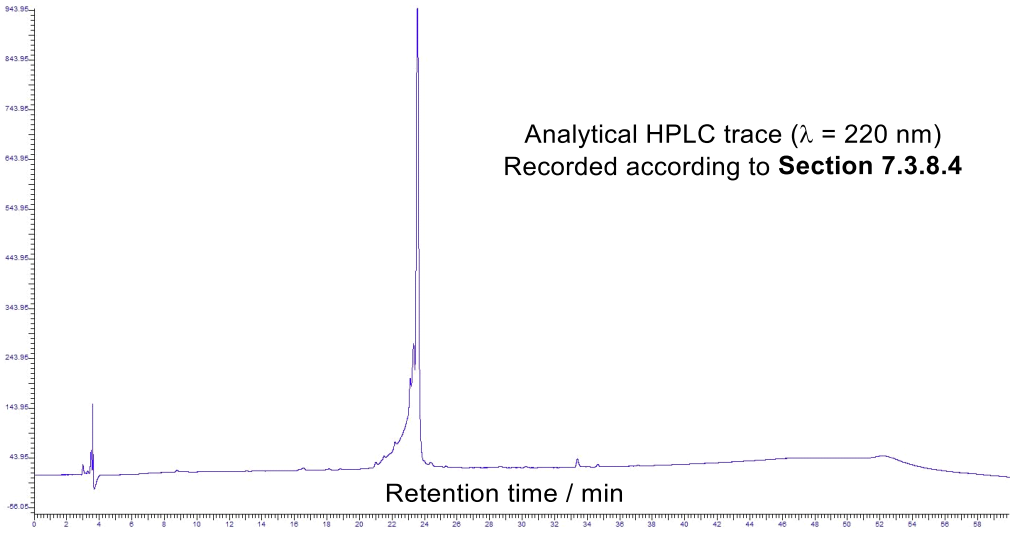

Synthesis of Caspase 2 Inhibitor 297

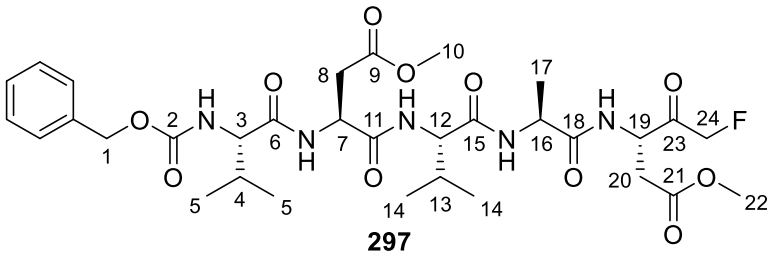

297

To a solution of Cbz-Val-Asp(OMe)-Val-Ala-OH (**306**) (0.20 g, 0.36 mmol) and HATU (0.14 g, 0.36 mmol) in DMF (1 ml) was added 2,4,6-trimethylpyridine (0.14 mL, 1.09 mmol). The mixture was left to pre-activate for about 1 minute before addition of ammonium salt **291** (0.74 mmol) in DMF (1.2 ml). The solution was then stirred at room temperature for 1.5 hours whilst being tracked by LCMS. Water was then added (25 ml) and the product extracted into ethyl acetate (8 x 15 ml). The organic phases were combined and concentrated under reduced pressure, affording the crude product, which was purified by HPLC x 2 according to **Section 7.3.8.2** and **7.2.8.3**, giving the product as a white solid (2.0 mg, 2.87 µmol, 0.8%). HRMS (ESI) *m/z* calculated for $[M+H]^+$ $C_{32}H_{47}N_5O_{11}F^+$ 696.3256, found 696.3274.

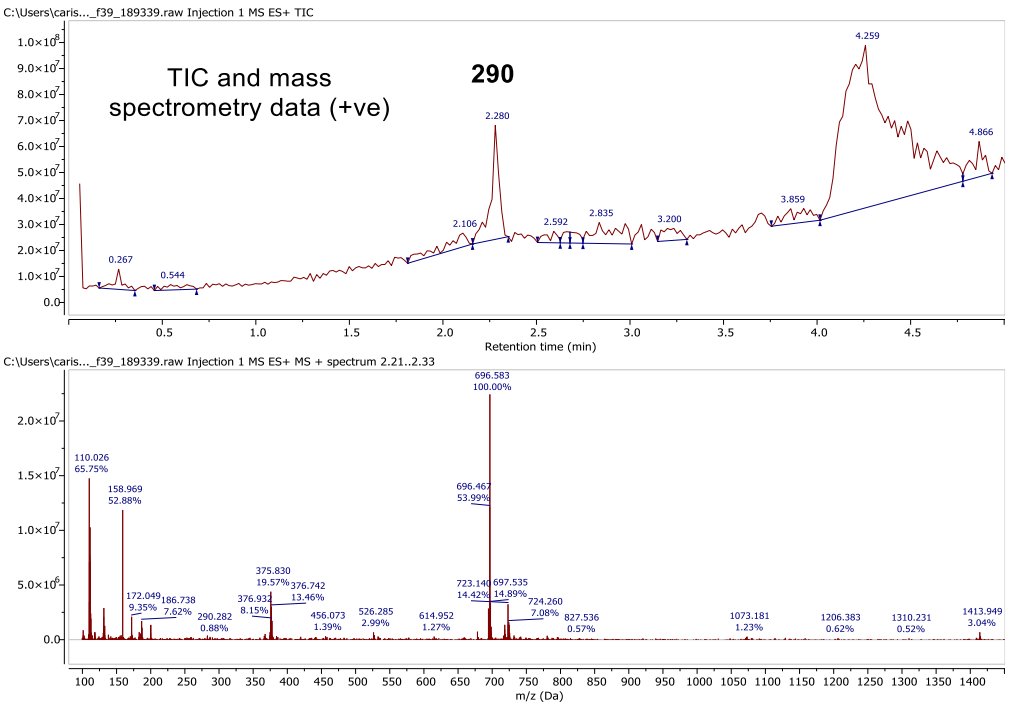

Synthesis of Caspase 3 Inhibitor 46

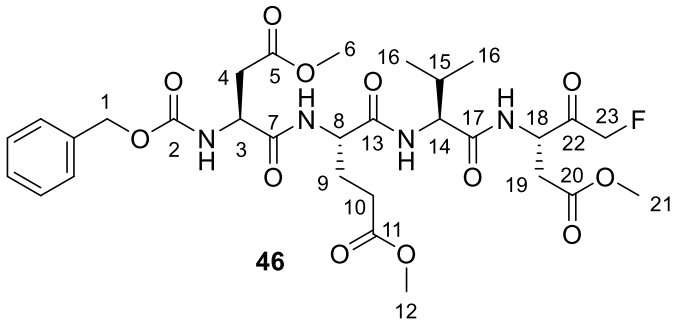

46

To a solution of Cbz-Asp(OMe)-Glu(OMe)-Val-OH (**307**) (0.20 g, 0.38 mmol) and HATU (0.15 g, 0.38 mmol) in DMF (1 ml) was added 2,4,6-trimethylpyridine (0.15 mL, 1.14 mmol). The mixture was left to pre-activate for about 1 minute before addition of ammonium salt **291** (1.13 mmol) in DMF (1.2 ml). The solution was then stirred at room temperature for 1.5 hours whilst being tracked by LCMS. Water was then added (25 ml) and the product extracted into ethyl acetate (8 x 15 ml). The organic phases were combined and concentrated under reduced pressure to afford the crude product, which was purified by HPLC x 2 according to **Section 7.3.8.3**, giving the product (along with the hydroxymethyl ketone analogue) as an off-white solid (34.2 mg, 50.8 µmol, 13%). ^{19}F NMR ($CDCl_3$, 376 MHz): δ (ppm) -234.15 (t, $^2J_{HF}$ = 46.8, C**23**-*F*), -233.87 (t, $^2J_{HF}$ = 47.0, C**23**-*F*). HRMS (ESI) *m/z* calculated for $[M+H]^+$ $C_{30}H_{42}N_4O_{12}F^+$ 669.2783, found 669.2786.

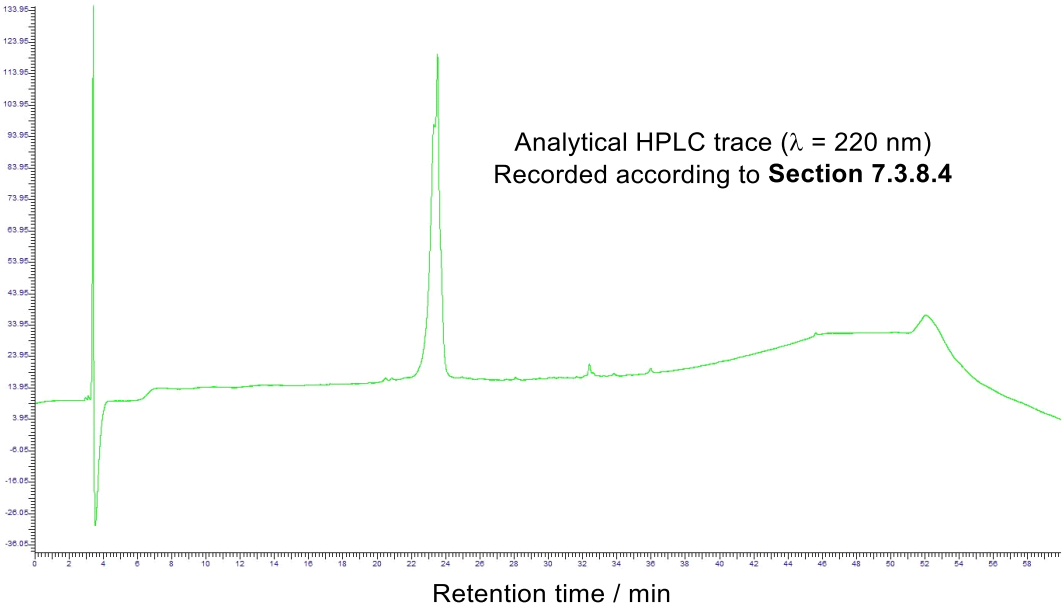

Synthesis of Caspase 6 Inhibitor 298

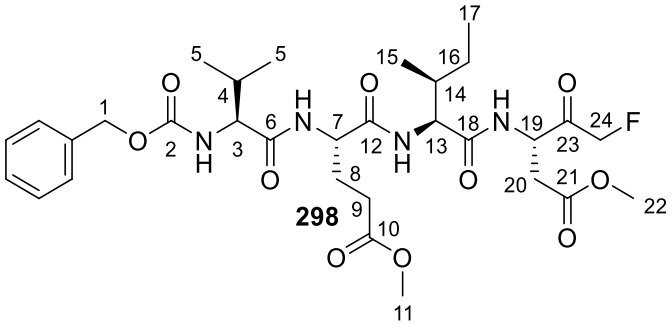

To a solution of Cbz-Val-Glu(OMe)-Ile-OH (**308**) (0.13 g, 0.26 mmol) and HATU (97.4 mg, 0.26 mmol) in DMF (1 ml) was added 2,4,6-trimethylpyridine (0.10 mL, 0.77 mmol). The mixture was left to pre-activate for about 1 minute before addition of ammonium salt **291** (1.13 mmol) in DMF (1.2 ml). The solution was then stirred at room temperature for 1.5 hours whilst being tracked by LCMS. Water was then added (25 ml) and the product extracted into ethyl acetate (8 x 15 ml). The organic phases were combined and concentrated under reduced pressure, affording the crude product, which was purified by HPLC x 2 according to **Section 7.3.8.3**, giving the product (along with the hydroxymethyl ketone analogue) as an off-white solid (4.94 mg, 7.57 µmol, 3%). ^{19}F NMR ($CDCl_3$, 376 MHz): δ (ppm) -214.94 (t, $^2J_{HF}$ = 48.4, C**24**-*F*). HRMS (ESI) *m/z* calculated for $[M+H]^+$ $C_{31}H_{46}N_4O_{10}F^+$ 653.3198, found 653.3218.

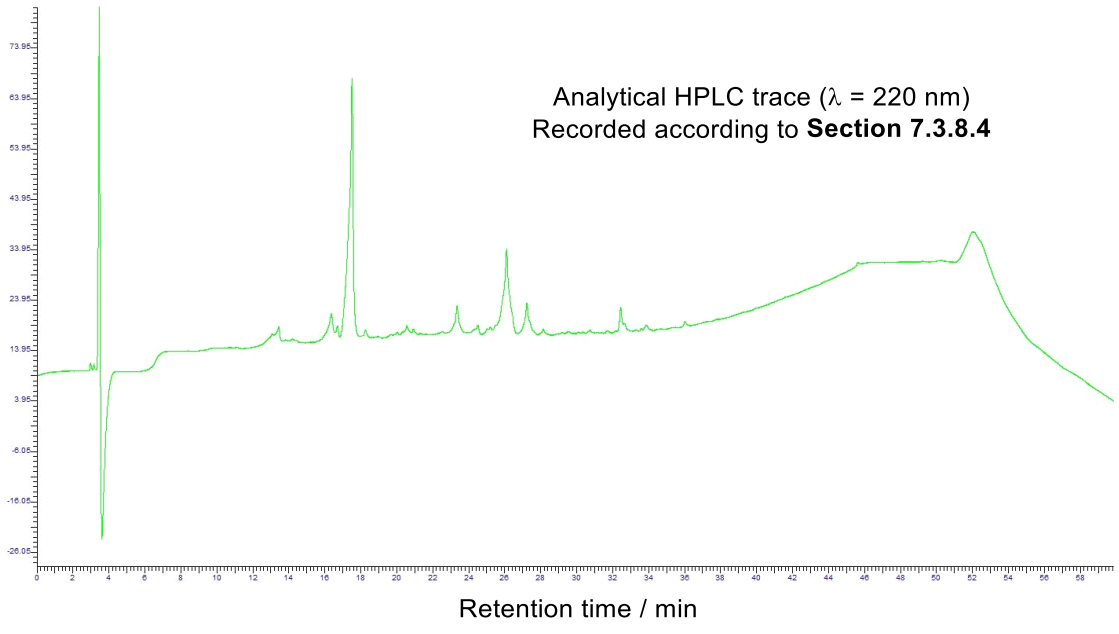

Synthesis of Caspase 8 Inhibitor 299

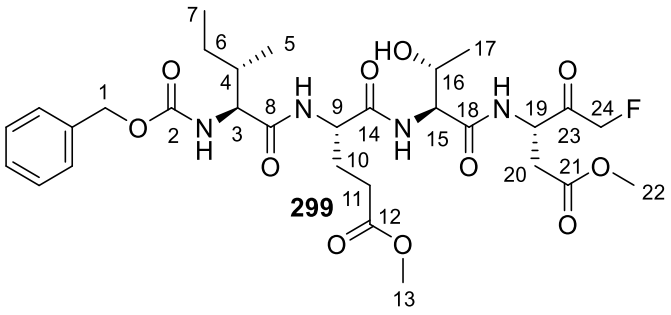

To a solution of Cbz-Ile-Glu(OMe)-Thr-OH (**309**) (0.29 g, 0.51 mmol) and HATU (0.20 g, 0.51 mmol) in DMF (1 ml) was added 2,4,6-trimethylpyridine (0.20 mL, 1.54 mmol). The mixture was left to pre-activate for about 1 minute before addition of ammonium salt **291** (0.74 mmol) in DMF (1.2 ml). The solution was then stirred at room temperature for 1.5 hours whilst being tracked by LCMS. Water was then added (25 ml) and the product extracted into ethyl acetate (8 x 15 ml). The organic phases were combined and concentrated under reduced pressure. Global deprotection was achieved through the addition of a solution of 2.5% H_2O in TFA (50 ml) for 1 hour. Subsequent concentration under reduced pressure afforded the crude product, which was purified by HPLC x 2 according to **Section 7.3.8.3**, giving the product (along with impurities) as a white solid (0.87 mg, 1.33 µmol, 0.3%). HRMS (ESI) *m/z* calculated for $[M+H]^+$ $C_{30}H_{44}N_4O_{11}F^+$ 655.2991, found 655.2975.

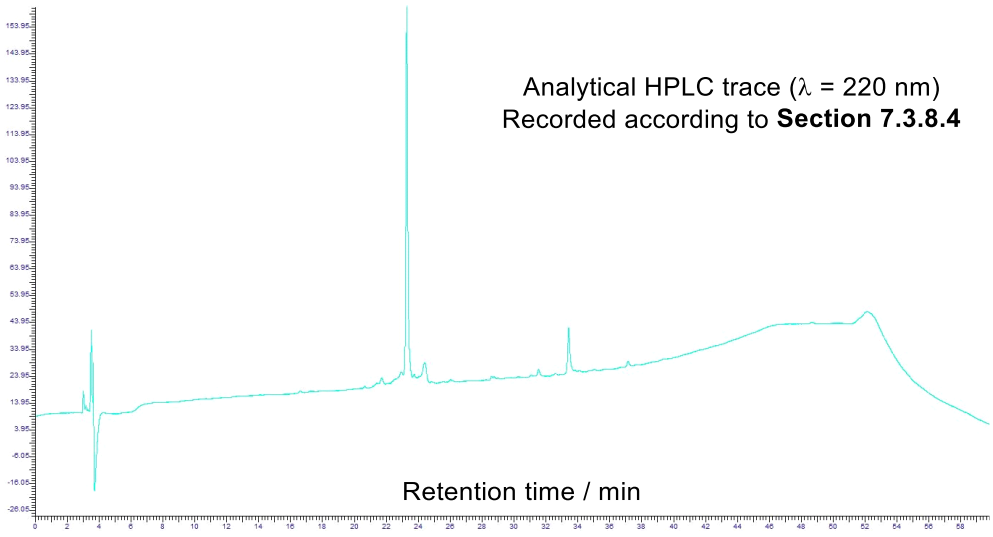

Synthesis of 315

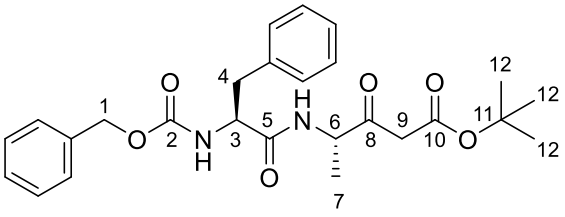

315

To a solution of Cbz-Phe-Ala-OH (**316**) (0.50 g, 1.35 mmol) in dry THF (3 ml) was added 1,1′-carbonyldiimidazole (0.22 g, 1.36 mmol) under an atmosphere of nitrogen. The reaction mixture was left to stir at room temperature for 1.5 h in order to generate the corresponding acyl imidazole *in situ*. Simultaneously a solution of *tert*-butyl acetate (0.56 mL, 4.17 mmol) in dry THF (1.5 ml) was added dropwise under nitrogen to a solution of 2 M lithium diisopropylamide in dry THF (2.1 mL, 4.18 mmol) which had been cooled to -78 °C. The resulting solution was left to stir at -78 °C for 20 min before the addition of the acyl imidazole-containing solution at -78 °C. The reaction mixture was stirred at -78 °C under inert conditions for a further 2 h before being quenched with 10 % *w/v* citric acid (15 ml) and extracted into EtOAc (3 x 10 ml). The combined organic phases were combined and concentrated *in vacuo*. Subsequent purification by silica gel flash column chromatography (hexane : ethyl acetate, 1 : 0 to 1 : 1) gave the product as a clear oil (48.0 mg, 0.10 mmol, 7%), as an apparent mix of rotamers. ^{1}H NMR ($CDCl_3$, 400 MHz): δ (ppm) 7.29 (10H, m, Ph-*H*), 6.54 (0.7H, d, $^{3}J_{HH}$ = 7.1, N-*H*, major rotamer), 6.33 (0.3H, d, $^{3}J_{HH}$ = 7.8, N-*H*, minor rotamer), 5.32 (0.3H, apps, N-*H*, minor rotamer), 5.26 (0.7H, m, N-*H*, $^{3}J_{HH}$ = 7.8, major rotamer), 5.09 (2H, s, C**1**-*H*), 4.59 (1H, m, C**6**-*H*), 4.43 (1H, m, C**3**-*H*), 3.37 (2H, m, C**9**-*H*, both rotamers), 3.05 (2H, m, C**4**-*H*), 1.46 (6.75H, s, C**12**-*H*, major rotamer), 1.44 (2.25H, s, C**12**-*H*, minor rotamer), 1.29 (2.25H, d, $^{3}J_{HH}$ = 7.1, C**7**-*H*, major rotamer), 1.18 (0.75H, d, $^{3}J_{HH}$ = 7.2, C**7**-*H*, minor rotamer). HRMS (ESI) *m/z* calculated for $[M+H]^+$ $C_{26}H_{33}N_2O_6^+$ 469.2339, found 469.2324.

Synthesis of 314 (reported as a mixture of diastereoisomers)

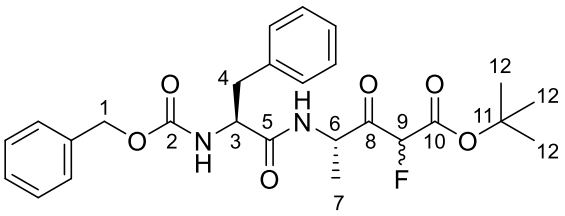

314

To a solution of *β*-ketoester **315** (45.0 mg, 96.0 µmol) and 19 mol % $CpTiCl_3$ (3.9 mg, 17.8 µmol) in MeCN (20 ml) was added F-TEDA (37.4 mg, 0.11 mmol). The reaction mixture was left to stir at room temperature overnight and subsequently concentrated under reduced pressure. The resulting crude material was purified by silica gel flash column chromatography (hexane : ethyl acetate, 1 : 0 to 3 : 7) to give the product (7.0 mg, 14.4 µmol, 15%). Reported as a mixture of diastereoisomers (dr ~ 43 : 57), as determined by ^{19}F NMR spectroscopy. ^{1}H NMR ($CDCl_3$, 700 MHz): δ (ppm) 7.28 (10H, m, Ph-*H*), 6.31 (1H, m, N-*H*), 5.37-5.24 (2H, m, N-*H* & C**9**-*H*), 5.10 & 5.08 (2H, ABq, $^{2}J_{AB}$ = 10.5, C**1**-*H*), 4.94 (0.5H, m, C**6**-*H*), 4.86 (0.5H, m, C**6**-*H*), 4.42 (1H, br m, C**3**-*H*), 3.11 (1H, m, C**4**-*H*), 3.04 (1H, m, C**4**-*H*), 1.52 (4.5H, s, C**12**-*H*), 1.50 (4.5H, s, C**12**-*H*), 1.29 (3H, m, C**7**-*H*). ^{13}C NMR ($CDCl_3$, 176 MHz): δ (ppm) 199.7 (m, C**8**), 170.6 (C**5**), 170.5 (C**5**), 162.5 (m, C**10**), 156.0 (C**2**), 136.2 (Ar), 129.5 (Ar), 128.9 (Ar), 128.7 (Ar), 128.4 (Ar), 128.2 (Ar), 127.4 (Ar), 90.3 (d, C**9**, $^{1}J_{CF}$ = 197.1), 85.3 (C**11**), 85.0 (C**11**), 67.3 (C**1**), 56.3 (C**3**), 56.1 (C**3**), 51.9 (C**6**), 51.4 (C**6**), 38.5 (C**4**), 28.1 (C**12**), 28.0 (C**12**), 17.1 (C**7**), 16.7 (C**7**). ^{19}F NMR ($CDCl_3$, 376 MHz): δ (ppm) -196.89 (dd, $^{2}J_{FH}$ = 48.8, $^{4}J_{FH}$ = 2.3, C**9**-*F*), -196.04 (d, $^{2}J_{FH}$ = 48.9, C**9**-*F*). HRMS (ESI) *m/z* calculated for $[M+H]^+$ $C_{26}H_{32}N_2O_6F^+$ 487.2244, found 487.2249.

Synthesis of 41

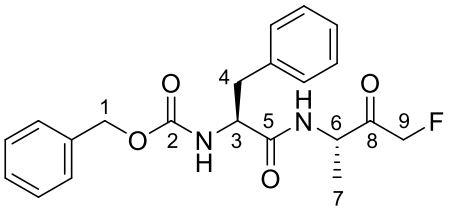

41

To a solution of *β*-ketoester **314** (8.8 mg, 18.1 µmol) was added 50% TFA in DCM (2.0 ml). The reaction mixture was left to stir at 40 ºC for 2 h before being concentrated under reduced pressure. The resulting crude material was purified by prep TLC (hexane : ethyl acetate, 7 : 3) to give the product (with some impurities still present) as a white solid (3.0 mg, 7.76 µmol, 43%), although impurities were evident by ^{1}H NMR spectroscopy. ^{1}H NMR ($CDCl_3$, 400 MHz): δ (ppm) 7.29 (10H, m, Ph-*H*), 6.32 (1H, d, $^{3}J_{HH}$ = 6.8, N-*H*), 5.26 (1H, br m, N-*H*), 5.10 (2H, apps, C**1**-*H*), 4.89 (2H, d, $^{2}J_{HF}$ = 47.2, C**9**-*H*), 4.76 (1H, m, C**6**-*H*), 4.42 (1H, br m, C**3**-*H*), 3.13 (1H, dd, $^{2}J_{HH}$ = 14.0, $^{3}J_{HH}$ = 6.4, C**4**-*H*), 3.03 (1H, dd, $^{2}J_{HH}$ = 13.7, $^{3}J_{HH}$ = 7.2, C**4**-*H*), 1.30 (3H, d, $^{3}J_{HH}$ = 7.2, C**7**-*H*). ^{19}F NMR ($CDCl_3$, 376 MHz): δ (ppm) -231.63 (t, $^{2}J_{FH}$ = 50.2, C**9**-*F*). HRMS (ESI) *m/z* calculated for $[M+H]^+$ $C_{21}H_{24}N_2O_4F^+$ 387.1720, found 387.1707.

Synthesis of 321

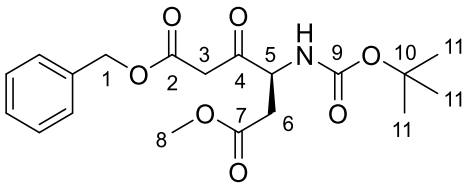

321

To a solution of Boc-Asp(OMe)-OH (4.00 g, 16.2 mmol) in dry THF (24 ml) was added 1,1'-carbonyldiimidazole (2.88 g, 17.8 mmol) under an atmosphere of nitrogen. The reaction mixture was left to stir at room temperature for 1.5 h in order to generate the corresponding acyl imidazole *in situ*. Simultaneously a solution of benzyl acetate (7.2 mL, 50.5 mmol) in dry THF (12 ml) was added dropwise under nitrogen to a solution of 2 M lithium diisopropylamide in dry THF (25 mL, 50.0 mmol) which had been cooled to -78 °C. The resulting solution was left to stir at -78 °C for 20 min before the addition of the acyl imidazole-containing solution at -78 °C. The reaction mixture was stirred at -78 °C under inert conditions for a further 1 h before being quenched with 10 % *w/v* citric acid (120 ml), extracted into EtOAc (3-4 x 60 ml) and washed with sat. $NaHCO_3$ (2 x 80 ml) and brine (1 x 80 ml). The combined organic phases were dried over anhydrous $MgSO_4$, filtered and concentrated *in vacuo*. Subsequent purification by silica gel flash column chromatography (hexane : ethyl acetate, 1 : 0 to 3 : 2) gave the pure product as a yellow oil (0.25 g, 0.66 mmol, 4%). ^{1}H NMR ($CDCl_3$, 400 MHz): δ (ppm) 7.35 (5H, m, Ph-*H*), 5.63 (1H, d, $^{3}J_{HH}$ = 9.1, N-*H*), 5.19 & 5.15 (2H, ABq, $^{2}J_{AB}$ = 12.0, C**1**-*H*), 4.56 (1H, dt, $^{3}J_{HH}$ = 9.3, $^{3}J_{HH}$ = 4.8, C**5**-*H*), 3.69 (2H, s, C**3**-*H*), 3.67 (3H, s, C**8**-*H*), 3.00 (1H, dd, $^{2}J_{HH}$ = 17.3, $^{3}J_{HH}$ = 5.0, C**6**-*H*), 2.76 (1H, dd, $^{2}J_{HH}$ = 17.3, $^{3}J_{HH}$ = 4.7, C**6**-*H*), 1.44 (9H, s, C**11**-*H*). ^{13}C NMR ($CDCl_3$, 101 MHz): δ (ppm) 201.5 (C**4**), 172.1 (C**7**), 166.9 (C**2**), 155.4 (C**9**), 135.4 (Ar), 128.7 (Ar), 128.6 (Ar), 128.5 (Ar), 82.2 (C**2**), 80.8 (C**10**), 67.4 (C**1**), 56.1 (C**5**) 52.3 (C**8**), 46.0 (C**3**) 35.3 (C**6**), 28.4 (C**11**), 28.0 (C**1**). HRMS (ESI) *m/z* calculated for $[M\text{-}Boc+H]^+$ $C_{14}H_{18}NO_5^+$ 280.1185, found 280.1188.

Synthesis of 43[12] (reported as a suspected mixture of rotamers)

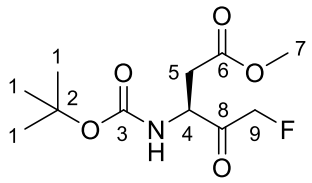

43

β-ketoester **320** (72.0 mg, 0.18 mmol) (also containing hydroxymethyl ketone) and 10% Pd/C (15 mg, 21% *w/w*) were mixed in absolute ethanol (1.0 ml) under an atmosphere of nitrogen for 5 mins. The resulting mixture was left to stir at room temperature for 1 h under an atmosphere of hydrogen before being left to stir at 40 ºC overnight in air. The catalyst was then removed through filtration with washings of ethanol and the resulting filtrate concentrated under reduced pressure to afford the crude material, which was then purified by silica gel flash column chromatography (hexane : ethyl acetate, 1 : 0 to 3 : 7). Due to the presence of impurities, two further purifications were attempted using prep TLC (hexane : ethyl acetate, 3 : 7 and 2 : 8) to give the product (as a suspected mixture of rotamers in a ratio of 0.6 : 0.4) as a clear oil (3.0 mg, 11.4 µmol, 6%), although some impurity peaks were still evident by ^{1}H NMR spectroscopy. ^{1}H NMR ($CDCl_3$, 400 MHz): δ (ppm) 5.64 (0.4H, d, $^{3}J_{HH}$ = 8.7, N-*H*, minor rotamer), 5.51 (0.6H, d, $^{3}J_{HH}$ = 8.8, N-*H*, major rotamer), 5.23 (1H, dd, $^{2}J_{HF}$ = 47.1, $^{2}J_{HH}$ = 16.4, C**9**-*H*), 5.11 (1H, dd, $^{2}J_{HF}$ = 47.4, $^{2}J_{HH}$ = 16.4, C**9**-*H*), 4.62 (0.6H, m, C**4**-*H*, major rotamer), 4.42 (0.4H, dt, $^{3}J_{HH}$ = 9.1, $^{3}J_{HH}$ = 4.7, C**4**-*H*, minor rotamer), 3.69 (3H, m, C**7**-*H*, both rotamers), 3.04 (1H, m, C**5**-*H*, both rotamers), 2.79 (1H, m, C**5**-*H*, both rotamers), 1.48 (9H, m, C**1**-*H*). ^{13}C NMR ($CDCl_3$, 151 MHz): δ (ppm) 171.9 (C**6**), 155.4 (C**3**), 84.3 (d, C**9**, $^{1}J_{CF}$ = 183.4), 81.0 (C**2**), 53.7 (C**4**), 52.4 (C**7**), 52.2 (C**7**), 35.6 (C**5**), 28.4 (C**1**). ^{19}F NMR ($CDCl_3$, 376 MHz): δ (ppm) -232.24 (td, $^{2}J_{FH}$ = 47.3, $^{4}J_{FH}$ = 1.8, C**9**-*F*). HRMS (ESI) *m/z* calculated for $[M\text{-}Boc+H]^+$ $C_6H_{11}NO_3F^+$ 164.0723, found 164.0717. Characterisation data was found to be consistent with the literature[12]; however, impurity peaks were present and some peaks doubled-up in this case, perhaps due to rotamers.

7.7 Experimental for Chapter 5

Synthesis of 372[13,14] (Reported as a mixture of keto/enol tautomers)

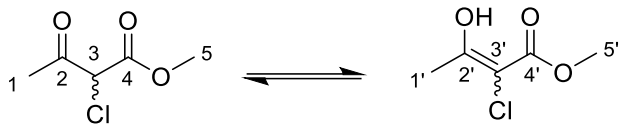

272 (keto) **372** (enol)

To a solution of methyl acetoacetate (**213**) (0.25 mL, 2.32 mmol) and 5 mol % $CpTiCl_3$ (24.7 mg, 0.11 mmol) in MeCN (10 ml) was added *N*-chlorosuccinimide (0.34 g, 2.55 mmol). The reaction mixture was left to stir at room temperature overnight and subsequently concentrated under reduced pressure. The resulting crude material was purified by silica gel flash column chromatography (hexane : ethyl acetate, 1 : 0 to 9 : 1) to give the pure product as a clear liquid 0.14 g, 0.93 mmol, 40%). Reported as a mixture of enol and keto tautomers (enol : keto, ~ 50 : 50). ^{1}H NMR ($CDCl_3$, 599 MHz): δ (ppm) 12.22 (1H, s, enol O-*H*), 4.77 (1H, s, C**3**-*H*), 3.83 (6H, s, C**5**-*H* & C**5'**-*H*), 2.38 (3H, s, C**1**-*H*), 2.17 (3H, s, C**1'**-*H*). ^{13}C NMR ($CDCl_3$, 151 MHz): δ (ppm) 196.7 (C**2**), 172.9 (C**2'**), 169.8 (C**4'**), 165.6 (C**4**), 96.9 (C**3'**), 61.2 (C**3**), 53.9 & 52.8 (C**5** & C**5'**), 26.4 (C**1**), 19.9 (C**1'**). GC-MS (EI^+) r.t. = 2.5 mins, *m/z* 150 [M^+], 108 [M-CH_3CO^+], 43 [CH_3CO^+]. Characterisation data was found to be consistent with the literature.[13,14]

Synthesis of 373 (Reported as a mixture of diastereoisomers and keto/enol tautomers)

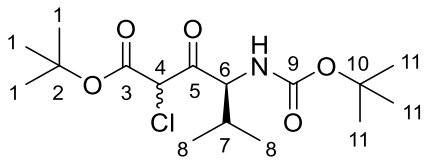

373

To a solution of *β*-ketoester **284** (1.22 g, 3.87 mmol) and 5 mol % $CpTiCl_3$ (42.4 mg, 0.19 mmol) in MeCN (50 ml) was added *N*-chlorosuccinimide (0.54 g, 4.04 mmol). The reaction mixture was left to stir at room temperature overnight and subsequently concentrated under reduced pressure. The resulting crude material was purified by silica gel flash column chromatography (hexane : ethyl acetate, 1 : 0 to 4 : 1) to give the product as a clear oil (0.74 g, 2.12 mmol, 55%). Reported as a mixture of enol and keto tautomers (enol : keto, ~ 20 : 80) and as a mixture of diastereoisomers (~ 40 : 60), as determined by ^{1}H NMR spectroscopy. ^{1}H NMR ($CDCl_3$, 400 MHz): δ (ppm) 12.63 (0.2H, s, enol O-*H*), 5.00 (1H, d, $^3J_{HH}$ = 9.5, N-*H* enol & keto), 4.98 (0.3H, s, keto C**4**-*H*), 4.90 (0.5H, s, keto C**4**-*H*), 4.71 (0.2H, m, enol C**6**-*H*), 4.63 (0.3H, dd, $^3J_{HH}$ = 9.6, $^3J_{HH}$ = 4.5, keto C**6**-*H*), 4.59 (0.5H, dd, $^3J_{HH}$ = 9.5, $^3J_{HH}$ = 4.3, keto C**6**-*H*), 2.27 (0.8H, m, keto C**7**-*H*), 1.98 (0.2H, m, enol C**7**-*H*), 1.49 (2H, s, enol C**1**-*H*), 1.44 (7H, m, keto C**1**-*H*), 1.40 (9H, m, C**11**-*H* keto & enol), 0.97 (2.4H, d, $^3J_{HH}$ = 6.8, keto C**8**-*H*), 0.93 (1.2H, m, enol C**8**-*H*), 0.79 (2.4H, m, keto C**8**-*H*). ^{13}C NMR ($CDCl_3$, 151 MHz): δ (ppm) 198.5 (keto C**5**), 198.0 (keto C**5**), 163.4 (keto C**3**), 163.2 (keto C**3**), 155.6 (keto C**9**), 155.6 (keto C**9**), 98.0 (enol C**4**) 84.9 (keto C**2**), 84.6 (keto C**2**), 84.0 (enol C**2**), 80.2 (keto C**10**), 79.6 (enol C**10**), 62.8 (keto C**6**), 62.0 (keto C**6**), 60.9 (keto C**4**), 58.8 (keto C**4**), 55.8 (enol C**6**), 31.5 (enol C**7**), 29.6 (keto C**7**), 29.5 (keto C**7**), 28.3 (C**11**), 28.1 (enol C**1**), 27.8 (C**1**), 27.7 (C**1**), 19.8 (keto C**8**), 19.7 (keto C**8**), 19.3 (enol C**8**), 18.1 (enol C**8**), 16.7 (keto C**8**), 16.6 (keto C**8**). HRMS (ESI) *m/z* calculated for $[M-H]^-$ $C_{16}H_{27}NO_5Cl^-$ 348.1578, found 348.1574.

Synthesis of 374

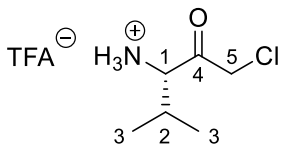

364

β-ketoester **373** (1.20 g, 0.86 mmol) was dissolved in 50% TFA in DCM (10 ml) and left to stir at 40 ºC for 2 h. Concentration under reduced pressure followed by lyophilisation gave the crude material in what was assumed to be a quantitative yield which was then rapidly used without further purification. HRMS (ESI) *m/z* calculated for $[M+H]^+$ $C_6H_{13}NOCl^+$ 150.0686, found 150.0694.

Synthesis of Ac-Ala-Tyr(O^{t}Bu)-Leu-OH (375)

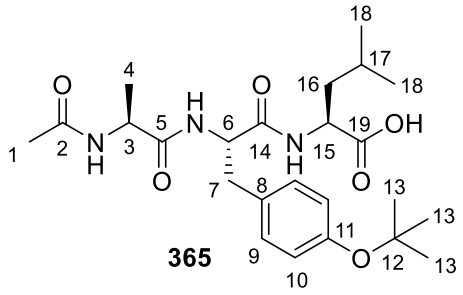

365

According to the general procedure described in **Section 7.3.1.1**, Fmoc-Leu-OH (5.0 equivalents with respect to the resin) was loaded onto 2-chlorotrityl chloride resin. Subsequently, amide couplings were carried out using PyBOP according to **Section 7.3.3** to afford the linear protected peptide **375** via manual Fmoc SPPS at room temperature on a 1.73 mmol scale. All couplings were single couplings, with an *N*-terminal acetylation being carried out as described in **Section 7.3.5**. Mild TFE cleavage of the resin was achieved according to **Section 7.3.7.3**, affording the desired peptide as a white solid (0.41 g, 0.50 mmol, 51%) with a crude purity of 86%, as determined by analytical HPLC (**Section 7.3.8.4**), which was used without purification. ^{1}H NMR (CD_3CN, 400 MHz): δ (ppm) 7.11 (2H, m, Ar-*H*), 7.01 (1H, d, $^3J_{HH}$ = 7.6, N-*H*), 6.89 (2H, m, Ar-*H*), 6.83 (2H, m, 2 x N-*H*),

4.52 (1H, td, $^{3}J_{HH}$ = 8.8, $^{3}J_{HH}$ = 4.6, C**6**-*H*), 4.31 (1H, m, C**15**-*H*), 3.98 (1H, m, C**3**-*H*), 3.16 (1H, dd, $^{2}J_{HH}$ = 14.1, $^{3}J_{HH}$ = 4.7, C**7**-*H*), 2.89 (1H, dd, $^{2}J_{HH}$ = 14.1, $^{3}J_{HH}$ = 9.2, C**7**-*H*), 1.87 (3H, s, C**1**-*H*), 1.60 (3H, m, C**17**-*H* & C**16**-*H*), 1.29 (9H, 2 x s, C**13**-*H*), 1.10 (3H, d, $^{3}J_{HH}$ = 7.2, C**4**-*H*), 0.92 (3H, d, $^{3}J_{HH}$ = 6.3, C**18**-*H*), 0.88 (3H, d, $^{3}J_{HH}$ = 6.2, C**18**-*H*). ^{13}C NMR (MeOD, 151 MHz): δ (ppm) 175.7 (C**19**), 174.8 (C**5**), 173.3 (C**9**), 173.2 (C**2**), 155.3 (C**11**), 133.5 (C**8**), 131.0 (C-**Ph**), 125.1 (C-**Ph**), 79.5 (C**12**), 55.6 (C**6**), 52.1 (C**15**), 50.6 (C**3**), 41.6 (C**16**), 37.8 (C**7**), 29.2 (C**13**), 25.9 (C**17**), 23.4 (C**18**), 22.4 (C**1**), 21.8 (C**18**), 17.8 (C**4**). HRMS (ESI) *m/z* calculated for $[M+H]^{+}$ $C_{24}H_{38}N_3O_6^{+}$ 464.2761, found 464.2739.

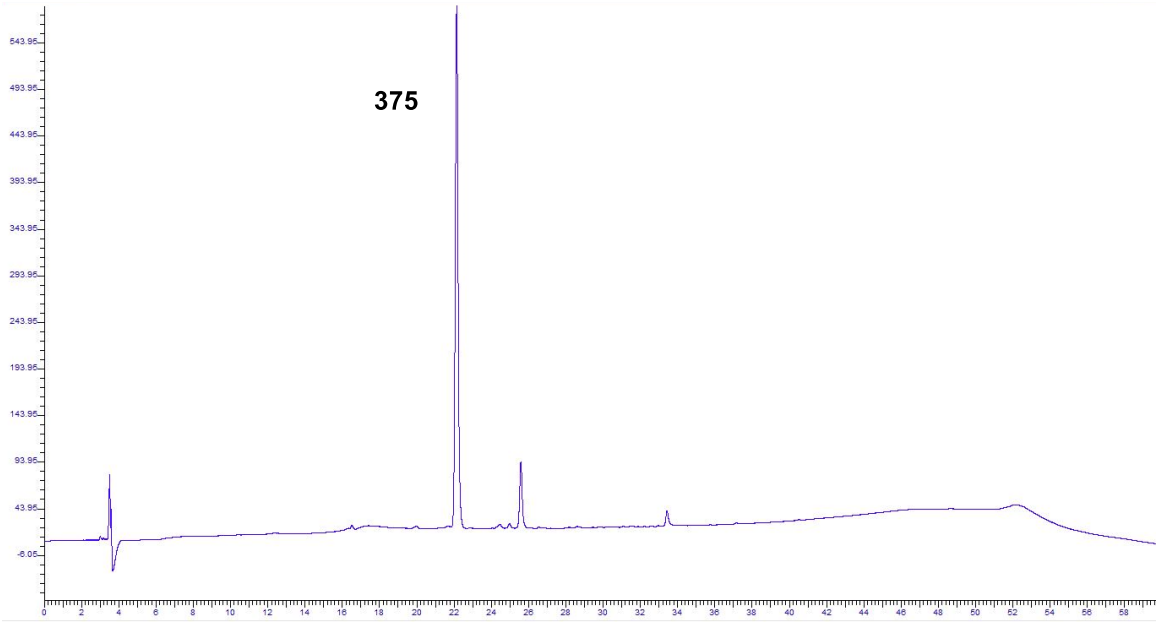

Synthesis of Ac-Ala-Tyr(O^{t}Bu)-Leu-Val-CMK (376) (Reported as a mixture of diastereoisomers)

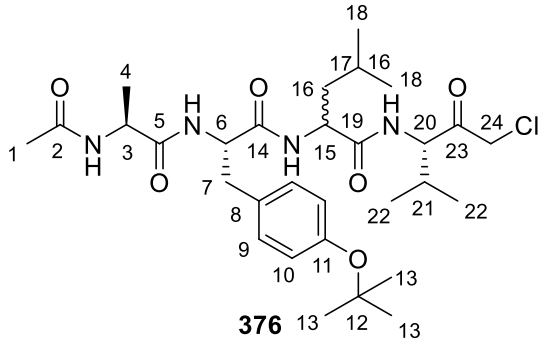

376

To a solution of Ac-Ala-Tyr(O^{t}Bu)-Leu-OH (**375**) (0.29 g, 0.63 mmol) and HATU (0.24 g, 0.63 mmol) in anhydrous DMF (2 ml) was added 2,4,6-trimethylpyridine (0.25 mL, 1.89 mmol). The mixture was left to pre-activate for about 1 minute before addition of CMK ammonium salt **374** in DMF (1.3 ml). The solution was then stirred at room temperature for 2 hours whilst being tracked by LCMS. Water was then added (35 ml) and the product extracted into ethyl acetate (3 x 25 ml). The organic phases were combined and concentrated under reduced pressure. The resulting crude material was purified by silica gel flash column chromatography (DCM : methanol, 1 : 0 to 98 : 2) to give the product as a white solid (0.28 g, 0.47 mmol, 75%). Reported as a mixture of diastereoisomers (~ 30 : 70), as determined by ^{1}H NMR spectroscopy. ^{1}H NMR (CD_3CN, 599 MHz): δ (ppm) 7.01 (8H, m, 4 x N-*H*, 4 x Ph-*H*), 4.32 (5H, m, C**24**-*H*, C**6**-*H*, C**20**-*H*, C**15**-*H*), 4.02 (0.3H, qd, $^3J_{HH}$ = 7.2, $^3J_{HH}$ = 5.3, C**3**-*H*), 3.89 (0.7H, qd, $^3J_{HH}$ = 7.2, $^3J_{HH}$ = 3.6, C**3**-*H*), 3.17 (0.3H, dd, $^2J_{HH}$ = 13.9, $^3J_{HH}$ = 6.1, C**7**-*H*), 3.10 (0.7H, dd, $^2J_{HH}$ = 14.3, $^3J_{HH}$ = 4.9, C**7**-*H*), 3.05 (0.7H, dd, $^2J_{HH}$ = 14.3, $^3J_{HH}$ = 7.9, C**7**-*H*), 2.95 (0.3H, dd, $^2J_{HH}$ = 13.9, $^3J_{HH}$ = 9.3, C**7**-*H*), 2.25 (1H, m, C**21**-*H*), 1.90 (1H, s, C**1**-*H*), 1.86 (2H, s, C**1**-*H*), 1.74 – 1.43 (3H, m, C**17**-*H* & C**16**-*H*) 1.30 & 1.29 (9H, 2 x s, C**13**-*H*), 1.19 (2H, d, $^3J_{HH}$ = 7.1, C**4**-*H*), 1.14 (1H, d, $^3J_{HH}$ = 7.1, C**4**-*H*), 0.88 (12H, m, C**18**-*H* & C**22**-*H*). ^{13}C NMR (CD_3CN, 151 MHz): δ (ppm) 202.0 (C**23**), 201.8 (C**23**), 175.2 (C**5**), 174.5 & 174.5 (C**5** & **19**), 174.1 (C**19**), 173.6 (C**2**), 172.5 (C**14**), 172.2 & 172.2 (C**2** & **14**), 155.6 (C-**Ph**), 155.2 (C-**Ph**), 133.4 (C**8**), 132.5 (C**8**), 130.7 (C-**Ph**), 130.7 (C-**Ph**), 125.0 (C-**Ph**), 124.9 (C-**Ph**), 79.3 – 78.7 (C**12**), 63.4 (C**20**), 63.2 (C**20**), 56.6 (C**6**), 56.0 (C**6**), 53.5 (C**15**), 53.2 (C**15**), 52.8 (C**3**), 51.1 (C**3**), 49.2 (C**24**), 49.2 (C**24**),

41.0 (C**16**), 40.8 (C**16**) 36.6 (C**7**), 36.1 (C**7**), 30.1 (C**21**), 30.0 (C**21**), 29.3 (C**13**), 25.4 (C**17**), 25.4 (C**17**), 23.7 (C**18** or **22**), 23.6 (C**18** or **22**), 23.1 (C**1**), 23.1 (C**1**), 21.7 (C**18** or **22**), 21.5 (C**18** or **22**), 20.0 (C**18** or **22**), 19.9 (C**18** or **22**), 18.6 (C**18** or **22**), 18.5 (C**18** or **22**), 17.4 (C**4**), 17.0 (C**4**). HRMS (ESI) *m/z* calculated for $[M+H]^+$ $C_{30}H_{48}N_4O_6Cl^+$ 595.3262, found 595.3263.

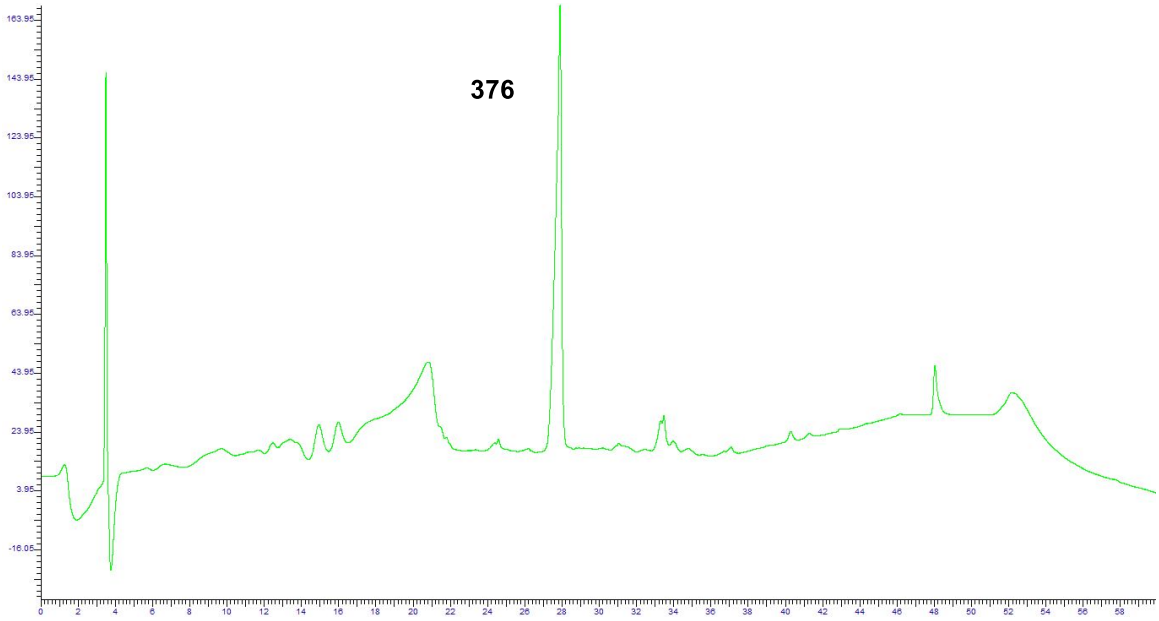

Synthesis of Ac-Ala-Tyr-Leu-Val-CMK (323a)

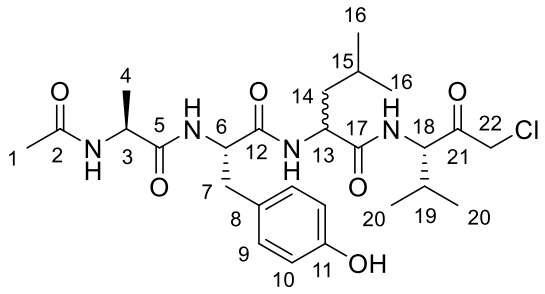

323a

^{t}Bu ester deprotection of Ac-Ala-Tyr(O^{t}Bu)-Leu-Val-CMK (**376**) (0.23 g, 0.39 mmol) was achieved through addition of a solution of 2.5% H_2O in TFA (20 ml) and subsequent stirring at room temperature for 1.5 hours. Concentration under reduced pressure, followed by lyophilisation afforded the product as a mixture of diastereoisomers in a ratio of 30 : 70, as determined by analytical HPLC (**Section 7.3.8.4**). Prep-HPLC purification (**Section 7.3.8.4**) allowed access to one (**323a**) of the two diastereoisomers as a white solid (17.6 mg, 32.6 µmol, 8%). [*Note* – the second diastereoisomer was also isolated but wasn't completely clean after attempted HPLC purification). ^{1}H NMR (CD_3CN, 400 MHz) data for **136a**: δ (ppm) 7.35 (1H, d, $^{3}J_{HH}$ = 8.1, N-*H*), 7.07 (2H, m, 2 x N-*H*), 7.01 (2H, d, $^{3}J_{HH}$ = 8.5, Ar-*H*), 6.78 (1H, d, $^{3}J_{HH}$ = 5.7, N-*H*), 6.72 (2H, m, Ar-*H*), 4.50 & 3.37 (2H, ABq, $^{2}J_{AB}$ = 16.0, C**22**-*H*), 4.28 (1H, dd, $^{3}J_{HH}$ = 8.1, $^{3}J_{HH}$ = 6.8, C**18**-*H*), 4.17 (2H, m, C**6**-*H* & C**13**-*H*), 4.06 (1H, m, C**3**-*H*), 3.05 (1H, dd, $^{2}J_{HH}$ = 13.8, $^{3}J_{HH}$ = 6.7, C**7**-*H*), 2.91 (1H, dd, $^{2}J_{HH}$ = 13.7, $^{3}J_{HH}$ = 8.6, C**7**-*H*), 2.23 (1H, C**19**-*H* [hidden behind H_2O peak]), 1.89 (3H, s, C**1**-*H*), 1.52 (2H, m, C**14**-*H*), 1.34 (1H, m, C**15**-*H*), 1.17 (3H, d, $^{3}J_{HH}$ = 7.1, C**4**-*H*), 0.92-0.77 (12H, m, C**16**-*H* & C**20**-*H*). HRMS (ESI) *m/z* calculated for $[M+H]^+$ $C_{26}H_{40}N_4O_6Cl^+$ 539.2636, found 539.2650.

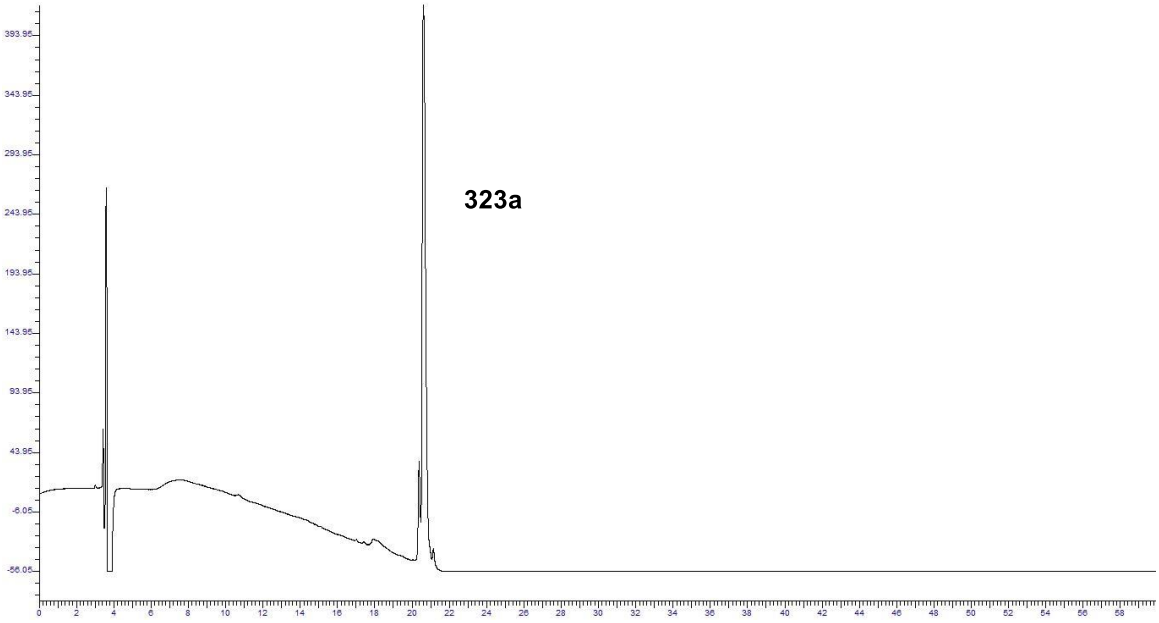

Synthesis of 377 (Reported as a mixture of diastereoisomers and keto/enol tautomers)

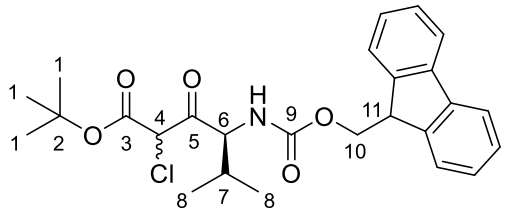

377

To a solution of *β*-ketoester **247** (0.12 g, 0.27 mmol) and 8 mol % $CpTiCl_3$ (4.6 mg, 21.0 µmol) in MeCN (20 ml) was added *N*-chlorosuccinimide (38.0 mg, 0.28 mmol). The reaction mixture was left to stir at room temperature overnight and subsequently concentrated under reduced pressure. The resulting crude material was purified by silica gel flash column chromatography (hexane : ethyl acetate, 1 : 0 to 4 : 1) to give the product as a clear oil (67.0 mg, 0.14 mmol, 52%). Reported as a mixture of enol and keto tautomers (enol : keto, ~ 10 : 90) and as a mixture of diastereoisomers (~ 50 : 50), as determined by ^{1}H NMR spectroscopy. ^{1}H NMR ($CDCl_3$, 400 MHz): δ (ppm) 12.71 (0.1H, s, enol O-*H*), 7.77 (2H, d, $^3J_{HH}$ = 7.6, Ar-*H*), 7.60 (2H, d, $^3J_{HH}$ = 7.5, Ar-*H*), 7.41 (2H, m, Ar-*H*), 7.32 (2H, m, Ar-*H*), 5.31 (0.5H, d, $^3J_{HH}$ = 9.7, N-*H*), 5.24 (0.5H, d, $^3J_{HH}$ = 9.5, N-*H*), 4.98 (0.5H, s, C**4**-*H*), 4.86 (0.5H, s, C**4**-*H*), 4.78 (0.5H, d, $^3J_{HH}$ = 4.3, C**6**-*H*), 4.76 (0.5H, d, $^3J_{HH}$ = 4.4, C**6**-*H*),

4.43 (1H, m, C**10**-*H*), 4.23 (1H, t, $^{3}J_{HH}$ = 6.8, C**11**-*H*), 2.33 (0.9H, m, keto C**7**-*H*), 2.05 (0.1H, m, enol C**7**-*H*), 1.55 (s, 1H, enol C**1**-*H*), 1.50 (4H, s, keto C**1**-*H*), 1.46 (4H, s, keto C**1**-*H*), 1.02 (3H, m, keto & enol C**8**-*H*), 0.84 (1.5H, d, $^{3}J_{HH}$ = 6.8, C**8**-*H*), 0.84 (1.5H, d, $^{3}J_{HH}$ = 6.6, C**8**-*H*). ^{13}C NMR ($CDCl_3$, 101 MHz): δ (ppm) 198.4 (C**5**), 197.9 (C**5**), 163.4 (C**3**), 163.0 (C**3**), 156.3 (C**9**), 143.8 (Ar), 141.5 (Ar), 127.9 (Ar), 127.9 (Ar), 127.3 (Ar), 125.2 (Ar), 120.2, (Ar), 120.2, (Ar), 85.4 (C**2**), 84.9 (C**2**), 67.3 (C**10**), 67.2 (C**10**), 63.2 (C**6**), 62.5 (C**6**), 60.8 (C**4**), 58.6 (C**4**), 47.4 (C**11**), 47.3 (C**11**), 29.9 (C**7**), 28.2 (C**7**), 27.9 (C**1**), 27.8 (C**1**), 19.9 (C**8**), 16.7 (C**8**), 16.6 (C**8**). HRMS (ESI) *m/z* calculated for $[M+H]^+$ $C_{26}H_{31}NO_5Cl^+$ 472.1891, found 472.1901.

Synthesis of CMK 382

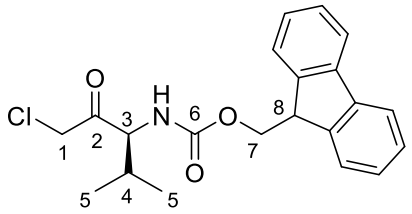

382

β-ketoester **377** (59 mg, 0.13 mmol) was dissolved in 30% TFA in DCM (5 ml) and left to stir at room temperature for 1.5 h before being concentrated under reduced pressure and subsequently lyophilised. The resulting material was then exposed to air for 72 h to ensure complete decarboxylation, giving the product as a white solid (25.2 mg, 67.8 µmol, 52%). ^{1}H NMR ($CDCl_3$, 400 MHz): δ (ppm) 7.77 (2H, d, $^{3}J_{HH}$ = 7.5, Ar-*H*), 7.59 (2H, d, $^{3}J_{HH}$ = 7.5, Ar-*H*), 7.41 (2H, m, Ar-*H*), 7.33 (2H, m, Ar-*H*), 5.31 (1H, d, $^{3}J_{HH}$ = 8.9, N-*H*), 4.53 (1H, dd, $^{3}J_{HH}$ = 8.9, $^{3}J_{HH}$ = 4.9, C**3**-*H*), 4.44 (2H, m, C**7**-*H*), 4.21 (3H, m, C**1**-*H* & C**8**-*H*), 2.21 (1H, m, C**4**-*H*), 1.02 (3H, d, C**5**-*H*), 0.85 (3H, d, $^{3}J_{HH}$ = 6.9, C**5**-*H*). ^{13}C NMR ($CDCl_3$, 101 MHz): δ (ppm) 201.5 (C**2**), 156.5 (C**6**), 143.8 (Ar), 141.5 (Ar), 127.9 (Ar), 127.2 (Ar), 127.2 (Ar), 125.2 (Ar), 125.1 (Ar), 120.2, (Ar), 67.1 (C**7**), 62.6 (C**3**), 47.4 (C**1**), 47.3 (C**8**), 30.3 (C**4**), 19.8 (C**5**), 17.1 (C**5**). HRMS (ESI) *m/z* calculated for $[M+H]^+$ $C_{21}H_{23}NO_3Cl^+$ 372.1366, found 372.1382.

7.8 References for Chapter 7

1. Sørensen, U. S., Falch, E. & Krogsgaard-Larsen, P. A Novel Route to 5-Substituted 3-Isoxazolols. Cyclization of N,O-DiBoc β-Keto Hydroxamic Acids Synthesized via Acyl Meldrum's Acids. *J. Org. Chem.* **65**, 1003–1007 (2000).

2. Kitamura, T. *et al.* Facile synthesis of 2-fluoro-1,3-dicarbonyl compounds with aqueous hydrofluoric acid mediated by iodosylarenes. *Synthesis (Stuttg)* **45**, 3125–3130 (2013).

3. Forrester, S. G., Foster, J., Robert, S., Salim, L. & Desaulniers, J. P. Efficient synthesis of the GABAA receptor agonist trans-4-aminocrotonic acid (TACA). *Bioorganic Med. Chem. Lett.* **27**, 4512–4513 (2017).

4. Theberge, C. R. & Zercher, C. K. Chain extension of amino acid skeletons: Preparation of ketomethylene isosteres. *Tetrahedron* **59**, 1521–1527 (2003).

5. Joshi, D. *et al.* An improved method for the incorporation of fluoromethyl ketones into solid phase peptide synthesis techniques. *RSC Adv.* **11**, 20457–20464 (2021).

6. Uyanik, M., Sahara, N., Tsukahara, M., Hattori, Y. & Ishihara, K. Chemo- and Enantioselective Oxidative α-Azidation of Carbonyl Compounds. *Angew. Chem. Int. Ed.* **59**, 17110–17117 (2020).

7. Preciado, A. & Williams, P. G. A Simple Microscale Method for Determining the Relative Stereochemistry of Statine Units. *J. Org. Chem.* **73**, 9228–9234 (2008).

8. da Costa, C. F., Pinheiro, A. C., de Almeida, M. v., Lourenço, M. C. S. & de Souza, M. V. N. Synthesis and Antitubercular Activity of Novel Amino Acid Derivatives. *Chem Biol Drug Des* **79**, 216–222 (2012).

9. Lee, H.-J., Huang, X., Sakaki, S. & Maruoka, K. Metal-free approach for hindered amide-bond formation with hypervalent iodine(iii) reagents: application to hindered peptide synthesis. *Green Chem.* **23**, 848–855 (2021).

10. Tian, J., Gao, W.-C., Zhou, D.-M. & Zhang, C. Recyclable Hypervalent Iodine(III) Reagent Iodosodilactone as an Efficient Coupling Reagent for Direct Esterification, Amidation, and Peptide Coupling. *Org. Lett.* **14**, 3020–3023 (2012).

11. Palomo, C., Palomo, A. L., Palomo, F. & Mielgo, A. Soluble α-Amino Acid Salts in Acetonitrile: Practical Technology for the Production of Some Dipeptides. *Org. Lett.* **4**, 4005–4008 (2002).

12. Witte, M. D. *et al.* Bodipy-VAD-Fmk, a useful tool to study yeast peptide N-glycanase activity. *Org. Bio. Chem.* **5**, 3690 (2007).

13. Sasaki, T., Hayakawa, K. & Ban, H. Photocyclization of methyl 2-arylthio- and 2-aryloxy-acetoacetates. *Tetrahedron* **38**, 85–91 (1982).

14. Allegretti, P. E., Schiavoni, M. M., di Loreto, H. E., Furlong, J. J. P. & della Védova, C. O. Separation of keto–enol tautomers in β-ketoesters: a gas chromatography–mass spectrometric study. *J. Mol. Struct.* **560**, 327–335 (2001).

Appendices

A1.1 X-ray Crystallography - General

For acquiring X-ray crystallography data, a single crystal was taken from the sample and analysed at 120.0 K. The data was collected using a Bruker D8 Venture, and the radiation source was Mo Kα (λ = 0.71073). The structure was solved by direct method and refined by full-matrix least squares on F^2 using Olex2. The refinement program was SHELXL 2017/1 (Sheldrick 2015) and the solution program was XS (Sheldrick 2008). Sample analysis and refinement was carried out by Dr Dmitry Yufit, Durham University.

A1.2 Crystal Structure Determination of Cbz-Val-Ala-OMe (303)

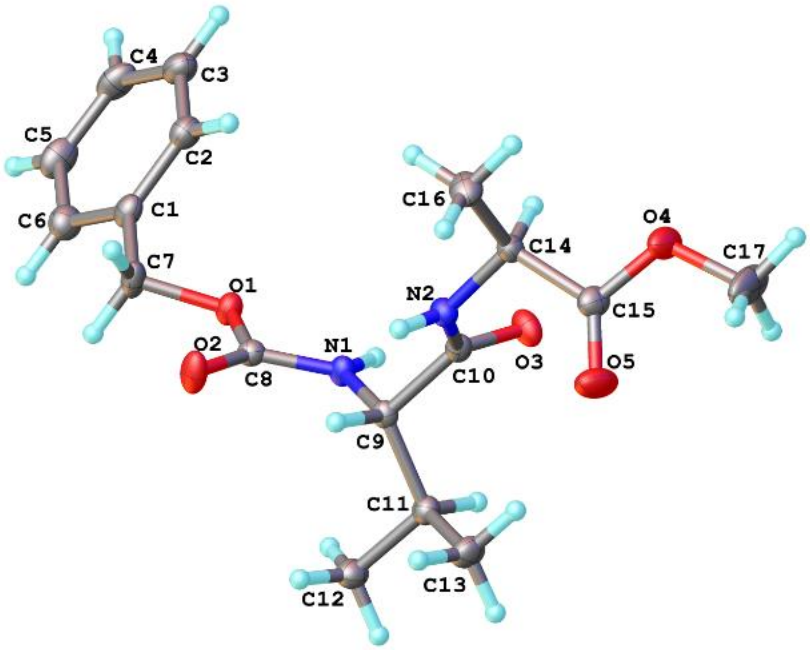

Figure A1.1 – Crystal structure of Cbz-Val-Ala-OMe (**303**), reported with a 50% thermal ellipsoid probability.

Table A1.1 – Crystal data and structure refinement for Cbz-Val-Ala-OMe (**303**).

Crystal data and structure refinement for 296	
Identification code	21srv385
Empirical formula	$C_{17}H_{24}N_2O_5$
Formula weight	336.38
Temperature/K	120.0
Crystal system	monoclinic
Space group	$P2_1$
a/Å	4.8245(3)
b/Å	11.0683(6)
c/Å	16.6992(9)
α/°	90
β/°	94.064(2)
γ/°	90
Volume/Å^3	889.48(9)
Z	2
ρ_{calc}g/cm^3	1.256
μ/mm^{-1}	0.093
F(000)	360.0
Crystal size/mm^3	0.35 × 0.06 × 0.05
Radiation	Mo Kα (λ = 0.71073)
2Θ range for data collection/°	4.89 to 54.992
Index ranges	-6 ≤ h ≤ 6, -14 ≤ k ≤ 14, -21 ≤ l ≤ 21
Reflections collected	13414
Independent reflections	4063 [R_{int} = 0.0571, R_{sigma} = 0.0605]
Data/restraints/parameters	4063/1/229
Goodness-of-fit on F^2	1.031
Final R indexes [I>=2σ (I)]	R_1 = 0.0437, wR_2 = 0.1043
Final R indexes [all data]	R_1 = 0.0479, wR_2 = 0.1070
Largest diff. peak/hole / e Å^{-3}	0.20/-0.19
Flack parameter	0.9(8)